TESIS DE LA UNIVERSIDAD DE ZARAGOZA
2024
26

Alejandra Vicente De Vera García

The Anthropocene signature in high altitude Pyrenean lakes: depositional variability, heavy metal dynamics and organic carbon fluxes

Director/es
Valero Garcés, Blas Lorenzo
Mata Campo, María Del Pilar

ISSN 2254-7606

Prensas de la Universidad
Universidad Zaragoza

ISSN 2254-7606

Universidad Zaragoza
1542

Tesis Doctoral

THE ANTHROPOCENE SIGNATURE IN HIGH ALTITUDE PYRENEAN LAKES: DEPOSITIONAL VARIABILITY, HEAVY METAL DYNAMICS AND ORGANIC CARBON FLUXES

Autor

Alejandra Vicente De Vera García

Director/es

Valero Garcés, Blas Lorenzo
Mata Campo, María Del Pilar

UNIVERSIDAD DE ZARAGOZA
Escuela de Doctorado

Programa de Doctorado en Geología

2023

Universidad Zaragoza
1542

Tesis Doctoral

The Anthropocene signature in high altitude Pyrenean lakes: depositional variability, heavy metal dynamics and organic carbon fluxes

Autor

Alejandra Vicente de Vera García

Director/es

Blas Lorenzo Valero Garcés
M. Pilar Mata Campo

Facultad de Ciencias / Escuela de doctorado
2023

The Antrophocene signature in high altitude Pyrenean Lakes

Depositional variability, heavy metal dynamics and organic carbon fluxes

PHD Thesis 2023

Alejandra Vicente de Vera Garcia

IPE CSIC

Universidad Zaragoza 1542

Grupo de Paleoambientes Cuaternarios
Departamento de Procesos Geoambientales
y Cambio Global
Instituto Pirenaico de Ecología (IPE-CSIC)
Consejo Superior de investigaciones Científicas
Avda. Montañana 1005 CP 50050
Zaragoza-España

Instituto Geológico y Minero de España
(CN IGME-CSIC)
Consejo Superior de investigaciones
Científicas
C/ La Calera, 1, Tres Cantos
Madrid-España

Los doctores M. Pilar Mata Campo y Blas Lorenzo Valero Garcés, investigadores del Centro Nacional Instituto Geológico y Minero de España (IGME-CSIC) y del Instituto Pirenaico de Ecología (IPE-CSIC) respectivamente, en calidad de co-directores de la tesis de doctorado de Alejandra Vicente de Vera García

Certifican:

Que Alejandra Vicente de Vera García ha realizado bajo nuestra dirección el trabajo que, para optar al grado de Doctor en Geología, presenta con el título: ***"The Anthropocene signature in high altitude Pyrenean lakes: depositional variability, heavy metal dynamics and organic carbon fluxes"***

Que el trabajo constituye un avance científico inédito y significativo en la temática tratada, cumple con los requisitos necesarios y se ajusta a los objetivos establecidos en el Plan de Investigación aprobado por la Comisión Académica del programa de Doctorado en Geología.

Y para que así conste, firmamos la presente Certificación en Zaragoza el 5 de Mayo de 2023 para los efectos que sean oportunos.

Dra. M.Pilar Mata Campo

Dr. Blas Lorenzo Valero Garcés

Agradecimientos

Esta tesis es una larga, increíble y agotadora historia de aventuras entre Zaragoza y todo el Pirineo Aragonés, que curiosamente, empezó en Madrid.

Mi primer contacto con este apasionante mundo, el estudio de los lagos, fue en 2014 en la Universidad Complutense de Madrid, de la mano de Mario Morellón y Juana Vegas, que me abrieron las puertas a la Limnología. Gracias Mario, por empezar todo esto, y por pensar en mí como futura doctora cuando Blas buscaba nuevas mentes que ilustrar.

Unos años después, en 2018, empezó esta locura de etapa, en la que tengo que agradecerles muchísimo, todo, a muchas personas:

En primer lugar, a mis directores de Tesis, Pili y Blas, os estaré eternamente agradecida por darme esta oportunidad. Gracias por el apoyo en el día a día, por estar ahí cualquier día de la semana y a cualquier hora, por toda la paciencia, comprensión y todo el cariño. Blas, me has enseñado infinitas cosas, pero ese optimismo abrumador es la mayor de todas.

A todo el equipo Paleo-IPE, somos mucho más que un equipo, somos una familia, y ¡Qué gran familia! A Ana, por todo tu cariño, apoyo, ayuda siempre que ha hecho falta. A Graciela, por ser compañera de locuras, apoyo emocional y científico a partes iguales. A Penélope, las charlas de coche eran la mejor vitamina para afrontar el día, gracias por todo tu cariño. A Jorge, por decir siempre “sí” a los campos y por dar unos abrazos estupendos. A Miguel Sevilla, por pasar de profe a amigo. A María y Miguel, dejasteis unos huecos en este despacho que son imposibles de llenar. A Juan, por aguantarme día a día sin rechistar (ni en chileno). A Ixeia, por levantarme en todas las bajonas y por todo el apoyo. A Marcel e Iván, por estar codo con codo en cada campaña. A Raquel, Elena e Inés, las mejores manos en el lab y las mejores escuchando mis dramas. A Fer, por tu paciencia infinita cuando aterricé en el IPE, por enseñarme tanto. Irene, Javi y Killian, muchas gracias por todo, ahora os paso el relevo, mucha suerte y a por todas!

A toda esa gente que también ha puesto piernas, espalda y ganas en las (muchas) campañas: Guillermo, Mónica, Álvaro, Ona, Reyes, Benito, Pedro...

Y a todos aquellos que el paso por el grupo, y este periplo científico, también ha cruzado en mi vida: A Rodri, por ser un hermano que no esperaba encontrar. A Josu, por todas las risas y buen rollo. To Mekbib, for always having a smile on your face.

A toda la gente del IPE, por acompañar en este viaje, por todas las risas, las comidas, los cafés, las sonrisas al cruzar los pasillos, alguna que otra salida, planes y cariño en general. A Clara, Fergus, Dani, Ana, Javi, Jesús, Antonio, Melani... Gracias a todo el mundo: administración, laboratorios, investigadores, pre-docs. Sin vosotros no hubiera sido posible, a todos, mil gracias.

A Pablo Corella, por ayudar siempre, por enseñarme a cortar los sondeos para hacer láminas y por todos los ánimos. A Matías Frugone y Josué M. Polanco por toda su ayuda y trabajo en los modelos de edad y en los análisis estadísticos. A Sergi Pla, por todas sus correcciones y el trabajo con las diatomeas. A Eduardo Vicente, por acogerme en su casa en Valencia y enseñarme todo lo que sé sobre clorofilas, y a Ricardo Prego, por todo su trabajo con la Sílice biogénica.

A todo el equipo REPLIM: País Vasco, Cataluña, Francia y Andorra. Que honor pertenecer a una unión de científicos tan extraordinaria.

A la gente de Aula Dei que me ha dedicado tanto tiempo y ayuda: Leticia Gaspar y Ana Navas, gracias por todo el tiempo invertido y recursos para realizar las granulometrías. A Carmen Castañeda, por todo su tiempo y esfuerzo con las láminas delgadas.

También mil gracias a todas esas personas que, aunque estuvieran fuera de las paredes del IPE, han sido fundamentales para sobrevivir a esta etapa:

Héctor y Andrea, gracias por haber sido la segunda y tercera pata de esta mesa coja, y además de eso, casa y lugar feliz. Héctor, gracias por tanto, esta tesis cuenta por los dos. Andrea, qué suerte hemos tenido de encontrarnos.

Marina gracias por estar siempre ahí, eres apoyo incondicional desde que recuerdo, qué afortunada soy.

A mis amigos de siempre, los que nunca fallan: Albert, Blanqui, Chris, Desy, Eri, Isa, Luis, Miri, Ro y Silvia, gracias por quererme tanto a pesar de estar poquito, qué increíble es teneros.

A Inés y Sara, por ser amigas, confidentes, paño de lágrimas, apoyo y coach emocionales, también por hacer algo de deporte, mil gracias.

A Muri, por estar siempre ahí, y por el mejor servicio de memes. A Marina B. por todo.

A mis Kikas, por aportar tantas risas y apoyo.

A Jony, por escucharme y aguantarme en esta montaña rusa. Por preparar los mejores viajes.

Y como no, a mi familia, por no soltarme nunca, por ser un apoyo absoluto siempre, en este y en todos los aspectos de la vida. Gracias mamá y papá por darme tantas oportunidades, con confiar tanto en mí, por ese amor incondicional. A Lau, por estar siempre pendiente de todo, por todo tu apoyo constante. A Ser, por dar tanta vidilla en casa. A mis tíos, Jesús y Andresa, por todo.

Esta tesis doctoral se ha realizado con una beca FPI de formación de personal investigador del Ministerio de Ciencia e Innovación asignada al proyecto MEDLANT (Depositional and geochemical dynamics of MEDiterranean Watershed-LAke Systems (WLS) during the ANThropocene: disentangling human and climate forcings, ref CGL2016-76215-R), y con el apoyo de otros proyectos relacionados desarrollados en el Instituto Pirenaico de Ecología (IPE), en particular REPLIM (Red de observatorios de ecosistemas sensibles (lagos, turberas) al cambio climático en el Pirineo, *2016-2019, EFA 056/15*).

A toda la gente que seguro me dejo en estas líneas y también tengo mucho que agradecer, gracias. Qué bonito ha sido mirar atrás y ver todo lo vivido, aprendido y disfrutado…

A mis padres

Abstract

High mountain lakes are one of the most iconic and valued elements of the mountain landscapes, but also one of the most vulnerable ecosystems. They are excellent indicators of global change, as their depositional and limnological dynamics are very sensitive to climatic and anthropogenic perturbations, and they archive in their sediments the complex signals of the interactions among the landscape, the surface geological and biological processes in the watersheds and the aquatic systems. More than a thousand high mountain lakes have been inventoried in the Pyrenees, and more than 200 have been cataloged in Aragon.

The aim of this thesis is to understand the multi-faceted nature of recent and past Global Changes in high mountain lakes in the Pyrenees and to evaluate depositional changes, sediment delivery, organic carbon accumulation and heavy metal deposition during the Anthropocene (last 2000 years). Six lakes have been selected in the western and central Pyrenees, as representative of the variety of high altitude lakes in terms of bathymetry, watershed, altitude and limnological characteristics. The lakes studied in this thesis are, from W to E: Acherito, La Sierra, Sabocos, Marboré, Urdiceto and Cregüeña.

To achieve the objectives of this PhD we have followed a multi-site, multidisciplinary approach (Chapter 2) and the following steps:

1. Characterization of some of the current processes in the lakes and the recent evolution of selected parameters (water and surface sediment composition, thermal regimes) through monitoring campaigns and surveys. The monitoring only spans 5 years, but highlights the variability of these ecosystems and provides a baseline of current status to assess the main impacts expected in physical, chemical and biological properties due to changes in water availability or increased temperatures (Chapter 3).
2. Identification of sedimentary facies, associations and depositional models from the study of sediment cores that could be applied to all high altitude Pyrenean lakes. The proposed depositional models provide the framework for reconstructing past environmental and climatic changes (Chapter 4).
3. Reconstruction of the depositional evolution of the lakes applying a multitude of analytical and absolute dating techniques to obtain high-resolution time series (Chapter 4).

4. Reconstruction of the Lithogenic and Organic carbon fluxes in the lakes for the last 1200 years (Chapter 5). The results demonstrate that prior to the 20th century, higher lithogenic fluxes occurred during periods of increased human pressure (such as the early Middle Ages) and during wetter phases of the Little Ice Age. The main changes in the studied high altitude lakes occurred synchronously but with different trends and ranges. All lakes show the largest changes during the last millennium in sediment input and organic carbon accumulation since 1850 and 1950 AD. The increase in sediment fluxes during the Great Acceleration (after 1950s CE) may be related to increased erodibility due to changes in precipitation seasonality (more winter rain versus snow). The recent increase in organic matter accumulation is likely due to increased productivity in the lakes, caused by higher temperatures, longer ice-free and growing seasons, and increased atmospheric nutrient inputs.
5. Reconstruction of the heavy metal deposition history in each lake for the last 2000 years (Chapter 6). Although all records show higher Enrichment Factors for Pb, Cu, Cd and Zn during the Roman, Medieval and Industrial revolution periods, the variable ranges and intensities indicates the important role of the characteristics of each lake, such as its location, altitude, sediment type, depth, watershed size, water composition, etc. Higher altitude lakes reflect global depositional trends and lower altitude lakes more regional and local signals.

This thesis demonstrates that high altitude Pyrenean lakes contain high-resolution archives of past climate variability and human activities during the Anthropocene. The reconstructed evolution of the depositional history of the lakes during the last two millennia underscores the uniqueness of the changes during the Great Acceleration (since mid 1950s). It provides the baseline data to assess the impact of current global warming and increased human activities in these vulnerable ecosystems and to implement conservation policies.

.

Resumen

Los lagos de alta montaña son uno de los elementos más emblemáticos y valorados de los paisajes montañosos, pero también uno de los ecosistemas más vulnerables. Son excelentes indicadores del cambio global, ya que su dinámica deposicional y limnológica es muy sensible a las perturbaciones climáticas y antropogénicas, y archivan en sus sedimentos las complejas señales de las interacciones entre el paisaje, los procesos geológicos y biológicos superficiales en las cuencas hidrográficas y los sistemas acuáticos. En los Pirineos se han inventariado más de mil lagos de alta montaña, y en Aragón se han catalogado más de 200.

El objetivo de esta tesis es comprender la naturaleza multifacética de los Cambios Globales recientes y pasados en los lagos de alta montaña de los Pirineos y evaluar los cambios deposicionales, la entrega de sedimentos, la acumulación de carbono orgánico y la deposición de metales pesados durante el Antropoceno (últimos 2000 años). Se han seleccionado seis lagos en los Pirineos occidentales y centrales, como representativos de la variedad de lagos de alta montaña en términos de batimetría, cuenca hidrográfica, altitud y características limnológicas. Los lagos estudiados en esta tesis son, de O a E: Acherito, La Sierra, Sabocos, Marboré, Urdiceto y Cregüeña.

Para alcanzar los objetivos de este doctorado hemos seguido un planteamiento multidisciplinar (Capítulo 2) en varias localizaciones y siguiendo estos pasos:

1. Caracterización de algunos de los procesos actuales en los lagos y de la evolución reciente de parámetros seleccionados (composición del agua y de los sedimentos superficiales, regímenes térmicos) mediante campañas de seguimiento y muestreos. El seguimiento sólo abarca 5 años, pero pone de manifiesto la variabilidad de estos ecosistemas y proporciona una línea base del estado actual para evaluar los principales impactos esperados en las propiedades físicas, químicas y biológicas debido a cambios en la disponibilidad de agua o al aumento de las temperaturas (Capítulo 3).
2. Identificación de facies sedimentarias, asociaciones y modelos deposicionales a partir del estudio de sondeos de sedimentos que podrían aplicarse a todos los lagos pirenaicos de gran altitud. Los modelos deposicionales propuestos proporcionan el marco para reconstruir los cambios ambientales y climáticos del pasado (Capítulo 4).

3. Reconstrucción de la evolución deposicional de los lagos aplicando multitud de técnicas analíticas y de datación absoluta para obtener series temporales de alta resolución (Capítulo 4).

4. Reconstrucción de los flujos litogénicos y de carbono orgánico en los lagos durante los últimos 1200 años (Capítulo 5). Los resultados demuestran que, antes del siglo XX, se produjeron mayores flujos litogénicos durante los periodos de mayor presión humana (como la Edad Media) y durante las fases más húmedas de la Pequeña Edad de Hielo. Los principales cambios en los lagos de gran altitud estudiados se produjeron de forma sincrónica pero con tendencias y rangos diferentes. Todos los lagos muestran los mayores cambios durante el último milenio en el aporte de sedimentos y la acumulación de carbono orgánico desde 1850 y 1950 d.C.. El aumento de los flujos de sedimentos durante la Gran Aceleración (después de 1950 d.C.) puede estar relacionado con el aumento de la erosión debido a los cambios en la estacionalidad de las precipitaciones (más lluvia invernal frente a nieve). El reciente aumento de la acumulación de materia orgánica se debe probablemente a la mayor productividad de los lagos, causada por el aumento de las temperaturas, la prolongación de las temporadas sin hielo y de crecimiento, y el incremento de los aportes de nutrientes atmosféricos.

5. Reconstrucción histótica de deposición de metales pesados en cada lago durante los últimos 2000 años (Capítulo 6). Aunque todos los registros muestran mayores Factores de Enriquecimiento para Pb, Cu, Cd y Zn durante los periodos romano, medieval y de la revolución industrial, los rangos e intensidades variables indican el importante papel de las características de cada lago, como su localización, altitud, tipo de sedimento, profundidad, tamaño de la cuenca, composición del agua, etc. Los lagos de mayor altitud reflejan tendencias deposicionales globales y los de menor altitud señales más regionales y locales.

Esta tesis demuestra que los lagos pirenaicos de gran altitud contienen archivos de alta resolución de la variabilidad climática pasada y de las actividades humanas durante el Antropoceno. La evolución reconstruida de la historia deposicional de los lagos durante los dos últimos milenios subraya la singularidad de los cambios durante la Gran Aceleración (desde mediados de la década de 1950). Proporciona los datos de referencia para evaluar el impacto del actual calentamiento global y el aumento de las actividades humanas en estos ecosistemas vulnerables y para aplicar políticas de conservación.

Contents

List of figures

1. INTRODUCTION

2. MATERIAL AND METHODS

3. MONITORING THE HIGH ALTITUDE PYRENEAN LAKES

4. SEDIMENTARY FACIES AND DEPOSITIONAL MODELS

5. ORGANIC CARBON AND LITHOGENIC FLUXES

6. THE HEAVY METAL DEPOSITION

List of tables

1. Introduction

Marboré Lake (October, 2020)

1. Introduction

1.1. Purpose of this PhD

The purpose of this PhD is to investigate the unique sediment records archived in high altitude Pyrenean lakes in order to assess the impact of climate and human activities in the recent past in sedimentary depositional environments, heavy metal pollution and changes in organic carbon and lithogenic fluxes. More than a thousand high mountain lakes, mostly between 2000 and 2500 m altitude, have been inventoried in the Pyrenees and only in Aragon, more than 200 *ibones* have been listed (Arruebo, 2014; CHE, 2023). These high mountain lakes in the Pyrenees are, in addition to iconic and threatened landscape elements, excellent indicators of the impacts of global change (Catalan et al., 2002, 2009, 2013; OPCC, 2019). Their depositional and limnological dynamics are highly sensitive to climatic and anthropogenic disturbances and they archived in their sediments the complex signatures of changes in the landscape, the aquatic system and the surface (geological and biological) processes. Recent research have shown significant alterations in lake depositional dynamics and regional flora and fauna over the last millennia in the central and western Pyrenees (see references in (Leunda et al., 2017; OPCC, 2019; Pérez-Sanz et al., 2013)) and also recent changes associated with rural exodus and new land uses, particularly increased tourism (Arruebo, 2014; CHE, 2023).

In this chapter we review the concept of the Anthropocene, how the climate and human activities are recorded in high altitude lakes and summarize the geological, geographic and limnological setting of the selected high altitude lakes studied in this PhD.

Fig.1.1. *Top. Photograph of Lake Acherito during the 2021 field campaign. Below, high-resolution photograph of an Acherito sediment core (REP-ACH17-1A-1G).*

1.1.1 The Anthropocene

The expansion of the humankind and its impact on the Planet in recent centuries has been staggering, largely due to technological advances (Turner et al., 1990) and the increase in population. According to McNeill, (2001), the human population has increased tenfold in the last three centuries to more than 8 billion, and quadrupled in the last century alone. This demographic growth has been accompanied by a 40-fold increase in livestock, the global economy, energy consumption, and industrial production (McNeill, 2001).

Within a few generations, Humankind is depleting fossil fuels that have taken hundreds of millions of years to accumulate. The burning of oil, carbon and natural gas has resulted in large emissions of CO_2 and other air pollutants (e.g., NOx, SO_2). For example, burning of fossil fuels releases about 160 Tg/year of SO_2 into the atmosphere, at least twice as much as all natural emissions combined, according to Houghton, (1996). Now emissions from fossil fuel and biomass combustion also exceed natural inputs, leading to the formation of photochemical ozone ('smog') over large regions of the world (Ehlers & Krafft, 2006).

Human activities have increased the rate of extinction in tropical rainforests by a factor of 1,000 to 10,000 (E. O. Wilson, 1992) and between 30% and 50% of the world's land area has been transformed according to (Vitousek et al., 1997). In the last century,

arable land has doubled at the expense of forests, which have declined by 20% (McNeill, 2001). More synthetic nitrogen fertilizer is now used in agriculture than is naturally fixed in all terrestrial ecosystems. Overuse of nitrogen fertilizers has led to eutrophication of surface and ground water in many regions of the world. Oxidation of SO_2 to sulfuric acid has led to acidification of precipitation and lakes, causing damage to biologically sensitive areas (Clair et al., 2004, 2011; Farmer, 1990; Tammi et al., 2003)

As a result of these human activities (Fig. 1.2), several 'greenhouse' gasses have increased substantially in the atmosphere over the last two centuries: CO_2 by more than 30% and CH_4 by more than 100% (Ehlers & Krafft, 2006), contributing significantly to the observed global average temperature increase of about 0.5˚C over the last century (IPCC, 2021).

The term "Global Change" refers to the environmental changes caused by human activities, specifically in processes that determine the functioning of the Earth system (Duarte et al., 2006). For millennia, biogeochemical processes have been co-varying in parallel with climate, but the multicomponent nature of the current global change, directly disturbing some biogeochemical cycles, creates new combinations that may have no past analogues (Catalan et al., 2013). Rockström et al., (2009) suggest that certain processes associated with global change have already surpassed the point of no return, jeopardizing the well-being of the planet and future generations. The exponential increase in resources consumption since the 1950s has been named as “The Great Acceleration” (Steffen et al., 2015).

The global impact of human activities in the Planet and their synergistic interactions with the biological and geological cycles – have even led to the proposal of the Anthropocene (Crutzen, 2002) (Fig 1.2). Given the various, significant and increasing impacts of human activities on the Earth and all the “spheres” at all scales, and the central role of humanity in geological and ecological processes, the term 'Anthropocene' has been proposed to refer to the current geological epoch (Crutzen, 2002; Crutzen & Stoermer, 2021; Steffen et al., 2015; Zalasiewicz et al., 2011, 2021). The onset of the Anthropocene could have occurred in the Early Holocene (Ruddiman et al., 2015), in the late 18th century, when analyses of air in polar ice revealed increasing global concentrations of carbon dioxide and methane or even after the first radionuclide peaks in the geological record with the use of thermonuclear bomb tests in the 1950s (Crutzen, 2002) (Fig.1.2). The geological definition of the Anthropocene as an epoch (Subramanian, 2019) or an event (Gibbard et al., 2022) has been in debate within the

Earth Science community for a long time and the nature of the Anthropocene and its use in the Earth Sciences Stratigraphy is not within the scope of this PhD thesis. The lake records included in this PhD span the last 2000 years, with a particular emphasis on the last two centuries when changes have been more intense.

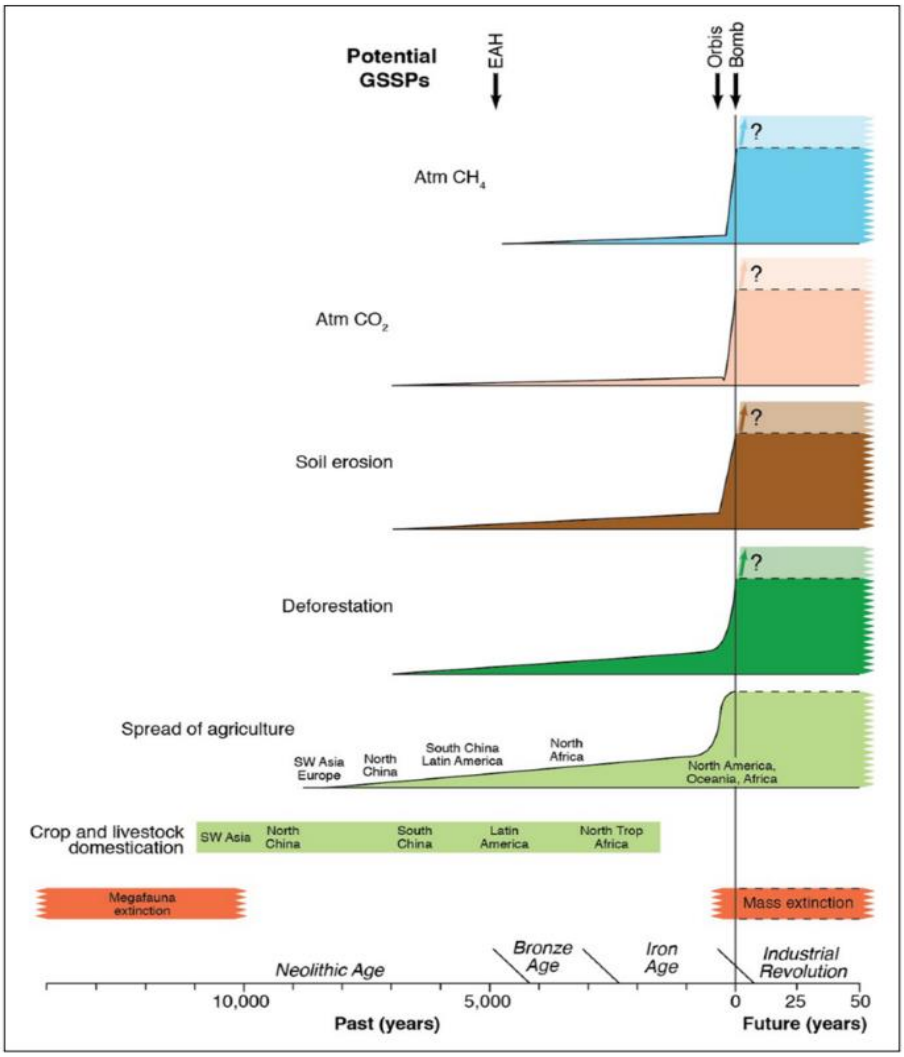

***Fig. 1.2**. The varied and increasing impacts of human activity on the Earth System and the onset of the Anthropocene. Within the long-term change of Earth, the beginning of the Anthropocene could be located at abrupt and global transitions as the Neolithic (EAH = Early Anthropogenic Hypothesis, (Ruddiman et al., 2015) the industrial Revolution or the Global Acceleration (modified from Lewis & Maslin, 2015).*

The impacts of all these changes occurring during the Anthropocene could be irreversible at a planetary scale (Fig.1.3) and, in some cases, they could lead to abrupt environmental shifts leading to a state less conducive to human development (Steffen et al., 2016). This PhD focuses on describing and interpreting the main impacts in alpine

lakes and watersheds during the Anthropocene, identifying their timing, synchronicity and intensity and the main drivers involved.

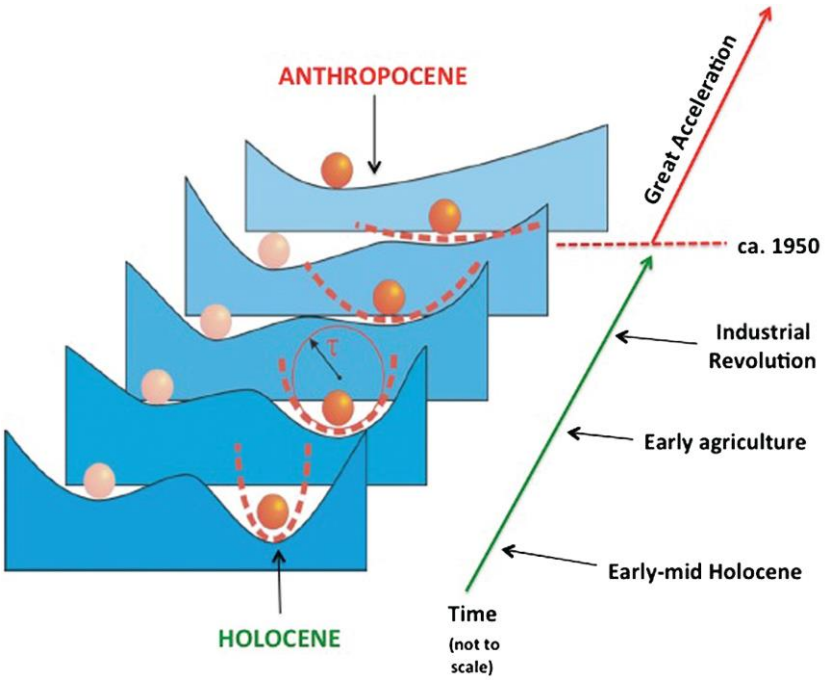

***Fig.1. 3**. A ball-and-cup depiction of regime shifts during the Holocene. The cup on the right represents a stable basin of attraction (the Holocene) and the orange ball the state of the Earth System. The cup on the left and the pink ball represent a potential state (the Anthropocene) of the Earth System. Under gradual anthropogenic forcing, the cup becomes shallower and finally disappears (a threshold, ca. 1950), causing the ball to roll to the left (the regime shift) into the trajectory of the Anthropocene toward a potential future basin of attraction. The symbol τ represents the response time of the system to small perturbations" (modified from Steffen et al., 2016, adapted from Lenton et al., 2008).*

1.1.2 Mountain regions in a changing world.

A responsible and sustainable use of the natural resources in a scenario of changing climate and increasing human pressure over the ecosystems is one of the main challenges for societies and science in the 21st century (Stern, 2006). The Anthropocene poses particular challenges in Mediterranean mountain areas as they are characterized by both a long history of human occupation, a strong seasonality of hydrological regimes and an annual water deficit (Lionello, 2012; Parry et al., 2007; Stocker, 2014). Mediterranean mountains occur in all continents (California, Chile, Australia, South Africa, circum-Mediterranean regions), providing a unique opportunity to investigate

Global Change processes during the Anthropocene in similar climate settings but with variable geographic and anthropic contexts. In this PhD we focus on the western and central Pyrenees dominated by Atlantic and Mediterranean climates, where predictive climatic models point to higher temperatures, lower precipitation and an increase in extremes (droughts, floods, heat waves) (Cuadrat et al., 2018; Pérez et al., 2010).

The effects of climate change in Mediterranean mountain watersheds have been analyzed from different perspectives: hydrology (Arnell & Gosling, 2013; Prudhomme et al., 2014), vegetation dynamics(Lenihan et al., 2003; Matesanz & Valladares, 2014; Vicente-Serrano et al., 2013), sediment dynamics (García-Ruiz, 2010; García-Ruiz et al., 2013; Syvitski et al., 2005), changes in biogeochemical cycles (Fowler et al., 2013; Frank et al., 2015), carbon storage (Muñoz-Rojas et al., 2015) and biodiversity (Hooper et al., 2012). In the context of more sustainable socio-economic growth, water availability, soil conservation and land degradation are key factors in Mediterranean mountain regions (Cramer et al., 2018; García-Ruiz et al., 2013; Meza et al., 2015) new activities and land uses (industry, tourism and agriculture) become main contributions of their economies (García-Ruiz, 2010). However, our knowledge of Mediterranean Mountain dynamics in the context of Global Warming and increased anthropogenic impact is hindered by the absence of integrated studies, both in space (including all the variety of basin contexts) and time (larger than a few decades time-span)(García-Ruiz et al., 2013; Sánchez-Canales et al., 2015).

Some of the areas most sensitive to these impacts of global change in Mediterranean areas are mountain regions. Mountains play a crucial role in providing essential ecological services such as freshwater, food, medicinal plants, timber, genetic resources, and habitats. Additionally, they are recognized for their exceptional geo-biodiversity, regulating climate, air quality, water flow, erosion, and natural hazards (Brilha et al., 2018; Egan & Price, 2017). Furthermore, mountain areas hold immense cultural heritage (García-Ruiz, Beguería, et al., 2015) and provide ample recreational and leisure opportunities, making them vital for social and economic functions (Debarbieux et al., 2014). Due to their unique environmental and climatic gradients (Körner, 2000), mountains offer exceptional opportunities to understand the dynamics of surface processes (geological and biological), and they require special attention for conservation and management.

Mountain environments are particularly vulnerable to global change, according to Krajick, (2004). Due to the steep ecological gradients in mountain areas, which are

characterized by a strong altitudinal gradient, several ecotones occur in small areas. This amplifies the impact of global climate signals (Beninston et al., 1997) and makes mountain regions some of the most evident indicators of global warming (Nogués-Bravo et al., 2007). While mountain regions may respond differently at regional to local scales to these changes, it is widely accepted that both mean and maximum temperatures will increase, along with an increase in the frequency of extreme events. Additionally, rising temperatures will likely decrease the proportion of precipitation that falls as snow (IPCC, 2021). The most significant changes are expected to occur in mountain regions at high and medium latitudes, as indicated by Egan & Price, 2017; IPCC, 2021, 2022,*https://www.ipcc.ch/report/ar6/wg1/downloads/report/IPCC_AR6_WGI_Full_Report.pdf*).

In the Pyrenees, the data compiled by the Pyrenean Observatory of Climate Change (OPCC) indicate and increase in temperature of +0.28 ºC per decade in the period 1959-2015 and a slight decrease in annual precipitation (approximately 2.5% per decade), but with large inter-annual variability (*Geoportal, Observatorio Pirenaico del Cambio Climático*, 2013)

1.1.3 Lakes as Anthropocene archives

Lakes are dynamic systems that are highly sensitive to local hydrology, the geology and biology processes and land cover and land uses changes of the drainage watershed, the regional climate and varied limnological processes (Renaut & Gierlowski-Kordesch, 2010). Lakes are distributed worldwide and, as such, can act as archives of surrounding environment conditions in many different geographical locations and climatic regions, capturing different aspects of climate change and surface processes in the watersheds (Bradley, 2015; Cohen, 2003; J. P. Smol, 2008). The sediment sequences are highly resolved archives of past global changes from geological scales to annual changes during recent times. Lake sediments are composed of two basic components: allochthonous material transported from the watershed and from global sources from atmospheric deposition, and autochthonous material produced within the lake itself (Fig. 1.4) (Bradley, 2015; J. Smol et al., 2001; Williamson et al., 2009).

Lakes have been shown to be reliable archives for reconstructing climate and environmental evolution on different time scales (from decades to million of years), as they are sensitive to both local landscape changes and global dynamics far beyond the lake itself (Arnaud et al., 2016; Barreiro-Lostres et al., 2015; Catalan et al., 2002, 2013;

González-Sampériz et al., 2017; Leunda et al., 2017; Renaut & Gierlowski-Kordesch, 2010).

Numerous studies have shown large ecological changes in lakes during the last centuries (Ho et al., 2019; Huang et al., 2022; Jane et al., 2021; Keck et al., 2020; Mammides, 2020; J. P. Smol, 2019; Steffen et al., 2007; Taranu et al., 2015) and particularly since the mid 20th century, including eutrophication (Jenny et al., 2016), biodiversity loss (Keck et al., 2020), and global changes in thermal dynamics (Maberly et al., 2020). The meta-analyses of 72 lakes worldwide based on integrated paleoecological records spanning 1850s - 2010s found that most abrupt ecological shifts had been asynchronous across the lakes, but with an increasing frequency after 1950 (Huang et al., 2022). According to this study, prior to the mid 20th century most shifts could be controlled by climate change, whereas both anthropogenic (nutrients, pollution, land use changes) and climate drivers were responsible for post 1950´s changes. However, it is worth noticing that in this study, the regional distribution of the lake records is biased to northern latitudes with few examples from the Alps and none in Mediterranean regions.

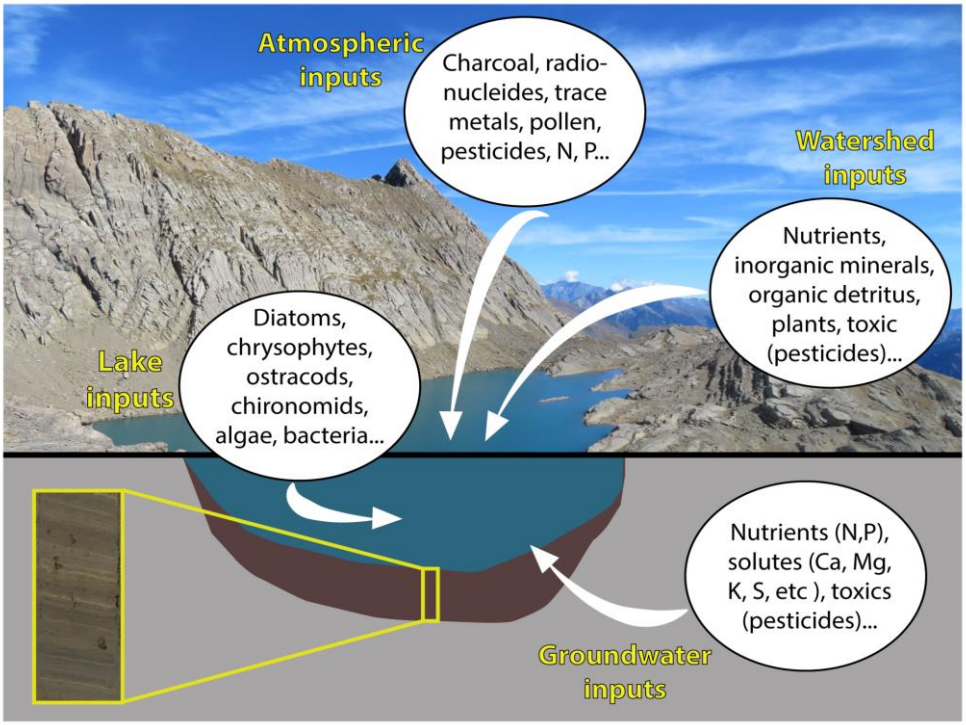

Fig. 1.4. *Sources of sedimentological, chemical and biological elements in lakes. Adapted from Smol (2001).*

High altitude mountain lakes are fragile environments due to their location in the cryosphere and the occurrence of extreme conditions and steep ecological gradients. These features give them particular limnological characteristics, as they are generally cold, oxygenated, poorly mineralized, moderately alkaline and low in nutrients (oligotrophic). These lakes are particularly sensitive to any changes in their environment due to their intrinsic characteristics, which include high UV radiation, low nutrient content and their remoteness from areas of high human activity. Furthermore, the study of disturbances is more straightforward in these types of lakes, as they are not affected by complex soil and vegetation responses (Catalan et al., 2006). For these reasons, high mountain lakes are excellent sentinels and recorders of past and present environmental changes (Catalan et al., 2006). Despite their remote location, we cannot consider these places as pristine, in fact only a few mountain lakes can be considered as such (Battarbee, 2005), as most have been affected by some direct and indirect anthropogenic changes, such as fertilization and atmospheric pollutants, grazing activities, deforestation and tourism (Camarero & Catalan, 2012; Catalan et al., 2017).

1.1.4 New Dynamics for Biogeochemical Cycles.

The new dynamics in Pyrenean high altitude watersheds and lakes caused by recent climate change and increase human pressure could have strong impacts on three main areas: sediment delivery (soil erosion, sediment mobilization), biogeochemical cycles and heavy metal deposition

i) Sediment Delivery. Experimental watersheds and catchments in Mediterranean mountains have helped to quantify some of the main parameters in soil erosion and sediment yield and their relationships with hydrometeorological factors, vegetation cover, available sediment sources and human activities (García-Ruiz et al., 2008). A recent review (García-Ruiz, Beguería, et al., 2015) showed an extraordinary high variability of erosion rates in Mediterranean watersheds, positive relationships with slope and annual precipitation and the paramount effect of land use. As most of the monitoring in experimental watersheds and plots span less than three years, the reliability of the estimated erosion rates reduces dramatically, given the highly non-normal behavior of soil erosion and its time dependency. Besides, González-Hidalgo et al., (2007) and Nadal-Romero et al., (2012) revealed that sediment mobilization in Mediterranean watersheds mostly occurs during flood events, increasing the uncertainty for the estimation of long-term sediment yields. And although most models suggest an increase of extreme events in Mediterranean regions (Sánchez et al., 2017), flood records from

annually resolved lake sequences in mid mountain areas (Montcortès Lake, Corella et al., 2014) do not show a recent increase in sediment delivery due to higher flood frequency. An integrated approach, linking experimental catchments and paleoflood records is strongly advised by the international community (*http://www.pages-igbp.org/ini/wg/floods/intro*). In this thesis we will use the novel approach pioneered by the Paleo_IPE group to compare sediment dynamics from monitored watersheds and lake records (Barreiro-Lostres et al., 2015) and quantify sediment fluxes in the Pyrenean lake basins.

ii) Bioproductivity and Carbon fluxes. Lakes are a central component of the carbon cycle, both mineralizing terrestrially derived organic matter (OM) and storing substantial amounts of organic carbon (OC) in their sediments (Anderson et al., 2009). Paleolimnological studies have shown large OC burial rate increases during the last century (Anderson et al., 2013), however, the rates and controls on OC burial by lakes remain uncertain, as do the possible effects of future global change processes. Land use changes and intensification of agriculture and associated nutrient loading together with atmospheric N-deposition are expected to enhance OC sequestration by lakes. Climate change also seems to be the main responsible behind an increased algal productivity since the end of the 19th century and during the late 20th century documented in lakes in the northern (Catalan et al., 2009; Enders et al., 2008; Pla et al., 2009; Rühland et al., 2015; Wolfe et al., 2006) and southern (Carrevedo et al., 2015; Michelutti et al., 2015) hemisphere. But many studies suggest a complex interaction of global warming and anthropogenic influences and it remains to be proven that climate is the only factor controlling these documented aquatic transitions (Catalan et al., 2013). Alternative causes as N (Galloway et al., 2008) and P increase in high altitude lakes (Camarero & Catalan, 2012), and catchment mediated processes could not be ruled out (Camarero & Catalan, 2012; Catalan et al., 2013; Elser et al., 2009; Fritz & Anderson, 2013; Pla et al., 2009).

In this PhD we reconstruct the TOC fluxes and compare them with several geochemical and biological proxies to better understand the main drivers of recent changes in carbon dynamics in Pyrenean lakes.

iii) Heavy metals loads. Global pollutants as lead associated to mining and metallurgy had a long history in the Iberian Peninsula where several records have shown the impact of diffuse atmospheric heavy metal deposition since Early Bronze age with peaks during Roman, Medieval and Contemporaneous times and a decrease since

regulation of Pb gasoline content (Camarero et al., 1998; García-Alix et al., 2013; Griffore et al., 2023; Hillman et al., 2017; Martín-Puertas et al., 2010; Mata Campo et al., 2013). The implications of recent changes in high altitude mountains for heavy metal cycling are not clear, but a remobilization of metals stored in the watersheds and changes in the accumulation in the lake sediments are likely (Bacardit et al., 2012; Bacardit & Camarero, 2009). Heavy metal stratigraphies allow evaluation of their mobilization and delivery to the watersheds in the past and recent periods and investigate if those phases could represent an analogue for the current times.

1.2. Scientific Strategy

1.2.1. A multidisciplinary strategy to investigate the Anthropocene signatures in lakes.

To understand the dynamics of Pyrenean basins and lakes during the Anthropocene we need to cover the whole spectrum of geographic/climatic/human settings and include a temporal scale able to capture the natural variability of the main processes. Sediment dynamics and biogeochemical cycles are controlled by three types of processes: i) Endogenic, related to the features of the depositional systems (relief, sediment availability and so on) and the C and heavy metal geochemical characteristics; ii) Climatic, as climate control changes in vegetation, frequency and intensity of rainfall, wind and temperature, iii) Anthropic, mainly through changes in the land uses, natural resources exploitation, infrastructure and industrialization.

The aim of this thesis is to understand the multi-faceted nature of recent and past Global Changes in high mountain lakes in the Pyrenees and to evaluate sediment delivery, organic carbon accumulation heavy metal deposition during the Anthropocene (last 2000 years).

To achieve such a goal a multi-site and multi-proxy strategy is needed to include a variety of systems, modern and past processes, and high-resolution records So, this thesis strategy relied in four axes:

1. A multi-site perspective: The selected lakes (Cregueña, Marboré, Urdiceto, La Sierra, Sabocos and Acherito) reflect the variety of Pyrenean lakes in terms of climate variability, geology, limnological properties and human impact. The transect will allow the

evaluation of its response during the last 2 ka to climatic and human impact, and to compare with the Great Acceleration in the context of the Anthropocene.

2. A paleoperspective. Most of the watersheds are now influenced by human activities and paleodata are the only possibility to define the baseline conditions (Bennion et al., 2011). Both, detailed reconstructions of climate variability and human activities are needed to evaluate the recent changes and impacts in the lakes and watersheds.

The time period spanning the records studied in this PhD includes several climatic variability phases: the IRHP (Iberian Roman Humid Period, 200 BCE – 400 CE), the Late Antiquity Age Age (400 - 800 CE), MCA (Medieval Climate Anomaly, 900-1300 CE), the LIA (Little Ice Age, 1300-1850 CE) and the recent warming (since 1850 CE) (see reviews in Carrevedo et al., 2015; Martín-Puertas et al., 2008; Morellón et al., 2012; Moreno et al., 2010 and references therein). Changes in solar insolation, North Atlantic dynamics (particularly NAO phases) and even African monsoon dynamics controlling the Westerlies and the Azores High location and intensities and also changes in volcanism have been suggested as drivers of climate variability in the western Mediterranean during the last 2000 years (Goodess & Jones, 2002; Moreno et al., 2010).

In relation to human activities during the last two millennia, there have been periods of higher human pressure in the Iberian Peninsula mountain landscapes, with a large increase in sediment delivery, intense deforestation and use of natural resources. A number of publications document these impacts in NW Spain (Redondo-Vega et al., 2017), the Somiedo Natural Park, (Morellón et al., 2016), the Iberian Range (Barreiro-Lostres et al., 2015), and the Pyrenees (Camarero et al., 1998; Pérez-Sanz et al., 2013).They mainly occurred: i) during the 13^{th}-16^{th} centuries, as a result of large land uses changes such as land clearing, in the context of increasing population and the deforestation for grazing with the development of powerful cattle ranger associations in Castilla (Mesta) and Aragón (Casa de Ganaderos), and ii) during the 18^{th}-19^{th} centuries, caused by the first industrialization phase. The research in the Iberian Range has demonstrated that in these highly human-modified landscapes, positive synergies between increasing human impact and more humid periods led to peaks in sediment delivery and heavy metal remobilization (Barreiro-Lostres et al., 2015).

3. High resolution records. To unravel the Anthropocene signatures in lake sequences we need high-resolution records containing detailed archives of past global changes. The IPE core repository and database provided a unique opportunity to

reconstruct the watersheds and lake evolution and to evaluate the response to both, the variable anthropogenic impacts and climate forcing during the last 2000 years. We will use sedimentary sequence from selected lakes with robust age models to obtain high-resolution time series of limnological changes in the lakes.

4. A multidisciplinary approach. In this PhD we followed a multi-proxy strategy including sedimentological, geochemical and biological techniques applied to watershed and lake sediment cores aimed to obtain long-term series of mountain landscape evolution, to quantify sediment delivery and erosion dynamics, heavy metal and carbon fluxes into the lakes.

1.2.2. Hypotheses and Research Goals

This doctoral thesis has been developed within the framework of the MEDLANT project (Depositional and geochemical dynamics of MEDiterranean Watershed-LAke Systems (WLS) during the ANThropocene: disentangling human and climate forcings), and with the support of other related projects developed at the Pyrenean Institute of Ecology (IPE). In particular monitoring activities have been included within the REPLIM project (Red de observatorios de ecosistemas sensibles (lagos, turberas) al cambio climático en el Pirineo) aimed to establish a network of lakes and peat bogs in the Pyrenees to serve as Global Change observatories.

The integrated research strategy stems from the idea that **past periods of global changes in Pyrenean lakes may serve as analogs to better understand, model, and predict the effects of the current period of global warming and increased human activities**. This main research is based onn several hypothesis:

H1. Sedimentation and lake dynamics is expected to change as a function of climate variability and human activities. We expect lower sediment delivery and organic carbon accumulation during colder and more arid periods and higher during warmer and more humid phases. In addition, the variable anthropogenic impact will modulate these signatures. We will investigate how climate variability during the last two millennia compares with the reconstructed changes in lake deposition in our lake sequences. The high-resolution reconstructions will help to answer the questions

whether past warmer periods or phases of intense human activities could be considered as analogue for the present global warming period.

H2. Synergistic effects between climate and human activities intensify erosion, heavy metal mobilization and C storage in high altitude mountain basins. Sediment fluxes maximize when human and climate factors reinforce each other. Strong human disturbances in Mediterranean mountain systems occurred during warmer periods. Low-resolution paleoreconstructions have suggested that in Mediterranean areas warmer periods have always been more arid and colder periods more humid (Morellón et al., 2012; Moreno et al., 2012). However, higher resolution paleoreconstructions (Corella et al., 2014) and climate models suggest that changes in precipitation seasonality may account for humid phases during relatively warmer periods (as the MCA) and arid phases during the LIA. Although an intensification of the hydrological cycle is expected during warmer periods (MCA, end of LIA, recent warming), these periods do not show the same response in available high-resolution records. For example, the only long varved record in Spain (annual resolution) shows an increase in sediment delivery – and flood frequency - during the MCA and a decrease in flood intensity and frequency during the last decades (Corella et al., 2014), illustrating the complexity of watershed response to climate and human activities. In recent times in the industrial period, increase in extreme events (Sánchez et al., 2017) and reforestation due to rural exodus (García-Ruiz et al., 2013) have opposite impacts in sediment delivery.

H3. The intensification of the hydrological cycle associated with recent global warming will lead to higher sediment mobilization and sediment delivery to the lake systems, increase in carbon fluxes and bioproductivity and an increase in metal mobilization from the watersheds. We will test these hypotheses by comparing recent changes in sediment delivery, carbon fluxes and metal mobilization with those during other warmer periods such as the IRHP, MCA and the end of the LIA. We will also investigate any significant changes in bioproductivity and C fluxes associated with the main phases of anthropic change.

The main objective of this PhD is to provide high-resolution, well-dated reconstructions of past global changes during the last two millennium along an altitudinal transects in the western and central Pyrenees based on a multiproxy study of lakes and watersheds.

The **specific objectives** are:

-To reconstruct the sedimentary dynamics of the Aragonese Pyrenean lakes during the last 2 millennia.

-To define a common depositional model for high altitude lake systems that could serve as a general framework to understand the impact of the drivers during the last 2 millennia.

-To characterize the current depositional patterns, limnological behavior and current characteristics of the lakes, through monitoring campaigns

-To reconstruct the response of Pyrenean lakes to the major climatic changes of the last millennium (Medieval Climate Anomaly, Little Ice Age, Recent Warming)

- To reconstruct the response to the variable anthropogenic impact during medieval, contemporary and recent rural abandonment.

- To identify, in each of these periods of rapid change, the synergies between climate and human activity

-To identify recent trends in changes in depositional dynamics (erosion and sediment transport from the catchment watersheds), biological productivity and deposition of pollutants (heavy metals) and to assess the role of climatic and anthropogenic changes in these trends.

-To evaluate the rates of change and trends in the aquatic systems caused by recent human activities (farming, tourism, hydroelectrical and mining activities) and by possible effects of recent warming.

-To increase our prediction capacity of the impacts of future global change in the high mountain watersheds and lakes of the Aragonese Pyrenees by analyzing the past responses of watersheds and lakes to climate variability and human intervention in the landscape and ecosystems.

- To contribute to improve the management and conservation policies of protected areas within more sustainable development strategies.

1.2.3. Structure of the PhD

To achieve the objectives of this PhD within the outlined research strategy, we have followed the following steps:

1. Characterization of some of the current processes in the lakes and the recent evolution of selected parameters (water and surface sediment composition, thermal regimes) through monitoring campaigns and surveys (Chapter 3).

2. Identification of sedimentary facies and associations and depositional models from the study of sediment cores that could be applied to all high altitude Pyrenean lakes (Chapter 4).

3. Reconstruction of the depositional evolution of the lakes applying a multitude of analytical and absolute dating techniques to obtain high-resolution time series (Chapter 4).

4. Reconstruction of the Lithogenic and Organic carbon fluxes in the lakes for the last 2000 years (Chapter 5).

5. Reconstruction of the heavy metal deposition history in each lake for the last 2000 years (Chapter 6).

1.3. Study area

1.3.1. Geological and geographic settings of Pyrenean lakes

All the lakes studied in this thesis are located in the Central and Western Pyrenees. The Pyrenees are an alpine mountain range stretching from the Atlantic Ocean to the Mediterranean Sea in the north of the Iberian Peninsula. The Pyrenees has a WNW-ESE orientation, it extends for about 450 km from the Bay of Vizcaya to the west, to the Gulf of Lion, Mediterranean Sea to the east, and it covers an area of approximately 45000 km^2. The Pyrenees has a maximum width of 130 km and the highest peaks are located in the central areas of the range, with the Aneto Peak (3404 m a.s.l.), Posets (3375 m a.s.l.), and Monte Perdido (3355 m a.s.l.). The Pyrenean range is flanked by the Aquitania Basin to the north and Ebro Depression to the south.

Since Mattauer, (1968) three main geological units have been considered in the Pyrenees: the North-Pyrenean zone, the Axial zone and the South-Pyrenean zone (Fig. 1.5). The structure of the range is asymmetric with a steeper and narrower French northern side and a much wider and more gently inclined, Spanish southern side (Belmonte-Ribas et al., 2014). The range is characterized by large thrusting structures involving the basement of the axial zone and part of its Mesozoic cover (Lakora, Gavarnie...) with displacements towards the south of more than 50 km in some cases.

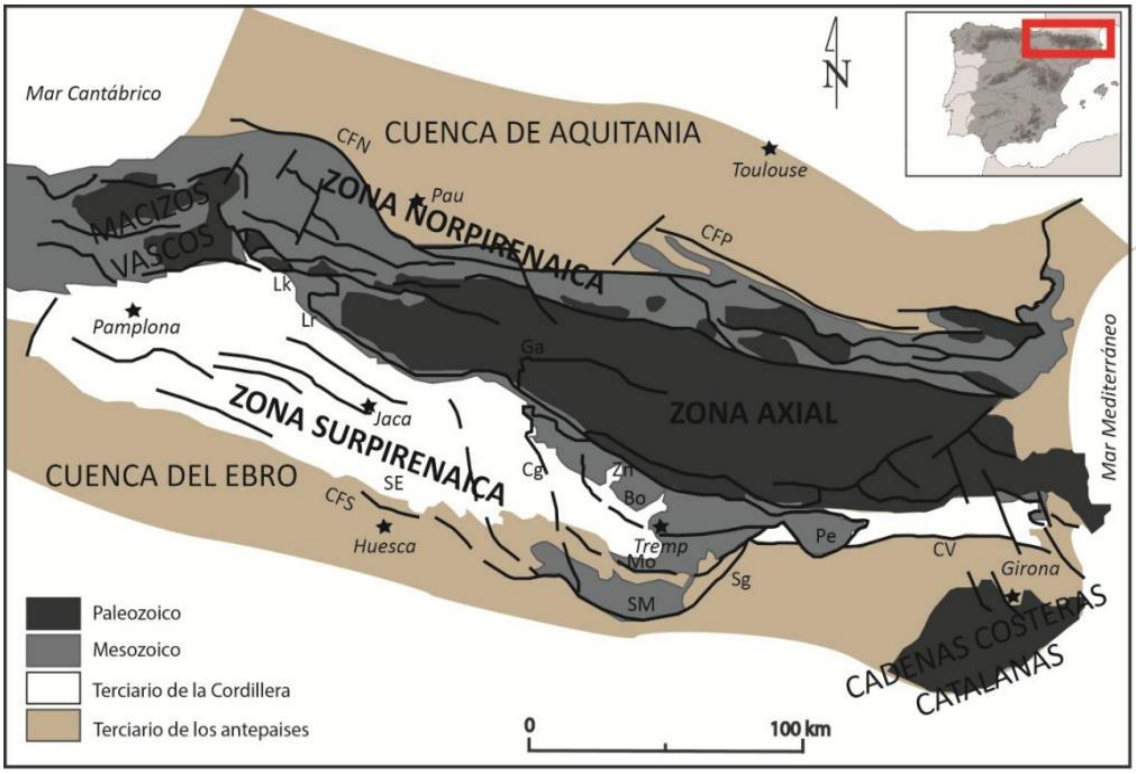

Fig. 1.5. *Structural diagram of the Pyrenees (Modified from Vera, (2004) with the location of the lakes studied in this PhD. Denomination of the main structures: CFS: South Pyrenean Frontal the main structures: CFS: South Pyrenean frontal overthrust, CFN: North Pyrenean frontal overthrust, CPP: Petites Pyrénées overthrust, LN: Lateral overthrust. Pyrenean frontal overthrust, CPP: Petites Pyrenees overthrust, Lk: Lakora overthrust, Lr: Lakora overthrust, Lk: Lakora overthrust, Lk: Lakora overthrust. Lakora Ridge, Lr: Larra Ridge, SE: Sierras Exteriores, Ga: Gavarnie Ridge, ZN: Nogueres zone, Bo: Bóixols overthrust, Mo: Montsec overthrust, SM: Sierras Marginales, Sg: Segre oblique ramp zone, Cg: Cinca oblique ramp zone (western boundary), Sg: Segre oblique ramp zone, Cg: Cinca oblique ramp zone (western boundary). Cinca (western limit of the Central South Pyrenean Unit), Pe: Pedraforca mantle, CV: Vallfogona thrust.*

The axial zone is composed by an extensive outcrop of the Variscan basement, immediately south of the North Pyrenean fault zone, where some of the highest peaks of the range are located. It is in this axial zone where the lakes of this thesis are located.

The Pyrenees Range was formed during the Alpine orogeny (Upper Eocene - Oligocene). Prior to this, sediment accumulated in large basins formed by distensional dynamics during the Lower Triassic of the Upper Permian (Puigdefàbregas & Souquet, 1986). From the Upper Cretaceous to the Middle Miocene (Muñoz, 1992) a tectonic inversion took place due to the collision between the Iberian and European Iberian plates that uplifted and formed this mountain range.

1.3.2 Climate variability

The main cause of climatic spatial variability in the Pyrenees is the topography of the terrain and the diversity of exposures that generate a wide range of local climates (Cuadrat Prats & Martín Vide, 2007). The main source of moisture for the Pyrenees is the North Atlantic, linked to the North Atlantic Oscillations, although there is also moisture from the western Mediterranean and northern Europe (Araguas-Araguas & Diaz Teijeiro, 2005; Lambs et al., 2013). The distribution of precipitation in this region is complex due to the orographic barriers (García-Ruiz, López-Moreno, et al., 2015). In general terms, three main bioclimatic regions can be identified along the Pyrenees. The Western Pyrenees is characterized by a humid climate, influenced by the Atlantic, while the Eastern Pyrenees has a drier and warmer summer season due to its Mediterranean influence. The Central Pyrenees, on the other hand, has characteristics of both climates, showing a more continental character with temperature contrasts and being drier than the western region (Batalla et al., 2018). The west - central part of the Pyrenees is a particularly sensitive transition zone between the Mediterranean and the Atlantic regions with an important altitudinal gradient, and varied topography, climate and vegetation.

Besides the Atlantic and Mediterranean influences, topography also plays an important role in Pyrenean climatic variability. Areas above 1,500 - 1,800 m altitude (the altitudinal limit will vary depending on orientation) have mountain climates, with the highest mean annual precipitation (MAP) values in the highest areas (2000-2500 mm/year). In the lower altitude areas, the highest MAP is found in the western regions, reaching 2000-2500 mm/year, but decreasing drastically towards the east, up to the Mediterranean coast (around 700 mm/year). Mean annual temperature (MAT) is related to elevation, with a temperature gradient of about 0.6 °C/100 m (García-Ruiz, López-

Moreno, et al., 2015). The AMR in the valleys is around 5-10 °C, while the AMR below 0 °C is found in the high massifs. The 0 °C isotherm is located at about 2726 m a.s.l. according to Del Barrio et al., (1990).

Regarding the climate variability over the last decades, the increase in temperature is one of the most outstanding features. According to the OPPC (*https://www.opcc-ctp.org/es/geoportal)* in the period 1959-2015, the average annual temperature had a rate of increase of +0.28 ºC per decade. This increase is general throughout the mountain range, with few differences between the northern and southern slopes (Fig.1.6).

Precipitation does not show such a clear evolution. From 1959 to the present, the data indicate a slight decrease in annual precipitation (approximately 2.5% per decade), but with large inter-annual variability (Fig.1.6).

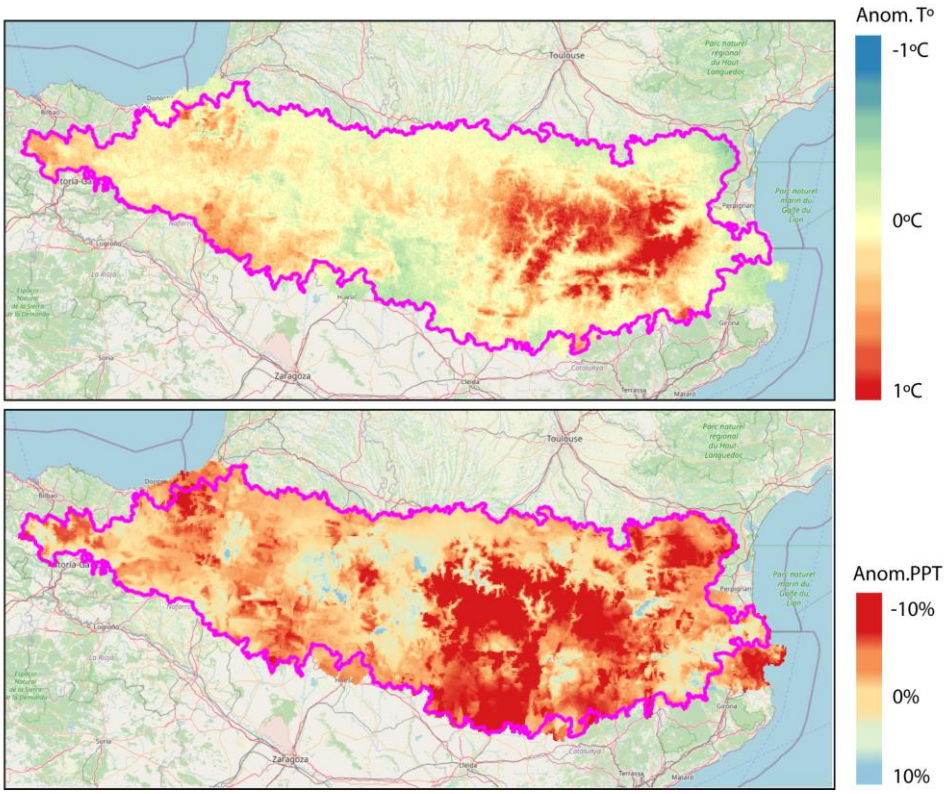

Fig. 1.6. *Maps obtained from the OPCC geoportal (https://www.opcc-ctp.org/es/geoportal) of the annual anomaly of average temperatures and precipitation for the period 2001-2010 compared with the average for the period 1961-1990. This indicator was calculated on the basis of the homogenized database for the entire Pyrenees (OPCC, 2019). The boundaries shown on the map correspond to the administrative boundaries of the Working Community of the Pyrenees generated from the aggregation of the municipalities that have joined it: Spain, France and Andorra.*

1.3.3 Anthropogenic activities

Despite the location of the high altitude mountain lakes in relatively remote areas in the Pyrenees, some of them have suffered direct impacts of anthropogenic activities during the last millennium. All the lakes are above the tree line and the vegetation cover is sparse, but some of them, those at lower altitudes, may have been affected to some extent by medieval deforestation for grazing (González-Sampériz et al., 2017). This deforestation took place in the upper valleys of the Gállego (this would affect the Sierra and Sabocos Lakes) and the Aragón Subordán (Acherito Lake).

Two of the lakes, Marboré and Urdiceto have been dammed during the early 20th century. In 1938, a dam was built in Marboré, but it never became operational and it was soon dismantled, so it has not affected the lake level, (Nicolás-Martínez, 1981). The Urdiceto dam has been exploited for hydrological power till recent years The administrative concession for the construction of the dam dates back to 1935. By 1938 the dam was in operation, although it was not fully completed until 1948. After the dam was built, the water depth increased from <10 m to 25 m. Materials from around the lake were used in the construction. Since then, several improvement and maintenance works have been carried out on the reservoir, such as waterproofing campaigns and dam enlargements (CHE, 1994).

Several areas in the Pyrenees have been the site of mining activities during several historic periods since Roman times. In the Parzan mines, lead ore was mined from the 16th century until the middle of the 20th century (Bielza et al., 1986; Corella et al., 2017) and iron and silver mining activities were carried out in the Alto Cinca in the first decades of the 20th century. Although minerals were not extracted directly in the watersheds of any of the lakes, the exploitation activities in the surrounding areas and the construction of infrastructure to support the mining activity had an impact on the environment. Global deposition from mining and metallurgical activities in the Iberian Peninsula and beyond has also had an impact on heavy metal deposition in high altitude lakes (Camarero et al., 1998).

More recent anthropogenic impacts are related to new economic activities in the region. Sabocos Lake is close to a ski resort (Panticosa Ski Resort) built in the 1980s. The construction likely had a limited direct impact on the watershed and the management of the resort claims that there is no direct impact on the hydrology of the lake. The proximity of the ski resort has increased winter and summer tourism. Evidence of direct,

recent impact in high altitude Pyrenean lakes because of increased hiking and tourism activities has been found in many lakes (Arruebo, 2014).

1.3.4 The alpine lakes in the Pyrenees

High altitude lakes are iconic elements of the Pyrenean landscape, greatly vulnerable to climate changes and increasing human impact. The main forecasted impacts on high elevation lakes are related to changes in physical, chemical and biological properties due to water availability changes and higher temperatures. According to Castillo Jurado, (2003), there are around 1000 Pyrenean lakes (>0.5 ha surface area) located in the alpine and montane vegetation belts, mostly between 2000 and 2500 m asl. The 17 largest lakes (surface area> 0.3 km^2) represent a total surface area of about 7.87 km^2; about 75% of Pyrenean lakes are smaller than 0.04 km^2; the average drainage basin surface area is about 1.67km^2 but the range is quite large between 0.1 km^2 (Gentianes, Gave de Pau) to 32.6 km^2 (Baños de Panticosa, Gállego River). Considering depth, there are two main categories: shallow (< 10-15 m maximum depth) and deep (> 15 m). In the Pyrenees we have 90 lakes deeper than 25 m, and 47 are deeper than 40 m. A survey during the summer of 2000 (Catalan et al., 2006) showed that 70 % of the Pyrenean lakes are ultraoligotrophic (TP < 4.7 µg L-1), 22 % oligotrophic (4.7 < TP < 9.3 µg L-1) and 6 % mesotrophic (9.3 < TP < 31 µg L-1)**.**

The annual cycle of high altitude lakes is greatly controlled by the ice phenology and the temperature changes (Sabás et al., 2021; Ventura et al., 2000) (Figure 1.7). During the ice-free season, in more than 75 % of the lakes light penetrates till the bottom, so autotrophic biota may develop. UV radiation can be quite high in these ecosystems, and many studies have shown its effects on micro-organism (Catalan et al., 2002; Rivera-Rondón & Catalan, 2020; Sabás et al., 2021). The lakes exhibit a dimictic behavior, where the surface waters become significantly warmer than the deeper waters during the summer. In contrast, during the winter, the deep waters maintain a higher temperature than the surface waters close to the ice. Two distinct periods exist in which the deep and surface waters become homogeneous, leading to the mixing of waters: one following the ice melting and the surface waters warming up during the summer, and another occurring in autumn (Fig. 1.7).

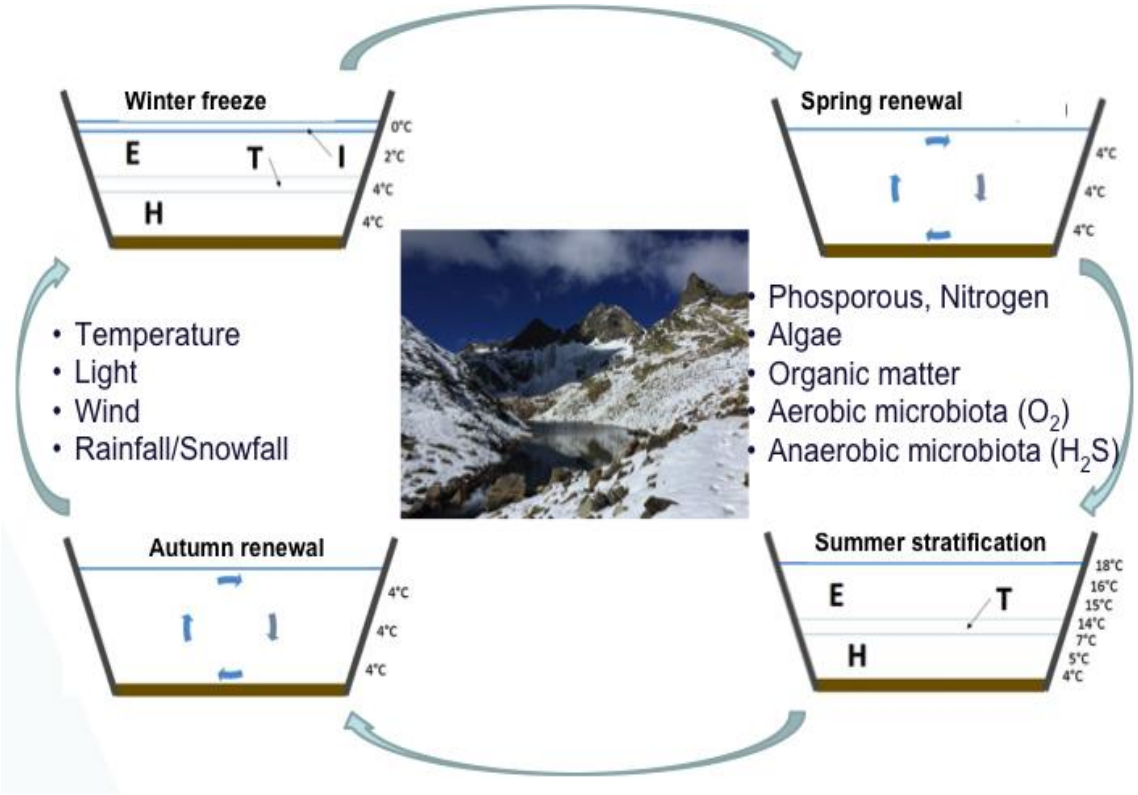

Fig. 1.7. *The seasonal cycle in high altitude lakes (from Ventura et al., 2000).*

Some of the high mountain lakes have been monitored by the Confederación Hidrográfica del Ebro (CHE) for the last decades (*https://www.chebro.es/en/web/guest/puntos-de-control-y-resultados*) and several reports have been published about their ecological status. The REPLIM project has implemented a monitoring network in lakes and peatlands where some basic but useful parameters have been measured to provide a regional picture of environmental and climate impacts in these ecosystems (*Geoportal, Observatorio Pirenaico del Cambio Climático*, 2013).

1.3.5. Study Sites

To investigate the nature of recent changes in high altitude Pyrenean watersheds, we selected six high altitude (1870-2630 m asl) lakes along a West - East transect in the Pyrenees (Fig. 1.8.): Acherito (ACH), La Sierra (SIE), Sabocos (SAB), Marboré (MAR), Urdiceto (URD), and Cregüeña (CRE). The lakes reflect the variety of Pyrenean lakes in terms of climate, geology, limnological properties and human impact. The main characteristics of the lakes are summarized in Table S1.1. The geology of the watersheds has been obtained from the MAGNA 1:50000 geological maps (*https://info.igme.es/cartografiadigital/geologica/Magna3S.aspx?language=es*).

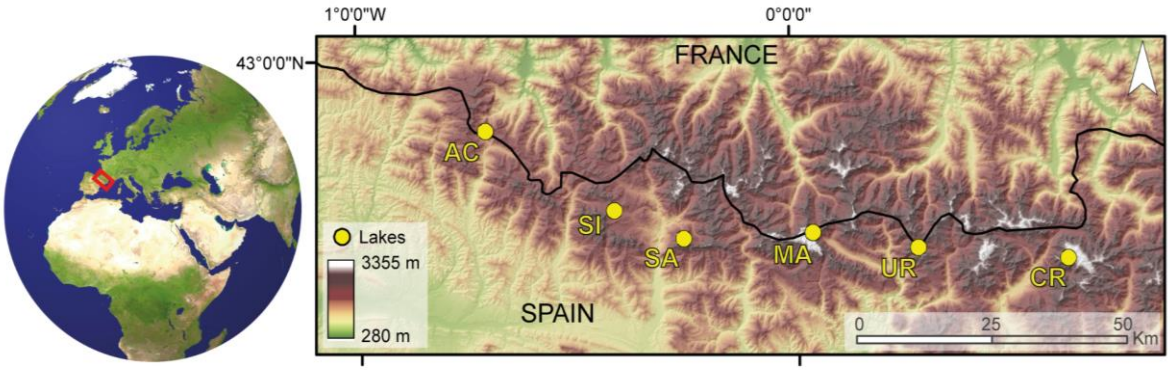

Fig. 1.8. *Location map of the selected lakes in a topographic map of the Pyrenees*

1.3.5.1. Cregueña

The lake is located in the Cregüeña valley and cirque, in the headwaters of the Esera River, within the Posets-Maladeta Natural Park in the Central Pyrenees. This narrow, rocky valley borders the southern slope of the Maladeta massif and contains the over-excavation basin of the Ibón de Cregüeña (42°38'N, 0°37'E). The lake is located at an altitude of 2,633 meters asl and characterized by its large surface area (44.5 hectares) and high depth (97 meters) (CHE, (2023), own data).

The 340.3 ha basin is formed by medium-grained granitic rocks, porphyroid with biotite, muscovite, cordierite and alkali feldspar megacrystals, emplaced during the Variscan orogeny (Cambro-Ordovician to Carboniferous (Ríos Aragües et al., 1991)). The landscape has been shaped by glacial activity the Pleistocene and by later

advances, such as during the Neoglacial phase (mid Holocene) and the Little Ice Age (LIA) (de Pisón Stampa, 1989) (Fig. 1.9).

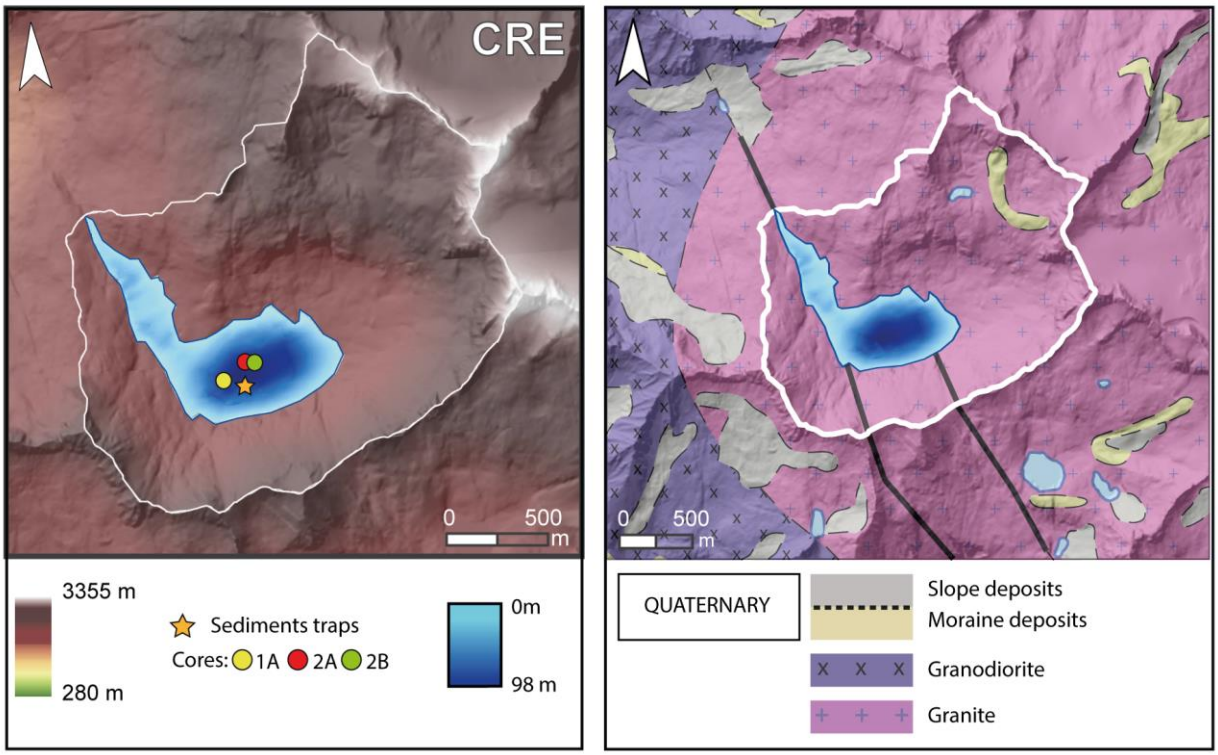

Fig. 1. 9. *Left. Topographic map and bathymetry of Cregueña with the location of selected cores and the sediment trap. Right. Geological map of the watershed and surroundings of the lake modified from 1:50000 MAGNA geological maps.*

In the upper part of the cirque, moraines associated with the LIA have been identified (Copons & Bordonau, 1997), which illustrates recent changes in the evolution of the ice extent in the basin, which may have had an impact on the sediment delivery to the lake. The watershed has slopes of 75%, which, together with the gelifraction processes, is responsible for active transportation processes of coarse granitic material to the lake (Cardiñanos, 2001, CHE, 2011).

According to CHE (*https://www.chebro.es/en/web/guest/puntos-de-control-y-resultados*) the ecological status of the lake is good.

1.3.5.2 Marboré

Lake Marboré (MAR) (42º41'N, 0º2'E) is located at an altitude of 2600 m in a glacial cirque within the Monte Perdido massif, the highest limestone massif in Europe. The lake and its watershed are included in the Ordesa y Monte Perdido National Park. Marboré Lake has a surface area of 8.8 ha, and is located in a catchment of 95.7 ha surface area. Its maximum depth is 26 m.

The Marboré Cirque is underlain by a synclinorium-like structure, composed by alternating limestone and sandstone layers of the Marboré Fm. (Fig.1.10). The Marbore Fm is composed of decimetric to metric-scale beds of gray, brown-weathered quartz-carbonate calcareous sandstone. It ranges from grain-supported quartz sandstones with sparse carbonate cementation to matrix-supported greywacke with quartz and calcite grains enclosed in a carbonate matrix (Souquet, 1967) (Fig.1.10).

Both the morphology and karst features of the Marboré cirque show structural control over the origin and evolution of the lake basin since deglaciation (B. Oliva-Urcia et al., 2018). The environmental, glacial and climate evolution of the area has been reconstructed based on sediment cores (Leunda et al., 2017; B. Oliva-Urcia et al., 2018) and geomorphological studies (García-Ruiz et al., 2013). There was a small snow and ice accumulation reaching the lake in the NW margin till early 20th century (García-Ruiz et al., 2013). One of the last remaining Pyrenean glaciers occurs in the northern slopes of the Monte Perdido (García-Ruiz et al., 2013, 2014), near the lake, but outside its watershed. The glacier was greatly reduced during the medieval times and expanded during the LIA and recent monitoring indicates it will disappear in the next decades (López-Moreno et al., 2019; Moreno et al., 2021).

According to CHE (*https://www.chebro.es/en/web/guest/puntos-de-control-y-resultados*) the ecological status of the lake is good.

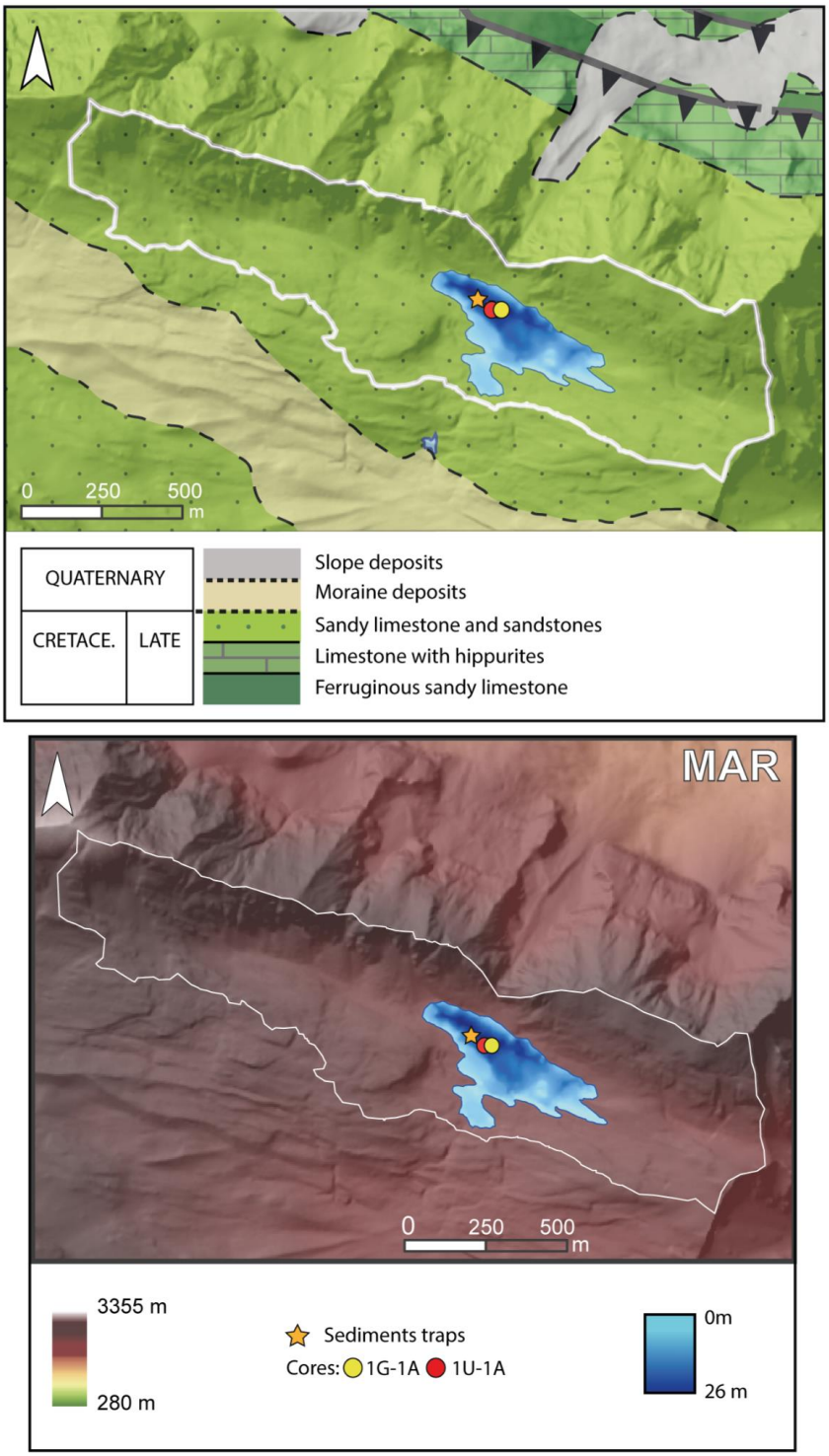

Fig. 1. 10. *Left. Topographic map and bathymetry of Marboré with the location of the selected cores and the sediment trap. Right. Geological map of the watershed and surroundings of the lake modified from 1:50000 MAGNA geological maps.*

1.3.5.3 Urdiceto

Urdiceto (42º39'N, 0º16' E) is situated at 2364 m asl. With a surface area of 26.6 ha, it is the second largest of the studied lakes, after Cregueña. The watershed covers 105.1 ha surface area and its maximum depth is 33 m.

The stratigraphic succession in the Urdiceto basin (Fig. 1.11) includes Ordovician, Permian, Triassic and Quaternary sedimentary materials, as well as granitic intrusions (Ríos Aragües et al., 1982). The Ordovician materials are yellowish-brown quartzites in decimetric layers in irregular contact with the Bielsa granite. The Permian and Triassic formations are red fine - to medium-grained sandstones and siltstones in 10-12 m thick beds. The Bielsa granite is composed of quartz, orthoclase, plagioclase (albite) and biotite, as well as apatite and zircon as accessories. Finally, the Quaternary occurs as slope debris deposits (Ríos Aragües et al., 1982) (Fig.1.11).

According to CHE (*https://www.chebro.es/en/web/guest/puntos-de-control-y-resultados*) the ecological status of the lake is good.

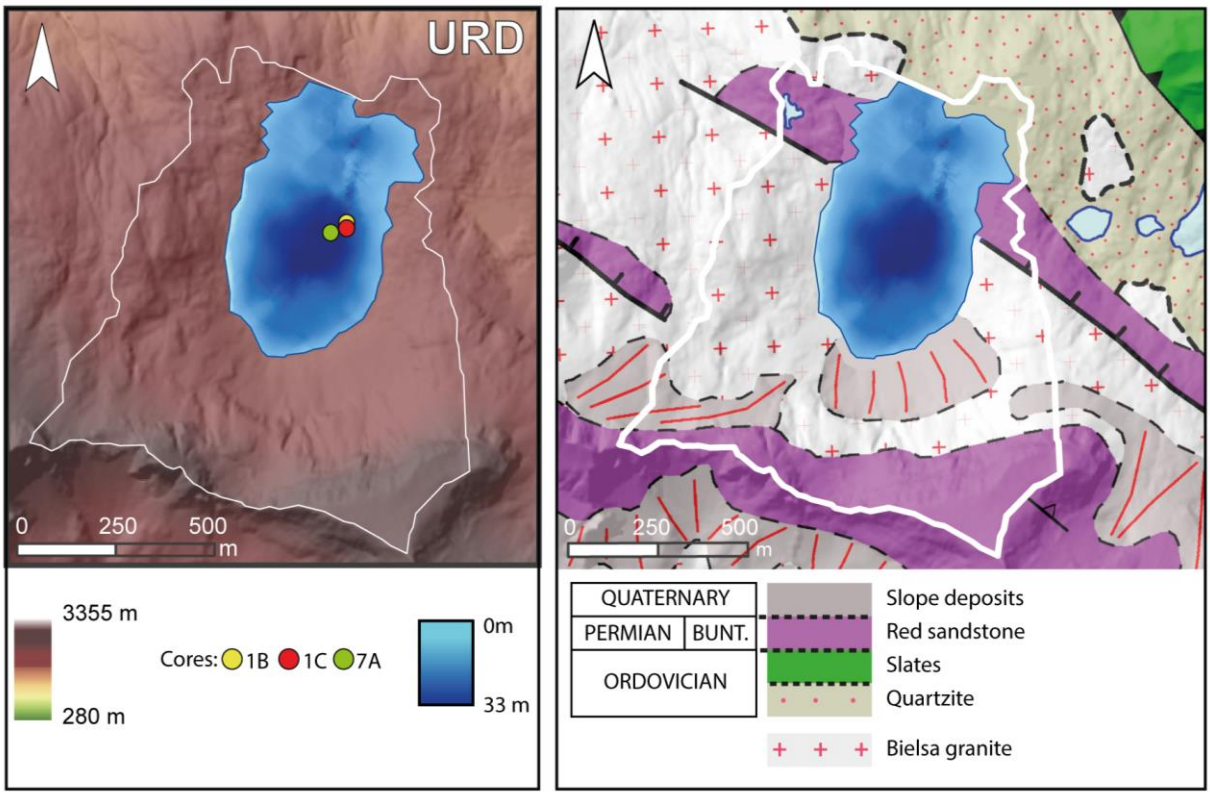

Fig. 1. 11. *Left. Topographic map and bathymetry of Urdiceto with the location of the selected cores and the sediment trap. Right. Geological map of the watershed and surroundings of the lake modified from 1:50000 MAGNA geological maps.*

1.3.5.4 La Sierra

La Sierra (42º44'N, 0º24' W) is the smallest of the lakes studied in this thesis, both in terms of surface area (1.3 ha) and maximum depth (7m). It is located in a 166 ha surface area basin at 2022 m asl.

The geological composition of the watershed only includes Carboniferous (Namurian and Westphalian) materials (Fig. 1.12). These materials are greywackes and shales (Culm facies) (Ríos Aragües et al., 1989). La Sierra Lake is near the Izas experimental catchment area where climate and hydrological features have been monitored for several decades (Alvera, 2000; Alvera & García-Ruiz, 2000; Lana-Renault et al., 2011).

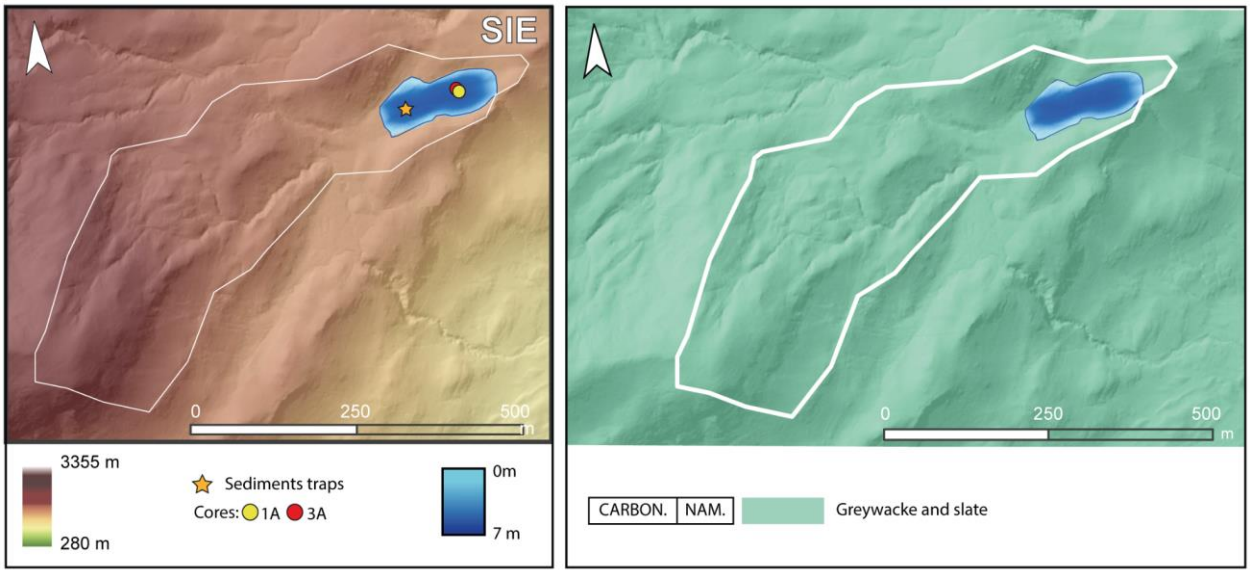

Fig. 1. 12. *Left. Topographic map and bathymetry of La Sierra with the location of the selected cores and the sediment trap. Right. Geological map of the watershed and surroundings of the lake modified from 1:50000 MAGNA geological maps.*

1.3.5.5 Sabocos

Sabocos Lake (42º41'N, 0º15' W) is situated at 1900 m asl in a catchment area of 231.7 ha. The surface area of the lake is 9.6 ha and its maximum depth is 32m. The watershed is geologically complex as there is a diversity of structures and formations. Tectonically the lake is located in a EW syncline formed by Lower Devonian materials, affected by N-S or NE-SW faults. To the south of the watershed, Cretaceous and Tertiary materials are uplifted by an E-W thrust fault (Fig. 1.13). The Devonian sequence is

composed by an alternation of calcareous shales and gray limestones in decimetric layers followed by black, limestones in decimetric to metric layers (Ríos Aragües et al., 1989). The Late Cretaceous rocks are mainly white to light gray massive limestones, followed by reddish ferruginous sandy limestones, light colored limestones and topped by the Marboré calcareous sandstone (Ríos Aragües et al., 1989). Concordantly over the Marboré sandstones are Palaeocene-Eocene fine-grained, gray-coloured dolomites in decimetric to metric layers, followed by massive limestones (Ríos Aragües et al., 1989) (Fig. 1.13).

According to CHE (*https://www.chebro.es/en/web/guest/puntos-de-control-y-resultados)* and Arruebo (2014) the ecological status of the lake is good.

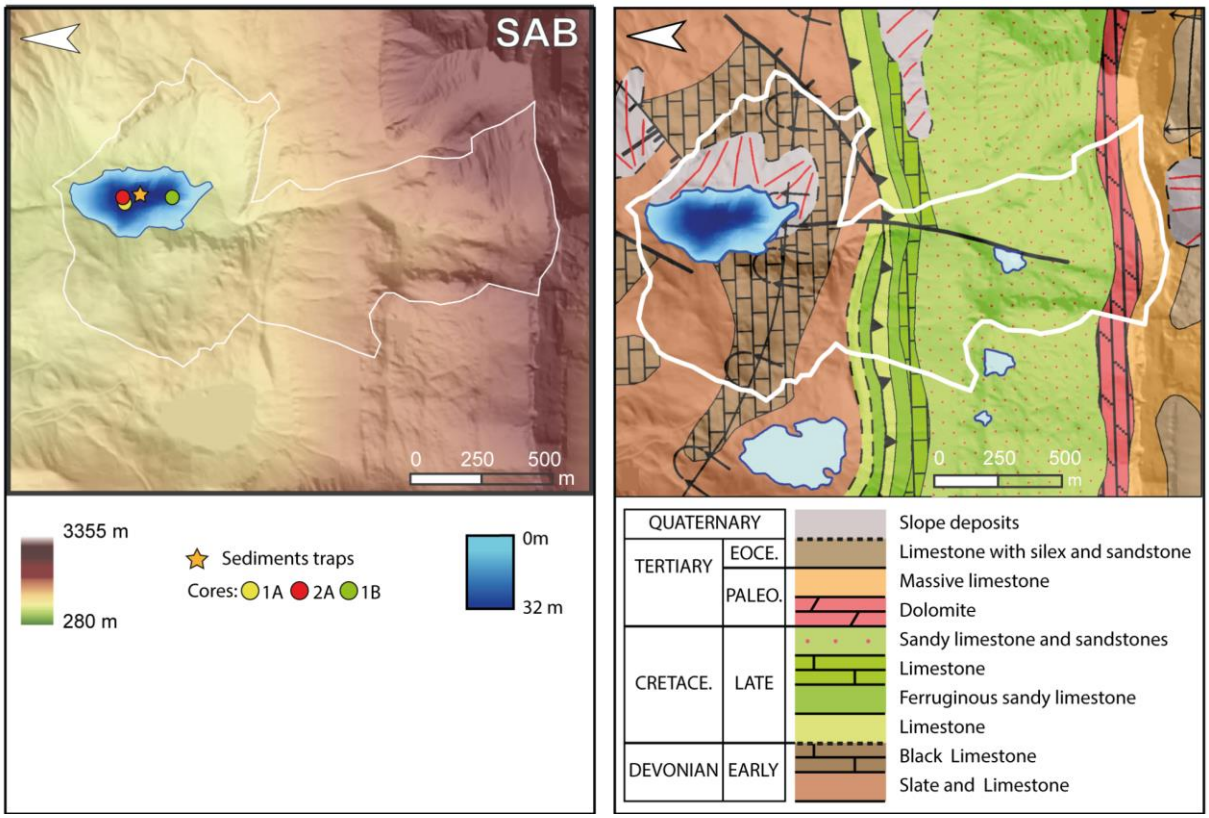

Fig. 1. 13*. Left. Topographic map and bathymetry of Sabocos with the location of the selected cores and the sediment trap. Right. Geological map of the watershed and surroundings of the lake modified from 1:50000 MAGNA geological maps.*

1.3.5.6 Acherito

Lake Acherito (42º52'N, 0º42' W) has a surface area of 5.8 ha, within a 56.9 ha watershed. It is located at the lowest altitude of the lake transect (1877 m asl) and it has a maximum depth of 29m.

The materials that outcrop in the Acherito basin are Carboniferous, affected by E-W and NE-SW faults (Fig. 1.14). The oldest materials are Lower Carboniferous (upper Tournaisian) and consist of "griotte" micritic reddish and gray limestones (Perret, 1988). They are overlain by Namurian black, laminated limestones in decimetric to metric layers. Most of the watershed is formed by sandstones and shales of the "Culm" facies, which occur as alternating centimetric to metric black sandstones and shales with occasional conglomerate intercalations (Teixell & García-Sansegundo, 1994).
According to the CHE reports (*https://www.chebro.es/en/web/guest/puntos-de-control-y-resultados*) the ecological status of the lake is good.

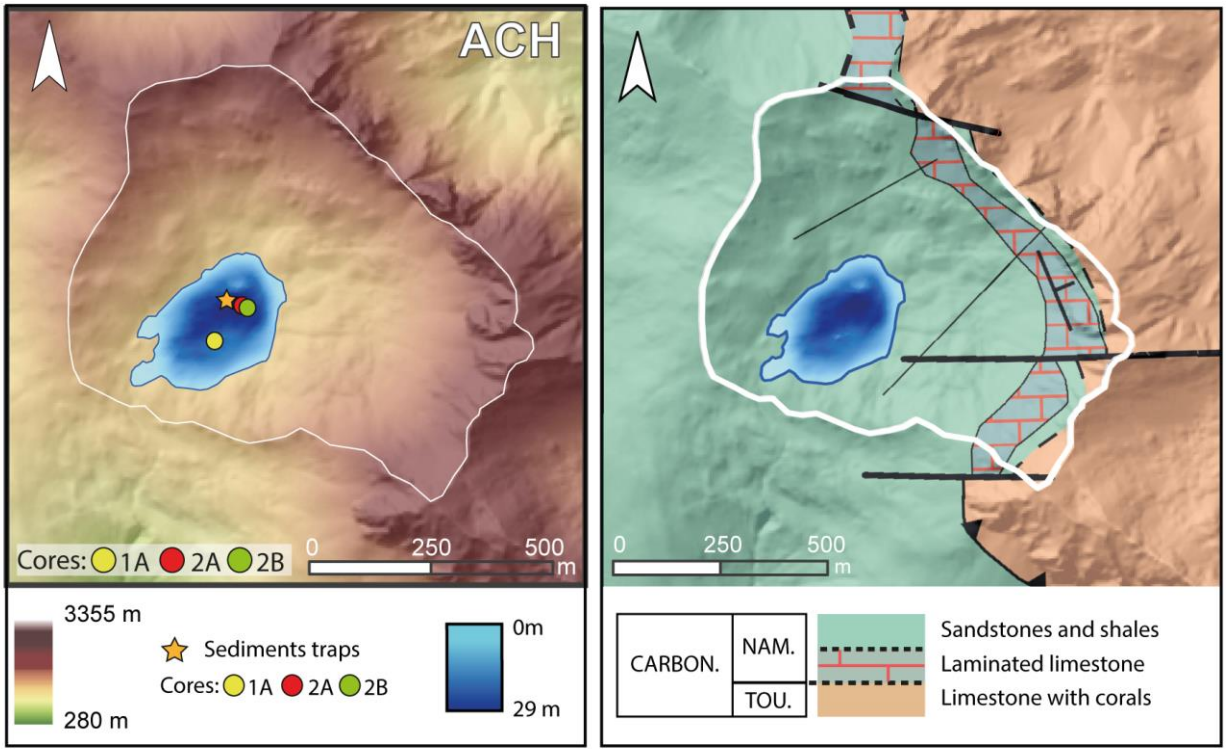

Fig. 1. 14. *Left. Topographic map and bathymetry of Acherito with the location of the selected cores and the sediment trap. Right. Geological map of the watershed and surroundings of the lake modified from 1:50000 MAGNA geological maps.*

1.4. Supplementary Information

Lake	Latitude	Longitude	Lake area (Km^2)	Catchment (Km^2)	Lake perimeter (Km)	Altitude (masl)	Max. Depth (m)	Lake volume (m^3)	Chlorophyll (µg/l) sup.	Trophic character	Conductivity (µS/cm)		Alkalinity (ppm)	
											sup.	max. deep	sup.	max. deep
Marboré (MA)	42,69546	0,04009	0,088	0,957	1,9486	2600	26	1379134	0,1436	Ultra-oligotrophic	69	77	58,6	57,5
Acherito (AC)	42,8797	-0,70705	0,058	0,569	1,0662	1877	29	583689	4,35	Mesotrophic	110	119	81,6	82,8
Sabocos (SA)	42,6926	-0,25741	0,096	2,317	1,364	1900	32	1183798	0,0818	Ultra-oligotrophic	169	209	117,4	141,6
Urdiceto (UR)	42,66524	0,2803	0,296	1,051	2,3276	2364	33	3557078	0,6118	Ultra-oligotrophic	35	35	34,6	36,5
Cregüeña (CR)	42,63766	0,62288	0,445	3,403	4,384	2633	98	20392626	0,315	Ultra-oligotrophic	14	14	15,9	13,9
Sierra (SI)	42,74221	-0,41502	0,013	1,66	0,46	2022	7	27081	2,71	Mesotrophic	18	19	22,3	23,2

Table S.1.1. *Main limnological features of the selected lakes*

2. Material and methods

Photograph of Urdiceto smear slide under the light microscope


BIE-URD12-1B-1G
cm 38
fire sand
Plan
0.30
Epi
DIC
40
50
60

2. Material and Methods

The sediment cores are the main material of study in this thesis, but in order to put the sediment sequences into context, the methodology has also included the study of the basins and the monitoring of some sedimentological, chemical, biological and limnological properties of the lakes. In order to characterize the hydrological and limnological functioning of the lake systems multiple field work campaigns and sampling have been carried out in each of the lakes. Selected surveys of the lake's basins, such as the vegetation or the sediments from the small streams feeding the lakes, have also been carried out. New sediment cores were obtained to complete those available at the IPE core repository. Subsequently, a wide variety of parameters have been measured on the sediment cores and researchers from different institutions have participated. The different physical, chemical and biological techniques applied for monitoring, sampling and analyses are detailed below.

2.1 Monitoring and field campaigns

Annual water and sediment sampling of the lakes has been carried out from 2018 to 2022 under the umbrella of the REPLIM project (EFA 056/15, 2016-2019) and following the protocols provided as a result of the project (see “Protocols for a correct identification and interpretation of the effects of climate change using lakes and peatlands located in high mountain areas”. REPLIM 2016-2019, EFA 056/15, Coordinated by B., Valero Garcés, Alberto de Diego, Laure Gandois, David Elustondo, David Amouroux, Lluis Camarero, Luis Ángel Fernández, Olaia Liñero, Fernando Barreiro, Sheila Izquieta (*http://www.ipe.csic.es/proyecto-replim*).

2.1.1 Multiparametric probe

The measurements along the entire water column of the lake were carried out from the boat anchored in the deepest part of the lake and using the multiparametric probe YSI EXO1 (*https://www.ysi.com/EXO1*) handheld control unit and field cable (Fig 2.1). The parameters measured are: Depth (m), Conductivity (Total Dissolved Solids(TDS), Salinity (S ‰)], pH, Oxidation Reduction Potential (ORP) and Optical Dissolved Oxygen (ODO). The probe is calibrated just before the measurements are taken. The probe is slowly lowered manually to the bottom of the lake and it is raised in

the same way, thus measuring the water column twice, which provides two comparable datasets.

Fig 2.1. *Using the YSI EXO1 multiparametric probe in the field*

2.1.2 Water Sampling

During the field campaigns, between 3 and 12 water samples were taken with a Niskin bottle at specific depths depending on the maximum depth of the lake. In total 3 samples of 1L were collected from each depth, one for chemistry laboratory analysis, one filtered in situ to characterize the organic matter and one for chlorophylls (Fig 2.2). The water samples were analyzed in the Pyrenean Institute of Ecology, and include conductivity, pH, total suspended solids, total dissolved solids, organic matter, alkalinity (carbonates and bicarbonates), total organic carbon, total nitrogen, soluble reactive phosphorus, anions (fluoride, chloride, nitrite, bromide, nitrate, phosphate and sulphate), cations (sodium, potassium, calcium and magnesium) and isotopes ($\delta^{18}O$ and $\delta^{2}H$). The analytical techniques followed the IPE protocols (*http://www.ipe.csic.es/laboratorios*) and they are summarized below.

Conductivity and pH were measured in situ with portable electrodes (YSI professional plus). For alkalinity, the potentiometric titration method is used (automatic titrator, Metrohm 798 MPT Titrino). For Total Suspended Solids, the water is filtered through a 0.45 mm pore membrane and the filter is subsequently dried at 105ºC. Organic matter is also obtained by gravimetric methods, but after filtration through a 0.45 mm

pore membrane, the sample is dried and then burned at 450ºC. For anions and cations, ion chromatography with chemical suppressor (Metrohm 861 Advanced Compact IC) is used. Phosphorus is obtained by the ascorbic acid chlorimetric method (Thermo Helios α spectrophotometer). Chlorophylls are first extracted with a glass fibre filter and then determined spectrophotometrically (Thermo Helios α spectrophotometer). Both total nitrogen and total organic carbon are obtained by catalytic combustion at high temperature (850°C) using a Multi-N/C 3100 analyser (Analytikjena ®), but nitrogen is subsequently detected by chemiluminescence (CLD) and carbon by non-dispersive infrared (MC-NDIR). All procedures are performed according to APHA protocols, 1989. Stable isotope analyses are performed by laser spectroscopy, using a Picarro L2130-i Liquid Water and Water Vapour Isotope Analyser.

Fig 2.2. *Left, collecting water samples with the Niskin bottle in field. Right, sampling bottles with labels.*

2.1.3 Temperature data loggers

During the first years of the REPLIM project, buoys were installed in the deepest areas of the lakes. These buoys were anchored to the bottom and a series of thermistors (Fig 2.3) were attached to the rope connecting the anchor to the buoy and programmed to measure and record the temperature on an hourly basis. The devices are HOBO Water Temperature Pro v2 Data Logger (ONSET) (*https://www.onsetcomp.com/products/data-loggers/u22-001*). The recorded data were

extracted during the summer campaigns with an optical reader and processed with the HOBOware software (*https://www.onsetcomp.com/support/help-center/software/hoboware*).

***Fig 2.3**. HOBO Water Temperature Pro v2 Data Logger (ONSET).*

2.1.4 Sediment traps

On the same rope where the thermistors were placed, a sediment trap was attached between 3 and 4 m above the anchor (except in La Sierra, where it was located at about 1.5 m from the bottom). The sediment traps were manufactured using two PVC tubes of 10 cm diameter and one meter long, and1L sample bottles at the bottom (Fig 2.4). The sediment accumulated in the sample bottles was collected annually during the summer surveys.

2.1.5 Bathymetry

Depth data were taken with a Garmin ECHOMAP UHD 62cv nautical GPS linked to an echo sounder that measured and recorded the tracks from a boat. The data points were analyzed with ArcMap 10.8 (ESRI) to produce the bathymetric maps.

2.1.6. Watershed vegetation and sediment sampling

Some representative plants in the watershed and in the immediate area around the lake were sampled, as well as some aquatic vegetation in the lake. Sediments from small streams entering the lake were also collected (Fig. 2.5). Samples were stored in labeled bags, and their location was recorded with a GPS. Both vegetation and sediment

samples were dried and crushed prior elemental (TC, TN) and isotope (d13N, d15N) analysis.

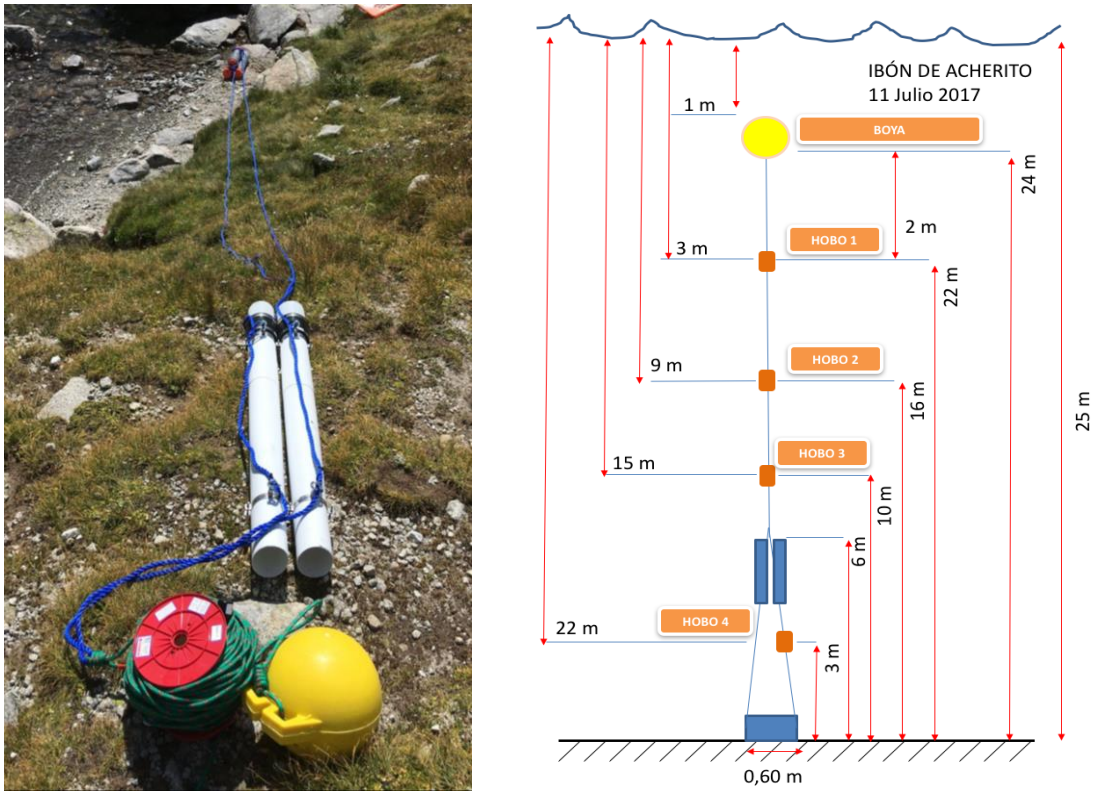

***Fig 2.4**. Left: field photograph showing the anchor in the background and the sediment trap next to the buoy. Right: diagram of the buoy system, with thermistors and sediment trap.*

***Fig 2.5**. Samples collected in the field, from left to right: vegetation in Urdiceto, sediment in Sabocos and lake vegetation (charophytes) in Urdiceto.*

2.2 Coring and surface sediment sampling

2.2.1 Core recovery

The sediment cores from Cregueña, Urdiceto, La Sierra, Sabocos and Acherito were taken in the framework of the REPLIM project. All the cores were retrieved from the deepest area of the lake from a boat with an Uwitec® gravity corer (Fig 2.6). The corer consists of a head, which holds a transparent PVC tube in a clamp. Surrounding this tube are also hollow cylindrical weights and hammers that can be moved vertically through the tube by striking the head (www.uwitec.ai). The corer is descended down the water column of the lake and it is let to fall in free fall a few meters before reaching the bottom. To retrieve longer cores, hammering is carried out by pulling on the ropes, holding the hammer and letting it fall. Once the corer is taken out of the water, the PVC tube is removed from the corer and kept in a vertical position. A cap is placed on its lower part, and on its upper part the water remaining in the tube is removed, a layer of floral foam is placed to prevent the movement of the core, and finally it is covered and taped.

Fig 2.6. *Photographs of the Uwitec® gravity corer, the recovery of a core from the boat and a series of recovered cores.*

The Marboré cores used in this thesis were obtained in August 2011 as part of the HORDA (83/2008) project. Besides short, gravity cores, in Marboré long cores were retrieved with a floating platform and a Uwitec® piston coring device (B. Oliva-Urcia et al., 2018).

A number or cores were retrieved in each lake to characterized deposition in the deepest part of the lakes. For higher resolution analytical work, representative cores were selected and a composite core sequence was obtained (Table 2.1). The location of the cores is shown in Table 2.1.

The notation for the cores follows the LRC protocol, for example REP - ACH17 - 1A - 1G, where:

REP is the project (REPLIM),
ACH the lake (Acherito),
17, the year of collection (2017),
1, the site,
A, the name of the core,
1, the section, and
G, the type of corer (gravity).

2.2.2. ^{210}Pb sampling

Sampling for ^{210}Pb dating was carried out in situ in the field, in order to avoid errors due to water loss and compaction of the sediment, or any type of small remobilization during transport. Two short parallel cores were collected in the same location and one was sampled in the field. Volumetric samples are obtained with the help of a cutting system at the top of the core and using a plunger inserted from the base of the corer and raised at 1 cm intervals. The samples were stored in hermetically sealed containers previously weighed and labeled (Fig. 2.7).

LAKE	CORE	TYPE	Water depth (m)	LOCATION
Acherito	REP-ACH17-1A-1G	Gravity	16,6	42.8793009649962
				-0.707078743726015
Acherito	REP-ACH17-2A-1G	Gravity	26,4	42.8800715133548
				-0.706239799037576
Acherito	REP-ACH17-2B-1G	Gravity	26,4	42.88071513354778
				-0.706239799037576
Cregueña	REP-CRE17-1A-1G	Gravity	91,0	42.6361703686416
				0.623441096395254
Cregueña	REP-CRE17-2A-1G	Gravity	89,7	42.6369894482195
				0.624630823731422
Cregueña	REP-CRE17-2B-1G	Gravity	85,9	42.6370166894048
				0.624739704653621
Marboré	MAR11-1U-1A	Piston	24,0	42.696078
				0.0395392390415385
Marboré	MAR11-1G-1A-4	Gravity	26,6	42.696106
				0.039373
Sabocos	SAB13-1B -1G	Gravity	23,0	42.693834
				-0.257476
Sabocos	REP-SAB18-1A-1G	Gravity	26,1	42.6931678131223
				-0.257350327447057
Sabocos	REP-SAB18-2A-1G	Gravity	26,6	42.6931535638869
				-0.25723272934556
La Sierra	REP-SIE18-1A-1G	Gravity	6,5	42.7421141881496
				-0.415113000199199
La Sierra	REP-SIR17-3A-1G	Gravity	6,6	42.7423394098878
				-0.414361730217934
Urdiceto	URD12-1B-1G	Gravity	28,0	42.665052
				0.281456
Urdiceto	URD12-1C-1G	Gravity	28,0	42.664972
				0.281429
Urdiceto	URD12-7A-1G	Gravity	30,0	42.664848
				0.280939

Table 2.1. *List of cores used in this thesis to compile the main composite sequence for each lake. It also includes the type of corer (gravity or piston Uwitec) and their location (latitude and longitude) and water depth. Other cores were used to characterize the facies and some specific analyses.*

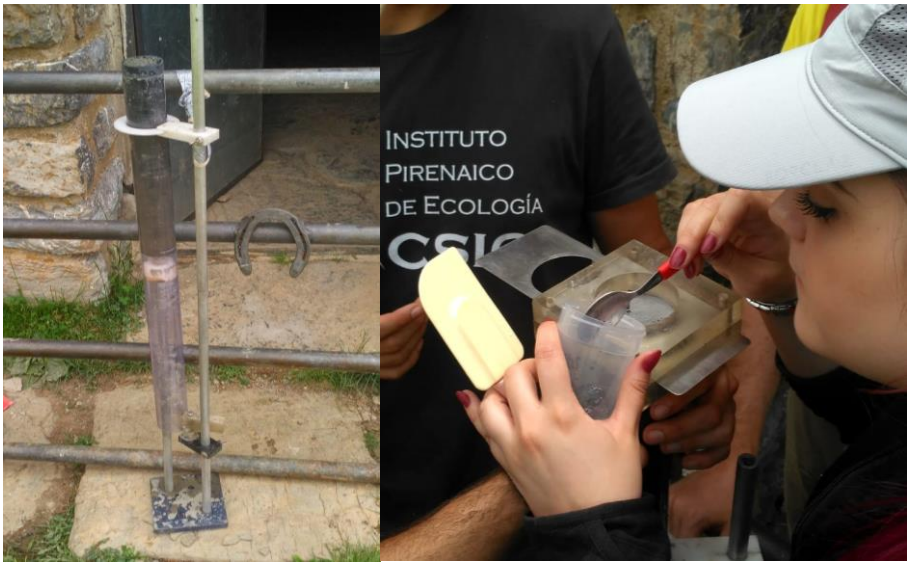

Fig 2.7. *Sampling of the Sabocos core for ^{210}Pb in the field. Left: the plunger and support system for core sampling. Right, the cutting and sampling system at the top of the core.*

2.2.3 Sediment Dredges

To characterize the recent sediments in the lakes, surface sediment samples were obtained with a dredge along depth transects (Fig. 2.8). The sampling was carried out with a Van VEEN sg-200 dredger (Aquatic BioTechnology) and only the upper 1 cm was collected. These samples were geolocated and the material was stored in sealed bags. The samples were then dried and ground prior to compositional and textural analysis.

Fig 2.8 *Sampling surface sediments with a dredge in Marboré.*

2.3 Analytical techniques

2.3.1 Core Imaging and geophysical properties

The cores in the PVC liner were cut longitudinally with a Geotek saw and divided into two equal parts, one of which is kept as an archive while the other half (working half) was used for the different studies and analyses. The two halves were properly wrapped in transparent film and then placed in a D-tube for optimal preservation at 4º C in the IPE-CSIC cold room.

The magnetic susceptibility (MS) was measured with a Geotek Multi-Sensor Core Logger (MSCL) with a Bartington loop sensor scanner at 1 cm resolution. High-resolution pictures were obtained with the Geotek MSCL. All these analyses were carried out at the IPE-CSIC Laboratory in Jaca.

2.3.2. Sedimentological analysis

For the sedimentological study, visual descriptions of the cores were carried out, supplemented by the high-resolution images. The detailed visual description include color, grain size, composition, sedimentary structures and textures and fossil content (if present).

In addition, smear slides and thin sections were prepared using the methodology described by (Schnurrenberger et al., 2003). Smear slides were prepared by placing a small sample of sediment on a glass slide, where it was spread with distilled water before drying on a hot plate. A coverslip was attached to the sample with a Norland Optical Adhesive P/N 6101) and a UV lamp. For the thin sections (Fig 2.9), core samples were cut and dehydrated, replacing the sample's water with acetone and avoiding the sample texture to be distorted. After impregnation with a cold-setting polyester resin, thin sections (mostly 135 mm x 58 mm) were prepared by the method of Guilloré (1985) using oil at all further stages of production to avoid contact with water. Finally, thin sections were scanned under polarized filters using an Epson Perfection V550 Photo flatbed scanner. Thin sections were prepared at the Soil Laboratory of the Estación Experimental de Aula Dei (EEAD – CSIC). An optical petrographic microscope at different magnifications and normal and polarized light was used to study the thin sections and the smear slides.

The integration of these sedimentological descriptions with thin sections, and subsequent analyses, such as texture and geochemical and mineralogical composition, allowed the definition of sedimentary facies, using four main criteria:

1) grain size; clay: 0.01 µm-2.0 µm, silt: 2.0 µm -63.0 µm and sand: > 63.0 µm,

2) main components as organic matter, silicates and carbonates calculated from the elemental data of organic and inorganic carbon:

% Carbonates = (100.09 * TIC) / 12.01;

% Organic matter =% TOC * 1,724 and

% silicates = 100 -% Carbonates -% MO.

3).Sedimentological features such as color, lamination (massive, banded, laminated or finely laminated), and grain size.

4) Geochemical composition, based on XRF scanner and ICP analyses. The process of defining and interpreting these facies is explained in Chapter 4.

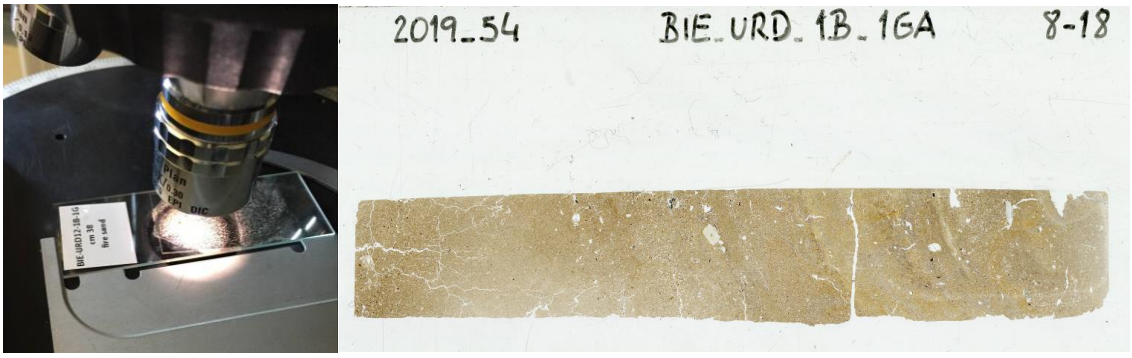

Fig. 2.9. *Left: Photograph of Urdiceto smear slide under the light microscope. Right. High resolution scan of Urdiceto thin section*.

2.3.3. Grain size

The grain size of the sediment samples was analyzed at the Soil and Water Department of the Aula Dei Experimental Station (EEAD-CSIC) using a Beckmann Coulter LS 13 320 grain size analyzer and at the IPE-CSIC laboratory using a MasterSizer 2000. Organic matter was removed from the samples using 3% H_2O_2 and kept 24h at 80ºC and, finally, $Na_2H_2P_2O_7$ was applied and kept in agitation for 24h to facilitate particle dispersion. The Coulter system is based on the different angle at which particles diffract light depending on their size. This instrument emits laser beams, which are transmitted to a lens that amplifies them and makes them pass through the place where the sample, suspended in filtered and distilled water, is placed. The suspended particles diffract the light at different angles, which are concentrated on the detector by

the action of lenses (Buurman et al., 1997). Shepard's textural diagram (Shepard, 1954) was applied to classify the samples into three categories according to their grain size: sand (>63 μm), silt (63 to 2 μm) and clay (< 2 μm).

2.3.4. Elemental Compositional Analyses: TC, TOC, TIC y TS

Organic carbon from organic matter and inorganic carbon mostly from carbonates are key components of lake sediments. Total Carbon (TC), Total Inorganic Carbon (TIC) and Total Sulfur were analyzed at 1 cm resolution in the sediment cores and in watershed and sediment trap samples at the IPE-CSIC (Zaragoza, Spain) using a LECO SC144 DR analyzer. For TIC analysis, organic matter was previously removed at 460 °C in a muffle furnace for 300 min. The Total Organic Carbon (TOC) was calculated as the difference between TC and TIC. Total Inorganic Carbon (TIC) represents the inorganic fraction of carbon, associated with carbonates. Total Organic Carbon (TOC) reflects the amount of organic matter in the sediment. Total Sulfur (TS) represents the total amount of sulfur in the sediment in different phases and minerals (organic matter, sulfates as gypsum, sulfides as pyrite...).

To analyze the samples, the concentration of CO_2 and SO_2 generated by the combustion of 100 mg of dry sediment at a temperature of 1,350ºC is measured. The samples are introduced into an oxygen-enriched furnace and placed in refractory ceramic vessels for a time varying between 60 and 300 seconds, depending on the concentrations of C and S present in each one. The resulting gases pass through particulate and moisture filters and are then analyzed in infrared detection cells.
To analyze TOC, the samples are acidified with HCl at 80ºC to remove carbonates and dried at 60ºC. The analysis uses certified C and S standards, and the analytical error is less than 5%. This method has proven to be more reliable than traditional methods such as Loss On Ignition (LOI) or calcimetry (Santisteban et al., 2004).

2.3.5. X-ray fluorescence (XRF) scanner

XRF scanners in cores are widely applied for palaeoclimatic / paleoenvironmental reconstructions on different time scales (Tjallingii, 2007). The results are semi-quantitative, but provide reliable records of the relative variability of the elemental composition of the core (Richter et al., 2006).

The XRF core scanner is a computer-controlled core-scanning tool that analyses the chemical composition of sediments directly on the surface of a longitudinally open core. XRF scanner measurements are non-destructive and provide near-continuous information.

The XRF analysis of the core was performed at the XRF-Core Scanner Laboratory of the University of Barcelona (UB, Spain), with an Avaatech X-Ray Fluorescence (XRF) scanner, at a resolution of 5 mm and under two different working conditions, first at an intensity of 10kV, in order to analyze the elements Al, Si, P, S, Cl, K, Ca, Ti, V, Cr, Mn, Fe, Rh and Ag; and the second, at an intensity of 30kV, to count Ni, Cu, Zn, Ga, Ge, As, Se, Br, Rb, Sr, Y, Zr, Nb, Au, Pb, Th and U according to Richter et al., (2006). The surface of the core was also carefully cleaned and optical images of each core section were taken with the high-resolution CCD camera attached to the equipment.

***Fig 2.10**. Avaatech X-Ray Fluorescence (XRF) from the XRF-Core Scanner Laboratory of the University of Barcelona (UB, Spain)*

2.3.6. Inductively coupled plasma mass spectrometry (ICP-MS)

In order to obtain a quantitative geochemical characterization of sedimentary facies and to verify the accuracy of the XRF core scanner analyses, the elemental

composition of major and trace elements was obtained by inductively coupled plasma mass spectrometry (ICP-MS). Quantitative chemical analyses were performed in the composite sequences at a lower resolution (every 1 cm, 150 mg weight sample) with an ICP-OES 720-ES (Varian) at the Experimental Station El Zaidin - CSIC (Granada, Spain). Samples were digested with HCl and HNO_3 (1:1:3 of H_2O: HCl: HNO_3) in a UltraWAVE (Milestone) at 220ºC during 15 minutes. Elements measured by ICP-OES were Al, As, Ca, Cd, Co, Cr, Cu, Fe, K, Li, Mg, Mn, Mo, Na, Ni, P, Pb, S, Se, Si, Sr, Ti, V, Zn.

2.3.7. X-Ray Difractometry (XRD)

The mineralogical composition of the samples was determined by X-ray diffraction (XRD) by the crystalline powder method with an X Ray diffractometer. The estimation of the relative abundance in each mineral phase was carried out using the intensity of the main peaks of each sample, following the standard process described by Chung, (1974) and applying the "method of reflective powers".

2.3.8. Scanning Electron Microscope (SEM)

Electron microscopy was used to obtain information of the components of the sediments, such as nature, surface texture of individual crystals and grains and the chemical composition of selected grains. Representative sediment samples from the cores and sediment traps have been analyzed. Images have been taken both in high or low pressure conditions, and carbon coating has been applied when necessary. Chemical composition of individual grains have been obtained by Energy dispersive analysis (EDS), the equipment is a Scanning electron microscope (SEM) Jeol 6110, that allow to work in variable pressure the CN IGME with JEOL microanalysis, and secondary and back scattered detectors.

2.3.9. Isotopes

The $\delta^{13}C_{OM}$ and $\delta^{15}N_{OM}$ in bulk organic matter were analyzed with a FlashEA 1112 (ThermoFinnigan) coupled with an interface ConfloII (ThermoFinnigan) to a mass spectrometer of isotopic ratios Deltaplus (ThermoFinnigan) at the University of A Coruña, Spain.

The analysis of $\delta^{13}C_{OM}$ in organic matter requires the prior elimination of the carbonates present in the sample (main source of CO_2 contamination from which the ^{13}C

isotopic contents will be measured). This removal was carried out by successive HCl treatments. First, a sample of approximately 0.5g was treated with 4M HCl (part of concentrated HCl (12M) diluted with two parts of distilled water) and left to react for at least 4 hours. Once the reaction is finished, the sample is properly washed with distilled water and it is left to dry in an oven at about 50ºC.

2.3.10 Organic Proxies

Biogenic silica (BioSi) was measured every 4 cm using the wet-alkaline leaching technique (Mortlock & Froelich, 1989) after carbonates and organic matter were removed by HCl 1M and peroxide. Then, BioSi was leached with Na_2CO_3 2M and solution separated from the remaining sediment by centrifugation and bicarbonate was neutralized with HCl. BioSi, as dissolved silicate, was measured by the molybdate blue colorimetric method using an AutoAnalyser Technicon II (Bernárdez et al., 2005). The analyses were carried out at the IIM-CSIC at the laboratory of Dr. Ricardo Prego.

Photosynthetic pigments in bulk sediment were analyzed at the University of Valencia, Spain, under the supervision of Dr. Eduardo Vicente with three successive pigment extractions measured with a spectrophotometer Beckman DU 640. The chlorophyll and the pheophytin in the sediment samples were calculated according the equations described in Lorenzen, (1967).

Sediment samples for diatom analysis were processed using hydrogen peroxide (33% H_2O_2) and HCL (2 ml 1 M) and mounted in Naphrax on a microscope slide following the method described in Battarbee et al., (2002). A minimum of 300 diatoms valves were identified per slide, and simultaneously we counted chrysophyte cysts to calculate C/D ratio (Chrysophyte / Diatoms ratio) using a Zeiss Axio Imager A1 microscope (Carl Zeiss Inc., Germany) equipped with a 100X objective (Zeiss Plan-Apo 1.4 numeric aperture) and differential interference contrast optics at 1,000 magnification. Diatoms concentration in sediment samples was estimated by adding a known number of microspheres (Battarbee et al., 2002). Diatom identifications were based mainly on (Rivera-Rondón & Catalan, 2017) and taxonomic references therein, with the currently accepted diatom names following the algabase database (*https://www.algaebase.org/*). Diatom analyses were performed by Dr. Sergi Pla Rabes (CREAF)

2.4 Age Models

The chronological model for the sedimentary sequences of the lakes is based on AMS ^{14}C dates (Table 2.2) and ^{210}Pb (Fig. 2.12 and 2.13) for the most recent part of the sequence. ^{137}Cs techniques were also used in the Marboré sequence. The combination of several absolute dating techniques has allowed us to generate a robust chronology for the lake sequences.

The first step to create the age models was to correlate the cores where the different dated samples were taken, because ^{14}C dates and ^{210}Pb samples were not always obtained in the same core. These correlations were made using visible and characteristic sedimentological features such as laminations, sedimentary facies or structures, and geochemical data as TC or TOC profiles. Figure 2.11 shows the correlation used to obtain the age models for the composite sequence for all lakes. The age model was applied to all samples taken for subsequent analyses.

Lake	DirectAMS code	Submitter ID	Sample type	Fraction of modern		Radiocarbon age	
				pMC	1 σ error	BP	1 σ error
AC	D-AMS 028339	REP-ACH17-2A-1G 49-50 cm	plant material	95.36	0.23	382	19
	D-AMS 028340	REP-ACH17-2A-1G 61-62 cm	plant material	90.97	0.33	760	29
SI	D-AMS 028338	REP-SIR17-3A-1G 45-46 cm	sediment (bulk)	86.59	0.23	1157	21
CR	D-AMS 028010	CRE17-2A-1G 9-10 cm	sediment (bulk)	85.04	0.27	1302	26
	D-AMS 028011	CRE17-2A-1G 14-15 cm	sediment (bulk)	83.74	0.27	1425	26
	D-AMS 028009	CRE17-1A-1G 22-23 cm	sediment (bulk)	78.17	0.25	1978	26
	D-AMS 028012	CRE17-2A-1G 40-41 cm	sediment (bulk)	66.14	0.22	3321	27
SA	D-AMS 037572	SAB13-1B-1G-1 (A), 2-3 cm	sediment (bulk)	85.01	0.41	1305	39
	D-AMS 037573	SAB13-1B-1G-1 (A), 47-48 cm	sediment (bulk)	68.86	0.24	2997	28
	D-AMS 037574	SAB13-1B-1G-1 (A), 88-89 cm	sediment (bulk)	63.87	0.22	3601	28
UR	D-AMS 024321	BIE-URD12-1B-1G	plant material	92.11	0.44	660	38
MA	D-AMS 001189	MAR11-1A-1U-1 cm 39-41	sediment (bulk)	73.13	0.23	2514	25
	D-AMS 1217-204	MAR11-1A-1U-2 cm 53-56	sediment (bulk)	63.79	0.22	3611	28

Table 2.2. *AMS ^{14}C dates included in the age models for the lake sequences.*

Age models were obtained combining ^{210}Pb -^{137}Cs techniques performed at St. Croix Watershed Research Station (Minnesota, USA) using gamma ray spectrometry (Fig. 2.12 and 2.13) and AMS ^{14}C dating from Direct AMS Laboratories (Seattle, USA) (Table 2.2). For ^{210}Pb the constant supply rate model was applied, which assumes a constant input of excess ^{210}Pb to the core, but allows the sediment flux to vary. We used Bayesian statistics to simulate the accumulation rate of the different lakes with the Bacon v2.5.8. Bayesian age-depth model (Blaauw & Christen, 2011) implemented in the geoChronR package v1.1.6 (McKay et al., 2021).

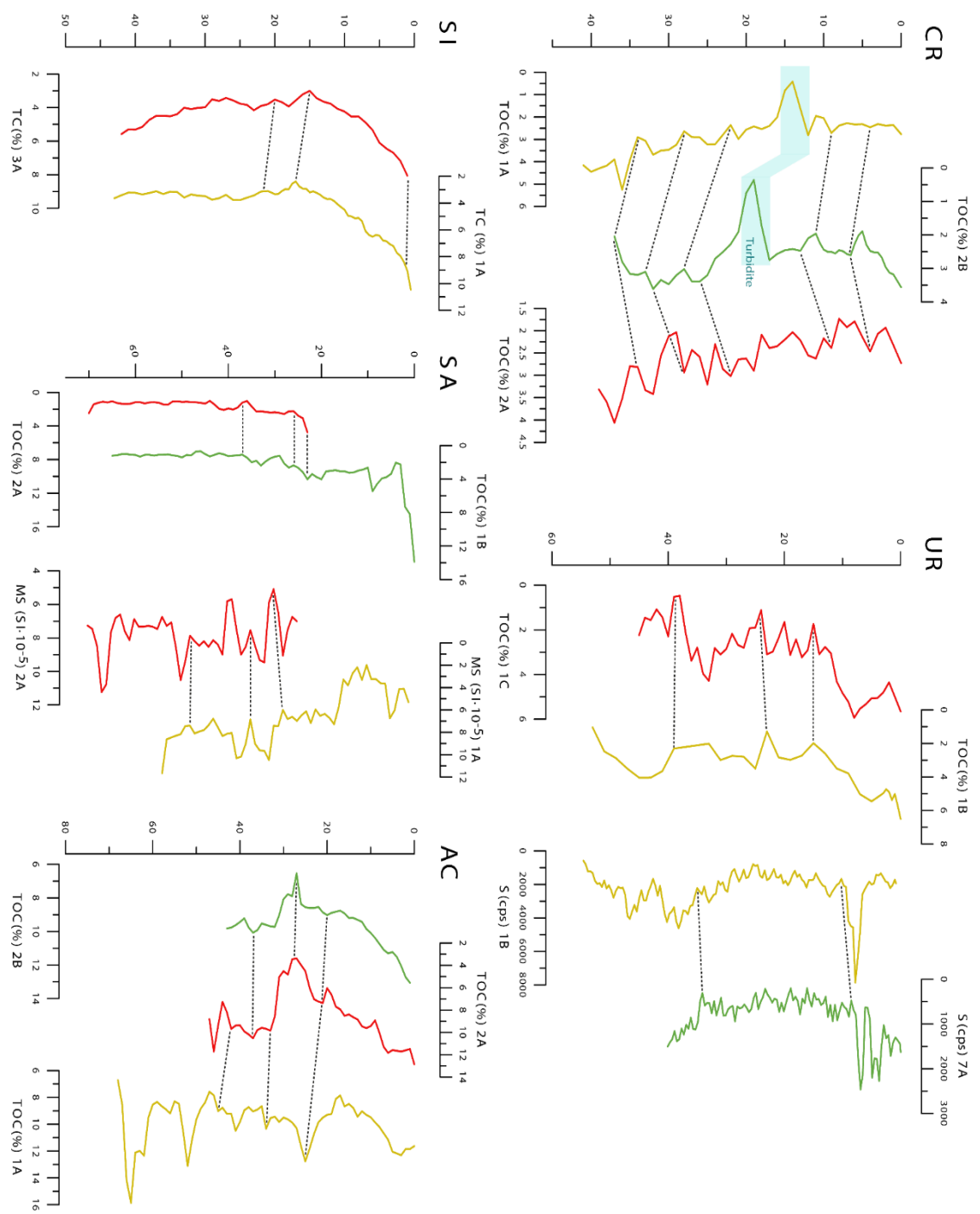

Fig. 2.11. *Core Correlations to obtain the master sequence to integrate ^{210}Pb and ^{14}C dates. CRE (REP-CRE17-1A-1G, REP-CRE17-2A-1G, REP-CRE17-2B-1G), URD (URD12-1B-1G, URD12-1C-1G, URD12-7A-1G), SIE (REP-SIE18-1A-1G, REP-SIR17-3A-1G), SAB (SAB13-1B -1G, REP-SAB18-1A-1G, REP-SAB18-2A-1G) and ACH (REP-ACH17-1A-1G, REP-ACH17-2A-1G, REP-ACH17-2B-1G).*

For Marboré, the age model used in this PhD thesis was obtained by Leunda et al., 2017. In this case, the chronology of the cores was determined using ^{210}Pb and ^{137}Cs and ^{14}C AMS. In the case of Marboré the ^{210}Pb age model is supported by the presence of a 137Cs peak at 6 cm (1963 AD).

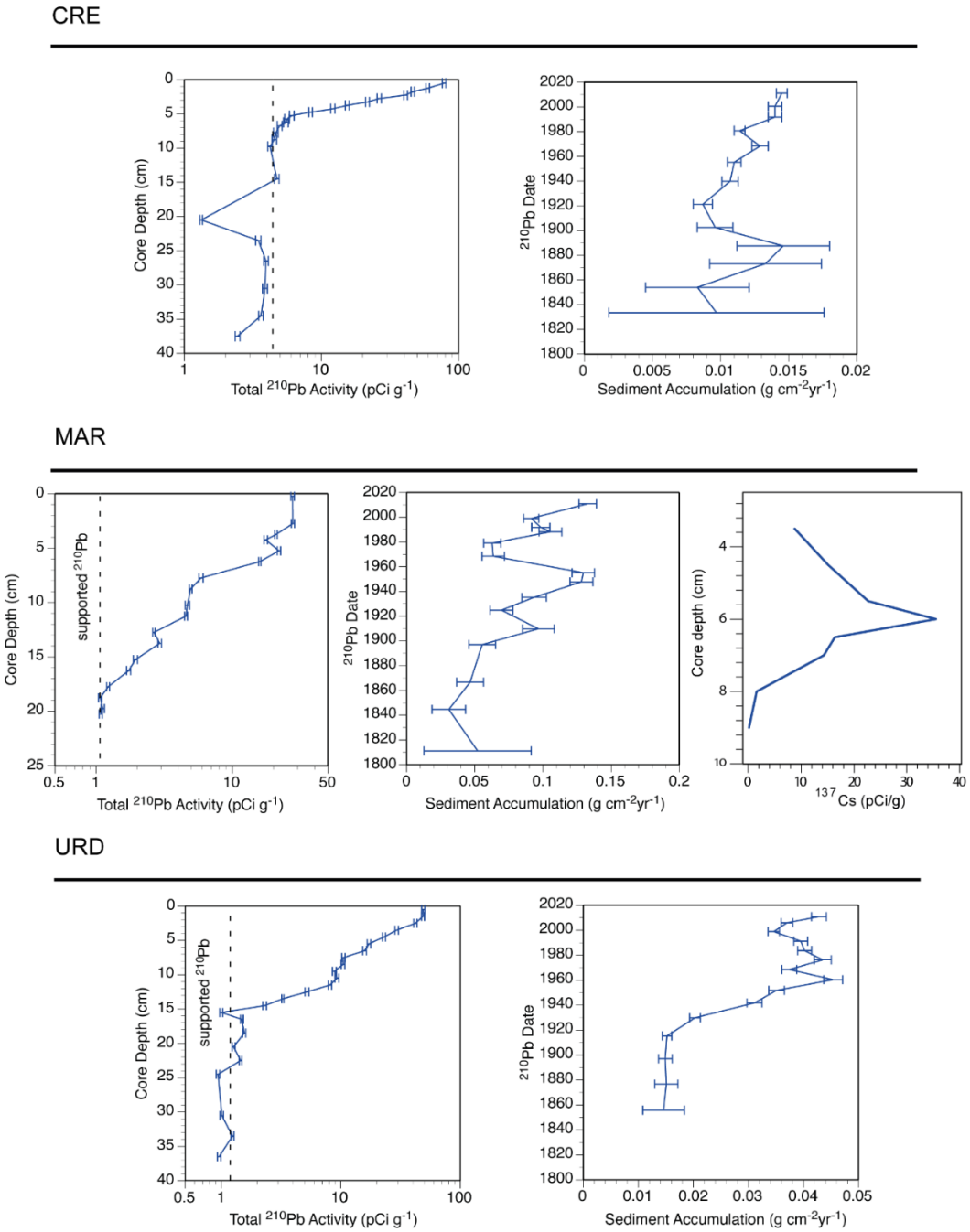

***Fig. 2.12**. Total ^{210}Pb activity (pCi g-1) and sediment accumulation (g cm-2 yr-1) for CR, MA and UR lakes. In the case of Marboré, the results of the total ^{137}Cs activity are also included*.

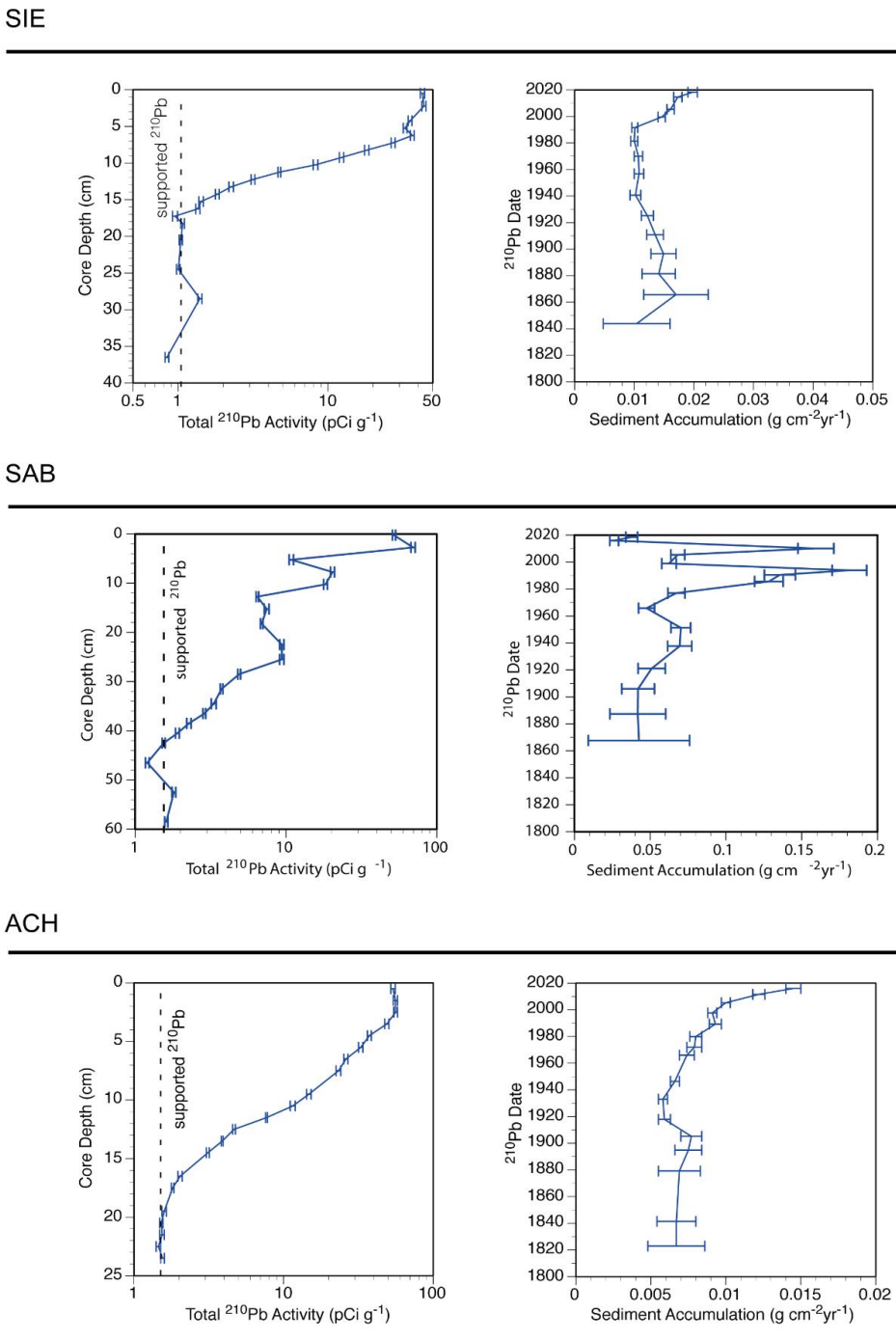

Fig. 2.13. *Total ^{210}Pb activity (pCi g-1) and sediment accumulation (g cm-2 yr-1) for SI, SA and AC lakes.*

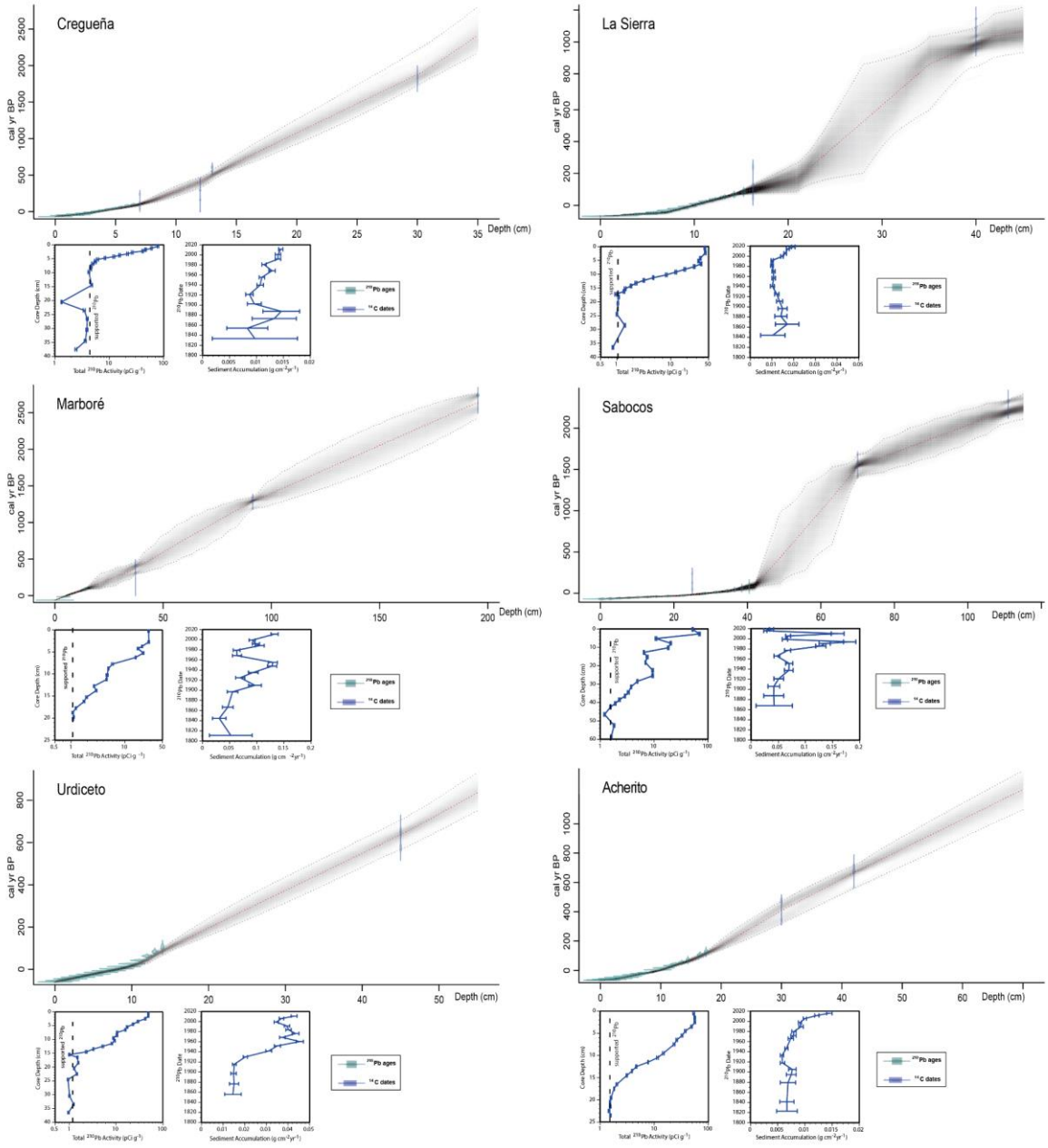

Fig. 2.14. *Depth- Age Models for the studied lakes. Total ^{210}Pb activity (pCi g-1) and Sediment Accumulation (g cm-2 yr-1) are shown in the insets*

2.5 Data Analysis Techniques

2.5.1 Statistical Analyses

To investigate the compositional relationships within the sediment sample data set, we calculated a “Compositional PCA" (PC_{comp}) including compositional (TOC, TIC), geochemical (elements measured in ICP) and grain-size data (% sand) (See more details in Chapter 5) and used the first $PC1_{comp}$ (explaining 53% of the variance) as an indicator of the lithogenic composition of the sediments.

To further investigate the organic and lithogenic components of the sediments, we used the geoChronR package v1.1.6 (McKay et al., 2021) to implement two “age-uncertain PCA” (Anchukaitis & Tierney, 2013) that were applied to two groups of variables: i) TOC_{flux}, C/N and $\delta^{13}C_{OM}$ and ii) L_{flux} and PCA_{comp}. GeoChronR uses a binning procedure to achieve this across multiple ensembles (McKay et al., 2021) and a probabilistic PCA (PPCA) approach using the pcaMethods package (Stacklies et al., 2007). Data analysis was performed by Dr. Matias Frugone (Pontificia Católica Universidad, Santiago, Chile).

The structure of the diatom assemblages was analyzed with a “diatom PCA”, based on Hellinger transformation (Legendre & Legendre, 2012) of diatoms counts (only diatoms with relative abundance higher than 1% and with at least two occurrences across the entire record) to extract the main components of variability in CR and AC. The PCA was performed using the R package Vegan (2.5-7) (Oksanen et al., 2019). Data analysis was performed by Dr. Sergi Pla (CREAF, Spain).

Two analytical techniques were applied to the time series to investigate the occurrence of periods of Change Points: Cumulative Sum and Generalized Additive Models. The analyses were performed by Dr. Josué Polanco (University of Salamanca). A cumulative sum (CumSum) of deviations of the mean (Ibanez et al., 1993) was applied to the time series of $\delta^{13}C_{OM}$, C/N, L_{Flux} and TOC_{flux}. A CumSum is the sequential sum of the successive elements of a variable after removing from each temporal observation the mean of the time series and plotting the cumulative sum of residuals. A positive slope of the CumSum indicates an above-average tendency in the data and a negative slope represents a below-average tendency, meanwhile changes in the slope of the cumulative sum curve from positive to negative or vice versa indicate phases for which the mean of the data is higher or lower than the mean of the original time series (Ibanez et al., 1993).

Not all the identified Change Points (CPs) have similar weight, and to evaluate their significance we have taken into consideration the change in slope and sign as well as the number of elements close to the CPs, as this technique works better for time series with more than 50 elements and ours contain between 38 and 83 points. The CumSum was programmed in R and the source code is available upon request.

The change point (CP) method proposed by Simpson, (2018) based on the use of GAMs (Generalized Additive Models) (Wood, 2017) fits a nonlinear trend to the time series and then estimates the first derivative of the function that represents this trend. It also estimates a confidence interval (95%) around the fitted function that is used to determine statistical significant temporal changes, i.e. periods of significant change are identified as those time points where the simultaneous (lower and upper) confidence interval on the first derivative does not include zero. These analyses were performed using the R packages “mgcv” (Wood, 2022) and “gratia” (Simpson, 2023) following the supplementary material provided in (Simpson, 2018).

3. Monitoring the high altitude Pyrenean Lakes

Uwitec® gravity corer on the boat, Sabocos (July, 2019)

3. Monitoring the High Altitude Pyrenean Lakes

The monitoring program implemented in this thesis has been carried out in the framework of the REPLIM project (Red de observatorios de ecosistemas sensibles (lagos, turberas) al cambio climático en el Pirineo. EFA056/15 Programa INTERREG V-A POCTEFA, España-Francia-Andorra) (2016-2019) (*https://www.opcc-ctp.org/es/replim*). The project started as a network of specialized scientific centers and managers from Spain, France and Andorra to cover the whole Pyrenean territory, and focused on the study of the dynamics of high mountain lakes and peatlands and their relationship with climate change. The REPLIM network created in the framework of this project continued with the ADAPYR project (2019-2022) (Capitalización, observación, transferencia y apropiación de estrategias de adaptación al cambio climático en los Pirineos en un contexto de cooperación transfronteriza. INTERREG – POCTEFA. 2019-2022). REPLIM has consolidated a Pyrenean network of lake and peatland observatories designed to tackle the challenge of assessing the impact of climate change in high mountain areas and provide robust scientific data to develop mitigation and adaptation policies. The network aims to enhance cooperation between beneficiaries (scientific centers) and associated actors (managers, citizens) from all Pyrenean territories. This PhD thesis is a contribution to such efforts.

3.1. Watershed and high altitude lake surveys

One of the main objectives of this PhD was to contribute to the REPLIM initiative to implement a monitoring network in lakes where some basic but useful parameters could be measured and to provide a regional picture of environmental and climatic impacts on these ecosystems. The REPLIM project concluded that the main expected impacts on high altitude lakes would be related to changes in physical, chemical and biological properties due to changes in water availability and rising temperatures. Governmental agencies, Water Authorities, Ministries of Spain, France and Andorra maintain a number of programs to analyze and monitor the ecological status of Pyrenean lakes (e.g., Confederación Hidrográfica del Ebro or the Agència Catalana de l'Aigua Agencia Catalana del Agua (*https://www.chebro.es/, https://aca.gencat.cat/),* but the REPLIM network has provided new and additional information on sediment and lake water composition and thermal regimes. This network includes sites where water, sediment and temperature monitoring programs are being carried out on an annual or biannual

basis (Figure 3.1). At these sites, waters, biota, and sediments have been characterized by annual sampling and sediment traps, and information from each node has been summarized and included in the OPCC geoportal (*https://opcc-ctp.org/es/geoportal*).

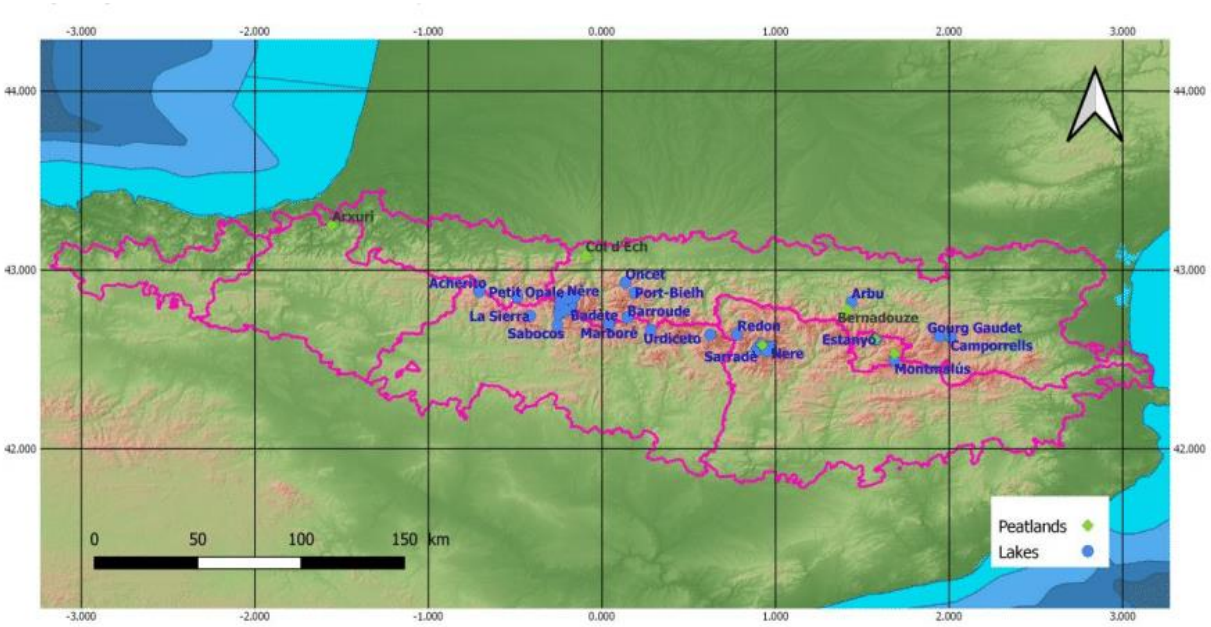

Fig. 3.1. *Location of the main sites in the REPLIM network (see geoportal for detailed location: https://opcc-ctp.org/es/geoportal)*

In the context of this PhD, the six selected watersheds were sampled for sediment, soil and vegetation characterization. The study in the selected lakes included a bathymetric survey and sediment characterization by coring and surface sediment sampling. New bathymetry maps were produced for each lake (Chapter 1). Sediment features for each lake are described in Chapter 4.

The lake monitoring included:

- sediment traps
- annual water sampling
- annual multiparameter probe measurements in the deepest area
- temperature sensors

3.2. Watershed surveys

Samples from vegetation, soils and sediments have been used to characterize the lithogenic and carbon input into the lakes. Isotope signatures of soil and vegetation and C/N ratios (Fig 3.2) show distinct groups been described in detail in the section of TOC fluxes. As in most sites, our watershed-lake survey shows that aquatic and terrestrial vegetation have similar $\delta^{13}C_{OM}$ range and lake sediments and POM have lower values. Watershed soil and vegetation samples have higher C/N but with high variability (12-70) and a relatively small $\delta^{13}C$ range (-30 to -25). Aquatic vegetation has relatively lower C/N values than terrestrial, although a large range (10-50) and similar $\delta^{13}C$ values. Soil samples have lower C/N values (12-23) than terrestrial and aquatic vegetation but similar $\delta^{13}C$ values as sediment and vegetation samples. Sediments collected in the creeks feeding the lakes have relatively low C/N values (5-20) and more positive $\delta^{13}C$ (-26 to -17). The lowest $\delta^{13}C_{om}$ values correspond to sediment traps (-33 to -25) and lake sediments (-26 to -17). Lake sediments and POM samples have the lowest C/N ratios. Information about mineral and geochemical composition of the sediment input into the lakes and the isotopic and C/N signature of watershed and lake samples is discussed in detail in Chapter 5 (Lithogenic and TOC fluxes).

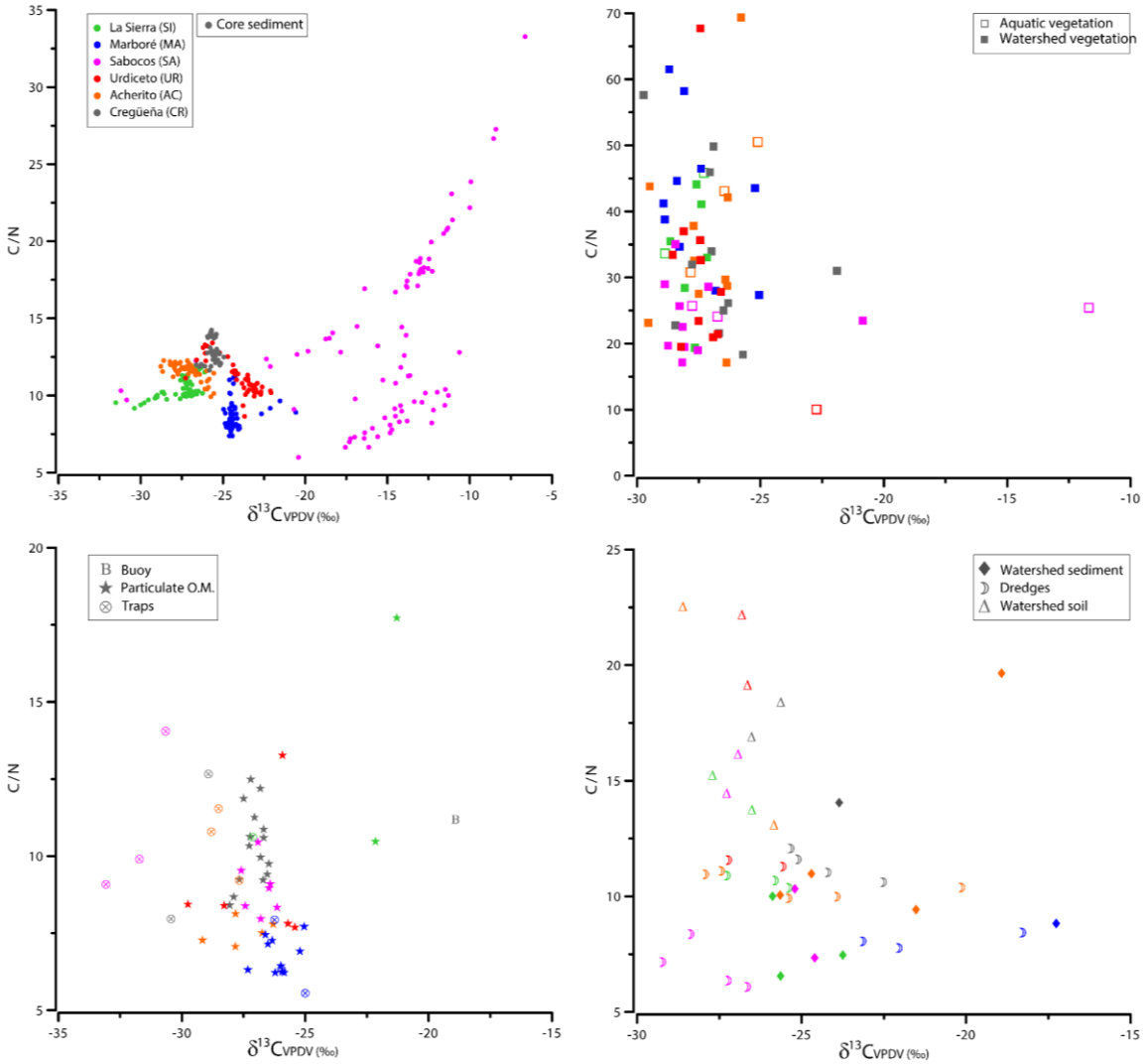

Fig. 3.2. *C/N vs δ¹³C (‰) for each lake considering sample type (core sediment, buoy, POM, sediment traps, dredges, aquatic vegetation) and for each watershed (vegetation, sediment and soil).*

3.3. Sediment traps

Sediment traps were installed in all lakes in the deepest areas (see Chapter 2) and the sediments were collected several times during the last years. The Urdiceto sediment trap could not be recovered after deployment as water level has been maintained higher than in previous years. Sediment fluxes were calculated and some compositional analyses performed in the recovered samples (Fig 3.4).

3.3.1. Sediment composition

The TOC of the sediment trap samples show a large range (1- 18 %) (Fig. 3.3). The C/N range (6 - 14) reflects the dominance of endogenous (in-lake) organic matter but with a variable contribution of exogenous organic matter from the catchments (Meyers & Teranes, 2002). Particulate organic matter in lake waters is higher in shallow lakes, such as La Sierra, where mixing is more intense. The wide range of δ ^{13}C and δ ^{15}N of recent organic matter accumulated in these lakes (Figure 3.3) underscores the interaction of varied sources and processes.

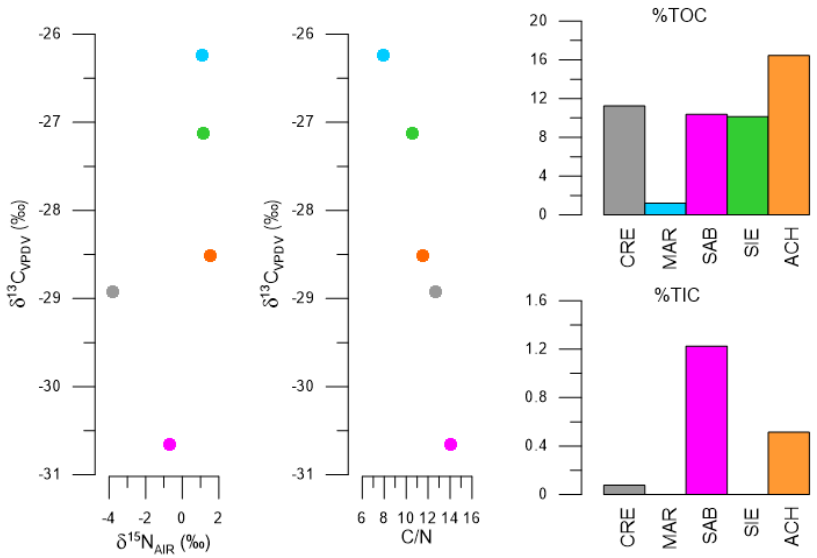

Fig 3.3. *Left. Biplots of δ^{13}C and δ^{15}N and δ^{13}C and C/N ratios in organic matter from sediment trap samples. Right: Total Organic and Inorganic Carbon content in samples from sediment traps from selected lakes.*

ICP analysis has been performed on some of the sediment trap samples and on the material recovered in the buoy in 2021 in Marboré (Fig 3.4). The results show the distinctive composition of each lake and also the varied range within the same lake, when data from several annual campaigns are available. Recent sediments from lakes in silicate watersheds as Cregüeña have higher content in lithogenic elements (Fe, Al, Ti, Mg) but also in heavy metals (Pb, Cu, Zn). As expected, samples from lakes on carbonate –bearing watersheds (Acherito, Sabocos) have higher Ca contents, except Marboré, which has the lowest Ca content, similarly to core sediment with almost no carbonate content (see Chapter 4).

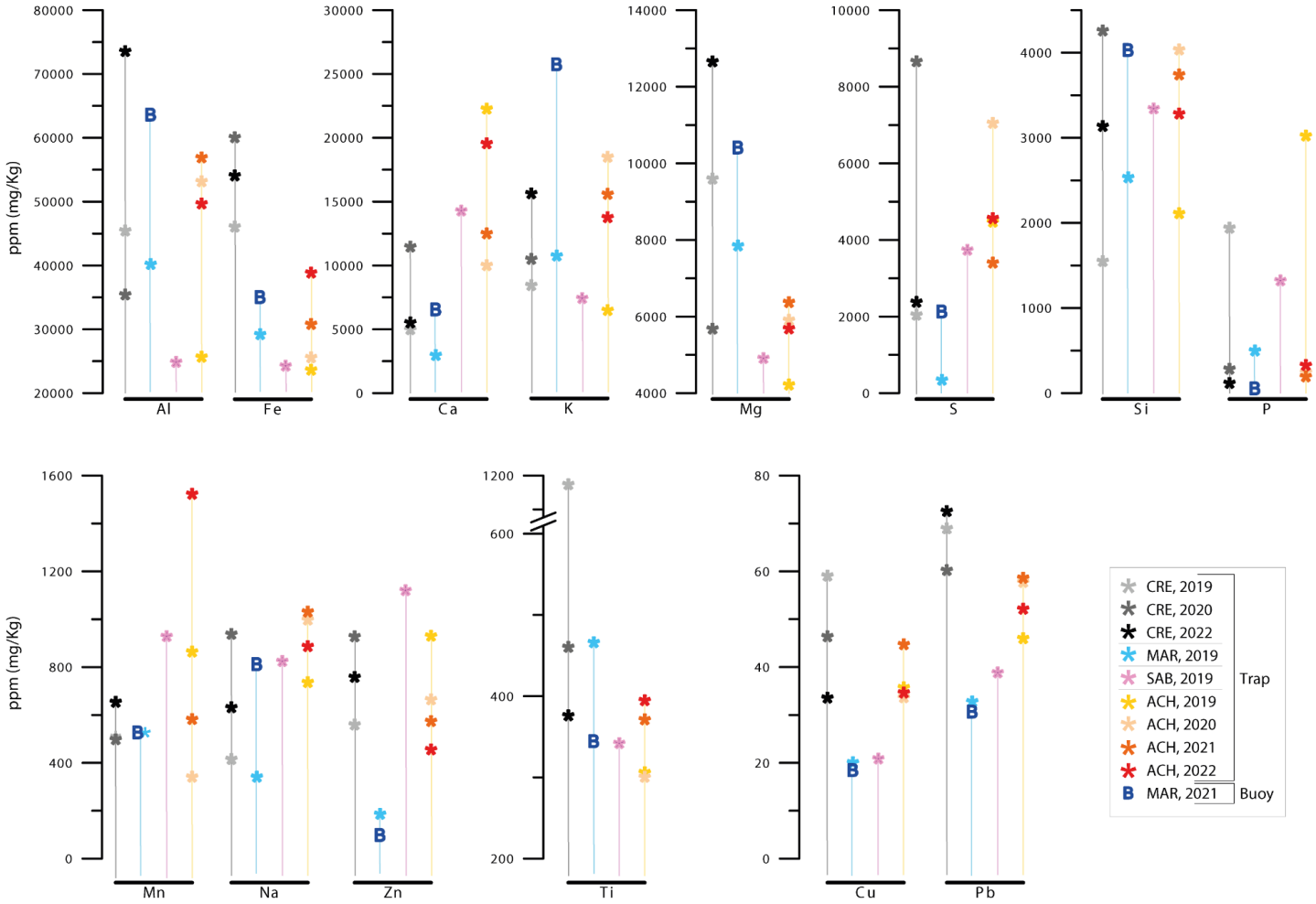

Fig 3.4. *Results of the ICP analysis on the Cregueña, Marboré, Sabocos and Acherito sediment trap samples in different years. The results of the Marboré buoy are also included.*

3.3.2. SEM Results

The observation with Scanning Electron Microscope on selected samples has helped to identify the main sediment components (Table 3.1 and figures 3.2 to 3.6).

	Diatom	Detrital	Carbonates	Other	Organics
Acherito	xxxx	xx (Qz, Mc)	No	Organic filaments, Fe-Oxides	Diatoms, chrysophyte cysts and organic-rich mass
Cregüeña	xx	xx (Qz, Mc)	No	Fe-Ox	Diatoms, chrysophyte cyst
Marboré	x	Very high Qz, Mc, Fds	No	Ti Oxides, circon. Monacite, apatite	Diatoms
Sabocos	xxxx	Low	Dolomite /ankerite	Fe-Oxides, Mn oxides	Diatoms, chrysophyte cysts and organic-rich mass
La Sierra	xxx	xx	Biogenic calcite	Ox Fe, plant remains	Diatoms, organic-rich mass, pollen grains

Table 3.1. *Main components of sediment from traps as identified by SEM. The number of "x" represents its relative abundance.*

3.3.2.1 Cregüeña

The Cregueña trap sediments were composed of 11 % TOC and no carbonates. The SEM observations show clayeyed and detrital siliciclastic grains, as well as organic components as diatoms and chrysophyte cyst (not very abundant). Small Fe-rich crystals have been detected over the sample, possibly of authigenic origin (Fig 3.5).

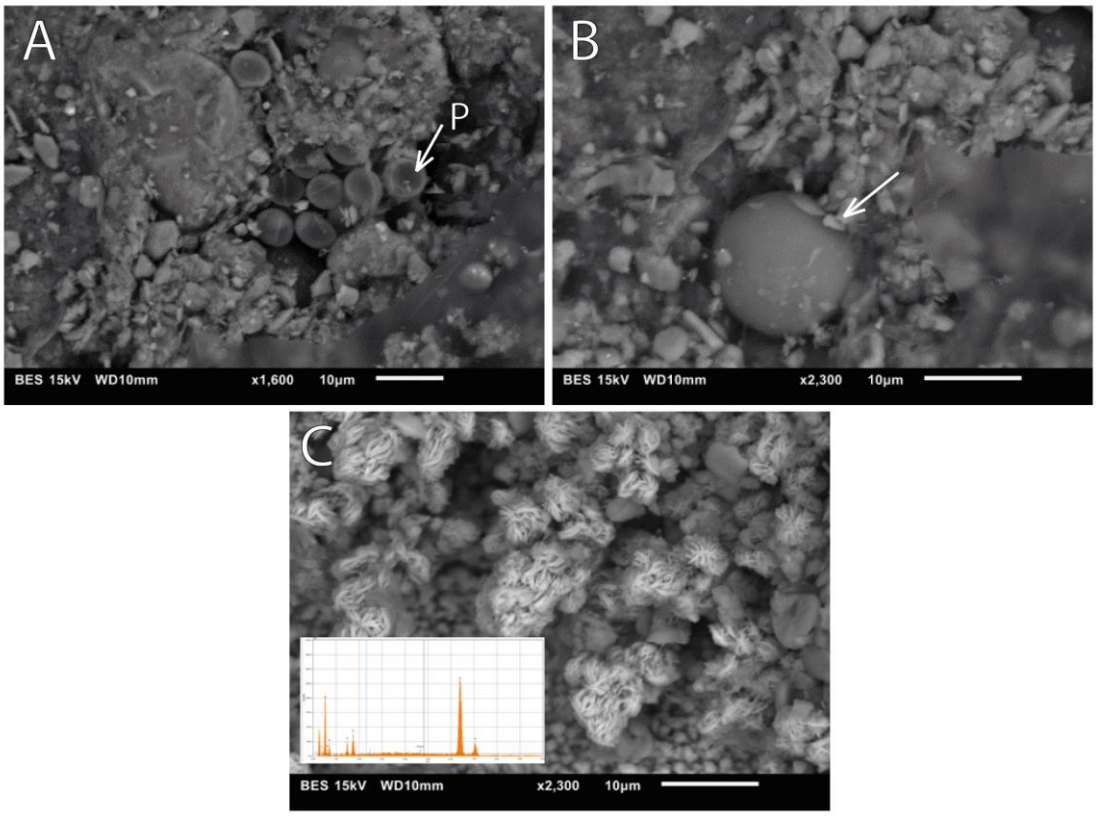

Fig. 3. 5*. A-C. Scanning electron microscopy images of samples from sediment trap taken in July / 2018 in Cregüeña. A) fine-grained matrix with biological debris and pollen grains (P). B) Siliceous cyst surrounded by detrital components. C) micrometric Fe-oxides with EDS spectra.*

3.3.2.2. Marboré

The sediments recovered in the sediment trap in Marbore had very low TOC (1 %) and no carbonate. The SEM study shows high content of silicate minerals and very low content of organic and algal components, in agreement with the low TOC values (Fig 3.6).

3.3.2.3. La Sierra

The sediment trap of La Sierra had moderate TOC values (10 %) and no carbonates. Abundant diatoms and clay particles in an organic-rich mass with iron oxides are identified in SEM images. Sporadic carbonate biological rests and clasts, and pollen grains have been also observed (Fig 3.7).

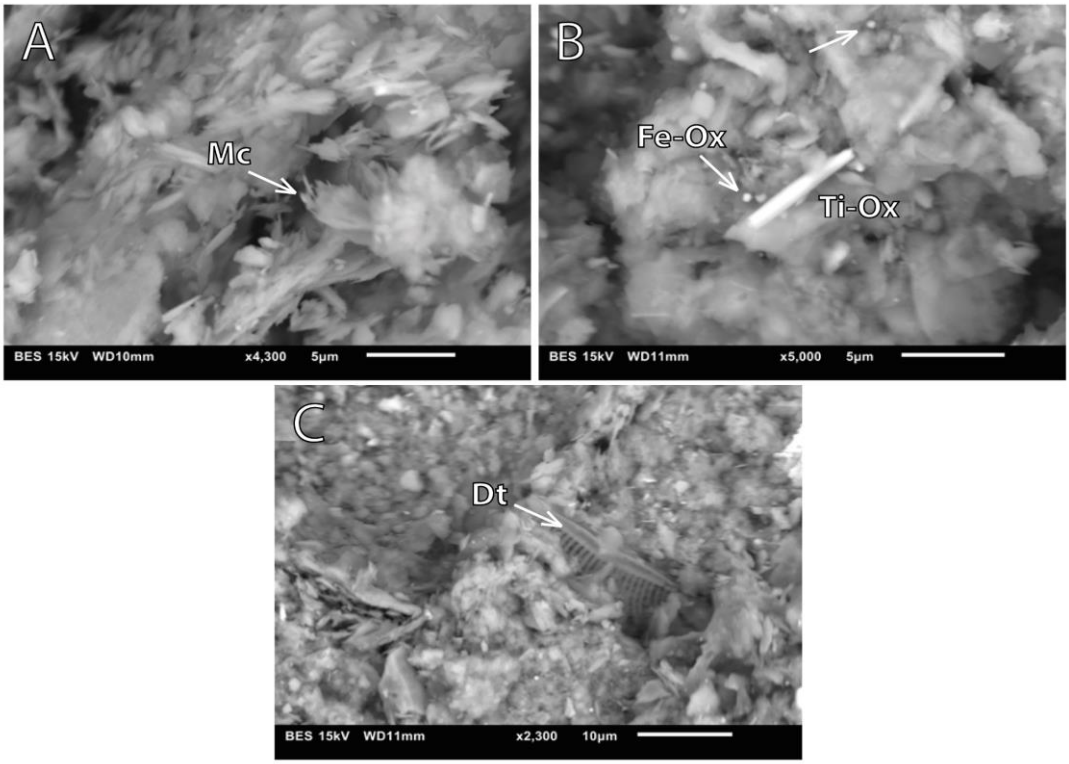

***Fig. 3.6**. A-C. Scanning electron microscopy images of samples from sediment trap of Marboré A) fine-grained matrix with abundant clays (Mc: micas). B) Clayey matrix with Ti-Oxides and sub-micron size Fe-oxides spheres C) Image of a diatom*

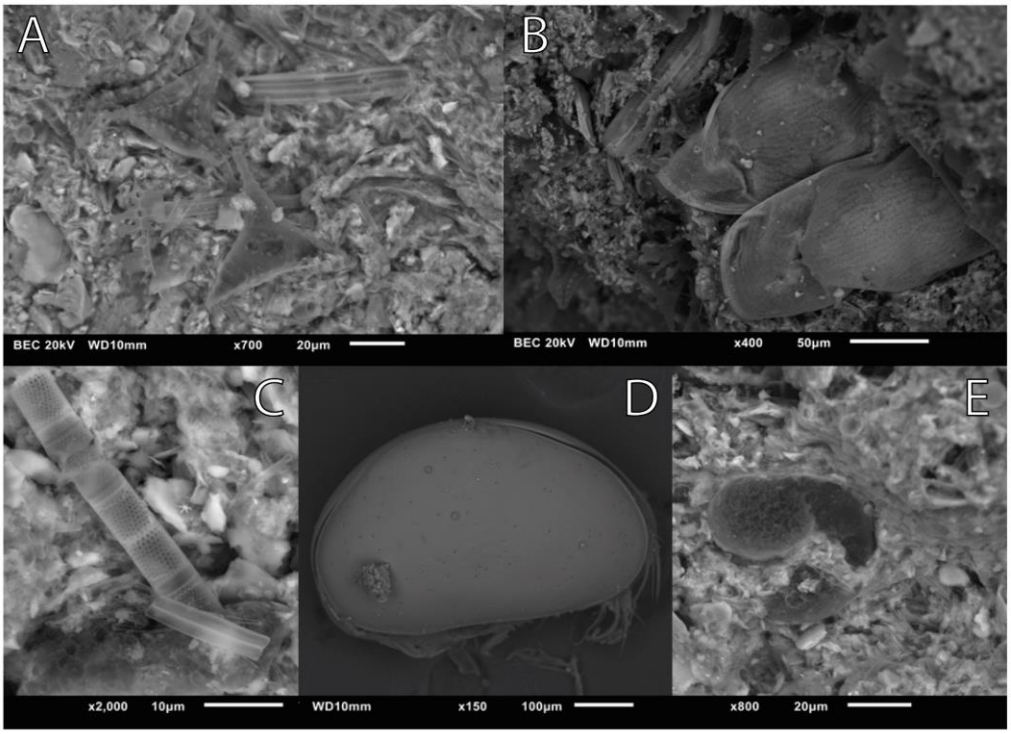

***Fig. 3.7.** A-E: BSE images of samples from sediment trap of La Sierra lake. A) BSE image showing abundant diatoms onto a fine-grained siliciclastic mass. B) plant remains. C) diatom and calcite crystals. D) ostracod E) pollen grain.*

3.3.2.4. Sabocos

The samples from the Sabocos sediment trap had higher TOC (12%) and the highest TIC (1.2 %) value of all lakes. The SEM images show abundant biological rest as diatoms, chrysophyte cysts and irregular organic masses with authigenic Ca-Mg-Fe carbonates. Mn oxides are also frequent as masses and Fe oxides as spherical submicron size particles possible of anthropogenic origin (Fig 3.8).

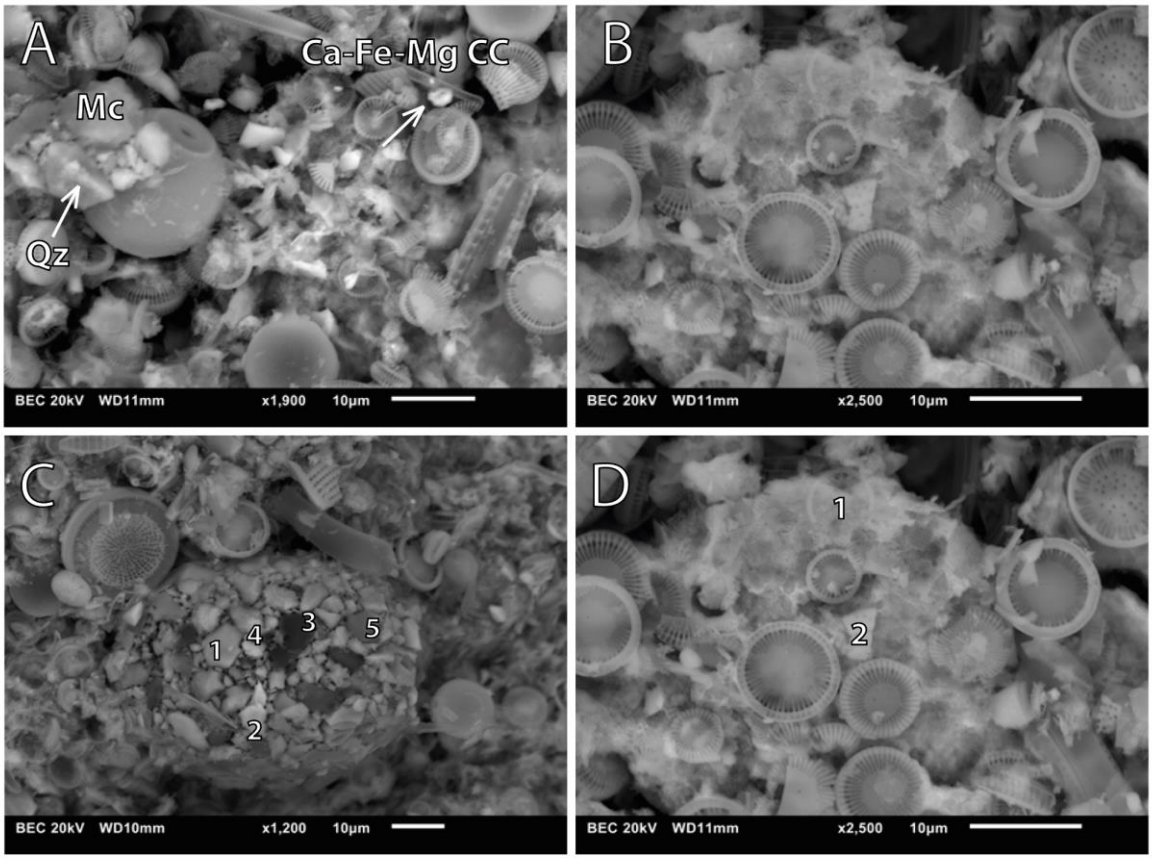

Fig. 3.8. *A-D: BSE images of samples from sediment trap of Sabocos lake. A) Abundant diatoms, cysts, detrital grains (quartz (qz); and Ca-Fe-Mg rich carbonates. B) general texture of the sample showing abundant diatoms and cysts; C) BSI image of a siliciclastic aggregate. 1: Na-Ca Feldspar (plagioclase); 2: calcite; 3: K-feldspar; 4: chlorite; 5: mica. D) diatoms over a Fe-Mg-Ca carbonated irregular mass (1) with calcite crystals (2).*

3.3.2.5. Acherito

Acherito sediment trap sample is characterized by the highest TOC of all lake samples (17 %) and some TIC (0.5 %). SEM images show a high abundance of diatoms and chrysophyte cyst, filaments and sporadic unidentified carbonate grains. Minor detrital grains are also present, as illite-type phyllosilicate, quartz, chlorite and Fe, Ti oxides. Phosphates and Fe oxides also occur (Fig 3.9).

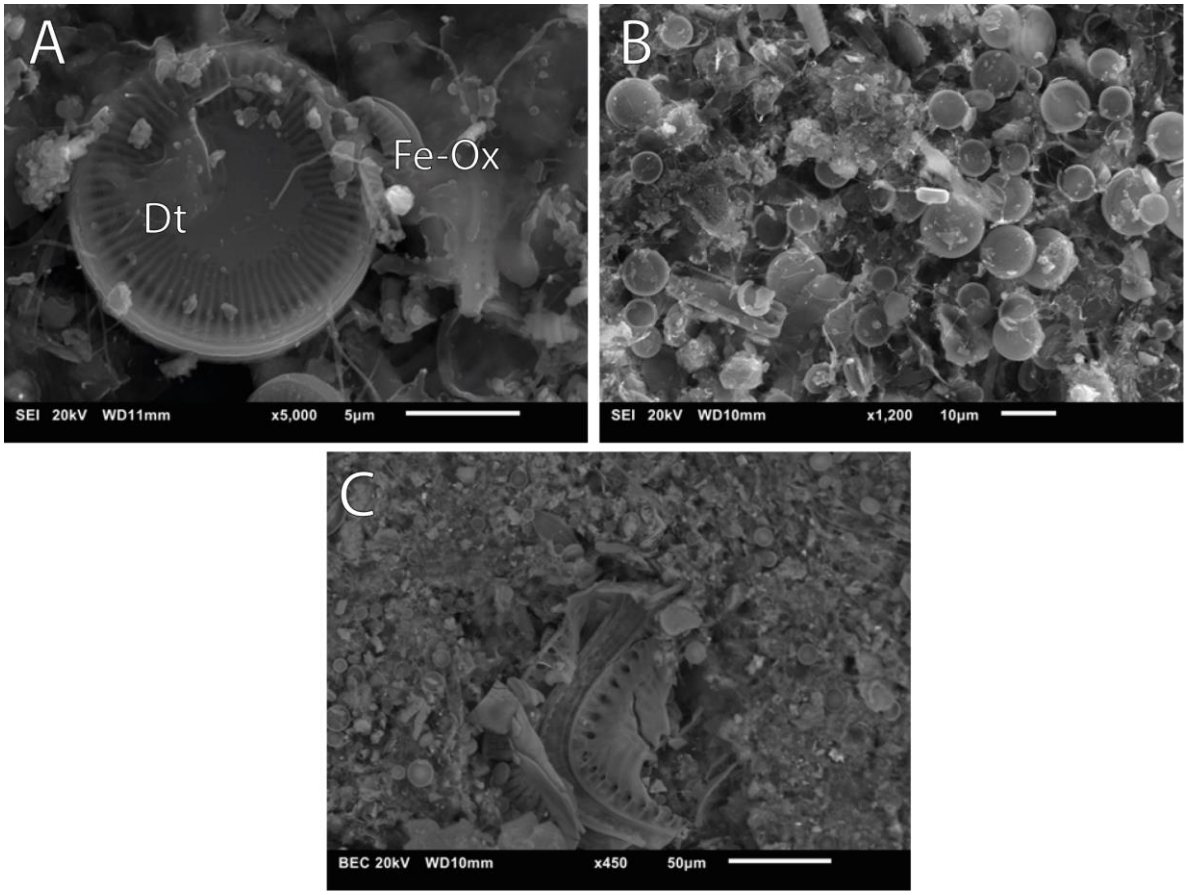

Fig. 3.9. *A-C. Scanning electron microscopy images of samples from sediment trap sample taken in july 2018 of Acherito lake. A) diatom with filaments and a Fe-oxide crystal. B) diatoms C) fine-grained matrix with biological debris.*

3.3.3 Sediment fluxes

Sediment fluxes into the high altitude lakes are strongly influenced by cryosphere processes in the watersheds (snow accumulation and melting, permafrost dynamics). The results from available sediment traps showed a large variability in sediment fluxes (Figure 3.10) from 18 to >400 g/m^2/yr. Total sediment fluxes calculated from sediment

traps are lower than those from the coretop of the sediment sequences (except Sierra and Acherito) likely due to the uncertainty of age models at the top of the sequences. High-altitude lakes in granite watersheds show the lowest sediment fluxes; lakes in lower altitudes and carbonate or mixed watersheds, the highest. The values of La Sierra are the highest (more than 400 g/m2/yr), but this is likely caused by the large remobilization of the bottom sediment due to the shallow depth of the lake (6 m). Lake Marboré has high sediment fluxes due to the large contribution of fine material washed into the lake from nearby moraines and slope accumulations. There is a large difference in sediment fluxes calculated from the core top (772 g/m2/yr) and the trap values (285.9 g/m2/yr) but we consider the sediment trap values more accurate as the core top ones are influenced by the sedimentation rate derived from the age model. Cregueña Lake has the lowest trap sediment flux, as the bioproductivity is small and the areas with possible sediment sources in the basin are limited. Only in Acherito, both top core and sediment trap values are comparable.

Lithogenic fluxes (L_{flux}) calculated from sediment traps are between 20 and 188 g m^{-2} yr^{-1} in silicate-dominated basins, and higher in carbonate basins (up to 544 g m^{-2} yr^{-1} in MA). Fluxes calculated from the first cm of the sediment cores range from 132 to 219 g m^{-2} yr^{-1} in lakes located in silicate watersheds (CRE, URD, SIE, ACH), and they are larger in carbonate – dominated watersheds (1274 in SA, 772 g m^{-2} yr^{-1} in MA).

	Sediment Flux (Trap) g/m2/yr	Sediment Flux (Top core) g/m2/yr
CREGÜEÑA	18,8	144,8
MARBORE	285,9	772,5
SIERRA	480,6	160,6
SABOCOS	65,5	289,2
ACHERITO	188,8	132,2

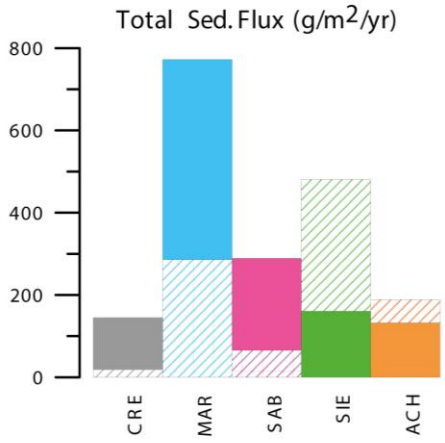

Fig. 3.10. *Left: Total sediment fluxes (g/cm2/yr) calculated from sediment traps (in 2018) and from top sediment core sequences. Right: In the sediment flux graph, the striped line shows the sediment flux data from the traps, while the solid color shows the data from the topcore sediment.*

3.4. Lake water surveys

3.4.1. Lake water results

As part of the REPLIM network, samples were collected since 2017 in the lakes, at different depths on an annual basis (in summer, between June and September). The analyses performed in the water samples included main anions and cations, chlorophyll concentration, conductivity, pH, organic matter concentration, alkalinity and phosphorus, and oxygen and hydrogen isotope. The same day of the water sampling, a continuous measurement along the water column of various physico-chemical properties was conducted with the use of a multiparametric probe.

Figure 3.11 shows a comparison of the surface waters (0 m) of all the lakes for conductivity, pH, alkalinity, organic matter and chlorophyll. The graph illustrates some clear differences among the lakes. Conductivity and pH show similar patterns: the highest values, and therefore slightly more alkaline waters, are found in Sabocos (Conductivity >160 us/cm and pH >8), followed by Acherito (Cond >110 us/cm and pH between 7 and 8). Marboré has a pH between 6.6 and 7 and a conductivity between 70 and 85 us/cm, and the other lakes have slightly more acidic and less concentrated waters: the pH of Cregueña, Sierra and Urdiceto surface waters ranges between 6 and 6.5, also their conductivity is lower, in Urdiceto between 30 and 50 us/cm, and Sierra and Cregueña around 20 us/cm.

The total alkalinity is low (between 5 and 35 ppm) for all lakes, except Sabocos (20 and 240 ppm). It depends on the amount of bicarbonates, since carbonates are absent, with the exception of Sabocos. On the other hand, there is a direct relationship between the organic matter content and the chlorophyll concentration in surface waters. The highest is La Sierra between 2 and 4.5% OM, and between 3 and 5 ug/l in chlorophyll. Acherito has high to moderate values between 0.5 and 1.3% OM and between 0.5 and 4.5 ug/l of chlorophyll. The rest of the lakes show low values for both indicators, less than 1% OM maximum values and around 0.5% in average and chlorophyll between 0 and 1.7 ug/l. According to chlorophyll and P contents, all these lakes are oligotrophic or ultra-oligotrophic.

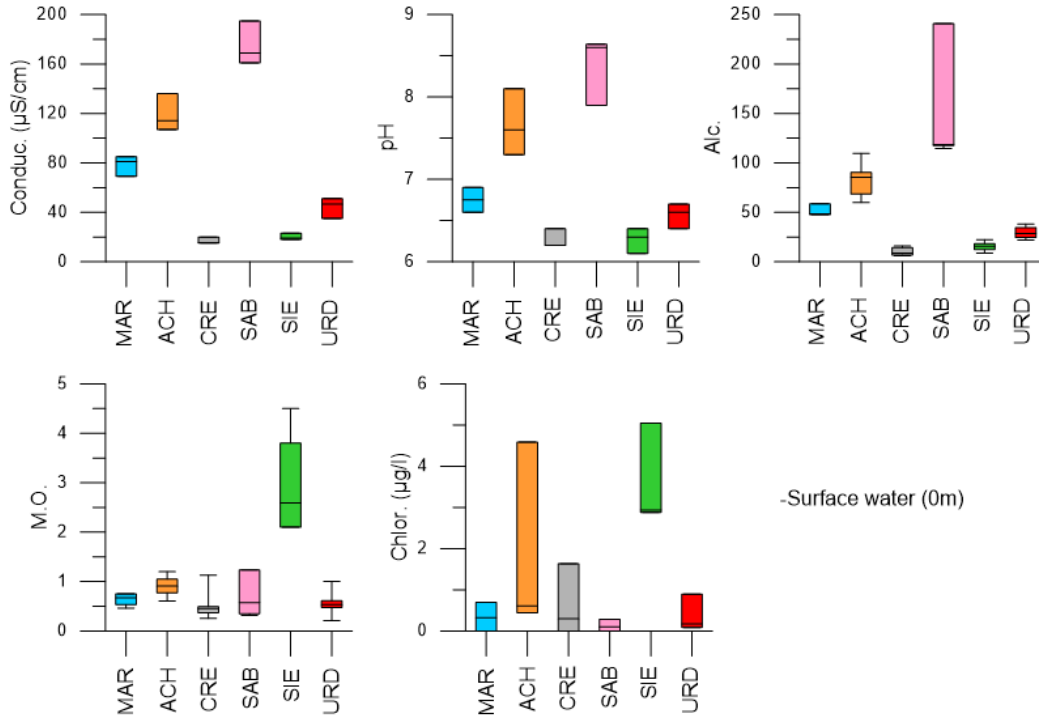

Fig. 3.11. *Surface lake water characterization based on conductivity, pH, alkalinity, organic matter, and chlorophyll content (lab analyses) measured from 2017 to 2022.*

3.4.1.1. Cregueña

Cregüeña is the lake located at the highest altitude (2633 m asl), with the greatest depth (98 m) and ultra-oligotrophic waters. The campaigns were carried out at different times between July and October from 2017 to 2022, illustrating different water stratification stages. Figure 3.12 shows the results obtained with the multiparametric probe in the campaigns carried out from 2017 to 2022.

The 2019 and 2020 campaigns were conducted when the lake was already mixed or it was in the process of mixing (autumn mixing) (see temperature graph in Fig. 3.12), while at the time of survey during the other campaings, the lake was stratified (normal summer stratification). The thermocline depth varies between the different profiles, but it is located approximately between 5 and 15 m deep. Conductivity values range between 6 and 12 µS/cm and subsequent laboratory results were somewhat higher. A slight trend of increasing conductivity is seen in recent years comparing probe profiles.

Conductivity varies very little along the water column, but when the lake is stratified the water in the epilimnion has slightly higher values. The ODO and pH values also define a chemocline between approximately 5 and 15m depth.

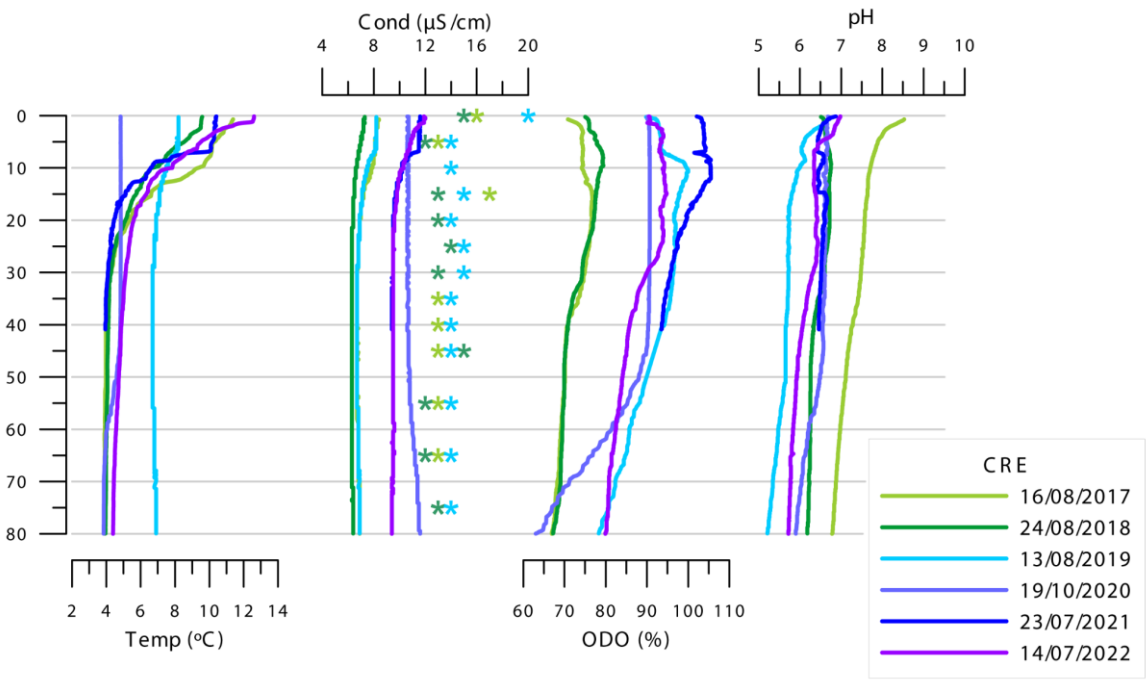

Fig. 3.12. *Parameters obtained from the multiparametric probe: temperature (ºC), conductivity (uS/cm), pH, and dissolved oxygen (% sat) during annual surveys (2017-2022). The conductivity results marked with (*) correspond to subsequent analysis in the laboratory.*

The hypolimnion waters are slightly more acidic and have less dissolved oxygen than surface waters, although the oxygen values are still relatively high at 80 m depth. The values of OM and SDT in the hypolimnetic waters are among the highest in the column, especially in the deeper waters and near the bottom. The $\delta^{18}O$ and $\delta^{2}H$ have a variable range but reach lower values in the hypolimnion too. In the metalimnion the pH is higher compared with hipolimnion, and alkalinity and ODO reach their highest values in the water column. The amount of chlorophyll, OM and phosphorus (SRP) is also higher in the metalimmnion compared to other depths. The epilimnion waters have the highest pH and conductivity values, and the ODO decreases compared to the metalimnion, but it is higher than in deeper waters. Surface waters present higher values in OM, chlorophyll, TDS, sulfates and Na. The $\delta^{18}O$ and $\delta^{2}H$ have a smaller range than in the hypolimnion but higher values (Fig 3.12 and 3.13).

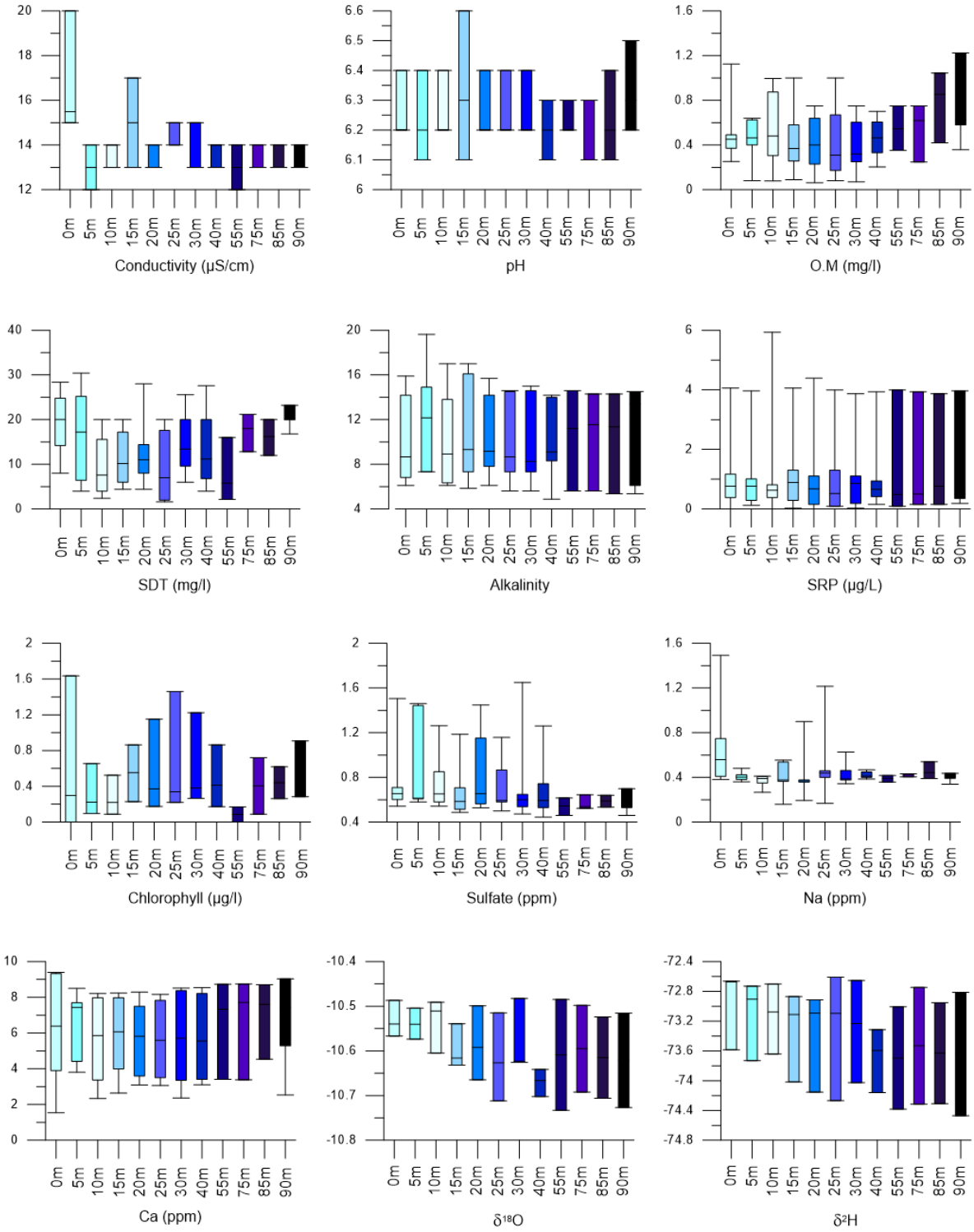

Fig. 3.13. *Characterization of Cregueña waters at different depths: Conductivity, pH, organic matter, Total dissolved solids (SDT), Alkalinity, Phosphorus (SRP), chlorophyll, sulfate, Na, Ca and $\delta^{18}O$ and $\delta^{2}H$.*

Our water surveys show consistent results with the 2011 reports of the CHE (Confederación Hidrográfica del Ebro) for this lake (*https://portal.chebro.es/ca/web/guest/puntos-de-control-y-resultados*). According to this report in 2010, Cregueña had a transparency of 20 m (based on the use of the Secchi disk), a conductivity lower thn 50 µS/cm, a pH of 7, and an alkalinity of <40 mg/L. They determined that the ecological status of this lake was good.

3.4.1.2. Marboré

Water analyses in the ibón of Marboré in samples collected during the period 2017- 2022 show little change in the composition in terms of alkalinity (40-80 ppm), pH (7-9) and trophic status (ultraoligotrophic) (Figure 3.14 and 3.15). These results are in agreement with the data obtained by Sánchez España et al., (2018).

The multiparametric probe data show the relatively low compositional variability of the waters during the ice-free period when measurements were taken (Figure 3.14). In general, the surveys show low and fairly stable conductivity values along the water column, and - despite thermal stratification during the summer - oxygen at the bottom waters, as the low biological activity did not consume it through the summer. The data of October 8, 2020 illustrate the autumn mixing with similar values of conductivity, pH and ODO in the entire volume of water. The data of October 9, 2019 show a deeper thermocline but homogeneous conductivity and ODO. The pH values are anomalous and likely due to calibration problems with the probe.

During the stratified summer period, the upper layer reached up to 5 to 8 m depth, and the thermocline was located from 4 to 10 meters. In the hypolimnion, OM values were somewhat higher, especially closer to the bottom, as are sulfates and TDS. In the metalimnion, conductivity and pH are higher; the increase in pH in the thermocline suggests higher biological activity at that depth, which corresponds with higher chlorophyll values. The epilimnion waters have higher conductivity and their isotopic values are also higher and less variable (Fig 3.14 and 3.15).

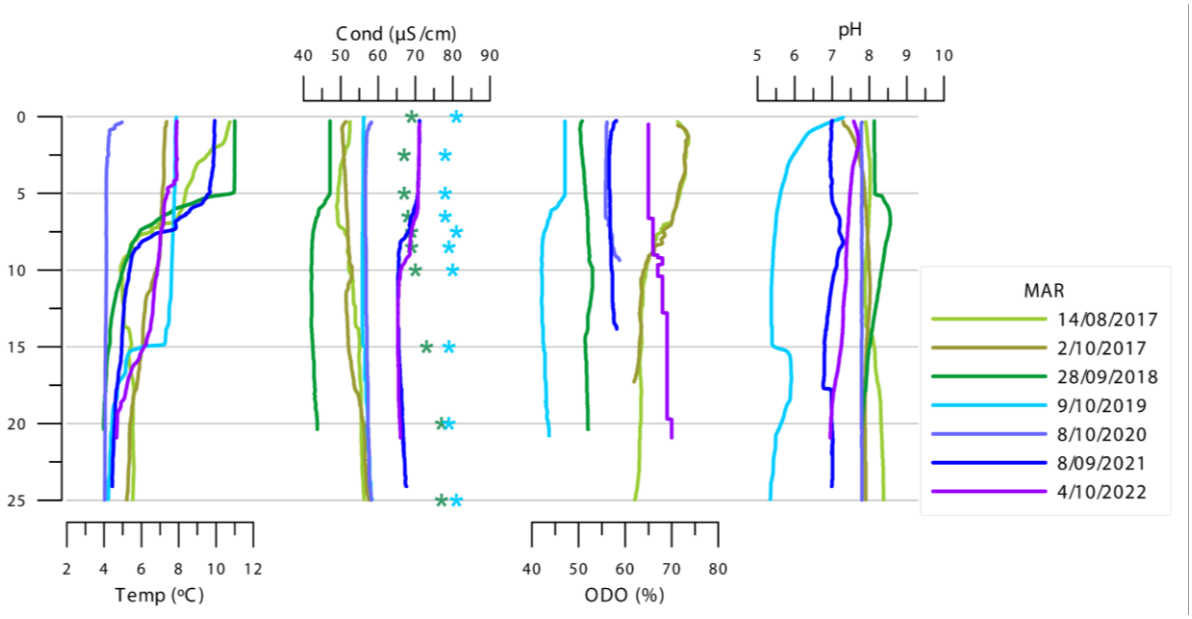

Fig. 3.14. *Parameters obtained from the multiparametric probe: temperature (ºC), conductivity (uS/cm), pH, and dissolved oxygen (% sat), during annual surveys (2017-2022). The conductivity results marked with (*) correspond to subsequent water analysis in the laboratory.*

The data obtained in this study are similar to the 2018 CHE reports (*https://portal.chebro.es/ca/web/guest/puntos-de-control-y-resultados*): conductivity of 68 µS/cm, a pH of 7.1 (at surface), an alkalinity of 35.5 mg/L, and Chlorophyll of 0.6 µg/L. They determined that the ecological status of this lake was good. Marbore lake has been the subject of a detailed study conducted from 2013 to 2015 (Sánchez España et al., 2018). Stratification dynamics and water chemistry values were very similar to our survey, but the pH for that period (7.0 and 7.8) was lower than measurements by CHE. Although previous studies in the Pyrenees did not find evidence of lake acidification (Catalan et al., 1992), others indicate moderate acidification related to burning of fossil fuels (Camarero & Catalan, 1998) and/or increased nitrogen loadings (Curtis et al., 2005). The variations of pH found in the surveys from 2013 to 2020 are not conclusive, but they suggests that vertical profiles of pH should be obtained regularly, in order to corroborate if an acidification process is taking place in this high-mountain lake.

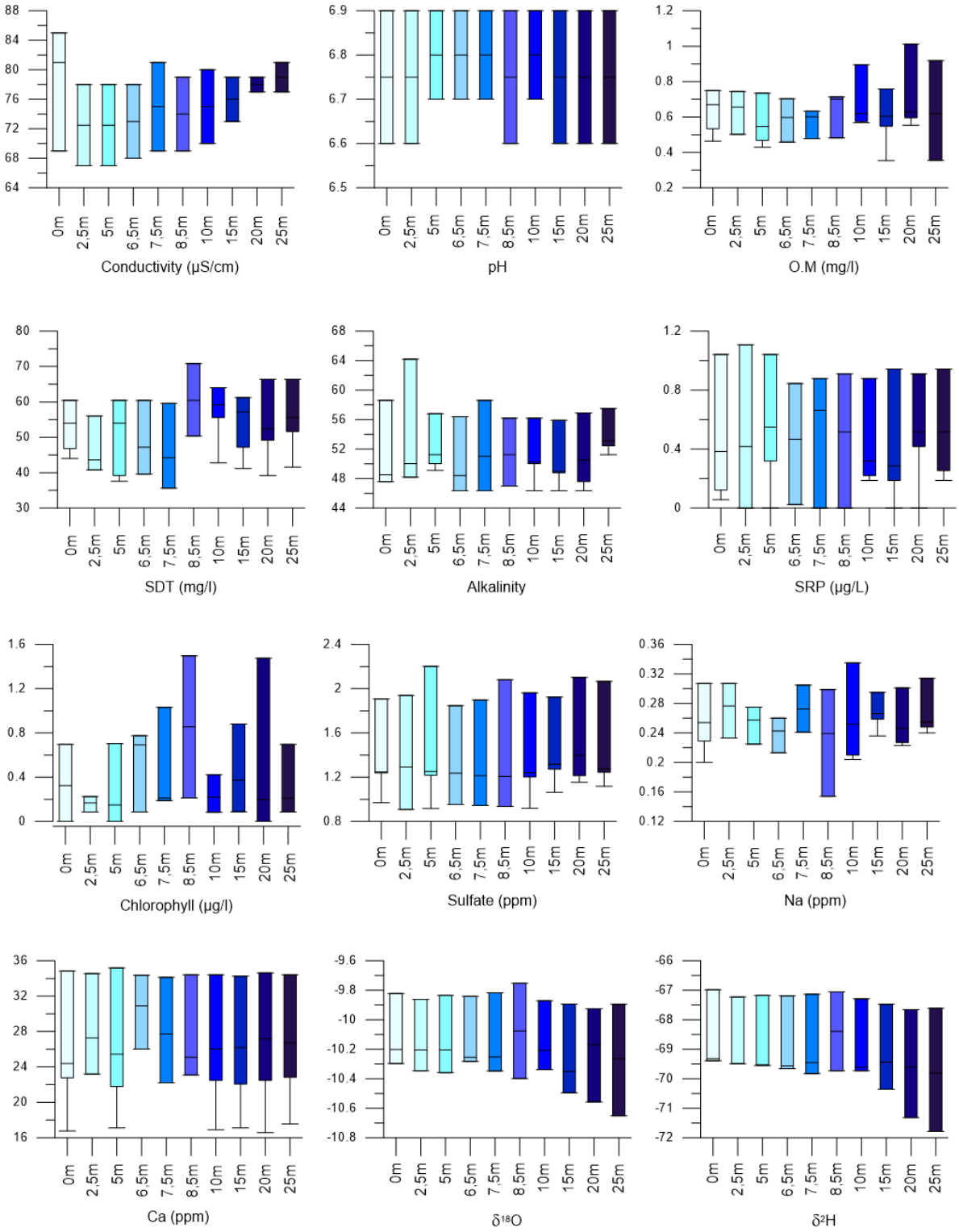

Fig. 3.15. *Characterization of Marboré waters at different depths: Conductivity, pH, organic matter, Total dissolved solids (TDS), Alkalinity, Phosphorus (SRP), chlorophyll, sulfate, Na, Ca and $\delta^{18}O$ and $\delta^{2}H$.*

3.4.1.3. Urdiceto

All water sampling in Urdiceto from 2017 to 2021 was done in July, during summer stratification and thus the temperature profiles are very similar to each other. The thermocline was between approximately 3 and 10 mm deep. Conductivity was low throughout the water volume and quite stable, only the 2021 sampling it had slightly higher values. With respect to its trophic state, it is an ultraoligotrophic lake (Fig 3.16). The pH values ranged between 6 and 8 with anomalously higher values in the surface waters in July 2019, that could also be caused by sensor malfunctioning.

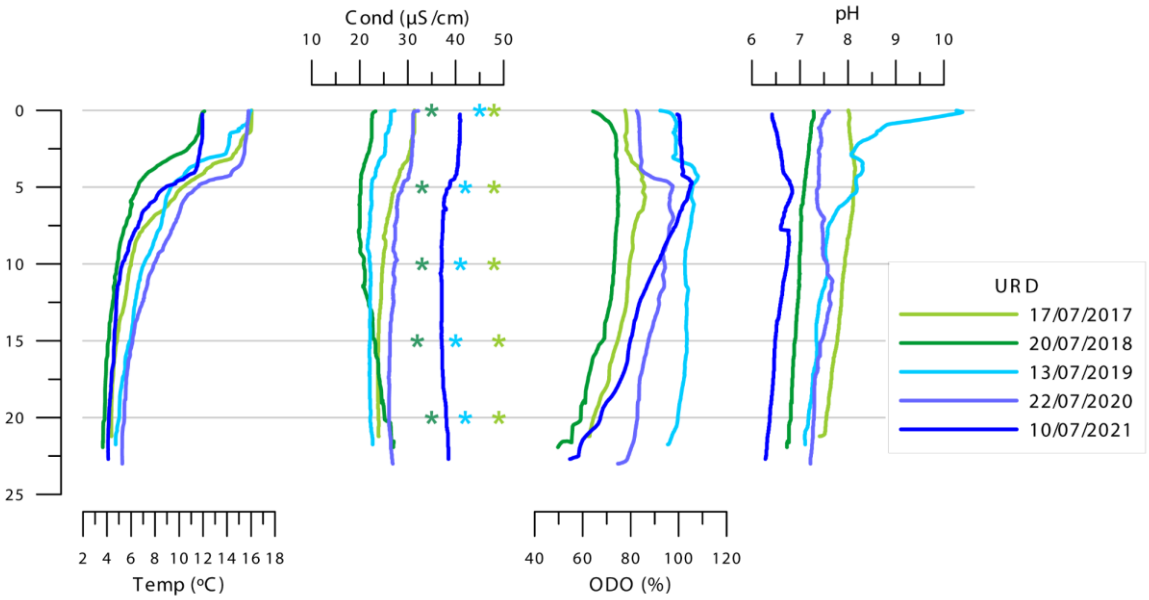

Fig. 3.16. *Parameters obtained with the multiparametric probe: temperature (ºC), conductivity (uS/cm), pH, and dissolved oxygen (% sat) during annual surveys (2017-2022). The conductivity results marked with (*) correspond to subsequent water analysis in the laboratory.*

Hypolimnion waters had higher OM, chlorophyll and phosphorus (SRP) values. They also had slightly higher amounts of sulfates, and $\delta^{18}O$ and $\delta^{2}H$ values were lower but with higher variability. The metalimnion waters have higher dissolved oxygen percentages, pH, OM and SDT values. Epilimnetic waters had somewhat higher conductivity, with low SDT and higher $\delta^{18}O$ and $\delta^{2}H$ isotopic values (Fig. 3.17).

The 2016 CHE report for Urdiceto (*https://portal.chebro.es/ca/web/guest/puntos-de-control-y-resultados*) had comparable results: a transparency between 4 and 10 m (based on the use of the Secchi disk), conductivity of 79 µS/cm, a pH of 8.5, an alkalinity of 24 mg/L and 2.54 µg/L of Chlorophyll . They determined that the ecological status of this lake was moderate.

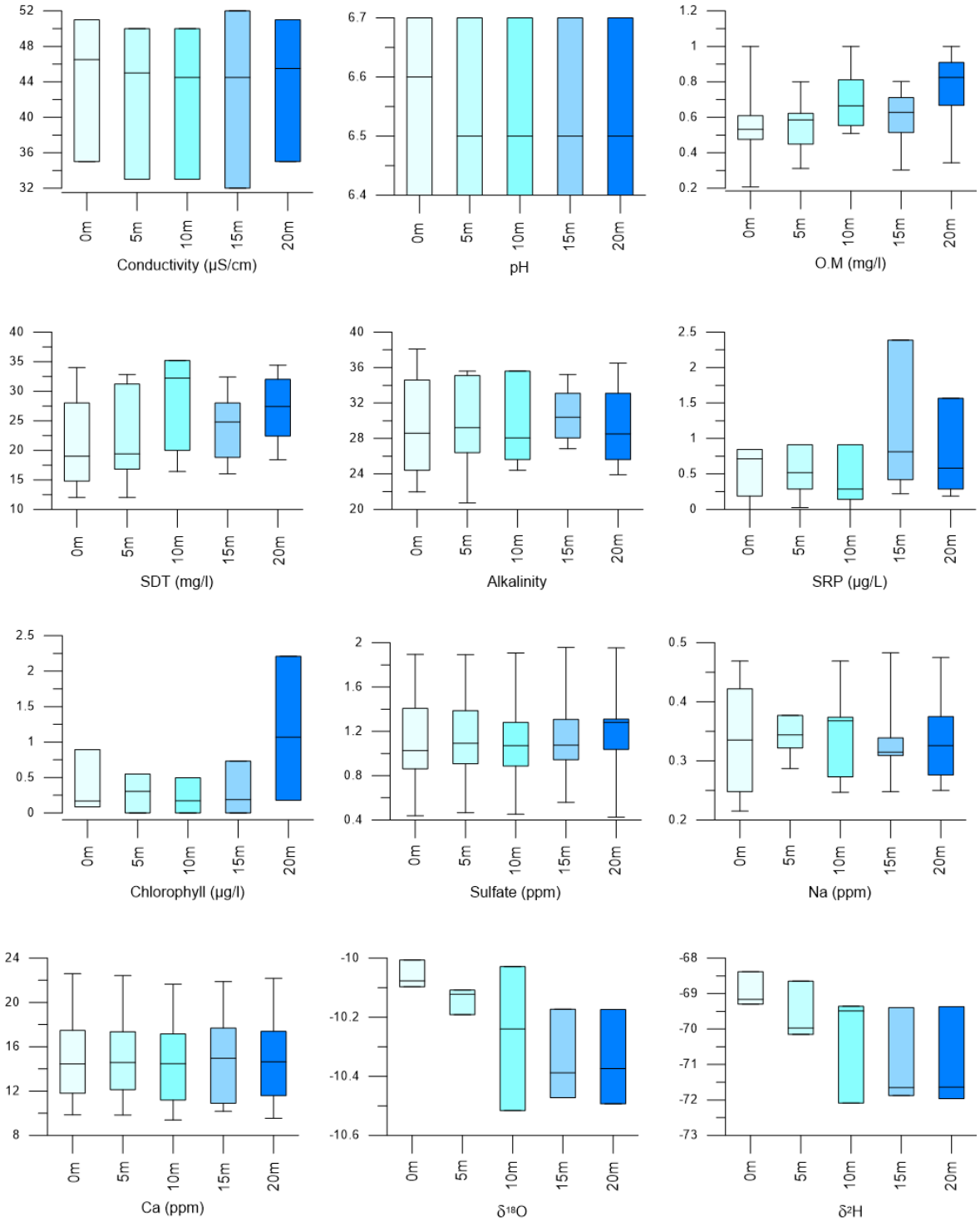

Fig. 3.17. *Characterization of Urdiceto waters at different depths: Conductivity, pH, organic matter, Total dissolved solids (TDS), Alkalinity, Phosphorus (SRP), chlorophyll, sulfate, Na, Ca and $\delta^{18}O$ and $\delta^{2}H$.*

3.4.1.4. La Sierra

The thermal profiles of La Sierra did not have a stratified structure, despite the fact that the sampling between 2017 and 2022 occurred on different dates between July and October (Figure 3.18). Only in 2019 there was a subtle temperature change between 3 and 4.5 m deep approximately. The absence of summer stratification is likely due to the shallow nature of this lake (maximum 6 m deep) that favors total water mixing. For the same reason, the temperature, conductivity, pH and ODO ranges between the bottom and the surface were small. The trophic state of the lake was mesotrophic.

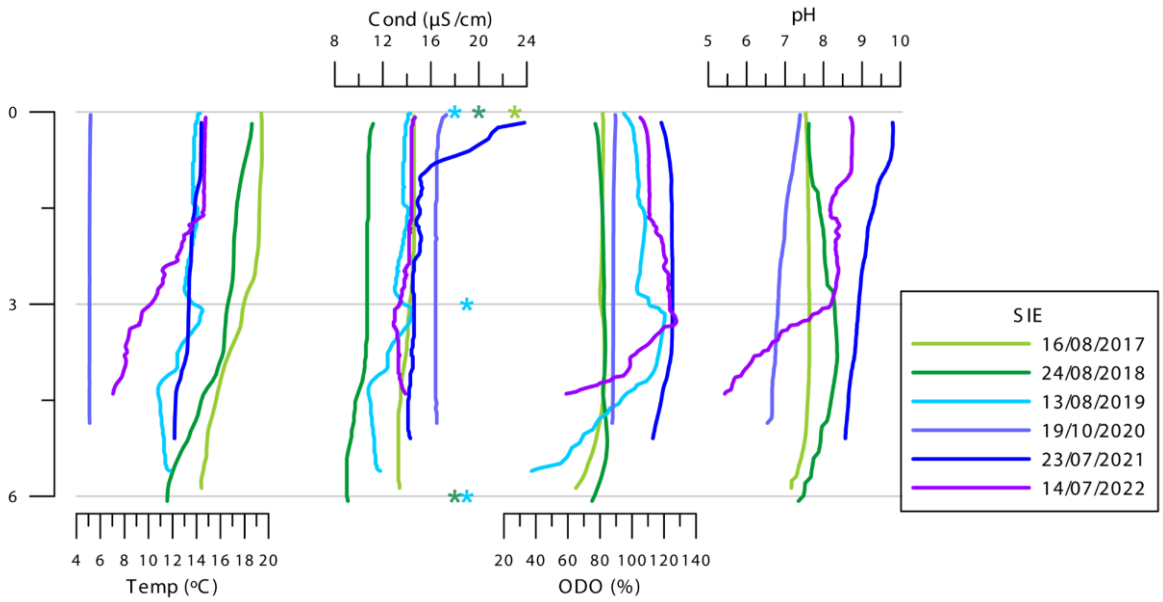

Fig. 3.18. *Parameters obtained by the multiparametric sonde: temperature (ºC), conductivity (uS/cm), pH, and dissolved oxygen (% sat) during annual surveys (2017-2022) The conductivity results marked with (*) correspond to subsequent analysis in the laboratory.*

The deeper waters had lower conductivity, pH, $\delta^{18}O$ and $\delta^{2}H$ values, and higher OM, chlorophyll and sulfate contents. In contrast, surface waters have higher conductivity, somewhat higher pH, more phosphorus (SRP), lower chlorophyll and OM concentration, and higher $\delta^{18}O$ and $\delta^{2}H$ values. THE ODO values are homogeneous along the whole water column and > 80 % in most surveys. Only in 2019, when the multiparametric probe profile showed some temperature and chemical stratification, the ODO increased at the thermocline and decreased in the bottom waters (Fig 3.18 and 3.19).

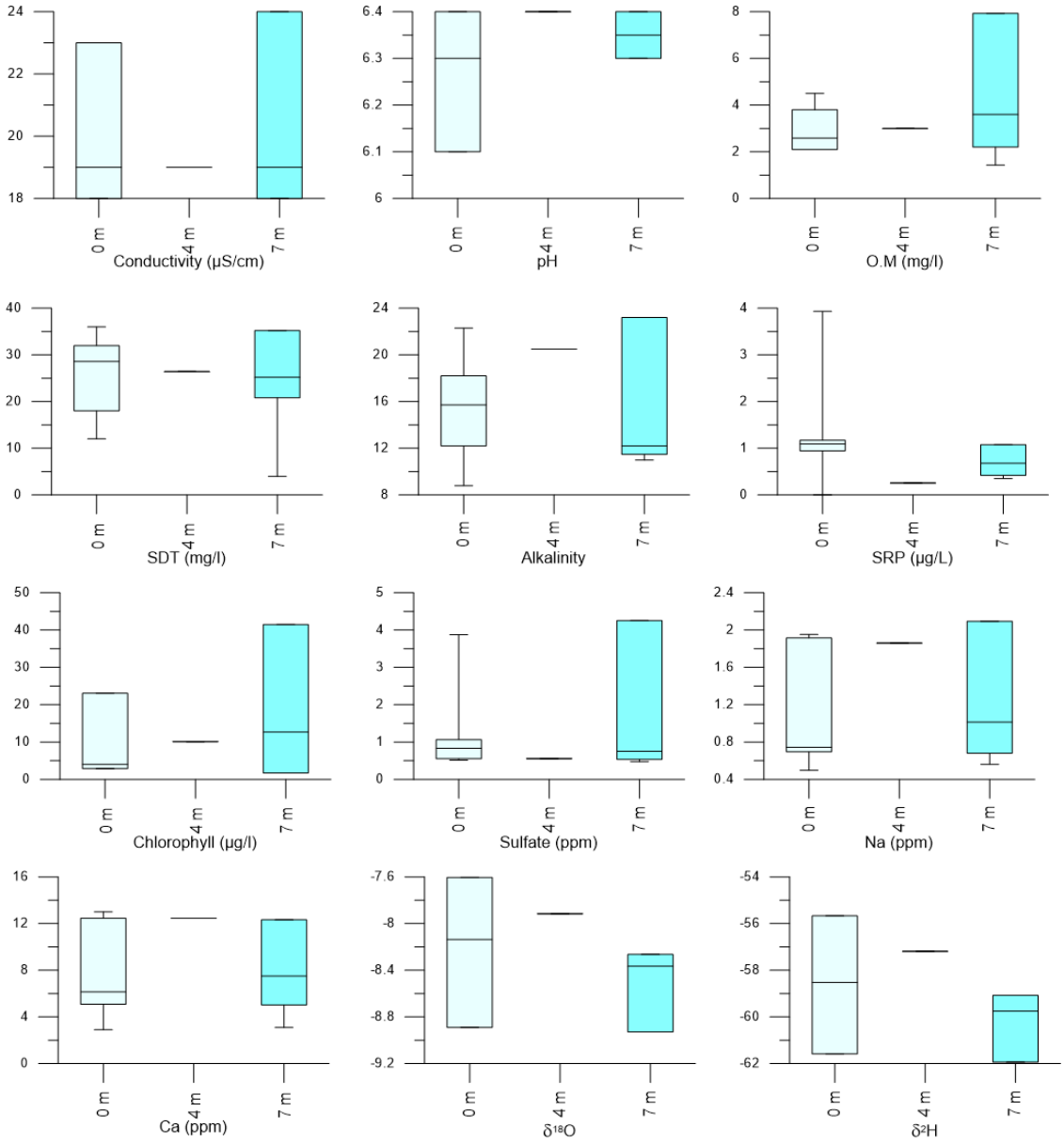

Fig. 3.19. *Characterization of La Sierra waters at different depths: Conductivity, pH, organic matter, Total dissolved solids (TDS), Alkalinity, Phosphorus (SRP), chlorophyll, sulfate, Na, Ca and $\delta^{18}O$ and $\delta^{2}H$.*

3.4.1.5. Sabocos

The Sabocos multiparametric probe profiles in November 2017 and October 2021 correspond to times of water mixing, while the other ones (between June and August) to thermal stratification stages. The thermocline was located between 3 and 10 m depth. Conductivity ranged between 90 and 200 uS/cm and pH between 7.5 and 10 (Fig 3.20). The trophic state was oligotrophic.

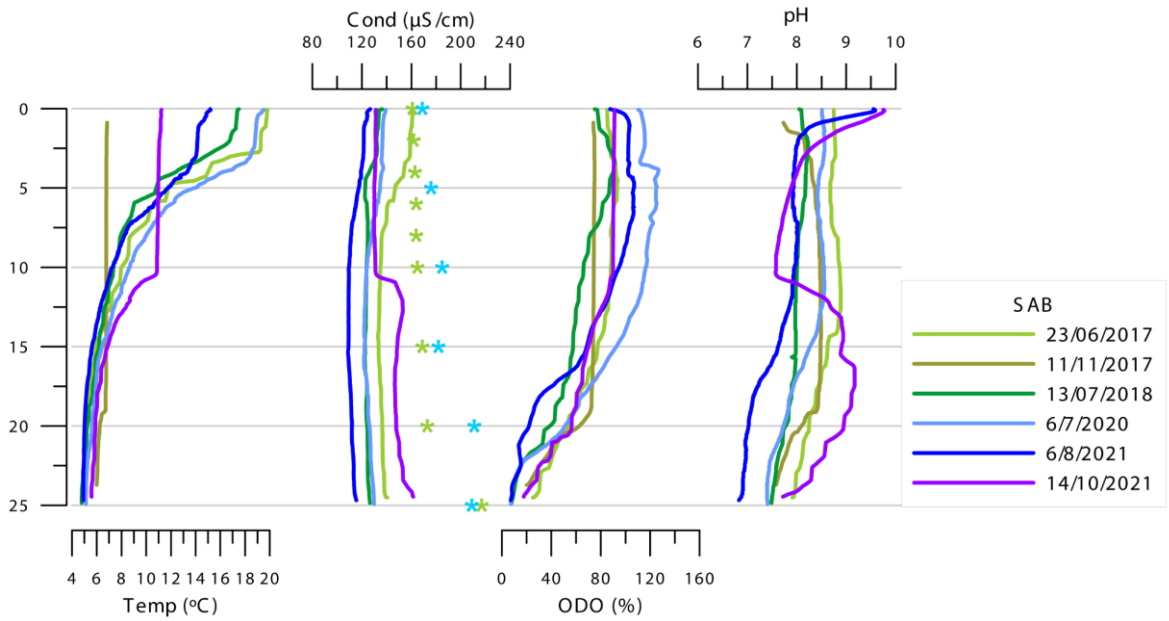

***Fig. 3.20**. Parameters obtained with the multiparametric probe: temperature (ºC), conductivity (uS/cm), pH, and dissolved oxygen (% sat) during annual surveys (2017-2022). The conductivity results marked with (*) correspond to subsequent water analysis in the laboratory.*

The hypolimnion waters had low ODO, and their pH values (at times of thermal stratification) were slightly more acidic. They have higher values of OM, chlorophyll and TDS, especially in the deeper waters and near the bottom; in addition bottom waters have higher alkalinity and Ca content. In the metalimnion, the ODO reaches the highest values in the water column, and pH, OM and chlorophyll have higher values. Epilimnion waters are slightly more concentrated, and their pH and ODO somewhat lower than in the metalimnion but higher than in deeper waters. OM and chlorophyll values were lower in surface waters (Fig 3.20 and 3.21).

The CHE 2020 report for this lake (*https://portal.chebro.es/ca/web/guest/puntos-de-control-y-resultados*) indicated a transparency of 10 m (based on the use of the Secchi disk), conductivity of 188 µS/cm, pH of 7.8, an alkalinity of 100 mg/L and higher

chlorophyll values, up to 2.4 µg/L. They determined that the ecological status of this lake was good.

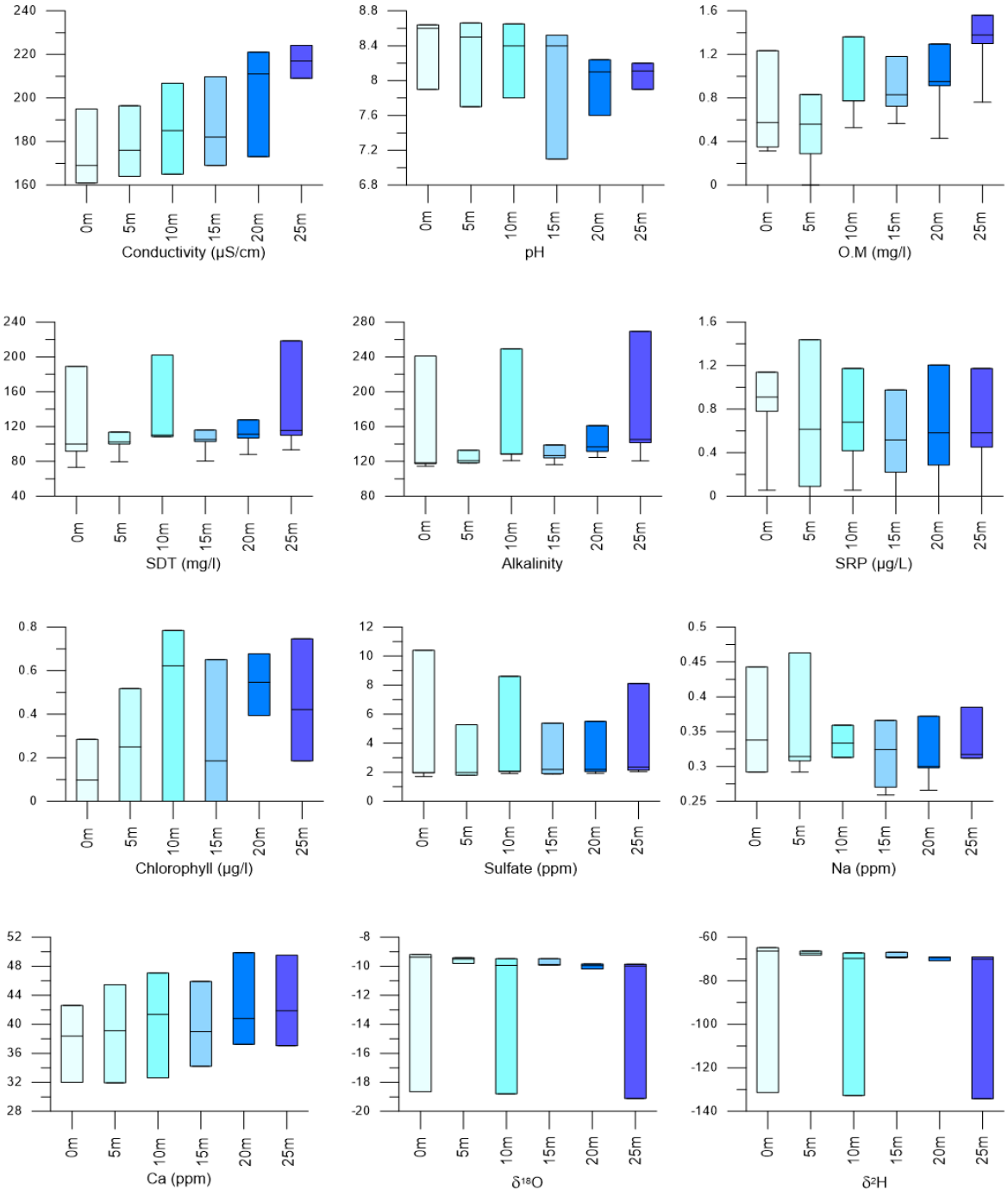

Fig. 3.21. *Characterization of Sabocos waters at different depths: Conductivity, pH, organic matter, Total dissolved solids (TDS), Alkalinity, Phosphorus (SRP), chlorophyll, sulfate, Na, Ca and $\delta^{18}O$ and $\delta^{2}H$.*

3.4.1.6. Acherito

Water sample collection in Acherito between 2017 and 2022 were done when the lake was stratified (July-August). The thermocline was established between approximately 4 and 12 m depth, but throughout the water column variability of conductivity and pH was small (Fig 3.22). The trophic state of this lake was oligotrophic. ODO was greater at the thermocline.

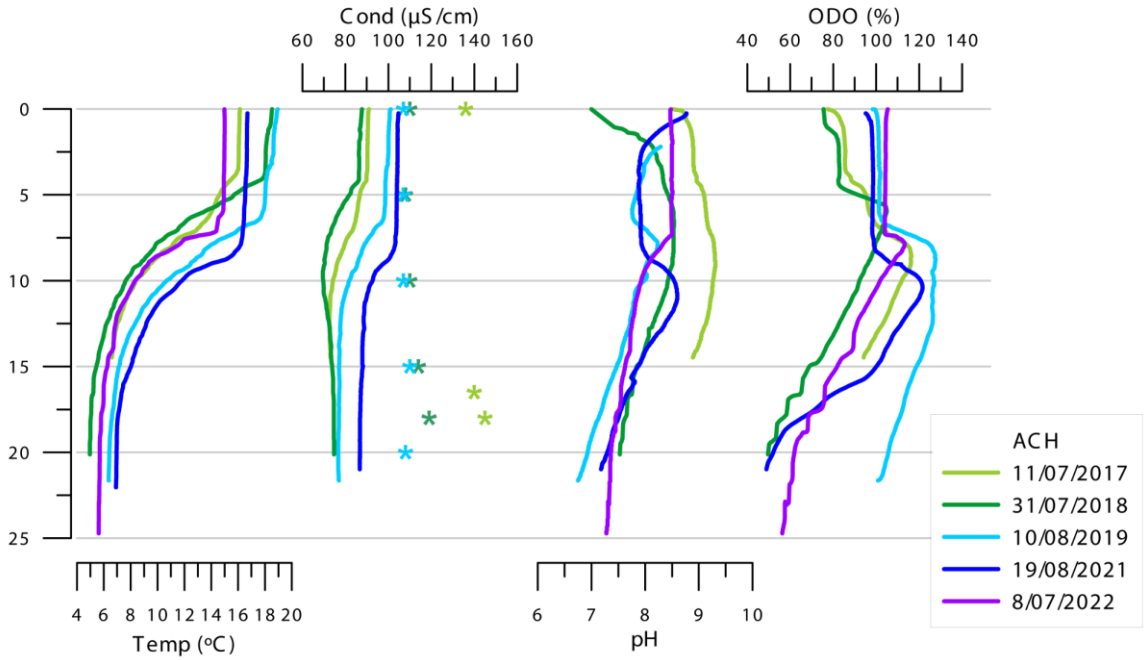

***Fig. 3.22**. Parameters obtained with the multiparametric probe: temperature (ºC), conductivity (uS/cm), pH, and dissolved oxygen (% sat) during annual surveys (2017-2022). The conductivity results marked with (*) correspond to subsequent water analysis in the laboratory.*

The waters of the hypolimnion were less concentrated, and had a lower ODO and pH than epilimnetic waters They also had somewhat higher values for OM, chlorophyll, TDS and phosphorus (SRP), but lower Na and sulfate. The $\delta^{18}O$ and $\delta^{2}H$ values were lower but with higher variability. The metalimnion waters had the highest ODO and pH, but lower OM and chlorophyll, while sulfates and Na increased slightly. In the epilimnion the waters were more concentrated and the pH was stable, higher than that of the deep waters and lower than that of the metalimnion. Surface waters had higher alkalinity, TDS, and chlorophyll; isotopic values were also higher and less variable (Fig. 3.22 y 3.23). This is similar to what is described in the 2017 CHE report for this lake (*https://portal.chebro.es/ca/web/guest/puntos-de-control-y-resultados*). According to this report, Acherito had a transparency of 3.6 m (based on the Secchi disk), conductivity of

100 µS/cm, a pH of 6.7 and an alkalinity of 100 mg/L. They determined that the ecological status of this lake was good.

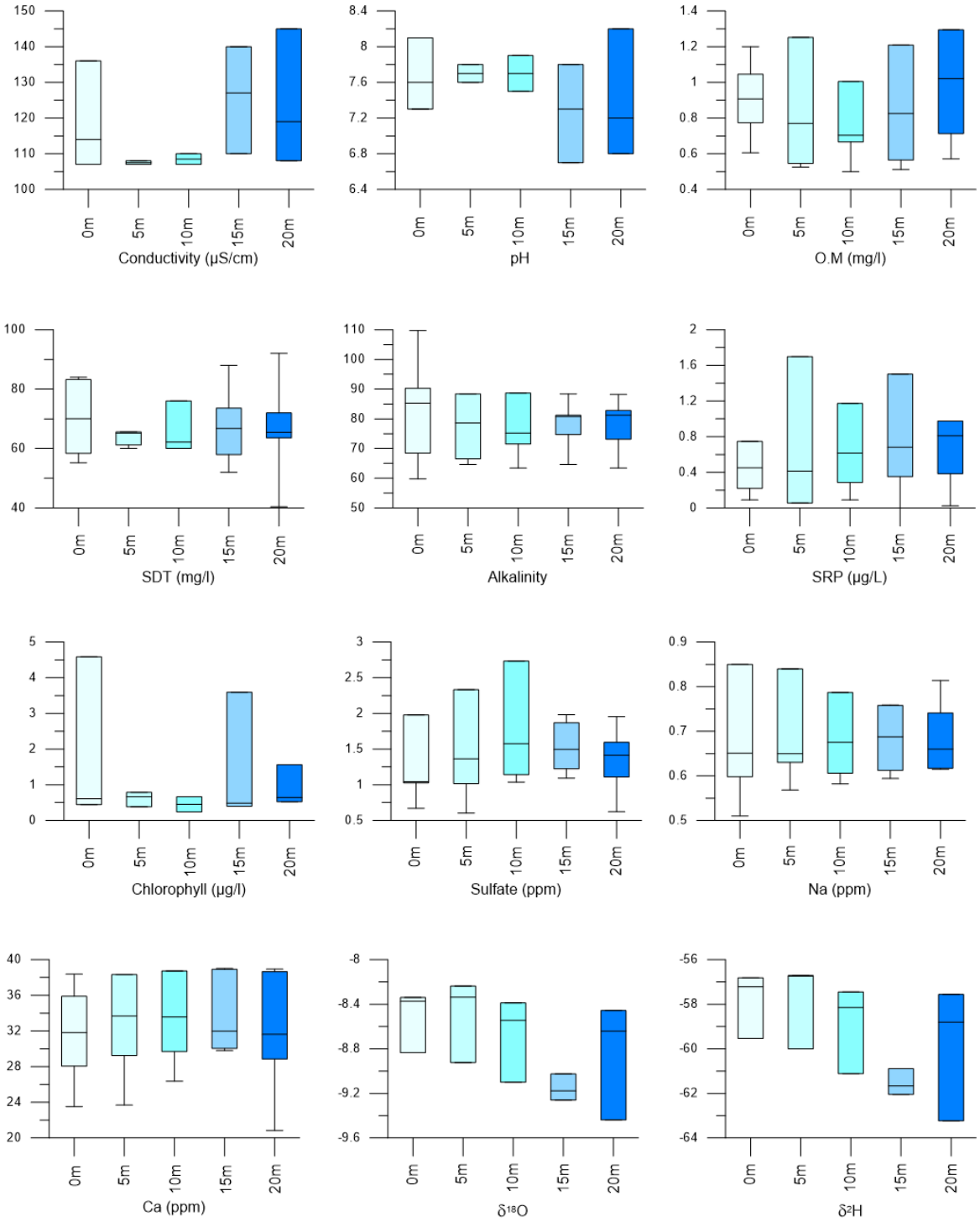

Fig. 3.23. *Characterization of Acherito waters at different depths: Conductivity, pH, organic matter, Total dissolved solids (TDS), Alkalinity, Phosphorus (SRP), chlorophyll, sulfate, Na, Ca and $\delta^{18}O$ and $\delta^{2}H$.*

3.4.2. Water composition variability

High altitude lakes are ecosystems with very dilute waters, low dissolved solids and solutes, oligotrophic to ultraoligotrophic and with high transparency. The watershed characteristics (topography, drainage network, surface) and bedrock geology (mainly carbonate versus siliceous formations) control the chemical composition of the water and the carbon cycle, as dissolved organic carbon responds mainly to soil type and abundance. Biogeochemical cycles are also influenced by bedrock properties (as they control alkalinity and carbon cycling, for example), and nutrients and contaminant deposition (as they exert great control over microbiota and macrobiota dynamics). In particular, water pH is an important factor in the development of algae and macrophytes and is mainly controlled by alkalinity and bedrock geology (Catalan et al., 2006).

Results from this PhD are in agreement with other studies in high mountain lakes, where watershed local erosion and nature of the basin, even within the same mountain range, partially controlled the dynamics of the lake, (Sánchez-España et al., 2019) in a study of 4 lakes of Somiedo Natural area, based on depth profiles of temperature, conductivity, pH and ORP, and dissolved oxygen, chlorophyll-a, organic carbon, nutrient and metal concentration, showed that most of the lakes have a stratification with vertical gradients as a result of different physical and (bio) geochemical processes. The 4 lakes studied, from 7-50 m depth in highs ranging from 1545-1640 m, showed differences respect to nutrient availability, primary productivity, or hypolimnetic oxygen deficit, with a range of trophic conditions between El Valle, (oligotrophic) to Calabazosa (eutrophic). These authors suggested that total phosphorus concentration (e.g., 10 µg/L P in El Valle vs. 35 µg/L P in Calabazosa) were responsible for these differences, and that the erosive processes in the catchment area may contribute to increase the oxygen consumption rate (terrestrial organic matter input).

Other mountain lakes studies, as those in the Central Range (Laguna Cimera or Peñalara Lake) (Granados & Toro, 2000; Toro et al., 2006) where long-term monitoring series have been obtained (Peñalara Lake) show a strong influence of human activity and increased sediment input to the lake on the limnology. In the actual scenario of global warming and increased human activities in the watersheds and lakes, changes of hydrochemistry of the lakes can be expected, but they will be also dependent on the nature of the catchment area, as climate change will induce different weathering processes according to the nature of the surrounding rocks (Rogora et al., 2003, 2018).

Although severe hypoxia/anoxia has not been observed in any of the studied lakes, future warmer and drier summers can reduce oxygen levels in deep waters by means of increasing or changing thermal stratification (Butcher et al., 2015; Foley, 2011). This increase is critical, as it can also influence the C and and N global cycles (Carey et al., 2022). This situation is already taking place in other mountain lakes in Spain such as in Lake Enol (PN Picos de Europa), where an increasing anoxia is occuring, due to combination of several factors, including thermal warming (Sánchez et al., 2017).

Our water surveys in the Pyrenean lakes have shown some variability in water composition and properties, but to determine if those changes are beyond seasonal and interannual variability, longer time series are needed.

3.5 Thermal regimes

3.5.1. Lake sites.

For the study of the thermal regimes of the lakes, a system of thermometers installed at various depths has been in place since 2017, with hourly temperature measurements (see Methodology chapter). The thermal regime graphs (Fig 3.24 to 3.34) show the temperature dynamics at depth during the surveyed period.

The lakes (with the exception of La Sierra) have a dimictic behavior. This means that during the summer the surface waters are much warmer than the deeper waters, behaving for practical purposes as two immiscible fluids. In winter the deep waters are kept at a higher temperature than the surface waters near the ice. There are two periods in which the temperatures of deep and surface waters are homogenized and therefore the mixing of waters occurs: one just after the ice melts and surface waters warm up during the summer and another during the autumn. The hourly temperature time series at several depths makes it possible to study parameters such as the duration of ice cover, the intensity and duration of mixing periods or the temperature difference between the warm surface waters in summer (epilimnion) and the deep, cold waters (hypolimnion). In the following sections we summarize the results for each lake.

3.5.1.1. Cregueña

The Cregueña data series since 2018 shows a similar winter behavior in the lake. Due to the ice cover that is maintained over a prolonged period of time, a positive temperature gradient at depth occurred in all winters with the exception of the winter of 2021, when the ice cover lasted less time and the water at depth remains mixed at a constant temperature. Differences also occur during the summers with normal stratification. For example, in 2018 the stratification period was shorter and lower temperatures were reached at lower depths while during other summers, such as 2021, temperatures were higher and stratification was better defined and lasted more days (Fig 3.24).

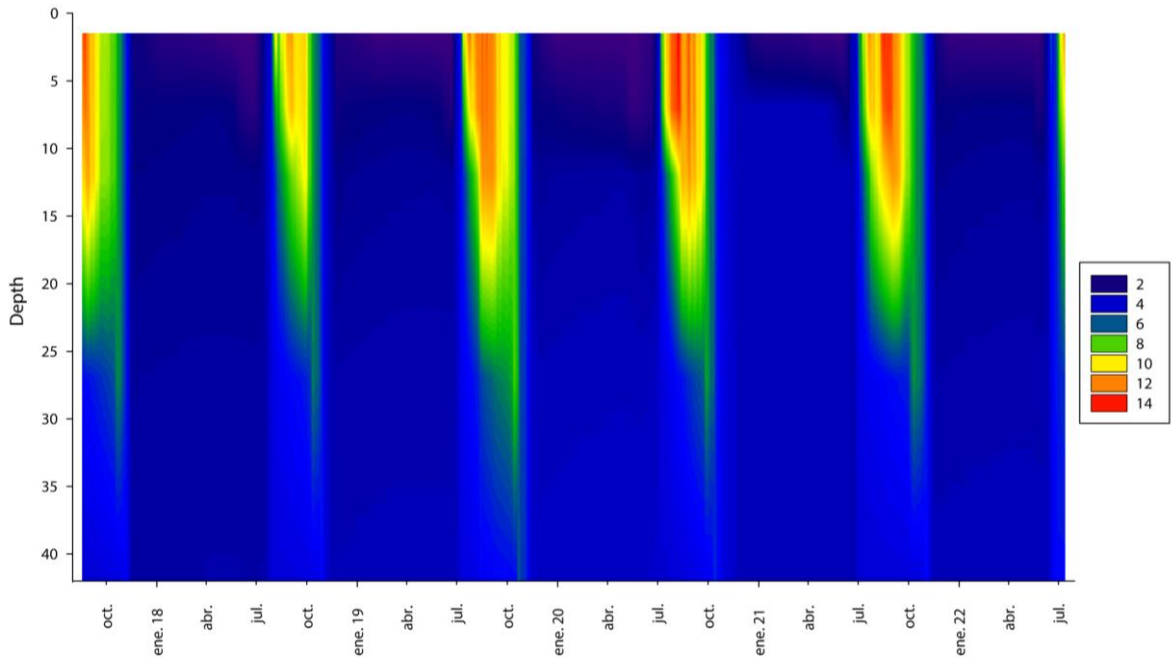

Fig 3.24. Thermal regime and water temperature changes at depth in Cregueña, based on hourly data collected with the thermistors installed in the lake at 1.5, 7, 12, 27 and 42 m deep. The graph legend is displayed in ºC.

During the survey period significant changes have occurred related to the duration of the different phases of the annual cycle of this lake. Most of the year, the lake is in reverse stratification (ice-covered winter), but the length of period has ranged from 193 to 236 days. Summer stratification varies between 88 and 121 days. The shortest periods were those of mixing, especially in spring/early summer. Autumn mixing spanned between 15 and 56 days, while spring mixing lasted only between 7 and 18 days (Fig. 3.25).

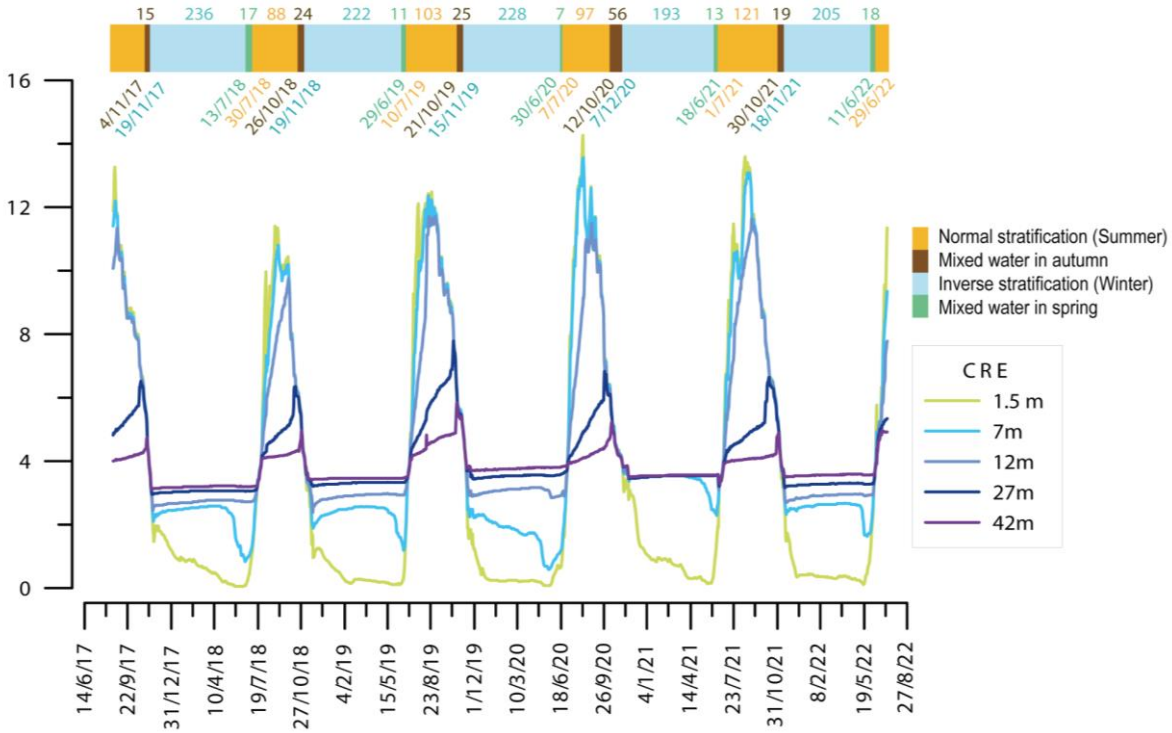

***Fig. 3.25**. Evolution of temperature and water mixing and stratification periods in Cregueña based on thermometers located at several depths*

3.5.1.2. Marboré

In the data series since 2018 (Fig 3.26 and 3.27) there were some winters (2019 and 2021) with homogeneous temperatures of around 3.5 ºC along the water column. In contrast, during the winters of 2018, 2020 and 2022 there was a positive temperature gradient at depth. Differences can also be seen between summer periods with normal stratification; summers such as 2019 and 2021 were warmer and higher temperatures were reached in deeper waters. The summer of 2022 was especially warm, maintaining higher temperatures throughout the water column and for a longer period. Also the duration of mixing periods were variable as can be seen in Figure 3.27.

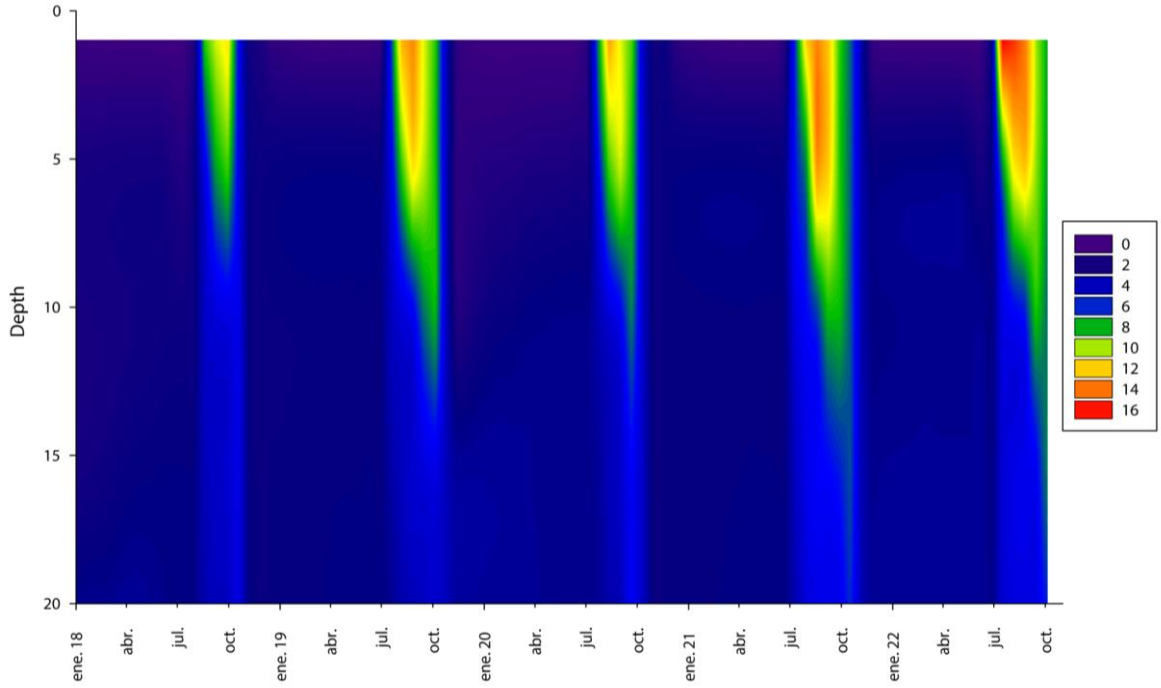

Fig 3.26. *Thermal regime and water temperature changes at depth in Marboré, based on hourly data collected with the thermistors installed in the lake at 1, 5, 10, 15 and 20 m deep. The graph legend is displayed in ºC.*

The thermal regime and mixing dynamics of the ibón de Marboré show slight changes since 2018 associated with higher summer temperatures in some years and the reduction of the ice cover period. The normal stratification period during summer varied between 57 and 101 days, the subsequent mixing period in autumn ranged between 21 and 68 days. Spring mixing periods were much faster, between 6 and 13 days, and the reverse stratification in winter, with ice cover, lasted between 208 and 267 days (Fig 3.27). Temperature records obtained by (Sánchez España et al., 2018), from 2013-2015 in Marbore Lake, also showed variations in the maximum temperature at the lake surface in the summer, ranging from 9-10 ºC (2013) to 17-18 ºC (2014-2015). The beginning of ice melting was recorded in July, similarly to other remote mountain lakes in Europe (e.g., (Catalan et al., 2002)).

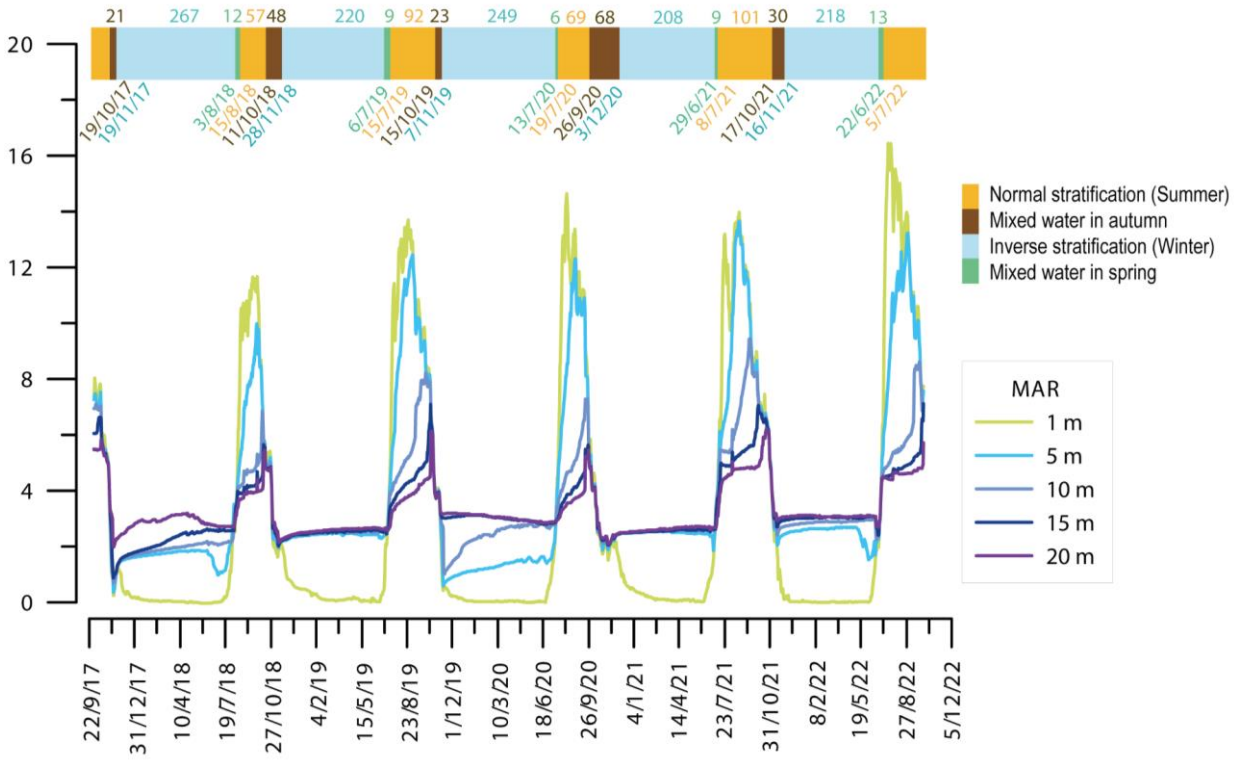

Fig. 3.27. *Evolution of temperature and water mixing and stratification periods in Marboré based on thermometers located at several depths*

3.5.1.3. La Sierra

La Sierra Lake has a thermal regime very different from the rest of the studied lakes due to its shallower nature (6 m max depth) that favors mixing, reducing the contrast between its surface and bottom waters. Despite the loss of data between the summer 2018 and the summer 2020, the time series showed mixing periods longer than in the other lakes, especially the autumn one, and periods of summer stratification (with little temperature gradient) interrupted by short periods of mixing.

The reverse stratification in winter is shorter than in the other lakes, between 106 and 149 days, and the autumn mixing phase is much longer, between 94 and 109 days (Fig 3.28 and 3.29).

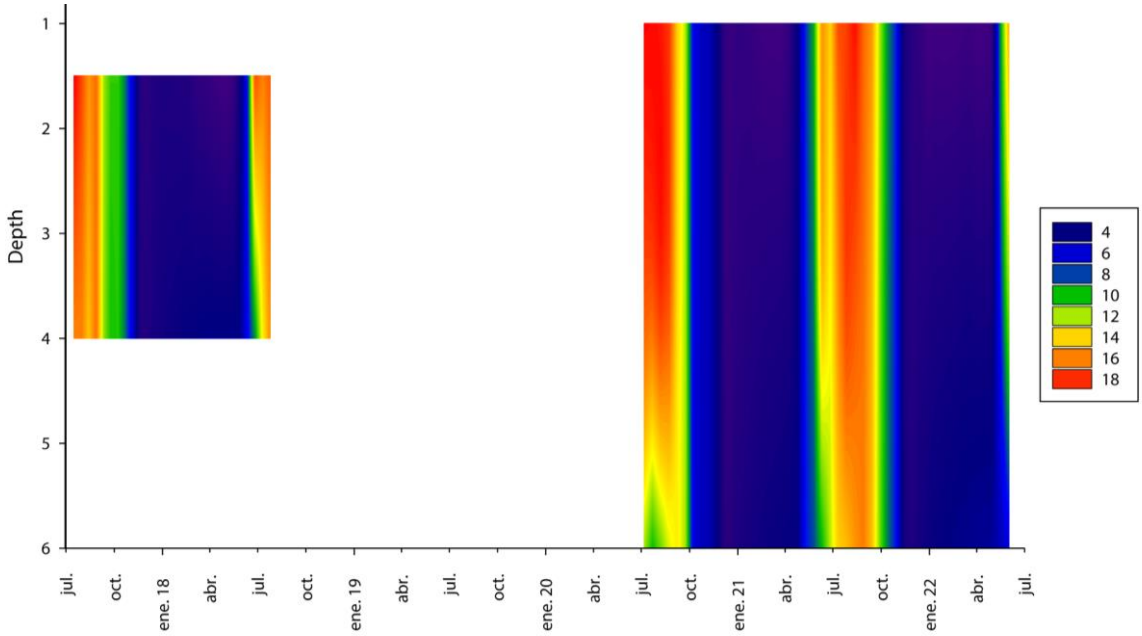

***Fig 3.28**. Thermal regime and water temperature changes at depth in La Sierra, based on hourly data collected with the thermistors installed in the lake at 1, 4 and 6 m deep. The graph legend is displayed in ºC.*

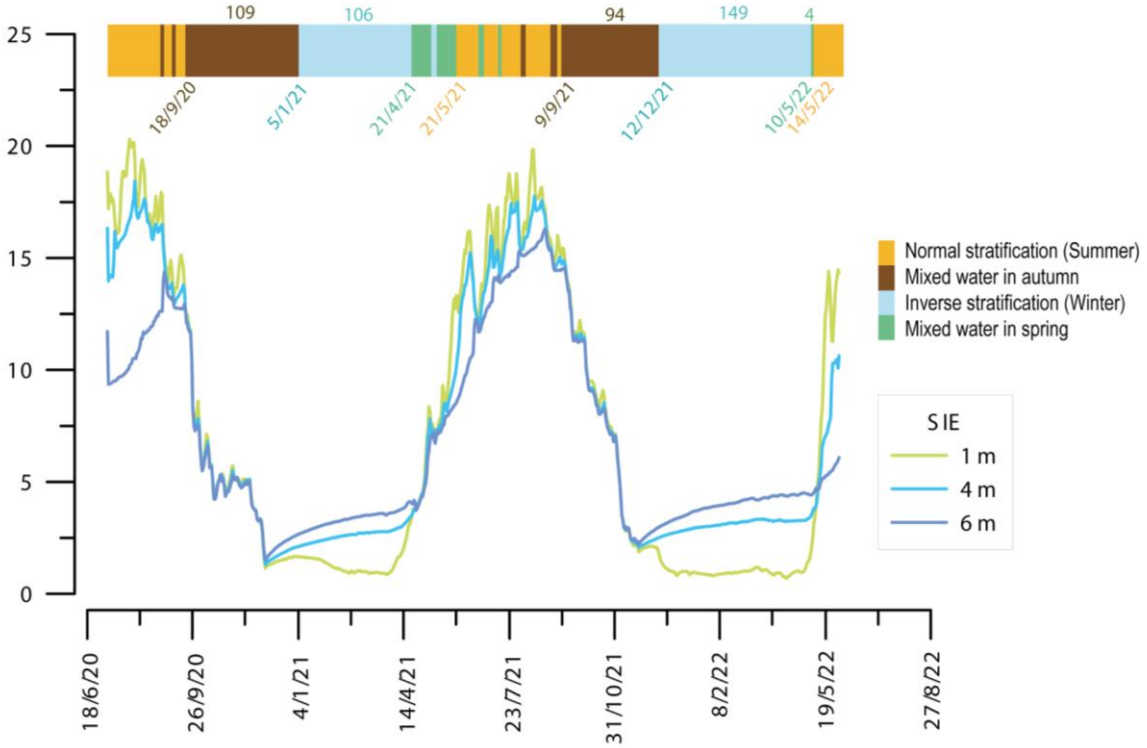

***Fig. 3.29.** Evolution of temperature, water mixing and stratification periods in La Sierra based on thermometers located at several depths*

3.5.1.4. Sabocos

The data collected between 2017 and 2021 (Fig 3.30 and 3.31) showed winter periods with a less marked reverse stratification compared with lakes such as Marboré or Cregueña. In the winter of 2018 the stratification was weak, with little difference in temperature between the shallow and deep waters. During the other winters (2019 and 2021), the stratification was not well defined, and rather there was a winter period with homogeneous low temperature water mixing.

Regarding the summers, 2018 was somewhat less warm than 2020 and 2021, reflected in higher temperatures reaching shallower depths and during less time.

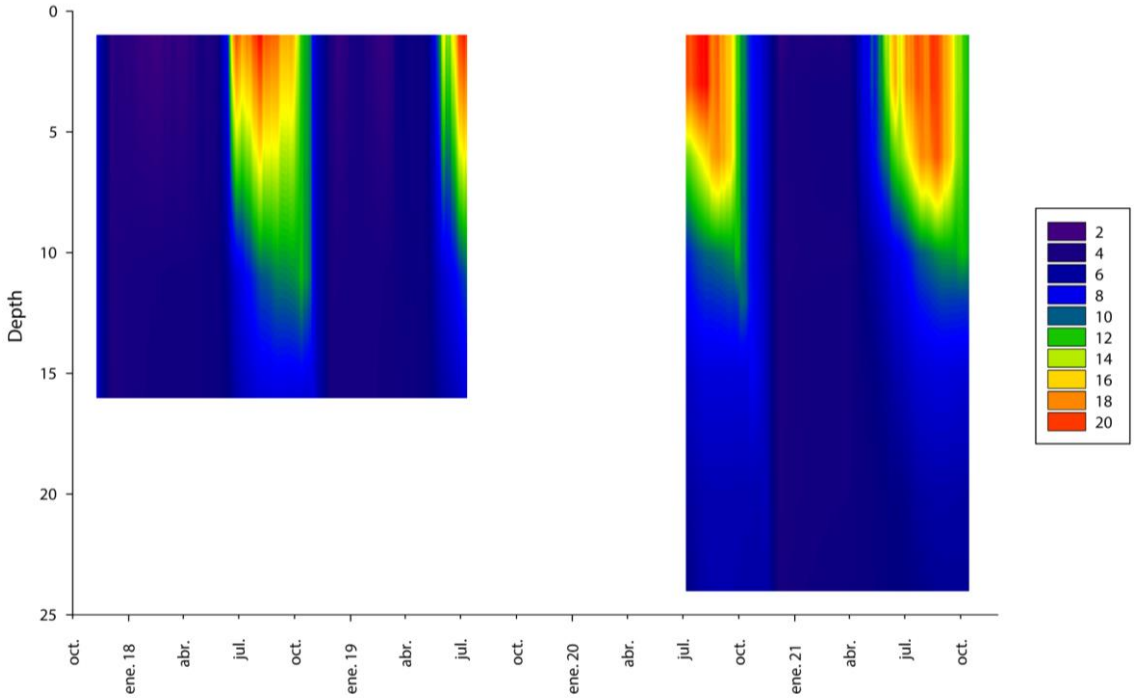

Fig 3.30. *Thermal regime and water temperature changes at depth in Sabocos, based on hourly data collected with the thermistors installed in the lake at 1, 3, 6, 10, 12, 15, 20 and 24 m deep. The graph legend is displayed in ºC.*

The duration of these periods has greatly varied during the last years. In 2018 the winter reverse stratification lasted 115 days followed by a mixing period of 42 days. The following year, 2019, the stratification was not well defined and lasted fewer days, (98) but the mixing period that followed was longer (62 days). And finally, during the winter of 2021 there was not a well-defined stratification, but it lasted longer (119 days), although the mixing period that followed was much shorter (10 days) (Fig 3.31).

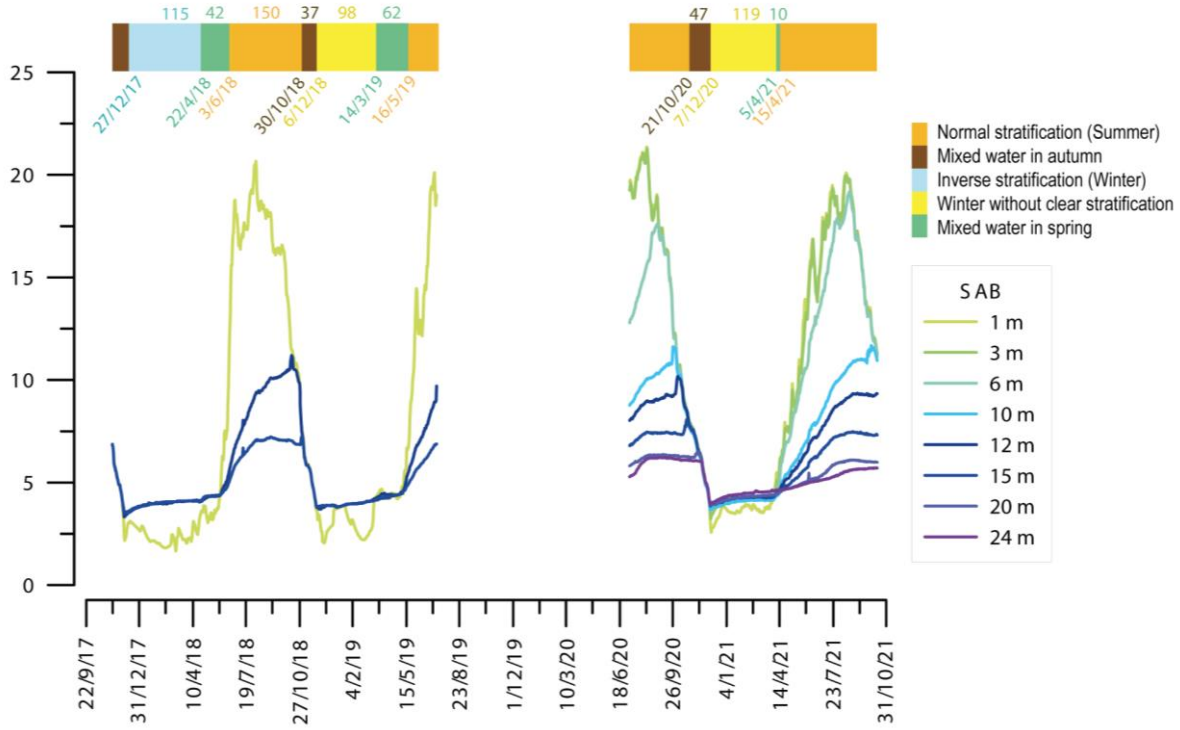

Fig. 3.31. *Evolution of temperature, water mixing and stratification periods in Sabocos based on thermometers located at several depths.*

3.5.1.5. Acherito

The Acherito data show that this is the warmest of the studied lakes. This is illustrated by the fact that there were more days per year of normal stratification and that the highest temperatures reached deeper waters in summer (Fig 3.32). There were certain differences between the winters, as 2019 and 2020 did not have a clear stratification, and the entire volume of water had lower and homogeneous temperatures, while the winters of 2021 and 2022 were slightly stratified. Due to malfunctioning of the upper thermometers there are not complete temperature profiles for 2018 and 2019. The summer of 2021 was the warmest of the series. The unstratified winter period of 2020 had a slightly shorter duration (123 days), and it was followed by a slightly longer spring mixing period (23 days), while the stratified winters of 2021 and 2022 were longer (138 and 163 days) with a shorter mixing period (2-13 days) (Fig 3.33).

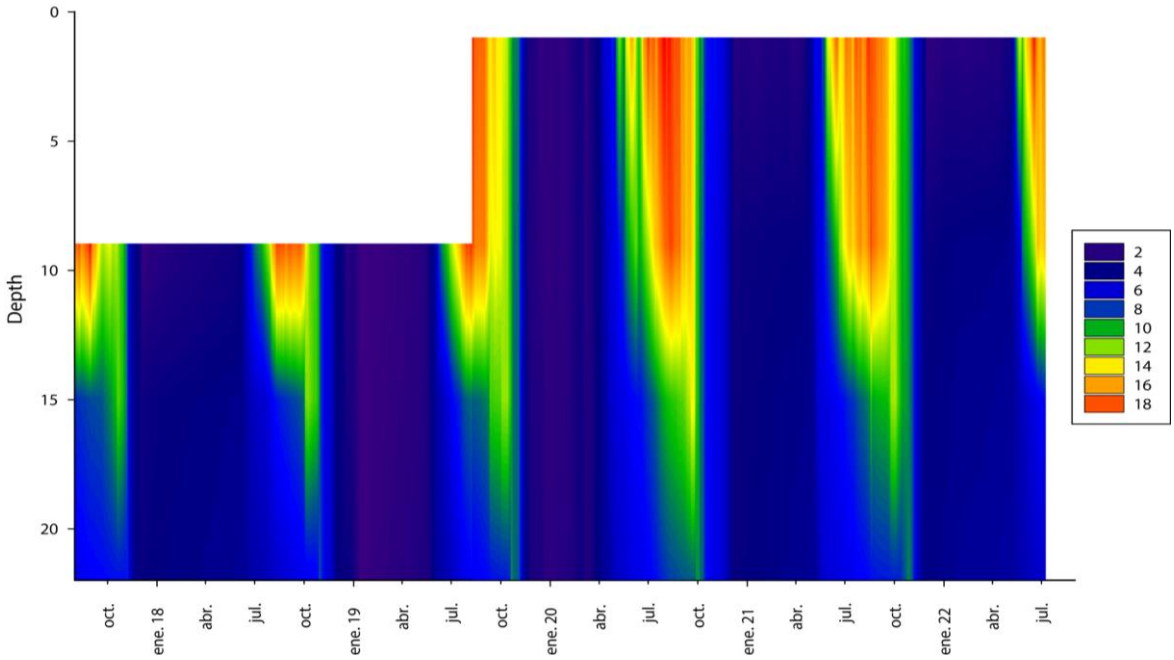

Fig 3.32. *Thermal regime and water temperature changes at depth in Acherito, based on hourly data collected with the thermistors installed in the lake at 1, 9, 15 and 22 m deep. The graph legend is displayed in ºC.*

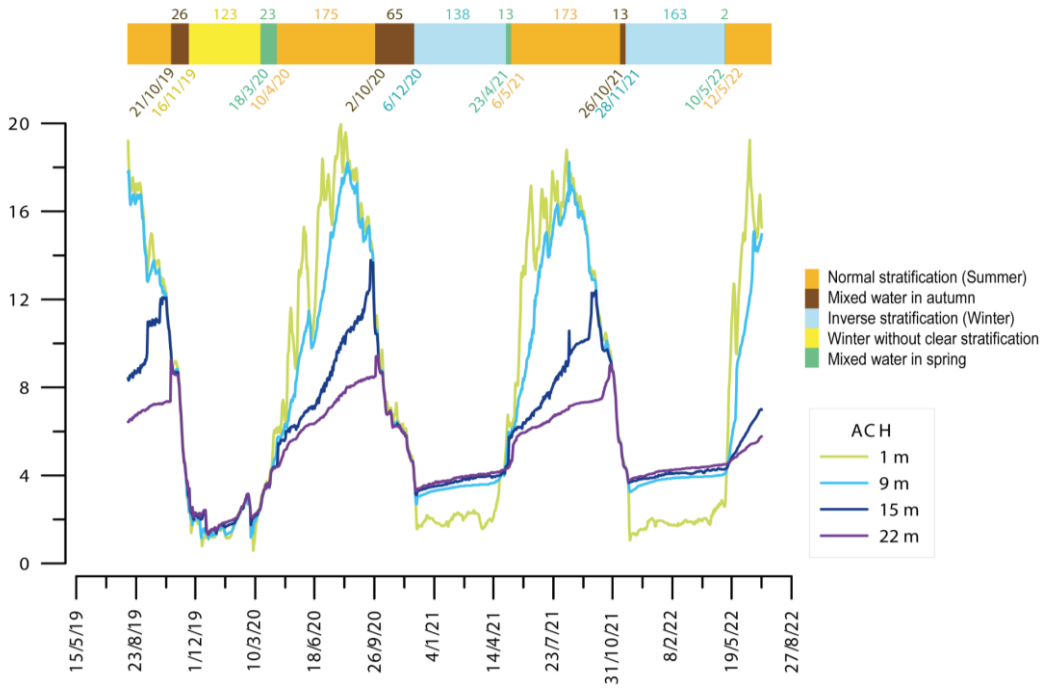

Fig. 3.33. *Evolution of temperature, water mixing and stratification periods in Acherito based on thermometers located at several depths.*

3.5.2 Changes in Thermal Regimes

Climate warming and therefore change in the water temperature of the lakes has been one of the most important issues regarding the recent dynamics of lakes (Beniston, 2003, 2005; Diaz & Bradley, 1997; Hock et al., 2019; Moser et al., 2019; Sabás et al., 2021). As the rate of warming is amplified with elevation, it is also expected that high-mountain lakes will experience more rapid changes than those located in lower altitude environments (Pepin et al., 2015; Rangwala & Miller, 2012). As temperature is a key environmental variable in lakes controlling biogeochemical processes (Sabás et al., 2021), the knowledge of how lake temperatures are changing is critical in the current global warming scenario in order to take the appropriate decisions by policymakers.

Redon Lake is the lake with the longest monitoring record in the Pyrenees (Aranda et al., 2016; Catalan et al., 2002). The records show a clear trend of increasing temperatures during the last century (Fig 3.34), especially higher during the last decades. During the summer and autumn, temperature increases have favored the proliferation of short-lived planktonic diatom species, such as *Fragilaria nanana* and *Cyclotella pseudostelligera*, as well as chrysophyte algae that form cysts in spring. The length of the ice-covered period has a direct influence on the composition of planktonic crustacean communities (Catalan et al., 2009).

Available data from the REPLIM network (REPLIM reports, 2021) show a clear increase in surface water temperature lakes, especially during summer and autumn. It is believed that these changes may have contributed to the observed changes in diatom communities and water chemistry by increasing alkalinity and nutrient concentrations (OPCC, 2019).

The surveys and lake time series in this thesis are not long enough to evaluate long-term climate impacts on lake dynamics, but they provide some information on how lakes are changing in recent years. In high altitude lakes, the impacts due to climate change are most likely mainly related to changes in temperature regimes (Catalan et al., 2002; OPCC, 2019).

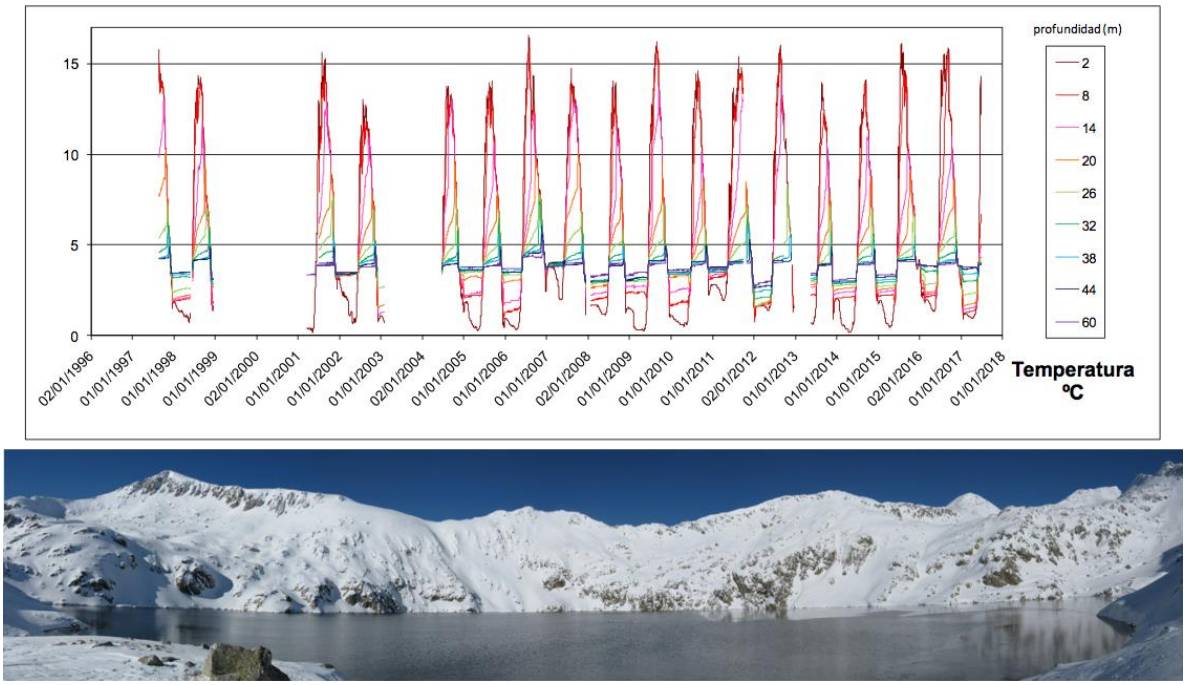

Fig 3.34. *Thermal regimen evolution of Redón since 1996 (Catalan et al., 2002; OPCC, 2019)*

Various studies throughout the Pyrenees indicate a clear increase in air temperatures in all seasons (El Kenawy et al., 2011; Esteban et al., 2012; López-Moreno et al., 2011; Maris et al., 2009; Spagnoli et al., 2002). In the central Spanish Pyrenees, Pérez-Zanón et al., (2017) defined regional anomalies of up to 0.57ºC / decade for maximum temperatures and 0.23 ºC / decade for minimum temperatures considering the period 1970-2013. These values are partly coincident with those observed on the French slope (Deaux et al., 2014).

The increase in temperature, the shorter duration of the ice-covered period in lakes and the decrease in snow accumulation in watersheds (Esteban et al., 2005; López-Moreno et al., 2009, 2011) may introduce drastic changes in the seasonal thermal regime of some lakes. The increases in both, annual and seasonal air temperatures translates directly into lake water temperature increases (D. M. Livingstone et al., 1999), although there are other variables involved such as radiation, wind speed, cloudiness and geographic/topographic features of the watersheds and the lakes (O'Reilly et al., 2015). Considering the temperatures along the water column, other factors are also significant as water transparency, water chemistry, bathymetry and lake basin morphology controlling mixing dynamics (Sabás et al., 2021).

Although the data series for the studied lakes are short (2017-2022) (Fig 3.35), they allow a preliminary evaluation on an annual basis of how climate variability has affected lake temperatures in each lake and along the lake transect.

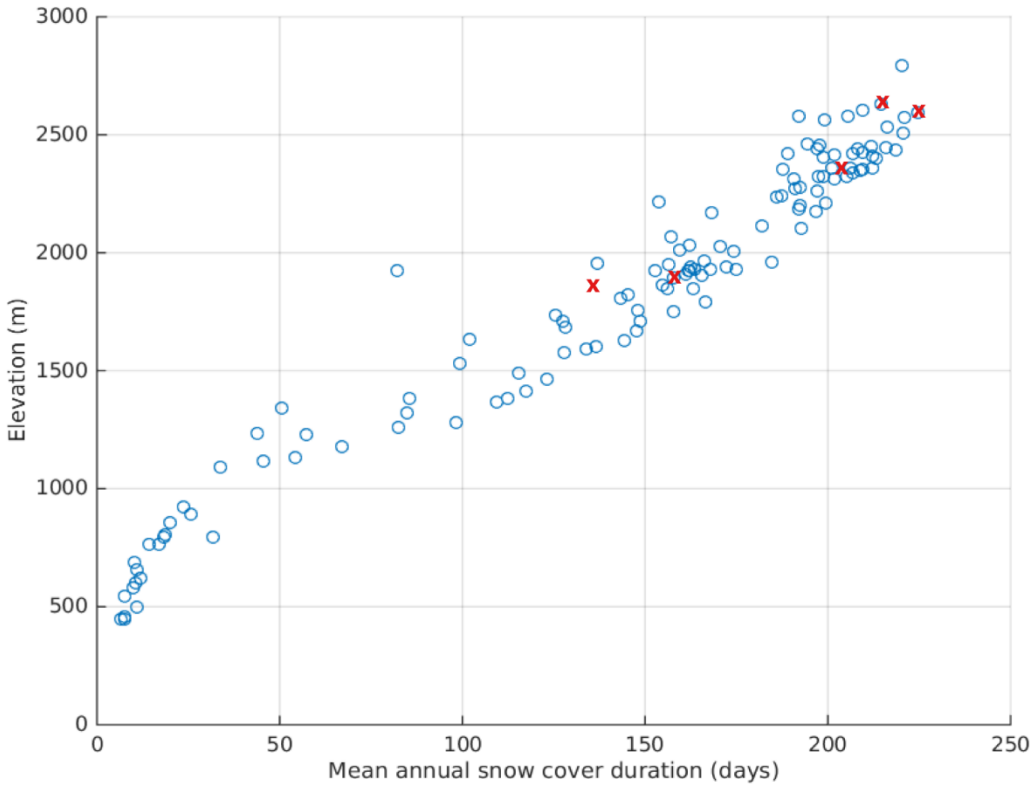

Fig. 3.35. *Mean annual snow cover vs. elevation at the location in Pyrenean Lakes (https://labo.obs-mip.fr/multitemp/snow-cover-duration-at-lakes-in-the-pyrenees/). From lowest to highest altitude: ACH, SAB, URD, MAR and CRE are located on the graph with red "x".*

Fig 3.36 compares lake surface water temperature data (thermistor at 1m depth) and days of snow cover data obtained by satellite images analyses (*https://labo.obs-mip.fr/multitemp/snow-cover-duration-at-lakes-in-the-pyrenees/* , (Gascoin et al., 2015)). The dotted lines show the mean annual temperature of each lake, and the solid line shows the maximum annual temperature. The top of the graph also shows the number of days when the lake is not completely covered with snow on a continuous basis (*https://labo.obs-mip.fr/multitemp/snow-cover-duration-at-lakes-in-the-pyrenees/*).

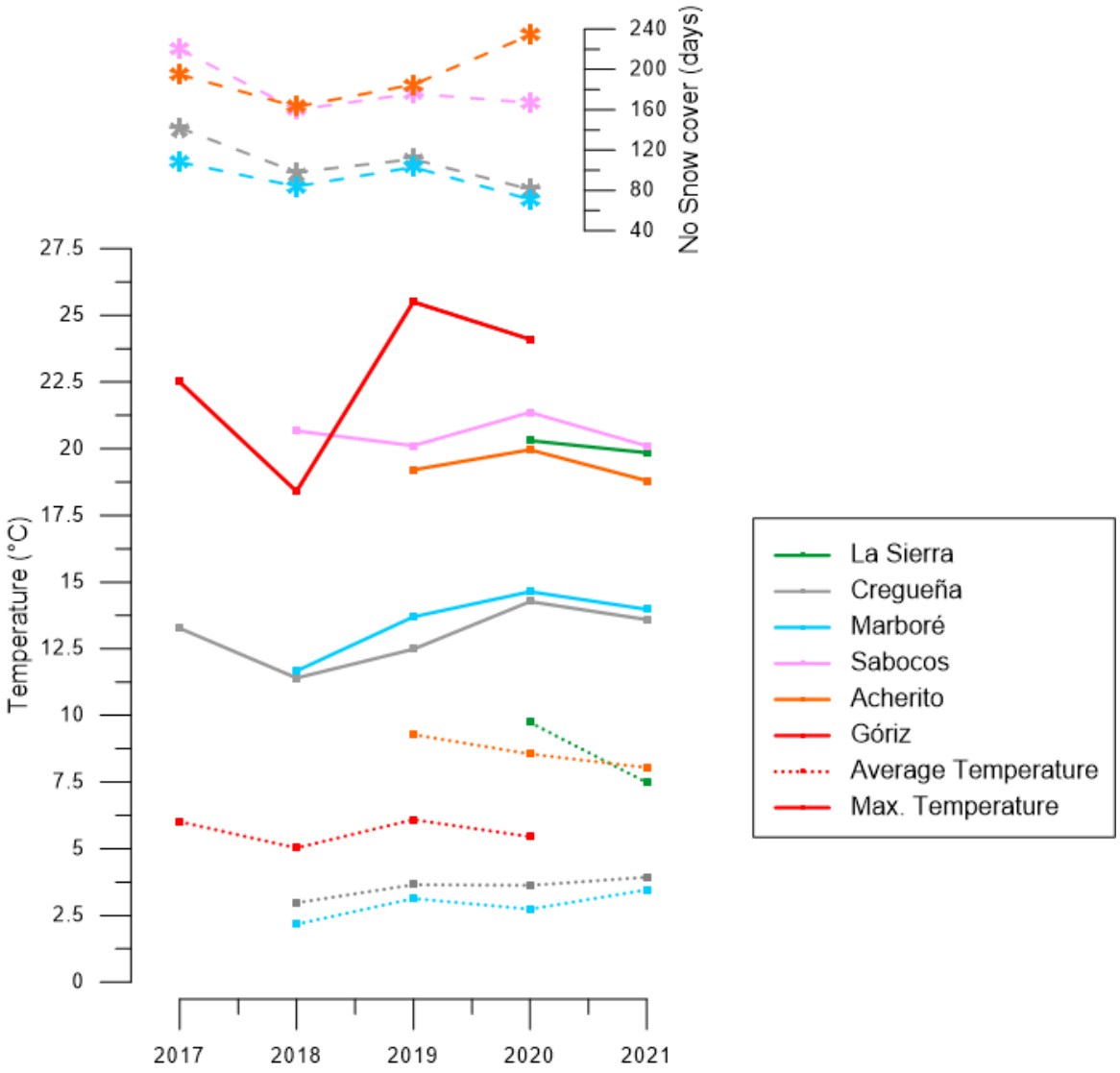

Fig 3.36. *Annual mean (dotted) and maximum (solid) temperature (ºC) obtained from the surface thermistor of each lake, and days without snow cover continuously in the lakes from 2017 to 2021. Data from the Goriz weather station, close to Marboré Lake are also included.*

The days without snow cover every year have been calculated based on data from Gascoin et al., (2015). This dataset contains the results of a gap-filling algorithm applied to MODIS snow products for the Pyrenees for 15 hydrological years. To calculate the number of days without snow we have taken the longest period of days in the year without snow, even though during the snow - free period there were interspersed days with snow. For comparison with a meteorological record, data from the Góriz weather station has also been used (located near Marboré, at 2200m altitude).

Some series do not have the annual mean temperature values because the record of the year was not complete due to sensor malfunctioning, but the maximum temperature record was complete because the missing data belonged to winter or spring.

According to the Góriz record (2200 m asl), the year with the lowest average and maximum temperature was 2018 (5 and 18.4 ºC respectively), and that was reflected in the surface water temperatures of Cregüeña (2633 m asl) and Marboré (2600 m asl), as the average (2.9 and 2.1ºC) and maximum (11.4 and 11.6 ºC) temperatures were also the lowest on our time series. In Sabocos located at a lower altitude (1900 m asl), the 2018 surface waters were not the coldest on record.

If we compare the warmest temperatures for Góriz (2019, 25.5 ºC maximum temperature and 6.1 ºC average), that was also the year (within the same period 2017-2020) with the highest average surface water temperature for Cregueña, Marboré and Acherito (3.7, 3.1 and 9.3 ºC), although their maximum temperatures were higher in 2020. 2021 was a warm year for the higher altitude lakes, as both Cregueña and Marboré reached their maximum mean temperatures (3.9 and 3.5 ºC). However, the lower altitude lakes, Acherito and Sabocos did not show the highest values. The maximum temperatures of all the lakes occurred in 2020. The pattern of days without snow cover on the lakes per year also reflects the surface temperature: the years with higher surface water temperatures coincide with years with shorter snow-covered periods.

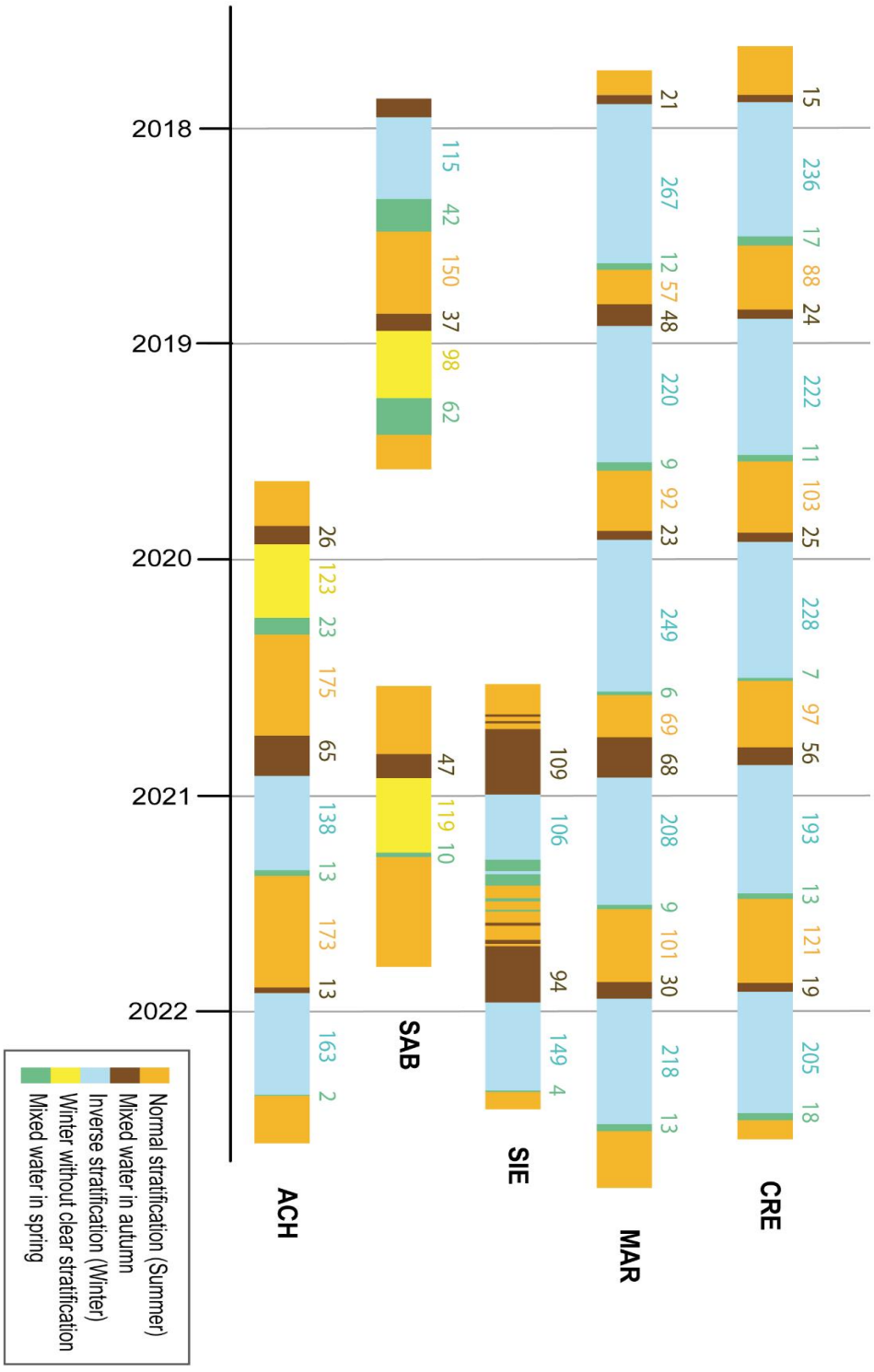

Fig 3.37. *Number of days of mixing and water stratification periods from winter 2017 to summer 2022 in all lakes*

This variability in terms of their maximum and average surface temperatures (strongly influenced by their altitude and air temperature) is also reflected in the length of their periods of mixing and stratification of their waters.

Fig. 3.37 y 3.38 shows the number of days of the different stratification and water mixing periods for each lake based on the temperature profiles

- **Normal stratification** is defined as the time when the lake has three thermally distinct zones: i) an upper (epilimnion) mixed and with higher temperatures, ii) a denser and colder zone at the bottom of the water column (hypolimnion) and iii) an intermediate layer with a strong temperature gradient (metalimnion). The period when the lakes were normally stratified has been defined, as the period when there was more than 1ºC difference between the shallowest and deepest thermometer during the summer months. During these months the difference between these thermistors ranges between 1 and 13 degrees.

- **Inverse stratification** is defined as the period when the lake had a positive temperature gradient towards the bottom. This happened when the lakes are ice-covered and there was more than 1ºC difference between the shallowest and deepest thermistor. This process occurs in winter, and the temperature difference in these lakes during inverse stratification was between 1 and 3°C.

- **Mixing periods** occurred during the transitions between normal and inverse stratification. During these periods, the shallow and deepest thermometers have less than 1ºC temperature difference.

As expected, the highest altitude lakes, Cregueña and Marboré, had the longest inverse stratification periods, between 193 and 267 days, and the shortest normal stratification, between 57 and 121 days. Whereas in the lakes located at lower altitudes, Sabocos and Acherito, winter stratification length varied and the temperature difference between surface and deep waters reached up to 3.4 degrees positive gradient from the surface waters to the deeper waters. However, in some years, a cold homogeneous water column occurred during the winter, with little difference between the surface waters and the bottom waters. In these lakes located at lower elevation, the normal summer stratification was longer, between 150 and 175 days.

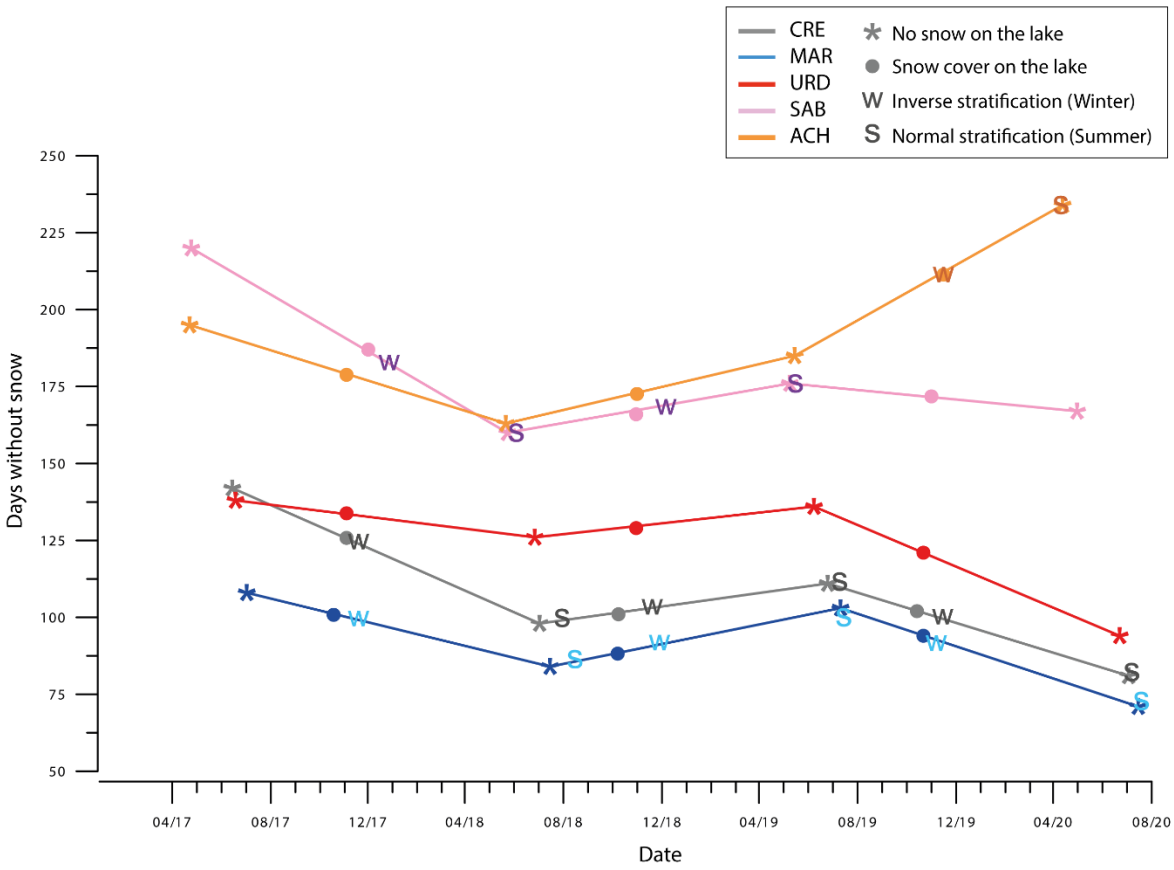

Fig 3.38. *Comparison of dates of snow cover and lake water stratification changes. Dates for snow –free lake (ice-off) and snow-covered lake based on Gascoin et al, (2015). Dates of winter and summer stratification onset based on thermistor dat. Data are plotted on a line connecting the number of snow-free days for each year at each lake.*

There was not much difference in the mixing periods (spring and autumn) between the lakes. Both higher and lower altitude lakes tend to have shorter spring mixing periods (between 2 and 62 days) than autumn mixing periods (between 15 and 68 days). The length of these periods is the same at all altitudes, for example, when a mixing period is longer in one year (as in autumn 2020) or shorter (spring 2021), all lakes have similar patterns of mixing periods.

The timing of the stratification also varies depending on altitude. Winter stratification began slightly earlier in the lakes located at higher altitudes, but only with a few days or weeks of difference. The onset of summer stratification occurred much earlier in lakes at lower altitudes than at higher altitudes. In the lower lakes it happened between April and June, while in the higher lakes, between July and August.

La Sierra had a different thermal regime from the rest because its lower depth. The described patterns on the functioning of the thermal regime of the lakes as a function

of their altitude more evident in the other lakes, did not apply to shallow lakes. In La Sierra, the mixing periods were longer than in the other lakes, especially the autumn one (94 to 109 days), and the normal summer stratification (with little temperature gradient) was repeatedly interrupted by short mixing periods.

The results obtained from the intense monitoring carried out during this thesis in selected lakes fit with the conclusions of the review of 59 lakes (Sabás et al., 2021) considering that altitude is the factor that most explains the variability of the temperature of the surface waters of the Pyrenean lakes. At a global scale, lake surface water temperature decreases linearly with altitude (D. M. Livingstone et al., 1999; O'Reilly et al., 2015; Sabás et al., 2021). Lower altitude lakes such as Sabocos and Acherito show a greater response to increasing spring air temperature, which favors a earlier snowmelt timing at lower than at higher altitudes. High altitude lakes such as Cregüeña and Marboré are less affected from earlier spring air temperature, as the ice cover stays for longer and it has an insulating effect (Šporka et al., 2006).

The water surface temperature is also strongly affected by the ratio of lake area to depth, the shallower the mixing depth (as in the case of La Sierra) the lower the thermal inertia and thus the larger the temperature range (Catalan et al., 2009; Gorham & Boyce, 1989; Woolway et al., 2015).

Morphological variables related to catchment characteristics, the ratio of total catchment to lake area (Sabás et al., 2021), topography and how it affects solar radiation (D. M. Livingstone et al., 1999; O'Reilly et al., 2015) or air variability (Catalan et al., 2002), are some of the characteristics that can affect the surface and whole water column temperature of lakes. Other geographic and climatic factors have to be considered too. For example, the total catchment to lake ratio also has an impact on the timing and the amount of cold snowmelt water reaching the lake and preventing a warming up of the epilimnion. The forecasted decrease in precipitation in some areas in the Pyrenees, the changes in the seasonal amounts and the changes from snow to rain precipitation may also lead to lower water renewal times, favoring higher temperatures in the lakes.

Our time series are too short to capture trends in interannual variability as those identified Lake Redo (Catalan et al., 2002). Summer temperatures are significant for mean water temperature, but actually, in the survey of Pyrenean lakes by Sabás et al., (2021), changes in spring temperatures explained more variability of the temperature records than summer temperatures. This is likely a consequence of the stronger effect

of late spring temperatures in thawing and ice-off and the beginning of the warming of surface waters. Other factors are cloudiness, precipitation, wind are also determinants in the interannual variability.

Looking ahead, some models and observations (Schneider & Hook, 2010) predict water surface temperature (epilimnion) increases of more than 10°C during the 21st century. These scenarios of limnological change in hydrology, ice cover and water temperature exceed the range of change over the last 11,700 years (Holocene period). Deeper lakes with higher thermal inertia (they take longer to warm and cool) as Cregüeña are expected to respond more slowly to new physical (temperature and density gradients), chemical (alkalinity, salinity, pH, nutrients) and biological (primary productivity, community composition) conditions. Lakes at lower altitudes would show a greater response to spring temperature increase and likely advances in the ice-off dates. In contrast, the expected increase in maximum annual temperatures in midsummer will have a higher impact in higher altitude lakes, as a consequence of the greater increase in air temperatures in altitude ("elevation-dependent warming", (Pepin et al., 2015)). In addition, the anoxic level of mountain lakes at mid altitudes may evolve in the future as a consequence of more acute and longer periods of stratification induced by global change (Sánchez España et al., 2018). As documented in other mountain areas (Sabás et al., 2021), these temperature increases and changes in the thermal regimes will likely drive changes in biological communities in Pyrenean lakes.

Longer time series from extended monitoring programs are needed to have identified trends and disentangle the drivers affecting thermal dynamics and ecological status of these lakes.

4. Sedimentary facies and depositional models

Photograph of core MAR11-1A-1U, taken with a high-resolution CCD camera attached to the XRF equipment.

4. Sedimentary Facies and Depositional Models

4.1 Introduction

Sedimentation in high mountain lakes is controlled by both watershed and lake processes. The sediment mineral matter can come from any part of the watershed - allochthonous origin - or originated and reworked within the lake -autochthonous origin. The organic matter that accumulates at the bottom of the lakes can also have the same sources: soil, vegetation and organic remains from the watershed, and originated in the lake by different organisms.

In addition to the variability of sediment sources and watershed characteristics, the sedimentation in the lakes is not homogeneous, and it is greatly controlled by the bathymetry of the lake, the physical features of the lake dynamics (currents, water circulation, river inputs…) and also the post–depositional processes. Over time, changes in the lake environment, the basin, and the climate generate a large diversity in the type and characteristics of the sediments that accumulate in the lake.

There are a number of studies dealing with sedimentation in high mountain lakes in the Iberian Peninsula (Moreno et al., 2011, 2012; B. Oliva-Urcia et al., 2018; B. Valero-Garcés et al., 2014; Vegas, 2007a; Vegas et al., 2006) and other areas in the Alps (Blass et al., 2007; Ohlendorf & Sturm, 2001) or Canada (Leonard & Reasoner, 1999) but to our knowledge, no previous studies have tried to synthesize the types of sedimentary facies and associations that can be found in high mountain lakes.

Sedimentary facies are defined as a set of sediment bodies with unique textural, compositional and structural characteristics that result from the accumulation within a particular sedimentary environment (Gressly, 1838). The objective of this chapter is to propose a methodology for the identification and definition of sedimentary facies applicable to high mountain lakes, so that they can be used for reconstructing the depositional processes in the lakes and the watersheds. As most cores were collected in the central, deeper areas of the lakes, the facies analyses presented in this chapter mostly represent deposition in distal sub environments of the lakes.

4.2 Material and methods

The high altitude Pyrenean lakes sedimentary facies have been defined through a multidisciplinary analysis including sedimentological and compositional techniques. The definition of sedimentary facies has followed three main criteria: i) grain size, ii) composition (% organic matter, silicate and carbonate) and iii) sedimentological features (such as color, sedimentary textures and structures as grading, lamination). Mineralogical (based on XRD, optics and scanning electron microscopy) and geochemical (based on XRF scanner and ICP analyses) were used to further define some of the facies.

Sediment cores were retrieved from the deepest areas of the lakes using a Uwitec short corer (see methodology chapter). The cores were curated at the IPE-CSIC cold room in Jaca and split lengthwise with a Geotek core splitter. The split cores were imaged with a GEOTEK camera and they were described based on sedimentological properties following LRC (*https://cse.umn.edu/csd/core-processing)* and IPE protocols (*http://www.ipe.csic.es/cambios-globales*). Smear slides and thin sections were used to identify components and describe sedimentary facies using an optical microscope and following Schnurrenberger et al., (2003). Samples for grain size analyses, about 1 gr weight, were taken every 1 cm and measured with a MasterSizer 2000 at the IPE-CSIC laboratories.

Total Carbon (TC), Total Inorganic Carbon (TIC) were analyzed at 1 cm resolution in the sediment cores and sediment trap samples at the IPE-CSIC (Zaragoza, Spain) using a LECO SC144 DR analyzer. For TIC analysis, organic matter was previously removed at 460 °C in a muffle furnace. The Total Organic Carbon (TOC) was calculated as the difference between TC and TIC.

X-Ray Fluorescence scanner analyses were performed at the University of Barcelona (Spain) with an AVAATECH X-Ray Fluorescence II core scanner at a resolution of 5 mm, with a counting time of 30s, and under two different working conditions, at 10 and 30 kV. Quantitative chemical analyses were performed at a lower resolution (every 1 cm, 150 mg weight sample) with an ICP-OES 720-ES (Varian) at the Experimental Station El Zaidin - CSIC (Granada, Spain). Elements measured were Al, As, Ca, Cd, Co, Cr, Cu, Fe, Hg, K, Li, Mg, Mn, Mo, Na, Ni, P, Pb, S, Se, Si, Sr, Ti, V and Zn.

The mineralogical composition of the samples was determined by X-ray diffraction (XRD) by the crystalline powder method with a X Ray diffractometer. The estimation of the relative abundance in each mineral phase was carried out using the intensity of the main peaks of each sample, following the standard process described by Chung, (1974) and applying the "method of reflective powers". Images and chemical composition by Energy dispersive analysis (EDS) of grains has been performed on selected samples by a Scanning electron microscope (SEM) Jeol 6110, of the CN IGME.

4.3 Facies criteria and classification

Grain size, composition and sedimentological characteristics have been used as primary criteria to define sedimentary facies.

Grain size.

A total number of 271 samples have been analyzed: 55 from Urdiceto, 42 from La Sierra, 63 from Sabocos, 42 from Cregueña and 69 from Acherito. The grain size ranges that have been used are the following: clay between 0.01 µm-2.0 µm, silt: 2.0 µm -63.0 µm and sand >63.0 µm. Samples have been plotted in a ternary diagram for clastic textural groups (Sand - Silt - Clay) according to the classification of Shepard (1954) (Figure 4.1). Most sediment samples are located at the bottom right of Shephard's ternary diagram and they correspond to Silty Sand, Sandy Silt, and Silt. Only some samples from Cregueña correspond to Sand and Clayey Silt.

Composition.

The main sediment components are organic matter, carbonate and silicate particles. To calculate percentages of each category we have used the TIC and TOC values, according with these equations:

%Carbonates= (100,09 * TIC) / 12,01

% OM =%TOC * 1,724

% Silicates= 100 - %Carbonates - %MO

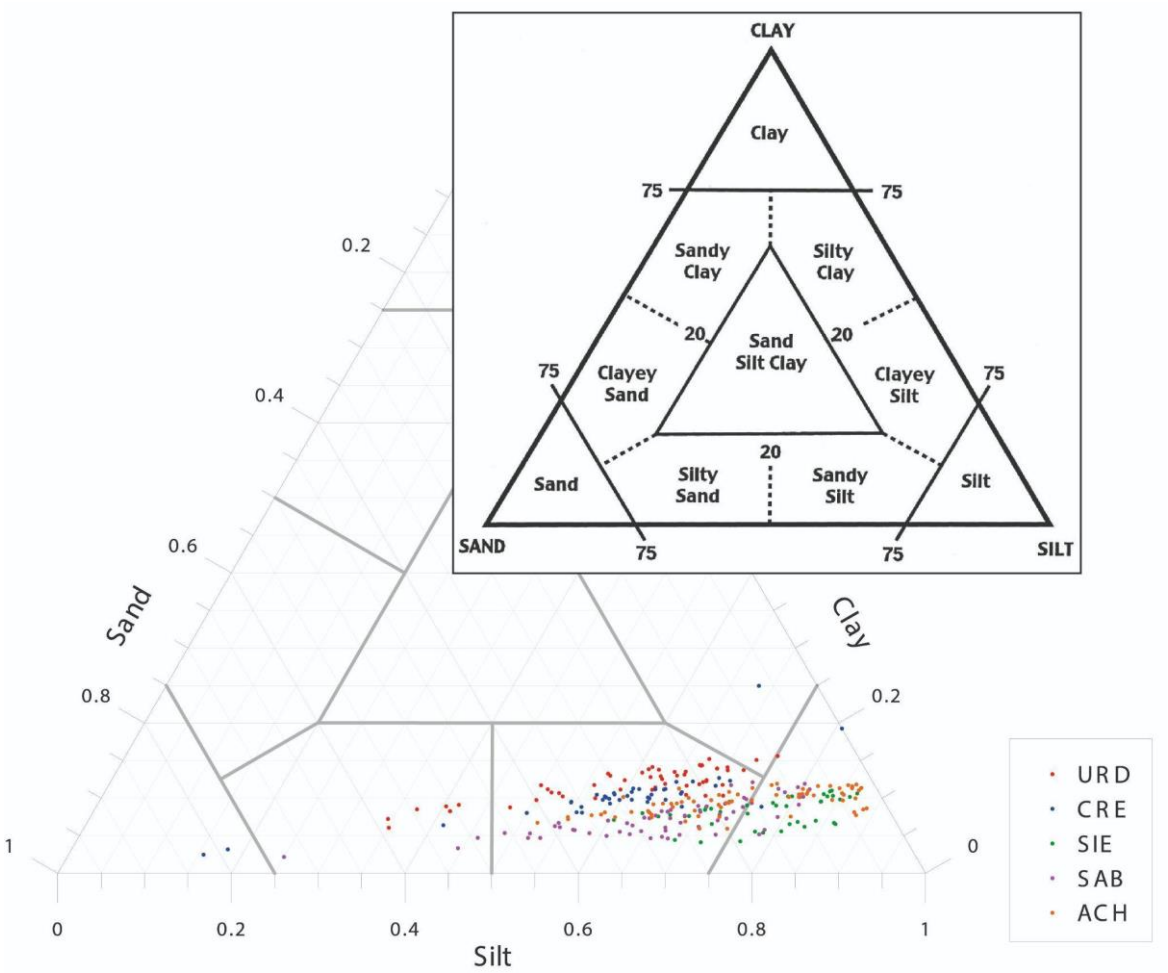

Fig.4.1. *Ternary diagram for clastic textural groups (Shephard, 1954) and location of samples for Pyrenean lakes (cores REP-ACH17-1A-1G, REP-SIR17-3A-1G, BIE-URD12-1B-1G, REP-CRE17-1A-1G, REP-SAB 18-2A-1G).*

Organic matter content in sediments of high mountain lakes is controlled by the low vegetation and edaphic cover of their basins and by their low productivity. The productivity of these lakes, in turn, depends on seasonality (ice-on season) and temperature (Catalan et al., 2002, 2009; Pla-Rabes & Catalan, 2005). Relatively high C/N ratios (7-15) suggest dominant algal sources but a variable contribution of terrestrial carbon. Increased organic carbon accumulation in lakes may respond to increased organic matter input from watersheds (higher C/N) during periods of increased erosion and/or runoff or to increased bioproductivity in the lake (lower C/N).

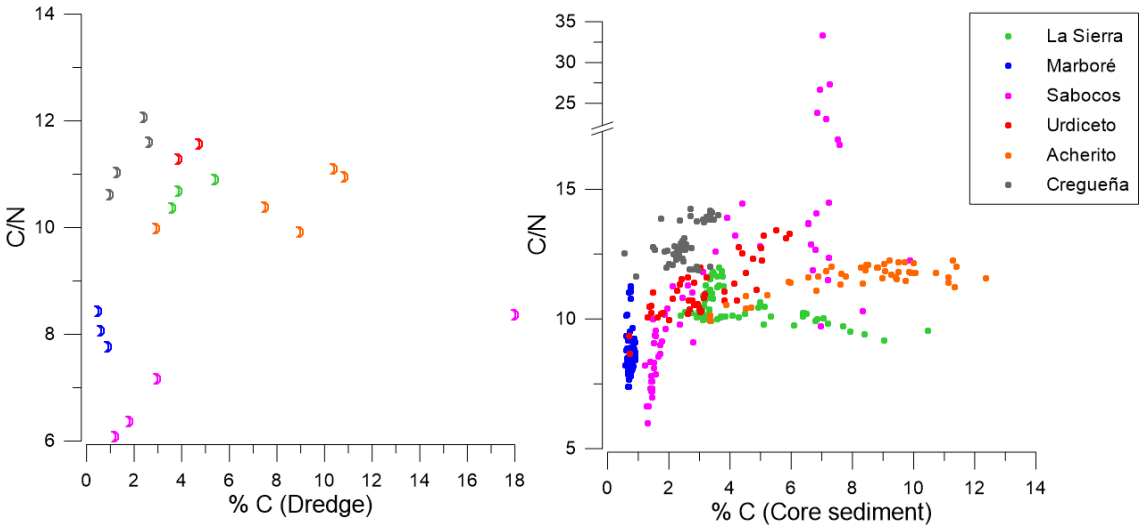

Fig. 4.2. *Scatter plot of C/N and % C values for dredge (left) and sediment cores (right) samples.*

We define **silicate facies** as those with more than 90% silicate content. They include two subgroups:

i) with 90 to 95% silicate (green color in the ternary diagram)
ii) with more than 95% (blue color).

The organic facies are those with more than 10% OM (orange color). Only a few samples reached up to 30% OM.

Carbonate-bearing facies are those with more than 2% carbonate content and we have differentiate 3 subgroups: i) with 2 to 25% carbonate content (purple color), ii) more than 25% carbonate (pink color) (up to 45%), and iii) with carbonate higher than 2.5 % but with more than 10% OM (yellow color) (Figure 4.3).

Sabocos is the only lake sequence mostly composed of carbonated facies, with carbonate content percentages between 2 and 45%. Marboré samples have the highest silicate mineral content, (> 95% silicate). Carbonate is absent in most Marboré sediments (0 to 1%), and only occurs in some thin laminae, where it can reach up to 14%. Cregueña, Urdiceto and Sierra have similar sediment composition, mostly silicate material with less than 10% of organic components. Acherito is the only lake with a significant organic component, between 10 and 30% OM.

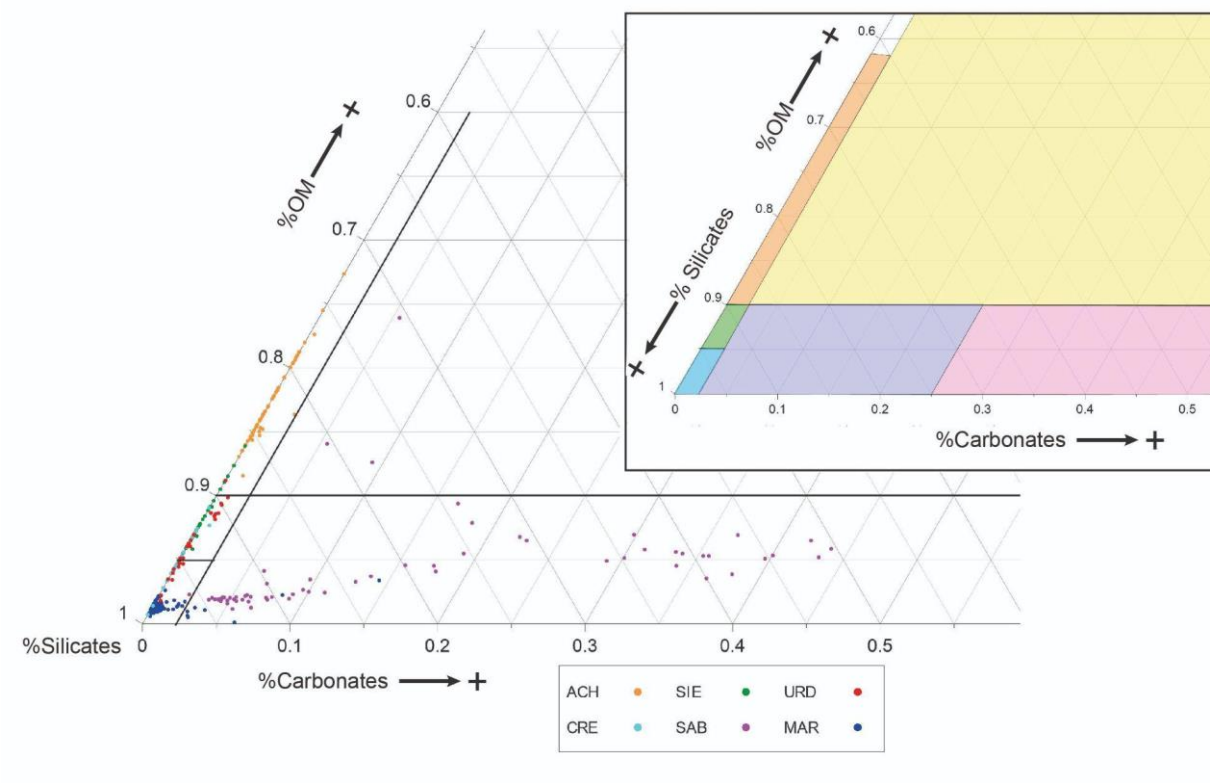

Fig.4.3. *Ternary compositional diagram including silicate, organic matter and carbonate components with Pyrenean lake samples from cores REP-ACH17-1A-1G, REP-SIR17-3A-1G, BIE-URD12-1B-1G, REP-CRE17-1A-1G, REP-SAB 18-2A-1G and MAR11-1U-1A-1).*

Sedimentological characteristics

To complete the description of the facies, other characteristics of the sediment were also taken into account, such as color (using the Munsell chart), lamination - massive, banded (> 1 cm), laminated (< 1 cm) or finely laminated (< 1 mm) - thickness of the layers, grading and presence of erosive surface.

Optical microscope observations of smear slides helped to identify and semi quantify minerals and types of organic matter and assess grain size distribution. Thin sections and scanning electron microscopy (SEM) images were also used to describe compositional and textural features of sedimentary facies.

4.4 Results

4.4.1 Sedimentary Facies

Considering the sedimentological and compositional criteria described in section 4.3, we defined a total of 13 facies in our set of Pyrenean lakes (Table 4.1). These facies occurred in cores of the central and deepest zones of the lakes, so they are all distal, profundal facies. We group them in three types: silicate, carbonate-bearing (mostly in Sabocos) and organic (mostly in Acherito). Average sedimentation rate also differentiate the three types (Figure 4.4).

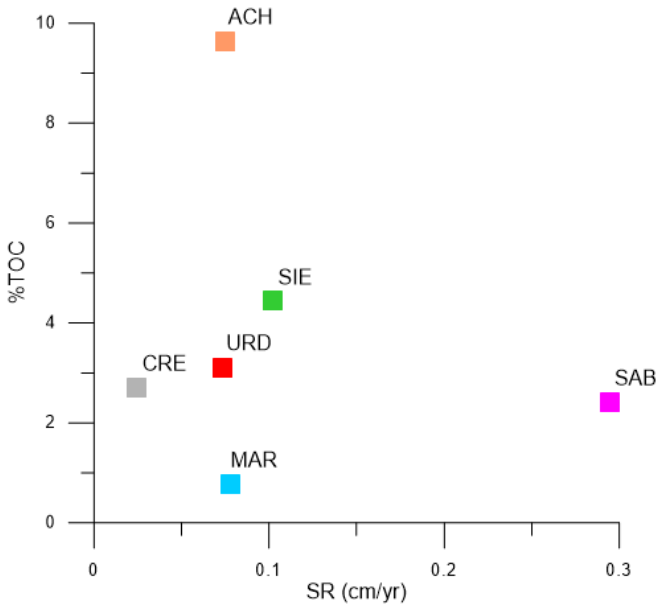

Fig. 4.4. *Average % TOC values of sediments for each lake and mean sedimentation rate (SR) for each lake sequence.*

4.4.1.1 Silicate Facies (> 90 % silicate component)

Facies.1. Brown to dark brown, slightly banded sandy silt

Description: F1 occurs as massive or slightly banded layers of 1 to several cm thick with gradational boundaries. This facies has more than 95 % of silicate component. F1 occurs in Cregueña and Urdiceto. In Cregueña, it corresponds to the sediments at the top 9 cm of the sequence. In Urdiceto, it appears throughout the sequence, in 1 to 6 cm thick layers.

Interpretation: This facies represents deposition in the deepest areas of the lake where organic productivity and accumulation is very low and clastic processes are dominant.

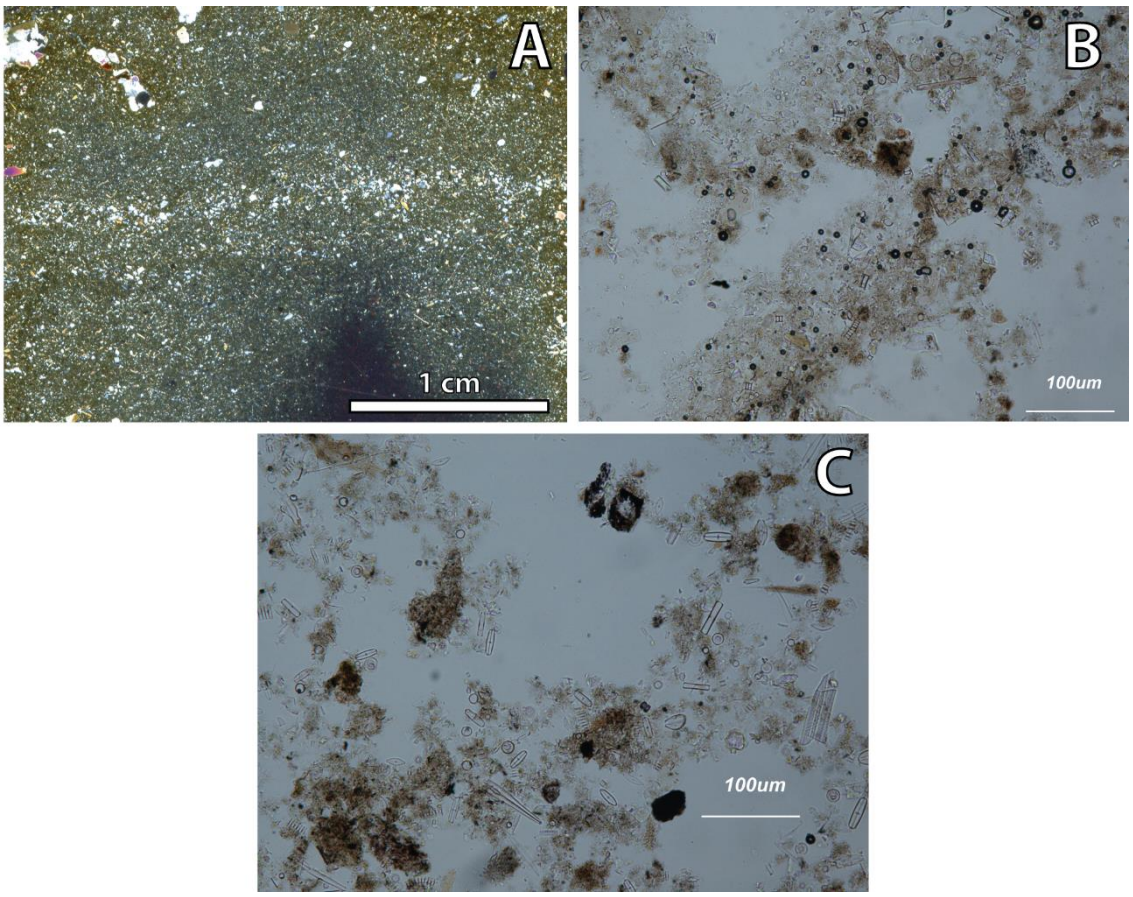

Fig. 4.5. *(A) High resolution thin section scan, Cregueña facies 1 (core CRE17-1A-1G) (crossed nicols). (B) Photograph (parallel nicols) taken of the smear slide corresponding to F1 (13 cm of CRE17-1A-1G). (C) Photograph (parallel nicols) taken of the smear slide corresponding to F1 (cm 35 of URD12-1B-1G).*

Facies 2. Grayish brown to dark brown, massive to banded sandy silt with organic matter

Description: F2 appears as massive or banded layers, one to several cm (up to 10 cm) thick, with gradational boundaries. This facies contains between 90 and 95% silicates and more organic matter than F1 (up to 10 %). Organic particles include some diatoms and small grains of unidentifiable algal material. F2 is the dominant facies in Cregueña, particularly in the lower part of the sequence. In La Sierra and Urdiceto, it appears in layers of 0.5 to 10 cm.

Interpretation. This facies reflects a similar environment as F1, dominated by deposition of watershed and littoral material transported to the distal areas of the lake

during the ice-free season after snow melting, rainfall or seasonal or torrential events. The main difference is the higher organic component originated in the lake, indicative of a higher productivity at the time of deposition.

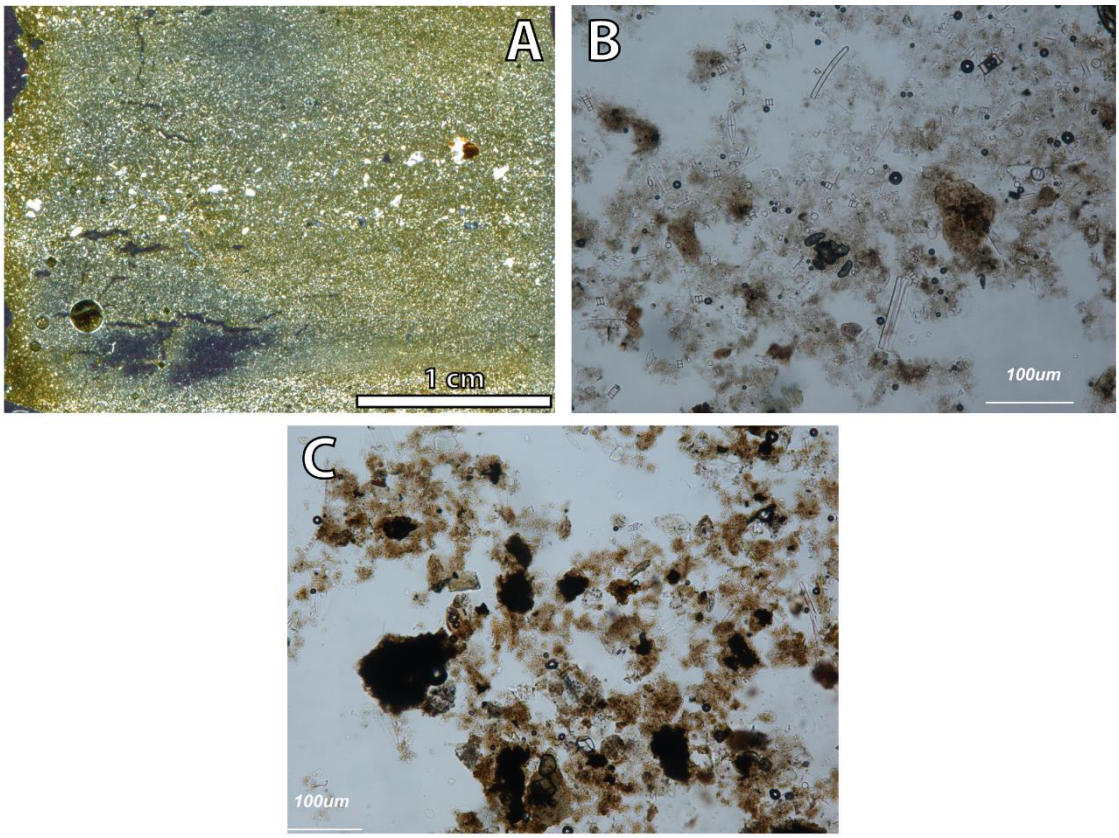

Fig. 4.6. *(A) High resolution thin section scan (crossed nicols), of Cregueña facies 2 (core CRE17-1A-1G). (B-C) Photograph in parallel nicols of F2. B) smear slide photograph (33 cm of CRE17-1A-1G). (C) Smear slide photograph (40 cm of SIE17-3A-1G).*

Facies 3. Grayish brown, banded silt

Description: F3 appears in layers 1 to 12 cm thick, slightly banded. The thickness of the banding is between 0.5 and 3 cm. Compositionally, F3 has between 90 and 95% silicates, and a relatively larger amount of OM (up to 10 %). Facies 3 only occurs in La Sierra, where it makes most of the sequence and it shows an increasing thickness layer upwards.

Interpretation: The finer and homogeneous grain size of these facies suggests deposition of clastic material at the bottom of the lake during periods not related to floods or torrential events.

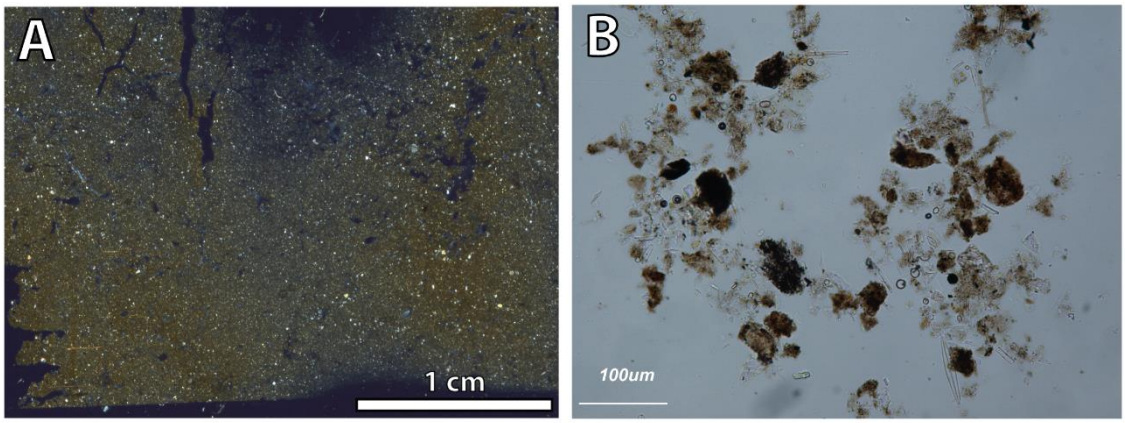

Fig. 4.7. *(A) High resolution thin section photograph in crossed nicols, of La Sierra facies 3 (core SIE17-3A-1G). (B) Photograph in parallel nicols of smear slide corresponding to F3 (9 cm of SIE17-3A-1G).*

Facies 4. Light brown massive silty sand

Description. Massive light brown silty sand, composed of 95% or more of silicates in layers of 1 to 2 cm with occasional fining upwards textures and sharp basal boundaries. It only occurs in Urdiceto.

Interpretation. The coarse nature of the sediments points to high - energy processes that transported clastic particles from the watershed and the littoral areas into the deepest part of the lakes. The coarser and fining upward texture suggest that this facies is related to energy decreasing process during extreme events (floods).

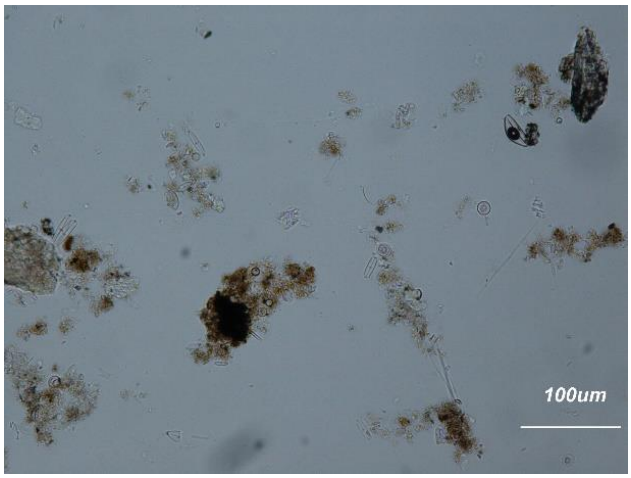

Fig. 4.8. *Photograph in parallel nicols taken of smear slide corresponding to F4 (57 cm of URD12-1B-1G).*

Facies 5. Dark brown, fining upward sand to clay silt

Description: F5 is composed of a single layer 6 cm thick, with dark brown sand at the base (2 cm thick), grading into brown silty sand, sandy silt, silt, and at the top clay silt. This facies only occurs in Cregüeña.

Interpretation. This facies is interpreted as deposited by turbidity currents. The age model for the Cregüeña sequence favors the Ribagorza earthquake (1373 CE) as the cause for talus des-stabilization and deposition of this turbidite unit.

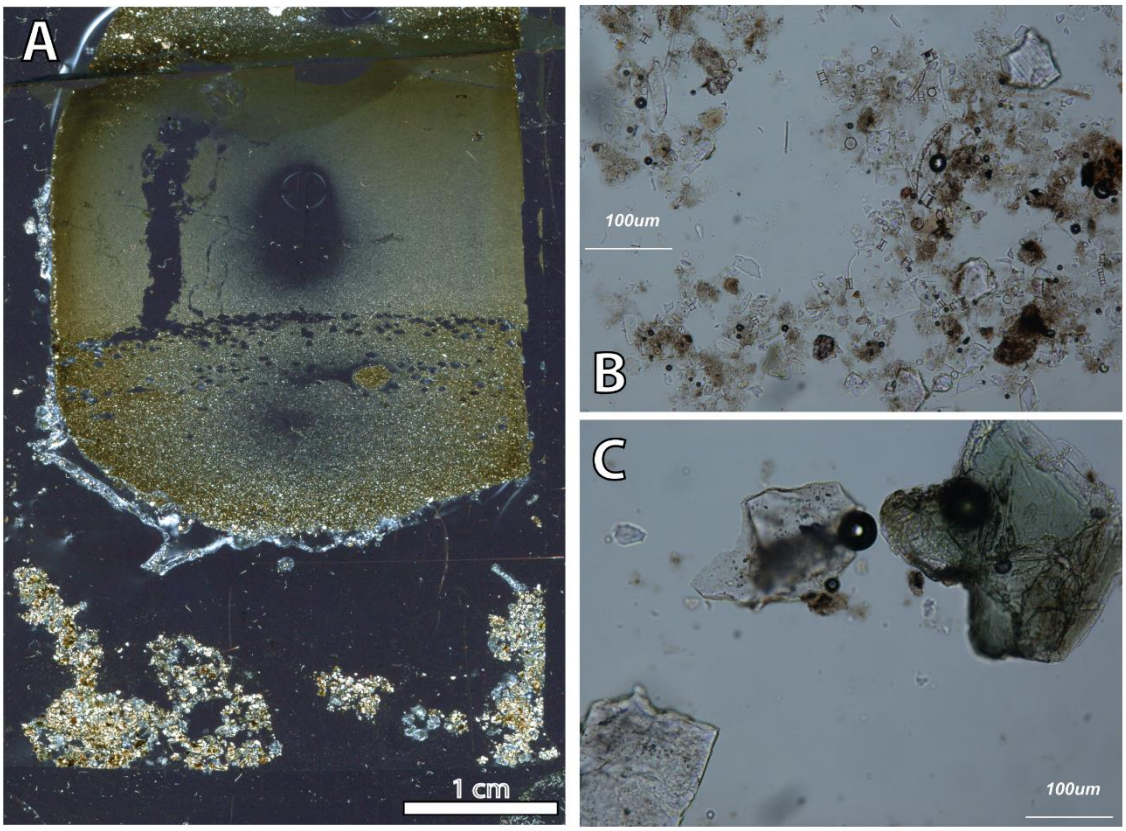

Fig. 4.9. *(A) High resolution thin section scan (crossed polars), from Cregueña facies 5 (core CRE17-1A-1G). (B-C) Photographs taken in parallel nicols of F5. B) smear slide (1 cm8 of CRE17-1A-1G. (C) smear slide (20 cm of CRE17-1A-1G).*

Facies 6. Laminated silts and silty clay

Description: Laminated silts and silty clays include brown, white, and gray millimeters thick laminae that occasionally are cm-thick. They only appear in Marboré. The layers have gradational boundaries and the main differences between them is their thickness and grain size: (1) the grayish layers have the finest grain size (between 2 and 5 μm) and they are usually the thickest laminate; (2) brown layers are coarser (20–70

μm) and they are usually thinner laminae than the gray layers, (3) the white layers have a composition similar to the grayish ones, but with coarser grain size range.

Interpretation. F6 is interpreted as rhythmites. Calcite-bearing, coarse silt/brown sand laminations deposited during warmer periods (thaw season, summer) and fine-grained, clay-rich, grayish laminations form during colder periods (when the lake is ice-covered). The Marboré laminations are not regular throughout the sequence, neither in their frequency nor in their thickness: the thicker brownish laminae do not always appear, the grayish laminae show a great variability in thickness and the whitish laminae are too thin to be measured or may even be absent. This variability is to be expected in high-altitude environments, where there may be periods of several years without a "warm" season long enough to melt the ice on the lake surface. During such periods of years (or decades) brown and white laminae would not be deposited (B. Oliva-Urcia et al., 2018). Similar rhythmic and laminated facies occur in current proglacial lakes (Carrivick & Tweed, 2013; S. J. Livingstone et al., 2012; Otto, 2019) and past proglacial sequences (Vegas, 2007a, 2007b).

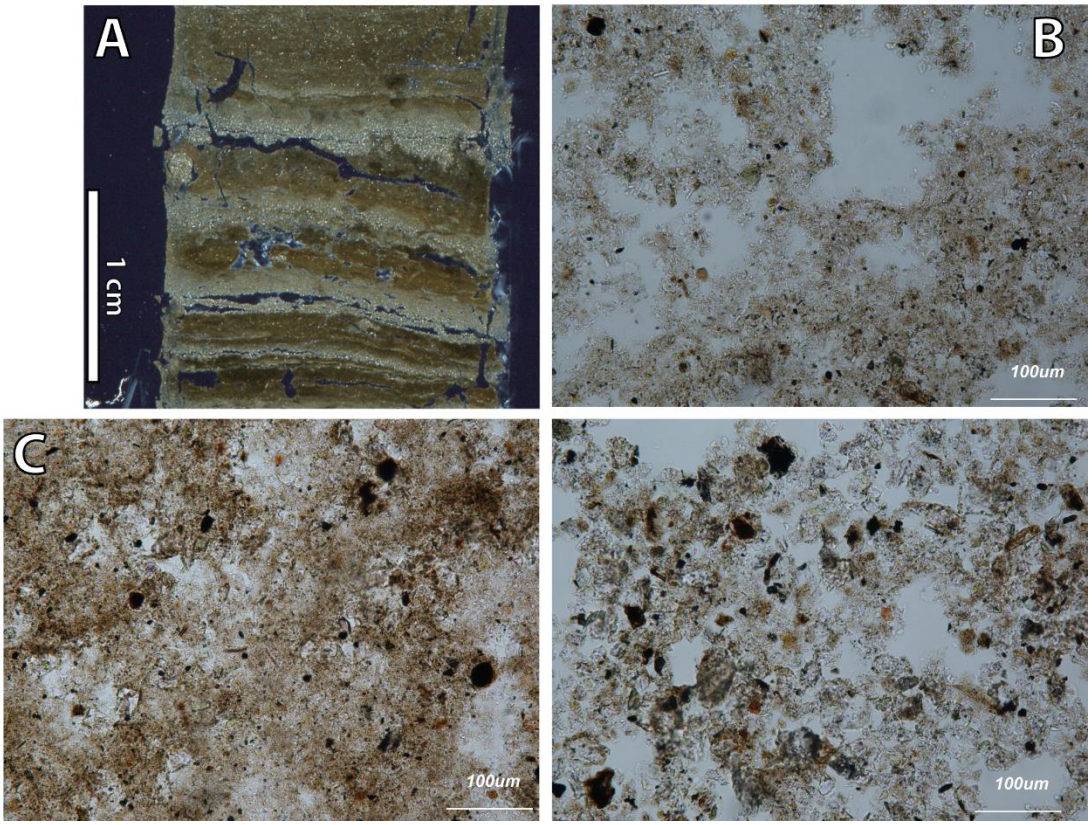

Fig. 4.10. *(A) High resolution thin section scan (crossed polars), of Marboré facies 6 (core MAR11-1U-1A-1). (B-D) Photographs taken in parallel nicols of smear slide corresponding to F6 (26-28 cm of MAR11-1U-1A-1, of a white (B), gray (C) and brown (D) lamina).*

4.4.1.2. Organic - rich facies (> 10 % OM)

Facies 7. Light brown massive, organic-rich sandy silt

Description. Facies 7 occurs in 2 to 7 cm thick layers, mostly massive although occasionally with diffuse lamination. The OM content ranges between 10 and 20%. This organic-rich facies occur mostly in Acherito.

Interpretation. This facies represent deposition in the distal areas in lakes with both higher organic productivity and higher input of detrital organic matter from the watershed.

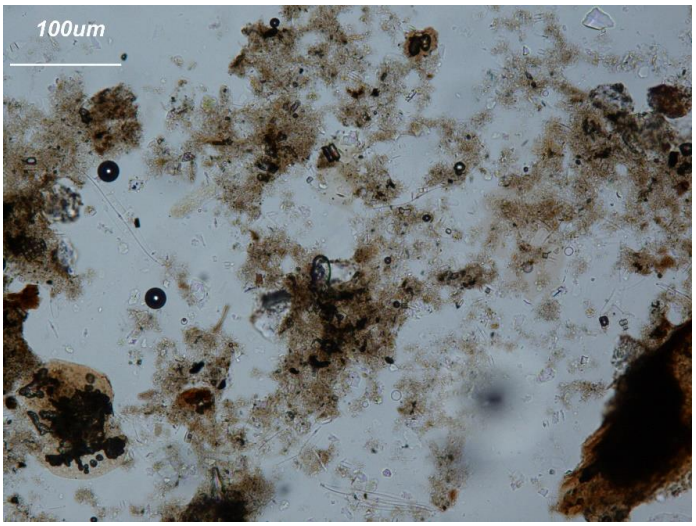

***Fig. 4.11**. Photograph in parallel nicols taken of smear slide corresponding to F7 (53 cm of ACH17-1A-1G).*

Facies 8. Grayish brown massive organic - rich silt

Description. F8 appears as 2 to 18 cm thick, massive layers in Acherito and at the top of La Sierra. The organic component is between 10 and 25%.

Interpretation. The high organic content and the fine grain size suggest deposition in distal areas during periods of higher organic productivity.

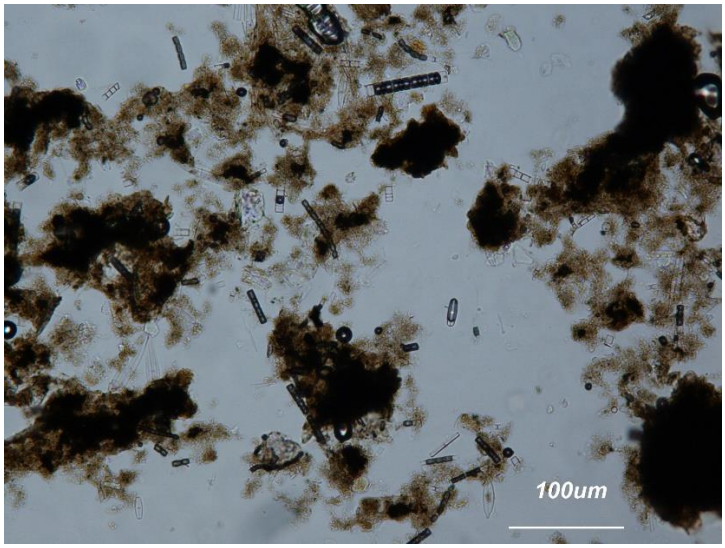

***Fig. 4.12**. Photograph in parallel nicols taken of smear slide corresponding to F8 (9 cm of SIE17-3A-1G).*

Facies 9. Dark grayish brown banded organic-rich sandy silt

Description. F8 occur in layers of 1 to 5 cm with diffuse banding and with OM content up to 30%. It only occurs in Acherito.

Interpretation. This is the most organic facies of the Pyrenean sequences and it represents deposition in a high productivity lake.

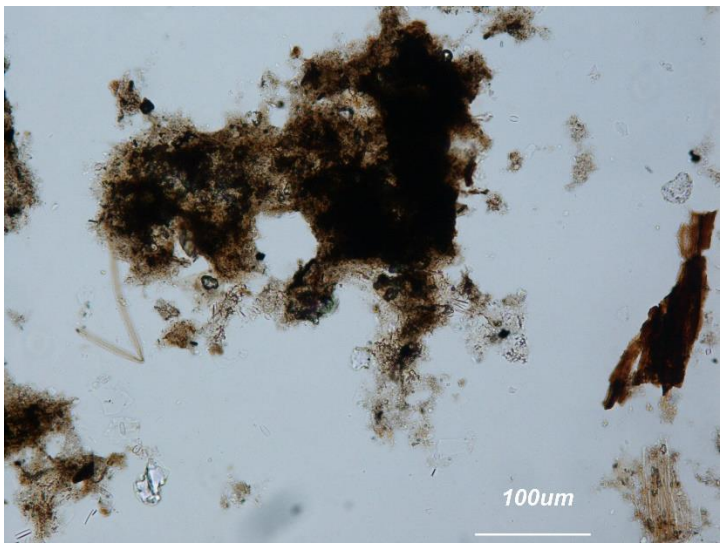

***Fig. 4.13.** Photograph in parallel nicols taken of smear slide corresponding to F9 (79 cm of ACH17-1A-1G)*

4.4.1.3. Carbonate-bearing facies (> 2 % carbonate component)

Sedimentary facies with some carbonate content only occur in Sabocos sequence, and occasionally, in Marboré.

Facies 10. Brown, finely laminated, organic-rich sandy silt with carbonate

Description. Finely laminated (mm) silt with 5 - 10% carbonate content, and 10 - 25% MO content. Carbonate particles include small charophyte remains and also detrital grains from the carbonate formations in the watershed.

Interpretation. Fine lamination and high organic content points to high organic productivity and deposition in distal areas with dominant anoxic conditions. Carbonate content and composition point to well-developed shallower littoral areas as main source of carbonate particles.

Facies11. Brown finely laminated carbonate sandy silt

Description. Finely laminated silt, mostly composed of carbonate particles (calcite and dolomite as determined by XRD) (15 - 45% carbonate content), and relatively lower organic content (4 - 9% MO).

Interpretation. This carbonate facies represent fine deposition in the deepest areas with dominant anoxic conditions. Carbonate content and composition point to well-developed shallower littoral areas as the main source of carbonate particles.

Facies12. Brown laminated carbonate sandy silt

Description. Dark brown, laminated sandy silt and silt in layers of several mm to cm thick. Some layers show fining upward grading. Compositionally they have 25 -45% carbonate and 4 - 9% OM.

Interpretation. Relatively coarse deposition in the deepest areas of the lake mostly composed of reworked material (charophytes …) from the littoral areas. Lower OM content suggest less productive littoral environments

Facies13. Brown, laminated to banded, sandy silt with carbonates.

Description. Laminated to banded sandy silts, in mm to 2 cm thick layers, although the average thickness is about 1 cm. The grain size of these layers can range from silt to silty sand. Compositionally they have between 2 and 25% carbonate, and less than 5% OM. This is the most common facies in Sabocos. The Marboré layers with < 1 % carbonate content have been included in these facies.

Interpretation. This facies represents deposition in the distal areas of a lake with a shallower littoral environment colonized by macrophytes and charophytes. Low organic content and dominant banded textures suggest oxic bottom waters.

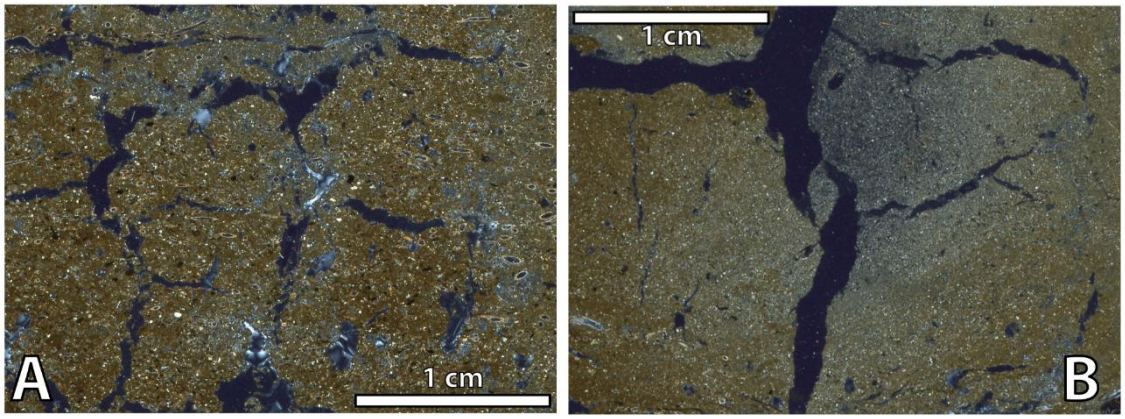

Fig. 4.14. *High resolution thin section photograph in crossed nicols, of Sabocos facies 13 (core SAB 18-1A-1G).*

	Facies	Legend	Composition	Granulometry	Description	Depositional Interpretation	Lakes
Clastic	1	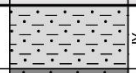	≥95% silicates	Sandy silt	Brown to dark brown slightly banded sandy silt	Clastic deposition in distal areas of the lake during periods of relatively higher (sandy facies) and lower (silty facies) energy, likely related to variable runoff and water and sediment delivery from the watershed	CR, UR
	2		90 to 95% silicates	Sandy silt	Grayish brown to dark brown massive to banded sandy silt with organic matter		CR, SI, UR
	3		91 to 95% silicates	Silt	Grayish brown banded silt		SI
	4		> 90 % silicates	Silty sand	Light brown massive silty sand		UR
	5	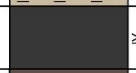	≥95% silicates	Sands to clayey silt	Dark brown fining upward sand to clay silt	Turbidite deposited after an earthquake	CR
	6	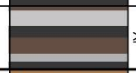	≥95% silicates	Silts and silty clay	Laminated silts and silty clays	Rhythmite: Clastic deposition controlled by seasonal to pluri-annual changes in run-off and sediment delivery from the watershed	MAR
Organics	7		10 to 20% OM	Sandy silt	Light brown massive, organic-rich sandy silts	Deposition in distal areas of the lakes with higher organic productivity	AC, UR
	8		10 to 25% OM	Silt	Grayish brown massive organic - rich silts		AC, SI
	9		10 to 30% OM	Sandy silt to silt	Dark grayish brown banded organic-rich sandy silts		AC
Carbonataded	10		5 to 10% carbonate 10 to 25% OM	Sandy silt	Brown, finely laminated organic-rich sandy silts with carbonates	Deposition in distal areas of the lake including sediment from the watersehd, carbonates and organics from the littoral areas (charophyte meadows)	SA
	11		15 to 45% carbonate 4 to 9% OM	Sandy silt	Brown finely laminated carbonate sandy silts		SA
	12		25 to 45% carbonate 4 to 9% OM	Sandy silt	Brown laminated carbonate sandy silts		SA
	13	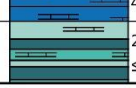	2 to 25% carbonate ≤ 5% OM	Sandy silt	Brown, laminated to banded, sandy silt with carbonates		SA

Table 4.1. *Sedimentary Facies in high altitude Pyrenean Lakes*

4.4.2. Facies Mineralogy (XRD data and SEM images)

Cregüeña

XRD data combined with the SEM study show the mineralogical composition of the Cregüeña sediments. Fig 4.15 shows the semiquantitative % of the main minerals as determined by XRD grouped as clays, quartz and feldspars. Clays are frequent (ranging from 24-53 % with average values of 38%) with illite/muscovite type minerals dominating over chlorite and possible kaolinite. Feldspars (both potassium feldspar and plagioclase) are present throughout the profile with quartz. There are no significant differences along the sequence. The turbidite unit (F5) is particularly rich both in clays and feldspars. Fig. 4.16 shows representative samples of F1, F5 and F2.

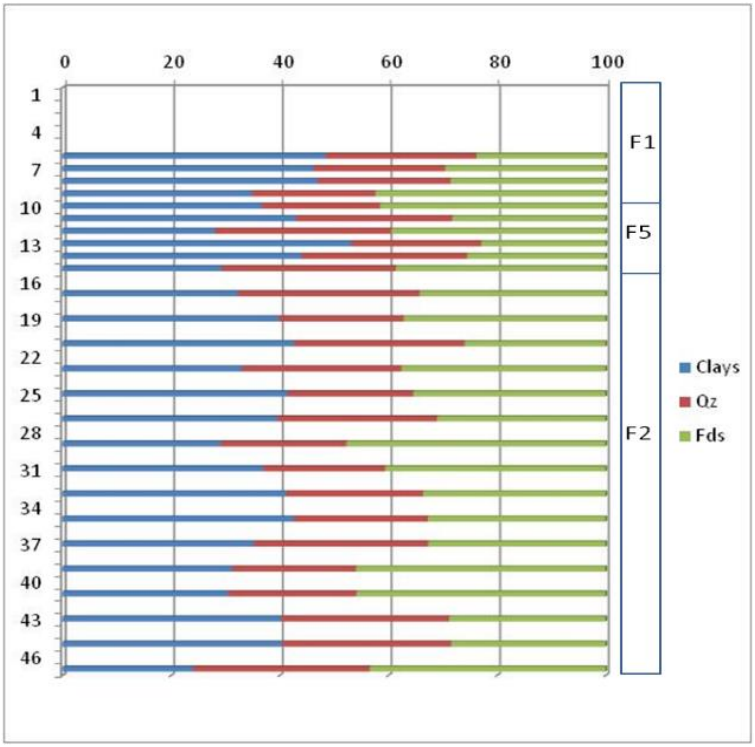

***Fig 4.15**. Semiquantitative % of the main minerals as determined by XRD grouped: clays, quartz and feldspars. The depth corresponds to the laboratory depth and it is not at scale.*

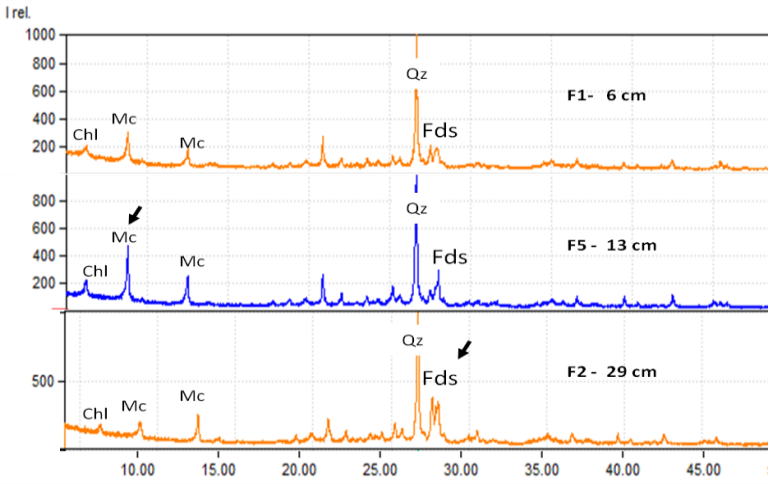

***Fig. 4.16**. XRD patterns of samples at 6, 13 and 29 cm, of F1, F5 and F2 respectively. Black arrows point to high-mica/feldspar contents in samples 13 and 29.*

The SEM study and EDS analysis on individual grains corroborate XRD data and optic study on smear slides. Main minerals are quartz, phyllosilicates (Chlorite and mica) and feldspars (both Na and K rich). At a microscopic scale, biogenic clast can be observed mainly as diatom debris. Minor minerals not detected by XRD, such as iron oxides, can also be seen.

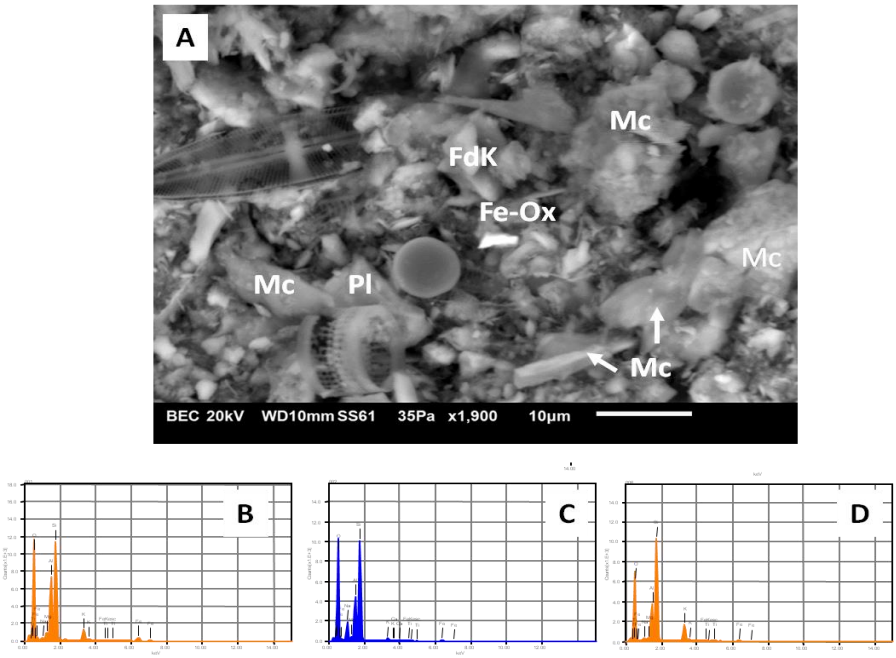

***Fig. 4.17.** A: BSE images of unit A (F1) (F2) Cregüeña. Image shows siliciclastic grains (Potassium feldspar, Na-rich plagioclase, micas, minor Fe-oxides and biogenic debris (diatom frustules). Mc: mica-like mineral; Qz Quartz; FdK: Potassium Feldspars. Chemical composition of the minerals has been assessed by means of EDS analysis. B-C-D. Representative EDS analysis of B: mica-like (muscovite), Na-Rich plagioclase and potassium feldspar.*

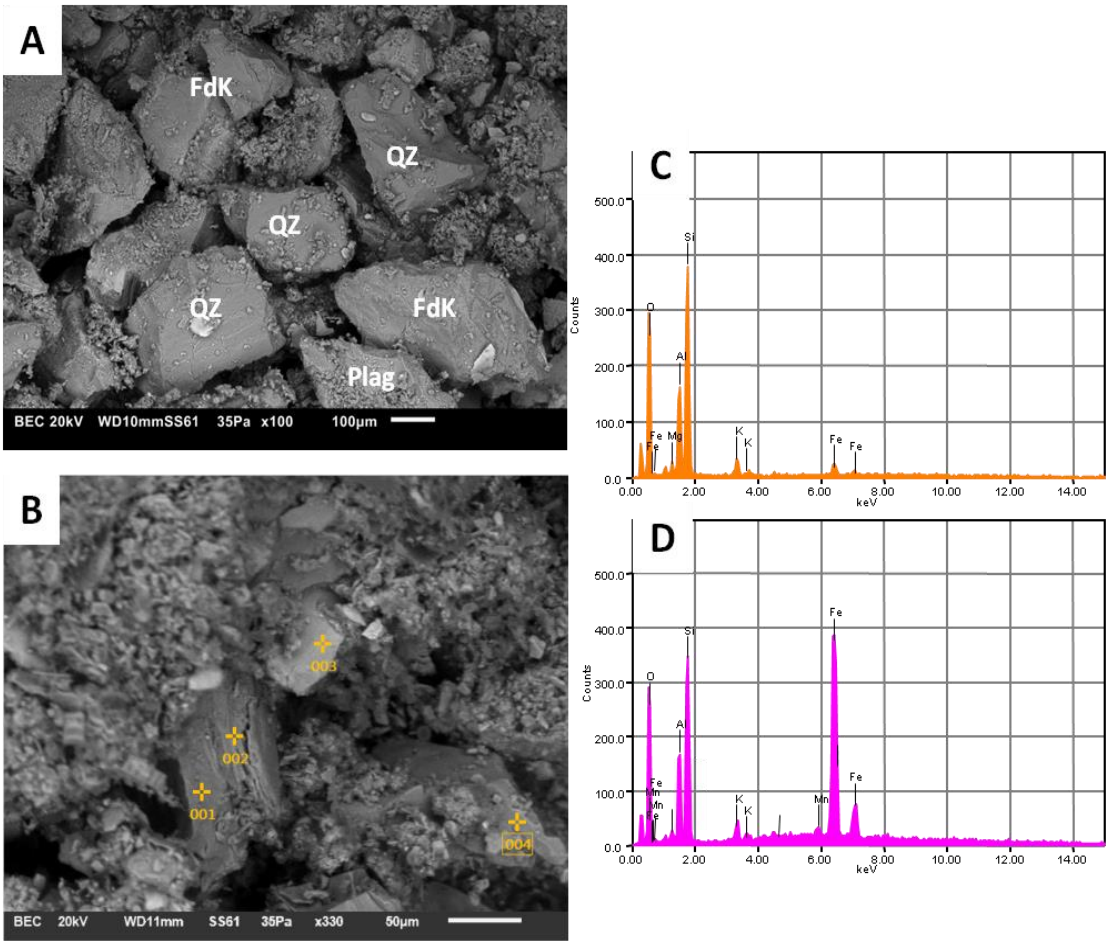

Fig. 4.18. *A-B: BSE images of unit C (F2) Cregüeña. A-B Images show siliciclastic grains. C-D: Show representative EDS analysis of mica and mica with iron oxides. Mc: mica-like mineral; Qz Quartz, FdK: Potassium Feldspars. Chemical composition of the minerals has been assessed by means of EDS analysis.*

Urdiceto

Semiquantitative percentages based on XRD data on representative samples along the core, show no significant differences and similar silicate mineralogical composition throughout the sequence. Quartz is the main mineral (33-68%) followed by clay minerals (42-19%) and feldspars (10-30%). Clays are minerals of the mica group (illites, muscovites, phengites and possibly biotite); chlorites have been observed, although the presence of small amounts of kaolinite is not ruled out. Feldspars of potassium and calco-sodic type are present in all samples but not in large quantities. The differences between the facies are mainly due to the content of quartz+Fds vs. phyllosilicates and related to grain size distribution.

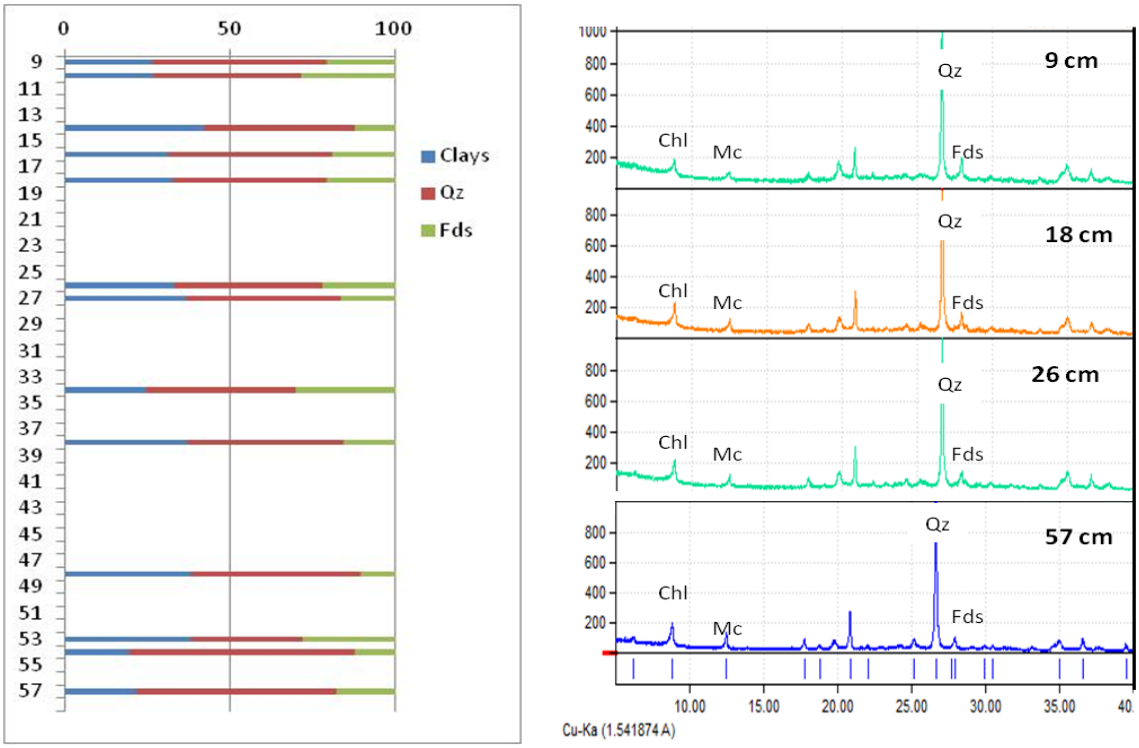

***Fig 4.19**. Left. Semiquantitative % of the main minerals in Urdiceto as determined by XRD grouped as clays, quartz and feldspars. The depth corresponds to the laboratory depth and it is not at scale. Right. XRD patterns of samples at 9, 18, 26 (F2) and 57 cm (F4).*

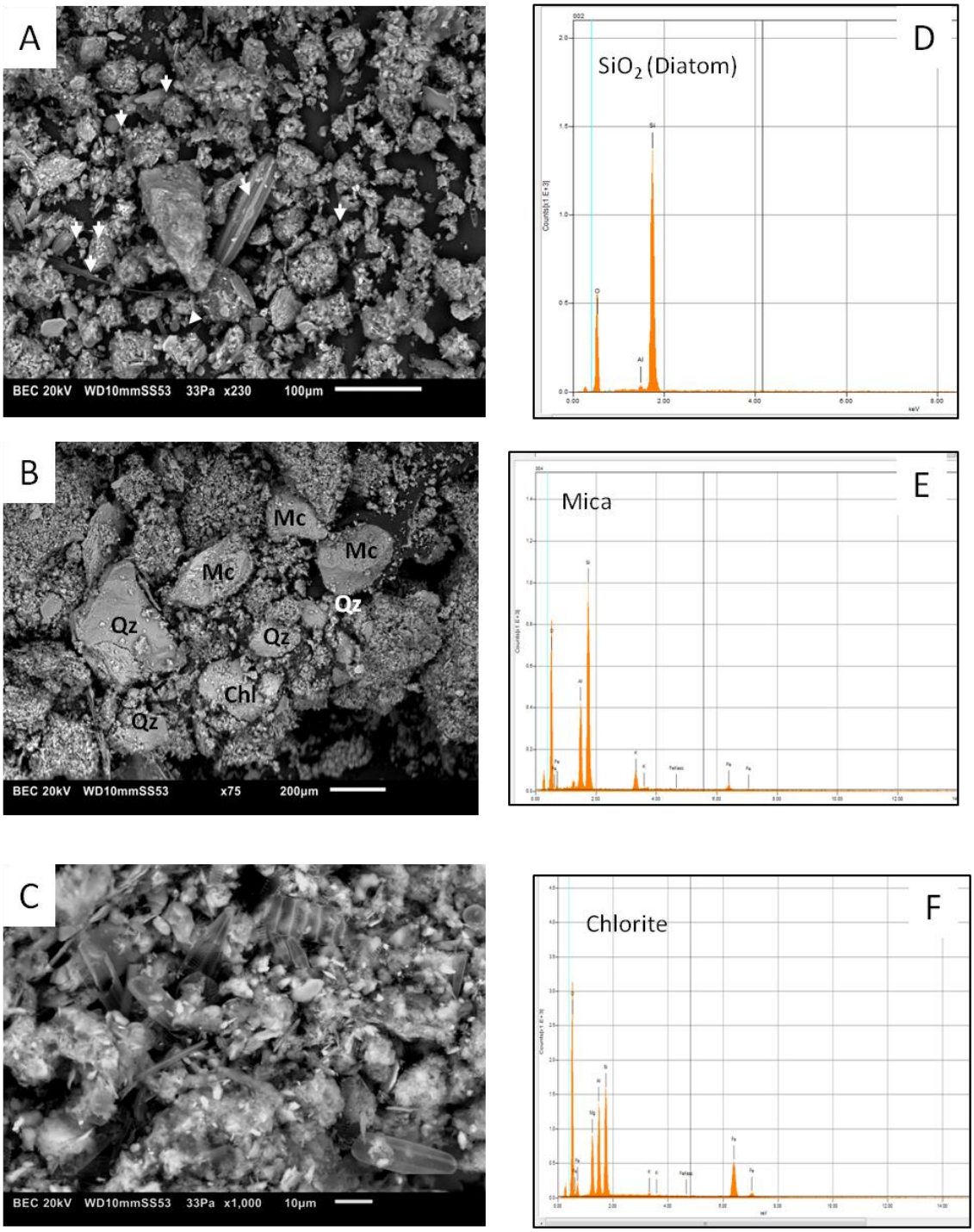

Fig. 4.20. *A-B: BSE images of unit F2 of Urdiceto. Images show a high content of siliciclastic coarser grains (micas quartz, chlorite) in a fine-grained (silty) siliciclastic silt with organic matter representative of facies 2. C: BSE image of a rich-diatom area with fine-grained siliciclastic grains. Mc: mica-like mineral; Qz Quartz, Chl: Chlorite. White arrows point to biogenic/bioclastic debris. D. Representative EDS analysis of a diatom; E: Representative EDS analysis of mica-like crystal E: Representative EDS analysis of a chlorite crystal.*

Sabocos

Fig 4.21 shows the mineralogy (XRD) and representative XRD patterns of different mineralogical associations in Sabocos. Carbonate-bearing facies have lower percentages of calcite and minor dolomite (less than 20%), quartz ranges from 50 to 61%, and illite/muscovite type minerals dominating over chlorite (see fig 4.21 representative XRD pattern at 54 cm). Carbonate-rich facies have up to 60% of calcite and 40% of dolomite (more abundant at the top of the sequence) (see Fig. 4.21, representative XRD pattern). Gypsum occurs sporadically in several samples as a possible alteration of the sulfides (framboidal pyrite) detected in the samples (Fig. 4.22).

SEM photos corroborate the mineralogy observed by XRD and the texture of the main components (siliciclastic, organic bioclastic). Calcite appears as bioclasts, larger detrital grains or small micrometric crystals. Dolomite occurs in large rhombohedrons but smaller crystals have also been observed that could have an autigenetic/diagenetic origin. Bioclasts (both carbonate and siliceous) are abundant in the facies of unit A. Framboidal pyrite is observed throughout the sequence, sometimes accompanied by Fe oxides and gypsum.

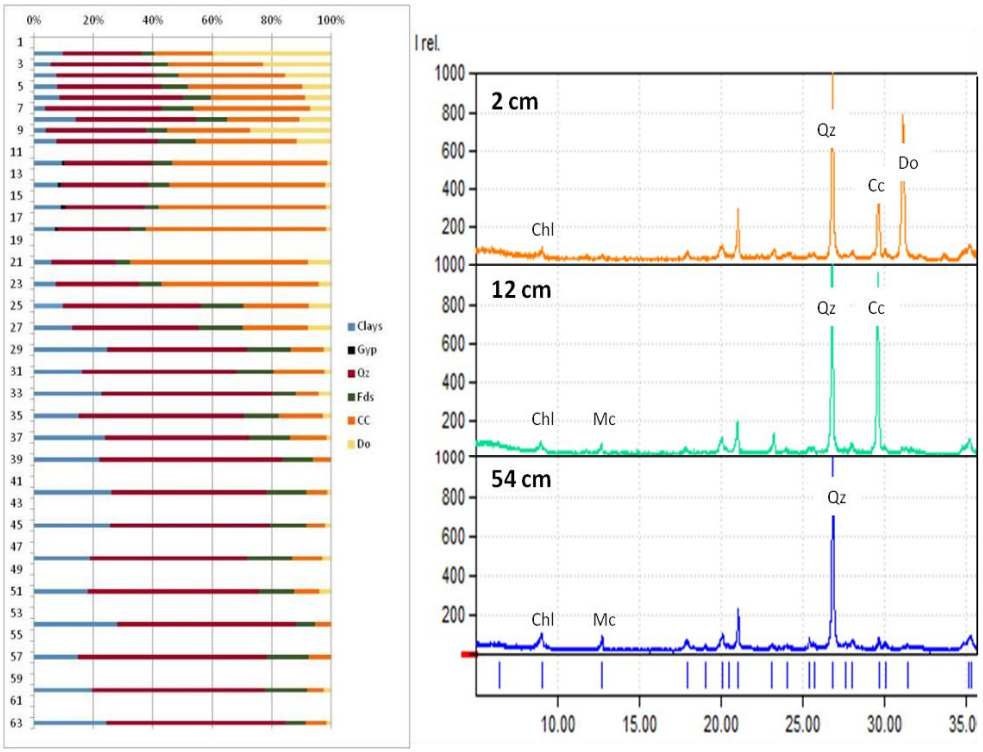

Fig. 4.21. *XRD semiquantitative values of mineralogy as determined by XRD in Sabocos. The depth corresponds to the laboratory depth and it is not at scale (left). Representative XRD patterns (right).*

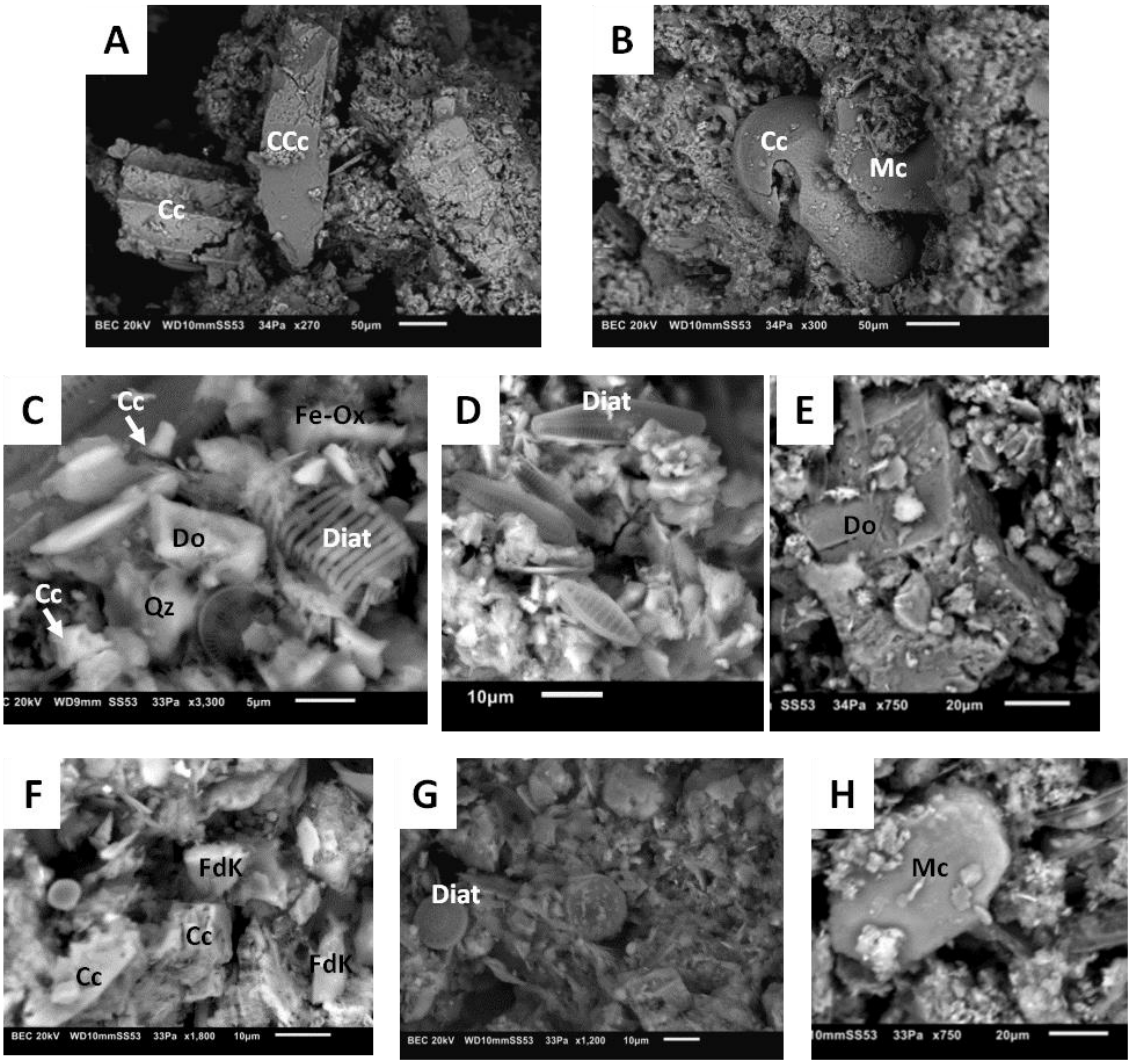

Fig. 4.22. *BSE images of samples of Sabocos. A-D Unit A (F10) A-B Images show calcitic bioclast s(Cc) C-D: Diatom frustules are abundant. Calcite and dolomite occur either as less than 5 microns (C), or as clear detrital grains (E). F-H: BSE images of unit A (F11) (Sabocos). Diat: Diatoms; Mc: mica-like mineral; Do: dolomite, Cc Calcite, Qz Quartz; FdK: Potassium Feldspars. The chemical composition of the minerals has been assessed by means of EDS analysis.*

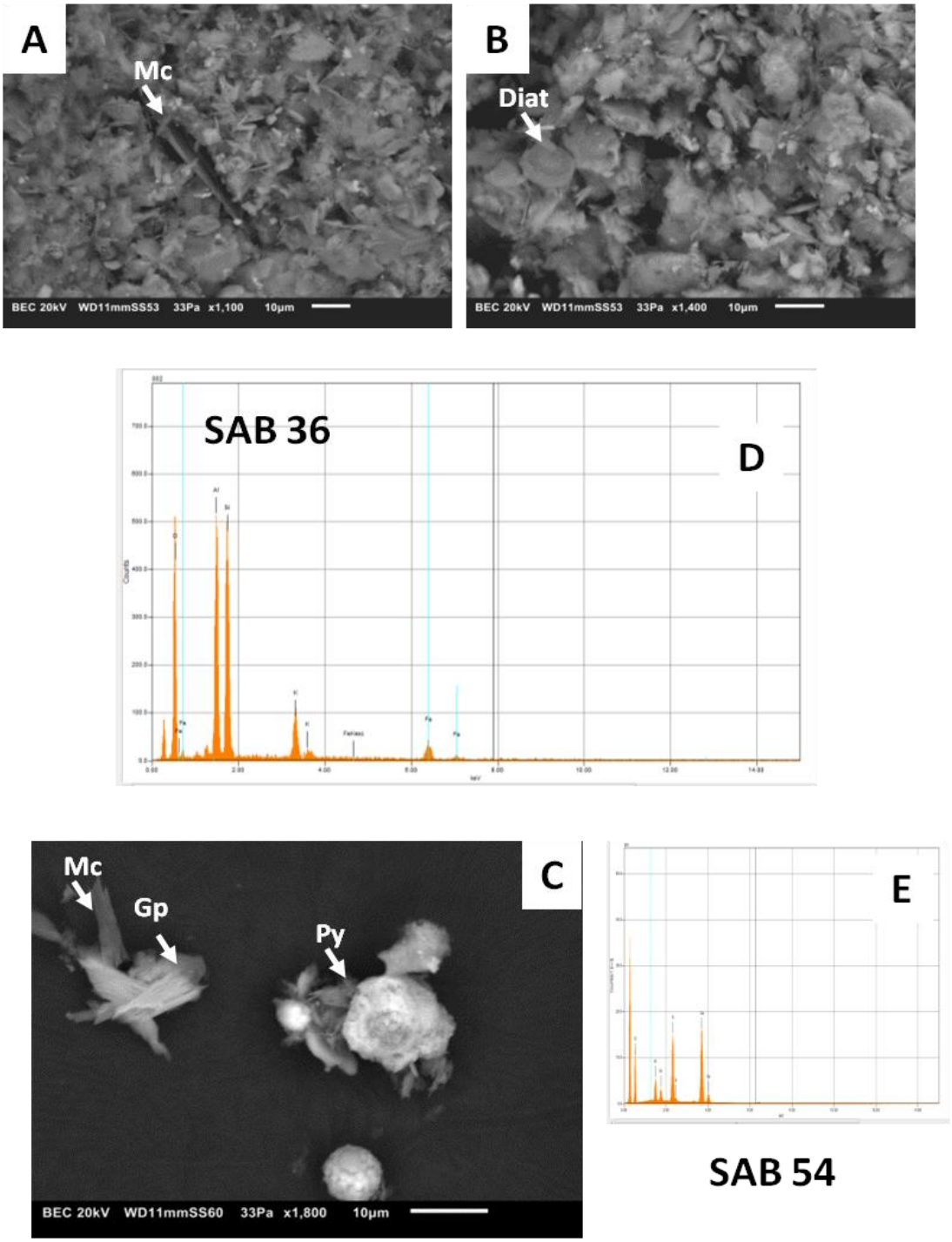

***Fig. 4.23**. BSE images of Sabocos. A-C: images of unit B (F11 and F13) of Sabocos. A-B Images show a fine-grained sediment, made of quartz, detrital micaceous minerals (illite - muscovite like), minor feldspars (K-feldspars) and sporadic pyrite. C: Iron oxides and gypsum have been detected by SEM as a possible alteration product of framboidal pyrite. D-E: EDS analysis of mica (image A) and Gypsum (Image B) Diat: Diatoms; Mc: mica-like mineral; Gp: Gypsum; Py: partially oxidized pyrite.*

Acherito

The mineralogy of Acherito sediments is composed of quartz, feldspars and clays, with no carbonates detected throughout the sequence. There are slight variations between clays/feldspars and quartz ratios, corresponding to the alternations between silty/sandy and clayey levels of the different facies. The quartz content can be up to 71%, clay minerals up to 31% and feldspars up to 28% (see figure showing representative XRD diagrams).

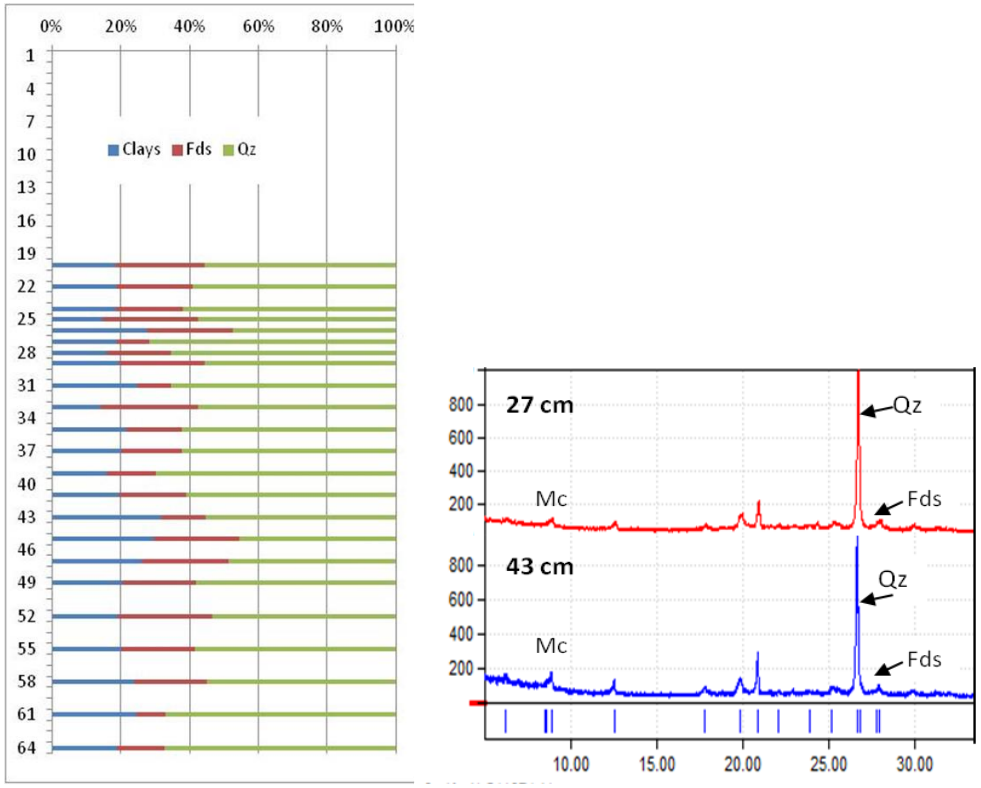

***Fig. 4.24**. XRD semiquantitative values of mineralogy as determined by XRD in Acherito. The depth corresponds to the laboratory depth and it is not at scale (left). Representative XRD patterns (right). Qz: quartz, Fds: feldspars and Mc: mica.*

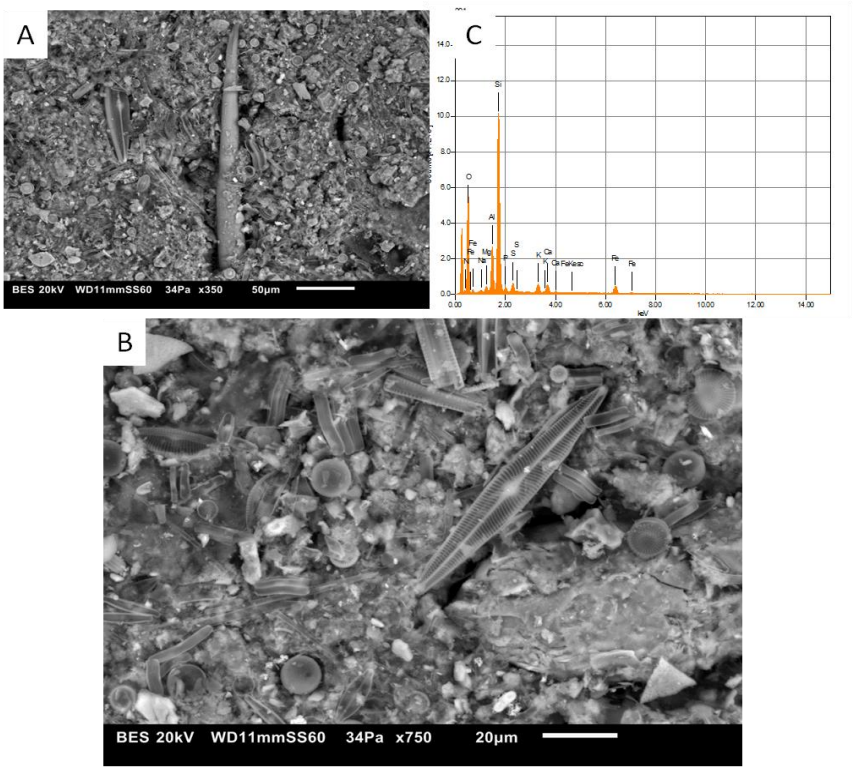

Fig. 4. 25. *A-B. BSE images of sample 17 cm from Acherito, Facies 8. A) fine-grained sediment with abundant diatoms and bioclasts. Besides main minerals detected by XRD (quartz, feldspars, clays) minor apatite, titanium oxides and pyrite crystals can be observed. C: General EDS spectra showing elements detected in area of image A (Si, Al, Mg, K, Ca, Fe, S, P and Na).*

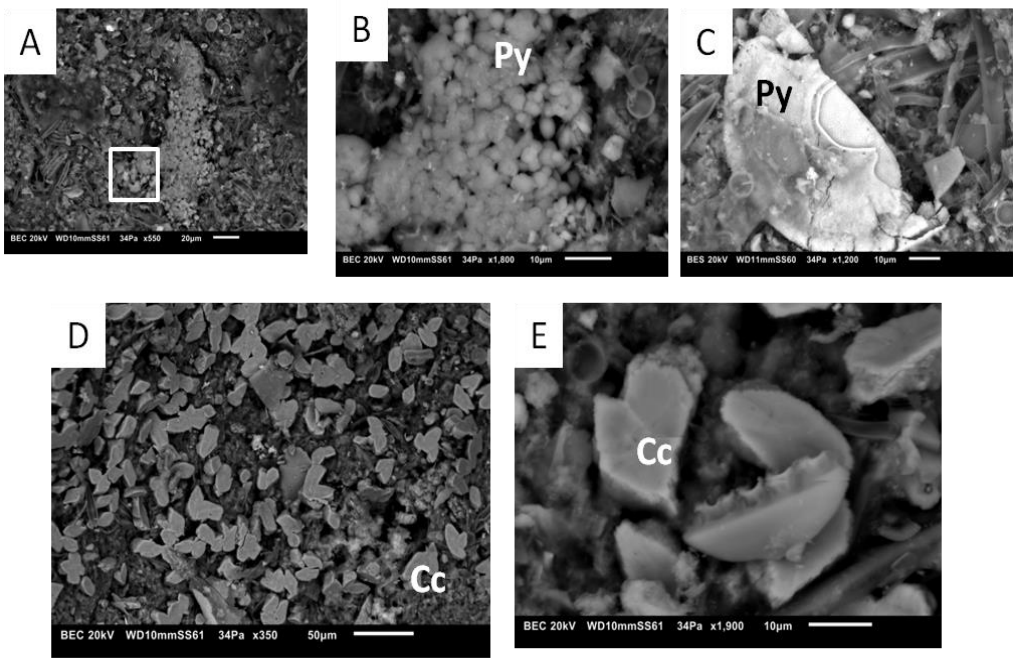

Fig. 4.26*. BSE images of Facies 8 (17 cm) A-B: diagenetic pyrite as framboids; (C) pyritized biological rest. D-E. BSE images of authigenic calcite crystals (not detected by XRD) over the surface of the siliciclastic sediment.*

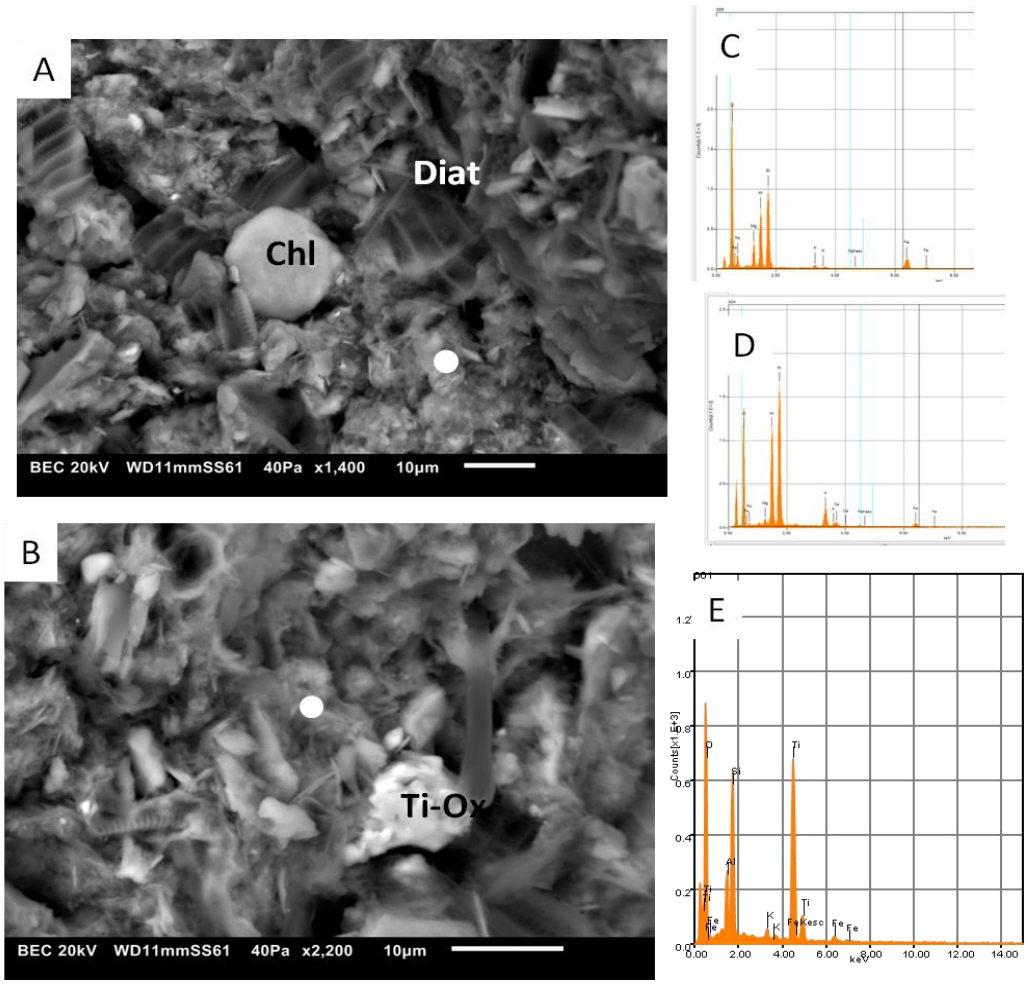

Fig. 4. 27*. BSE images of sample 17 (facies 7). A) General texture with abundant diatom frustules. C:) EDS spectra of chlorite plate: D): Spectra of white circle showing average chemical composition of the clayey matrix, E): Titanium oxide mineral in the matrix.*

La Sierra

The mineralogy of all samples is similar and consists of quartz, ranging from 43-73 %, with average values of 58%, followed by phyllosilicates, mainly mica group minerals and chlorite, kaolinite being sporadic, (from 14-44 with average values of 27%) and feldspars, mainly sodic and calco-sodic (with values ranging from 7% to 25% and average of 15%).

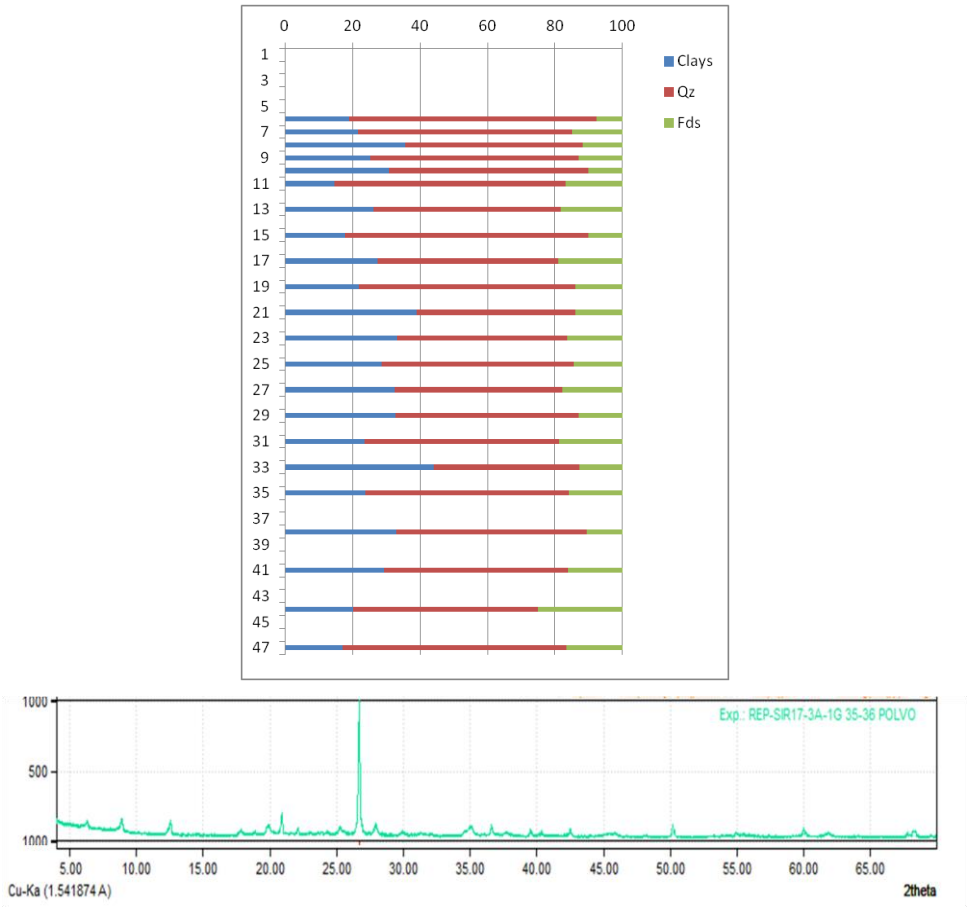

Fig. 4.28. *XRD semiquantitative values of mineralogy as determined by XRD in La Sierra. The depth corresponds to the laboratory depth and it is not at scale (left). Representative XRD pattern of sample from La Sierra 35-36 cm.*

4.4.4. Facies Geochemistry

4.4.4.1. Geochemical indicators

Geochemical composition may help to better define the sedimentary facies and refine the environmental and depositional interpretations. In this PhD thesis we have used the following ratios:

1) K/Ti as an indicator of clastic sediment input to the lakes (Arnaud et al., 2016).

2) Fe/Mn, as an indicator of dominant oxidizing or reducing conditions at the lake bottom and surface sediment environment. The lower Fe/Mn ratios are interpreted as a predominance of more oxidizing conditions at the bottom of the lake (Corella et al., 2012; Schaller & Wehrli, 1996).

2) Ca/Ti, as an indicator of the relative proportion of total carbonates (allochthonous and endogenic) compared to detrital materials (Corella et al., 2013; Morellón et al., 2014). The higher the values of this ratio, the higher the endogenous carbonate formation.

3) Rb/Zr, is considered an indicator of grain size in the terrigenous, silicate materials. Higher values are associated with greater amounts of finer clay minerals as Rb is present in clay minerals and Zr in zircon (coarse fractions) (Dypvik & Harris, 2001; Kylander et al., 2011; Wu et al., 2020).

4) Br/Ti reflects the relationship between organic matter and silicate content, as Br is associated with organic compounds. Higher Br/Ti values reflect a greater amount of organic matter in the sediment (Ziegler et al., 2008).

5) C/N indicates possible sources of OM. Relatively lower C/N ratios indicate algal sources of OM in lakes and lower terrestrial carbon contributions. Whereas a higher input of organic matter derived from the watershed would cause higher C/N values (Meyers & Teranes, 2002).

4.4.4.2. XRF scanner facies composition

Data from XRF scanners provide a larger number of analyses per facies than ICP. The range for the selected ratios varied: between 0.3 and 6 for K/Ti, 7 and 2620 for Fe/Mn, 0 and 0.43 for Br/Ti, 0.25 and 1.6 for Rb/Zr and 0.3 and 22 for Ca/Ti.

Silicate Facies

Facies 1 is characterized by a variable K/Ti ratio, with some samples with the lowest values for all facies and other with the highest (1.3 to 5). It also has a wide range in the Rb/Zr ratio (0.5 to 1.3). The Fe/Mn ratio is low, but similar to what we find in most facies. As the K/Ti ratio increases, the Fe/Mn also increases, but maintaining similar values to the rest of the facies (31 to 229). The Br/Ti is generally low (0.007 to 0.16), increasing slightly as the K/Ti ratio decreases.

Facies 2 behaves geochemically very similar to facies 1, but the K/Ti values are somewhat lower (0.7 to 4.7) and the Fe/Mn has a larger range of variability (20 to 1148). There is no clear increasing relationship between K/Ti and Fe/Mn.

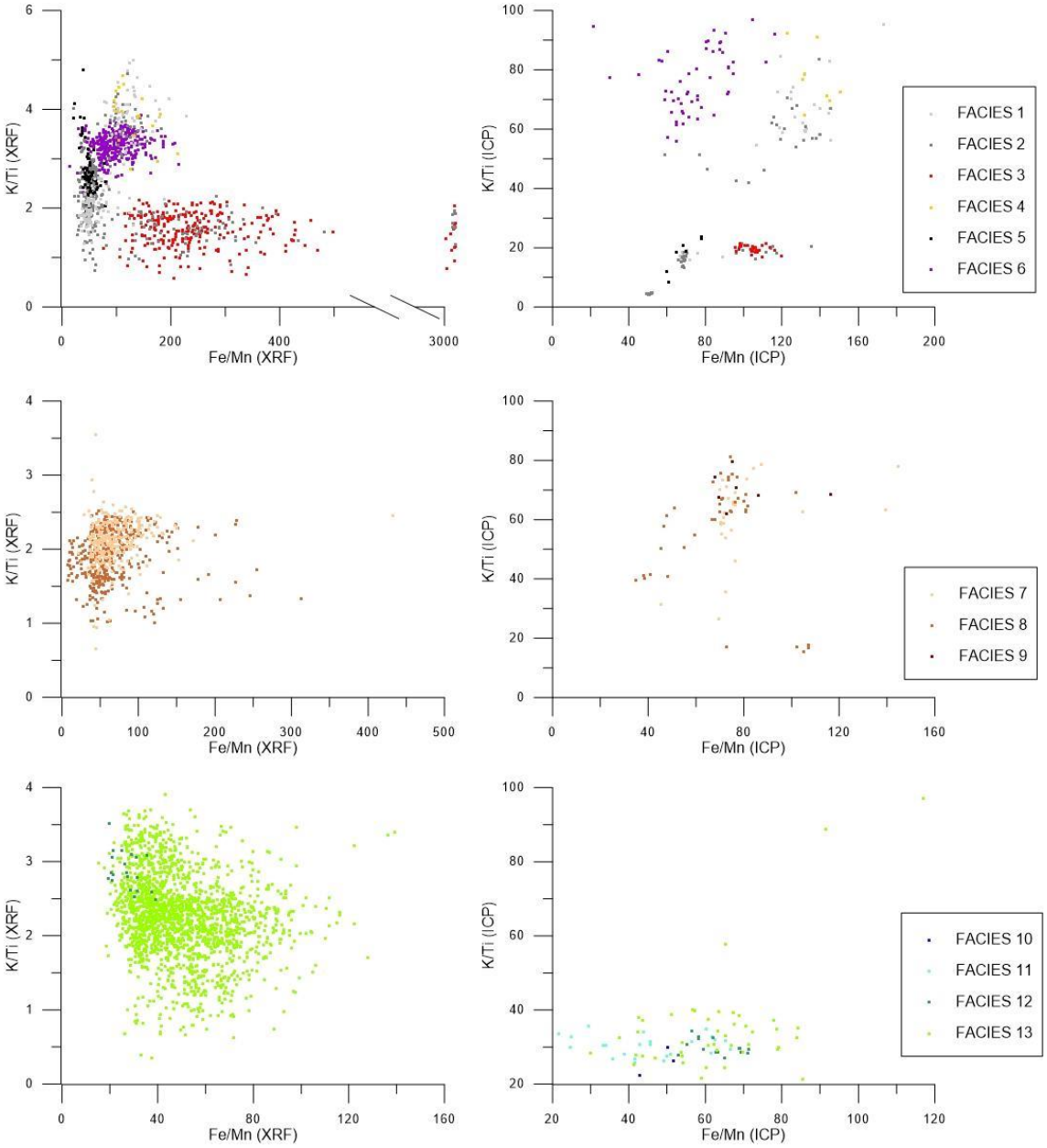

Fig.4.29. *Scatter plots by facies groups: silicate (F1 to F6), organic (F7, F8, F9) and carbonate (F10 to F13). The data includes all the lakes studied (Cregueña, Marboré, Urdiceto, La Sierra, Sabocos, Acherito). The plots show the K/Ti and Fe/Mn ratios obtained from XRF scanner and ICP analyses.*

Facies 3 has a low K/Ti ratio (0.6 to 2.2) and large Br/Ti variability (0.006 to 0.19). Rb/Zr has little variability (0.5 to 0.8), but this is similar to what we see in other facies. Facies 3 is similar to Facies 2 in terms of the wide range in Fe/Mn ratio (75 to 2620), well above the rest of the facies.

Facies 4 has a high K/Ti ratio (2.8 to 4.7) and slightly higher Fe/Mn ratio values (95 to 212), although within the range of most facies (except facies 2 and 3). The Br/Ti ratio is lower than most facies and with little variability (0.006 to 0.02). And the Rb/Zr has slightly higher values than most facies, but similar to facies 1, 2 and 6 (0.9 to 1.2).

Facies 5 has a K/Ti ratio with intermediate values (1.9 to 4.8), similar to most facies. The Fe/Mn (21 to 80) and Br/Ti (0.01 to 0.06) are lower and within a smaller range. The Rb/Zr is variable, with most values similar to the rest of the facies but with some samples with higher ratios (0.4 to 1.6).

Facies 6 has intermediate K/Ti values (2 to 3.8) and Rb/Zr values similar to the rest of the facies (0.26 to 1). The Fe/Mn ratios have a somewhat greater range of variability (14 to 214), but similar to facies 1 and 2. The Br/Ti is very low, the lowest and with the least variability of all the facies (0 to 0.007).

Organic Facies

Facies 7 has variable but intermediate values in K/Ti (0.6 to 3.5), Rb/Zr (0.5 to 1) and Fe/Mn (20 to 432), but a wider range in high Br/Ti values (0.02 to 0.28).

Facies 8 behaves similarly to facies 7, although it can reach even higher values in the Br/Ti ratio (0.04 to 0.43), and lower values in Fe/Mn, although with a large variability (7 to 312).

Facies 9, 10 and 11 have no XRF data.

Carbonate Facies

Facies 12 has intermediate K/Ti values (2.5 to 3.5) and high Ca/Ti values (11 to 21). Fe/Mn ratio (2.5 to 3.5) and Rb/Zr (0.3 to 0.5) are low. The Br/Ti ratio reaches average values like those seen in the silicate facies (0.01 to 0.06).

Facies 13 has a great variability in the K/Ti ratio (0.3 to 3.9) and includes samples with the lowest values. The Ca/Ti (0.3 to 22) is also highly variable, increasing as K/Ti also increases. The Fe/Mn is generally low, although some samples can also have similar values as other organic or silicate facies (15 to 139). The Br/Ti (0.01 to 0.06) and an Rb/Zr (0.25 to 1.37) have intermediate values.

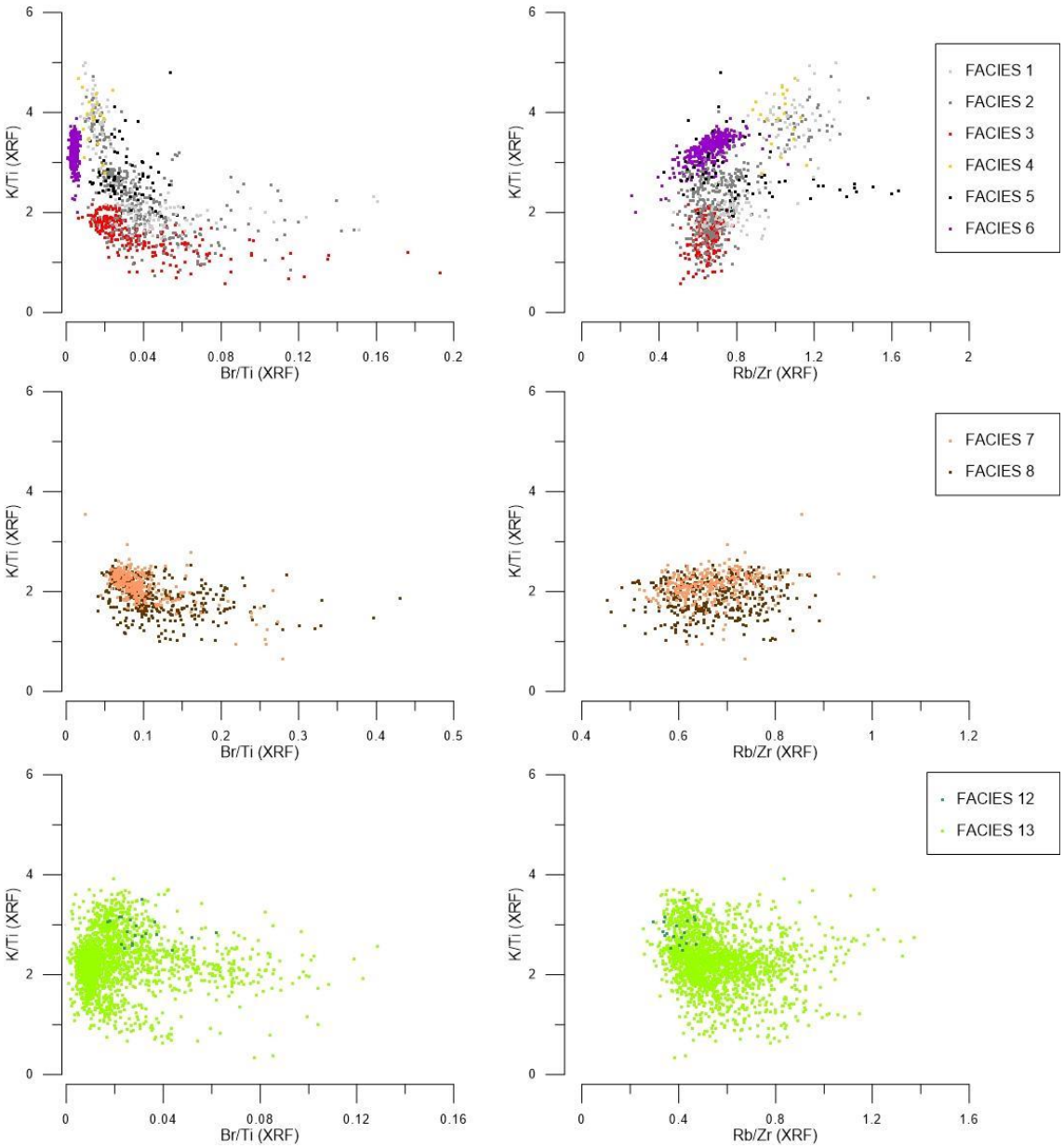

Fig.4.30. *Scatter plots by facies groups: silicate (F1 to F6), organic (F7, F8, F9) and carbonate (F10 to F13). The data include all the lakes studied (Cregueña, Marboré, Urdiceto, La Sierra, Sabocos, Acherito). The plots show the K/Ti, Rb/Zr and Br/Ti ratios. All graphs are based on XRF core-scan data.*

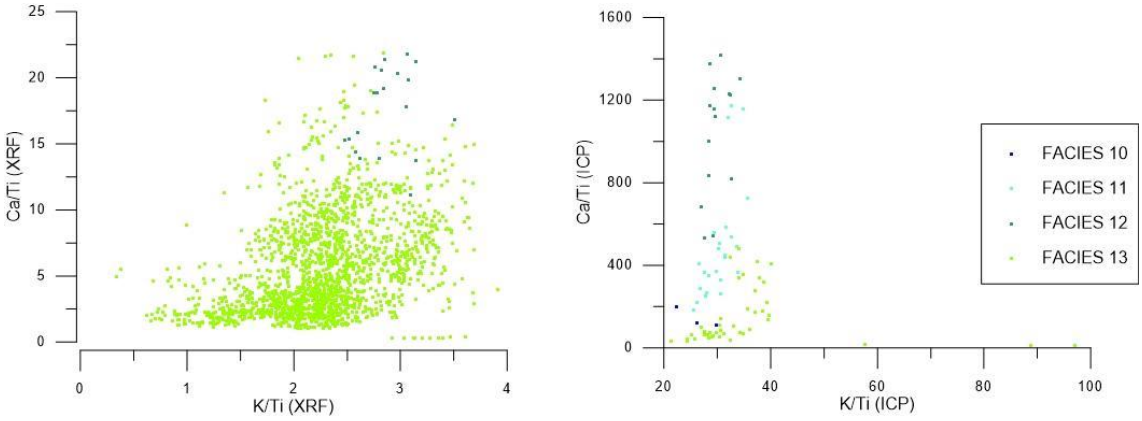

Fig.4.31. *Scatter plots of carbonate facies: F10 to F13 from Marboré and Sabocos (the only lakes with this type of facies). The plots show the K/Ti and Ca/Ti ratios obtained from XRF scanner and ICP analyses.*

4.4.4.3. ICP facies composition

The ICP analyses provide quantitative compositional data for the identified facies. However, the number of analyses is smaller and some elements (Br) have not been analyzed. The selected ratios used to describe the facies have the following ranges considering the ICP data: K/Ti between 4 and 99.5, Fe/Mn between 21 and 202 and Ca/Ti between 9 and 1420. The results for each facies are described below.

Silicate Facies:

Facies 1 has a very large variability in K/Ti ratio, with the highest and lowest values in the whole facies dataset (15 to 95). Fe/Mn ratio also has high variability (66 to 173). K/Ti increases as the Fe/Mn ratio increases.

Facies 2 also has a wide range in K/Ti with slightly lower values than facies 1 (4 to 83). Fe/Mn ratio is highly variable (49 to 145) but within values occurring in other facies.

Facies 3 has a smaller K/Ti and Fe/Mn value range, with lower values in K/Ti (16 to 22) and slightly higher in Fe/Mn (95 to 120) compared to the rest of the facies.

Facies 4 has higher values in both K/Ti (64 to 92) and Fe/Mn (122 to 150) than other facies.

Facies 5 has lower K/Ti values (8 to 24) and intermediate Fe/Mn (59 to 78).

Facies 6 has high K/Ti ratio values (55 to 97) and moderate, but variable Fe/Mn (21 to 116).

Organic Facies

Facies 7, 8 and 9 show intermediate values in the K/Ti ratio (between 26 and 79 for F7, 15 and 81 for F8 and 62 and 79.6 for F9). The Fe/Mn is variable (between 45 and 145 in F7, 35 and 107 in F8 and 67 and 116 in F9), but with values within the same range to other facies.

Carbonate Facies

Facies 10 and 11 are the only carbonate facies with available ICP data. Facies 11 has a larger and higher range (183 to 1171) than facies 10 (109 to 198) for Ca/Ti. Both have relatively low K/Ti (between 22 to 30 in F10 and 25 to 36 in F11) and Fe/Mn (between 42 to 51 in F10 and 21 to 66 in F11).

Facies 12 is the carbonate facies with the highest Ca/Ti ratio (between 531 and 1419). It also has low Fe/Mn (52 to 71) and K/Ti (27 to 34) values with little variability. Facies 13 has low Ca/Ti ratios (between 10 and 480) and K/Ti ratio (21 to 97) with some of the lowest values of the carbonate facies. The Fe/Mn ratio has greater variability than the rest of the carbonate facies, reaching values somewhat higher (29 to 116).

4.4.4.4. XRF versus ICP facies composition

The large difference in the number of XRF and ICP samples makes some comparisons difficult to draw. In addition, we can only compare the results between the ratios of elements available in both analyses, i.e. K/Ti, Fe/Mn and Ca/Ti.

In the siliciclastic facies there are notable differences between XRF and ICP results. Facies 1 and 4 have similar results in both types of analyses, but Facies 2 and 3 show larger differences. This is particularly evident in the Fe/Mn ratio, with XRF ratios showing greater variability and values well above the rest of the facies, while ICP ratios are much less variable and within average values. Facies 5 have both XRF and ICP

highest K/Ti ratio, although XRF values are more differentiated from the rest of the facies. The Fe/Mn based on XRF analyses has average values similar to the other facies, but ICP ratios are the highest. Facies 6 has intermediate K/Ti (XRF) values while ICP ratios are lower.

Organic facies tend to have lower K/Ti values in XRF than in ICP. Carbonate facies, on the contrary, have lower K/Ti values in ICP, while XRF ratios are higher and more variable.

We only have Ca/Ti data for two facies and the difference in the number of samples for each type of analyses is large. XRF ratios in facies 13 and 14 are similar, but the highest Ca/Ti (ICP) values of facies 14 are never higher than the lowest values of facies 13.

4.4.4.5. Sedimentary sequences and units

In order to better understand the relationships among geochemical composition and sedimentary facies we have carried out Principal Component Analysis (PCA) for each lake integrating data from ICP, granulometry (% sand) and TOC. The Principal Component Analysis (PCA) is a statistical method that allows simplifying the complexity of sample spaces with many dimensions but preserving its information. Therefore, it allows "condensing" the information provided by multiple variables into just a few components. PC1 in these lakes explains more than 37 % of the variability, although the percentage varies in each lake: 53.6% in Sabocos, 48.4% in La Sierra, 43.1% in Acherito, 42.6% in Urdiceto, 39.9% in Cregueña, and 37.5% in % in Marbore.

The PC1 in most of the lakes shows a clear differentiation of organic versus siliciclastic components. In general, the sand % is positively associated with elements such as Al, K or Na, and other elements depending on each lake (such as Si and Ti in La Sierra and Sabocos), defining the silicate and clastic component. The TOC is associated with Ca, S, Mn and P, defining the organic component. The higher altitude lakes show a different behavior, probably because in this case the organic factor is less relevant. In Marboré, PC2 differentiates better these two components (siliciclastic vs. organic), but in this lake Ca is associated with the detrital component, together with Al, K or Na. In Cregueña the organic component is minimal and PC1 differentiates grain size, separating the coarse from the fine fractions. The coarse fraction is associated with TOC, Ca, P, Ti, while the fine fraction is associated with Al, K, Mn and Fe.

In the following sections we describe the sedimentary sequences in each lake, with the defined facies, units and main compositional and geochemical indicators.

Cregueña

Cregueña is the lake located at the highest altitude (2633 masl) and the deepest (99 m) of the studied transect. Cregueña lies in a granitic watershed and has little facies variability (Fig. 4.33), dominated by siliciclastic facies with very low organic content. We have identified three facies (F1, F2 and F5) and three sedimentary units based on the intercalation of an event unit (B) (Figure 4.33).

Unit C (26 cm thick) is formed by massive, grayish brown to dark brown sandy silt (facies 2). The top boundary with unit B is sharp and erosive. PC1 indicates mainly siliciclastic origin of the sediments (Figure 4.32) and TOC values decreased towards the top of the unit. Unit B is formed by facies 5 (Turbidite event) in a single 6 cm layer with a fining-upward sequence also marked by the Rb/Zr ratio. The top of the core (Unit A) is composed of facies 1 (Brown to dark brown sandy silt, slightly banded), finer and more organic-rich towards the top. Higher PC1 values reflect the TOC increase at the top of the sequence.

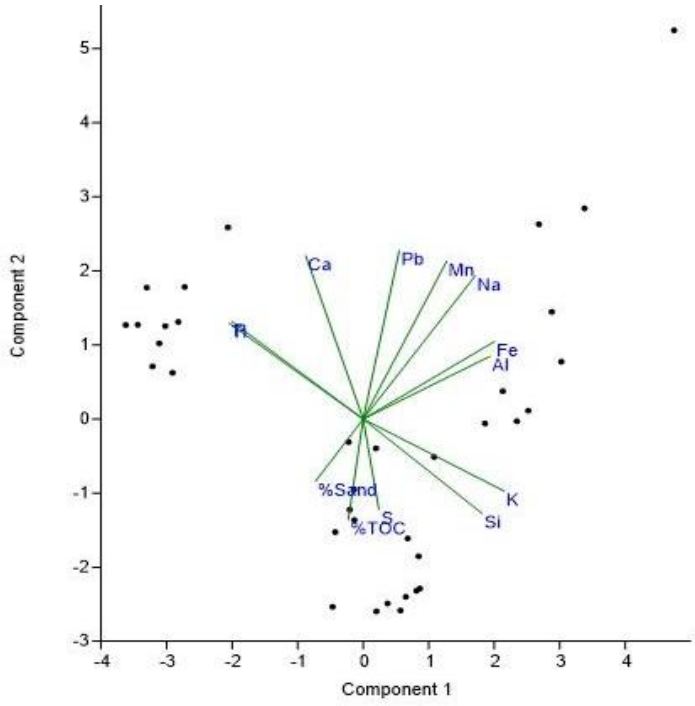

Fig. 4.32. *Cregueña Principal Component 1 vs Principal Component 2. The data set includes data from ICP, granulometry (% sand) and TOC (%).*

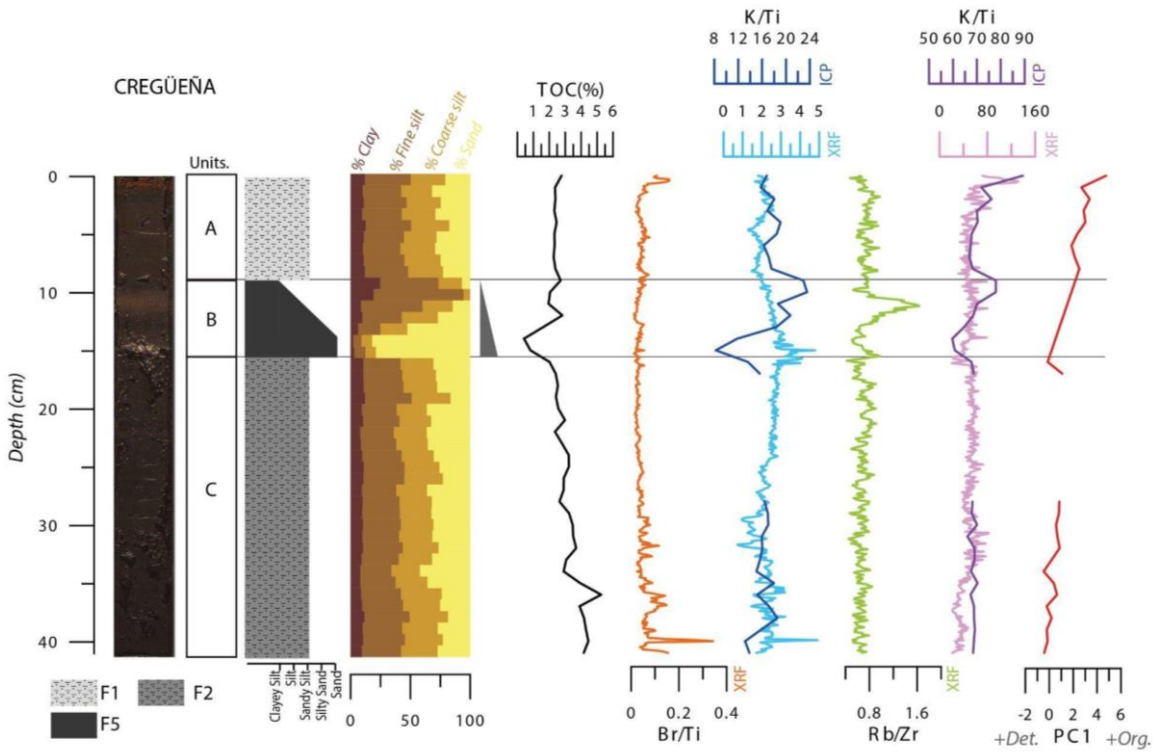

***Fig. 4.33**. Core REP-CRE17-1A-1G, photograph, sedimentary units, sedimentary facies, granulometry, Total Organic Carbon (TOC%), Br/Ti and Rb/Zr by XRF, K/Ti and Fe/Mn by XRF and ICP, Principal Component 1 (PC1).*

Marboré

Marboré is located at 2600 masl, in a carbonate watershed and with a maximum depth of 31 m. Marboré is the only one of the lakes that presents a sequence of rhythmites (facies 6, Laminated silt and silty clay). Occasionally thin layers (from millimeters up to 2 centimeters) of facies 13 (Brown sandy silt, from laminated to banded, with the presence of carbonates) intercalate. We have defined only one unit (A). Most of the sequence (subunit A2) shows little variability. Considering geochemical and compositional criteria, the upper 6 cm have been grouped into subunit A1 with a small increase in TOC, TIC and Ca/Ti and higher K/Ti, pointing also to higher siliciclastic input (Figure 4.35). In Marboré, the PC2 better differentiates siliciclastic vs. organic (Figure 4.34) and in this lake Ca is associated with the detrital component, together with Al, K and Na.

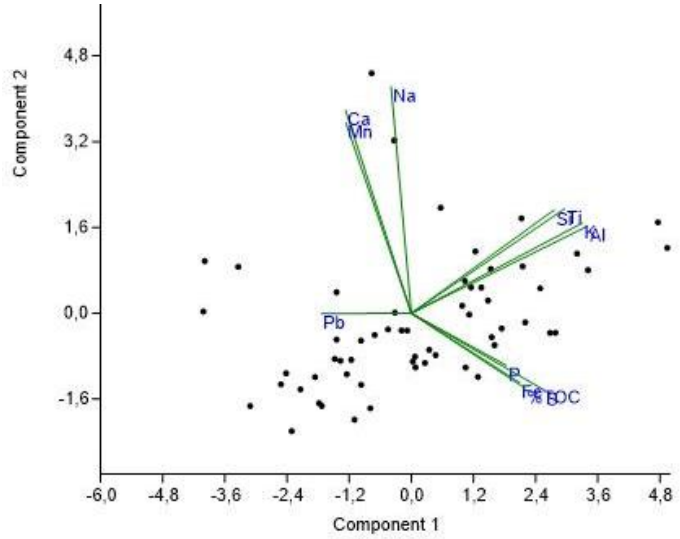

***Fig. 4.34**. Marboré Principal Component 1 vs Principal Component 2. The data set includes data from ICP, granulometry (% sand) and TOC (%).*

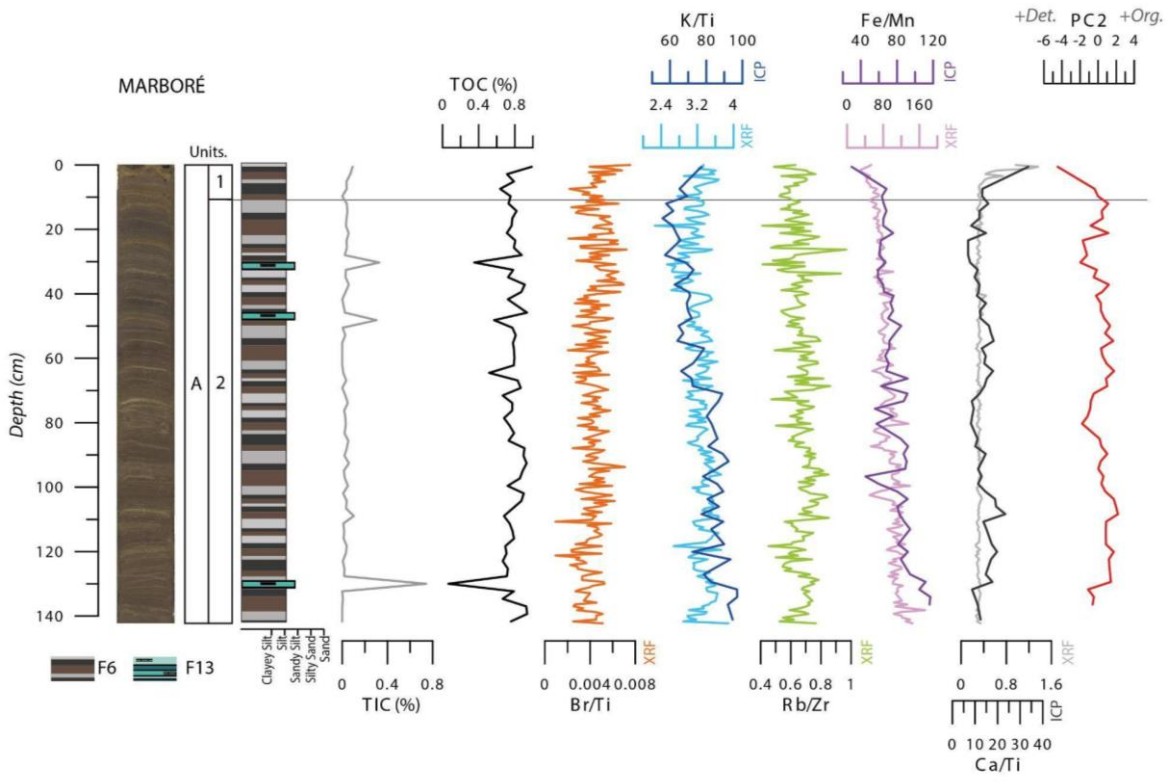

***Fig. 4.35.** Core photo (MAR11-1U-1A-1), sedimentary units and subunits, sedimentary facies, granulometry, Total Inorganic Carbon (TIC%), Total Organic Carbon (TOC%), Br/Ti and Rb/Zr by XRF, K/Ti, Ca/Ti and Fe/Mn by XRF and ICP, Principal Component 2 (PC2).*

Urdiceto

The Urdiceto Lake is located at 2364 m asl in a watershed composed of mixed silicate-rich sedimentary and granitic rocks. The sequence includes four facies and it has been divided into two units. The lower unit (B) is an alternation of facies 1 (Brown to dark brown sandy silt, slightly banded), 2 (Grayish brown to dark brown sandy silt) and 4 (Massive light brown silty sand). It is characterized by low TOC values, although with some variability, and the PC1 indicates a mainly clastic origin.

Unit B (54-14 cm) is divided into three different subunits (B1, B2 and B3) according to facies composition. Subunit B3 is composed of facies 1, in layers of approximately one cm and with several intercalated fining-upward layers of facies 4. Subunit B2 presents an alternation of F1 and F2, with layers ranging from 0.5 to 6 cm. Subunit B1 contains F1, F2 and F4, in layers of 1 to 4 cm, with F1 and F2 being the thickest. Facies 4 may occur in fining-upward sequences.

Unit A (14 – 0 cm) is composed of F2, topped by facies 7 (Light brown sandy silt, massive and with more abundant OM). Geochemical indicators mark an increase in the organic component (higher PC1, TOC, Br/Ti) at the top of the sequence.

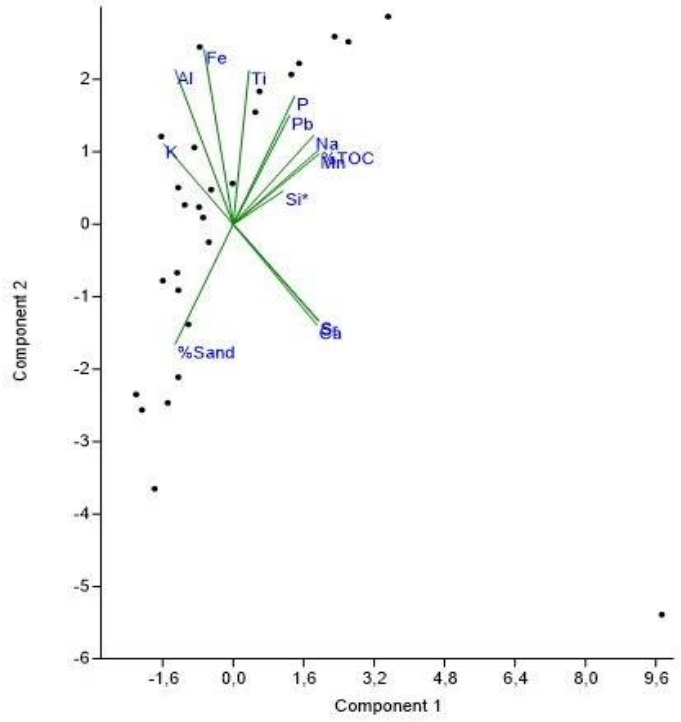

Fig. 4.36. *Urdiceto Principal Component 1 vs Principal Component 2. The data set includes data from ICP, granulometry (% sand) and TOC (%)*

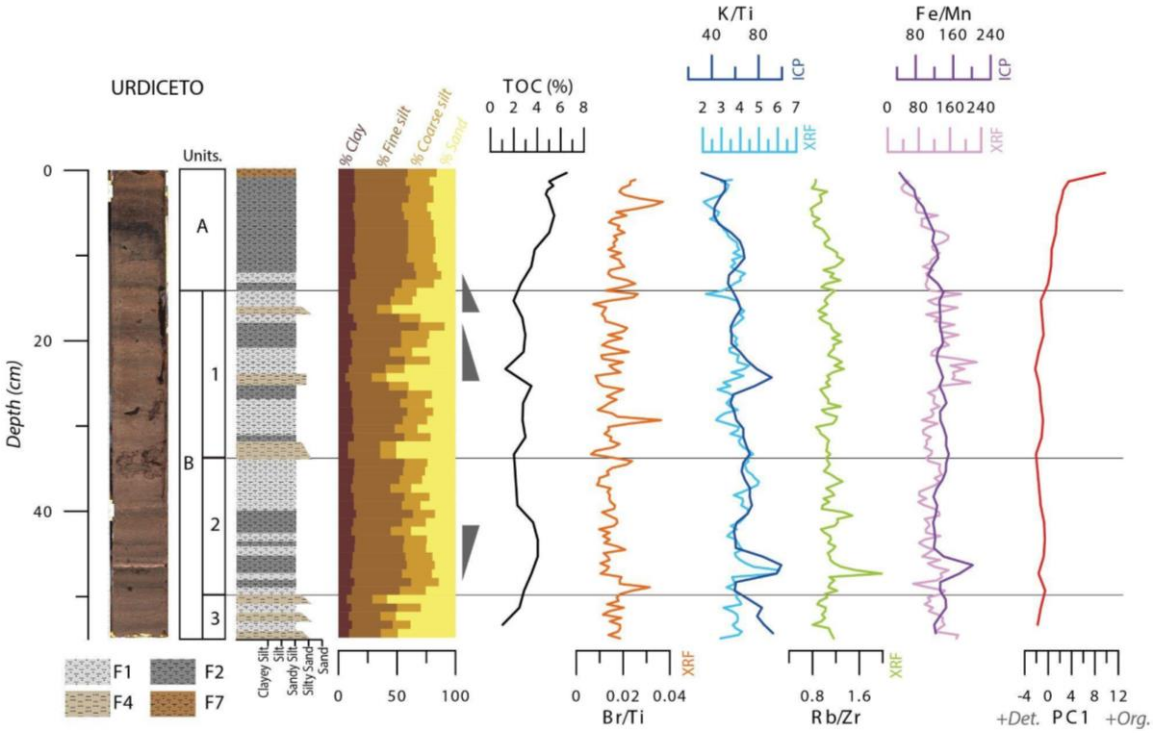

***Fig. 4.37**. Core photo (REP-URD12-1B-1G), sedimentary units, sedimentary facies, granulometry, Total Organic Carbon (TOC%), Br/Ti and Rb/Zr by XRF, K/Ti and Fe/Mn by XRF and ICP, Principal Component 1 (PC1).*

La Sierra

La Sierra is the smallest (0,013 ha) and shallowest (7m) of the lakes. It is located at 2022 masl in a silicate formation watershed. We have identified three facies and the sequence is divided into two units. Unit B (42-17 cm) is composed by an alternation of facies 2 (Grayish brown to dark brown sandy silt) and facies 3 (Banded grayish brown silt) in layers 1 to 4 cm thick. Facies 2 layers are thinner and less frequent towards the top. This unit is characterized by a slightly decreasing TOC towards the top.

Unit A (0 – 17 cm) is composed by banded facies 3 and it is topped by facies 9, the most organic facies of the sequence. TOC increases along this unit, Fe/Mn decreases slightly and PC1 shows a rather marked and rapid increase of the organic component at the top.

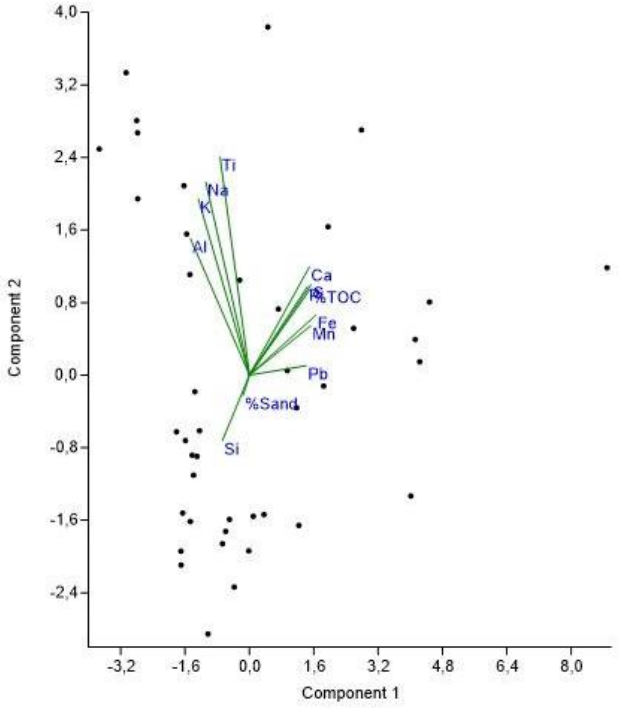

Fig. 4.38. *La Sierra Principal Component 1 vs Principal Component 2. The data set includes data from ICP, granulometry (% sand) and TOC (%)*

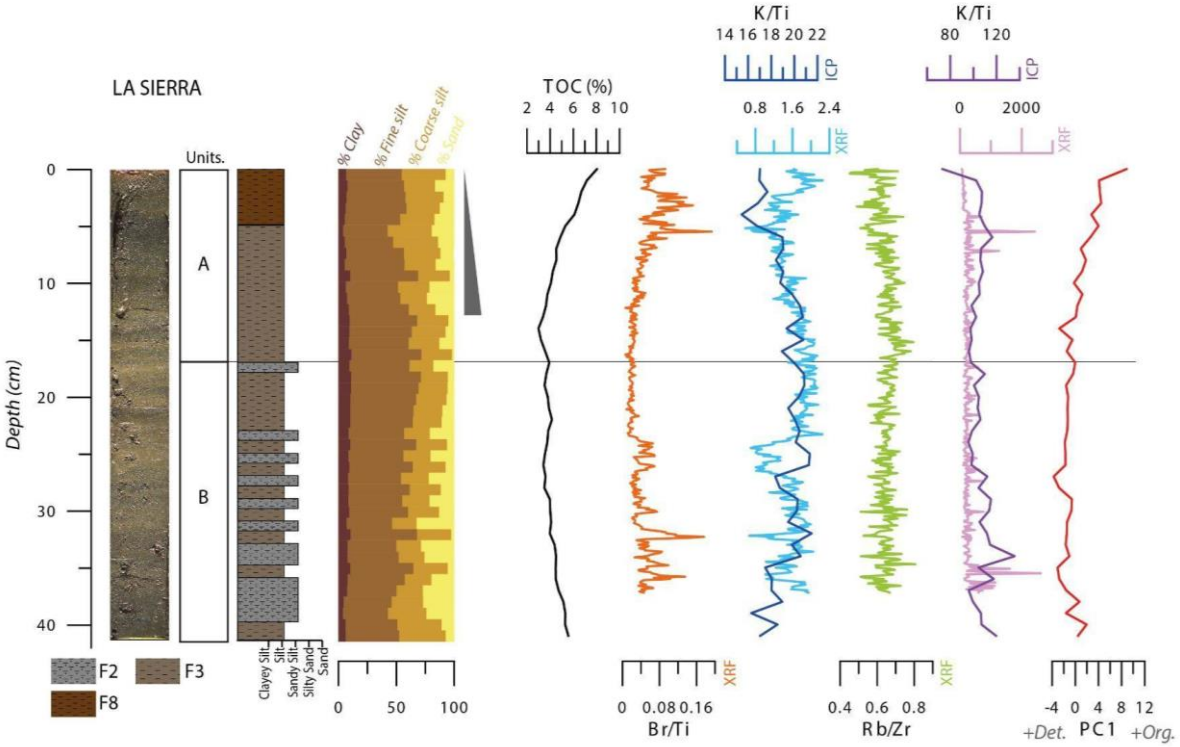

Fig. 4.39. *Core photo (REP-SIR17-3A-1G), sedimentary units, sedimentary facies, granulometry, Total Organic Carbon (TOC%), Br/Ti and Rb/Zr by XRF, K/Ti and Fe/Mn by XRF and ICP, Principal Component 1 (PC1).*

Sabocos

Sabocos is the only lake with carbonate facies. The lake is located at 1900 m asl in a carbonate watershed. The sedimentary sequence is divided into two units. Unit B (63- 23 cm) is only composed of facies 13 (Brown sandy silt, from laminated to banded, with the presence of carbonates) in layers several cm thick and ranging from silt to silty sand. Unit A (23-0 cm) starts with facies 12 (Brown sandy silts, laminated and with abundant carbonates), continues with facies 11 (Finely laminated brown sandy silts with abundant carbonates) and ends at the top with facies 10 (Finely laminated brown sandy silts with presence of carbonates and abundant OM).

Unit B has low and relatively constant TOC and TIC values, low Ca/Ti ratios, and low PC1 values indicating a higher detrital portion. In unit A, all these proxies increase, showing a higher organic fraction and an increase in carbonates.

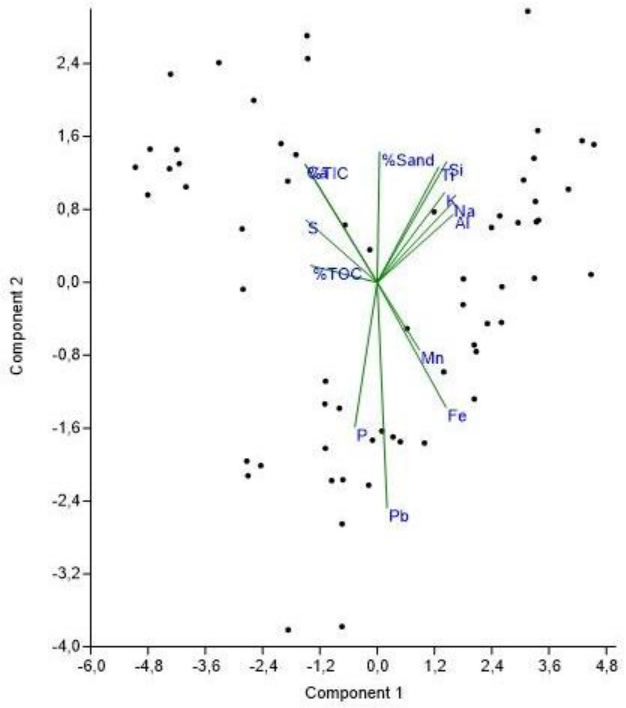

***Fig. 4.40**. Sabocos Principal Component 1 vs Principal Component 2. The data set includes data from ICP, granulometry (% sand) and TOC (%)*

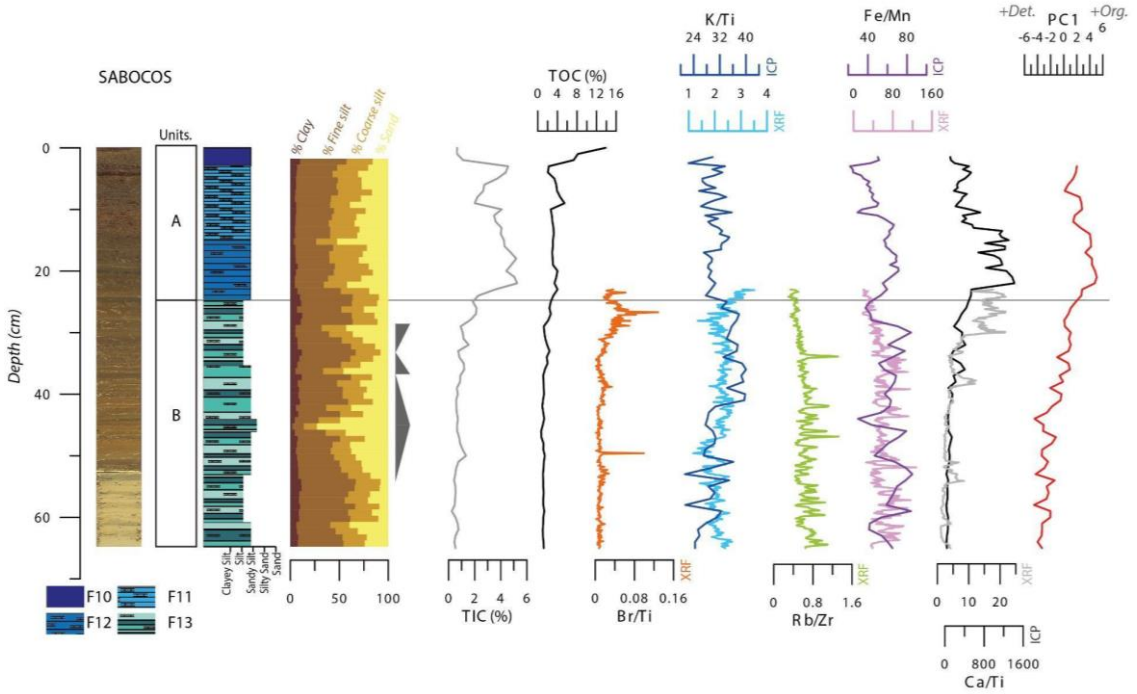

Fig. 4.41. *Core photo (SAB 18-2A-1G and SAB13-1B-1G-1), sedimentary units and subunits, sedimentary facies, granulometry, Total Inorganic Carbon (TIC%), Total Organic Carbon (TOC%), Br/Ti and Rb/Zr by XRF, K/Ti, Ca/Ti and Fe/Mn by XRF and ICP, Principal Component 1 (PC1).*

Acherito

Acherito is located at 1877 masl in a mixed carbonate and silicate watershed. The Acherito sequence included three facies and it is divided into two main units. The lower unit B (68- 19 cm) is an alternation of facies 7 (Light brown sandy silt, massive and with abundant MO), 8 (Massive grayish brown silt with plenty of MO) and 9 (Dark grayish brown sandy silt, banded and with abundant MO). Facies 9 is more abundant at the base of this unit while layers of facies 7 are thicker and more frequent towards the top of this unit. Unit A (19 – 0 cm) is exclusively composed by facies 8.

PC1 shows a lower organic component in unit B, and an increasing trend in unit A, paralleled with higher Br/Ti, and a decrease in Fe/Mn.

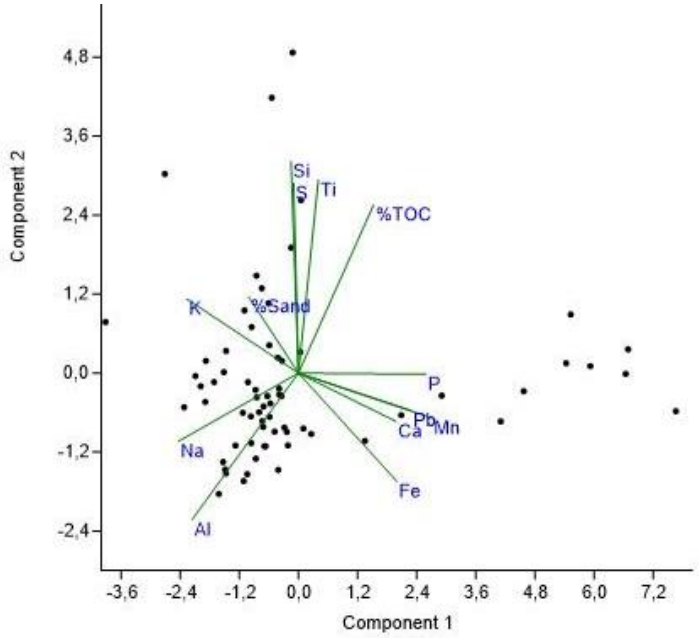

Fig. 4.42 *Acherito Principal Component 1 vs Principal Component 2. The data set includes data from ICP, granulometry (% sand) and TOC (%)*

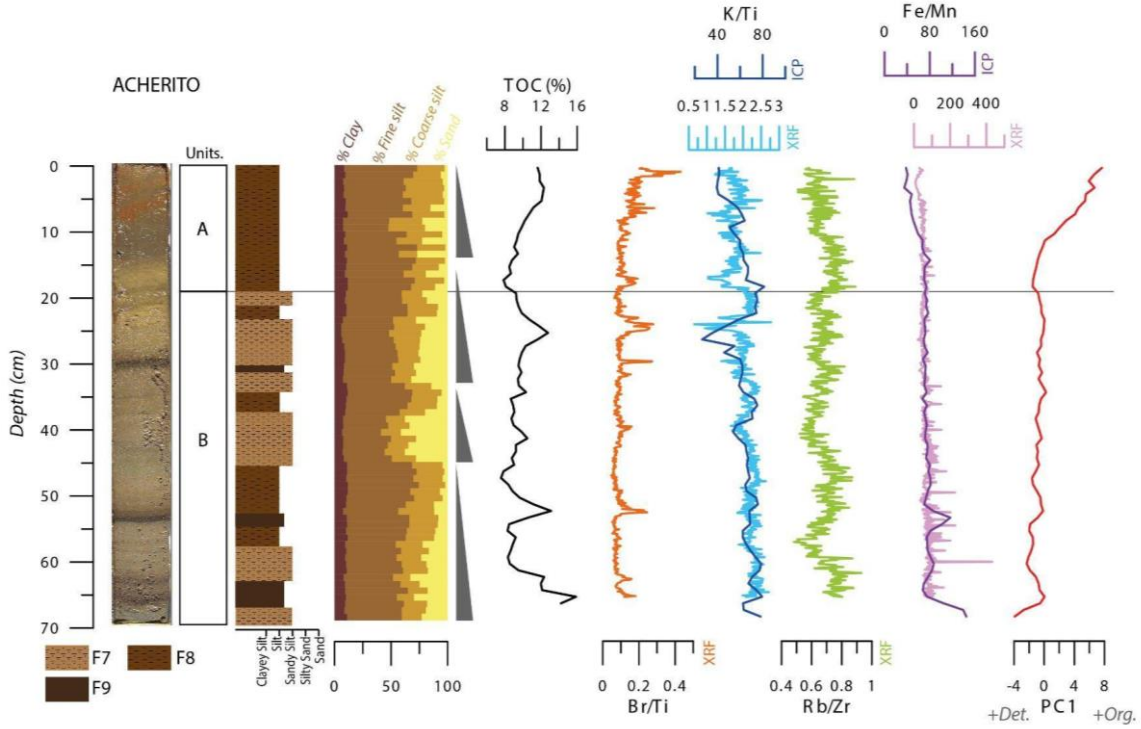

Fig. 4.43 *Core photo (REP-ACH17-1A-1G), sedimentary units, sedimentary facies, granulometry, Total Organic Carbon (TOC%), Br/Ti and Rb/Zr by XRF, K/Ti and Fe/Mn by XRF and ICP, Principal Component 1 (PC1).*

4.5. Facies associations and Depositional Model

4.5.1. Facies Associations

We group the 13 facies in 5 main facies associations:

Facies Association A: Sandy silt and silt, banded to massive with variable organic content. It includes F1, F2, F3, F7 and F8.
Interpretation: Distal deposition in siliciclastic lakes

Facies Association B: Rhythmites. It includes facies 6 and 13.
Interpretation: Seasonal deposition (ice covered- ice free) in high sedimentation rate siliciclastic lake

Facies Association C: Carbonate-rich banded sand and silt. It includes Facies 10 and 13.
Interpretation: Distal deposition in carbonate lakes.

Facies Association D: Carbonate-rich, laminated silt. It includes F 11 and 12.
Interpretation: Distal deposition in carbonate lakes with well developed charophyte - macrophyte meadows in littoral areas.

Facies Association E: Massive to banded, organic rich sandy silt and silt. It includes F7, F8 and F9.
Interpretation: Distal deposition in moderate productivity lakes.

Considering these facies associations, two main depositional facies model can be identified in Pyrenean lakes: i) clastic and ii) carbonate. Clastic lakes are divided according to sediment yield and organic productivity into four types: a) low organic productivity and low sedimentation rate (Cregüeña); b) low organic productivity and high sedimentation rate (Marboré); c) moderate organic productivity and low sedimentation rate (Urdiceto, La Sierra) and d) moderate organic productivity and high sedimentation rate (Acherito) (Figure 4.44).

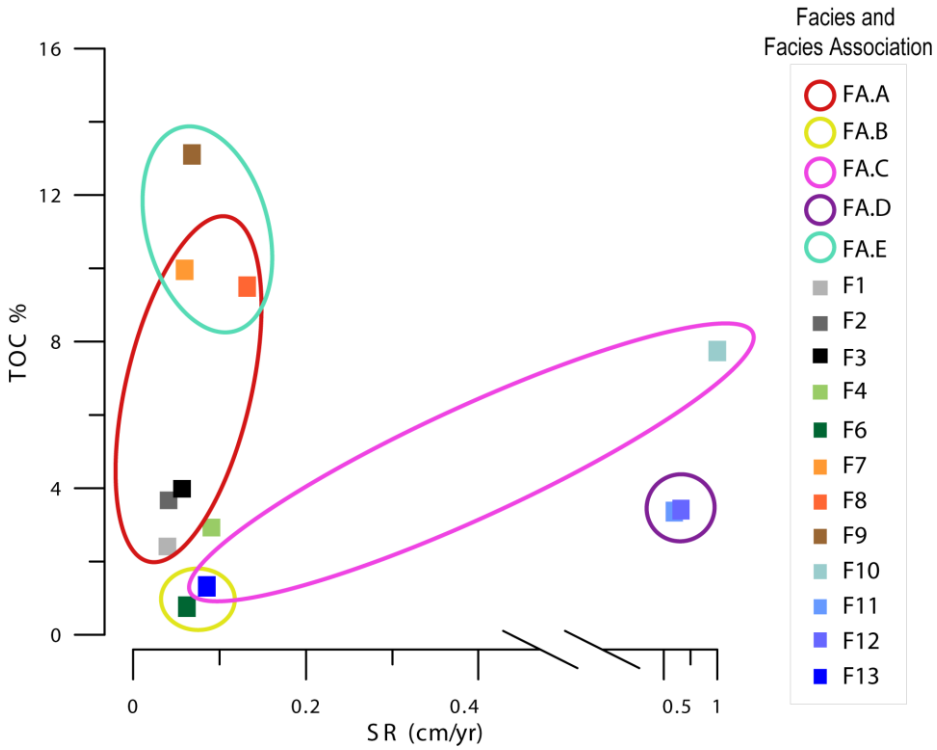

***Fig. 4.44**. Facies and facies association, according to sedimentation rate and average %TOC*

4.5.2 Depositional Models

Lake basins are originated by a multitude of geological processes: tectonic, aeolian, fluvial, glacial, volcanic, karstic, impacts, anthropogenic (Cohen, 2003; Renaut & Gierlowski-Kordesch, 2010). There are multiple lacustrine depositional models described in the literature (Cohen, 2003; W. Dean, 1981; W. E. Dean & Fouch, 1983; Eugster & Kelts, 1983; Gierlowski-Kordesch & Kelts, 2000; Kelts & Hsü, 1978; Renaut & Gierlowski-Kordesch, 2010). Some of the lacustrine depositional models studied in the literature are carbonate–rich lakes (Platt & Wright, 1991; Talbot & Allen, 1996; B. Valero-Garcés et al., 2014). There are case studies of high altitude, glacial and periglacial lakes (Catalan et al., 2002; Davaud & Girardclos, 2001; Kelts & Hsü, 1978; Moreno et al., 2011, 2012; Moscariello, 2021; B. Oliva-Urcia et al., 2018; Vegas, 2007a, 2007b), but not a synthetic model of high altitude mountain lakes.

In this section we integrate the facies described previously into several facies associations and depositional models for mountain lakes. The available sedimentary sequences from our lake transect are from relatively small lakes (0,013 – 0,445 km^2 surface area), shallow (less than 7 m) to deep (up to 98 m), but they occur in a variety of geographic (altitude from 1877 to 2633 m asl) and geologic (carbonate, silicate and

mixed bedrock) context. Current climate is of high mountain type (Cuadrat Prats & Martín Vide, 2007; García-Ruiz et al., 2015) and most watersheds have very thin soils and vegetation is very scarce.

Lake facies and sequences identified in this PhD are from distal areas. The open water-profundal environments include the transitional talus and the central, deepest, and relatively flat areas. Distal areas are characterized by deposition of massive to laminated fine-grained silt. The transitional talus is a narrow area characterized by steep morphology, and the occurrence of small mass movements as a result of sediment destabilization. Transport processes are dominant over sedimentation in this spatially-restricted environment. Slope instability in the talus is more common in deeper lakes with steeper morphologies (Cregüeña). In addition, turbidite currents frequently remobilize and erode talus sediments and bring the eroded material to distal areas. Littoral environments are characterized by coarser siliciclastic sedimentation and higher energy processes. Only in Sabocos, the littoral platform has been colonized by macrophytes and charophytes that produce large amounts of carbonates that are transported to the talus and the distal areas.

The lakes correspond to two main depositional systems:

i) siliciclastic lakes with low and moderate organic productivity and variable sedimentation rate

ii) carbonate lakes

Due to the fact that these facies have been identified and described in lakes with different depositional and limnological characteristics, they could be applied to other high mountain lakes.

4.5.2.1. Siliciclastic lake depositional model

Siliciclastic lakes are divided according to sediment yield and organic productivity into four types: i) low organic productivity and low sedimentation rate (Cregüeña); ii) low organic productivity and high sedimentation rate (Marboré); iii) moderate organic productivity and low sedimentation rate (Urdiceto, La Sierra) and iv) moderate organic productivity and high sedimentation rate (Acherito).

Grain size also discriminate facies in siliciclastic lakes:

Coarse clastic facies (gravel, sand and coarse silt size) occur in the littoral areas of the studied lakes, but they are almost absent in the distal areas.

Massive and Graded Facies are common in distal areas. In most lakes they occur as i) mm-thick laminae and ii) cm to dm thick layers. Coarse facies arranged in fining upward sequences represent deposition during flooding events (Urdiceto) or associated to turbidite currents after an earthquake (Cregüeña). The cm- to dm-thick layers show fining-upward textures, erosive basal surfaces with plant remains, and a sandy basal sub-layer. The sedimentological features of graded and massive facies are characteristic of turbidite-type or storm-related deposits (Mangili et al., 2007; Martín-Puertas et al., 2009; Moreno et al., 2008; Noren et al., 2002). The graded nature indicates deposition by turbidity currents that separate the coarse bed load from the fine grains in suspension. The coarse basal layer and the erosional surfaces likely result from underflow current processes (Sturm & Matter, 1978). Fine particles with a fining upwards texture would have been deposited by settling afterwards. The fine, massive texture of some facies indicates rapid deposition in distal areas of the lake of suspended clay-rich materials that were transported by creeks that drain the catchment during flooding episodes. These facies are similar to those described in alpine lakes (Wilhelm et al., 2012).

Finely laminated sediments (layers thinner than 1 cm) are the most characteristic lacustrine facies, but they are not common in high altitude mountain lakes. They vary in thickness and lateral extent (continuous to discontinuous) and form when sediment supply changes with time (seasonally, annually) and preservation conditions are met (Glenn & Kelts, 1991). These occur in Marboré, in a sequence of rhythmites, and in some intervals in Acherito.

There are three main facies associations (A, B and E) in siliciclastic lakes. The F.A A (Alternating sandy silt and silt facies, banded to massive with variable organic content) includes F1, F2, F3 (Fig.4.45), F7 and 8 (Fig.4.46). The facies distribution can be highly variable depending on the productivity of the lake and the sediment yield. At times of higher lake productivity, the facies with higher organic components (F7 and F8) dominate. On the contrary, at times of lower productivity, facies F1, F2 and F3 are most common.

The facies association E (Massive to banded, organic rich sandy silt and silt) represents deposition when biological productivity in the lake is higher. It includes F7, F8 and F9. The only lake with this association is Acherito. These facies associations may include layers of other “event” facies, such as F4 and F5, deposited due to flood events (F4) or after an earthquake (F5) (Fig. 4.45).

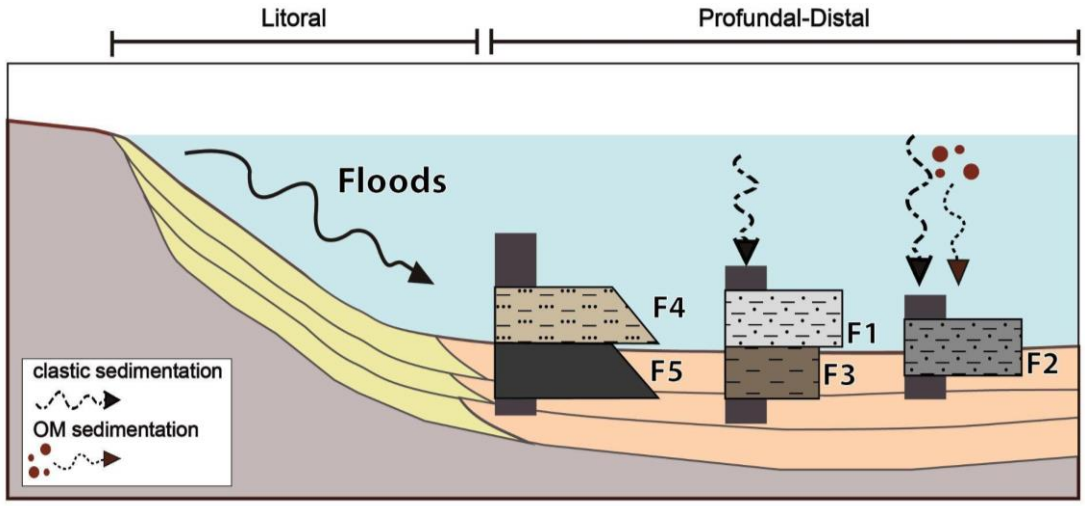

Fig. 4.45. *Depositional model of silicate facies in siliciclastic lakes with low organic productivity.*

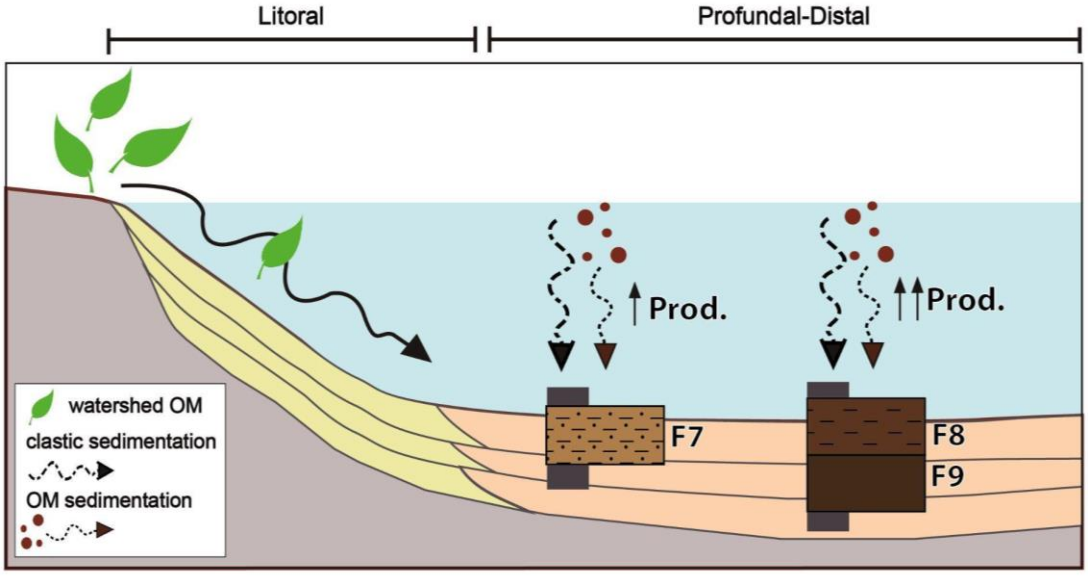

Fig. 4.46*. Depositional model of organic facies in siliciclastic lakes with higher organic productivity.*

Facies Association B (Rhythmites) includes laminated, clastic, carbonate-poor facies that only occur in Marboré. In this sequence, the Holocene sediments are composed of banded to laminated, carbonate-poor, coarse and fine silts. Carbonate content is low (TIC < 1 %) and composition is dominated by quartz and clay minerals,

with low organic matter content. Finer-grained laminae are lighter in color and coarser laminae are darker and with more Fe-bearing minerals, as biotites. Despite these lakes being placed in carbonate watersheds, TIC percentages are surprisingly low (2-3 %). Sedimentological and textural features of the Marboré facies are similar to proglacial lake sediments (Leonard & Reasoner, 1999; Ohlendorf et al., 2003). They are interpreted as rhythmites deposited in lakes fed by glacier meltwater with a strong seasonality: the calcite-rich, coarse silt laminae deposit during the melting season and the fine-grained clay-rich laminae during the winter, when the lake was ice-covered. Coarser laminae deposited during years with stronger melting pulses. In proglacial environments, better development of laminated sediments would occur during periods of stronger seasonality with higher melting and run-off discharges during spring and summer and longer ice-covered winters. More massive facies are finer-grained, clay-rich and with no carbonate. They would deposit during periods with less marked seasonality (colder summers), less available water for run off when only fine glacial sediment were mobilized ("glacial flour"). In the Iberian Peninsula we have other examples of glacially influenced lakes with siliciclastics rhythmite (Vegas, 2007a, 2007b). In another alpine lake (Enol), lower carbonate content in proglacial sediments is clearly associated with coarser sediment fraction (Moreno et al., 2011). In Marboré lamination reflects changes in annual clastic input to the lake and changes in the seasonality: coarse clastic materials are delivered to the lake during the summer and finer sediments are deposited during the ice-covered winter. (Fig.4.47)

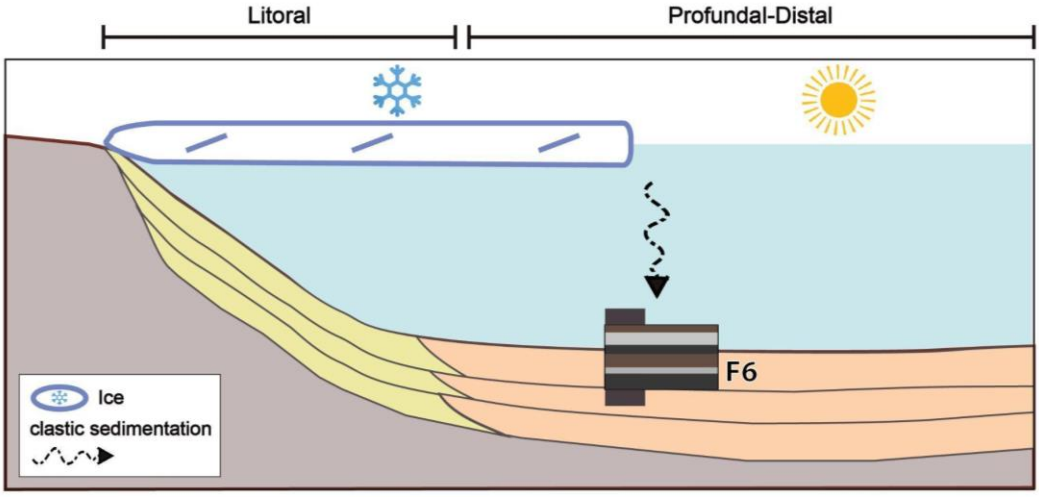

***Fig 4.47**. Depositional model of rhythmites in clastic lakes.*

4.5.2.2. Carbonate lake depositional model

Sabocos depositional model includes two Facies Association (F.A.):

- Facies Association C: Carbonate sand and silt. It includes Facies 10 and 13 and it is interpreted as distal deposition in carbonate lakes.

- Facies Associationn D: Carbonate, laminated silt with charophyte. It includes F11 and 12 and it is interpreted as distal deposition in carbonate lakes with well developed charophyte meadows in littoral areas.

Carbonate sediments in F.A C are composed of banded sand and coarse silt with variable carbonate content (coarse-silt calcitic detrital particles, charophytes), silicate minerals, macrophytes and terrestrial organic matter. Carbonates are biogenic grains (Chara fragments, carbonate coatings) and small crystals derived from the reworking of particles produced in the littoral environments and from the carbonate watershed.

Carbonate-rich sands and silts (FA C) are common facies in Iberian lakes (Barreiro-Lostres et al., 2017; González-Sampériz et al., 2020; Rull et al., 2021; B. Valero-Garcés et al., 2014; Vegas et al., 2006, 2010; Vegas-Vilarrúbia et al., 2022) but rarely occur in high altitude mountain lakes, even in carbonate terrains. In Enol, another high-altitude lake in a carbonate watershed in Picos de Europa, Holocene sediments are also carbonate-rich (López-Merino et al., 2011; Moreno et al., 2010, 2011; B. Oliva-Urcia & Moreno, 2019).

F.A. C reflects deposition in a distal environment closely connected to a carbonate-producing littoral environment with restricted clastic input from the watershed. The lack of sedimentary textures is interpreted as the result of bioturbation in well-oxygenated waters. (Fig. 4.48).

Finely banded to laminated carbonate silts (F.A. D) are deposited in more distal, relatively deeper and permanent or seasonally anoxic areas of Sabocos (Fig. 4.48). Finely banded sediments represent reworking and redeposition of the charophyte meadows and other carbonate-encrusted littoral formations. The generation of laminites requires variability in sediment supply over time (seasonality), anoxic hypolimnion and good preservation conditions (Glenn & Kelts, 1991).

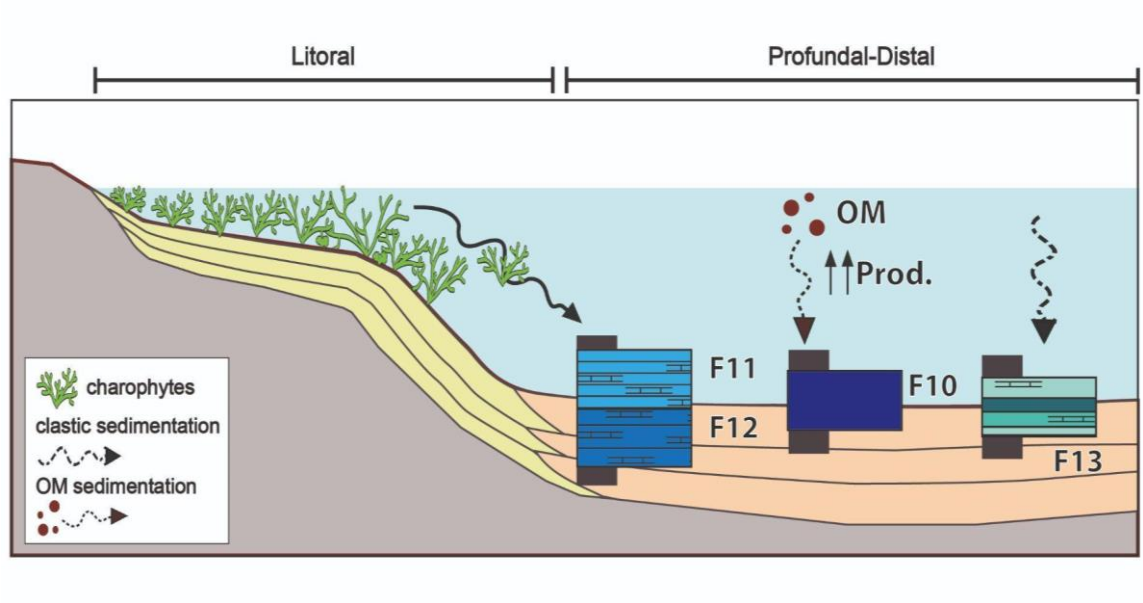

***Fig. 4.48**. Depositional model of carbonate facies in carbonate lakes.*

4.5.2.3 Controls on deposition in mountain lakes

Lake sediments greatly reflect the geology, hydrology and surface features of the watershed. The amount of sediments reaching the lake from the catchment depends on several factors: i) the size of the watershed, ii) the availability of erodible materials and iii) the existence of an organized drainage network. The availability of sediments in the catchment area is determined by the size of the watershed, geology, climate, vegetation cover and in more recent times, land uses and human impact. Lakes with smaller watersheds and not well-developed surface drainage network (ACH, URD) have lower clastic input to the distal areas, mostly as coarse materials from the littoral zones. Lakes with larger watersheds (CRE, SAB, SIE) have better developed clastic facies, both coarse and fine.

Pyrenean mountain lake sequences are characterized by a large variability of facies and depositional subenvironments. Several factors control sedimentation in these lakes, such as basin morphology, hydrology, thermal regime and sediment delivery to the lake (Morellón et al., 2009; B. L. Valero-Garcés & Kelts, 1995).

Lake morphology and glacier processes. Lake morphology determines the surface extent of depositional environments, particularly littoral versus distal, and the occurrence of talus des-stabilization processes in deep lakes such as Cregüeña.

Watershed. The geology of the watershed influences the type of clastic supply to the lake and the hydrochemistry of the waters.

Hydrology. In the lakes studied, water level has been a minor factor affecting the facies evolution, with the exception of the recent anthropogenic changes in Urdiceto. Hydrological balance and watershed geology greatly determine water chemical composition and dissolution processes of clastic carbonates. Rhythmites in Marboré have a very low carbonate content, in spite of the dominant carbonate composition of the rock formations and the moraines in the catchment. The Lateglacial and Holocene moraines in the catchment are carbonate - rich (up to 11 % TIC) while the laminated sediments are carbonate-free (< 0.1 % TIC). Recent studies show that the water column in Marbore Lake remains undersaturated with respect to calcite, being calcite unstable and therefore, tends to dissolve. The fluctuations found in the record would be the result of seasonal and pH variations in the water column (B. Oliva-Urcia et al., 2013, 2018; Sánchez España et al., 2018).

Climate. Climatic factors are key to explain surface processes responsible for clastic facies as an increase in storminess or higher precipitation is directly related to higher run-off or rapid floods events. Warmer periods may also increase the amount of organic matter reaching the lake and the productivity of the lake.

Water stratification. Lake depth is the main parameter controlling thermal stratification and development of anoxic conditions. The development of seasonal or permanent thermal stratification requires a minimum water depth of 6 m (Shaw et al., 2002). Water stratification may help to reduce oxygen content at the hypolimnion and cause anoxic conditions more prone to laminae preservation.

The depositional evolution in each lake during the last 2000 years will be summarized in Chapter 5 with the integration of the sedimentary facies analyses and the geochemical indicators.

4.6 Conclusions

Pyrenean mountain lakes are small lake systems with a large variability of facies and depositional subenvironments. Silicate minerals are main sediment components because of the dominant geology of the watersheds and the lake water hydrochemistry. The profundal- distal facies that show a large variability of banded and laminated facies. Endogenic carbonate formation occurs only in Sabocos Lake, mostly in the littoral areas, associated with charophyte/macrophyte meadows. Detrital input is a major contribution to the sediment budget in these lakes. The sedimentary sequences illustrate trends related to climate variability and human impact in the watershed.

The proposed Sedimentary Facies unifies the analysis of the sedimentary dynamics of mountain lakes in the Pyrenees, and allows comparing and reconstructing the processes of erosion, transport and sedimentation at the basin scale. Integration with other indicators is essential to use these records as archives of climatic and environmental variability on a regional scale.

Detailed sedimentary facies of these systems provides the framework to reconstruct past environmental and climate changes. These Pyrenean lakes may serve as facies analogs for larger systems and help to identify sources and processes controlling lacustrine deposition in modern lakes and pre-Quaternary lacustrine formations. The facies analyses and depositional models could help to detangle the endogenic and clastic contribution to sediment budgets. These depositional models provide a dynamic framework for integrating all paleolimnological data necessary to decipher the high-resolution paleoenvironmental information archived in these lake sequences.

5. Organic Carbon and Lithogenic Fluxes

Acherito Lake (July, 2018)

5. Organic Carbon and Lithogenic Fluxes

This chapter has been submitted to the journal Scientific Reports as a manuscript entitled "*Unprecedented recent regional increase in organic carbon and lithogenc fluxes in high altitude Pyrenean Lakes*" and co-authored by Alejandra Vicente de Vera, María Pilar Mata-Campo, Sergi Pla, Eduardo Vicente, Ricardo Prego, Matías Frugone-Álvarez, Josué Polanco-Martínez, Marcel Galofré and Blas Lorenzo Valero-Garcés and it is currently under second review.

5.1. Introduction

Lakes are a central component of the carbon cycle and several paleolimnological studies have shown organic carbon burial rate increases during the last centuries, although the causes for regional variability and the specific involved processes remain uncertain, as also the future scenarios (Anderson et al., 2013, 2020). At a global scale, recent changes in mountain lake dynamics have been related to climate variability, direct human impact in the watersheds (Battarbee et al., 2002; Catalan et al., 2002, 2013) and increased global deposition rates of nutrients (Galloway & Cowling, 2002), altering their structure, functioning and diversity (Penuelas et al., 2013) and causing eutrophication and pollution (Camarero et al., 2009; McLauchlan et al., 2013).

To assess the recent rates of response and vulnerability of ecosystems and territories to rapid shifts of the Earth System they have to be evaluated in the context of the Anthropocene (Crutzen, 2002) and the current Great Acceleration (Steffen et al., 2015) (GA). In particular, Mediterranean mountains face great environmental risks as temperature and precipitation regimes (IPCC, 2021) and human pressure increased (Barreiro-Lostres et al., 2015; Catalan et al., 2002, 2013) have changed during the last century. A clear example of such trends are documented in the Pyrenees where, since 1959, annual temperature has increased more than 1.6 °C and summer temperature more than 2.3 °C. The decrease in annual precipitation has been small (-2.5%, last 50 years) but winter rainfall events are now more frequent (OPCC, 2019).The high altitude lakes in the Pyrenees provide an opportunity to investigate the role of climate change and human activities in carbon and sediment dynamics, as past climate variability (Catalan et al., 2002, 2009, 2014; Corella et al., 2018; Giralt et al., 2017; Leunda et al., 2017; Morellón et al., 2012; Pérez-Sanz et al., 2013; Pla-Rabes & Catalan, 2005, 2011) and the history of human impacts are relatively well known (González-Sampériz et al.,

2017). Human activities had a restricted impact till the onset of the ca.12th century deforestation phase (González-Sampériz et al., 2017; Rull et al., 2021). The abandonment of traditional agropastoral activities has led to large socioeconomic changes since the mid 20th century, and currently, lakes provide numerous services for new infrastructure development for energy resources, ski resorts and tourism (García-Ruiz et al., 2020; González-Sampériz et al., 2017).

Some of the observed hydrological changes caused by recent climate change in the Pyrenees include melting glaciers and decreased snow cover (Vidaller et al., 2021), increased sediment dynamics (García-Ruiz et al., 2015) and ecological changes in high altitude lakes (Catalan et al., 2002, 2013). However, the absence of long-term series and high-resolution reconstructions along geographic transects have impeded the evaluation of the regional nature of these recent observations within the context of past periods of rapid change. To investigate the nature of recent changes in high altitude Pyrenean watersheds, we reconstruct past organic carbon and depositional dynamics in six high altitude (1870-2630 m asl) lakes along a West - East transect in the Pyrenees: Acherito (AC), La Sierra (SI), Sabocos (SA), Marboré (MA), Urdiceto (UR), and Cregüeña (CR). The selected lakes reflect the variety of Pyrenean lakes in terms of climate, geology, limnological properties and human impact. We evaluate their response during the last 1.2 ka to climate and human impact, and characterize the uniqueness of the Great Acceleration against the backdrop of the Anthropocene.

Historic human impact in the watersheds is varied. Medieval deforestation for grazing occurred in the upper Gállego (SI, SA) and Aragón Subordán (AC) valleys. UR was dammed in the 1930s and water depth increased from <10 m up to 25 m. A dam was also built in the 1940s in MA, but it was decommissioned early on, and it did not affect lake level. SA is close to a ski area built in the 1980s. All lakes are located above tree line and vegetation cover is scarce. Although all originated after the last deglaciation, glacier expansion documented by moraine deposition during the Little Ice Age (1200-1850 CE) only occurred in the CR watershed (Cía et al., 2005). MA watershed is not connected to the Monte Perdido Glacier but documentary evidence showed a smaller snow and ice accumulation in the NW shore till the mid 1950s (García-Ruiz et al., 2014).

5.2. Material and Methods

For a detail description of the material and methods used in this Chapter, see Chapter 2

Data used in is Chapter included Total Carbon (TC), Total Inorganic Carbon (TIC) and Total Organic Carbon (TOC) and $\delta^{13}C_{OM}$ in bulk organic matter analyzed at 1 cm resolution in the sediment cores. Quantitative chemical analyses (ICP) were performed in the composite sequences at 1 cm resolution. Samples for grain size analyses were measured with a MasterSizer 2000. Biogenic silica (BioSi) was measured every 4 cm using the wet-alkaline leaching technique and measured by the molybdate blue colorimetric method using an AutoAnalyser Technicon II. Photosynthetic pigments in bulk sediment were analyzed at the University of Valencia, Spain. Sediment samples for diatom analysis were processed at CREAF laboratories

TOC fluxes were calculated as:

TOC_{flux} = density * Sedimentation rate* %TOC.

Lithogenic Flux were calculated as:

L_{flux}= density * SR * (100 - %TOC -%TIC). [SR was obtained from the age models].

Age models were obtained combining ^{210}Pb-^{137}Cs techniques performed at St. Croix Watershed Research Station (Minnesota, USA) using gamma ray spectrometry and AMS ^{14}C dating, and the Bacon v2.5.8 Bayesian age-depth model implemented in the geoChronR package v1.1.6

PCAs were calculated with several datasets: i) a “Compositional PCA" (PC_{comp}) including compositional (TOC, TIC), geochemical (elements measured in ICP) and grain-size data (% sand), ii) “age-uncertain PCAs” were applied to two groups of variables: i) TOC_{flux}, C/N and $\delta^{13}C_{OM}$ and ii) L_{flux} and PCA_{comp}, iii) a “diatom PCA”, based on Hellinger transformation of diatoms counts using the R package Vegan (2.5-7)

Two statistical techniques were applied to the time series: 1) A cumulative sum (CumSum) of deviations of the mean and 2) the change point (CP) method based on the use of GAMs (Generalized Additive Models).

5.3. Results

5.3.1. Altitudinal transect of lake depositional systems

The sedimentary sequences have been analyzed using a multiproxy approach including detailed sedimentological, compositional, geochemical, and isotope analyzes. Age models based on ^{210}Pb, ^{137}Cs, and ^{14}C dates were obtained with Bayesian age-depth models (Blaauw & Christen, 2011; McKay et al., 2021). The sedimentary sequences of the lakes with the main proxies are shown in figure 5. 1. A, B, C.

Deposition in **Acherito** is characterized by organic-rich silt facies 7, 8 and 9, more organic-rich during warmer periods (MCA) and with more intercalated coarser clastic facies during colder periods (LIA). A transition to sediments to lower C/N started around 1400 CE and led to minimum values between 1500-1650 CE, a period with lower BioSi (1500-1650 CE), maximum $\delta^{13}C$ values, and a peak in Chlorophyll (around 1700 CE). Two other periods with decreasing C/N intervals occurred around 1800 – with synchronous $\delta^{13}C$ positive excursion, higher Br/Ti and no changes in chlorophyll- and during the GA, with a decreasing $\delta^{13}C$ trend and a peak in chlorophyll and Br/Ti.

La Sierra sequence is characterized by an alternation of coarser and finer silts, with higher frequency of coarser silt layers during the LIA and finer, more organic-rich deposition since 1850 CE. The lower unint B with facies 2 annd 4 shows a decreasing trend towards the top of the unit. The interval with the highest C/N values and MS suggest higher watershed disturbance during 1200-1650 CE. Both Br/Ti and chlorophyll have higher values during warmer periods as the MCA and since 1850 CE. The top unit A composed of Facies 3 and 9 shows a large increase in TOC content and a Fe/Mn decrease. The $\delta^{13}C$ showed a sharp negative trend since mid 20^{th} century with decreasing C/N values.

The **Sabocos** sequence is the only with carbonate facies. The basal unit B is composed of facies 13 and coarser carbonate silts deposited during the LIA compared with finer silts during the MCA and since the end of the LIA. The largest changes occurred during the 20^{th} century with deposition of facies 12, 11 and 10. The last decades showed an exponential increase in Br/Ti and PC1 and a negative $\delta^{13}C$ excursion. C/N reaches the highest values (up to 35) between 1950-2013 CE and slightly decreases afterwards up to 9. After 1980, finely laminated facies 11 deposited in the deepest areas suggesting more dominant anoxic conditions. During the last decades, an increase in charophyte

and macrophyte meadows could have acted as a sediment trap and reduce coarse sediment delivery towards the deepest part of the lake.

In **Marboré**, finely laminated facies 6 were deposited during the last two millennia. The second part of the LIA (1600-1850) had higher Br/Ti. The end of the LIA is a period of rapid change marked by higher PC1, positive C/N and Ch excursions). The chlorophyll profiles show increased productivity during the MCA and the transition to the LIA (1000-1300 CE) - with no changes in C/N and $\delta^{13}C$ - and during the 1800s (with higher C/N and lower $\delta^{13}C$). Deposition during the GA is characterized by higher Br/Ti, lower PC1 and chlorophyll, moderate C/N values and a very large positive $\delta^{13}C$ excursion with a subsequent decrease.

In **Urdiceto** the lower unit (B) is an alternation of Facies 1, 2 and 4 with low TOC values, although with some variability, and the PC1 indicates dominant clastic processes. Coarse layers deposited during the LIA. Chlorophyll shows higher values during 1500-1700 CE and 1800-1930 CE and lower during the last phase of the LIA and the GA. The end of the LIA is marked by an increase in some productivity indicators (Br/Ti and $\delta^{13}C$). The largest C/N positive excursion corresponds to the watershed disturbance during the dam construction in the early 1930s; a secondary peak around 1500 CE points to some watershed disturbance during medieval times. The GA is marked by relatively high but decreasing C/N, the lowest $\delta^{13}C$, increasing BioSi values and relatively low chlorophyll.

The **Cregüeña** sequence comprises fine massive silts (F1 and F2) with low organic content and an intercalated 7 cm thick fining upward layer (F5), deposited around 1370 CE. This layer is interpreted as a co-seismic turbidite caused by the largest historical earthquake in the central Pyrenees, the Ribagorza earthquake (1375 CE). Chlorophyll values are higher during warmer periods: IRHP, MCA and the last century and relatively lower PC1 values occurred during 500 - 1300 CE and since the end of the LIA. The largest decrease in C/N values started just before the deposition of the turbidite and accelerated in the second phase of the LIA, after 1550 with more positive values of PC1. The changes in Biogenic silica demonstrate a further increase in diatom productivity in the lake after the LIA. The two periods with the lowest C/N values correspond to ca. 1600 CE (secondary peak in chlorophyll) and the Great Acceleration. The $\delta^{13}C$ shows little variability prior to 1000 CE, increasing values up to 1500, and decreasing since then, particularly during the GA. The interval with the less negative $\delta^{13}C$ values corresponds with the lowest C/N values around 1500- 1650 CE, likely associated to changes in organic matter source. Biogenic silica identifies the LALIA, the

second half of the LIA and the GA as the periods with higher diatom productivity. The last 50 years are characterized by increasing TOC, decreasing $\delta^{13}C$ and C/N and increasing BioSi.

In AC, SI, CR and UR, deposition is dominated by silt facies with some intercalated coarser facies, more frequent during the Little Ice Age (LIA) and with finer, more organic-rich facies since 1850 CE. In MA, rhythmite facies deposited during the last two millennia, reflecting the dominance of seasonal ice cover dynamics. Dam construction in the early 1930s in UR favored finer deposition in the profundal area since then; however, no significant impact was detected in MA after dam construction in the 1940s. The CR sequence comprises an intercalated 7 cm thick fining upward layer, interpreted as a co-seismic turbidite caused by the largest regional earthquake during the last millennium (the Ribagorza earthquake, 1375 CE). The SA sequence is the only one with carbonate facies, but it also shows coarser silts during the LIA and finer silts since then. In this lake, a depositional change occurred after the 1980s, with more carbonate –rich facies in the littoral areas and finely laminated facies in the deepest areas, suggesting expansion of the charophyte and macrophyte littoral meadows and dominant anoxic conditions in the profundal areas.

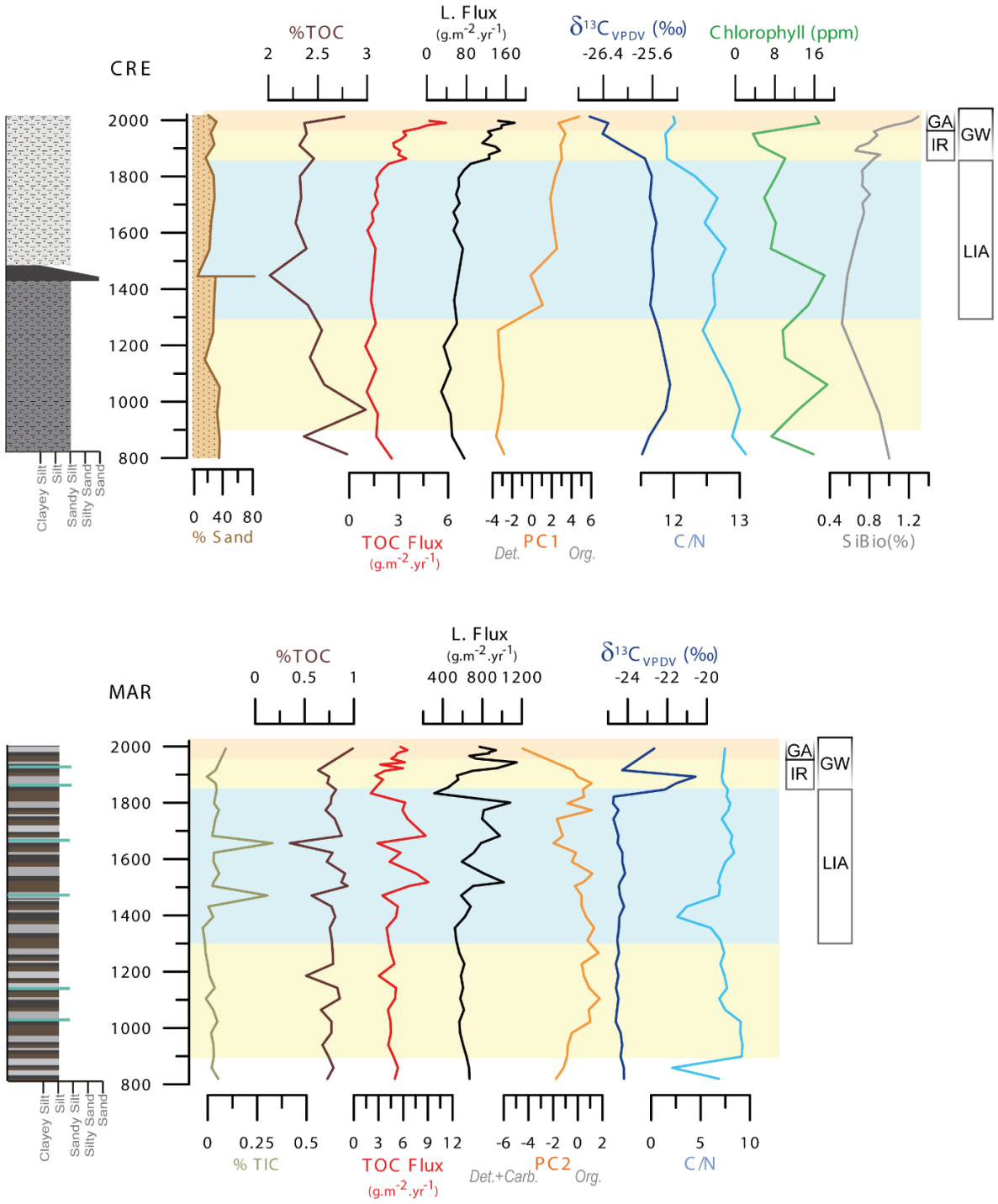

Fig. 5. 1.A *Sedimentological facies (see description in table S.2), % sand (light brown), %TOC (dark brown), %TIC (dull green), TOC flux (red), Lithogenic flux (black), $PC1_{comp}$ (orange), $\delta^{13}C_{om}$ (dark blue), C/N (light blue), chlorophyll (green) and biogenic silica (gray) from Cregueña and Marboré. Climate phases (Little Ice Age, LIA Recent Global Warming, GW) and global change phases (Industrial Revolution, IR and Great Acceleration, GA) are also indicated.*

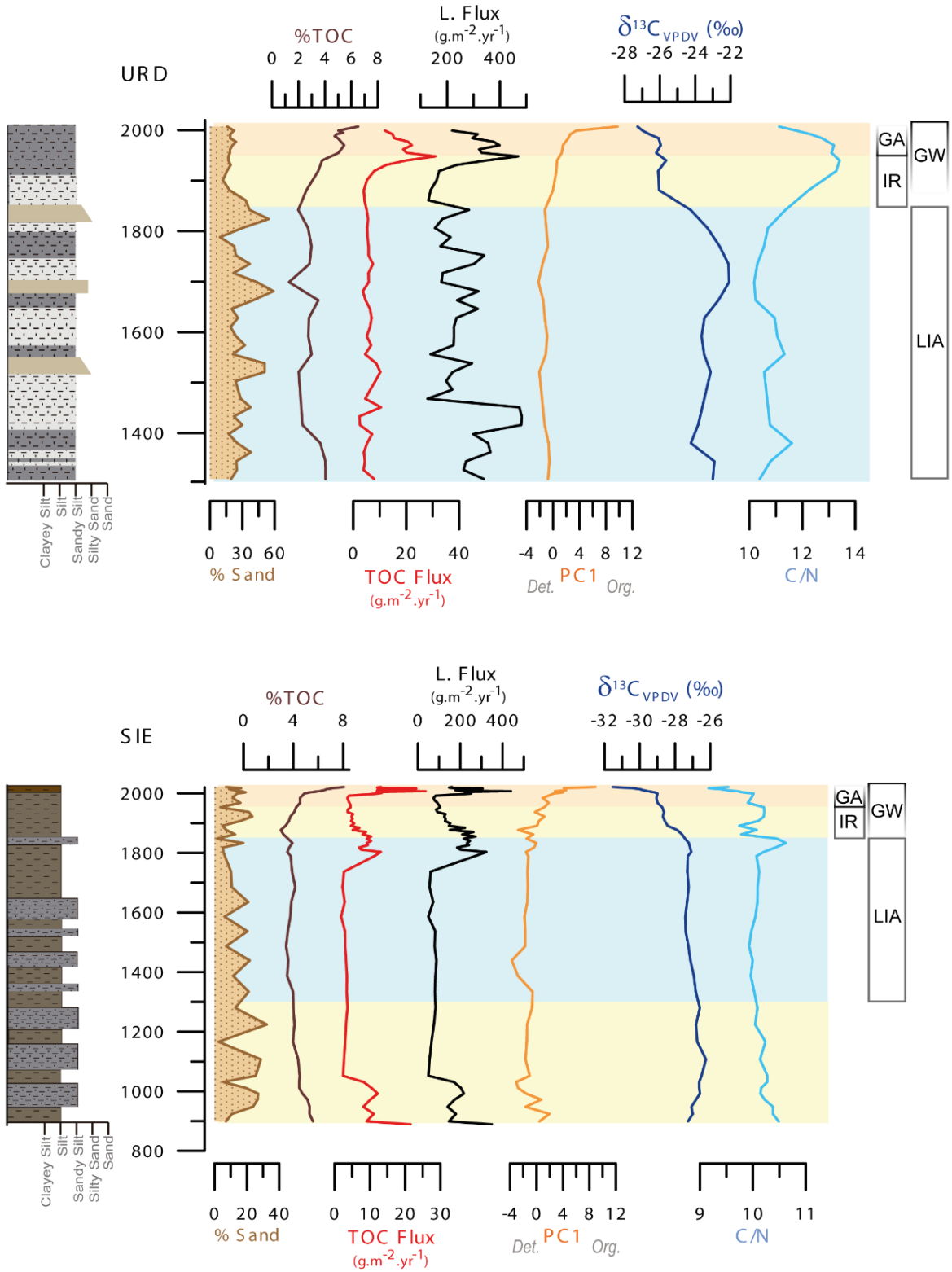

Fig. 5.1.B *Sedimentological facies (see description in table S.2), % sand (light brown), %TOC (dark brown), TOC flux (red), Lithogenic flux (black), $PC1_{comp}$ (orange), $\delta^{13}C_{om}$ (dark blue) and C/N (light blue) from Urdiceto and La Sierra. Climate phases (Little Ice Age, LIA Recent Global Warming, GW) and global change phases (Industrial Revolution, IR and Great Acceleration, GA) are also indicated.*

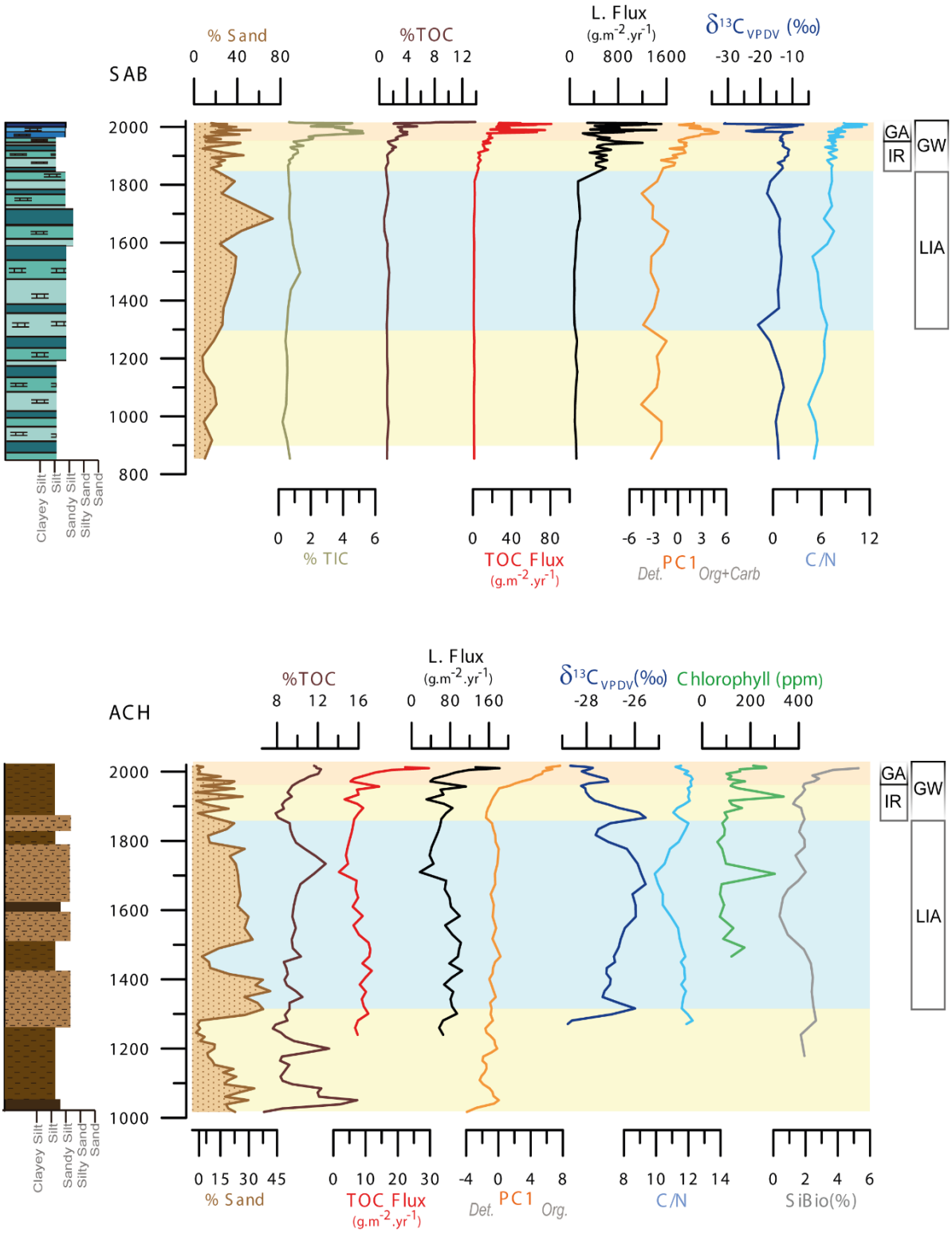

Fig. 5.1.C *Sedimentological facies (see description in table S.2), % sand (light brown), %TOC (dark brown), %TIC (dull green), TOC flux (red), Lithogenic flux (black), $PC1_{comp}$ (orange), $\delta^{13}C_{om}$ (dark blue), C/N (light blue), chlorophyll (green) and biogenic silica (gray) from Sabocos and Acherito. Climate phases (Little Ice Age, LIA Recent Global Warming, GW) and global change phases (Industrial Revolution, IR and Great Acceleration, GA) are also indicated.*

5.3.2 Lithogenic flux, Organic Carbon flux and depositional and productivity proxies

The following formulae have been used to calculate the fluxes:

$$TOC_{flux} = density * Sedimentation\ rate * \%TOC.$$

$$L_{flux} = density * SR * (100 - \%TOC - \%TIC).\ [SR\ was\ obtained\ from\ the\ age\ models].$$

Lithogenic fluxes (L_{flux}) calculated from sediment traps are between 20 and188 g m^2 yr^{-1} in silicate-dominated basins, and higher in carbonate basins (up to 544 g m^{-2} yr^{-1} in MA). Fluxes calculated from the first cm of the sediment cores range from 132 to 219 g m^{-2} yr^{-1} in lakes located in silicate watersheds (CR, UR, SI, AC), and they are larger in carbonate – dominated watersheds (1274 in SA, 772 g m^{-2} yr^{-1} in MA). Flux trends calculated from the sediment sequences directly reflect the age models, and consequently they have variable uncertainties and time-resolution during the last 1200 years. L_{flux} plots with the associated time uncertainty (Fig. 5.2) show large variability for the last 1200 years. In this study, we focus on the last 200 years, as the age models for our sequences are more robust for this period. L_{flux} for SI shows a high value pre-LIA phase coherent with the medieval human impact in the Gállego valley (González-Sampériz et al., 2017). UR and AC have moderate to high L_{flux} during the first part of the LIA. Both MA and SI have high sediment fluxes prior to the end of the LIA, contrary to AC and UR. SA and CR do not show significant changes prior to 1850 CE. In spite of this variability, all lakes show a change in L_{flux} patterns after 1850 CE and the highest L_{flux} at some point during the last 200 years. SI values increased at the end of the LIA and since 1950, but lower values occurred during 1850-1950. MA shows an abrupt decrease at the end of the LIA and a recovery in the 20th century. UR fluxes were the highest during dam construction (ca. 1940) but the values remained high during the last decades. In spite of the different nature of the depositional processes and the expected variability among all lakes, late 20th century L_{flux} values were among the highest fluxes observed in all records.

The periods with higher sediment fluxes prior to 1850 CE are coherent with changes in sedimentary facies, as they correspond with coarser sediments and more frequent coarser layers deposited during some phases of the LIA. To obtain a geochemical proxy of sediment input we calculated a “Compositional PCA " including TOC, TIC, geochemical (all elements measured by ICP) and grain size (%sand) data (Fig. 5.1.A,B,C). The first $PC1_{comp}$ explains up to 53% of the variance. We interpret this

first principal component as related to changes in the lithogenic composition of the sediments. Lakes at lower altitude show a relatively greater detrital component in the sediments before 1850 CE, followed by an abrupt increase in the organic component, particularly marked since the mid 20th century. The two lakes at higher altitudes show somewhat different patterns: CR trends are similar, but with smaller ranges, and in MA, $PC2_{comp}$ better reflects the silicate component, although it only explains 25% of total variance.

The TOC_{flux} based on sediment trap data ranges between 2.8 g m^{-2} yr^{-1} (CR) to 46 g m^{-2} yr^{-1} (AC), and the values are similar to those calculated from core-top sediment samples (from 4.8 g m^{-2} yr^{-1} in CR to 49 g m^{-2} yr^{-1} in SA). Sediment traps have higher TOC content and lower C/N (5-15) and $\delta^{13}C_{OM}$ (-33‰ to -25‰) values than surface and downcore sediment samples. The TOC content in the lake sediments ranges between 0.06 (MA) and 13% (AC). TOC_{flux} and L_{flux} trends are similar, with generally lower TOC_{flux} values prior to 1850 CE, and the most prominent changes associated to the LIA and the GA. TOC_{flux} are high in early medieval times (SI) and during some phases of the LIA (AC, MA, UR). The 1850 CE transition is marked by an increase in TOC_{flux} in three lakes (AC, CR, SA), a decrease in MA and SI and no changes in UR. However, values during the GA are the largest in all cases. The largest increase in TOC_{flux} occurred in the 1970s in SA (from 14 to 66 g m^{-2} yr^{-1}) and even though it has decreased afterward, still remained high (> 40 g m^{-2} yr^{-1}).

In SI, the largest change occurred around 1980 CE (from 4 to 12 g cm^{-2} yr^{-1}). In CR, after a small increase in TOC_{flux} around 1850 CE, it also intensified during the GA (from 3,1 to 4,9 g m^{-2} yr^{-1}). MA is the only lake with similar values during the GA (4,5 to 6,5 g m^{-2} yr^{-1}) and the LIA (2 to 9 g m^{-2} yr^{-1}). The highest values in UR occurred after the damming in the 1940s (from 12 to 31 g m^{-2} yr^{-1}) and although later decreased, still remained at relatively high values (Fig. 5.2).

The TOC_{flux} trends are coherent with other organic proxies such as C/N molar ratio, $\delta^{13}C_{OM}$ in bulk organic matter, diatoms, biogenic silica (BioSi) and chlorophyll. Our survey shows that soil and watershed vegetation have higher C/N values with high variability (12-70) and a relatively small $\delta^{13}C_{OM}$ range (-30‰ to -25 ‰), while lake sediments and Particulate Organic Matter (POM) samples have the lowest C/N ratios (mainly from 6 to 15, except for SA sediments that reach values of up to 35) (Fig. 5.3).

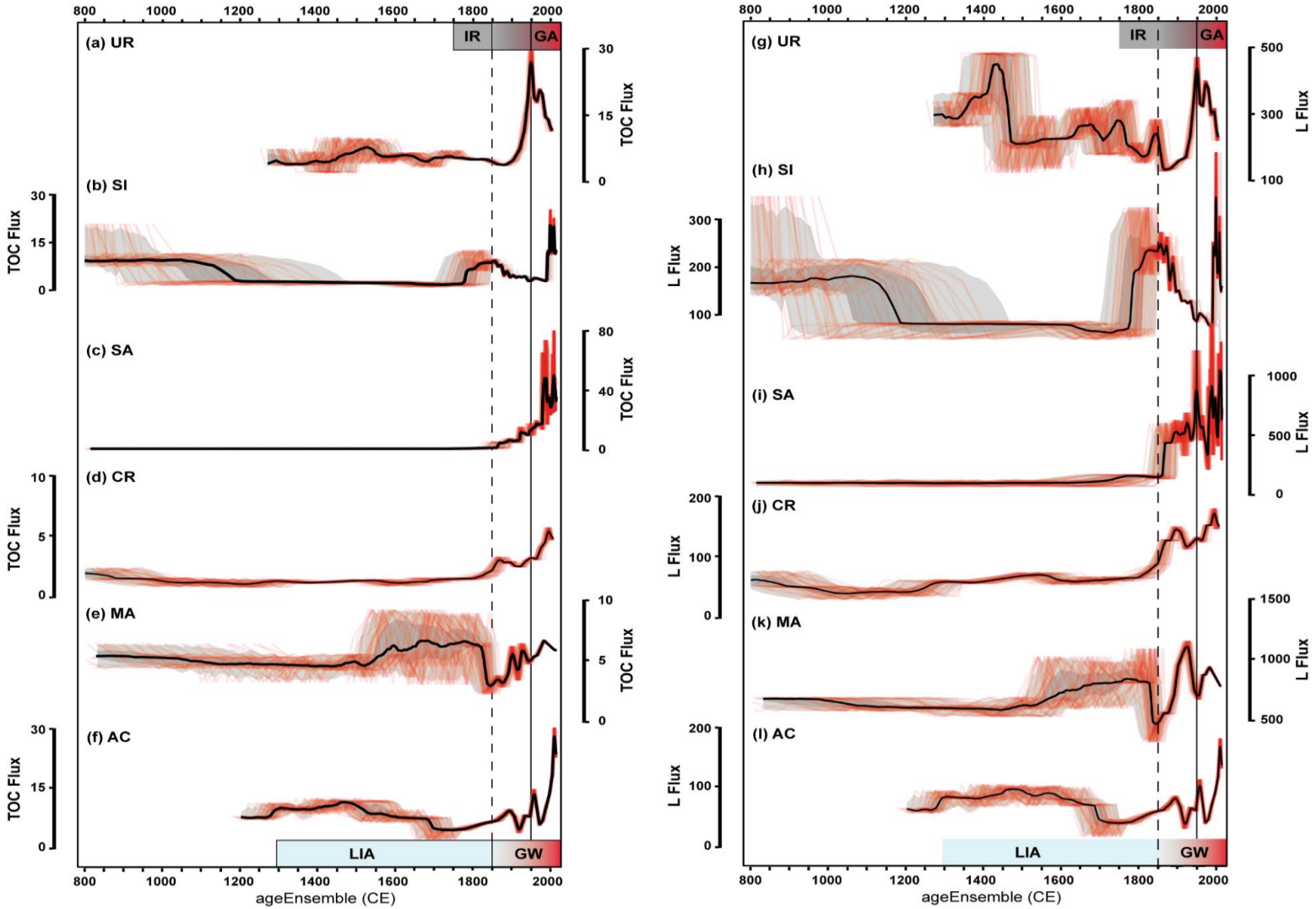

Fig. 5.2. *Lithogenic and TOC fluxes for the last 1200 years in the studied lake sequences. The climate phases (Little Ice Age, LIA Recent Global Warming, GW) and the global change phases (Industrial Revolution, IR and Great Acceleration, GA) are also indicated. Shaded areas reflect the uncertainty of the age models.*

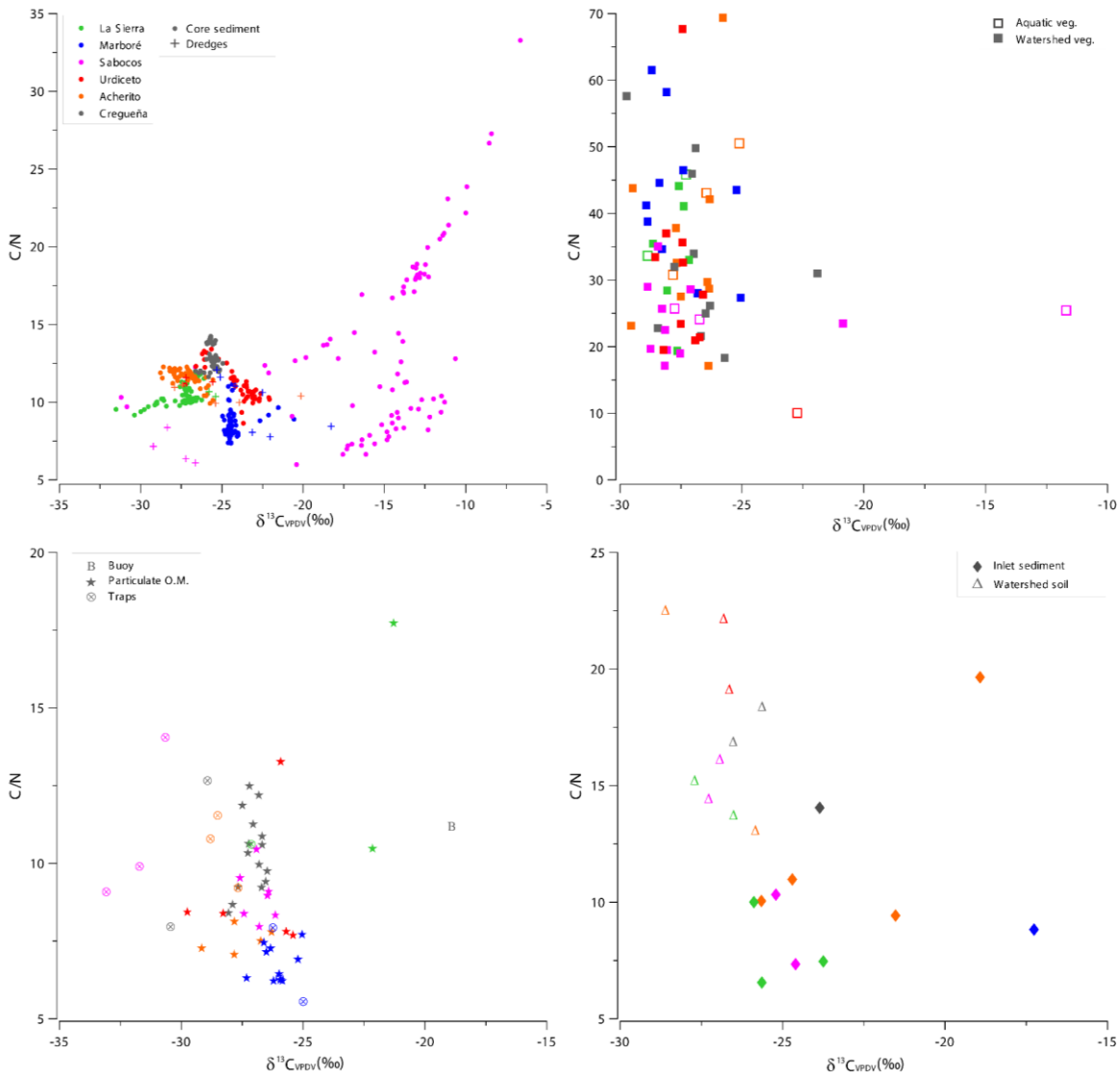

***Fig 5.3**. C/N vs δ¹³C (‰) for each lake considering sample type (core sediment, buoy, POM, sediment traps, dredges, aquatic vegetation) and for each watershed (vegetation, sediment and soil).*

CR has the highest C/N values and MA the lowest. The complexity of organic matter sources (Meyers and Teranes, 2002) is illustrated by the varied trends in C/N ratios in the lakes along the last 1200 years and particularly during the last 2 centuries. However, compared with pre-industrial values, C/N values are lower in the 20th century and some show decreasing trends (UR, CR, SI, AC), except in carbonate-watershed lakes with no trend (MA) or increasing values (SA).

The lowest $\delta^{13}C_{OM}$ values correspond to sediment traps (-33‰ to -25‰), lake sediments (-26‰ to -17‰) and POM (-30‰ to -25‰). Aquatic and terrestrial vegetation have similar $\delta^{13}C_{OM}$ values, but aquatic samples have relatively lower C/N values than

terrestrial, although the range is large (10-50). Soil samples have lower C/N values (12-23) than terrestrial and aquatic vegetation, but similar $\delta^{13}C_{OM}$ signatures as sediment and vegetation samples. Sediments collected in the creeks feeding the lakes have relatively low C/N values (5-20) and more positive $\delta^{13}C_{OM}$ (-26‰ to -17‰). A sample from a biofilm in CR buoy has the highest $\delta^{13}C_{OM}$ value (-18‰). Most lake sediment samples – except SA – plot in the same $\delta^{13}C_{OM}$ (-32‰ to -20‰) *vs* C/N (7-15) graph, but each lake has a distinctive distribution (Fig. 5.3). Higher altitude lakes have relatively higher $\delta^{13}C_{OM}$ (UR>MA>CR) than lower altitude sites. SA samples have the largest C/N (5 to 35) and $\delta^{13}C_{OM}$ ranges distributed in two distinct populations with some of the highest $\delta^{13}C_{OM}$ values (up to -7‰). Among the other sites, small, shallow SI has the largest $\delta^{13}C_{OM}$ range (-32‰ to -26‰). MA and UR also have large C/N ranges and among the highest $\delta^{13}C_{OM}$ ranges (-27‰ to -21‰). CR and SI have relatively more negative $\delta^{13}C_{OM}$ values (-29‰ to -25‰). In spite of the $\delta^{13}C_{OM}$ variability in each lake during the last 1200 years (Fig. 5.1. A, B ,C) all time series (except MA) show a conspicuous decrease trend starting mid 19th century (end of the LIA) and intensifying since the mid 20th century. In CR, the $\delta^{13}C_{OM}$ decrease is about 1 ‰ associated with rather constant C/N values. UR had a larger $\delta^{13}C_{OM}$ decline (-6 ‰) but started earlier (around 1700 CE) with an increasing C/N till 1950 and decreasing afterwards. SI also has a large $\delta^{13}C_{OM}$ decline (-6 ‰) associated with variable but decreasing C/N values. AC showed a -2 ‰ decrease with lower C/N values during the GA. Carbonate lakes showed a different behavior: SA had an increasing $\delta^{13}C_{OM}$ (6 ‰) during the IR and a large decline with abrupt shifts (up to 20 ‰) during the GA. MA also showed increasing $\delta^{13}C_{OM}$ (up to -4 ‰) between 1850 and 1950 and then decreasing during the GA with little changes in C/N. Some of the observed decline in $\delta^{13}C_{OM}$ during the last two centuries could be due to the documented decrease in $\delta^{13}C_{OM}$ value for atmospheric CO_2 from pre-industrial (-6.4‰) to recent times (-8.4‰ in 2014) ("Suess effect") (Keeling et al., 2016). However, as the $\delta^{13}C_{OM}$ range in our data set is larger (from 1 in CR, to 20 ‰ in SA) it is likely that other factors (OM sources, changes in productivity rates, and exchange with atmosphere) (Gu et al., 2006; Teranes & Bernasconi, 2005) have contributed to these recent patterns.

Diatom assemblages have been analyzed in surface sediments of all lakes and four core sequences (AC, MA, SA and CR), although diatoms were poorly preserved in MA. The CR, AC and SA diatom records show recent rapid changes in diatom assemblages. All three records started with benthic and thycoplanktonic taxa dominance, but all three lakes show an unprecedented recent increase in small planktonic diatoms (*Cyclotella spp., Discotella spp., Pantocsekiella spp.* and planktonic

Fragilaria spp.) (Fig. 5. 4. A, B, C). Biogenic silica and chlorophyll content have been measured in AC and CR sequences (Fig. 5. 4.A, B, C). Both have lower values in the high altitude, silicate watershed site (CR<1.5% BioSi, 18 ppm chlorophyll) and higher in the intermediate altitude AC (BioSi up to 6% and 337 ppm chlorophyll). Both sites show increasing BioSi since 1950 reaching the highest values in the records at the top of the sequence. Chlorophyll concentrations have also been higher since 1950, but there were similar prior peaks in CR and even with larger values in AC (Fig. 5. 4.A, B, C).

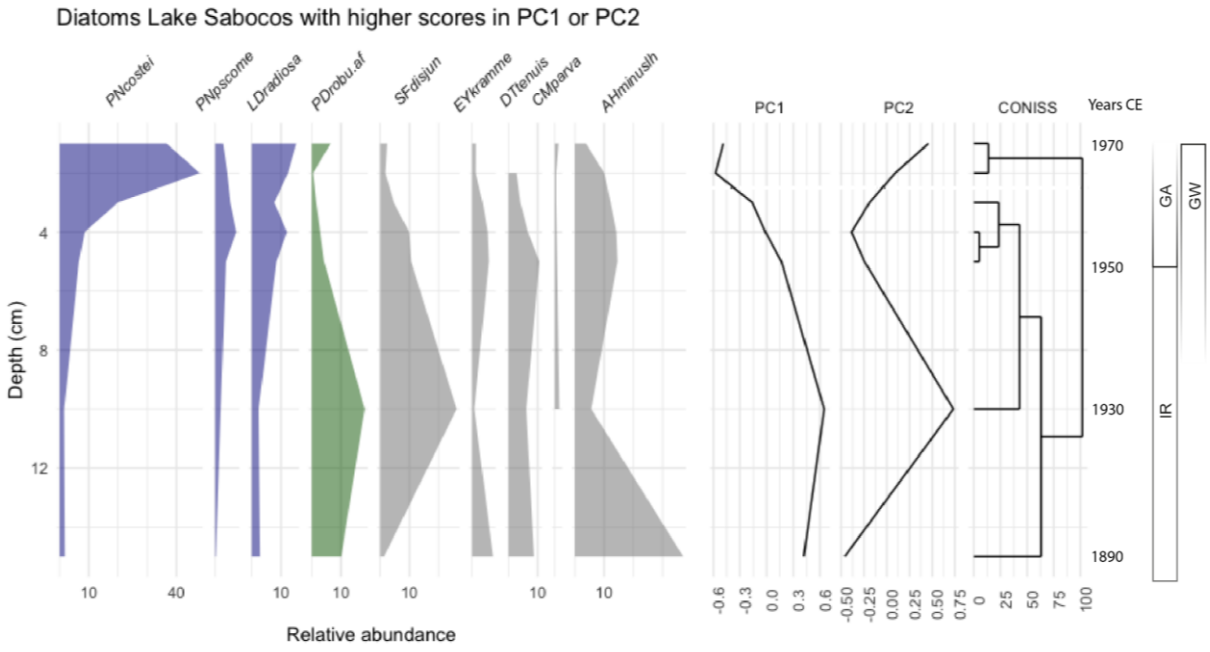

Fig. 5. 4. A. *Diatom stratigraphy for Sabocos (SA) sequence. The climate phases (Recent Global Warming, GW) and the global change phases (Industrial Revolution, IR and Great Acceleration, GA) are also indicated.*

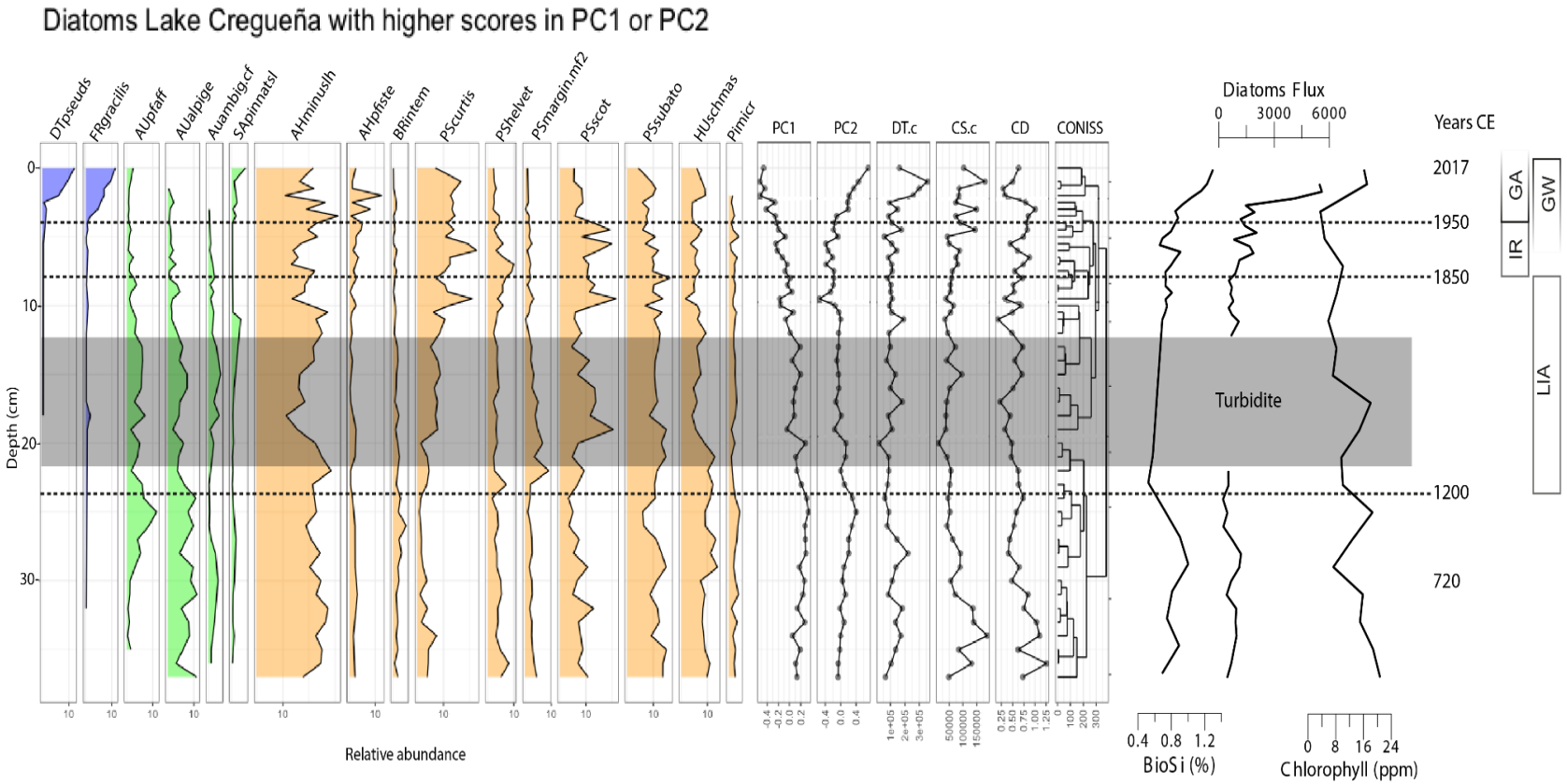

Fig. 5. 4. B*. Diatom stratigraphy, diatom flux, biogenic silica (%), and chlorophyll (ppm) for Cregueña (CR). The climate phases (Little Ice Age, LIA Recent Global Warming, GW) and the global change phases (Industrial Revolution, IR and Great Acceleration, GA) are also indicated*

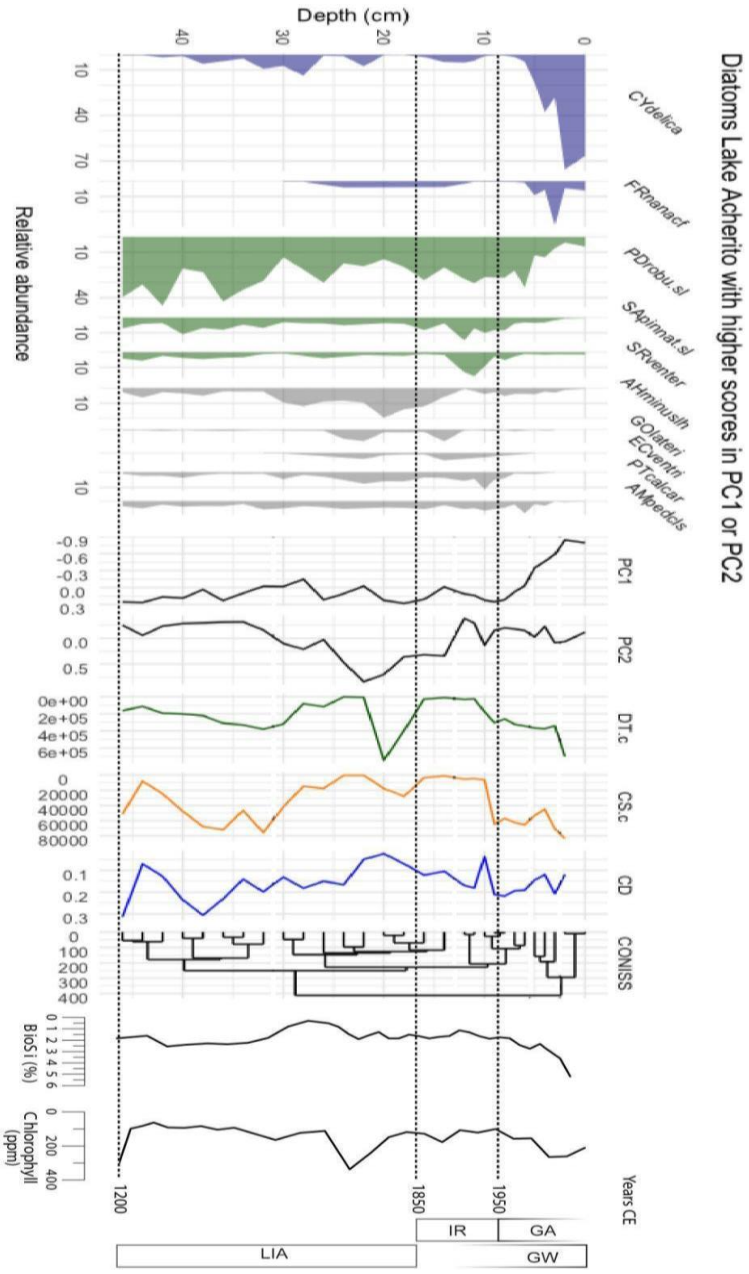

Fig. 5. 4.C. *Diatom stratigraphy, biogenic silica (%), and chlorophyll for Acherito (AC) sequence. The climate phases (Little Ice Age, LIA Recent Global Warming, GW) and the global change phases (Industrial Revolution, IR and Great Acceleration, GA) are also indicated.*

5.4. Discussion

5.4.1. Variability in depositional evolution and lithogenic fluxes

The different timing and intensity of sediment input variability may reflect local responses of the watersheds and lakes to varied climate and human pressure in mountain environments during the last millennium (Barreiro-Lostres et al., 2015;

González-Sampériz et al., 2017; B. Oliva-Urcia et al., 2018). Periods with higher L_{flux} during medieval times in lower altitude lakes (SI, between 800-1200 CE; AC, between 1300-1500 CE) (Fig. 5.2) and the site located close to a mountain pass (UR, 1300-1500 CE) (Fig. 5.2) could be related to the deforestation for summer grazing pastures that started in the 12th century with the socio-economic changes brought by the expansion of the Aragon Crown (González-Sampériz et al., 2017). During the LIA (1300-1850 CE) the human presence in higher altitude areas was reduced (Pérez-Sanz et al., 2013; Rull et al., 2021) and another peak in human population was reached after the mid 19th century. Rural exodus since the mid 20th century again decreased human pressure in mid mountains (García-Ruiz, Beguería, et al., 2015).

At higher altitude sites, sediment fluxes are mostly controlled by hydrological and cryospheric processes, as snowmelt is responsible for mobilization of sediment in the watershed and deposition in the lakes. Monitoring data in the Izas experimental watershed (Alvera, 2000; Lana-Renault et al., 2011) and reconstructions of past cryospheric activity (Lana-Renault et al., 2011; Morán-Tejeda et al., 2017) have shown that in the Pyrenees, periods with more precipitation - either as snow in winter or rainfall the rest of the year - and higher seasonality (rapid spring-summer snowmelt) are conducive to higher run-off, erosion and sediment delivery in the watersheds. On the other hand, during colder episodes lake bioproductivity is reduced (Lana-Renault et al., 2011; Lasanta-Martínez et al., 2005; Morellón et al., 2012; B. Oliva-Urcia et al., 2018; Pérez-Sanz et al., 2013; Pla-Rabes & Catalan, 2005). The maximum extent of LIA glaciers in the Pyrenees occurred during the last decades of the17th century (Maunder Minimum) minor re-advances between 1750 and 1800, and a significant expansion until 1830 (Dalton Minimum) (M. Oliva-Urcia et al., 2018). In our records we have identified periods with higher L_{flux} and higher bioproductivity that we relate to dominantly wetter and warmer conditions respectively. L_{flux} time series show that greater sediment delivery did not occur during the coldest periods as the Maunder minimum (1620-1715 CE), but prior to 1570 CE and after 1715 CE (Fig. 5. 2). We do not expect L_{flux} variability to follow global regional glacier expansion and retreat during the LIA in the watersheds that have been glacier-free during the last millennia (AC, SI, SA, UR). In MA and CR several moraines show active glaciers during the LIA but the Equilibrium Line Altitudes (ELA) fluctuated at higher elevations, between 2620 and 2945 m asl and the ice was never in contact with the lakes (M. Oliva-Urcia et al., 2018). MA, the only lake with a small snow and ice accumulation reaching the lake in the NW margin till early 20th century - is the only one with an important increase in sediment input during the second phase of the LIA (1750- 1850 CE).

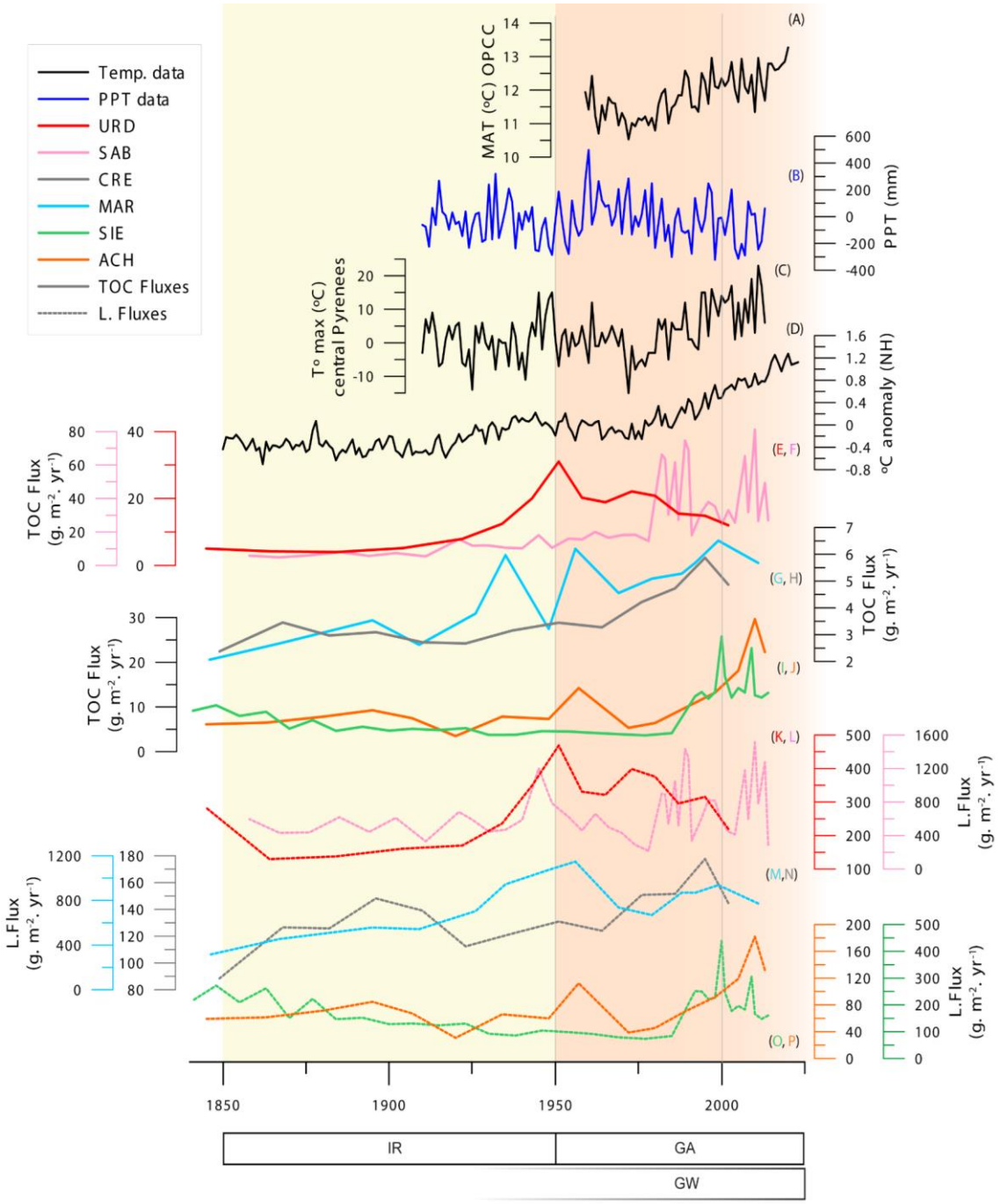

Fig. 5. 5. *Lithogenic fluxes, TOC fluxes and climate reconstructions based on instrumental data since 1850 CE. (A) Mean annual temperature in the Pyrenees obtained by OPCC (https://www.opcc-ctp.org/sites/default/files/documentacion/en_informe_opcc_adapyr.pdf); (B, C) Regional climate series of precipitation and temperature over the central Pyrenees between 1910 and 2013* (Pérez-Zanón et al., 2017) *and (D) gridded temperature anomaly averages for the northern hemisphere from the HadCRUT global temperature dataset (Morice et al. (2021); Osborn et al. (2021)). (E to J) TOC fluxes and K to P) lithogenic fluxes. Lakes are grouped into 1) more anthropized (UR in red and SA in pink), 2) higher altitude (CR in gray and MA in blue) and 3) lower altitude (SI in green and AC in orange). Climate phases (Recent Global Warming, GW) and global change phases (Industrial Revolution, IR and Great Acceleration, GA) are also indicated.*

The second large increase in L_{flux} during the last 1200 years occurred during the last century and particularly during the last decades. This is somehow unexpected as the watersheds have not been directly affected by large land use changes or direct human activities and changes in precipitation amount have been relatively small. Since the 1950s, agropastoralism pressure in the Pyrenees has been greatly reduced and new socioeconomic activities (tourism) have become the main agents of landscape transformation (Lasanta-Martínez et al., 2005). In absence of direct changes in land cover, we propose that new precipitation regimes could be responsible for this trend. The data from the high altitude Izas experimental basin - including SI watershed - (Lana-Renault et al., 2011) shows the paramount relevance of the short (two-month) snowmelt period as it is responsible for about 50% of the total annual runoff and 35–43% of the total solute and suspended sediment yield. Higher temperatures also increase the probability of larger runoff events in spring and more frequent rain events with higher erodibility impact than snow (Sánchez-López et al., 2016). The reconstructions and instrumental temperature data for central Pyrenean area (Fig. 5.5) show the recent increase in annual mean temperature and the variability of precipitation (Morice et al., 2021; OPCC, 2019; Osborn et al., 2021; Pérez-Zanón et al., 2017). The recent increases in L_{flux} in most sites suggest these regional changes in hydrology are affecting sediment transport and delivery simultaneously across the Pyrenees at various altitudes.

5.4.2. Variability in Organic Matter fluxes

Organic accumulation in high altitude Pyrenean lakes is limited by the reduced vegetation and soil cover in their watersheds and by the low productivity, which strongly depends on seasonality (ice-free season) (Catalan et al., 2002, 2009). Relatively low C/N ratios (7-15) suggest dominant algal sources, and variable contribution of terrestrial carbon. Periods with increased organic carbon accumulation may respond to higher input of watershed-derived organic matter (higher C/N) during periods of higher erosion and/or run-off and/or increased lake bioproductivity (lower C/N, higher BioSi, chlorophyll). The C/N records have a large variability, but during the GA, all those located in silicate – watersheds showed decreasing trends. MA values have remained constant during the last centuries and SA is the only one with an increasing trend, likely related to macrophyte development in the littoral areas. An increase in BioSi and chlorophyll and changes in diatom assemblages also occurred in CR, SA and AC during the last decades (Fig. 5. 4. A,B,C). As in most studies (Meyers & Teranes, 2002), our watershed-lake survey shows that aquatic and terrestrial vegetation have similar $\delta^{13}C_{OM}$ range and lake sediments and POM have lower values (Fig. 5.3). Changes in productivity greatly affect

$\delta^{13}C_{OM}$ values (Meyers & Teranes, 2002; Torres et al., 2012) as during carbon uptake, phytoplankton preferentially assimilates the lighter isotope ^{12}C (Gu et al., 2006). Under conditions of low to moderate primary productivity, plankton preferentially uptake the lighter ^{12}C, resulting in lower $\delta^{13}C_{OM}$ values (Torres et al., 2012). The $\delta^{13}C_{OM}$ shows a large decrease at the end of the LIA and the onset of the Industrial Revolution (IR) and reaching the most negative values during the last decades. The two lakes with carbonate-facies and dominant carbonate formations in the watersheds (MA and SA) show a distinctive large increasing $\delta^{13}C_{OM}$ trend in recent times, which points to other sources of DIC in these lakes. In MA, more DIC from carbonate bedrock could reach the lake during warmer periods (B. Oliva-Urcia et al., 2018). In SA, recent development of charophyte meadows has shifted the type of organic matter accumulation and contributed to higher $\delta^{13}C_{OM}$. The ice-cover period could be another factor as shorter ice cover decreases the accumulation of CO_2 during winter in the water column, which also decreases CO_2 exchange between the lake and the atmosphere leading to more positive $\delta^{13}C_{OM}$ (Catalan et al., 2009).

Prior to the unprecedented recent increase in the diatom planktonic component, the tichoplanktonic taxa were abundant in CR, AC and SA. In CR, the deepest lake, *Aulacoseira spp.* showed higher abundance prior to the mid 20th century (Fig. 5. 4. A, B,C). These species are very abundant during spring and autumn overturn periods in dimictic lakes. Hence, their recent decrease suggests shorter overturn and longer summer stratification periods (Pla-Rabes & Catalan, 2005). In lake AC small fragilaroids dominate the tychoplankton, and the abundance of these species is sensitive to shoreline water turbulence and temperatures (Schmidt et al., 2004). In lake SA, the small fragilaroid *Pseudostaurosira cf. robusta* also showed a peak ca. 1970 CE just before the increasing trend of planktonic diatoms, suggesting a lake/catchment disturbance likely related to the ski resorts constructions.

5.4.3. The uniqueness of the Great Acceleration

Both L_{flux} and TOC_{flux} indicate unique patterns in the six lakes since 1850 CE and particularly during the last decades, suggesting changes in the depositional regimes. Identification of potential Change Points (CP) in our time series using statistical tools is hampered by the non-regular nature of the data and the relatively low number of cases. We applied two methodologies to the L_{flux}, TOC_{flux}, C/N ratio and $\delta^{13}C_{OM}$ time series, one based on GAMs (Generalized Additive Models) (Simpson, 2018; Wood, 2017) (Fig. 5.6) and other on Cumulative Sum (CumSum) (Ibanez et al., 1993) (Fig. 5.7). Both are

statistical models intended to estimate nonlinear trends and to identify periods of significant temporal changes (or simply change points – CP) in unevenly spaced paleoenvironmental time series. Each technique has pros and cons in terms of identification of CPs, quality and readability of graphic outputs.

Both GAM and CumSum identified several CPs prior to 1850 and some during the 20th century. The CumSum (Fig. 5.7) L_{flux} plots showmain L_{flux} CPs in the 19th century (1850 CR, 1813 MA, 1878 SI, 1813 SA, 1885 AC) and in the 20th century (1928, MA; 1925 and 1935, UR; 1940 and 1985, SA; 1989 AC). Despite the numerous CPs identified, most of them occurred in the mid to late 20th century and at the end of the LIA (ca 1850 CE). Other CPs are associated with dam construction - MA and UR, 1920-1940 -, a LIA phase in MA (the only lake with a direct connection with a small ice accumulation) and documented medieval deforestation in some low altitude lakes (SI, AC, UR). The GAM analysis (Fig. 5.6) identified the most significant CPs during the 20th century, around the mid 19th century (end of the LIA) and some smaller in the previous centuries (CR, ca. 1750; SI, ca.1670-1790 and ca. 1830-1900; UR, around1870; SA, around 1750; AC, around 1570-1700 and 1850). As we discussed before, prior to the 20th century, periods of higher sediment input in the high-altitude Pyrenean lakes would be related to wetter and/or higher seasonality climate phases during the LIA and increased human pressure (12th-13th centuries and late 1800s - early 1900s) (Fig. 5.6 and 5.7).

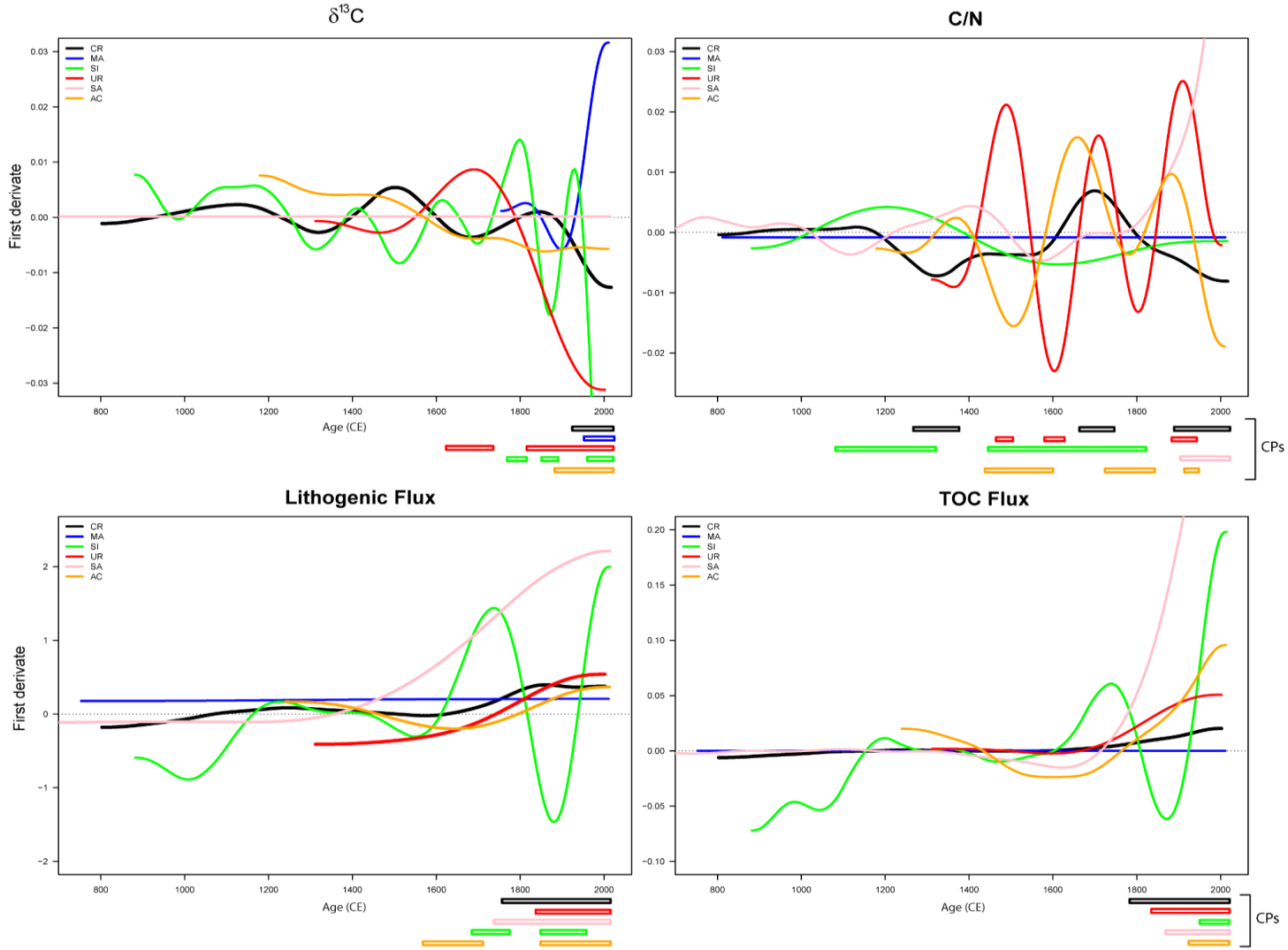

Fig. 5.6. *Estimated first derivatives (black lines) of the GAM trends fitted to Lflux and TOC flux, C/N and $\delta^{13}C_{OM}$ time series and location of the significant temporal changes. The 95% simultaneous confidence intervals of the first derivatives are in supplementary information, fig.S.5.3 and S.5.4)*

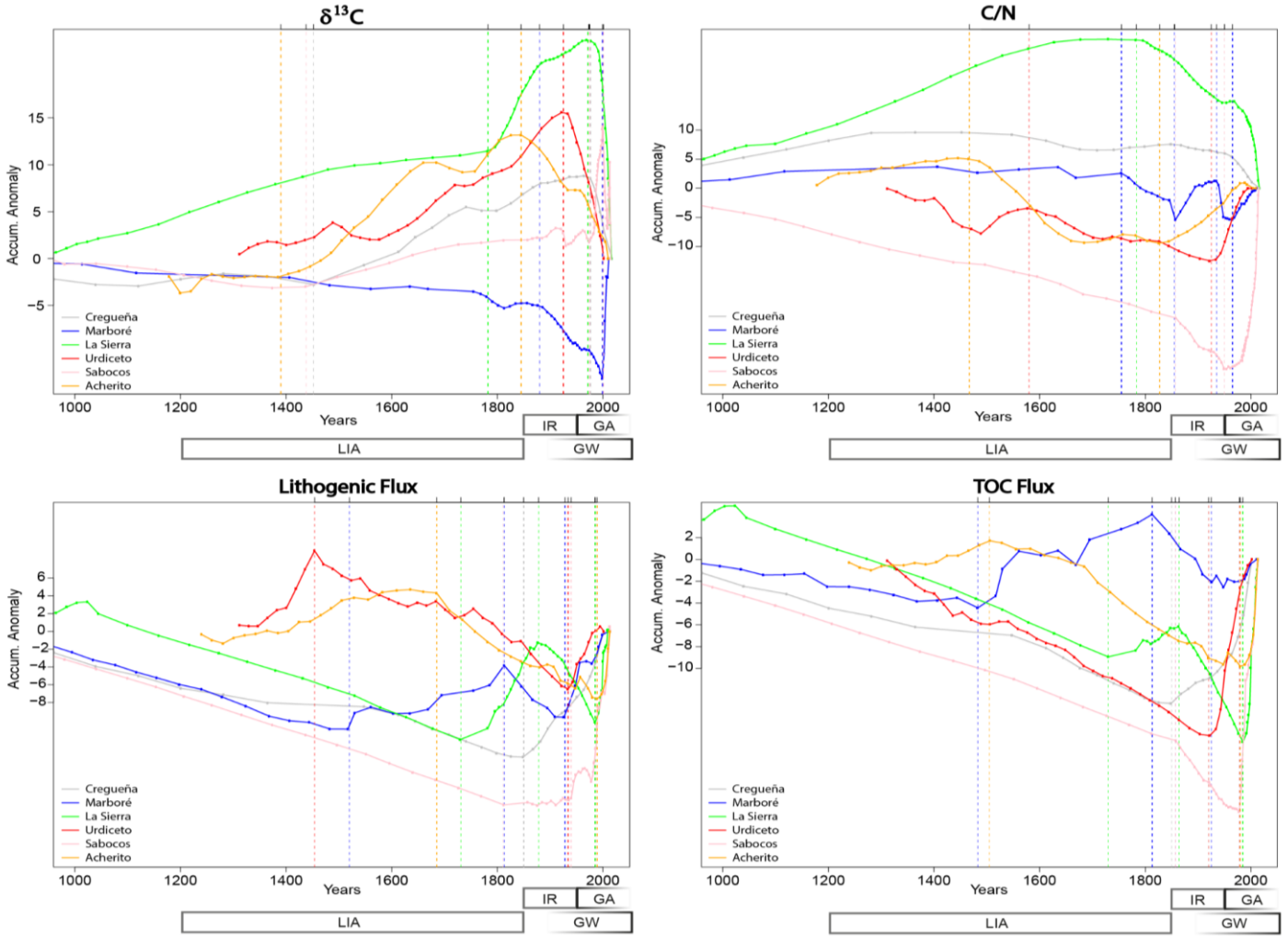

Fig 5.7. *Accumulated anomalies from the mean value of each variable ($\delta^{13}C$, C/N, L_{flux}, TOC_{flux}) obtained through the CumSum method. Vertical lines indicate the years when changes in trend occur.*

During the last century, a common feature of the lake records is the rapid increase in L_{flux}, and both techniques identified CPs. This supports an intensification of surface processes (erosion, run-off) in the watersheds. Similar trends have been described in other settings with reduced recent human disturbance in the watersheds (Great Plain in the US; New Zealand) and they have been ascribed to higher dust deposition (Brahney et al., 2015, 2019). Dust could be a contributing factor in Pyrenean lakes as Saharan dust fluxes in the southern Pyrenees are the highest in the Iberian Peninsula (Pey et al., 2020). In the case of the Pyrenean mountains, the documented trends of overall decrease in the duration of the snowpack, earlier snowmelt and the increasing frequency of winter rain events (Morán-Tejeda et al., 2017) could be potentially responsible for increasing erodibility and runoff in alpine basins, conducive to higher sediment delivery to the lakes.

The TOC fluxes during the last decades are the largest in the records (Fig. 5.2, 5.5) and both techniques identified most CPs during the last 200 years (Fig. 5.6, Fig. 5.7). GAM analyses for lakes located at lower altitudes show main CPs during the 20th century (SI, ca. 1950, UR, early 1900; SA 1950; AC ca 1910-20). In CR the main CP occurred earlier, and MA data could not be adjusted to a GAM model. The CumSum analysis also found earlier CPs (800-1200 and 1700-1800 CE in SI; 800-1100 and 1500-1800 in MA, 1700-1800 in SA). Some of them correlate with warmer phases during the Medieval Climate Anomaly and others during periods of higher soil watershed disturbance during medieval and modern times.

GAM analyses show the most important change in isotope signatures in the 20th century in most lakes (CR, MA, SI, UR), except in AC that occurred at the end of the LIA and MA with no model adjustment. CumSum showed CPs in 1975 CE in CR, SI and SA and a little bit later (2000 CE) in MA. MA and AC have CPs at the end (1880) and the mid 19th century, respectively. GAM analyses showed an earlier CP for AC and CumSum for SI and CR (1452, 1782 CE) coinciding with CPs identified with other proxies. The analyses for the C/N record show more CPs prior to the 20th century than for the other time series, but still most occurred in the mid to late 20th century (CR, UR and AC) and in the late 19th century (SA and SI). Some of the variability in CPs could be attributed to the age uncertainty associated with the Bayesian age models. Biological evidence suggests that the increase in organic carbon accumulation during the last decades has been driven by increased productivity (Fig. 5. 4. A,B,C).

To understand the temporal evolution associated with the range of variability in lake age-depth models in terms of organic matter accumulation and sediment input, we implemented two main component analyses of uncertain age (PC_{AU}) using two sets of variables (Anchukaitis & Tierney, 2013) 1) TOC_{flux}, CN, and $\delta^{13}C_{OM}$ that were interpreted as indicators of organic matter accumulation and sources (PC_{AUorg}) and 2) L_{flux} and $PC1_{comp}$ that represent sediment delivery to lakes (PC_{AUlit}) (see Fig. 5.8). The two first principal components ($PC1_{AUorg}$ and $PC1_{AUlit}$) explained 52% and 49% of the variance. This means that for the same age assemblage, more than half of the variability in the data associated with sediment and organic matter input increases simultaneously. Fig. 5.8 shows that the main changes for all lakes occurred around 1850, 1900 and 1950 CE, both in terms of a rapid increase in organic matter accumulation and sediment flux into the lakes. We run similar PCA analyses excluding UR and SA time series, - the two lakes that could have been more affected by dam and ski resort construction, respectively – and the results are comparable (Fig. 5.8), although the % of variance explained by the first components changed: 68 % for PC_{AUorg} and only 26 % for PC_{AUlit} . The $PC1_{AUorg}$ y $PC1_{AUlit}$ versus age plots show similar structure, with larger positive values around the end of the LIA (1850), 1950 and recent decades (see Supplementary Material for details of both PCAs, Fig S.5.5 to S.5.8). Interestingly, the $PC1_{AUorg}$ variability was larger if SA and UR were not included in the data and positive peaks were more clearly associated to warmer periods at the end of the LIA and during the 20th century (Figure 5.5 and references). However, we note that the time at which the loadings exceed the 95% probability density region (blue region in the Fig. 5.8) coincides with the timing when both trends became faster and exponential after 1950 CE.

The individual uncertain age PCA (PC_{AU}) for the four variables used in this study ($\delta^{13}C_{OM}$, C/N, L_{flux} and TOC_{flux}) show similar patterns and the % of variance explained by each PC1 was between 54 and 80 % (Fig. 5.9). The structure of these PC1 versus age plots was similar to the general $PC1_{AUorg}$ y $PC1_{AUlit}$ and confirmed that the main changes occurred during the mid 19th century and mid 20th century. For organic accumulation (PC1 TOC_{flux} and PC1 $\delta^{13}C_{OM}$) the periods with the largest deviations occurred during the early and mid to late 20th century and for sediment delivery (PC1 C/N and PC1 L_{flux}) during the mid 19th century (end of LIA) and late 20th century, although variability was larger.

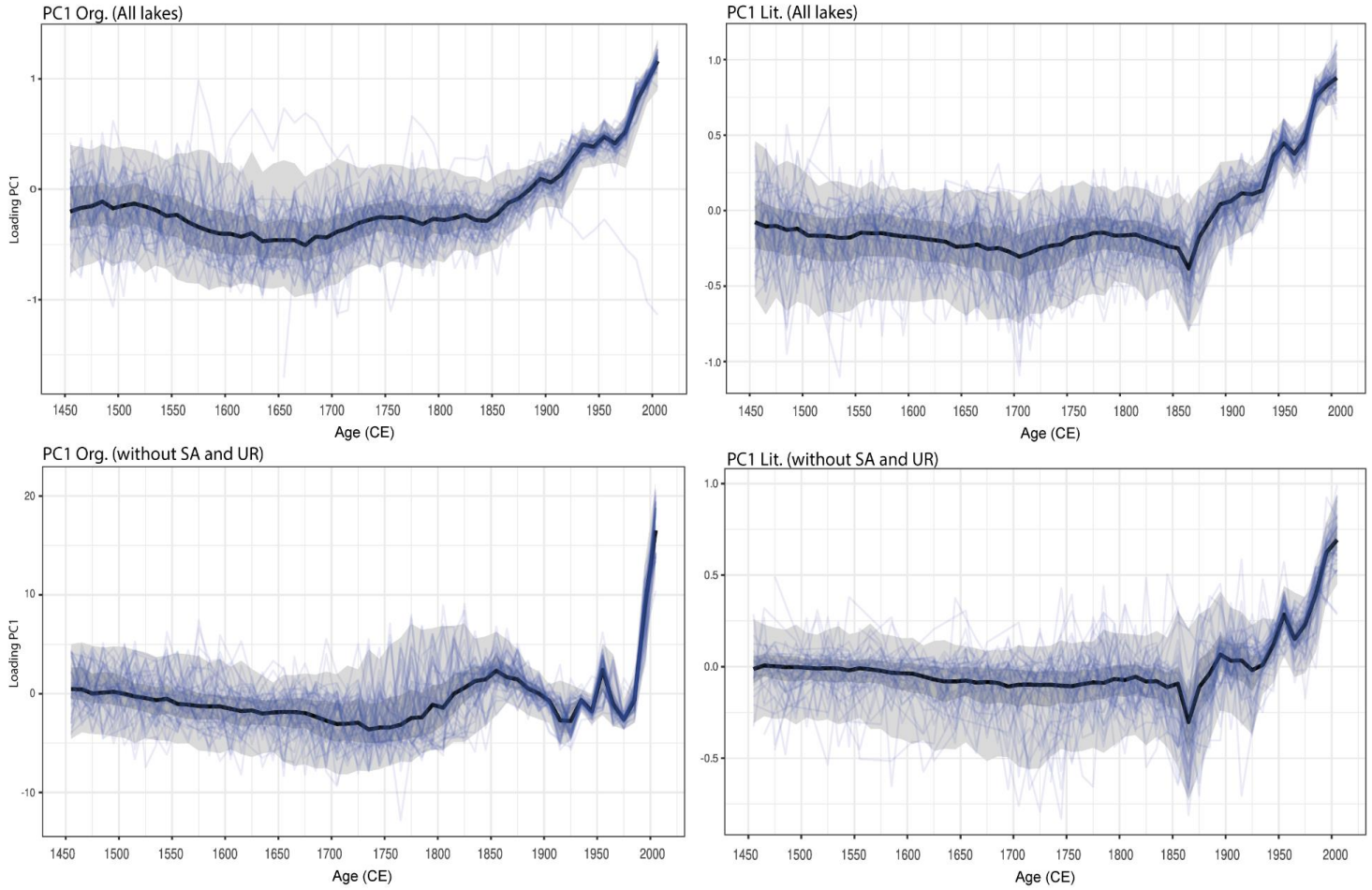

Fig. 5.8. *Principal component analysis for all proxies from all lakes datasets (left) and excluding SA and UR (right) of (top) organic matter variables (C/N, $\delta^{13}C_{OM}$ and TOC fluxes) and (bottom) sediment delivery (Lithogenic fluxes and "compositional PC1" (see methodology and Fig. 5.1). The median ensemble member is shown in black, with the 50 % and 95 % highest-density probability ranges shown in dark and light gray, respectively. Age-uncertain organic matter and sediment delivery ensemble members are shown in blue.*

The similarities in sites located at higher (CR) and lower (AC) altitude and with different bedrock geology (carbonate *vs* siliceous) supports global processes in lake ecology as main factors explaining TOC_{flux} and shifts in diatom assemblages during the GA (Fig. 5. 4. A, B, C and 5.1. A, B, C). A similar recent rapid increase on the planktonic component in another Pyrenean lake (Redon) has been correlated with higher air temperatures at the end of summer and more stable stratification (Catalan et al., 2002). Similar increases in planktonic diatoms have been related to climate warming (Rühland et al., 2015), and increasing nutrient availability (Catalan et al., 2002, 2013; Pla et al., 2009). Higher atmospheric CO_2, temperatures, nitrogen and phosphorus deposition all increase primary productivity (Catalan et al., 2013; Penuelas et al., 2013). Both, longer and more stable summer stratification and the observed increase in lithogenic mobilization from lake catchment would change lake nutrients availability for phytoplankton growth (Pla-Rabes & Catalan, 2011). The decrease in C/D ratio (Chrysophyte / Diatoms ratio) and the increase in BioSi observed in lake CR reinforce the idea of an increase in lake trophic state. Other factors, as faster C burial favoring C preservation due to higher Lflux and incomplete organic matter decomposition near the sediment-water interface, may have amplified the effects of increased bioproductivity and resulted in overestimation of recent TOC_{flux},

Hence, higher $L_{flux,}$ $TOC_{flux,}$ and planktonic diatoms in high altitude lakes identify the GA as a unique period with higher bioproductivity and sediment delivery caused by the synergistic effects of increasing temperatures, higher erodibility, and nutrient availability.

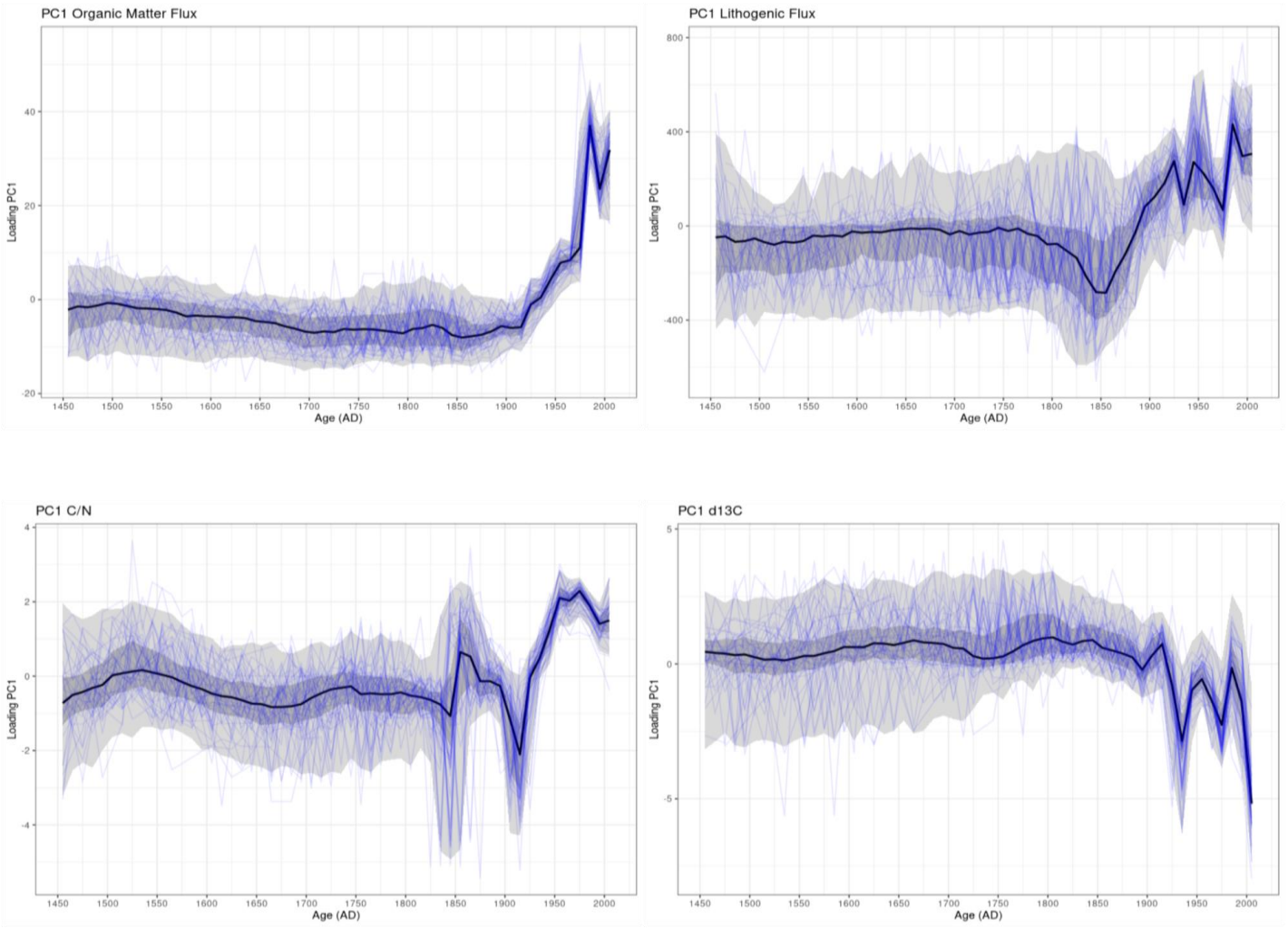

Fig. 5. 9. *First Principal Component for PCA obtained for C/N, $\delta^{13}C$, TOC fluxes and lithogenic fluxes, including all lakes. The median ensemble member is shown in black, with the 50 % and 95 % highest-density probability ranges shown in dark and light gray, respectively. The PC1 explained most of the variance for each variable: 80 % for TOC fluxes, 68 % for L flux, 58 % for $\delta^{13}C$ and 54 % for C/N. Age-uncertain ensemble members are shown in blue.*

5.5. Conclusions

High altitude Pyrenean lakes show the greatest changes in sediment delivery and organic carbon accumulation since 1850 and 1950 CE over the last 1200 years.
Prior to the 20th century, higher lithogenic fluxes occurred during periods of increased human pressure (early medieval times, late 19th century) and wetter phases of the LIA. Lakes at lower altitudes (AC, SA, SI) show higher TOC_{flux}, lower $\delta^{13}C_{OM}$ and C/N during medieval times, after 1850 CE and an accelerating trend since 1950, all indicative of increase in carbon burial and bioproductivity. Main periods of change in higher altitude lakes occurred at the same periods, but with variable trends and smaller ranges. The $\delta^{13}C_{OM}$ trends in alkaline lakes suggest additional sources of Dissolved Inorganic Carbon during the Great Acceleration from the watershed carbonate formations.

Increased sediment fluxes to the lakes during the last decades may be related to changes in seasonality, leading to longer ice-free periods and higher erodibility of rainfall versus snow precipitation. Increased organic accumulation is driven by higher algal productivity, primarily controlled by higher temperatures and longer ice-free and growing season, although higher atmospheric input of nutrients could also be a significant factor. The exponential increase in lithogenic and organic carbon fluxes in all lakes since the mid 20th century is a unique feature in the last 1200 years.

5.6. Supplementary Information

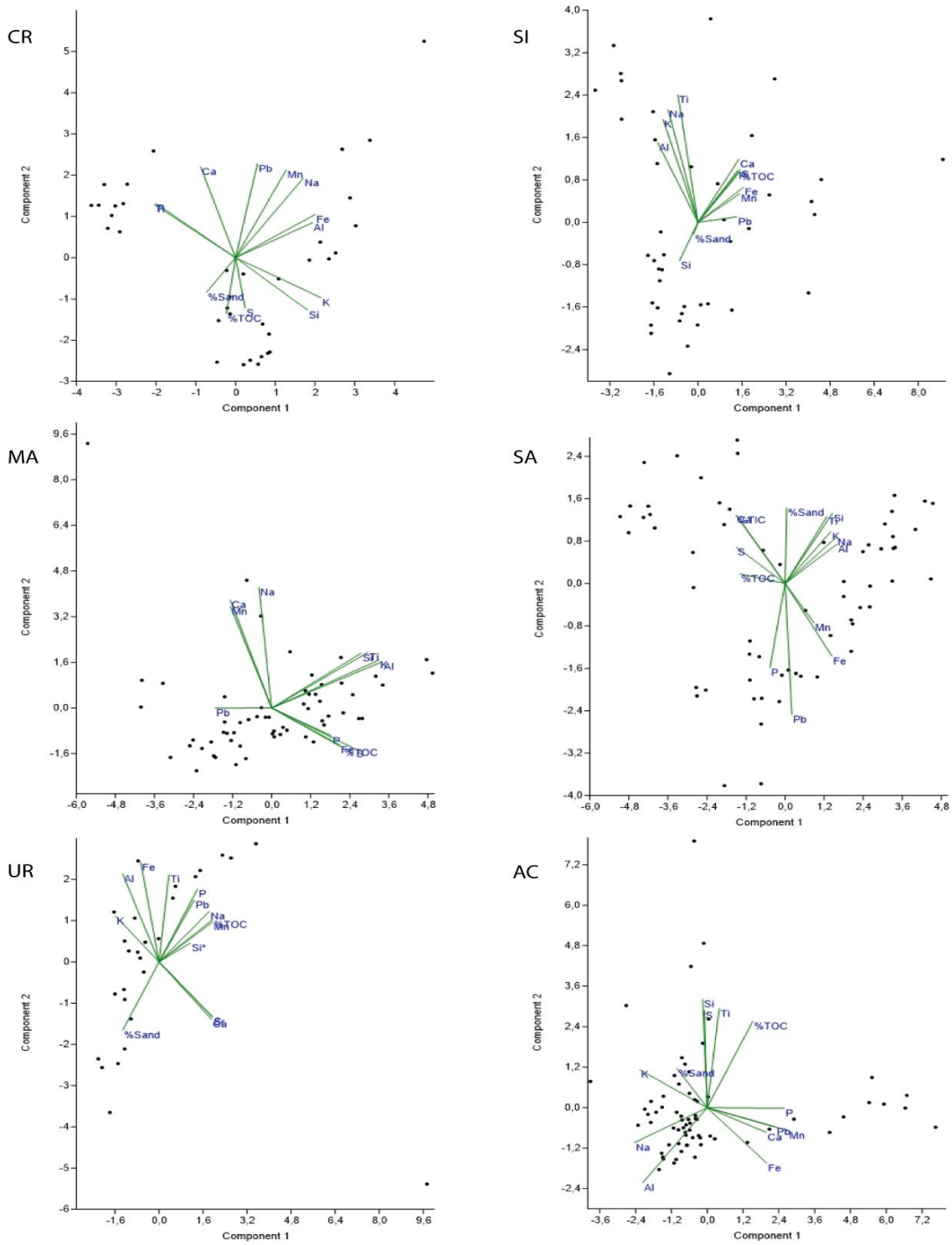

S.5.1. *PC1 and PC2 components for the Compositional PCA (PCcomp) obtained from geochemical data (ICP), %TOC, %Sand and %TIC (in MA and SA). The PC1 of each lake explains between 53.5% and 37.5% of variance (SA 53.5%, SI 48.4%, AC 43.1%, CR 39.9%, MA 37.5%).*

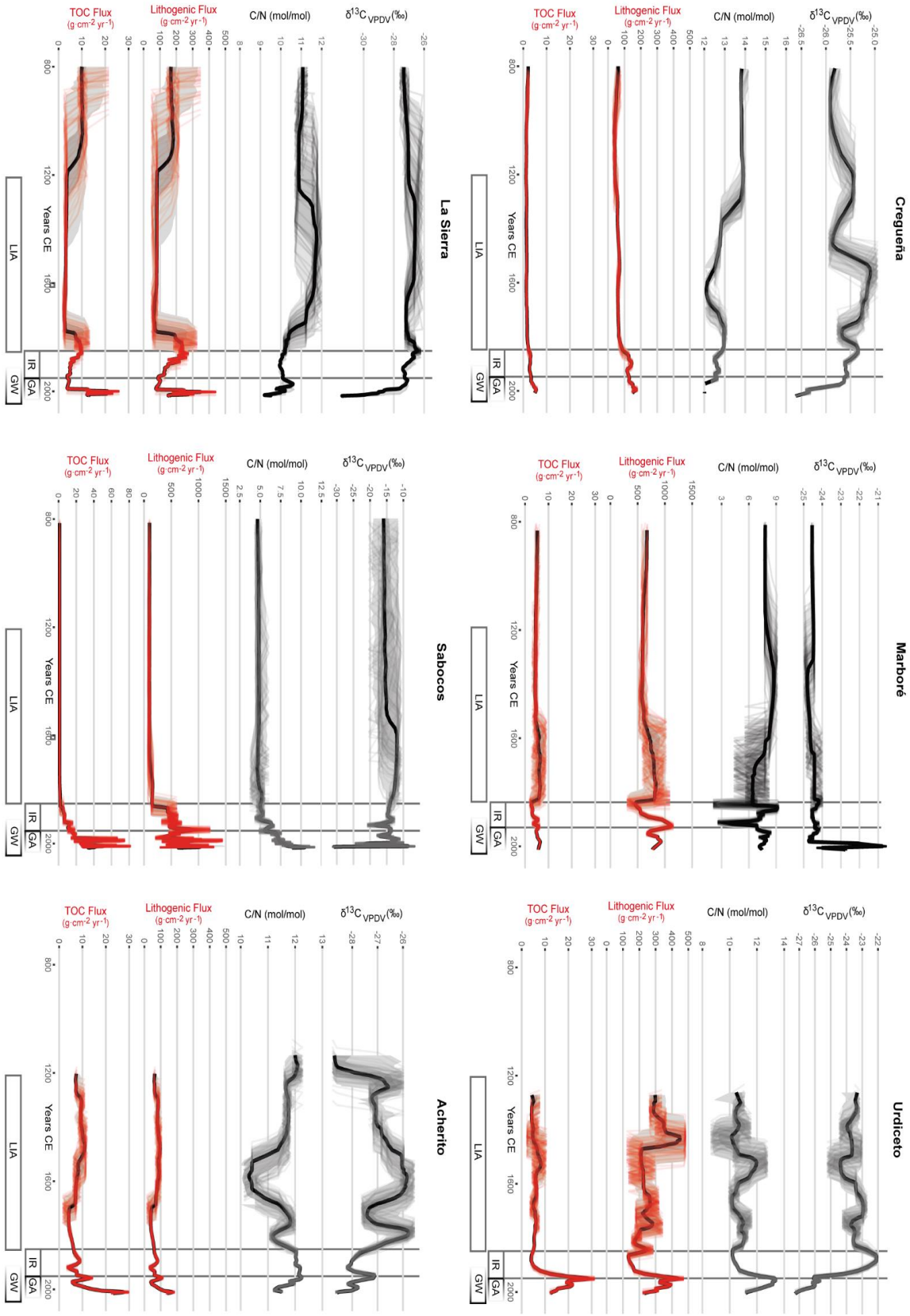

S.5.2. *Lithogenic and TOC fluxes (red), C/N and δ^{13}C (black) for the last 1200 years in the studied lake sequences (CR, MA, UR, SI). The climate phases (Little Ice Age, LIA Recent Global Warming, GW) and the global change phases (Industrial Revolution, IR and Great Acceleration, GA) are also indicated. Shaded areas reflect the uncertainty of the age models.*

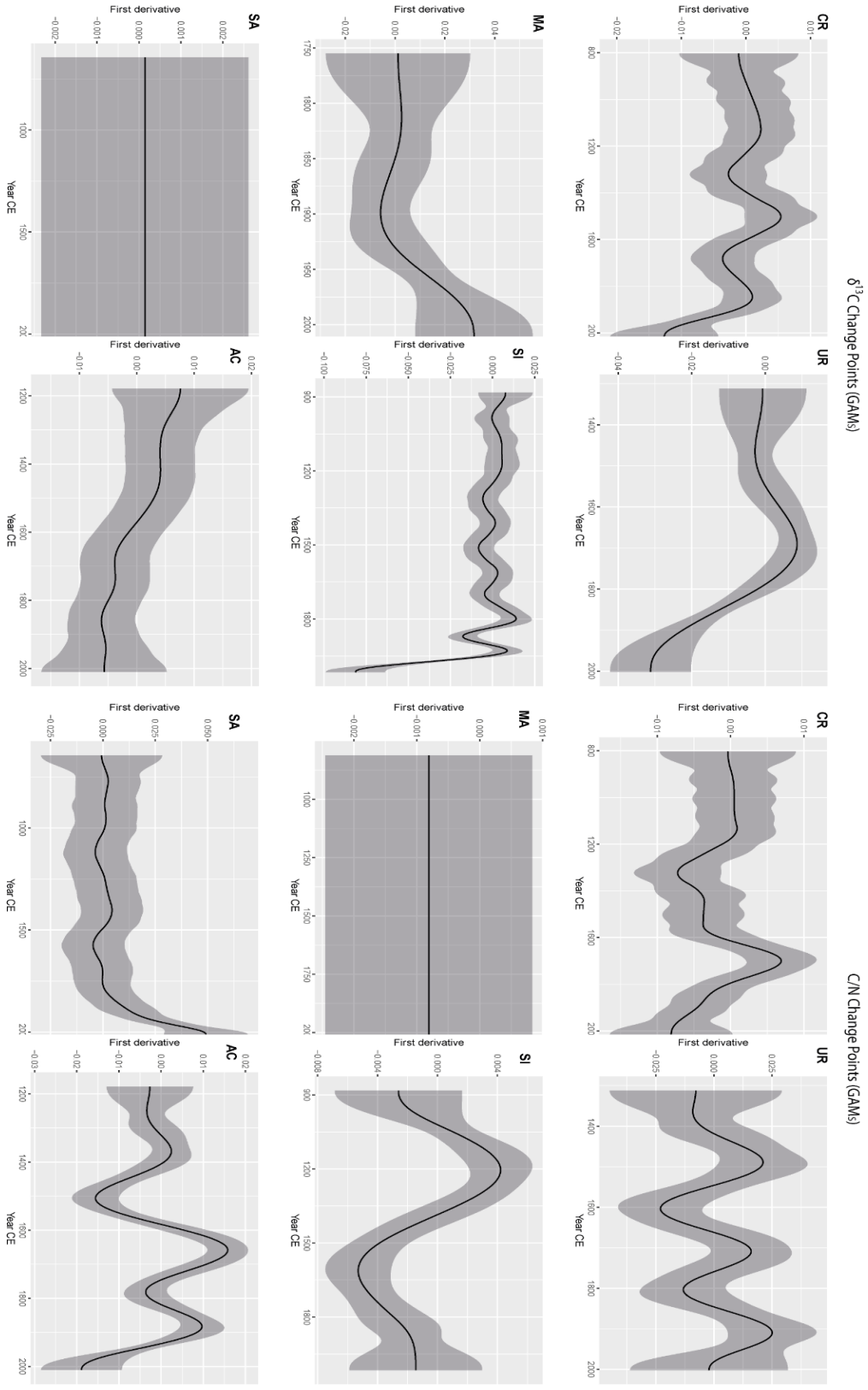

***S.5.3**. Estimated first derivatives (black lines) and 95% simultaneous confidence intervals of the GAM trends fitted to dC13 and C/N time series. Where the simultaneous interval does not include 0, the models detect significant temporal change in the response.*

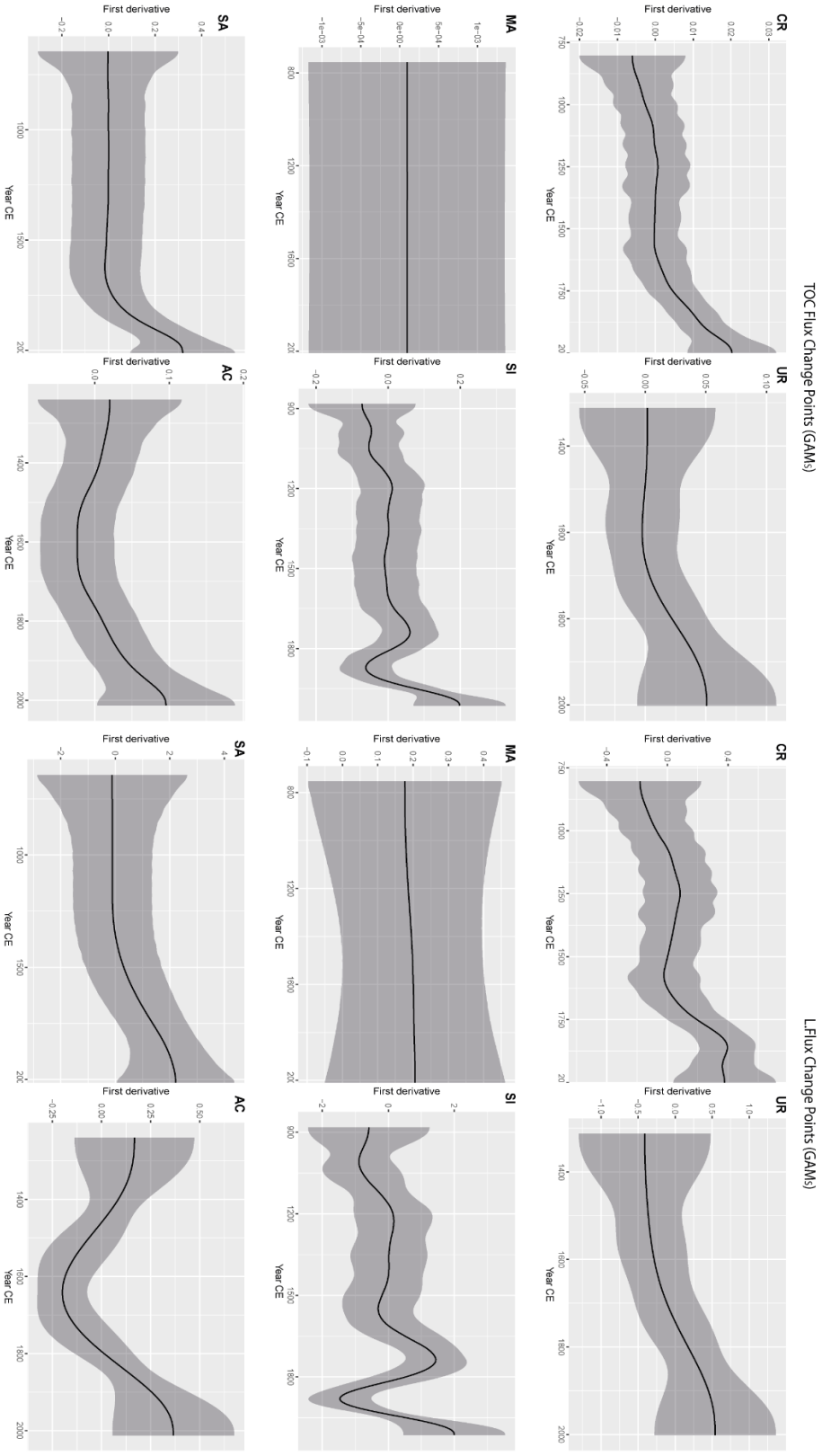

S.5.4. *Estimated first derivatives (black lines) and 95% simultaneous confidence intervals of the GAM trends fitted to LFlux and TOCflux time series. Where the simultaneous interval does not include 0, the models detect significant temporal change in the response.*

Age- uncertainty PCAs for Organic accumulation, sediment delivery and individual variables.

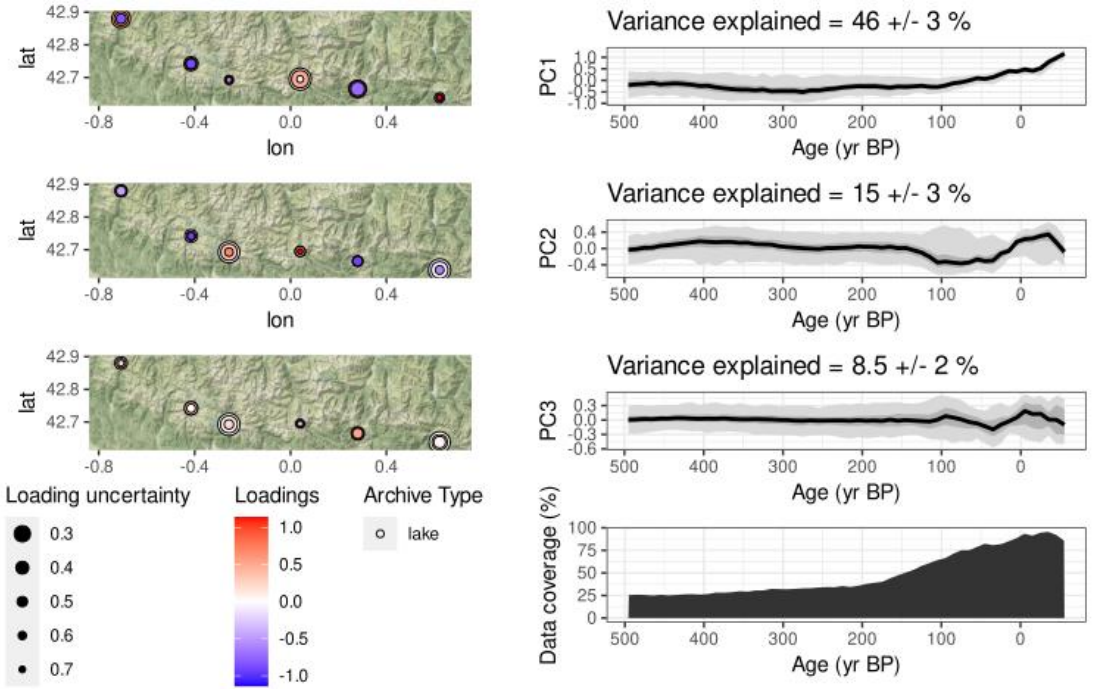

***S.5.5**. Principal component analysis for organic accumulation (all lakes)*

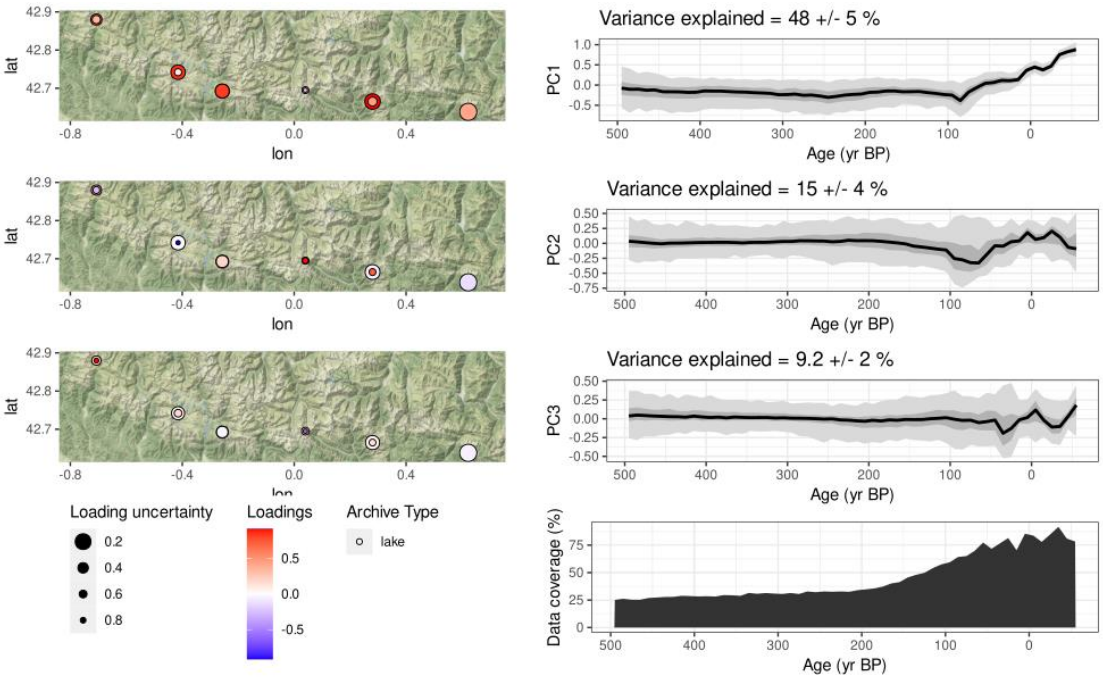

***S.5.6**. Principal component analysis for sediment delivery (all lakes).*

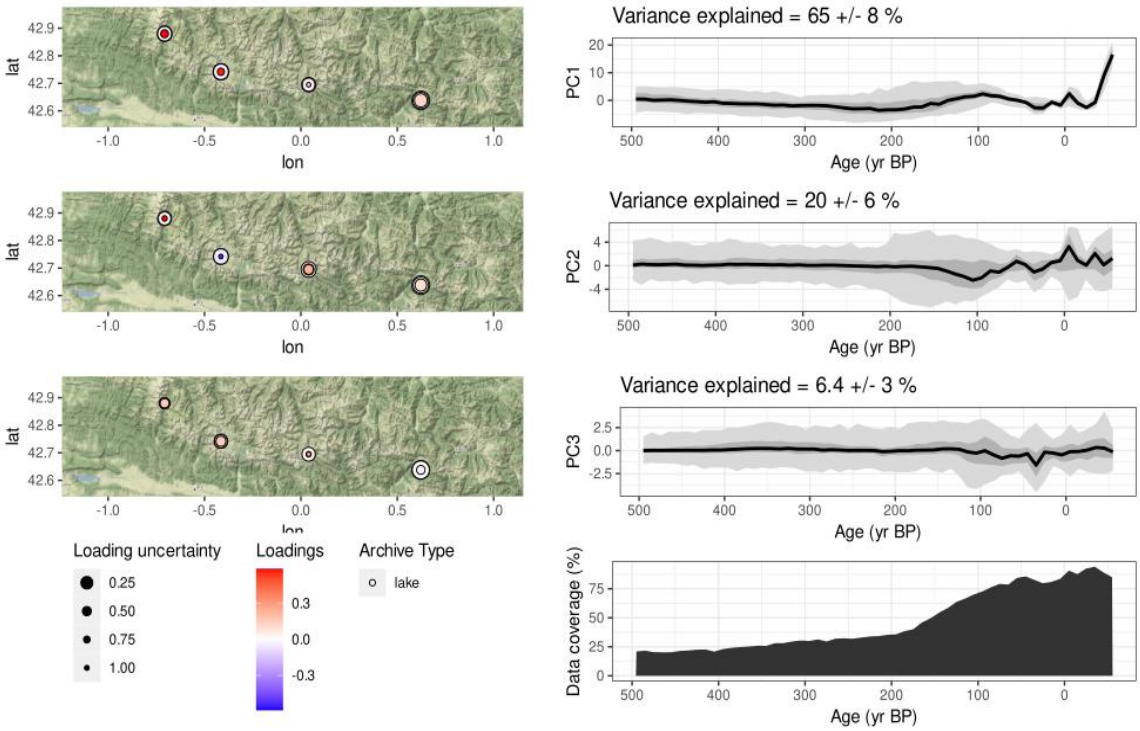

S.5.7. *Principal component analysis for organic matter sources, excluding URD and SAB.*

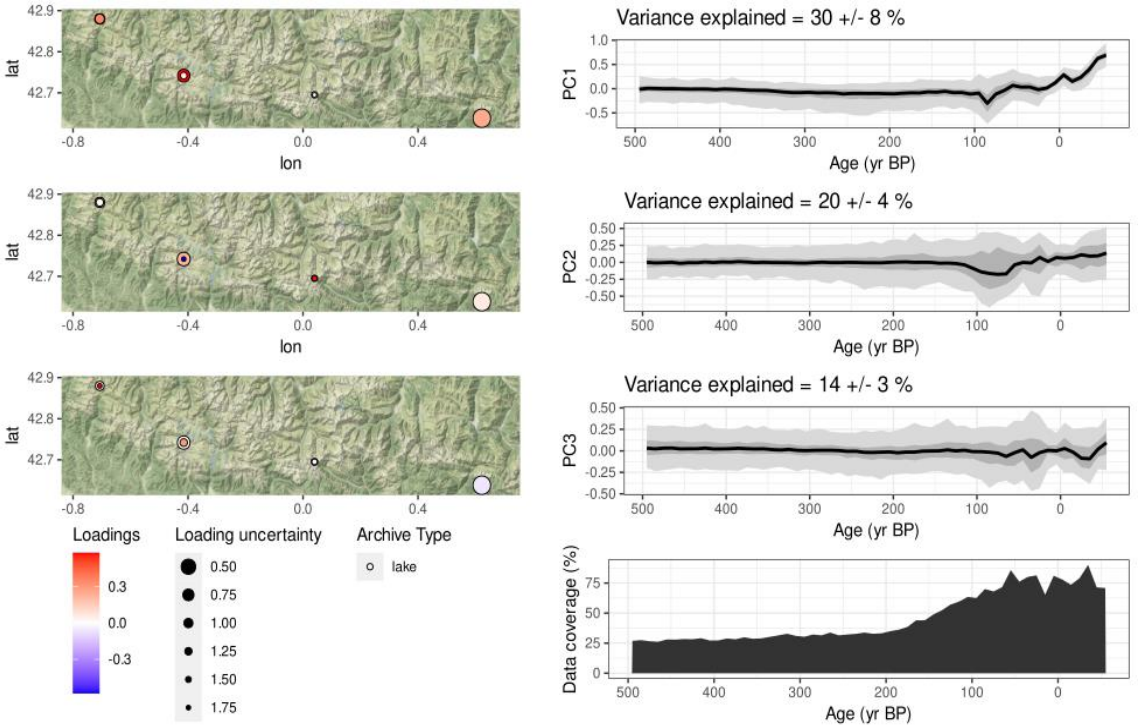

S.5.8. *Principal component analysis for sediment delivery, excluding URD and SAB.*

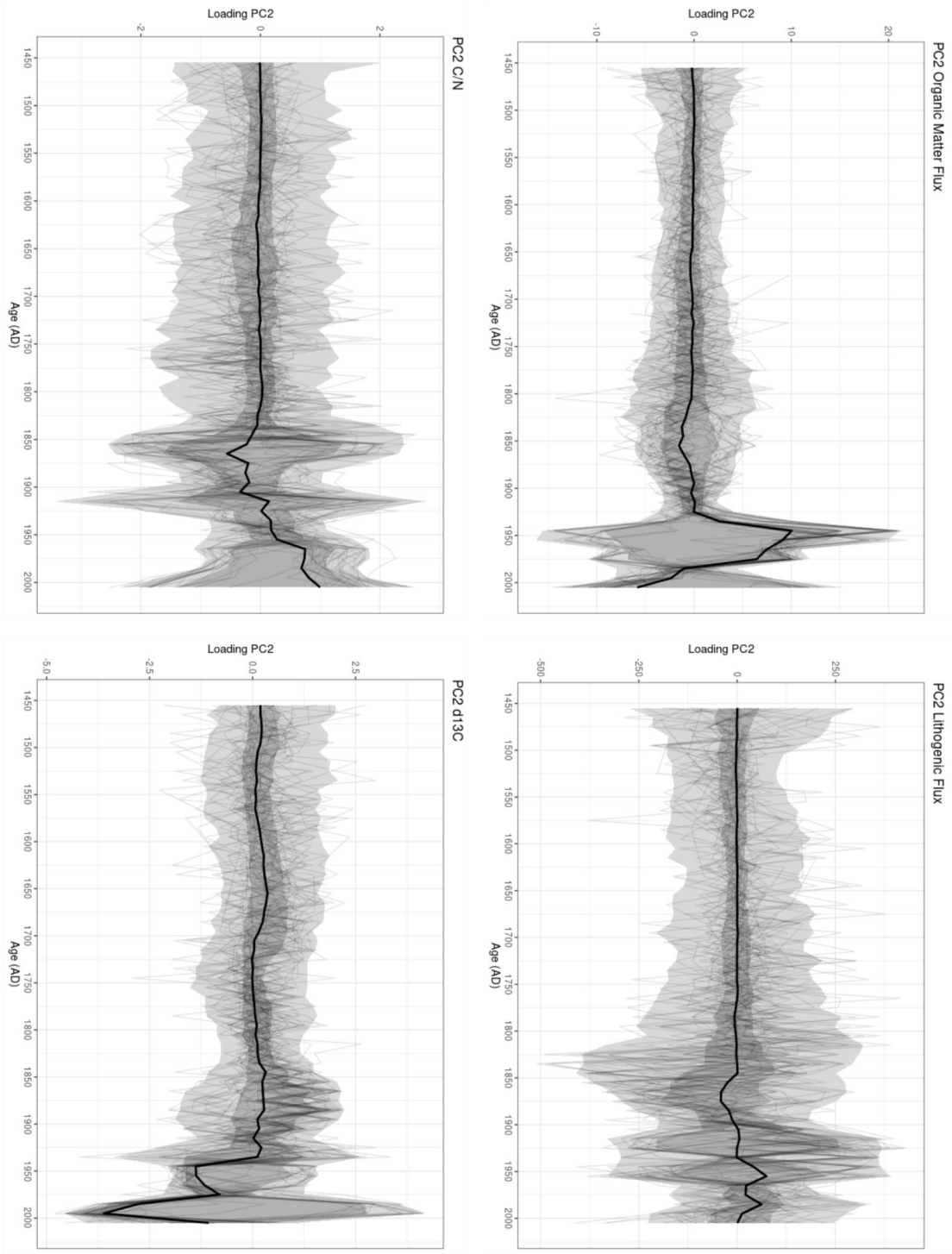

S.5.9. *Second Principal Component for C/N, $\delta^{13}C$, TOC fluxes and lithogenic fluxes (all lakes). The median ensemble member is shown in black, with the 50 % and 95 % highest-density probability ranges shown in dark and light gray, respectively. Age-uncertain ensemble members are shown in gray.*

6. Heavy metal deposition

Cregüeña Lake (July, 2018)

6. The heavy metal deposition

6.1. Introduction

Although metals are important as micronutrients for ecosystems, they are also toxic substances with public health relevance (European Water Framework Directive, EWFD, 2019). They have both natural, as part of the biogeochemical cycles and weathering processes of the lithosphere, and anthropogenic origin, as a result of agricultural, industrial and mining activities. High altitude lakes are considered pristine ecosystems as they are located far away from population centers and industrial areas and the absence of local pollution sources makes them good candidates to archive global signals of pollution (Smol, 2008). Nevertheless, high - mountain lakes show clear evidence of chemical pollution that have toxic impacts (Machate et al., 2023) and references therein; Camarero et al., 2017; Compte-Port et al., 2018). Heavy metal pollutants associated to mining and smelting had a long history in the Iberian Peninsula where several records have shown the impact of diffuse atmospheric heavy metal deposition since Early Bronze age with peaks during Roman, Medieval and Modern Age (Camarero et al., 1998; Corella et al., 2018; García-Alix et al., 2013; Hillman et al., 2017; Le Roux et al., 2020; Martínez Cortizas et al., 2013; Martín-Puertas et al., 2010; Mata Campo et al., 2013).

In the Pyrenees, the study in Redón lake (Camarero et al., 1998) was the first to show historical variations in lead fluxes with a large increase in Medieval and Modern times. More studies (Bacardit & Camarero, 2010; Camarero, 2003; Camarero et al., 2017) have documented high concentrations in heavy metal content in a number of Pyrenean lake surface and core sediments and the varied impact of orography, altitude and wet and dry deposition (Bacardit, 2011; Catalan et al., 2013). The inventories of trace metals in soils and sediments and geochemical modeling have allowed the identification of the main transfer processes from watersheds to lakes during the ice-free season in the Pyrenean lakes (Bacardit & Camarero, 2010) and the apportioning of anthropogenic and natural contributions (Bacardit et al., 2012). An altitudinal study in three lakes in the Central Pyrenees (Corella et al., 2018) demonstrated the occurrence of the main pollution phases (Roman, Medieval, Contemporaneous and Recent times) in all records, but pointed out significant differences for each metal and in each lake, suggesting a role for location (altitude and geology) and limnological features of the systems (size, depth, and depositional tipology mostly).

Several geochemical surveys including As, Cd, Cu, Hg, Pb, Se and Zn of Pyrenean lakes (Bacardit, 2011; Bacardit & Camarero, 2009; Camarero, 2003; Le Roux et al., 2020; Rodriguez-Iruretagoiena et al., 2016) have shown concentrations beyond "natural" background values and higher concentration in surface sediments from eastern regions, interpreted as a response to historical and more intense recent industrialization. Data from the Spanish sites demonstrate the global reach of past mining and smelting activities all over the Iberian Peninsula, although the intensity of the heavy metal pollution in the records shows a large spatial and temporal variability. Recent changes in climate and land uses in the watersheds may have implications for heavy metal cycling, as a remobilization of metals stored in the watersheds is likely (Bacardit et al., 2012; Bacardit & Camarero, 2009)

In this chapter we describe the results of the W-E transect of lake records in the western and central Pyrenees spanning the last 2000 years. The heavy metal stratigraphies allow evaluation of input, storage and mobilization in the watersheds - lakes since Roman times, and investigate if previous accumulation phases could represent an analogue for the present period.

6.2. Material and methods

We have selected a representative core for the study of heavy metals in each lake: Cregüeña (REP-CRE17-1A-1G), Marboré (MAR11-1A-1U-1 and 2), Urdiceto (BIE-URD12-1B-1G), Sierra (REP-SIR17-3A-1G), Acherito (ACH17-1A-1G) and Sabocos (REP-SAB18-2A-1G). The cores were taken from the deepest areas of the lakes and the location is shown in Table 2.1, Chapter 2. The age-depth models for the last 2000 years are based on ^{137}Cs, ^{210}Pb and AMS ^{14}C radiometric dating techniques, and the chronologies have been created using BACON software (Blaauw & Christen, 2011). The details of the age models are explained in Chapter 2.

Data from two different techniques, XRF core-scanner and ICP, were used to determine the concentration of selected metals. X-Ray Fluorescence analyses were performed at the University of Barcelona (Spain) with an AVAATECH X-RayFluorescence II core scanner at a resolution of 4 mm, with a counting time of 30s, and under two different working conditions, 10 and 30kV. The results are given in counts per second (cps) and they are semi-quantitative. Quantitative chemical analyses were

performed in the lake sequences at a lower resolution (every 1 cm, 150 mg weight sample) with an ICP-OES 720-ES (Varian) at the Experimental Station El Zaidin - CSIC (Granada, Spain). Elements measured were Al, As, Ca, Cd, Co, Cr, Cu, Fe, Hg, K, Li, Mg, Mn, Mo, Na, Ni, P, Pb, S, Se, Si, Sr, Ti, V, Zn.

Enrichment factors (EF) have been calculated following published methodologies (Corella et al., 2018). First, we normalized the selected heavy metals with aluminum (Al) to better identify the variability in metal concentrations not related to changes in the run-off detrital input. Al was selected for normalization, as this lithogenic element is immobile (i.e., geochemically stable) in sediments (Boës et al., 2011; Tylmann, 2005) and had higher concentrations in our sediments than other elements (Ti, for example) due to the predominant siliciclastic nature of the sediments. EFs were calculated using average sediment concentrations at the base of the core representing reference conditions. As the time span of the sediment sequences is not the same, we have checked that the values at the base were indeed among the lowest of the whole sequence.

$$EF = \frac{(Mcm)/\,(Alcm)}{(Mbottom)/(Albottom)}$$

where [Mcm] and [Alcm] are the metal and aluminum concentrations at the same depths of the sediment cores, and [Mbottom] and [Albottom] are the metal and aluminum concentrations in the sediments at the base of the sediment cores.

6.3. Results

6.3.1 Heavy metal concentrations and XRF vs ICP data

For the selected lake sequences we have acquired both, high-resolution (4 mm) semi quantitative XRF core-scanner and quantitative ICP data on discrete samples. Considering the higher resolution and easier acquisition lab procedures for scanner XRF, it is useful to know whether XRF data could be a viable option for chemical stratigraphies under some circumstances. For the selected heavy metals, Zn has the higher concentration range (67-300 ppm), followed by Pb (16-270 ppm), Cu (9-49 ppm) and Cd (0.4-3.7 ppm). These values are within the ranges of previous surveys (Camarero, 2003, in 75 surface sediments) and sites (Zaharescu et al., 2009 in Respumoso Lake). In Respumoso Lake (located at 2200 masl in the central Pyrenees), the trace metal data in the catchment sediment fraction is Zn (32-183 ppm), Pb (10-152), Cu (0-30) and Cd (0.6-

3.2). This study concludes that sediment-bound trace elements constitute a considerable metal load in this catchment. Average Pb concentrations are above values considered to produce toxicological effects (30-70 ppm, (DelValls & Chapman, 1998).

Our data set for core sediment shows a large variability pointing to a greater role of local conditions compared to altitude or geographic location. Camarero (2003) reported higher heavy metal content in the eastern Pyrenean sites but we have not found significant differences in heavy metal content between the western (ACH, SIE, SAB) and central (MAR, URD, CRE) lakes.

The correlations among the XRF data set and some compositional (TOC) and textural (% sand and % silt) are shown in supplementary information. For Pb and Pb/Ti there are few significant positive correlations, and they are related to organic (TOC, Br/Ti, Fe/Mn) or textural (Rb/Zr and grain size) components. In most lakes, both parameters have negative correlations with lithogenic, detrital elements as Al, Ti and Ca, and more positive with organic related and fine-grained indicators.

The correlations among ICP data (including TOC and % sand) are shown in supplementary material. Pb, Cu, Cd, Zn show a significant correlation among them and with other metals (As, Cr, Ni), indicative of some common sources. Cu and Cd show better correlations with some lithogenic elements (Al, Si, Ca) than Pb.

Correlation with TOC is significant in all cases except in Acherito. No correlation with textural (% sand) data and low correlation with lithogenic elements, point again to a major role of atmospheric deposition sources for these metals. Only, in La Sierra, Pb and % sand have a significant positive correlation.

Overall our data are in agreement with previous surveys (Bacardit & Camarero, 2009) suggesting a lithogenic origin for Al, Fe, T, K, Ca and Mn, (as corroborated by the mineral composition data) and an additional anthropogenic source for Pb, Cu, Zn and Cd. Calcium has endogenic sources in Acherito and particularly in Sabocos, where primary carbonate productivity has increased recently. The relatively high concentrations of Arsenic (6 - 50 ppm) have also been found in other Pyrenean lakes (Camarero, 2003; Catalan et al., 2006) and explained as a result of natural high As content in the watersheds due to pyrite and arsenopyrite occurrences (Subías et al., 2015; Zaharescu et al., 2009).

Figures 6.1.A and 6.1.B show the correlation between XRF scanner and ICP data for Pb, Zn and Cu, as they are the only metals analyzed by both techniques. The ICP values range for Pb is between 15 and 270 ppm and cps reach up to 3300. Pb is the metal that shows the best correlation between XRF and ICP, and it is also better in the lakes with higher cps - Urdiceto (up to 3300 cps and with correlation coefficient of 0.91) and Marboré (up to 2300 cps, with correlation coefficient of 0.85) - than in those with intermediate values (Cregueña, La Sierra and Acherito, up to 850 cps and with correlation coefficients of 0.74, 0.88 and 0.81). Sabocos, with maximum values of 310 cps does not show any relationship (correlation coefficient of -0.19).

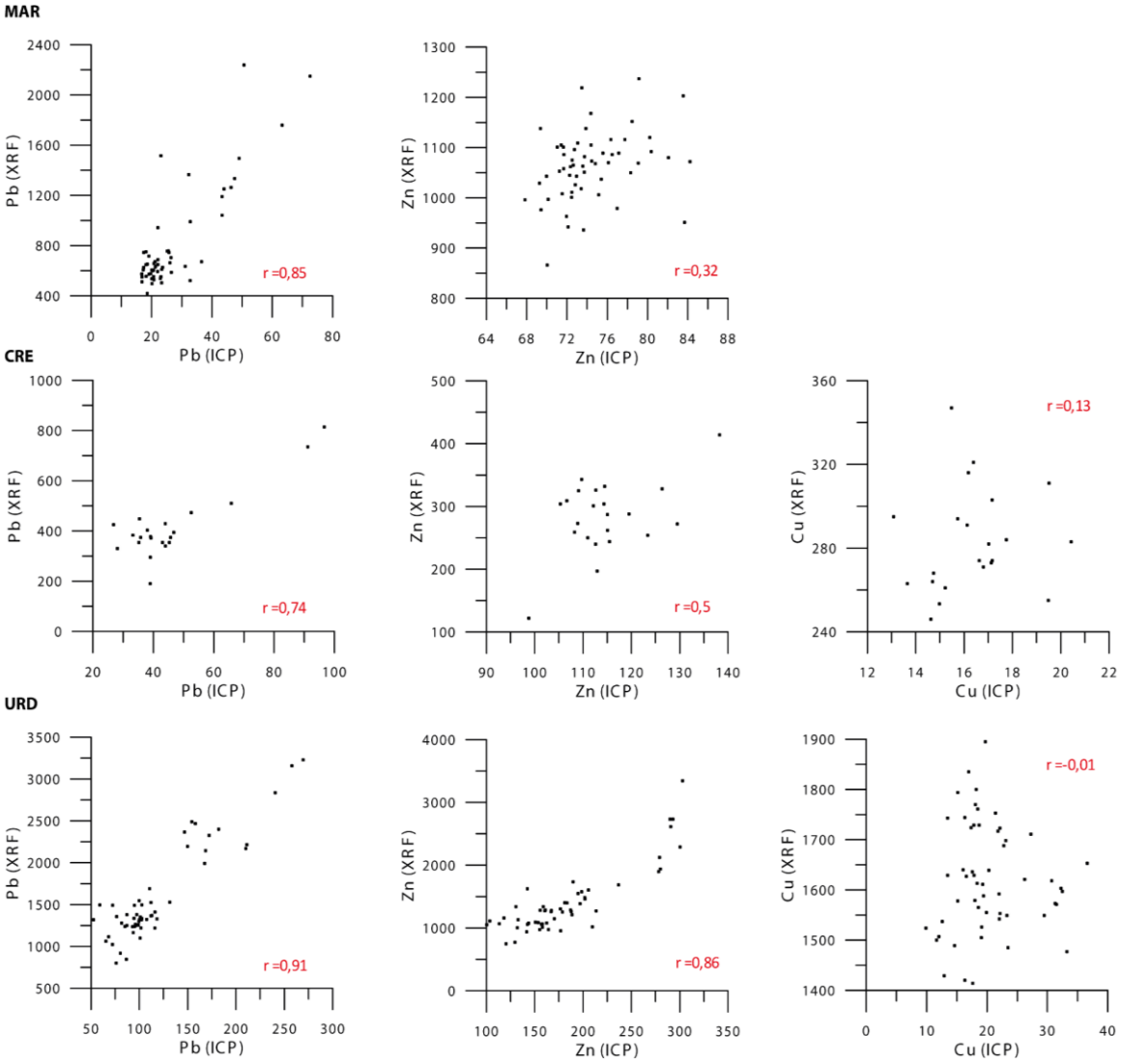

Fig 6.1.A. *Scatter plots of data from discrete (ICP, in ppm) and core scanner (XRF, in counts per second) samples and correlation coefficients for Marboré, Cregueña and Urdiceto.*

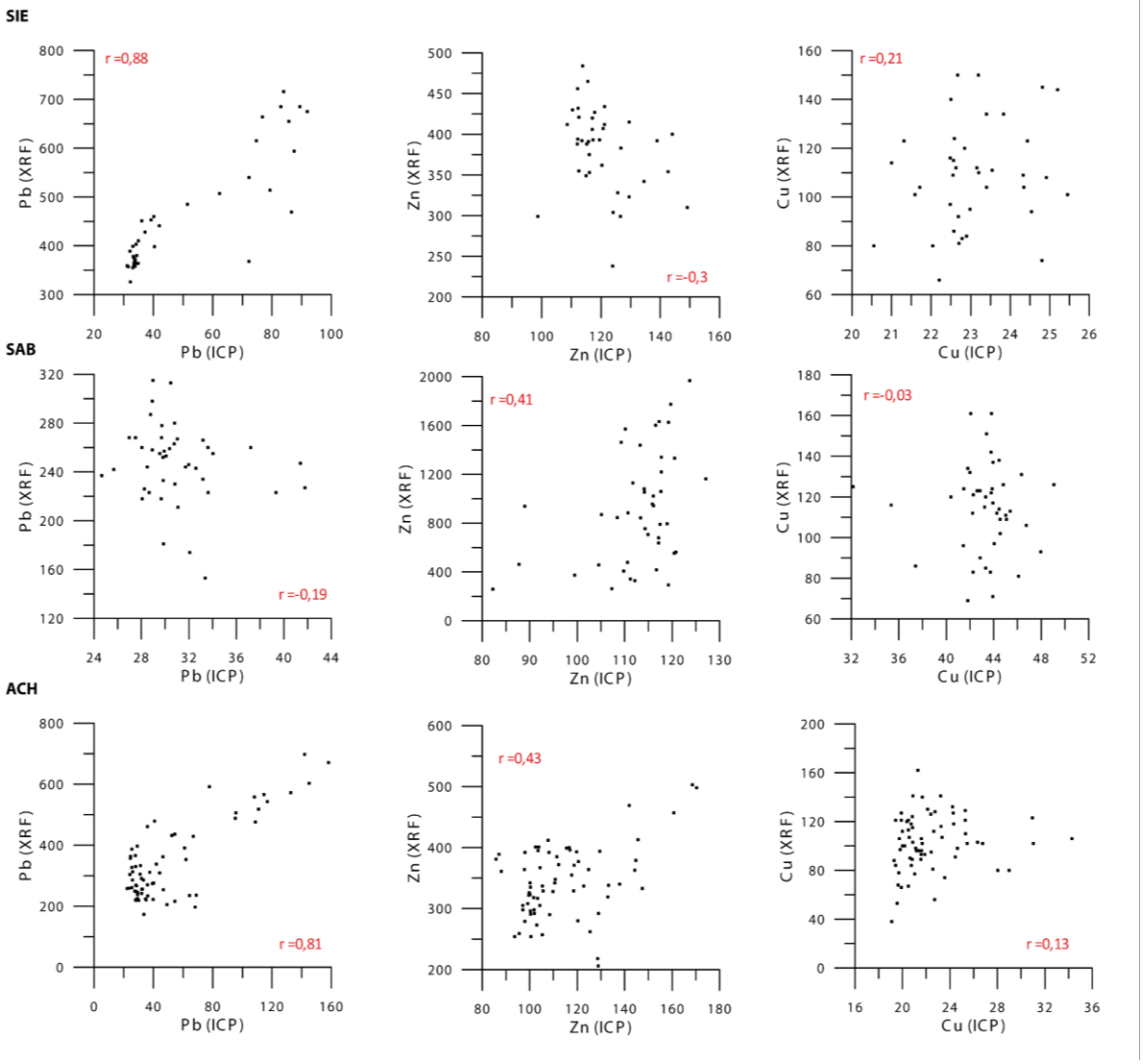

Fig 6.1.B. *Scatter plots of data from discrete (ICP, in ppm) and core scanner (XRF, in counts per second) samples and correlation coefficients for La Sierra, Sabocos and Acherito.*

Considering Zn, the only lake sequence that shows a significant relationship between ICP and XRF data is Urdiceto, with XRF values up to 3500 cps, although most of them are below 2000. Zn concentrations (ICP) in Urdiceto range between 100 and 320 ppm. Correlation coefficient between XRF and ICP values is 0.86. The rest of the lakes have lower cps (from 150 to 500 cps in most of them), and correlation coefficients are low (-0.3 to 0.5). However, in the case of Sabocos, the Zn values are relatively high (up to 2000 cps) but there is no significant relationship between XRF and ICP data (correlation coefficient is 0.41). Copper has very low cps in most lakes (< 350) and consequently, graphs show scatter plots and no correlation. Even in the case of Urdiceto

with higher cps (up to 1900), there is no correlation (correlation coefficient from -0.03 to 0.21).

Figure 6.2 shows all the data from figures 6.1.A and 6.1.B but grouped by metal. Pb shows variability between lakes, but despite this the overall correlation is high (correlation coefficient 0.77). Zn correlation is not significant (0.47) and for Cu it is even lower (correlation coefficient -0.32).

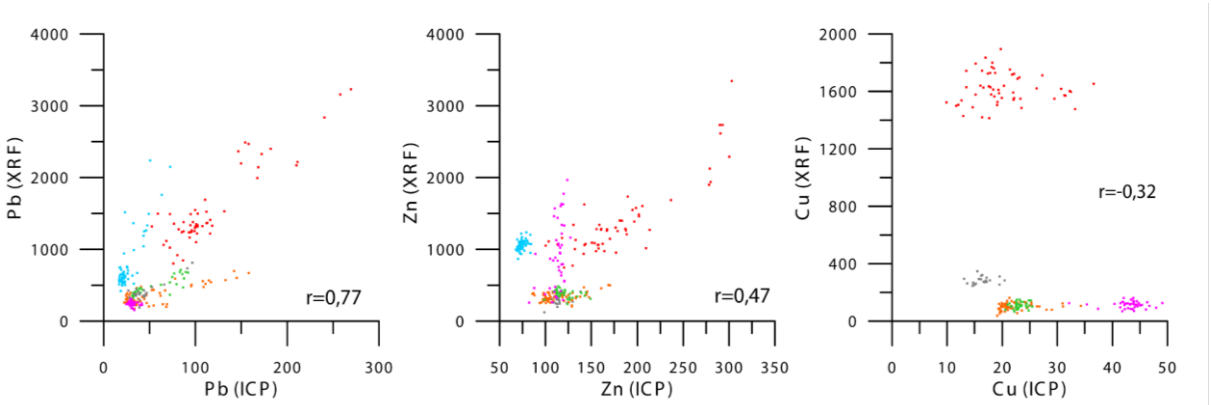

Fig 6.2. *Scatter plots of data from discrete (ICP, in ppm) and core scanner (XRF, in counts per second) samples and correlation coefficients for Cregüeña (gray) Marboré (blue), Urdiceto (red), La Sierra (green), Sabocos (pink) and Acherito (orange).*

In conclusion, the correlation between XRF core scanner and ICP data for Pb, Zn and Cu is only significant when cps values are high and the ICP range is also large. These results are expected due to matrix effects in natural samples such as water content, grain size and lack of homogeneity, being therefore necessary for XRF spectrometry, the standard preparation procedures. Pb is the only metal with a significant correlation, supporting the use of semi-quantitative XRF data as a proxy for quantitative ICP data.

6.3.2 Heavy metal geochemical trends

Figure 6.3 summarizes the heavy metal stratigraphies for the lakes. In Cregueña we have a data gap from 500 to 1300 yr CE. Pb and Cd have similar patterns, maintaining low values and low variability (26 to 104 ppm in Pb, 1.5 to 4.6 ppm to Cd) during the whole sequence, except during the Roman Period and since the IR. The RP showed small peaks around the 100 and 300 yr CE (39 for Pb and 2.3 for Cd). But the largest

change in both metals began at the onset of the 20th century (1915 yr CE), where Cd already reached values similar to those of the RP, and Pb surpassed them (66 ppm). However, it is during the GA when both increased more rapidly and reached their highest values (4.6 for Cd, 104 for Pb).

Cu and Zn have similar patterns than Cd and Pb, but the ranges are smaller: between 14 and 17 for Cu and 105 - 130 for Zn during the RP and between 16 and 20 ppm for Cu and 108 - 140 for Zn during the last decades.

In Marboré, Pb concentrations are very low throughout the record (between 10 and 20 ppm) except for the RP (150-330 yr CE) when they reached up to 50 ppm, and at the beginning of the IR (1860 yr CE), up to 72 ppm. After the sharp increase at the beginning of the IR, Pb concentrations dropped until the mid 20th century, but increased again during GA, remaining stable at values around 30 ppm till recent times. Cu and Zn have similar patterns to each other, showing higher values and greater variability during the last decades but within the range of other previous periods (e.g. medieval times). Finally, Cd shows a different pattern from the other metals, with a sharp increase at 1400 yr CE and then a very slight increase until the present. However, the values are too low, close to the detection limit, so the trends are not reliable, beyond the suggestion of higher values during medieval times.

The heavy metals in Urdiceto show high variability during the medieval ages but a similar behavior during the MCA and the LIA. In general, the values were somewhat higher during the MCA, and then decreased slightly in the LIA. After the IR, all metals increased, but in the case of Cd, Cu and Zn the values are not much higher than during the previous periods (Cd increased from 2.8 ppm during the LIA to 3.6 ppm at the end of the IR, Cu from 15 to 30 ppm, and Zn from 150 to 210 ppm). Pb content doubled from 100 to 260 ppm at the onset of the LIA. At the beginning of the GA (1950 yr CE), both Cd and Cu increased during the first decade: Cd reached similar values than during the MCA (around 4 ppm), and Cu reached the maximum values of the record (37 ppm). Subsequently, both metal contents decreased slightly and remained high and stable from the middle of the GA (1970 yr CE) to the present. The Pb content started to decrease already at the end of the 19th century and the trend continued up to the 1970s, reaching values around 150 ppm. The Pb concentrations have remained stable until the present. Zn content reached the highest values at the end of the IR and maintained them till the turn of the 20th century when they rapidly decreased.

In La Sierra, heavy metals profiles show similar patterns during the Medieval and Modern Ages, including the MCA and the LIA, but with lower variability than in other lakes. During the first part of the MCA (900 to 1000 yr CE), the values were somewhat higher than during the LIA. During the IR, Cu and Zn had some peaks, but the ranges were similar to those from the rest of the record, and they did not show a clear increase. On the contrary, Cd and Pb concentrations were higher during this period. Cd content reached higher values than during the MCA, but still low (3 ppm in the LIA, 4 ppm during the IR, 5 during the GA). Pb concentrations did have a large increase, from 35 to 85 ppm during the IR. During the GA, Cu content remained stable, even decreasing slightly, Pb remained at high values, and Zn increased, reaching 150 ppm. From the year 2000 CE onwards, all metal concentrations showed a decrease.

In Sabocos, the general trends are similar to those from the other lakes: little variability and somewhat higher values during the MCA, although also with some peaks during the LIA. The most important changes in this lake occurred after the IR: Cu and Pb increased and reached their highest values (49 ppm for Cu, 41 ppm for Pb) during the early to mid 20th century (1910 - 1970 yr CE). Cu values were only slightly higher than in the rest of the record, but Pb values were much higher than previously. However, both dropped abruptly to the lowest values of the record in the middle of the GA (around 1980 yr CE, 27 ppm for Cu, 22 ppm for Pb) to rise again in the last decades, up to 44 ppm for Cu and 35 ppm for Pb. On the contrary, Cd and Zn have a different pattern, with higher variability since the beginning of the IR, although their values decreased until the end of the 20th century (1990 yr CE). During the last decades, both increased, but concentrations were not higher than during former periods.

Acherito metal stratigraphies show greater variability during medieval times than modern ages, with slightly higher values during the early medieval times, but also some peaks during the LIA. All metals content remained fairly stable during the IR, without showing a clear increase. The main change occurred after the onset of the GA when Cd, Pb and Zn increased rapidly, reaching their maximum values, especially Zn and Pb (3.2 ppm for Cd, 160 ppm for Pb, 170 ppm for Zn). Copper did not show increasing trends during the GA, even a slight decrease. By the late 20th century (1980 yr CE) the heavy metal content decreased but continued to maintain high values up to the present.

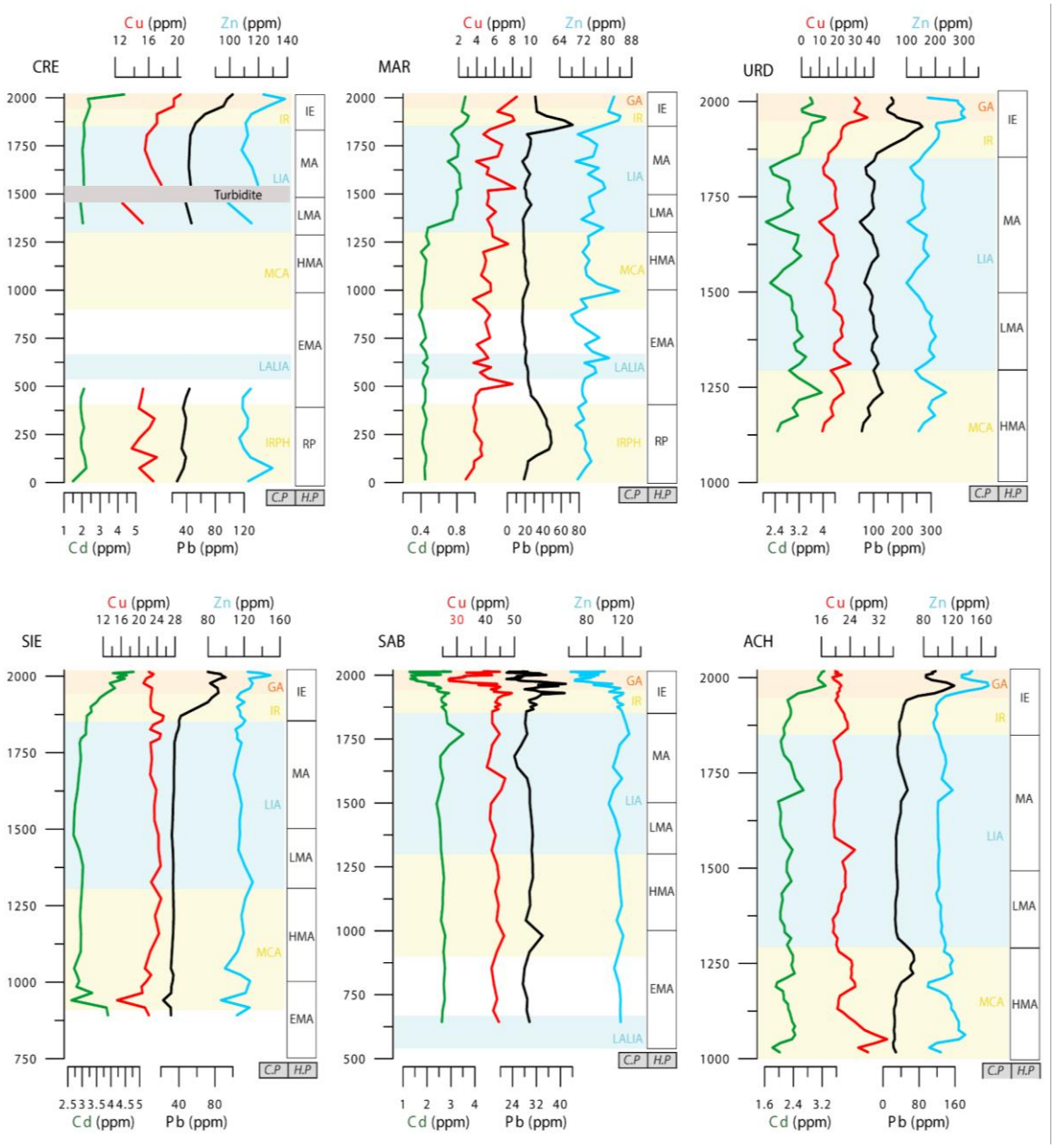

Fig 6.3. *Heavy metal (Pb, Cu, Zn, Cd) concentrations for Acherito, La Sierra, Sabocos, Marboré, Urdiceto and Cregüeña. The climatic (C.P) and historical (H.P) periods are indicated. The main climate phases are: IRHP, LALIA, MCA, LIA and Recent Warming. The historical periods are Roman period (RP, 200 BCE – 400 CE), Early Middle Ages (EMA, 400 - 1000 CE), High Middle Ages (HMA, 1000 – 1300 CE), Late Middle Ages (LMA, 1300 – 1492 CE), Modern Ages (MA, 1492 – 1850 CE), Industrial Era (IE, 1850 CE – Current) including the Industrial Revolution (IR, 1850 – 1950 CE) and Great Acceleration (GA, 1950 – current CE).*

6.3.3. Heavy metal enrichment factors

Enrichment Factors reflect better the variability of heavy metal dynamics in mountain lakes than changes in absolute concentrations, avoiding those effects due to changes in the main lithogenic (or mineralogical) components. An EF value higher than 2 has been considered as an indication of non-natural input and the occurrence of anthropogenic pollution (Camarero, 2003). Figure 6.4 illustrates the EF evolution in the six lakes. All lakes show EF < 2 prior to the onset of the Industrial Revolution and a sharp increase during the last century and particularly since the mid 20th century. A Medieval period with higher EFs occurred in most lakes, but the timing and the heavy metals involved are different. Finally, a decrease in EF during the last decades is more pronounced in some metals and lakes, but also with a large variability.

In Cregüeña, all heavy metals EFs show little variability prior to the late 19th century, and only Pb EF increased up to 1.5 during the RP. We have no data for the LALIA and the MCA periods to check if there was a decrease during that time, but values remained low during the LMA and the MA and only started to increase around 1870 yr CE up to the present day: Cd from 1.2 to 2.7, Cu from 0.8 to 1.2, Pb from 1.5 to 3.6 and Zn from 0.9 to 1.13.

The EFs in Marboré have the largest variability of all lakes. During the RP there was an increase in all EF, especially Pb (0.7 to 2.8), but also for Cd, Cu and Zn (< 1 to 1.6). During the LALIA, the EFs for Pb, Cd and Zn decreased and, in the case of Pb, reached their lowest values (0.5). EF Cu remained stable but with large variability, even with a peak at the beginning of LALIA (ca 500 yr CE) up to 2.7. All EFs began to increase around the year 1000 CE, particularly Cu, reaching EF 2. After the 1300 yr CE, all EFs decreased but did not reach values as low as those during the LALIA. During the late 19th century, EFs started to increase, and they reached the highest values of the record (Cd, 2.8; Pb, 3.5; Cu 2.8); only Zinc EF showed a smaller increase (1.5). During the GA (from 1950 onwards) the EF values decreased with respect to the IR, but maintained relatively high values.

In Urdiceto, the EF values during the Medieval ages were somewhat higher than during the Modern age, although within similar ranges. In the case of Pb, the highest value during the early medieval times was 1.8, and during the LIA, 1.4. These somewhat lower values remained relatively stable during the Modern age, till mid 19th century, when they increased rapidly, reaching higher values than in previous times: Pb from 1

to 3.4, Cd from 0.8 to 1.2, Cu from 0.9 to 1.7 and Zn from 0.6 to 1.7. The Pb EF shows a sharp decrease during the mid 20th century, while all the other metals continued to increase during the first decades of the GA (until 1960 CE). After the 1960s, all showed a slight decrease, followed by a subsequent sharp increase, until reaching their current maximum values (Cd, 2; Cu, 3.5; Pb, 3.8 and Zn, 1.7).

La Sierra also shows little EF variability for all metals until the beginning of the IR. The values during the early medieval times (MCA) are somewhat higher than those of the modern Age (LIA), but within the same range. The largest change occurred after the onset of the IR and particularly during the GA, when all EFs increased both in values and in variability, and the trend continued till the present. From the 1850s to the present, Cd, Cu and Zn showed similar increases: from 0.8 to 2 for Cd, from 1 to 1.6 for Cu, and from 1 to 1.8 for Zn. Pb increase was threefold, from 1.2 to 4.4. The increasing trends continued for Cd, Cu and Zn EFs till the present. In the case of Pb, the highest value (4.4) occurred in 1996, and it decreased to 3.7 later.

Sabocos EFs did not show significant changes until 1850 yr CE. As in the other lakes, the EFs increased during the IR reaching values higher than before. From 1850 till the 1950s, the EFs increased from 1.4 to 2.4 for Cd, 1.2 to 2.4 for Cu, 1.1 to 2.8 for Pb and 1.2 to 2.3 for Zn. The maximum EFs generally occurred around 1960 yr CE: 2.5 for Cu, 3.6 for Pb and 2.4 for Zn. Interestingly, since then and until the present times, the EF values have slightly decreased, although with great variability. The changes in the depositional system described in previous chapters (higher carbonate productivity in the lake) may be partially responsible for this trend.

Acherito showed relatively low values close to EF 1 (lower for Cu, about 0.7) during most of the sequence, except for three periods: around the 13th, 18th and mid 19th centuries till present. Around 1200 yr CE, Pb and Cu showed higher EFs: (0.9 for Cu and 2.2 for Pb), but values for Zn and Cd barely changed. The next peak occurred around 1700 yr CE, when briefly all metal EFs increased from previous lower values: up to 1.5 for Cd, 0.8 for Cu, 2.1 for Pb and 1.3 for Zn. The most recent EF peak, started with a slight increase during the IR, reaching values similar to the peak around 1700 yr CE, and increasing more rapidly later, with the beginning of the GA, when all metals show their maximum EFs: 2 for Cd, 1 for Cu, 6.1 for Pb and 1.9 for Zn. During the last decades EFs show a slight decline.

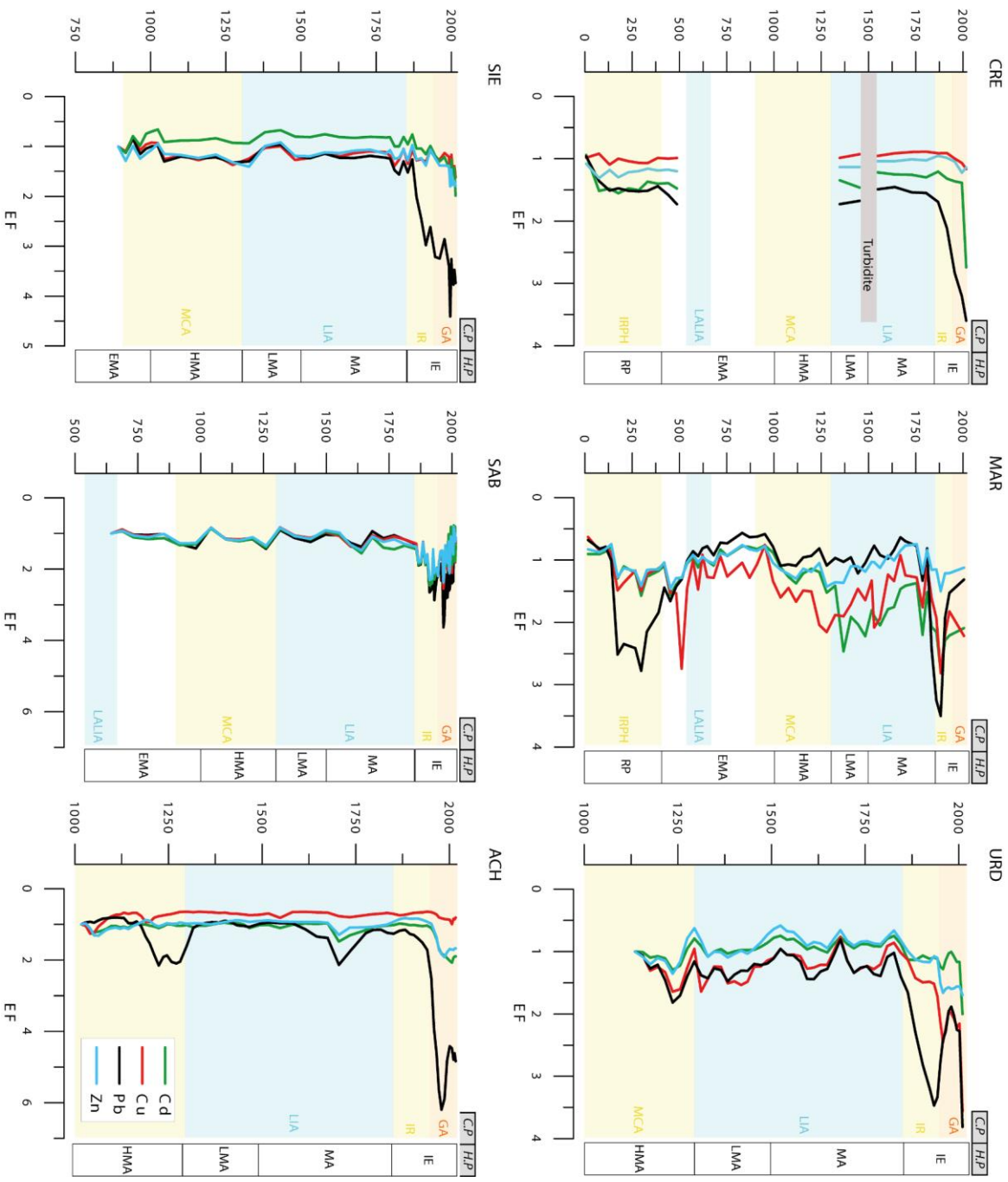

Fig. 6.4. *Enrichment factors (EF) of heavy metals (Cd, Cu, Pb and Zn) in all lakes. The climatic (C.P) and historical (H.P) periods are indicated. The historical periods are Roman period (RP, 200 BCE – 400 CE), Early Middle Ages (EMA, 400 - 1000 CE), High Middle Ages (HMA, 1000 – 1300 CE), Late Middle Ages (LMA, 1300 – 1492 CE), Modern Ages (MA, 1492 – 1850 CE), Industrial Era (IE, 1850 CE – Current) including the Industrial Revolution (IR, 1850 – 1950 CE) and Great Acceleration (GA, 1950 – current CE).*

6.4. Discussion

6.4.1. Heavy metal deposition in Pyrenean lakes during the last 2000 years

Only two lakes in the transect (CRE and MAR) include the Roman Period and both show some evidence of higher heavy metal pollution. In MAR, Pb reached an EF of 3, while in CRE remained at 1.5. The EFs of the other metals show smaller increases during this period for both lakes. The higher EFs occurred between 100 - 300 yr CE, the period of the maximum expansion of the Roman Empire in the Mediterranean and also in Hispania (Hanebuth et al., 2018; Hansson et al., 2017; Hillman et al., 2017; Rosman et al., 1997). The Pb EF was the highest of the last 2000 years during the RP.

During the EMA, Pb, Cd and Zn EFs decreased in both records; Cu remained at similar values in MAR than during the RP and even reached 2.7 around 500 CE. Another increase in heavy metal EFs occurred at the turn of the millennium, roughly around the beginning of the MCA and the HMA. In MAR, Pb had relatively low EF values (0.9 - 1.2, between 1000 and 1300), although somewhat higher than those during the EMA (0.5 - 1, between 600 and 1000 yr CE). In ACH and URD the increase occurred later, between 1200 and 1300 CE approximately (ACH Pb EF increased from 1 to 2.2 and URD from 1 to 1.9). SAB and SIE did not show any significant changes in Pb EF during the HMA. In the case of copper, EF increased in MAR and ACH (peaked between 1050 - 1200 CE), but changes in the other lakes were small (SIE) or not significant (SAB and URD). For Cd, EF had a continuous increase in MAR, similar to that of Cu. Zn showed a subtle increase in MAR, the same peaks at 1050 and 1200 yr CE for ACH and somewhat higher values for URD.

A small lowering of EF values in most records marks the transition to the Late Medieval Ages and the onset of the LIA. Pb EF only changed significantly in MAR, where it started to increase rapidly at the beginning of the 19th century (EF 0.8 in 1810, and 3.2 in 1850 yr CE), and ACH with a peak of EF 2.1 in 1700 yr CE. Cu values remained within the same ranges as before, but with more variability, particularly in URD and SAB. CRE and MAR showed a decrease in their EF Cu during the LMA and especially the MA, although with some peaks (such as 1530 yr CE for MAR). Around 1800 yr CE, the decreasing trends stopped and the lakes began to enrich in Cu. Cd increased greatly in MAR, both during the LMA and in the last decades of the MA. Also in ACH and SAB the Cd enrichment was notable during the MA. Zn had a greater variability during these

periods, although the EFs were smaller. In spite of the variability, the tendency of increasing EF during the middle and late MA was maintained in MAR, SIE and SAB.

Although some of the EFs had already started to increase during the late Modern Age, the onset of the IR witnessed the most abrupt change in all records, with large positive EF shifts. In the case of Pb, the increase was almost synchronous in all lakes, at around 1850 yr CE; in URD and MAR it started somewhat earlier.

All lakes maintained higher Pb EF during the late 19th and early 20th century, except MAR that peaked in 1880 yr CE (3.5 EF), and then rapidly decreased, so at the beginning of the 20th century, the EF was 1.94. The Cu profile also marked the onset of the IE, more evident in URD, SAB and MAR, and subtler in CRE and SIE. Similarly to Pb, the increase started earlier in URD and MAR, and peaked in the first decades in MAR (EF 2.7). Cd and Zn also showed the same patterns with increases in all lakes and a distinctive peak in MAR.

During the GA, most EFs had rapid increasing trends and reached their maximum values, but there are differences between the timing among metals and lakes. In the case of Pb, CRE and SIE had a fairly continuous EF increase since the onset of the GA. CRE started the GA with Pb EF of 2.5 and reached 3.6 by our current decade. SIE had a mid 20th century EF of 3.2, slightly lower than the current 3.7, but it had some higher values (up to 4.4) at 1996 yr CE. In ACH, Pb EF reached its highest peak (6.2) around 1990 and declined afterwards. In contrast, MAR and SAB had lower EF Pb during the GA, compared to the previously maximum values. MAR Pb EFs continued the decline since the peak in 1880 yr CE and SAB decreased, although with greater variability since its maximum EF in 1970 (EF 3.4). Cu increased during the GA in all lakes except SAB, where it showed the same trend as Pb. In URD, the maximum Cu EF values also occurred during the GA, with an EF of 3.8. Cd and Zn also had similar increasing trends during this period, except in SAB and MAR where there are subtle decreases.

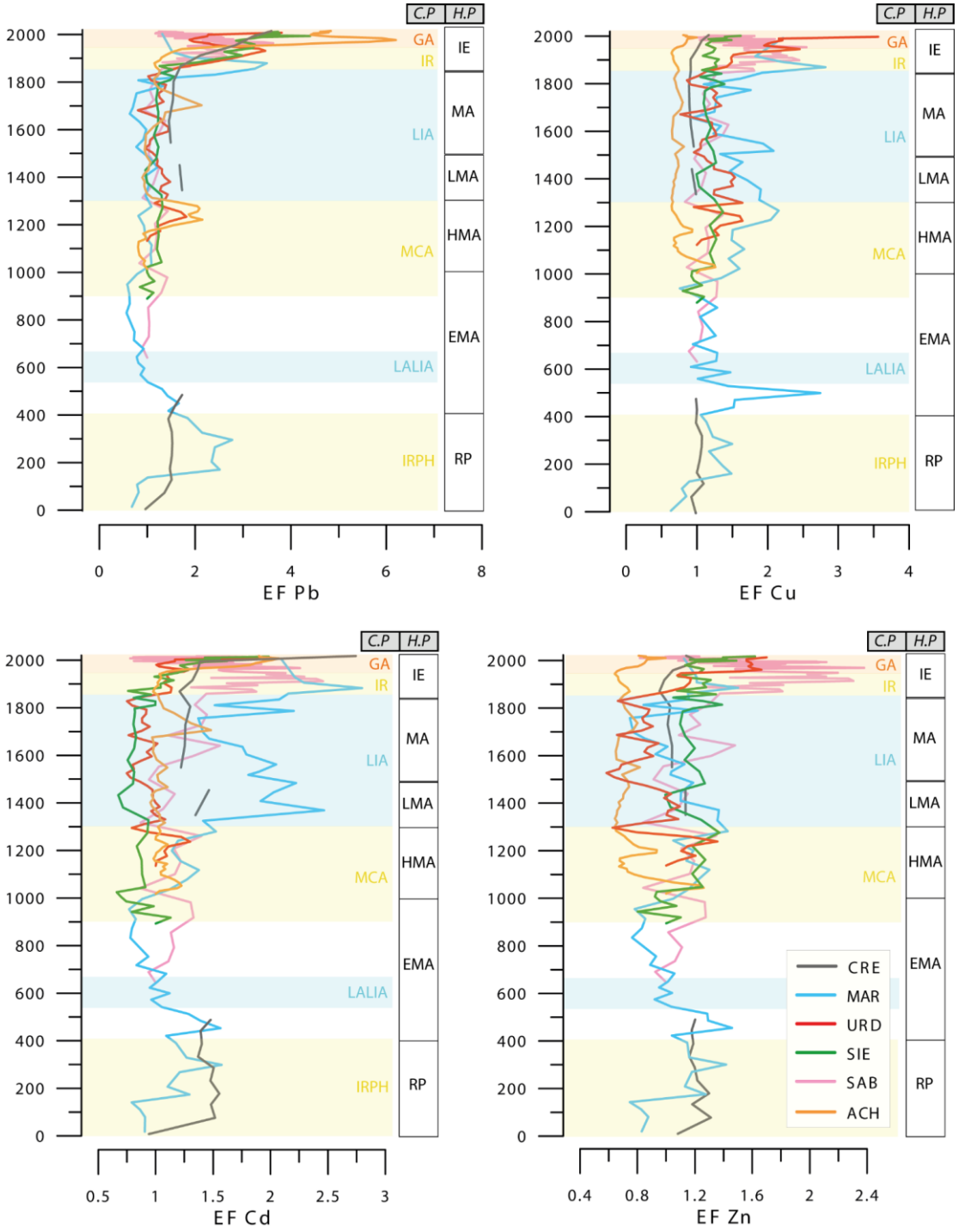

Fig. 6.4. *Enrichment factors (EF) of anthropogenic heavy metals (Cd, Cu, Pb and Zn) in Cregueña (CRE), Marboré (MAR), Urdiceto (URD), La Sierra (SIE), Sabocos (SAB) and Acherito (ACH) during the last 2000 years. The climatic (C.P) and historical (H.P) periods are indicated. The historical periods are Roman period (RP, 200 BCE – 400 CE), Early Middle Ages (EMA, 400 - 1000 CE), High Middle Ages (HMA, 1000 – 1300 CE), Late Middle Ages (LMA, 1300 – 1492 CE), Modern Ages (MA, 1492 – 1850 CE), Industrial Era (IE, 1850 CE – Current) including the Industrial Revolution (IR, 1850 – 1950 CE) and Great Acceleration (GA, 1950 – current CE).*

The data presented in this section demonstrate a large variability of EFs, both considering the lake and the specific heavy metals during the last 2000 years (Fig. 6.5). The EF for Pb had the maximum values in all lakes. In CRE Pb had 3.6, followed by Cd (2.7), Zn and Cd (1.2 and 1.1, respectively). In MAR, Pb EF was 3.5, followed by Cu and Cd (2.8 both), and Zn (1.5). URD EF Pb and Cu (3.8 and 3.5) were followed by Cd and Zn (2 and 1.7, respectively). The Pb EF of SIE (4.4) is much larger than any other metal (Cd 1.9, Zn 1.8 and Cu 1.6). In ACH the EF Pb (6.2) also has a large difference with the rest of metals (Cd 2.1, Zn 1.7 and Cu 1.3). Finally, all SAB EF are >2 (Cu 2.5, Cd 2.4 and Zn 2.3), with higher values for EF Pb (3.6).

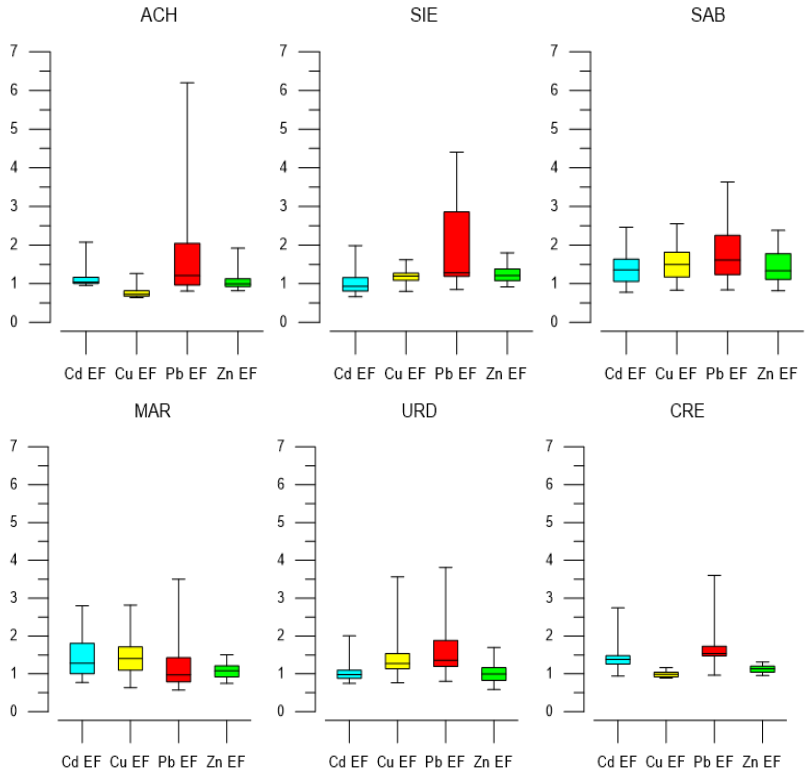

Fig. 6.5. *Box-whisker plot graphs with the minimum, maximum, median, lower quartile, and upper quartile of the heavy metal enrichment factors for each metal in each lake, for the last 2000 years. The caps at the end of each box indicate the extreme values (minimum and maximum), the box is defined by the lower and upper quartiles, and the line in the center of the box is the median.*

Figure 6.6 summarizes the EFs for each lake during the main cultural phases. The EFs in the studied lakes are similar to those calculated in other Pyrenean lakes and alpine regions of Europe (Bacardit & Camarero, 2010; Camarero, 2003; Camarero et al., 2009, 2017; Corella et al., 2017, 2018; Rosman et al., 2000; Schwikowski et al., 2004; Shotyk et al., 1998). Similarly to our records, Pb has the highest EF of all metals.

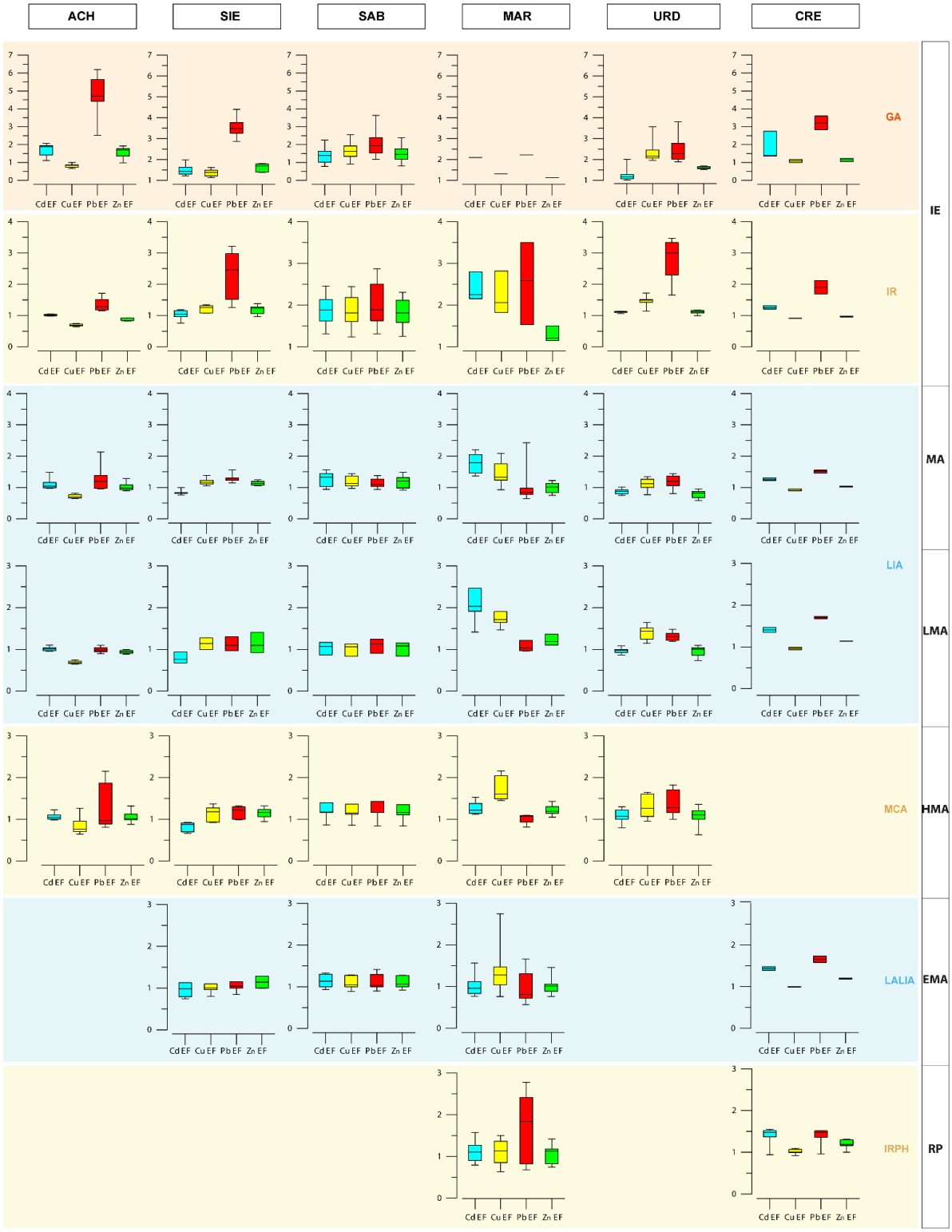

Fig. 6.6. *Box-whisker plot graphs with the minimum, maximum, median, lower quartile, and upper quartile of the heavy metal enrichment factors data for the last 2000 years for the main cultural and climate periods. The caps at the end of each box indicate the extreme values (minimum and maximum), the box is defined by the lower and upper quartiles, and the line in the center of the box is the median.*

6.4.2. Lake processes, altitudinal effects and watershed influence on heavy metal deposition

Several surveys (Bacardit et al., 2012; Bacardit & Camarero, 2009, 2010; Camarero, 2003; Camarero & Catalan, 1998; Corella et al., 2017, 2018) have demonstrated that the concentration of heavy metals in surface sediments of Pyrenean lakes is unexpectedly high, considering that they are in relatively remote locations, where contaminants input is almost exclusively through atmospheric deposition. The concentration in these lakes for some heavy metals and other pollutants is similar to that found in areas affected by urban, industrial or wastewater discharges (Camarero et al., 2009). There are several lake processes that contribute to these high concentrations in high altitude mountain lakes (REPLIM Report 2021, *http://www.ipe.csic.es/proyecto-replim*): i) the lakes are the final sink of their watersheds and therefore pollutants accumulate in these sediments; ii) lakes located in intermediate altitudes have moderate organic content and this facilitates the ability to bind metal cations and metalloids; and iii) sedimentation rates in these high altitude lakes are usually low, so the enrichment effect increases

The time series of concentration and enrichment factors for Pb, Cu, Cd and Zn in the six Pyrenean lakes show similar patterns, but a large variability in timing and intensity, likely reflecting diverse sources (regional and global), and local factors, such as depositional processes in the lake and watershed features, including altitude, geology and drainage patterns.

The **geology of the basin** and the water chemistry could be a significant factor in metal accumulation. Carbonate and organic deposition facilitates metal accumulation in the sediments (Morellón et al., 2011; Pérez-Sanz et al., 2013; Roberts, 2015; J. P. Smol, 2008). In our Pyrenean transect, MAR, ACH and SAB have carbonate formations in the watershed. MAR is located in a Cretaceous - Tertiary carbonate watershed with carbonate-bearing Quaternary glacial sediments (moraines between 30 and 86% of $CaCO_3$ (García-Ruiz et al., 2014), however, the lake waters are undersaturated in calcite and the carbonate content in the lake sediments is < 1 %. Endogenic calcite precipitation in the lake is unlikely and even if small calcite particles form in the lake, they dissolve before they reach the bottom without being able to trap trace metals (Oliva-Urcia et al., 2018; Sánchez España et al., 2018). In the case of Marboré, Sanchez-España et al. 2018 describe anomalous content of Iron and zinc in the water-column of Marboré Lake during 2013 to 2015, at a depth of 7 m with concentrations of 4500 µg/L Fe and 900 µg/L

Zn. This anomaly was not accidental and represents a common process in the lake. This increase might be related to an increase of weathering processes (e.g., increase in temperature and thawing of the ice cover) as a result from weathering reactions involving sulfides. Minor minerals as sulfides can therefore provide a minor contribution of heavy metals content as Fe, As, Zn or Cu.

There are no major differences in heavy metal compositions between lakes with carbonate watersheds and lakes with silicate or mixed watersheds. MAR, ACH and SAB located in carbonate watersheds do not show a higher concentration or enrichment of heavy metals than URD, CRE and SIE in silicate watersheds. This is probably due to the fact that the percentage of carbonate in the sediments is generally low (only in Sabocos reaches 45% of carbonates, although it is usually less than 25%, and in the rest of the lakes less than 2% of carbonate). Other factors besides watershed composition are more relevant to control the accumulation of heavy metals in these lakes.

Elevation is also an important factor as mountains intercept long-range, global contamination and differences in altitude generate strong climatic gradients that control dry versus wet deposition (Bacardit & Camarero, 2010). Several studies conducted at higher altitude lakes (> 2500 m asl) as Marboré and Cregüeña (Bacardit & Camarero, 2010; Corella et al., 2018) indicate that these higher altitude lakes are representative of global background contamination, since long-range atmospheric transport of contaminant metals occurs at altitudes above the mixing limit.

(Bacardit & Camarero, 2010a, 2010b) found higher enrichments of Ni, Cu, Zn and Pb in lower elevation sites due to the influence of local factors that were not observed in soils and snowpack at higher elevations. In the study conducted in an altitudinal transect of lakes in the Central Pyrenees, including Marboré, 2600 mm asl, Basa de la Mora, 1914 m asl, and Estaña, 670 masl, (Corella et al., 2018), lower metal concentrations were found in lakes located at lower altitudes.

The varied **depositional processes in the lakes** have also been considered as a possible explanation for the variability of accumulation of heavy metals (Blais & Kalff, 1995; Lehman, 1975; Mackay et al., 2012). In particular organic matter accumulation facilitates the ability to bind metal cations and metalloids and higher heavy metal concentrations are expected in lakes with higher O.M. content (Sánchez España et al., 2018). In the three carbonate-lakes in the central Pyrenees studied by Corella et al. (2018), the site located at the lower elevation (670 m asl) and with the highest OM

content had higher heavy metal concentrations. However, other factors such as higher endogenic carbonate formation and local sources (mining) could also have enhanced the atmospheric signatures preserved in the lake record (Corella et al., 2018; Morellón et al., 2011).

6.4.3. Heavy metals and anthropogenic activities

The main factor controlling deposition of heavy metals in Pyrenean lakes is the varied anthropogenic input (mining, smelting, industrial activities, fossil fuels). Our study and previous regional records show high EFs for heavy metals in the Pyrenees during Roman Period, the Medieval Ages and since the Industrial Revolution (Camarero et al., 1998; Corella et al., 2018; Hansson et al., 2017; Mata Campo et al., 2013; B. Oliva-Urcia et al., 2018).

The heavy metal pollution in Marboré during the Roman Period was higher than during the industrial revolution. The signature in Cregüeña also points to increased lead input during the RP, but EF was still lower than 2. The source of Pb pollution in Marboré could be both global and local mining/smelting activities. This great environmental impact of Roman mining has also been documented also in the French Pyrenees and in the Northwest and South of Spain (García-Alix et al., 2013; Hanebuth et al., 2018; Hansson et al., 2017; Hillman et al., 2017; Martín-Puertas et al., 2010). The high levels of Pb during the RP suggest that the main source of contamination was large-scale mining, as there is an absence of historical records and infrastructures that document Roman mining in this region (Irabien et al., 2012; Urteaga, 2014). There are also no records of impacts associated with mining (deforestation and fires) in regional and local paleoenvironmental reconstructions (González-Sampériz et al., 2017; Leunda et al., 2017, 2020; Pèlachs et al., 2009). However, the similar Pb isotopic signatures of Marboré lake sediment and some ore samples from mines close to Marboré (Parzán, Bizielle, Cierco, Palouma) suggest that local exploitation of Pb and Ag in the region could have contributed to the heavy metal pollution (Corella et al., 2021).

All of available data suggest that most of the heavy metal contamination came from large-scale regional mining sources. During the RP, the Rio Tinto and Mazarrón mines were the most important in the Roman Empire, and it has been estimated that around 70% of the total atmospheric Pb released into the environment at that time would have originated from these mines (Rosman et al., 1997). Therefore, the enrichment in

the Pyrenees would be a reflection of large-scale mining in southern Spain (Corella et al., 2021). In addition, this would not only affect the deposition of Pb, but would also be reflected in the parallel enrichment of Cd and Zn, since they are two by-products of Pb in mining and smelting techniques (Dudka & Adriano, 1997), and in Cu, which also had a large production, not only in Rio Tinto, but also in other mines in the NW of the peninsula (Wilson, 2002). At a global scale, the maximum levels of Cu in the atmosphere occurred at the end of the RP perhaps due to the increased demand for Cu for coinage when the Roman monetary system changed to a bimetallic coin composed of an alloy of Au and Cu (McConnell et al., 2018; A. Wilson, 2002). In MAR, the EF for Cu reached 2.7 in 510 CE. The concentrations of Pb, Zn and Cd decrease progressively at the end of this period, coinciding with the decrease in Roman mining in the Iberian Peninsula, largely attributed to the socio economic crises of the Roman Empire (McConnell et al., 2018).

The next increase in Cu, Pb, and their associated metals, occurred between the 11th and 13th century, during the HMA and LMA and it was more likely related to the exploitation of local mines. SIE and MAR show this increased around 1000 yr CE and the other lakes a little later. The boom in demand for Pb at these times coincides with the first historical evidence of local mining at Parzan, after Aragon kings Alfonso II and Jaime II granted permits for ore extraction to local nobles in 1277 and 1293 yr CE (Bielza et al., 1986). These new activities could explain the Pb peaks in ACH and URD in the 13th century and the beginning of a new phase of Cu enrichment in MAR. The use of local furnaces for smelting Cu, Ag, Pb and Fe are also documented during these periods (Nieto Callén, 1996), which could explain the Cu increase during the LMA.

In addition to the correlation of metal deposition and anthropic record, there is also a correspondence between the EFs periods and the climatic phases. Warmer periods, with a longer season without snow favored the exploitation of mineral resources in mountainous areas. The extractive mining period during the HMA and LMA coincided with the MCA, a warm and arid period in the Iberian Peninsula between 900 and 1300 yr CE (Moreno et al., 2012). In contrast, there was a decline in Pb during the EMA and MA coincided with the LALIA and LIA, both cold periods in the Iberian Peninsula (Corella et al., 2012, 2013; Morellón et al., 2012; B. Oliva-Urcia et al., 2018). This relationship between climatic phases and mining activities in alpine environments was also observed in the Western Alps (Guyard et al., 2007), as in this region mining was only possible when glaciers retreated.

The Industrial Era atmospheric deposition of metals in all lakes follows the increasing trend of lead pollution in Europe (Rosman et al., 2000; Schwikowski et al., 2004; Shotyk et al., 1998). At a more regional level, increased coal combustion in Europe since 1850 yr CE has been proposed as the main source of increased Pb deposition in coastal sediments and peatlands in northern Spain (Leorri et al., 2014; Martínez Cortizas et al., 2013). Copper mines also were more active in northern Spain during the 19th century (Nieto Callén, 1996). Many studies show the impact of industry in estuaries to the W of the Pyrenees and the increase of heavy metals in recent decades (Fdez-Ortiz de Vallejuelo et al., 2010; Fernández et al., 2008; Garmendia et al., 2019; Rodriguez-Iruretagoiena et al., 2016).

Although, as previously stated, there are some indications of Roman activities and documentary evidence of late medieval mining in the central Pyrenees, the main impact in the central Pyrenees area from local mining was derived from the Parzan and Cierco galena mines and it occurred between 1860 and 1930 yr CE. The agreement between Pb isotope ratios of MAR sediments and galena samples suggest the intense large-scale Pb mining activities in the Southern Central Pyrenees was a main factor controlling deposition of Pb, Cd and Zn in Marboré, Urdiceto and Cregüeña lakes during Modern times (Camarero et al., 1998; Corella et al., 2017; Nieto Callén, 1996). In the 1930s there was a sharp decline with a return to near pre-industrial values of Zn, Cd and Pb in MAR (and a little later, around 1940 in URD), probably related to the economic recession of the time, the impact of the Spanish Civil war and the closure of the mines.

The overall impact of the usage of leaded fuels, which increased greatly since 1950 (Schwikowski et al., 2004), is clearly documented in all lakes, more notable in those where local mining was not the main input. In ACH, the Pb enrichment factors during the GA are much higher than in the rest of the lakes and this could be due to the fact that it is the lake located at lower altitude, and pollution due to road transport may be more effective (von Storch et al., 2003). However, it is also possible that sedimentation in the lake has become more organic and that this has facilitated Pb accumulation in the sediments. The higher Pb enrichments in the late 1980s (after mines closure) in URD CRE or SIE, are consistent with the global increase of lead emissions in Spain (Eurostat, 1998; Pacyna et al., 2007). The drastic reduction in Pb during the last decades - particularly in ACH or SIE - would reflect the ban of leaded gasoline in Spain in 2001.

With respect to Zn, the increase seen in these lakes in the industrial era could be due to higher emissions on a global scale associated with the increase in industrial and agricultural activities with fertilizers (Nriagu, 1979, 1996).

6.5. Conclusions

The characteristics of each lake such as location, altitude, sediment type, depth, watershed size, water characteristics, etc., influence the ability of the system to store heavy metals transported by atmospheric fallout both from regional sources and over long distances. The record of heavy metal deposition in the Pyrenean lakes shows a large variability, with different timings and intensities due to local and lake-specific processes. However, all show positive enrichments of Pb, Cu, Cd and Zn during Roman, Medieval and Industrial revolution times.

The historical mining -mainly during the RP, and later, HMA and LMA - was the main anthropogenic impact in relation to metal deposition on the environment. There is a clear relationship between these periods of higher impact and climatic periods, since mining was more active in temperate and warmer phases, allowing the extraction of minerals, and decreased in colder climatic conditions (LALIA and LIA).

Our study supports that lakes located at higher altitudes register better the global atmospheric deposition of heavy metals over long distances, while in lakes at lower altitudes, biogeochemical processes (such as the greater deposition of organic matter) and local factors (regional climatic variability, pollution due to their proximity to populated areas and infrastructure) are more significant. In our transect, the increase in Pb enrichment during the industrial era started earlier in MAR and CRE, followed closely by URD (the lakes located at higher altitudes), and later one in the other three located at lower altitude.

With respect to variation in heavy metal deposition due to their location in the W-E transect, we have not detected major changes during present and past high accumulation phases. In Pb, the lakes with the highest enrichment are ACH and SIE, located further west, but this increase is probably due to their more organic composition and their higher capacity to retain these metals. The rest of the lakes have, although at different times, similar EF. With respect to Cu, although also with great variability, the

lakes with the highest EF are URD, MAR and SAB, those located further east, where there has been historically a higher level of industrialization.

The trend of increase of these metals in different periods correlates well with other nearby records and with regional and global emission inventories, suggesting a mixed signal between local and global sources of trace metal contamination.

6.6. Supplementary Information

Correlation coefficients between XRF, XRF ratios, %TOC and %Sand data for each lake:

-CRE

0	TOC	%ARN	%LIMO	Al	Ca	Ti	Mn	Fe	Pb	Fe/Mn	Br/Ti	Ca/Ti	Rb/Zr	K/Ti	Pb/Ti
TOC	0	0,0062406	0,00223	0,029052	0,00022331	0,0018354	0,96394	0,0016327	0,74981	0,017502	0,00023191	0,28167	0,096062	0,040856	0,0017221
%ARN	-0,45332	0	2,87E-38	0,66383	0,11491	0,74078	0,93017	0,53333	0,039656	0,42008	0,3994	0,26076	0,20942	0,12376	0,27318
%LIMO	0,4999	-0,997	0	0,58197	0,080194	0,61067	0,86805	0,67942	0,051415	0,56782	0,31649	0,29156	0,24757	0,10041	0,22073
Al	-0,36922	0,076124	-0,096334	0	2,41E-11	9,96E-09	0,04366	2,28E-06	0,33401	0,033397	0,028134	0,65782	0,002787	1,64E-06	0,035715
Ca	-0,58502	0,2713	-0,29977	0,86364	0	2,14E-16	0,17603	6,55E-09	0,59034	0,00071614	3,29E-05	0,18748	0,018349	5,45E-05	3,85E-05
Ti	-0,50803	0,057977	-0,089123	0,79721	0,93481	0	0,20129	1,06E-15	0,11729	4,74E-06	1,69E-06	0,0074406	0,0019361	0,011296	4,34E-06
Mn	-0,0079303	-0,015369	0,029134	0,34303	0,23402	0,22135	0	0,23619	0,78805	0,0079275	0,35975	0,4465	0,31674	0,20736	0,23231
Fe	-0,51282	-0,10894	0,072389	0,70488	0,80282	0,92795	0,20555	0	0,0024794	6,90E-08	3,72E-06	0,001419	0,00014254	0,067383	8,74E-05
Pb	-0,05589	-0,34939	0,33192	0,16824	0,094216	0,26961	0,047129	0,49539	0	0,0091931	0,12862	0,023022	0,012669	0,58291	0,85474
Fe/Mn	-0,39925	-0,14072	0,099949	0,36048	0,54473	0,68894	-0,44151	0,76875	0,43399	0	0,00056389	0,0063992	0,011875	0,64173	0,0045152
Br/Ti	0,58379	-0,147	0,17435	-0,3712	-0,64147	-0,71104	-0,15961	-0,69434	-0,26186	-0,55342	0	2,36E-09	0,056678	0,9908	5,47E-18
Ca/Ti	0,18716	0,19535	-0,18342	-0,077573	-0,22813	-0,44468	-0,13293	-0,51848	-0,38333	-0,4521	0,81585	0	0,0525	0,0067852	1,15E-08
Rb/Zr	-0,28579	-0,21751	0,20074	0,49034	0,39656	0,50582	0,17426	0,59924	0,41713	0,4206	-0,32513	-0,33048	0	0,51079	0,14463
K/Ti	-0,34743	0,26512	-0,28227	0,71173	0,6276	0,42325	0,21847	0,31273	-0,096096	0,081475	-0,0020225	0,44924	0,11496	0	0,99557
Pb/Ti	0,51065	-0,19043	0,21233	-0,35619	-0,6372	-0,69093	-0,20722	-0,614	-0,032102	-0,46867	0,94812	0,79519	-0,25173	0,00097303	0

-MAR

0	TIC	TOC	Al	Ca	Ti	Mn	Fe	Pb	Fe/Mn	Br/Ti	Ca/Ti	Rb/Zr	K/Ti	Pb/Ti
TIC	0	3,84E-12	0,63516	0,52792	0,91194	0,7675	0,091573	0,43305	0,87596	0,1845	0,56611	0,6482	0,61228	0,4229
TOC	-0,75321	0	0,29939	0,27057	0,060114	0,68979	0,28593	0,11431	0,43799	0,6385	0,12494	0,21504	0,93268	0,14395
Al	0,06251	-0,13621	0	0,00067737	2,26E-10	0,54609	0,027471	0,069501	0,016945	0,04729	0,047896	0,98854	1,64E-12	0,21842
Ca	0,083092	0,14453	0,42656	0	0,7471	0,0074944	0,81113	0,25385	0,024069	0,09391	3,74E-39	0,81559	0,0053341	0,26281
Ti	0,014584	-0,24415	0,70924	0,042506	0	0,22275	0,093885	0,031498	0,021779	7,35E-05	0,1637	0,90177	0,0075529	0,19054
Mn	0,038973	0,0526	-0,079478	0,34194	-0,15975	0	0,010258	0,018719	2,51E-23	0,023492	0,0057737	0,44824	0,77684	0,010783
Fe	0,21976	-0,14003	0,2847	-0,031505	0,21825	0,32904	0	0,015773	0,5597	0,74064	0,45968	0,53528	1,11E-07	0,025482
Pb	0,10311	-0,206	0,23598	0,14963	0,27801	0,30273	0,31045	0	0,51634	0,55536	0,60064	0,67842	0,2164	2,34E-56
Fe/Mn	-0,020582	-0,10201	0,30724	-0,29104	0,29574	-0,90604	-0,076806	-0,085428	0	0,029261	0,0078869	0,45812	0,065447	0,36666
Br/Ti	0,17367	0,061895	-0,25718	0,21823	-0,48901	0,29219	-0,043629	0,077655	-0,28163	0	0,012007	0,62672	0,38543	0,29776
Ca/Ti	0,07556	0,20028	0,2565	0,97412	-0,18213	0,35227	-0,097273	0,06895	-0,33987	0,32236	0	0,80346	0,042961	0,49472
Rb/Zr	-0,060114	0,16241	-0,0018939	-0,030748	0,016276	-0,099756	-0,081621	-0,054636	0,097608	0,064071	-0,032811	0	0,53691	0,65822
K/Ti	0,066762	0,01114	0,76136	0,35534	0,34162	0,037365	0,62226	0,16194	0,23939	-0,11408	0,26223	0,081295	0	0,34623
Pb/Ti	0,10539	-0,19092	0,16124	0,14687	0,17134	0,32693	0,28832	0,99346	-0,11863	0,13667	0,089864	-0,058287	0,12374	0

-URD

0	TOC	%LIMO	%ARENAS	Al	Ca	Ti	Mn	Fe	Pb	Br/Ti*	Pb/Ti*	Fe/Mn*	Ca/Ti	K/Ti	Rb/Zr
TOC	0	0,00035766	8,87E-05	0,62582	0,0076647	0,23291	0,00012596	0,14451	0,0048286	0,16018	0,093063	0,0026848	0,010723	0,07169	0,32124
%LIMO	0,63653	0	1,15E-21	0,80306	0,20079	0,88528	0,03377	0,16165	0,00035047	0,059972	0,0023636	0,068876	0,057346	0,35956	0,5793
%ARENAS	-0,68221	-0,98769	0	0,95781	0,16304	0,84239	0,017402	0,2117	0,00022457	0,040421	0,0018552	0,030953	0,045489	0,21508	0,90992
Al	0,098265	0,050347	-0,010687	0	0,00030837	0,00059668	0,28995	0,019977	0,55846	0,00075219	0,17224	0,99827	0,65003	4,31E-07	0,0080433
Ca	0,50174	0,25416	-0,27627	0,64177	0	4,39E-07	0,00011685	0,020768	0,11786	0,034466	0,23667	0,038126	0,055915	0,19751	0,67553
Ti	0,23751	0,029139	-0,04015	0,61772	0,80394	0	0,12847	0,00052132	0,29463	0,00014003	0,022881	0,99454	0,21754	0,09652	0,91249
Mn	0,67143	0,40979	-0,45389	0,21134	0,67377	0,29997	0	0,35201	0,016325	0,41308	0,24053	6,11E-06	0,0011057	0,26888	0,34302
Fe	0,28846	0,27714	-0,24832	0,44515	0,44265	0,6228	0,18636	0	0,030635	0,080239	0,86445	0,055197	0,24254	0,23575	0,069654
Pb	0,52603	0,63726	-0,65264	0,11779	0,30816	0,20935	0,45787	0,41662	0	0,149	3,15E-06	0,1213	0,37161	0,23509	0,87942
Br/Ti*	0,27808	0,36663	-0,39683	-0,60879	-0,40834	-0,66808	0,16422	-0,34259	0,28541	0	9,93E-05	0,078092	0,041722	0,00011717	0,17121
Pb/Ti*	0,3297	0,56041	-0,57128	-0,27058	-0,23566	-0,43634	0,23379	-0,034476	0,76639	0,67878	0	0,099126	0,12495	0,035369	0,92399
Fe/Mn*	-0,55453	-0,3554	0,4159	0,00043759	-0,40109	0,001382	-0,75198	0,37319	-0,30544	-0,3449	-0,32407	0	0,00049926	0,10227	0,07608
Ca/Ti	0,48294	0,37018	-0,38805	0,091463	0,37218	-0,24527	0,59334	-0,23282	0,17902	0,39449	0,30263	-0,62441	0	0,66022	0,56577
K/Ti	-0,35208	-0,1835	0,24655	0,80428	0,25596	0,32646	-0,22058	0,23611	-0,23643	-0,67369	-0,4065	0,32126	-0,08863	0	0,00012386
Rb/Zr	-0,19837	0,11164	-0,022851	0,4991	-0,084402	-0,022198	-0,1898	0,35447	-0,030638	-0,2712	0,019271	0,34711	-0,11562	0,67195	0

-SIE

0	TOC	%_ARENAS	%LIMOS	Al	Ca	Ti	Mn	Fe	Pb	Fe/Mn	Br/Ti	Ca/Ti	Rb/Zr	K/Ti	Pb/Ti
TOC	0	0,61883	0,73126	0,047588	0,0005719	0,00037951	0,049383	0,049595	0,1097	0,5983	6,96E-06	3,23E-09	0,12557	0,83816	2,53E-06
%_ARENAS	0,082205	0	1,17E-26	0,18461	0,24669	0,58469	0,048537	0,59579	0,78657	0,0070325	0,96285	0,95735	0,51806	0,72095	0,5563
%LIMOS	0,0568	-0,97764	0	0,49276	0,48391	0,88011	0,055892	0,47091	0,26587	0,012378	0,42808	0,43858	0,73198	0,93592	0,20388
Al	-0,31925	-0,21696	0,11316	0	0,5296	2,84E-12	0,078016	2,07E-05	0,10966	0,65282	6,58E-07	9,97E-05	0,0050621	5,29E-09	4,87E-05
Ca	0,52671	0,18998	-0,11548	0,10376	0	0,86808	0,084755	0,47272	0,088797	0,83248	0,4786	0,0037653	0,56335	0,034358	0,36221
Ti	-0,54074	-0,090275	-0,024961	0,85836	-0,027486	0	0,50785	9,09E-09	0,2506	0,82181	2,03E-13	5,94E-10	0,0037516	1,10E-05	2,60E-12
Mn	0,31684	-0,31797	0,30867	0,28558	0,27958	0,10927	0	0,91324	0,62254	5,39E-09	0,65782	0,25688	0,64571	0,068806	0,32911
Fe	-0,31656	0,087629	-0,11891	0,62542	0,11843	0,77135	-0,018032	0	0,23548	0,016341	3,98E-06	2,22E-08	0,028881	0,00011694	9,52E-10
Pb	0,28016	-0,044793	0,1826	-0,26019	0,27616	-0,18845	-0,081339	0,19448	0	0,64239	0,20001	0,21312	0,74481	0,37803	0,71691
Fe/Mn	-0,087034	0,42478	-0,39683	-0,074352	-0,034999	0,037263	-0,77852	0,38221	0,076744	0	0,3325	0,20522	0,37422	0,85007	0,1258
Br/Ti	0,65181	-0,0077514	0,1306	-0,70137	0,11687	-0,87835	0,073212	-0,66441	0,20974	-0,15937	0	7,62E-12	0,016802	0,0015369	6,32E-16
Ca/Ti	0,78529	0,0088506	0,12768	-0,58259	0,45318	-0,80806	0,18602	-0,677	0,2039	-0,20739	0,85	0	0,04717	0,038421	6,63E-18
Rb/Zr	-0,2495	-0,10667	0,056642	0,44001	0,095428	0,45334	-0,075982	0,35013	-0,053834	0,14628	-0,38071	-0,31982	0	0,059728	0,036674
K/Ti	0,033797	-0,059068	0,013306	0,77876	0,33971	0,64112	0,29447	0,57788	-0,14513	0,03128	-0,49017	-0,33283	0,3042	0	0,0074204
Pb/Ti	0,67423	-0,097147	0,20799	-0,60286	0,14996	-0,85907	0,16048	-0,80052	0,059959	-0,24936	0,91237	0,93213	-0,33571	-0,42221	0

-SAB

0	%LIMO	%ARENAS	%_TIC	%_TOC	Al	Ca	Fe	Mn	Pb	Ti	Pb/Ti*	Fe/Mn*	Ca/Ti	K/Ti
%LIMO	0	6,20E-56	0,97588	0,25744	0,49216	0,98145	0,90379	0,59423	0,0094463	0,52926	0,24077	0,47003	0,97423	0,40838
%ARENAS	-0,99162	0	0,5224	0,66302	0,76615	0,50889	0,49054	0,36874	0,0057085	0,67042	0,29563	0,50147	0,59501	0,30319
%_TIC	-0,0038878	0,082095	0	6,70E-13	6,44E-09	1,04E-55	1,86E-36	0,0006313	0,00054545	0,0016252	0,16955	0,019656	1,18E-20	0,50181
%_TOC	0,14482	-0,055977	0,7575	0	1,15E-06	1,45E-13	1,08E-10	0,024651	0,86837	0,0095727	0,049781	0,023635	8,29E-09	0,52137
Al	-0,088135	0,038222	-0,6534	-0,56892	0	3,37E-09	1,41E-07	0,0018071	0,92092	7,92E-29	1,06E-14	0,61786	1,76E-13	3,98E-06
Ca	-0,0029889	0,08477	0,99148	0,77101	-0,66239	0	2,97E-33	0,00017172	0,00039693	0,0010248	0,13555	0,05835	2,45E-23	0,478
Fe	0,01554	-0,088464	-0,96305	-0,70545	0,60607	-0,95271	0	1,10E-05	0,00035027	0,0057158	0,28727	0,060623	1,40E-15	0,43686
Mn	0,068407	-0,11517	-0,419	-0,28293	0,38552	-0,45617	0,52294	0	0,062114	0,0066495	0,07133	5,36E-09	2,19E-05	0,81155
Pb	0,32459	-0,34441	-0,42339	0,021304	-0,012762	-0,43274	0,43634	0,23642	0	0,31068	0,00029658	0,90208	0,0057953	0,0055758
Ti	-0,080752	0,054671	-0,38905	-0,32405	0,93333	-0,404	0,34436	0,33854	-0,12978	0	1,11E-18	0,44535	3,77E-07	1,63E-12
Pb/Ti*	0,14996	-0,13385	0,17523	0,24826	-0,79215	0,19014	-0,13617	-0,22876	0,44108	-0,85062	0	0,31757	0,00020728	4,01E-10
Fe/Mn*	-0,092677	0,086257	-0,29329	-0,28488	0,064072	-0,23981	0,23774	-0,65598	0,015817	-0,097882	0,12796	0	0,68778	0,48909
Ca/Ti	0,0041531	0,068262	0,8727	0,64981	-0,76933	0,8973	-0,80697	-0,50741	-0,34384	-0,58923	0,45105	-0,051632	0	0,59652
K/Ti	0,10599	-0,13179	-0,086188	-0,082298	-0,54442	-0,091029	0,099709	-0,030646	0,34531	-0,74925	0,68985	0,088759	0,067984	0

-ACH

0	TOC	%ARN	%LIMO	Al	Ca	Ti	Mn	Fe	Pb	Fe/Mn	Br/Ti	Ca/Ti	Rb/Zr	K/Ti	Pb/Ti
TOC	0	0,6267	0,97264	0,00024275	0,75585	1,23E-05	0,034779	0,00078991	0,10649	0,028821	7,07E-08	2,52E-12	0,77301	0,66022	0,0028041
%ARN	0,05959	0	6,13E-63	0,54257	0,36073	0,23952	0,039079	0,54478	1,64E-05	0,53614	0,025443	0,1482	0,19638	0,65149	0,00041406
%LIMO	-0,0042053	-0,99252	0	0,25473	0,24863	0,10115	0,0099923	0,68531	2,75E-06	0,28365	0,004761	0,066077	0,3293	0,42553	8,16E-05
Al	-0,42814	0,074566	-0,13898	0	3,56E-11	1,27E-25	0,03694	2,13E-10	0,00054808	1,07E-05	3,17E-10	7,82E-06	0,96814	7,26E-14	2,30E-09
Ca	0,038114	0,11173	-0,14077	0,69472	0	2,21E-12	0,86367	6,68E-10	0,19011	0,007428	0,0003954	0,97889	0,7865	2,19E-09	0,00056832
Ti	-0,49982	0,14348	-0,199	0,89829	0,72337	0	0,017249	4,05E-15	0,00048634	4,50E-07	3,01E-15	1,29E-09	0,95074	2,34E-08	4,65E-12
Mn	0,25457	-0,24902	0,30817	-0,25172	0,021054	-0,28589	0	0,15844	0,001573	9,41E-08	7,17E-05	3,82E-05	0,31474	0,16587	0,0015174
Fe	-0,39472	-0,074159	0,049661	0,67431	0,66038	0,77732	0,17166	0	0,73664	0,018133	0,00019129	0,0024984	0,98993	6,80E-05	0,0018625
Pb	0,19602	-0,49359	0,53052	-0,40545	-0,15964	-0,40888	0,37348	-0,041222	0	0,016983	0,00028003	2,05E-06	0,45259	0,0074164	3,98E-22
Fe/Mn	-0,2633	0,075755	-0,13091	0,50285	0,31961	0,564	-0,59026	0,28377	-0,28655	0	1,53E-05	0,00015348	0,075977	0,00042781	0,00011473
Br/Ti	0,59482	-0,26895	0,33602	-0,66955	-0,41474	-0,77955	0,45939	-0,43448	0,42427	-0,49508	0	2,28E-12	0,15114	5,39E-05	1,68E-11
Ca/Ti	0,72209	-0,17592	0,22254	-0,5094	0,0032453	-0,652	0,47443	-0,35837	0,53617	-0,44024	0,72307	0	0,44188	0,086156	2,10E-12
Rb/Zr	-0,035359	-0,15743	0,1192	0,0048979	-0,033205	0,0075753	-0,12281	-0,0015472	-0,091911	0,21505	-0,17467	-0,094093	0	0,56203	0,26785
K/Ti	-0,053868	0,055347	-0,097484	0,7543	0,64509	0,61177	-0,16869	0,46066	-0,31967	0,41252	-0,46628	-0,20812	0,071013	0	2,03E-06
Pb/Ti	0,35448	-0,41344	0,45621	-0,64442	-0,4044	-0,71603	0,37462	-0,36804	0,86875	-0,4477	0,70278	0,72389	-0,13525	-0,53639	0

Correlation coefficients between ICP, %TOC and %Sand data for each lake:

-CRE

	Al	As	Ca	Cr	Cu	Fe	K	Li	Mg	Mn	Na	Ni	P	Pb	S	Si	Ti	V	Zn	%TOC	%Sand
Al		0,0001257	0,1894	6,53E-26	3,39E-19	3,94E-10	2,15E-10	1,96E-08	4,39E-22	1,39E-05	6,37E-12	3,04E-21	0,10526	0,00024134	0,0097225	0,1013	0,035115	1,26E-12	7,18E-11	0,092592	2,13E-11
As	0,56333		0,31566	0,00084486	8,45E-05	1,68E-06	2,36E-05	0,0471	0,00014043	0,0042934	0,0028288	0,0004808	0,025349	0,0012917	0,1393	0,011306	0,0008547	9,81E-09	0,0006920	0,0035307	
Ca	0,20915	0,16066		0,054272	0,031649	0,90579	0,30492	0,001279	0,039404	0,00020534	0,094791	0,14784	0,00020494	0,029267	0,71626	0,075666	0,0005803	0,00091968	0,013376	0,0044969	0,010295
Cr	0,97122	0,50116	0,30285		4,89E-24	4,40E-07	1,47E-08	2,33E-07	1,02E-21	1,64E-05	3,26E-09	1,64E-28	0,49046	0,0001001	0,0015014	0,26455	0,22081	2,77E-17	6,14E-12	0,036979	2,21E-13
Cu	0,93534	0,57488	0,33615	0,96997		2,97E-06	2,14E-07	4,49E-06	1,69E-16	8,81E-05	5,31E-08	9,86E-23	0,6681	4,42E-05	0,0002577	0,50517	0,36367	5,94E-18	5,76E-13	0,0048763	4,63E-14
Fe	0,7986	0,66978	-0,019072	0,69584	0,65772		1,35E-14	1,12E-05	8,01E-11	1,20E-05	5,23E-10	1,69E-06	5,10E-06	0,020324	0,076865	5,38E-05	1,66E-06	0,00029822	3,63E-07	0,6010	0,00099062
K	0,80541	0,60926	-0,16421	0,75176	0,70888	0,88606		0,015413	6,42E-10	0,0059346	6,70E-06	5,38E-09	9,25E-06	0,061623	0,00014176	5,65E-06	1,15E-06	3,32E-05	1,21E-07	0,26312	8,52E-05
Li	0,74756	0,31111	0,4859	0,70741	0,64872	0,62768	0,37597		4,87E-10	5,22E-13	5,44E-15	8,57E-06	0,80426	2,48E-05	0,61499	0,83371	0,91432	1,43E-06	2,80E-05	0,86073	8,19E-05
Mg	0,95443	0,56003	0,32302	0,95236	0,91003	0,81599	0,79291	0,79617		1,90E-09	6,08E-13	1,93E-18	0,24632	8,12E-05	0,0047322	0,07309	0,13601	6,13E-15	2,19E-14	0,13647	8,95E-11
Mn	0,62247	0,43685	0,54844	0,61845	0,57371	0,62597	0,42244	0,86093	0,77958		4,16E-10	6,53E-05	0,51724	1,61E-05	0,19248	0,42277	0,52323	1,75E-07	8,42E-08	0,86541	0,00058186
Na	0,84031	0,45457	0,26442	0,77264	0,73222	0,79534	0,63971	0,89155	0,85977	0,79799		2,74E-08	0,30318	1,20E-07	0,42351	0,072618	0,19846	2,29E-07	2,04E-07	0,71485	8,72E-05
Ni	0,94956	0,52084	0,23008	0,97891	0,95785	0,66958	0,76591	0,63402	0,92911	0,58215	0,74247		0,58375	4,83E-05	8,52E-05	0,31426	0,2901	2,89E-17	1,61E-12	0,052625	5,03E-14
P	-0,25666	-0,34895	0,5485	-0,11079	-0,069015	-0,64588	-0,63223	0,039925	-0,18522	0,10408	-0,1648	-0,088129		0,027674	0,96939	3,92E-07	1,23E-28	0,29101	0,61778	0,81539	0,84639
Pb	0,54338	0,31873	0,34072	0,57001	0,59283	0,36121	0,29449	0,60801	0,57603	0,61882	0,71885	0,59044	0,34394		0,073393	0,61032	0,088625	4,56E-06	5,05E-05	0,59011	0,00776318
S	0,3992	0,56252	0,058524	0,4798	0,5413	0,27941	0,55975	-0,080924	0,43258	0,20773	0,12845	0,57465	0,0061841	0,28262		0,17847	0,75079	2,36E-05	7,90E-06	0,0001787	0,00137433
Si	0,25952	0,23491	-0,2805	0,17836	0,10708	0,58752	0,64357	0,033824	0,28213	0,12865	0,28335	0,16111	-0,69798	-0,081991	0,2143		2,14E-07	0,73513	0,22915	0,89201	0,85586
Ti	-0,32999	-0,39176	0,5144	-0,19541	-0,14561	-0,66998	-0,67738	0,017337	-0,23683	0,10261	-0,20503	-0,16926	0,97921	0,26931	-0,05115	-0,70886		0,51912	0,40628	0,89646	0,8946
V	0,85403	0,50074	0,4981	0,91832	0,92474	0,53662	0,60046	0,67304	0,89085	0,71236	0,70765	0,91813	0,16894	0,6484	0,60932	0,05448	0,10362		1,11E-13	0,0051892	1,31E-13
Zn	0,81713	0,75758	0,38328	0,84064	0,86017	0,69943	0,71872	0,6049	0,88305	0,72475	0,7097	0,85205	-0,080287	0,58923	0,63592	0,19199	-0,13324	0,87226		0,0134833	3,34E-09
%TOC	0,26613	0,50826	0,43483	0,32688	0,43126	0,084121	0,17888	-0,028268	0,23655	0,02731	-0,058827	0,30484	0,037613	-0,086649	0,55273	0,021876	-0,020969	0,42849	0,38288		0,0029168
%Sand	-0,82918	-0,44528	-0,3964	-0,86734	-0,8782	-0,49539	-0,57466	-0,57577	-0,81484	-0,51431	-0,57399	-0,87764	-0,031212	-0,4108	-0,48318	-0,029268	0,02135	-0,87108	-0,77229	-0,4533	

-MAR

	Al	Ba	Ca	Cd	Co	Cr	K	Mg	Mn	Na	P	Pb	S	Si	Ti	As	B	Cu	Fe	Mo	Ni	Sr	Zn	Zr	TOC
Al		4,48E-52	0,56952	0,70788	0,12858	4,27E-12	1,10E-48	1,54E-16	0,2624	0,00039036	0,11092	0,025014	0,038352	2,15E-13	1,04E-20	0,0086135	1,33E-23	0,85255	0,020966	0,097338	0,21028	5,86E-08	0,58066	1,76E-13	0,09057
Ba	0,998422		0,46197	0,13736	2,43E-14	3,78E-39	5,82E-17	0,17009	0,00020361	0,15275	0,033078	0,076331	0,033734	1,91E-24	0,59545	0,022107	0,039226	0,24862	6,19E-09	0,54604	1,37E-15	0,0006207	0,0035307		
Ca	0,079129	0,10223		0,0046679	0,34606	0,071584	0,67109	0,089628	1,28E-10	2,85E-12	0,97879	0,5597	0,78292	0,92056	0,40952	0,11416	0,21536	0,00042142	0,48347	0,21287	0,17745	4,35E-09	0,00076466	0,11018	0,0075019
Cd	0,052178	0,13394	0,36616		0,35061	2,04E-07	0,83163	0,0033882	0,00025628	0,039227	0,42632	0,062049	0,28382	0,53812	0,012495	1,08E-05	0,051316	9,07E-07	0,017182	6,76E-09	0,12677	2,32E-05	5,72E-05	2,03E-05	0,57782
Co	0,20941	0,2048	0,13073	0,12951		0,097295	0,19963	0,0081057	0,057483	0,38636	0,70639	0,80785	2,42E-08	0,46678	0,20643	0,96774	0,058825	0,25772	0,082243	0,34292	2,21E-09	0,0312333	0,053861	0,067263	0,01409
Cr	0,77841	0,82238	0,24715	0,63858	0,22799		1,73E-09	9,18E-21	0,0014186	0,00020097	0,27491	0,34084	0,18379	6,03E-05	1,23E-19	4,47E-07	1,35E-19	0,013025	1,68E-05	1,37E-06	0,043037	8,59E-15	0,012851	1,01E-30	0,053762
K	0,99219	0,98173	0,059121	-0,029619	0,1773	0,71078		7,13E-13	0,47952	0,00041548	0,15482	0,025924	0,081795	2,95E-14	7,18E-17	1,52E-18	0,029187	1,52E-18	0,49661	0,106	0,2851	0,4116	1,69E-06	0,89261	1,82E-10	0,16781
Mg	0,85625	0,86194	0,23324	0,39183	0,35671	0,90339	0,7949		0,0053084	0,00035761	0,074399	0,12781	0,0032806	3,52E-06	4,63E-16	0,0006042	6,94E-24	0,028633	5,16E-06	0,00027768	0,00093882	1,26E-13	0,00229931	1,96E-21	0,0016772
Mn	0,15522	0,18943	0,74268	0,47376	0,26012	0,4235	0,098287	0,37422		7,66E-06	0,5812	0,74841	0,41949	0,78154	0,030615	0,0055168	0,012305	5,55E-05	0,0019755	0,068581	0,18922	1,02E-09	0,00591111	0,00094836	0,017889
Na	0,46545	0,48474	0,78225	0,28146	0,12027	0,48511	0,46354	0,46812	0,56744		0,79086	0,1366	0,80354	0,0010963	0,001598	0,34304	0,0050978	0,050022	0,55352	0,079988	0,43544	3,19E-11	0,011759	0,0036739	0,013624
P	0,21941	0,19728	-0,0037051	-0,11051	0,052457	0,15126	0,19631	0,24461	0,076752	0,03694		0,13369	0,01577	0,71552	0,21006	0,23443	0,047241	0,90458	0,007866	0,94871	0,22227	0,25679	0,61462	0,20817	0,056794
Pb	-0,30482	-0,29062	0,081143	0,25567	-0,033879	-0,13214	-0,30303	-0,20982	-0,04467	-0,20521	-0,19684		0,031401	0,0046557	0,12297	0,016849	0,086294	0,3225	0,53752	0,94107	0,49149	0,46568	0,096988	0,149	0,68516
S	0,28268	0,24325	-0,038378	-0,14851	0,67334	0,18363	0,23898	0,39306	0,11214	0,034653	0,32709	-0,25323	0,19983	0,14741	0,14515	0,95774	0,0073691	0,6223	3,93E-05	0,57193	1,02E-07	0,0863599	0,11058	0,055587	4,92E-05
Si	0,80515	0,79984	0,013897	-0,085831	0,10114	0,51797	0,82094	0,58424	0,038627	0,41938	0,050751	-0,37947		3,73E-09	3,13337	2,47E-08	0,19667	0,55449	0,27473	0,49045	0,00061185	0,953571	1,74E-06	0,7205	
Ti	0,9029	0,93323	0,11454	0,33776	0,17469	0,89269	0,86073	0,84954	0,29455	0,41934	0,17333	-0,21246	0,20093	0,70045	3,57E-05	1,23E-20	0,28803	0,0046475	0,0039211	0,30934	7,45E-11	0,43261	3,05E-24	0,23022	
As	0,35411	0,392	0,21748	0,55978	-0,0056359	0,62461	0,29701	0,45184	0,37267	0,13155	0,16455	0,32399	0,0073941	0,13979	0,53131	1,36E-05	0,025055	9,27E-06	0,00062083	0,37266	2,92E-05	0,0090263	2,95E-06	0,14254	
B	0,92566	0,9312	0,17136	0,26662	0,25878	0,89229	0,88113	0,92757	0,33845	0,4572	0,27127	-0,23563	0,36073	0,67303	0,90224	0,55448	0,34514	6,07E-07	0,0041946	0,023678	3,30E-12	0,090459	7,54E-21	0,0090782	
Cu	-0,025894	0,011286	0,46311	0,61138	0,15673	0,33588	-0,094517	0,29799	0,52014	0,26806	-0,016702	0,1372	0,068559	-0,17846	0,14724	0,30474	0,13088	0,072812	0,0099317	0,0097919	0,00039683	7,35E-08	0,015365	0,030259	
Fe	0,31353	0,31094	0,097411	0,32307	0,23864	0,54953	0,22241	0,5761	0,41181	0,082419	0,35738	-0,085757	0,52892	0,082219	0,37954	0,56319	0,61896	0,24612	0,005777	0,00094242	0,00014747	0,0048502	1,85E-05	3,30E-05	
Mo	0,22796	0,28146	0,17228	0,69213	0,13158	0,60934	0,14812	0,47622	0,24973	0,24037	-0,008963	0,010301	0,078636	0,15132	0,46531	0,46315	0,38358	0,34795	0,3708	0,03648	0,00013753	0,014777	3,19E-06	0,40985	
Ni	0,17325	0,15973	0,18627	0,21038	0,07054	0,27642	0,11404	0,43751	0,18981	0,10836	0,16894	-0,09564	0,65044	0,095869	0,14095	0,12375	0,30755	0,34857	0,4378	0,28535	0,010883	5,82E-06	0,026644	0,00050949	
Sr	0,65947	0,69339	0,69832	0,5419	0,23951	0,83001	0,59924	0,80957	0,7176	0,79807	0,15703	-0,10139	0,23559	0,45144	0,74883	0,53627	0,78088	0,46495	0,49389	0,49584	0,34393	0,00049247	4,52E-15	0,00077946	
Zn	0,075247	0,083974	0,44426	0,51936	0,26386	0,3365	0,018809	0,39653	0,36986	0,34049	0,070072	0,2282	0,21961	-0,0081132	0,10902	0,3521	0,23266	0,6558	0,37784	0,33011	0,57349	0,45828	0,018799	0,0037691	
Zr	0,80584	0,84261	0,21985	0,54508	0,25089	0,96109	0,73868	0,90932	0,43717	0,4673	0,17404	-0,19807	0,26206	0,5986	0,9299	0,58792	0,90415	0,32536	0,54721	0,58627	0,30165	0,83454	0,31879	0,049247	
TOC	0,23258	0,20472	0,35998	0,077438	0,3323	0,26397	0,19043	0,41764	0,32116	0,33384	0,26082	-0,05645	0,52321	-0,049824	0,16602	0,20222	0,35185	0,29515	0,53324	0,11446	0,45722	0,44963	0,38774	0,26894	

-URD

	Al	As	Ca	Cd	Cr	Cu	Fe	K	Li	Mg	Mn	Mo	Na	Ni	P	Pb	S	Si	Sr	Ti	V	Zn	%Sand	%TOC
Al		0,17489	7,43E-07	0,70453	6,94E-08	0,67245	4,38E-08	1,11E-05	4,71E-05	0,33078	0,32412	0,10748	0,60351	0,76483	0,47253	0,71943	1,24E-06	0,56419	1,40E-06	0,0032328	3,66E-11	0,46004	0,50553	0,50787
As	0,26897		0,86401	3,53E-08	0,0019923	2,34E-05	0,00053927	0,68949	0,16524	0,075496	0,11898	0,0088158	0,052271	0,0034757	0,0026872	3,04E-05	0,71685	0,95797	0,80386	0,035936	0,015817	0,00065382	6,22E-05	0,0069958
Ca	-0,79462	0,034588		0,34153	0,0037948	0,20685	0,0010543	0,00079341	0,0027437	0,005741	0,037937	0,52735	0,11684	0,13148	0,72755	0,42154	3,04E-35	0,10685	3,13E-40	0,29506	0,00017824	0,83815	0,24133	0,0098512
Cd	0,076491	0,84258	0,19037		0,0035862	1,16E-08	0,010976	0,43252	0,16723	0,0050889	0,00060201	0,011487	0,0010773	1,64E-05	2,11E-05	2,05E-06	0,26043	0,32734	0,30118	0,035386	0,034155	2,12E-07	3,33E-06	0,00028124
Cr	0,8331	0,56812	-0,53803	0,54078		0,0049592	4,45E-11	0,0076874	3,38E-05	0,85571	0,2324	0,03008	0,11409	0,040432	0,0031709	0,023194	0,0059162	0,70071	0,005679	1,92E-05	1,52E-17	0,0019838	0,004215	0,14472
Cu	0,085251	0,71954	0,25089	0,85688	0,52467		0,059354	0,2363	0,037393	0,040876	2,18E-06	0,31541	5,44E-06	3,17E-11	4,34E-11	5,17E-05	0,15266	0,050482	0,1689	0,017832	0,030712	4,18E-09	8,82E-05	1,79E-07
Fe	0,83963	0,62154	-0,59529	0,48159	0,91049	0,36745		0,00070497	0,0012883	0,67027	0,83261	0,0099727	0,53289	0,43432	0,10776	0,026907	0,0017285	0,81988	0,0015025	0,0017666	4,49E-11	0,051355	0,02069	0,76306
K	0,73818	0,08058	-0,6067	-0,15756	0,50158	-0,23584	0,61132		0,53157	0,35764	0,01102	0,13102	0,016738	0,024087	0,24504	0,29584	0,00067633	0,84465	0,00079376	0,36549	0,0035231	0,16682	0,93762	0,077392
Li	0,70064	0,27489	-0,55352	0,27365	0,70976	0,4025	0,58698	0,12587		0,96637	0,29719	0,81805	0,14088	0,037059	0,0052132	0,11844	0,0040171	0,25997	0,0037878	0,0052628	2,16E-06	0,0023881	0,24532	0,50434
Mg	-0,19458	0,34776	0,51713	0,52336	0,036721	0,396	0,085853	-0,18423	0,0085178		0,047589	0,29145	0,21318	0,2689	0,53591	0,008312	0,0049876	0,48688	0,0054743	0,8517	0,85585	0,37192	0,0080409	0,10874
Mn	-0,19722	0,30727	0,40145	0,61738	0,23776	0,774	0,042677	-0,48136	0,20827	0,38464		0,95295	6,62E-13	3,86E-07	5,83E-06	0,0017791	0,031767	0,0066642	0,030137	0,1245	0,45638	6,61E-05	0,0068663	1,06E-05
Mo	0,31673	0,49403	-0,12716	0,47895	0,41789	0,20073	0,48709	0,29807	0,046448	0,2107	-0,011919		0,60602	0,93945	0,81883	0,72314	0,56421	0,69329	0,54765	0,048648	0,060458	0,3265	0,089609	0,83536
Na	-0,10463	0,37744	0,30897	0,59441	0,31121	0,75456	0,12547	-0,45631	0,29098	0,24754	0,93682	-0,1039		3,08E-08	3,97E-06	8,74E-05	0,096306	0,036513	0,096285	0,04922	0,25882	5,66E-05	0,0033521	3,81E-05
Ni	-0,060375	0,5423	0,29773	0,72858	0,39681	0,91299	0,15695	-0,43295	0,40315	0,22058	0,80614	-0,015343	0,84444		1,30E-13	0,00030899	0,095888	0,094874	0,10521	0,011361	0,14895	9,42E-10	0,00054564	5,08E-08
P	0,14435	0,55449	0,070289	0,72215	0,5467	0,91069	0,31649	-0,23162	0,52212	0,12456	0,75302	0,046246	0,76146	0,94471		0,0024968	0,62207	0,041974	0,64932	0,0039586	0,014002	4,52E-12	0,0013067	3,07E-06
Pb	0,072471	0,71261	0,1613	0,7752	0,43545	0,69799	0,42552	-0,20884	0,3077	0,49729	0,57313	0,071474	0,68265	0,6417	0,55789		0,33688	0,68942	0,38029	0,085774	0,075292	0,00028104	3,76E-05	0,0021892
S	-0,78508	0,073166	0,999	0,22442	-0,51557	0,28297	-0,57439	-0,61292	-0,53523	0,52438	0,41409	-0,11608	0,32666	0,32705	0,099327	0,19218		0,11359	1,06E-37	0,33566	0,0003096	0,96359	0,19791	0,0065128
Si	-0,11609	-0,010647	0,31726	0,19594	0,077526	0,38013	-0,045973	0,039569	-0,22463	0,13976	0,50928	-0,079545	0,40422	0,32799	0,39405	0,0806	0,31162		0,099551	0,3174	0,81566	0,349	0,13302	0,023473
Sr	-0,78278	0,050139	0,9996	0,20659	-0,5177	0,27262	-0,58046	-0,60668	-0,53812	0,5196	0,41776	-0,12102	0,32668	0,31868	0,09166	0,17585	0,99936	0,32369		0,3479	0,00030608	0,9122	0,20972	0,0067001
Ti	0,54578	0,40536	-0,20917	0,40646	0,72453	0,45236	0,57344	0,18129	0,52163	-0,037753	0,30297	0,38296	0,38207	0,47959	0,53596	0,33685	-0,19266	0,19992	-0,18792		3,86E-05	0,0088279	0,0020026	0,02099
V	0,91195	0,45981	-0,6603	0,40899	0,97355	0,41645	0,91043	0,54164	0,77418	-0,036685	0,14961	0,36598	0,22516	0,28544	0,46723	0,34798	-0,64163	0,047069	-0,64203	0,70613		0,0092898	0,038068	0,44013
Zn	0,14841	0,61423	-0,041246	0,81605	0,56831	0,86885	0,3788	-0,2739	0,55993	0,17891	0,69092	0,19627	0,69544	0,8844	0,92597	0,64499	-0,0092203	0,1875	-0,022273	0,49395	0,4911		0,0012314	0,00020812
%Sand	-0,13389	-0,69271	-0,2334	-0,76522	-0,53285	-0,68239	-0,4429	0,015809	-0,23149	-0,49912	-0,50768	-0,33304	-0,54404	-0,62109	-0,58639	-0,70685	-0,25574	-0,2966	-0,24936	-0,56789	-0,4012	-0,58888		8,83E-05
%TOC	-0,13316	0,50668	0,48778	0,64497	0,28832	0,81881	0,060843	-0,34566	0,13426	0,31565	0,73923	0,041965	0,70652	0,83755	0,76689	0,56389	0,5105	0,43466	0,50899	0,44197	0,155	0,65518	-0,68234	

-SIE

	Al	As	Ca	Cd	Cr	Cu	Fe	K	Li	Mg	Mn	Na	Ni	P	Pb	S	Si	Ti	V	Zn	%Sand	TOC
Al		0,0005249	0,023981	0,0002694	1,86E-33	0,25318	0,00074115	1,91E-21	2,32E-07	2,81E-10	0,0023116	1,13E-17	0,0013505	0,0079319	0,00025663	0,0028811	0,082475	1,33E-09	2,28E-35	0,053288	0,59851	0,00069587
As	-0,51222		4,66E-08	6,04E-19	0,00049467	0,79117	1,19E-16	0,0043303	4,73E-06	0,0036392	5,09E-10	0,062826	0,28342	1,50E-05	2,56E-15	1,05E-08	0,2625	0,23622	0,0012491	0,00025169	0,10604	2,78E-05
Ca	-0,34787	0,72805		2,75E-11	0,01872	0,43661	5,95E-10	0,14681	1,58E-06	0,021586	1,70E-10	0,53056	0,65103	1,30E-08	9,00E-06	1,26E-08	0,076208	0,65838	0,052192	4,92E-08	0,29827	8,46E-10
Cd	-0,53411	0,92967	0,82108		0,00024393	0,61221	9,82E-30	0,0050633	1,39E-07	0,0035542	1,07E-08	0,045994	0,49604	2,01E-06	1,78E-13	2,12E-15	0,069368	0,38067	0,00067836	3,90E-07	0,2999	5,25E-08
Cr	0,98712	-0,51423	-0,36133	-0,53725		0,041843	0,00092821	1,04E-15	7,77E-09	9,10E-14	0,0033691	1,17E-13	6,91E-05	0,004103	0,00037316	0,0012888	0,024796	1,57E-07	8,55E-40	0,10029	0,5196	0,00023221
Cu	0,18031	-0,042111	-0,1233	-0,080521	0,31547		0,91633	0,63216	4,70E-05	3,53E-06	0,85329	0,70896	2,40E-09	0,071094	0,90936	0,033737	3,83E-05	0,081926	0,085076	0,30722	0,012107	0,0071526
Fe	-0,50029	0,90745	0,78787	0,98016	-0,49227	-0,016713		0,00718	1,51E-06	0,0087124	2,18E-09	0,058705	0,62676	2,57E-07	1,45E-10	3,88E-14	0,11252	0,3702	0,0020536	4,21E-06	0,19786	2,14E-07
K	0,9477	-0,43148	-0,22779	-0,42465	0,89629	-0,076051	-0,40886		0,0009514	1,36E-05	0,007362	1,59E-28	0,062817	0,085828	0,001763	0,075512	0,65732	1,15E-17	2,00E-17	0,085049	0,98266	0,051889
Li	0,70114	-0,64134	-0,66464	-0,71008	0,75471	0,58513	-0,6656	0,49138		4,61E-13	8,76E-05	0,0064202	2,91E-06	2,76E-07	2,88E-05	2,05E-10	1,98E-05	0,40539	2,85E-07	0,0081573	0,24901	9,73E-14
Mg	0,79657	-0,43892	-0,35365	-0,43992	0,86859	0,6478	-0,39979	0,61691	0,85666		0,0074528	8,80E-05	2,67E-12	0,00013919	0,016413	0,00099942	0,00062477	0,014892	1,46E-11	0,90669	0,36234	1,98E-05
Mn	-0,4576	0,78971	0,80215	0,75014	-0,44217	0,029416	0,77183	-0,4077	-0,5679	-0,40713		0,086515	0,42664	9,75E-13	6,58E-05	0,00011363	0,37431	0,19803	0,0071549	0,002955	0,093773	1,12E-05
Na	0,91813	-0,28962	-0,099534	-0,30964	0,86682	-0,059334	-0,29408	0,97716	0,414	0,56777	-0,26771		0,090367	0,28307	0,023989	0,18612	0,70143	1,07E-19	6,19E-16	0,16627	0,71072	0,13961
Ni	0,47846	-0,16943	-0,071874	-0,10799	0,57458	0,77056	-0,077256	0,28963	0,65196	0,84243	-0,12598	0,26461		0,024359	0,51384	0,12131	0,0092907	0,51926	0,00035527	0,057608	0,15998	0,0031602
P	-0,40422	0,61444	0,74735	0,65971	-0,43381	-0,28133	0,69938	-0,26828	-0,69807	-0,5544	0,85077	-0,16955	-0,347		0,032912	2,16E-06	0,010714	0,89918	0,011766	0,065735	0,40539	1,30E-09
Pb	-0,53565	0,89125	0,62666	0,86378	-0,5236	-0,018112	0,80393	-0,46828	-0,59805	-0,36826	0,57596	-0,34785	-0,1036	0,32983		2,86E-07	0,33674	0,15147	0,00075381	3,86E-06	0,62689	0,00072448
S	-0,44867	0,75046	0,74785	0,89234	-0,48021	-0,32838	0,87442	-0,27721	-0,80007	-0,48959	0,56038	-0,20805	-0,24279	0,6582	0,69742		0,003838	0,73934	0,0037414	1,09E-05	0,83539	2,94E-12
Si	0,27109	-0,17687	-0,27658	-0,283	0,34601	0,59063	-0,24851	0,070494	0,60762	0,50625	-0,14065	0,060943	0,39672	-0,38982	-0,15195	-0,43666		0,30439	0,041825	0,33689	0,17922	0,0029757
Ti	0,77808	-0,1868	0,070262	-0,13881	0,70804	-0,27155	-0,14185	0,91805	0,1318	0,3733	-0,20267	0,93568	0,10227	-0,020156	-0,22527	0,052902	-0,16232		7,66E-09	0,71245	0,71503	0,78154
V	0,98967	-0,48138	-0,30167	-0,50339	0,99381	0,2689	-0,46231	0,91566	0,69753	0,82717	-0,40902	0,89909	0,52521	-0,3852	-0,49969	-0,43775	0,3155	0,75492		0,12376	0,50819	0,0013661
Zn	-0,30034	0,53626	0,72717	0,69183	-0,25706	0,16139	0,64393	-0,26892	-0,4029	-0,018648	0,44762	-0,2176	0,29531	0,28661	0,64586	0,62225	-0,1519	-0,05859	-0,24126		0,67223	0,00019282
%Sand	-0,083628	-0,25295	-0,16436	-0,16382	-0,10219	-0,38378	-0,20274	0,0034574	-0,18188	-0,14417	-0,26195	-0,05896	-0,22079	-0,1318	-0,077228	0,033053	-0,21128	0,058042	-0,10498	-0,067239		0,66285
TOC	-0,5025	0,59896	0,78365	0,72616	-0,53879	-0,40904	0,70258	-0,30204	-0,86812	-0,60765	0,62158	-0,23182	-0,44484	0,77834	0,50109	0,84159	-0,44734	0,044101	-0,47802	0,54455	0,069284	

-SAB

	Al	As	Ca	Cd	Cr	Cu	Fe	K	Li	Mg	Mn	Na	Ni	P	Pb	S	Si	Ti	V	Zn	%_TOC	%Sand
Al		0,0052384	3,37E-09	1,07E-06	2,60E-57	1,61E-05	1,41E-07	1,92E-35	2,75E-19	0,077995	0,001807	6,56E-53	3,25E-08	0,081449	0,92103	4,98E-08	9,67E-17	7,92E-29	4,22E-55	2,65E-07	1,14E-06	0,76615
As	0,34767		8,88E-09	2,79E-10	0,000708	1,78E-07	3,01E-10	0,032114	0,002391	0,068977	0,0040123	0,018378	3,25E-06	0,022267	0,0016561	0,0075263	0,077446	0,11754	0,00050623	4,71E-06	0,047316	0,2748
Ca	-0,66239	-0,64883		7,15E-30	4,48E-10	3,72E-25	2,97E-33	1,95E-05	8,67E-15	0,0023979	0,00017172	1,81E-08	3,19E-31	0,94308	0,00039674	6,45E-21	2,50E-06	0,0010248	1,53E-11	1,33E-31	1,43E-13	0,50889
Cd	0,57026	0,69428	-0,93854		1,86E-07	2,16E-18	5,22E-62	0,0010201	2,58E-12	3,50E-05	4,72E-06	1,95E-06	7,29E-26	0,74326	0,00025952	9,87E-15	3,30E-05	0,013955	9,36E-09	8,21E-31	2,86E-10	0,46513
Cr	0,99245	0,41551	-0,68852	0,60147		2,67E-06	2,25E-08	7,97E-35	5,74E-18	0,1039	0,0006555	2,57E-39	1,72E-08	0,2732	0,73188	1,67E-07	1,56E-14	1,02E-27	2,32E-58	1,07E-07	7,01E-06	0,85385
Cu	0,51438	0,60216	-0,91107	0,84703	0,55248		4,25E-19	0,00068907	3,57E-07	0,47904	4,75E-06	0,00013824	2,49E-17	0,4088	5,68E-06	2,48E-15	0,0014049	0,027658	2,11E-07	3,10E-18	2,89E-10	0,14658
Fe	0,60607	0,69337	-0,95271	0,99471	0,63518	0,8556		0,00030823	1,68E-13	3,94E-05	1,10E-05	2,60E-07	1,33E-27	0,80909	0,00035019	3,29E-15	1,05E-05	0,0057159	9,70E-10	6,69E-31	1,07E-10	0,49054
K	0,96005	0,27036	-0,51012	0,40415	0,95811	0,41634	0,43999		1,33E-11	0,93402	0,00049401	7,76E-28	0,00023872	0,23753	0,62325	7,85E-05	8,96E-13	1,10E-33	2,15E-30	0,00070531	0,00083543	0,84029
Li	0,85781	0,37599	-0,79365	0,74483	0,84162	0,59016	0,76976	0,72836		7,17E-05	0,0084713	4,42E-21	3,11E-18	0,0082066	0,81702	4,16E-15	2,64E-18	1,41E-09	2,11E-19	5,92E-15	2,09E-14	0,065939
Mg	-0,2237	-0,23064	0,37589	-0,49645	-0,2068	-0,090814	-0,49363	-0,010644	-0,4789		0,064248	0,012584	8,92E-06	0,10604	0,45738	0,021265	0,10115	0,71953	0,066892	1,84E-06	0,011468	0,64466
Mn	0,38552	0,35758	-0,45617	0,54093	0,41786	0,54078	0,52294	0,42633	0,32899	0,23457		0,012462	0,0084971	0,69246	0,062118	0,00056775	0,0070223	0,0066495	0,00029686	0,0021027	0,024594	0,36874
Na	0,98946	0,2963	-0,63842	0,55867	0,97033	0,46196	0,59572	0,92796	0,877	-0,31272	0,31313		2,13E-08	0,019062	0,65763	4,48E-08	6,80E-18	9,20E-26	5,25E-41	2,49E-07	2,84E-07	0,63042
Ni	0,62956	0,54854	-0,94466	0,9159	0,63915	0,83309	0,92664	0,44716	0,84504	-0,52746	0,32886	0,636		0,21828	0,030085	2,87E-23	1,89E-07	0,0048303	5,42E-10	2,47E-36	1,63E-19	0,98369
P	-0,22122	0,28763	0,0091785	-0,042091	-0,14017	0,10589	-0,031053	-0,15098	-0,33026	0,20556	0,050817	-0,29467	-0,15729		0,00040305	0,012915	3,00E-05	0,16611	0,15465	0,39949	0,00029949	0,074759
Pb	-0,012745	0,38843	-0,43275	0,44483	0,044027	0,53705	0,43635	-0,063093	-0,02974	-0,095326	0,23642	-0,056932	0,27351	0,43229		0,11933	0,00968	0,31073	0,6538	0,0011605	0,86689	0,0057104
S	-0,62294	-0,33369	0,87536	-0,79267	-0,60323	-0,8029	-0,80084	-0,47663	-0,79914	0,28973	-0,42219	-0,62462	-0,89674	0,31162	-0,19825		7,02E-09	0,002656	3,54E-09	7,69E-20	9,43E-31	0,73579
Si	0,82476	0,22411	-0,55376	0,49785	0,78916	0,39385	0,52401	0,75483	0,84593	-0,20843	0,33641	0,84066	0,60121	-0,50012	-0,3236	-0,65218		3,80E-11	1,70E-15	1,15E-05	2,31E-10	0,0091396
Ti	0,93333	0,1992	-0,404	0,30832	0,92728	0,27752	0,34436	0,95426	0,67401	-0,04614	0,33854	0,91523	0,35072	-0,17663	-0,12977	-0,37233	0,71716		3,56E-24	0,011845	0,0095688	0,67042
V	0,99108	0,42561	-0,72691	0,64807	0,99303	0,59926	0,67881	0,94098	0,85912	-0,23234	0,44105	0,97393	0,68615	-0,18146	0,057611	-0,66169	0,80561	0,9039		3,90E-09	2,34E-07	0,98348
Zn	0,59541	0,54098	-0,94626	0,94287	0,61072	0,84506	0,94326	0,41563	0,79653	-0,55981	0,38039	0,59643	0,9627	-0,108	0,40004	-0,86405	0,52191	0,31526	0,66036		2,48E-14	0,65537
%_TOC	-0,56897	-0,2509	0,7711	-0,69396	-0,53261	-0,69386	-0,70551	-0,41041	-0,78688	0,31661	-0,28304	-0,59415	-0,86041	0,4408	0,021545	0,9426	-0,69651	-0,32407	-0,59751	-0,7855		0,66221
%Sand	0,038222	-0,13971	0,08477	-0,093699	0,023679	-0,18502	-0,088464	0,025904	0,23314	-0,05924	-0,11517	0,061796	-0,0026276	-0,22611	-0,3444	0,04336	0,32593	0,054671	-0,0026616	-0,057333	-0,05612	

-ACH

	Al	As	Ca	Cd	Cr	Cu	Fe	K	Li	Mg	Mn	Na	Ni	P	Pb	S	Si	Sr	Ti	V	Zn	%_TOC	%Sand
Al		6,72E-08	0,023826	3,52E-07	6,83E-27	0,62682	0,16534	1,0037E-08	7,6666E-35	6,0861E-16	3,4683E-07	1,3581E-26	0,0064715	2,7095E-08	2,0227E-05	4,6988E-05	0,14618	9,8377E-08	0,032769	7,0987E-34	7,1539E-05	4,5736E-10	0,30706
As	-0,59922		0,036632	0,0098467	0,0042946	0,079788	0,91377	0,65767	2,6756E-11	0,00064537	0,21983	0,012072	0,043545	0,021221	0,077553	3,3608E-08	3,6382E-10	0,38692	1,0984E-08	0,0010967	0,14798	0,0018298	0,19245
Ca	-0,27387	-0,25397		7,69E-08	0,0001192	0,20558	4,5444E-05	6,3208E-06	0,43886	0,00002651	2,137E-09	2,5437E-05	0,0019115	3,3975E-07	3,2904E-06	0,024599	0,1464	0,37586	0,90757	0,0017338	1,2157E-06	1,2281E-05	0,92225
Cd	-0,57177	0,31098	0,59707		9,72E-08	0,13967	1,0312E-14	3,2922E-05	1,5028E-06	1,8883E-05	7,5262E-24	1,0369E-07	0,0047709	1,2403E-18	2,7756E-21	0,68506	0,49128	0,39875	0,045621	2,0248E-06	6,0678E-23	0,00082808	0,0028914
Cr	0,90974	-0,34213	-0,44975	-0,59331		0,017758	0,0039464	6,1048E-19	5,4986E-14	1,3392E-20	7,6296E-12	5,1724E-41	3,9423E-08	1,9949E-10	7,6584E-07	0,16581	0,91887	7,3628E-07	0,29798	2,5623E-43	0,00052745	1,5511E-06	0,13626
Cu	0,060021	0,21395	-0,15545	-0,18099	0,28673		0,00014536	0,004642	0,54723	0,3042	0,0011433	0,051016	5,2718E-07	0,017111	0,017806	3,39E-09	0,4666	0,089975	0,083486	0,084373	0,79724	0,0078452	0,90901
Fe	-0,17016	0,013379	0,47348	0,77374	-0,34513	-0,44465		0,00049861	0,4175	0,025481	4,9874E-19	0,015272	0,0001245	2,3599E-14	5,377E-09	4,5392E-05	0,85762	0,044517	0,16816	0,060335	1,1277E-05	0,94666	0,00059766
K	0,62781	0,054712	-0,51714	-0,48103	0,83697	0,33934	-0,41099		0,00037319	1,6389E-10	8,7235E-11	3,0179E-17	3,1603E-19	2,9759E-07	7,5296E-07	0,50261	0,00017053	3,4558E-05	0,012279	9,0493E-18	0,0092347	0,020642	0,078846
Li	0,94915	-0,70153	-0,09543	-0,54553	0,76026	-0,074268	-0,099925	0,41923		2,91E-09	5,97E-05	3,04E-14	0,27312	5,2151E-07	0,00041892	4,0215E-08	0,047668	2,4426E-06	0,014844	2,5536E-17	1,7706E-05	3,6234E-09	0,24723
Mg	0,79459	-0,40348	-0,48601	-0,49366	0,85619	0,12644	-0,27085	0,68112	0,64501		3,39E-08	5,98E-16	0,0019096	7,3727E-08	0,00018627	0,1403	0,19071	0,0111	0,050299	2,9863E-16	0,038131	7,0189E-11	0,16025
Mn	-0,57205	0,15074	0,64911	0,88714	-0,71473	-0,38618	0,83805	-0,68841	-0,46694	-0,60982		2,25E-10	5,3908E-07	1,9115E-28	6,2441E-14	0,051979	0,66782	0,39852	0,18429	9,2169E-09	2,6381E-10	0,0048438	0,0032504
Na	0,90775	-0,30282	-0,48695	-0,59227	0,96723	0,23764	-0,29312	0,81437	0,76513	0,79471	-0,67737		1,4558E-06	1,8219E-09	1,1053E-06	0,077272	0,73366	2,6357E-10	0,5325	4,1109E-39	5,3288E-05	5,8158E-08	0,21813
Ni	0,32712	0,24556	-0,36979	-0,33835	0,60752	0,56471	-0,44864	0,84047	0,13479	0,36982	-0,56431	0,54613		0,00026163	0,00014858	0,003084	3,9266E-05	0,033201	0,0042394	4,1167E-07	0,097273	0,29191	0,22178
P	-0,61323	0,279	0,57241	0,8331	-0,67881	-0,28832	0,76719	-0,57469	-0,5649	-0,59774	0,91939	-0,65121	-0,42904		2,80E-09	0,53334	0,76629	0,36821	0,052139	4,2666E-08	5,9215E-09	0,00036694	0,0036578
Pb	-0,49212	0,21552	0,53036	0,86339	-0,55801	-0,28662	0,6366	-0,55832	-0,41597	-0,43815	0,7592	-0,55128	-0,44408	0,64553		0,47209	0,85517	0,50753	0,34025	2,6295E-06	2,1032E-14	0,07419	0,00026689
S	-0,47268	0,60996	-0,27244	-0,050081	-0,16998	0,64292	-0,4735	0,082691	-0,60722	-0,1807	-0,23669	-0,21572	0,35374	-0,076853	-0,088674		0,29361	6,1737E-05	0,62981	0,013624	0,85077	7,7298E-05	0,91537
Si	-0,17811	0,67159	-0,17802	0,084888	0,012585	-0,089772	-0,022164	0,44048	-0,24106	-0,16062	-0,052987	0,042023	0,47692	0,036713	-0,02255	0,12922		0,016344	4,71E-28	0,83985	0,94492	0,098714	0,24259
Sr	0,59312	-0,1066	-0,10909	-0,10398	0,55872	-0,20722	0,24447	0,47991	0,53622	0,3062	-0,10403	0,67549	0,25864	-0,11084	-0,081744	-0,46613	0,29026		0,0066233	5,1575E-09	0,050117	0,0005603	0,83657
Ti	-0,25926	0,62651	-0,014345	0,24326	-0,12807	-0,21143	0,16905	0,30212	-0,29431	-0,23836	0,16295	-0,07701	0,34259	0,23653	0,11743	0,059501	0,91706	0,32625		0,4941	0,47292	0,039639	0,55623
V	0,94551	-0,38747	-0,37297	-0,53985	0,97216	0,21084	-0,22899	0,8217	0,81541	0,79948	-0,62902	0,9625	0,56907	-0,6063	-0,53478	-0,29787	0,024966	0,63718	-0,08434		0,00050351	1,4939E-06	0,33067
Zn	-0,46253	0,17733	0,54951	0,8793	-0,40937	-0,031736	0,50494	-0,3135	-0,49509	-0,25204	0,67548	-0,46968	-0,20275	0,63526	0,76811	0,023242	-0,0085362	-0,23854	0,088508	-0,41071		0,0028126	0,08707
%_TOC	-0,66879	0,37122	0,5031	0,39605	-0,54493	0,31982	0,0082665	-0,28022	-0,64202	-0,69088	0,3378	-0,60148	0,12967	0,4197	0,21795	0,46063	0,2019	-0,40762	0,25016	-0,54564	0,35689		0,65574
%Sand	0,1257	-0,16	0,012059	-0,35595	0,18254	0,01412	-0,40574	0,21461	0,14224	0,1722	-0,35192	0,15129	0,15011	-0,34781	-0,4285	-0,01313	0,14363	0,025483	0,072612	0,11976	-0,20907	0,05504	

7. Conclusions

La Sierra Lake (June, 2021)

7. Conclusions

The multidisciplinary analyses of sediment cores from a transect of six high altitude lakes in the central and western Pyrenees combined with monitoring surveys of the lakes allowed us to reconstruct the sedimentation and lake dynamics for the last 2000 years, document the synergistic effects of climate and human activities and demonstrate the uniqueness of recent changes within the last two millennia. We summarize the main conclusions of this PhD related to: 1) Depositional facies models, 2) Lithogenic and Carbon fluxes, 3) Heavy metal deposition, and 4) Recent trends.

7.1. Depositional facies models

a) A detailed sedimentary analysis of the six lakes along the transect has provided depositional models for distal sedimentation that could be applied to high altitude lakes in other mountain settings.

b) Pyrenean mountain lakes are small lake systems but with a large variability of facies and depositional subenvironments. Silicate minerals are main sediment components because of the dominant geology of the watersheds and the lake water hydrochemistry. Detrital input is a major contribution to the sediment budget in these lakes. The most common profundal - distal facies are banded and laminated, although event deposits (flood layers, turbidite layers) are also present. Endogenic carbonate formation occurs only in Sabocos Lake mostly in the littoral areas, associated to charophyte/macrophyte meadows.

c) The proposed Depositional models provide the frameworks to reconstruct past environmental and climate changes and allow comparing and reconstructing the processes of erosion, transport and sedimentation at the basin scale.

d) These Pyrenean lakes may serve as facies analogs for larger systems and help to identify sources and processes controlling lacustrine deposition in modern lakes and pre-Quaternary lacustrine formations.

e) The sedimentary sequences illustrate trends related to climate variability and human impact in the watershed. These depositional models provide a dynamic framework for integrating all paleolimnological data necessary to decipher the high-resolution paleoenvironmental information archived in these lake sequences.

7.2. Lithogenic and Organic Carbon fluxes

f) The high-resolution analyses and the robust age models have allowed the reconstruction of lithogenic and organic carbon fluxes during the last 1200 years.

g) High altitude Pyrenean lakes show the greatest changes in sediment delivery and organic carbon accumulation since 1850 and 1950 CE over the last 1200 years.

h) Prior to the 20th century, higher lithogenic fluxes occurred during periods of increased human pressure (early medieval times, late 19th century) and wetter phases of the LIA. Lakes at lower altitudes (AC, SA, SI) show higher TOC_{flux}, lower $\delta^{13}C_{OM}$ and C/N during medieval times, after 1850 CE and an accelerating trend since 1950, all indicative of increase in carbon burial and bioproductivity. Main periods of change in higher altitude lakes occurred at the same periods, but with variable trends and smaller ranges.

i) The $\delta^{13}C_{OM}$ trends in alkaline lakes suggest additional sources of Dissolved Inorganic Carbon during the Great Acceleration from the watershed carbonate formations.

j) Increased sediment fluxes to the lakes during the last decades may be related to changes in seasonality, leading to longer ice-free periods and higher erodibility of rainfall versus snow precipitation. Increased organic accumulation is driven by higher algal productivity, primarily controlled by higher temperatures and longer ice-free and growing season, although higher atmospheric input of nutrients could also be a significant factor.

k) The exponential increase in lithogenic and organic carbon fluxes in all lakes since the mid 20th century is a unique feature in the last 1200 years.

7.3. Heavy metal deposition

l) The record of heavy metal deposition in the Pyrenean lakes during the last 2000 years shows a large variability, with different timing and intensities due to local and lake-specific processes. However, all show positive enrichments of Pb, Cu, Cd and Zn during Roman, Medieval and Industrial revolution times.

m) The characteristics of each lake such as location, altitude, sediment type, depth, watershed size, water characteristics, etc., control how the system stores heavy metals from local, regional and global sources.

n) The historical mining and metallurgy activities, mainly during the RP, and later, HMA and LMA were the main anthropogenic inputs of metal deposition into the lakes. There is a clear relationship between these periods of higher impact and climatic periods, since mining was more active in temperate and warmer phases, allowing the extraction of minerals, and decreased in colder climatic conditions (LALIA and LIA).

o) Lakes located at higher altitudes register better the global atmospheric deposition of heavy metals over long distances, while lakes at lower altitudes, biogeochemical processes (such as the greater deposition of organic matter) and local factors (regional climatic variability, pollution due to their proximity to populated areas and infrastructure) are more significant. In our transect, the increase in Pb enrichment during the industrial era started earlier in MAR and CRE, followed closely by URD (the lakes located at higher altitudes), and later in the other three lakes located at lower altitude.

p) We have not detected major changes during present and past high accumulation phases due to location in the W-E transect. Considering Pb, the lakes with the highest enrichment are ACH and SIE, located further west, but this increase is probably due to their more organic composition of their sediments. With respect to Cu, although also with great variability, the lakes with the highest EF are URD, MAR and SAB, those located further east, where there has been historically a higher level of industrialization.

q) The past phases of heavy metal increases correlates well with other nearby records and with regional and global emission inventories, suggesting a mixed signal between local and global sources of trace metal contamination.

7.4. Recent trends

r) The results obtained from the intense monitoring carried out during this thesis in the lakes confirm that altitude is the factor that better explains the temperature variability of the surface waters of the Pyrenean lakes. Lower altitude lakes such as Sabocos and Acherito show a greater response to increasing spring temperature, which favors a greater advance in the timing of snowmelt at lower altitudes than at higher altitudes. High altitude lakes such as Cregüeña and Marboré are insulated for longer from spring air temperature, as the ice cover has an insulating effect.

s) Other morphological variables related to catchment characteristics, the ratio of total catchment to lake area, topography, solar radiation and air temperature variability also affect the surface and whole water column temperature.

t) Available thermal regimes in lakes show a large variability in stratification and mixing periods.

u) To confirm the changes in thermal regimes it would be advisable to continue the monitoring of these lakes in order to have more robust data on how global change may be affecting their thermal dynamics and ecological status.

v) Deeper lakes with higher thermal inertia (they take longer to warm and cool) as Cregüeña are expected to respond more slowly to new physical (temperature and density gradients), chemical (alkalinity, salinity, pH, nutrients) and biological (primary productivity, community composition) conditions.

w) The anoxic level of mountain lakes at mid altitudes may evolve in the future as a consequence of more acute and longer periods of stratification induced by global climate change.

7. 5. Future actions

This PhD has:

1) Reconstructed the sedimentary dynamics of the Aragonese Pyrenean lakes during the Anthropocene.
2) Defined a common depositional model for high altitude lake systems that could serve as a general framework to understand the impact of the drivers during the Anthropocene.
3) Described the current depositional patterns and limnological behavior of the lakes through monitoring campaigns.
4) Demonstrated that Pyrenean lakes have responded to the major climatic changes of the last millennium (Medieval Climate Anomaly, Little Ice Age, Recent Warming) and to the variable anthropogenic impact during medieval, contemporary and recent rural abandonment.
5) Identified recent trends in changes in depositional dynamics (erosion and sediment transport from the catchment watersheds), biological productivity and deposition of pollutants (heavy metals) and to assess the role of climatic and anthropogenic changes in these trends.
6) Demonstrated the changes in the lakes and watersheds caused by recent human activities (farming, tourism, hydroelectrical and mining activities) and by recent warming.

To sum up, this PhD thesis has demonstrated that high altitude Pyrenean lakes contain high - resolution archives of climate variability and human activities during the Anthropocene and proven that the three main hypotheses stated prior to the beginning of the research were accurate.

H1. The organic carbon and lithogenic fluxes reconstructions demonstrate that sedimentation and lake dynamics have changed as a function of climate variability and human activities, with lower sediment delivery and organic carbon accumulation during colder/more arid periods and lower anthropogenic input and higher during warmer/more humid phases and higher human activities.

H2. The records show how synergistic effects between climate and human activities have intensified erosion, heavy metal mobilization and C storage in high altitude mountain basins. Sediment fluxes maximize when human and climate

factors reinforce each other. Stronger human disturbances have occurred during warmer periods.

H3. The intensification of the hydrological cycle (flood intensity and frequency) associated with recent global warming have led to higher sediment mobilization and sediment delivery to the lake systems, increase in carbon fluxes and bioproductivity and an increase in metal mobilization from the watersheds. The results illustrate the uniqueness of the Great Acceleration and the current Global Warming compared to other changes during the last 2000 years.

This PhD and the REPLIM network have documented important changes in the Pyrenean lakes and peatlands during the last millennia, due presumably to positive feedback between the increase inhuman activities and global warming. One of the main challenges is the ascription of the observed changes and trends to either climate change or anthropic pressure. On the other hand, the lack of detailed information to characterize these ecosystems and their internal processes (from detailed inventories of biodiversity to quantification of biogeochemical processes) hampers our ability to understand their resilience against climate and human impact.

Observation and monitoring protocols have to be included in a more integral management of the territory to warrant the preservation of vulnerable ecosystems and a more sustainable use of the mountain resources. Maintaining monitoring networks is essential in order to anticipate changes in the ecological status of lakes and raise awareness of the impacts of Climate Change and human activities in high mountain ecosystems.

7.1 Conclusiones

Los análisis multidisciplinares de sondeos de sedimentos en un transecto de seis lagos de gran altitud en los Pirineos centrales y occidentales, combinados con estudios de monitorización de los lagos, nos permitien reconstruir la sedimentación y la dinámica lacustre de los últimos 2000 años, documentar los efectos sinérgicos del clima y las actividades humanas y demostrar la singularidad de los cambios recientes en los últimos 2000 años. Resumimos las principales conclusiones de este doctorado relacionadas con: 1) Modelos de facies deposicionales, 2) Flujos litogénicos y de carbono, 3) Deposición de metales pesados y 4) Tendencias recientes.

7.1. Modelos de facies deposicionales

a) Un análisis sedimentario detallado de los seis lagos a lo largo del transecto ha proporcionado modelos deposicionales para la sedimentación distal que podrían aplicarse a lagos de gran altitud en otros entornos de montaña.

b) Los lagos de montaña pirenaicos son sistemas lacustres pequeños pero con una gran variabilidad de facies y subambientes deposicionales. Los minerales siliciclásticos son los principales componentes de los sedimentos debido a la geología dominante de las cuencas hidrográficas y a la hidroquímica del agua. El aporte de detritos es una contribución importante al balance de sedimentos en estos lagos. Las facies profundas y distales más comunes son bandeadas y laminadas, aunque también están presentes depósitos de eventos (capas de inundación, capas turbidíticas). La formación endógena de carbonatos sólo se produce en el lago Sabocos, principalmente en las zonas litorales, asociada a praderas de carófitos/macrófitos.

c) Los modelos deposicionales propuestos proporcionan los marcos para reconstruir los cambios medioambientales y climáticos del pasado y permiten comparar y reconstruir los procesos de erosión, transporte y sedimentación a escala de cuenca.

d) Estos lagos pirenaicos pueden servir como facies análogas para sistemas mayores y ayudar a identificar fuentes y procesos que controlan la deposición lacustre en lagos modernos y formaciones lacustres pre-cuaternarias.

e) Las secuencias sedimentarias muestran tendencias relacionadas con la variabilidad climática y el impacto antrópico en la cuenca. Estos modelos deposicionales proporcionan un marco dinámico para integrar todos los datos paleolimnológicos necesarios para descifrar la información paleoambiental de alta resolución archivada en estas secuencias lacustres.

7.2. Flujos litogénicos y de carbono orgánico

f) Los análisis de alta resolución y los modelos de edad robustos han permitido reconstruir los flujos litogénicos y de carbono orgánico durante los últimos 1200 años.

g) Los lagos pirenaicos de mayor altitud muestran los mayores cambios en la aportación de sedimentos y en la acumulación de carbono orgánico desde 1850 y 1950 EC durante los últimos 1200 años.

h) Antes del siglo XX, se produjeron flujos litogénicos más elevados durante los periodos de mayor presión humana (principios de la Edad Media, finales del siglo XIX) y las fases más húmedas de la LIA. Los lagos situados a menor altitud (AC, SA, SI) muestran un mayor flujo de TOC, menores $\delta^{13}C_{OM}$ y C/N durante la época medieval, después de 1850 CE y una tendencia acelerada desde 1950, todo ello indicativo de un aumento del enterramiento de carbono y de la bioproductividad. Los principales periodos de cambio en los lagos de mayor altitud se produjeron en los mismos periodos, pero con tendencias variables y rangos menores.

i) Las tendencias de δ^{13}COM en los lagos alcalinos sugieren fuentes adicionales de Carbono Inorgánico Disuelto durante la Gran Aceleración a partir de las formaciones carbonatadas de la cuenca.

j) El aumento de los flujos de sedimentos hacia los lagos durante las últimas décadas puede estar relacionado con cambios en la estacionalidad, que han dado lugar a periodos más largos sin hielo y a una mayor erosionabilidad de las precipitaciones de lluvia frente a las de nieve. El aumento de la acumulación orgánica se debe a una mayor productividad de las algas, controlada principalmente por el aumento de las temperaturas y la prolongación de los periodos sin hielo y de crecimiento, aunque un mayor aporte atmosférico de nutrientes también podría ser un factor importante.

k) El aumento exponencial de los flujos litogénicos y de carbono orgánico en todos los lagos desde mediados del siglo XX es una característica única en los últimos 1200 años.

7.3. Deposición de metales pesados

l) El registro de deposición de metales pesados en los lagos pirenaicos durante los últimos 2000 años muestra una gran variabilidad, con diferentes momentos e intensidades debido a procesos locales y específicos de cada lago. Sin embargo, todos muestran enriquecimientos positivos de Pb, Cu, Cd y Zn durante las revoluciones romana, medieval e industrial.

m) Las características de cada lago, como su ubicación, altitud, tipo de sedimento, profundidad, tamaño de la cuenca, características del agua, etc., controlan la forma en que el sistema almacena los metales pesados procedentes de fuentes locales, regionales y globales.

n) Las actividades mineras y metalúrgicas históricas, principalmente durante el RP, y posteriormente, la HMA y la LMA fueron los principales aportes antropogénicos de deposición de metales en los lagos. Existe una clara relación entre estos periodos de mayor impacto y los periodos climáticos, ya que la minería fue más activa en las fases templadas y cálidas, permitiendo la extracción de minerales, y disminuyó en las condiciones climáticas más frías (LALIA y LIA).

o) Los lagos situados a mayor altitud registran mejor la deposición atmosférica global de metales pesados a larga distancia, mientras que en los lagos situados a menor altitud son más significativos los procesos biogeoquímicos (como la mayor deposición de materia orgánica) y los factores locales (variabilidad climática regional, contaminación por su proximidad a zonas pobladas e infraestructuras). En nuestro transecto, el aumento del enriquecimiento en Pb durante la era industrial comenzó antes en MAR y CRE, seguidos de cerca por URD (los lagos situados a mayor altitud), y más tarde en los otros tres lagos situados a menor altitud.

p) No hemos detectado cambios importantes durante las fases de alta acumulación actual y pasada debido a la ubicación en el transecto W-E. Considerando el Pb, los lagos con mayor enriquecimiento son ACH y SIE, situados más al oeste, pero este incremento se debe probablemente a la composición más orgánica de sus

sedimentos. Respecto al Cu, aunque también con gran variabilidad, los lagos con mayor EF son URD, MAR y SAB, los situados más al este, donde históricamente ha habido un mayor nivel de industrialización.

q) Las fases pasadas de aumento de metales pesados se correlacionan bien con otros registros cercanos y con los inventarios de emisiones regionales y globales, lo que sugiere una señal mixta entre fuentes locales y globales de contaminación por metales traza.

7.4. Tendencias recientes

r) Los resultados obtenidos del intenso seguimiento realizado durante esta tesis en los lagos confirman que la altitud es el factor que mejor explica la variabilidad de la temperatura de las aguas superficiales de los lagos pirenaicos. Lagos de menor altitud como SAB y ACH muestran una mayor respuesta al aumento de la temperatura primaveral, lo que favorece un mayor adelanto en el momento del deshielo a menor altitud que a mayor altitud. Lagos de gran altitud como CRE y MAR se aíslan durante más tiempo de la temperatura primaveral del aire, ya que la capa de hielo ejerce un efecto aislante.

s) Otras variables morfológicas relacionadas con las características de la cuenca, la relación entre la cuenca total y la superficie del lago, la topografía, la radiación solar y la variabilidad de la temperatura del aire también afectan a la temperatura de la superficie y de toda la columna de agua.

t) Los regímenes térmicos disponibles en los lagos muestran una gran variabilidad en los periodos de estratificación y mezcla.

u) Para confirmar los cambios en los regímenes térmicos sería aconsejable continuar el seguimiento de estos lagos con el fin de disponer de datos más sólidos sobre cómo el cambio global puede estar afectando a su dinámica térmica y a su estado ecológico.

v) Se espera que lagos más profundos y con mayor inercia térmica (tardan más en calentarse y enfriarse) como Cregüeña respondan más lentamente a nuevas condiciones físicas (gradientes de temperatura y densidad), químicas (alcalinidad,

salinidad, pH, nutrientes) y biológicas (productividad primaria, composición de la comunidad).

w) El nivel anóxico de los lagos de montaña a altitudes medias puede evolucionar en el futuro como consecuencia de periodos más agudos y prolongados de estratificación inducidos por el cambio climático global.

7. 5. Acciones futuras

Esta tesis doctoral ha:

1) Reconstruido la dinámica sedimentaria de los lagos pirenaicos aragoneses durante el Antropoceno.
2) Definido un modelo deposicional común para sistemas lacustres de gran altitud que podría servir como marco general para entender el impacto de los impulsores durante el Antropoceno.
3) Describir los patrones deposicionales actuales y el comportamiento limnológico de los lagos mediante campañas de monitorización.
4) Demostrado que los lagos pirenaicos han respondido a los principales cambios climáticos del último milenio (Anomalía Climática Medieval, Pequeña Edad de Hielo, Calentamiento Reciente) y al impacto antropogénico variable durante el abandono rural medieval, contemporáneo y reciente.
5) Identificado las tendencias recientes de los cambios en la dinámica deposicional (erosión y transporte de sedimentos desde las cuencas hidrográficas de captación), la productividad biológica y la deposición de contaminantes (metales pesados) y evaluado el papel de los cambios climáticos y antropogénicos en estas tendencias.
6) Demostrar los cambios en los lagos y las cuencas causados por las actividades humanas recientes (agricultura, turismo, actividades hidroeléctricas y mineras) y por el calentamiento reciente.

En resumen, esta tesis doctoral ha demostrado que los lagos pirenaicos de gran altitud contienen archivos de alta resolución de la variabilidad climática y las actividades humanas durante el Antropoceno y ha demostrado que las tres hipótesis principales planteadas antes del inicio de la investigación eran correctas.

H1. Las reconstrucciones del carbono orgánico y de los flujos litogénicos demuestran que la sedimentación y la dinámica de los lagos han cambiado en función de la variabilidad climática y de las actividades humanas, con menor aporte de sedimentos y acumulación de carbono orgánico durante los periodos más fríos/áridos y menor aporte antropogénico, y mayor durante las fases más cálidas/húmedas y de mayor actividad humana.

H2. Los registros muestran cómo los efectos sinérgicos entre el clima y las actividades humanas han intensificado la erosión, la movilización de metales pesados y el almacenamiento de C en las cuencas montañosas de gran altitud. Los flujos de sedimentos se maximizan cuando los factores humanos y climáticos se refuerzan mutuamente. Las perturbaciones humanas más intensas se han producido durante los periodos más cálidos.

H3. La intensificación del ciclo hidrológico (intensidad y frecuencia de las inundaciones) asociada al reciente calentamiento global ha conducido a una mayor movilización y entrega de sedimentos a los sistemas lacustres, a un aumento de los flujos de carbono y de la bioproductividad y a un incremento de la movilización de metales desde las cuencas hidrográficas. Los resultados ilustran la singularidad de la Gran Aceleración y el actual Calentamiento Global en comparación con otros cambios ocurridos durante los últimos 2000 años.

Este doctorado y la red REPLIM han documentado importantes cambios en los lagos y turberas pirenaicas durante los últimos milenios, debido presumiblemente a la retroalimentación positiva entre el aumento de las actividades humanas y el calentamiento global. Uno de los principales retos es la atribución de los cambios y tendencias observados al cambio climático o a la presión antrópica. Por otro lado, la falta de información detallada para caracterizar estos ecosistemas y sus procesos internos (desde inventarios detallados de la biodiversidad hasta la cuantificación de los procesos biogeoquímicos) dificulta nuestra capacidad para entender su capacidad de recuperación frente al impacto climático y humano. Los protocolos de observación y seguimiento deben incluirse en una gestión más integral del territorio para garantizar la preservación de los ecosistemas vulnerables y un uso más sostenible de los recursos de las montañas. El mantenimiento de redes de seguimiento es esencial para anticipar cambios en el estado ecológico de lagos y concienciar sobre los impactos del Cambio Climático y las actividades humanas en los ecosistemas de alta montaña.

8. References

Urdiceto Lake (July, 2018)

8. References

Alvera, B. (2000). La cuenca experimental del Izas, Pirineo Aragonés.

Alvera, B., & García-Ruiz, J. M. (2000). Variability of Sediment Yield from a High Mountain Catchment, Central Spanish Pyrenees. Arctic, Antarctic, and Alpine Research, 32(4), 478-484. https://doi.org/10.1080/15230430.2000.12003392

Anchukaitis, K. J., & Tierney, J. E. (2013). Identifying coherent spatiotemporal modes in time-uncertain proxy paleoclimate records. Climate Dynamics, 41(5), 1291-1306. https://doi.org/10.1007/s00382-012-1483-0

Anderson, N. J., D'Andrea, W., & Fritz, S. C. (2009). Holocene carbon burial by lakes in SW Greenland. Global Change Biology, 15(11), 2590-2598. https://doi.org/10.1111/j.1365-2486.2009.01942.x

Anderson, N. J., Dietz, R. D., & Engstrom, D. R. (2013). Land-use change, not climate, controls organic carbon burial in lakes. Proceedings of the Royal Society B: Biological Sciences, 280(1769), 20131278. https://doi.org/10.1098/rspb.2013.1278

Anderson, N. J., Heathcote, A. J., Engstrom, D. R., & Globocarb data contributors. (2020). Anthropogenic alteration of nutrient supply increases the global freshwater carbon sink. Science Advances, 6(16), eaaw2145. https://doi.org/10.1126/sciadv.aaw2145

Araguas-Araguas, L. J., & Diaz Teijeiro, M. F. (2005). Isotope composition of precipitation and water vapour in the Iberian Peninsula: First results of the Spanish network of isotopes in precipitation. International Atomic Energy Agency Technical Report, 1453, 173-190.

Aranda, C. M., Gracia, I. M., Sala, D. N., Moreno, J. E. N., & Inurrigarro, R. O. (2016). Tercer informe sobre el canvi climàtic a Catalunya.

Arnaud, F., Poulenard, J., Giguet-Covex, C., Wilhelm, B., Révillon, S., Jenny, J.-P., Revel, M., Enters, D., Bajard, M., Fouinat, L., Doyen, E., Simonneau, A., Pignol, C., Chapron, E., Vannière, B., & Sabatier, P. (2016). Erosion under climate and human pressures: An alpine lake sediment perspective. Quaternary Science Reviews, 152, 1-18. https://doi.org/10.1016/j.quascirev.2016.09.018

Arnell, N. W., & Gosling, S. N. (2013). The impacts of climate change on river flow regimes at the global scale. Journal of Hydrology, 486, 351-364.

Arruebo, T. (2014). Valoración integral de los lagos glaciares del Pirineo aragonés: Una propuesta para su gestión [Http://purl.org/dc/dcmitype/Text, Universidad de Zaragoza]. https://dialnet.unirioja.es/servlet/tesis?codigo=203702

Bacardit, M. (2011). Trace elements biogeochemistry in high mountain lake catchments: Identifying anthropogenic versus natural components from the atmospheric contamination legacy in remote natural areas. TDX (Tesis Doctorals En Xarxa). https://dugi-doc.udg.edu/handle/10256/4819

Bacardit, M., & Camarero, L. (2009). Fluxes of Al, Fe, Ti, Mn, Pb, Cd, Zn, Ni, Cu, and As in monthly bulk deposition over the Pyrenees (SW Europe): The influence of meteorology

on the atmospheric component of trace element cycles and its implications for high mountain lakes. Journal of Geophysical Research: Biogeosciences, 114(G2).

Bacardit, M., & Camarero, L. (2010). Major and trace elements in soils in the Central Pyrenees: High altitude soils as a cumulative record of background atmospheric contamination over SW Europe. Environmental Science and Pollution Research, 17(9), 1606-1621. https://doi.org/10.1007/s11356-010-0349-4

Bacardit, M., Krachler, M., & Camarero, L. (2012). Whole-catchment inventories of trace metals in soils and sediments in mountain lake catchments in the Central Pyrenees: Apportioning the anthropogenic and natural contributions. Geochimica et Cosmochimica Acta, 82, 52-67.

Barreiro-Lostres, F., Brown, E., Moreno, A., Morellón, M., Abbott, M., Hillman, A., Giralt, S., & Valero-Garcés, B. (2015). Sediment delivery and lake dynamics in a Mediterranean mountain watershed: Human-climate interactions during the last millennium (El Tobar Lake record, Iberian Range, Spain). Science of The Total Environment, 533, 506-519. https://doi.org/10.1016/j.scitotenv.2015.06.123

Barreiro-Lostres, F., Moreno, A., González-Sampériz, P., Giralt, S., Nadal-Romero, E., & Valero-Garcés, B. (2017). Erosion in Mediterranean mountain landscapes during the last millennium: A quantitative approach based on lake sediment sequences (Iberian Range, Spain). CATENA, 149(P3), 782-798. https://doi.org/10.1016/j.catena.2016.05.024

Batalla, M., Ninyerola, M., & Catalan, J. (2018). Digital long-term topoclimate surfaces of the Pyrenees mountain range for the period 1950–2012. Geoscience Data Journal, 5(2), 50-62.

Battarbee, R. W. (2005). Mountain lakes, pristine or polluted? Limnética, 24(1-2), 001-008.

Battarbee, R. W., Thompson, R., Catalan, J., Grytnes, J. A., & Birks, H. J. B. (2002). Climate variability and ecosystem dynamics of remote alpine and arctic lakes: The MOLAR project. Journal of Paleolimnology, 28, 1-6.

Belmonte-Ribas, A., Sancho, C., Moreno, A., Lopez-Martinez, J., & Bartolome, M. (2014). Present-day environmental dynamics in ice cave A294, Central Pyrenees, Spain. Geografia Fisica e Dinamica Quaternaria, 37(2), 131-140.

Beniston, M. (2003). Climatic Change in Mountain Regions: A Review of Possible Impacts. En H. F. Diaz (Ed.), Climate Variability and Change in High Elevation Regions: Past, Present & Future (pp. 5-31). Springer Netherlands. https://doi.org/10.1007/978-94-015-1252-7_2

Beniston, M. (2005). The Risks Associated with Climatic Change in Mountain Regions. En U. M. Huber, H. K. M. Bugmann, & M. A. Reasoner (Eds.), Global Change and Mountain Regions: An Overview of Current Knowledge (pp. 511-519). Springer Netherlands. https://doi.org/10.1007/1-4020-3508-X_51

Beniston, M., Diaz, H. F., & Bradley, R. S. (1997). Climatic Change at high elevation sites: An overview. Climatic Change, 36(3), 233-251. https://doi.org/10.1023/A:1005380714349

Bennion, H., Battarbee, R. W., Sayer, C. D., Simpson, G. L., & Davidson, T. A. (2011). Defining reference conditions and restoration targets for lake ecosystems using palaeolimnology: A synthesis. Journal of Paleolimnology, 45, 533-544.

Bernárdez, P., Prego, R., Francés, G., & González-Álvarez, R. (2005). Opal content in the Ría de Vigo and Galician continental shelf: Biogenic silica in the muddy fraction as an accurate paleoproductivity proxy. Continental Shelf Research, 25(10), 1249-1264. https://doi.org/10.1016/j.csr.2004.12.009

Bielza, V., Corral, J. L., Escolano, S., Laliena, C., Sesma, A., & Ubieto, A. (1986). Estudio histórico-geográfico del valle de Bielsa (Huesca). Huesca, Instituto de Estudios Altoaragoneses, 10, 224.

Blaauw, M., & Christen, J. A. (2011). Flexible paleoclimate age-depth models using an autoregressive gamma process. Bayesian Analysis, 6(3), 457-474. https://doi.org/10.1214/11-BA618

Blais, J. M., & Kalff, J. (1995). The influence of lake morphometry on sediment focusing. Limnology and Oceanography, 40(3), 582-588. https://doi.org/10.4319/lo.1995.40.3.0582

Blass, A., Bigler, C., Grosjean, M., & Sturm, M. (2007). Decadal-scale autumn temperature reconstruction back to AD 1580 inferred from the varved sediments of Lake Silvaplana (Southeastern Swiss Alps). Quaternary Research, 68(2), 184-195. https://doi.org/10.1016/j.yqres.2007.05.004

Boës, X., Rydberg, J., Martinez-Cortizas, A., Bindler, R., & Renberg, I. (2011). Evaluation of conservative lithogenic elements (Ti, Zr, Al, and Rb) to study anthropogenic element enrichments in lake sediments. Journal of Paleolimnology, 46(1), 75-87. https://doi.org/10.1007/s10933-011-9515-z

Bradley, R. S. (2015). Chapter 9—Lake Sediments. En R. S. Bradley (Ed.), Paleoclimatology (Third Edition) (pp. 319-343). Academic Press. https://doi.org/10.1016/B978-0-12-386913-5.00009-0

Brahney, J., Ballantyne, A. P., Kociolek, P., Leavitt, P. R., Farmer, G. L., & Neff, J. C. (2015). Ecological changes in two contrasting lakes associated with human activity and dust transport in western Wyoming: Dust-P controls on alpine lake ecology. Limnology and Oceanography, 60(2), 678-695. https://doi.org/10.1002/lno.10050

Brahney, J., Ballantyne, A. P., Vandergoes, M., Baisden, T., & Neff, J. C. (2019). Increased Dust Deposition in New Zealand Related to Twentieth Century Australian Land Use. Journal of Geophysical Research: Biogeosciences, 124(5), 1181-1193. https://doi.org/10.1029/2018JG004627

Brilha, J., Gray, M., Pereira, D. I., & Pereira, P. (2018). Geodiversity: An integrative review as a contribution to the sustainable management of the whole of nature. Environmental Science & Policy, 86, 19-28. https://doi.org/10.1016/j.envsci.2018.05.001

Butcher, J. B., Nover, D., Johnson, T. E., & Clark, C. M. (2015). Sensitivity of lake thermal and mixing dynamics to climate change. Climatic Change, 129(1), 295-305. https://doi.org/10.1007/s10584-015-1326-1

Buurman, P., Pape, T., & Muggler, C. C. (1997). Laser grain-size determination in soil genetic studies 1.Practical problems. Soil Science, 162(3), 211.

Camarero, L. (2003). Spreading of trace metals and metalloids pollution in lake sediments over the Pyrénées. Journal de Physique IV (Proceedings), 107, 249-253. https://doi.org/10.1051/jp4:20030289

Camarero, L., Bacardit, M., de Diego, A., & Arana, G. (2017). Decadal trends in atmospheric deposition in a high elevation station: Effects of climate and pollution on the long-range flux of metals and trace elements over SW Europe. Atmospheric Environment, 167, 542-552. https://doi.org/10.1016/j.atmosenv.2017.08.049

Camarero, L., Botev, I., Muri, G., Psenner, R., Rose, N., & Stuchlik, E. (2009). Trace elements in alpine and arctic lake sediments as a record of diffuse atmospheric contamination across Europe. Freshwater Biology, 54(12), 2518-2532. https://doi.org/10.1111/j.1365-2427.2009.02303.x

Camarero, L., & Catalan, J. (1998). A simple model of regional acidification for high mountain lakes: Application to the Pyrenean lakes (N-E Spain). Water Research, 32(4), 1126-1136. https://doi.org/10.1016/S0043-1354(97)00291-1

Camarero, L., & Catalan, J. (2012). Atmospheric phosphorus deposition may cause lakes to revert from phosphorus limitation back to nitrogen limitation. Nature Communications, 3(1), 1118. https://doi.org/10.1038/ncomms2125

Camarero, L., Masqué, P., Devos, W., Ani-Ragolta, I., Catalan, J., Moor, H. C., Pla-Rabes, S., & Sanchez-Cabeza, J. A. (1998). Historical variations in lead fluxes in the Pyrenees (Northeast Spain) from a dated lake sediment core. Water, Air, and Soil Pollution, 105, 439-449.

Carey, C. C., Hanson, P. C., Thomas, R. Q., Gerling, A. B., Hounshell, A. G., Lewis, A. S. L., Lofton, M. E., McClure, R. P., Wander, H. L., Woelmer, W. M., Niederlehner, B. R., & Schreiber, M. E. (2022). Anoxia decreases the magnitude of the carbon, nitrogen, and phosphorus sink in freshwaters. Global Change Biology, 28(16), 4861-4881. https://doi.org/10.1111/gcb.16228

Carrevedo, M. L., Frugone, M., Latorre, C., Maldonado, A., Bernárdez, P., Prego, R., Cárdenas, D., & Valero-Garcés, B. (2015). A 700-year record of climate and environmental change from a high Andean lake: Laguna del Maule, central Chile (36 S). The Holocene, 25(6), 956-972.

Carrivick, J. L., & Tweed, F. S. (2013). Proglacial lakes: Character, behaviour and geological importance. Quaternary Science Reviews, 78, 34-52. https://doi.org/10.1016/j.quascirev.2013.07.028

Castillo Jurado, M. del. (2003). Morfometría de lagos. Una aplicación a los lagos del Pirineo. Universitat de Barcelona.

Catalan, J., Ballesteros, E., Camarero, L., Felip, M., & Gacia, E. (1992). Limnology in the Pyrenean Lakes. Limnetica, 8. https://doi.org/10.23818/limn.08.03

Catalan, J., Camarero, L., Felip, M., Pla, S., Ventura, M., Buchaca, T., Bartumeus, F., Mendoza, G. de, Miró, A., Casamayor, E., Medina-Sánchez, J., Bacardit, M., Altuna, M., Bartrons, M., & Quijano, D. (2006). High mountain lakes: Extreme habitats and witnesses of environmental changes. Limnetica, 25, 551-584. https://doi.org/10.23818/limn.25.38

Catalan, J., Curtis, C. J., & Kernan, M. (2009). Remote European mountain lake ecosystems: Regionalisation and ecological status. Freshwater Biology, 54(12), 2419-2432. https://doi.org/10.1111/j.1365-2427.2009.02326.x

Catalan, J., Ninot, J. M., & Aniz, M. M. (Eds.). (2017). High Mountain Conservation in a Changing World (Vol. 62). Springer International Publishing. https://doi.org/10.1007/978-3-319-55982-7

Catalan, J., Pla, S., Rieradevall, M., Felip, M., Ventura, M., Buchaca, T., Camarero, L., Brancelj, A., Appleby, P. G., Lami, A., Grytnes, J. A., Agustí-Panareda, A., & Thompson, R. (2002). Lake Redó ecosystem response to an increasing warming the Pyrenees during the twentieth century. Journal of Paleolimnology, 28(1), 129-145. https://doi.org/10.1023/A:1020380104031

Catalan, J., Pla-Rabés, S., García, J., & Camarero, L. (2014). Air temperature-driven CO2 consumption by rock weathering at short timescales: Evidence from a Holocene lake sediment record. Geochimica et Cosmochimica Acta, 136, 67-79. https://doi.org/10.1016/j.gca.2014.04.005

Catalan, J., Pla-Rabés, S., Wolfe, A. P., Smol, J. P., Rühland, K. M., Anderson, N. J., Kopáček, J., Stuchlík, E., Schmidt, R., Koinig, K. A., Camarero, L., Flower, R. J., Heiri, O., Kamenik, C., Korhola, A., Leavitt, P. R., Psenner, R., & Renberg, I. (2013). Global change revealed by palaeolimnological records from remote lakes: A review. Journal of Paleolimnology, 49(3), 513-535. https://doi.org/10.1007/s10933-013-9681-2

CHE. (1994). Inspección y examen de las presas de Pineta, Plandescun, Urdiceto y Laspuña, en el río Cinca e IP en el río Aragón. Ref: 0045B.

CHE. (2023). Lagos. Portal CHEbro. https://www.chebro.es

Chung, F. H. (1974). Quantitative interpretation of X-ray diffraction patterns of mixtures. II. Adiabatic principle of X-ray diffraction analysis of mixtures. Journal of Applied Crystallography, 7(6), 526-531. https://doi.org/10.1107/S0021889874010387

Cía, J. C., Andrés, A. J., Sánchez, M. A. S., Novau, J. C., & Moreno, J. I. L. (2005). Responses to climatic changes since the Little Ice Age on Maladeta Glacier (Central Pyrenees). Geomorphology, 68(3), 167-182. https://doi.org/10.1016/j.geomorph.2004.11.012

Clair, T. A., Dennis, I. F., Amiro, P. G., & Cosby, B. J. (2004). Past and future chemistry changes in acidified Nova Scotian Atlantic salmon (Salmo salar) rivers: A dynamic modeling approach. Canadian Journal of Fisheries and Aquatic Sciences, 61(10), 1965-1975.

Clair, T. A., Dennis, I. F., & Vet, R. (2011). Water chemistry and dissolved organic carbon trends in lakes from Canada's Atlantic Provinces: No recovery from acidification measured after 25 years of lake monitoring. Canadian Journal of Fisheries and Aquatic Sciences, 68(4), 663-674. https://doi.org/10.1139/f2011-013

Cohen, A. S. (2003). Paleolimnology: The history and evolution of lake systems. Oxford University Press.

Compte-Port, S., Borrego, C. M., Moussard, H., Jeanbille, M., Restrepo-Ortiz, C. X., de Diego, A., Rodriguez-Iruretagoiena, A., Gredilla, A., Fdez-Ortiz de Vallejuelo, S., Galand, P. E., Kalenitchenko, D., Rols, J.-L., Pokrovsky, O. S., Gonzalez, A. G., Camarero, L., Muñiz, S., Navarro-Navarro, E., & Auguet, J.-C. (2018). Metal contaminations impact archaeal community composition, abundance and function in remote alpine lakes. Environmental Microbiology, 20(7), 2422-2437. https://doi.org/10.1111/1462-2920.14252

Corella, J. P., Benito, G., Rodriguez-Lloveras, X., Brauer, A., & Valero-Garcés, B. L. (2014). Annually-resolved lake record of extreme hydro-meteorological events since AD 1347 in NE Iberian Peninsula. Quaternary Science Reviews, 93, 77-90. https://doi.org/10.1016/j.quascirev.2014.03.020

Corella, J. P., Brauer, A., Mangili, C., Rull, V., Vegas-Vilarrúbia, T., Morellón, M., & Valero-Garcés, B. L. (2012). The 1.5-ka varved record of Lake Montcortès (southern Pyrenees, NE Spain). Quaternary Research, 78(2), 323-332. https://doi.org/10.1016/j.yqres.2012.06.002

Corella, J. P., Saiz-Lopez, A., Sierra, M. J., Mata, M. P., Millán, R., Morellón, M., Cuevas, C. A., Moreno, A., & Valero-Garcés, B. L. (2018). Trace metal enrichment during the Industrial Period recorded across an altitudinal transect in the Southern Central Pyrenees. Science of The Total Environment, 645, 761-772. https://doi.org/10.1016/j.scitotenv.2018.07.160

Corella, J. P., Sierra, M. J., Garralón, A., Millán, R., Rodríguez-Alonso, J., Mata, M. P., de Vera, A. V., Moreno, A., González-Sampériz, P., Duval, B., Amouroux, D., Vivez, P., Cuevas, C. A., Adame, J. A., Wilhelm, B., Saiz-Lopez, A., & Valero-Garcés, B. L. (2021). Recent and historical pollution legacy in high altitude Lake Marboré (Central Pyrenees): A record of mining and smelting since pre-Roman times in the Iberian Peninsula. Science of The Total Environment, 751, 141557. https://doi.org/10.1016/j.scitotenv.2020.141557

Corella, J. P., Stefanova, V., El Anjoumi, A., Rico, E., Giralt, S., Moreno, A., Plata-Montero, A., & Valero-Garcés, B. L. (2013). A 2500-year multi-proxy reconstruction of climate change and human activities in northern Spain: The Lake Arreo record. Palaeogeography, Palaeoclimatology, Palaeoecology, 386, 555-568. https://doi.org/10.1016/j.palaeo.2013.06.022

Corella, J. P., Valero-Garcés, B. L., Wang, F., Martínez-Cortizas, A., Cuevas, C. A., & Saiz-Lopez, A. (2017). 700 years reconstruction of mercury and lead atmospheric deposition in the Pyrenees (NE Spain). Atmospheric Environment, 155, 97-107.

Cramer, W., Guiot, J., Fader, M., Garrabou, J., Gattuso, J.-P., Iglesias, A., Lange, M. A., Lionello, P., Llasat, M. C., Paz, S., Peñuelas, J., Snoussi, M., Toreti, A., Tsimplis, M. N., & Xoplaki, E. (2018). Climate change and interconnected risks to sustainable development in the Mediterranean. Nature Climate Change, 8(11), 11. https://doi.org/10.1038/s41558-018-0299-2

Crutzen, P. J. (2002). Geology of mankind. Nature, 415(6867), 23-23. https://doi.org/10.1038/415023a

Crutzen, P. J., & Stoermer, E. F. (2021). The 'anthropocene'(2000). Springer.

Cuadrat, J. M., Valero-Garcés, B., Moreno, A., Verfaillie, D., Galop, D., & Rodríguez, E. (2018). El cambio climático en los Pirineos: Impactos, vulnerabilidades y adaptación.

Cuadrat Prats, J. M., & Martín Vide, J. (2007). La Climatología española. Pasado, presente y futuro. Prensas de la Universidad de Zaragoza.

Curtis, C. J., Emmet, B. A., Grant, H., Kernan, M., Reynolds, B., & Shilland, E. (2005). Nitrogen saturation in UK moorlands: The critical role of bryophytes and lichens in determining retention of atmospheric N deposition. Journal of Applied Ecology, 42(3), 507-517. https://doi.org/10.1111/j.1365-2664.2005.01029.x

Davaud, E., & Girardclos, S. (2001). Recent Freshwater Ooids and Oncoids from Western Lake Geneva (Switzerland): Indications of a Common Organically Mediated Origin. Journal of Sedimentary Research, 71(3), 423-429. https://doi.org/10.1306/2DC40950-0E47-11D7-8643000102C1865D

de Pisón Stampa, E. M. (1989). Morfología glaciar del valle de Benasque (Pirineo aragonés). Ería, 18, 51-64.

Dean, W. (1981). Carbonate minerals and organic matter in sediments of modern north temperate hard-water lakes. Recent and ancient nonmarine depositional environments: models for exploration, 213-231. https://doi.org/10.2110/pec.81.31.0213

Dean, W. E., & Fouch, T. D. (1983). Lacustrine Environment. En P. A. Scholle, D. G. Bebout, & C. H. Moore (Eds.), Carbonate Depositional Environments (Vol. 33, p. 0). American Association of Petroleum Geologists. https://doi.org/10.1306/M33429C6

Deaux, D., Soubeyroux, J.-M., Cuadrat, J., Cunillera, J., Esteban, P., Prohom, M., & Serrano-Notivoli, R. (2014). Homogénéisation transfrontalière des températures sur le massif des Pyrénée. Climatologie, 24, 67-78.

Debarbieux, B., Oiry Varacca, M., Rudaz, G., Maselli, D., Kohler, T., & Jurek, M. (2014). Tourism in mountain regions: Hopes, fears and realities. Department of Geography and Environment, University of Geneva; Centre for Development and Environment, University of Bern.

Del Barrio, G., Creus, J., & Puigdefábregas, J. (1990). Thermal seasonality of the high mountain belts of the Pyrenees. Mountain Research and development, 227-233.

DelValls, A., & Chapman, P. (1998). Site-Specific Sediment Quality Values For The Gulf Of Cádiz (Spain) And San Francisco Bay (Usa), Using The Sediment Quality Triad And Multivariate Analysis. Ciencias Marinas, 24. https://doi.org/10.7773/cm.v24i3.753

Diaz, H. F., & Bradley, R. S. (1997). Temperature Variations During the Last Century at High Elevation Sites. En H. F. Diaz, M. Beniston, & R. S. Bradley (Eds.), Climatic Change at High Elevation Sites (pp. 21-47). Springer Netherlands. https://doi.org/10.1007/978-94-015-8905-5_2

Duarte, C. M., Alonso, S., Benito, G., Dachs, J., Montes, C., Pardo Buendía, M., Ríos, A. F., Simó, R., & Valladares, F. (2006). Cambio Global. Impacto de la actividad humana sobre el sistema Tierra. CSIC. Consejo superior de investigaciones científicas.

Dudka, S., & Adriano, D. C. (1997). Environmental Impacts of Metal Ore Mining and Processing: A Review. Journal of Environmental Quality, 26(3), 590-602. https://doi.org/10.2134/jeq1997.00472425002600030003x

Dypvik, H., & Harris, N. B. (2001). Geochemical facies analysis of fine-grained siliciclastics using Th/U, Zr/Rb and (Zr+Rb)/Sr ratios. Chemical Geology, 181(1), 131-146. https://doi.org/10.1016/S0009-2541(01)00278-9

Egan, P., & Price, M. F. (2017). Mountain ecosystem services and climate change: A global overview of potential threats and strategies for adaptation. UNESCO.

Ehlers, E., & Krafft, T. (2006). Earth system science in the anthropocene. Springer.

El Kenawy, A., López-Moreno, J. I., & Vicente-Serrano, S. M. (2011). Recent trends in daily temperature extremes over northeastern Spain (1960–2006). Natural Hazards and Earth System Sciences, 11(9), 2583-2603. https://doi.org/10.5194/nhess-11-2583-2011

Elser, J. J., Andersen, T., Baron, J. S., Bergström, A.-K., Jansson, M., Kyle, M., Nydick, K. R., Steger, L., & Hessen, D. O. (2009). Shifts in lake N: P stoichiometry and nutrient limitation driven by atmospheric nitrogen deposition. science, 326(5954), 835-837.

Enders, S. K., Pagani, M., Pantoja, S., Baron, J. S., Wolfe, A. P., Pedentchouk, N., & Nunez, L. (2008). Compound-specific stable isotopes of organic compounds from lake sediments track recent environmental changes in an alpine ecosystem, Rocky Mountain National Park, Colorado. Limnology and Oceanography, 53(4), 1468-1478.

Esteban, P., Jones, P. D., Martín-Vide, J., & Mases, M. (2005). Atmospheric circulation patterns related to heavy snowfall days in Andorra, Pyrenees. International Journal of Climatology, 25(3), 319-329.

Esteban, P., Prohom, M., & Aguilar, E. (2012). Tendencias recientes e índices de cambio climático de la temperatura y la precipitación en Andorra, Pirineos (1935-2008). Pirineos, 167, 87-106. https://doi.org/10.3989/Pirineos.2012.167005

Eugster, H. P., & Kelts, K. (1983). Lacustrine chemical sediments. Chemical sediments and geomorphology, 321-368.

Eurostat. (1998). Data Sets about Gasoline Sales and Lead Content in Gasoline in 12 EU-Nations, Statistical Office of the European. Communities, Brussels (1998).

Farmer, A. M. (1990). The effects of lake acidification on aquatic macrophytes—A review. Environmental Pollution, 65(3), 219-240. https://doi.org/10.1016/0269-7491(90)90085-Q

Fdez-Ortiz de Vallejuelo, S., Arana, G., de Diego, A., & Madariaga, J. M. (2010). Risk assessment of trace elements in sediments: The case of the estuary of the Nerbioi–

Ibaizabal River (Basque Country). Journal of Hazardous Materials, 181(1), 565-573. https://doi.org/10.1016/j.jhazmat.2010.05.050

Fernández, S., Villanueva, U., de Diego, A., Arana, G., & Madariaga, J. M. (2008). Monitoring trace elements (Al, As, Cr, Cu, Fe, Mn, Ni and Zn) in deep and surface waters of the estuary of the Nerbioi-Ibaizabal River (Bay of Biscay, Basque Country). Journal of Marine Systems, 72(1), 332-341. https://doi.org/10.1016/j.jmarsys.2007.06.009

Foley, B. (2011). Controls and consequences of oxygen depletion in lakes. University of Ulster.

Fowler, D., Coyle, M., Skiba, U., Sutton, M. A., Cape, J. N., Reis, S., Sheppard, L. J., Jenkins, A., Grizzetti, B., Galloway, J. N., Vitousek, P., Leach, A., Bouwman, A. F., Butterbach-Bahl, K., Dentener, F., Stevenson, D., Amann, M., & Voss, M. (2013). The global nitrogen cycle in the twenty-first century. Philosophical Transactions of the Royal Society B: Biological Sciences, 368(1621), 20130164. https://doi.org/10.1098/rstb.2013.0164

Frank, D., Reichstein, M., Bahn, M., Thonicke, K., Frank, D., Mahecha, M. D., Smith, P., van der Velde, M., Vicca, S., Babst, F., Beer, C., Buchmann, N., Canadell, J. G., Ciais, P., Cramer, W., Ibrom, A., Miglietta, F., Poulter, B., Rammig, A., … Zscheischler, J. (2015). Effects of climate extremes on the terrestrial carbon cycle: Concepts, processes and potential future impacts. Global Change Biology, 21(8), 2861-2880. https://doi.org/10.1111/gcb.12916

Fritz, S. C., & Anderson, N. J. (2013). The relative influences of climate and catchment processes on Holocene lake development in glaciated regions. Journal of Paleolimnology, 49, 349-362.

Galloway, J. N., & Cowling, E. B. (2002). Reactive Nitrogen and The World: 200 Years of Change. AMBIO: A Journal of the Human Environment, 31(2), 64-71. https://doi.org/10.1579/0044-7447-31.2.64

Galloway, J. N., Townsend, A. R., Erisman, J. W., Bekunda, M., Cai, Z., Freney, J. R., Martinelli, L. A., Seitzinger, S. P., & Sutton, M. A. (2008). Transformation of the nitrogen cycle: Recent trends, questions, and potential solutions. Science, 320(5878), 889-892.

García-Alix, A., Jiménez-Espejo, F. J., Lozano, J. A., Jiménez-Moreno, G., Martínez-Ruiz, F., Sanjuán, L. G., Jiménez, G. A., Alfonso, E. G., Ruiz-Puertas, G., & Anderson, R. S. (2013). Anthropogenic impact and lead pollution throughout the Holocene in Southern Iberia. Science of the total environment, 449, 451-460.

García-Ruiz, J. M. (2010). The effects of land uses on soil erosion in Spain: A review. CATENA, 81(1), 1-11. https://doi.org/10.1016/j.catena.2010.01.001

García-Ruiz, J. M., Beguería, S., Nadal-Romero, E., González-Hidalgo, J. C., Lana-Renault, N., & Sanjuán, Y. (2015). A meta-analysis of soil erosion rates across the world. Geomorphology, 239, 160-173. https://doi.org/10.1016/j.geomorph.2015.03.008

García-Ruiz, J. M., López-Moreno, J. I., Lasanta Martínez, T., Vicente Serrano, S. M., González-Sampériz, P., Valero-Garcés, B. L., Sanjuán, Y., Beguería, S., Nadal-

Romero, E., & Lana-Renault, N. (2015). Los efectos geoecológicos del cambio global en el Pirineo Central español: Una revisión a distintas escalas espaciales y temporales.

García-Ruiz, J. M., Nadal-Romero, E., Lana-Renault, N., & Beguería, S. (2013). Erosion in Mediterranean landscapes: Changes and future challenges. Geomorphology, 198, 20-36. https://doi.org/10.1016/j.geomorph.2013.05.023

García-Ruiz, J. M., Palacios, D., de Andrés, N., Valero-Garcés, B. L., López-Moreno, J. I., & Sanjuán, Y. (2014). Holocene and 'Little Ice Age' glacial activity in the Marboré Cirque, Monte Perdido Massif, Central Spanish Pyrenees. The Holocene, 24(11), 1439-1452. https://doi.org/10.1177/0959683614544053

García-Ruiz, J. M., Regüés, D., Alvera, B., Lana-Renault, N., Serrano-Muela, P., Nadal-Romero, E., Navas, A., Latron, J., Martí-Bono, C., & Arnáez, J. (2008). Flood generation and sediment transport in experimental catchments affected by land use changes in the central Pyrenees. Journal of Hydrology, 356(1), 245-260. https://doi.org/10.1016/j.jhydrol.2008.04.013

García-Ruiz, J. M., Tomás-Faci, G., Pilar, D.-B., Montes, L., Domingo, R., Sebastián, M., Lasanta Martínez, T., González-Sampériz, P., López-Moreno, J. I., Arnáez, J., & Beguería, S. (2020). Transhumance and long-term deforestation in the subalpine belt of the central Spanish Pyrenees: An interdisciplinary approach. https://doi.org/10.13039/501100010067

Garmendia, M., Fdez-Ortiz de Vallejuelo, S., Liñero, O., Gredilla, A., Arana, G., Soto, M., & de Diego, A. (2019). Long term monitoring of metal pollution in sediments as a tool to investigate the effects of engineering works in estuaries. A case study, the Nerbioi-Ibaizabal estuary (Bilbao, Basque Country). Marine Pollution Bulletin, 145, 555-563. https://doi.org/10.1016/j.marpolbul.2019.06.051

Gascoin, S., Hagolle, O., Huc, M., Jarlan, L., Dejoux, J.-F., Szczypta, C., Marti, R., & Sánchez, R. (2015). A snow cover climatology for the Pyrenees from MODIS snow products. Hydrology and Earth System Sciences, 19, 2337-2351. https://doi.org/10.5194/hess-19-2337-2015

Geoportal, Observatorio Pirenaico del Cambio Climático. (2013). https://opcc-ctp.org/es/geoportal

Gibbard, P. L., Bauer, A. M., Edgeworth, M., Ruddiman, W. F., Gill, J. L., Merritts, D. J., Finney, S. C., Edwards, L. E., Walker, M. J., & Maslin, M. (2022). A practical solution: The Anthropocene is a geological event, not a formal epoch. Episodes Journal of International Geoscience, 45(4), 349-357.

Gierlowski-Kordesch, E. H., & Kelts, K. R. (2000). Lake Basins Through Space and Time. American Association of Petroleum Geologists. https://doi.org/10.1306/St46706

Giralt, S., Moreno, A., Cacho, I., & Valero-Garcés, B. (2017). A comprehensive overview of the last 2,000 years Iberian Peninsula climate history. CLIVAR Exchanges, 7, 6-11.

Glenn, C., & Kelts, K. (1991). Sedimentary Rhythms in Lake Deposits.

González-Hidalgo, J. C., Peña-Monné, J. L., & de Luis, M. (2007). A review of daily soil erosion in Western Mediterranean areas. CATENA, 71(2), 193-199. https://doi.org/10.1016/j.catena.2007.03.005

González-Sampériz, P., Aranbarri, J., Pérez-Sanz, A., Gil-Romera, G., Moreno, A., Leunda, M., Sevilla-Callejo, M., Corella, J. P., Morellón, M., Oliva, B., & Valero-Garcés, B. (2017). Environmental and climate change in the southern Central Pyrenees since the Last Glacial Maximum: A view from the lake records. CATENA, 149, 668-688. https://doi.org/10.1016/j.catena.2016.07.041

González-Sampériz, P., Gil-Romera, G., García-Prieto, E., Aranbarri, J., Moreno, A., Morellón, M., Sevilla-Callejo, M., Leunda, M., Santos, L., Franco-Múgica, F., Andrade, A., Carrión, J. S., & Valero-Garcés, B. L. (2020). Strong continentality and effective moisture drove unforeseen vegetation dynamics since the last interglacial at inland Mediterranean areas: The Villarquemado sequence in NE Iberia. Quaternary Science Reviews, 242, 106425. https://doi.org/10.1016/j.quascirev.2020.106425

Goodess, C. M., & Jones, P. D. (2002). Links between circulation and changes in the characteristics of Iberian rainfall. International Journal of Climatology: A Journal of the Royal Meteorological Society, 22(13), 1593-1615.

Gorham, E., & Boyce, F. M. (1989). Influence of Lake Surface Area and Depth Upon Thermal Stratification and the Depth of the Summer Thermocline. Journal of Great Lakes Research, 15(2), 233-245. https://doi.org/10.1016/S0380-1330(89)71479-9

Granados, I., & Toro, M. (2000). Recent warming in a high mountain lake (Laguna Cimera, Central Spain) inferred by means of fossil chironomids. Journal of Limnology, 59 (suppl. 1), 109-119. https://doi.org/10.4081/jlimnol.2000.s1.109

Gressly, A. (1838). Observations géologiques sur le Jura soleurois. Petitpierre.

Griffore, M. P., Shiel, A. E., Rutila, E. C., Hillman, A. L., Barreiro-Lostres, F., Valero-Garcés, B. L., Morellón, M., & Abbott, M. B. (2023). Lead isotope fingerprinting techniques help identify and quantify 3000 years of atmospheric lead pollution from Laguna Roya, northwestern Iberia. Anthropocene, 42, 100375.

Gu, B., Chapman, A. D., & Schelske, C. L. (2006). Factors controlling seasonal variations in stable isotope composition of particulate organic matter in a softwater eutrophic lake. Limnology and Oceanography, 51(6), 2837-2848. https://doi.org/10.4319/lo.2006.51.6.2837

Guyard, H., Chapron, E., St-Onge, G., Anselmetti, F. S., Arnaud, F., Magand, O., Francus, P., & Mélières, M.-A. (2007). High-altitude varve records of abrupt environmental changes and mining activity over the last 4000 years in the Western French Alps (Lake Bramant, Grandes Rousses Massif). Quaternary Science Reviews, 26(19), 2644-2660. https://doi.org/10.1016/j.quascirev.2007.07.007

Hanebuth, T. J. J., King, M. L., Mendes, I., Lebreiro, S., Lobo, F. J., Oberle, F. K., Antón, L., Ferreira, P. A., & Reguera, M. I. (2018). Hazard potential of widespread but hidden historic offshore heavy metal (Pb, Zn) contamination (Gulf of Cadiz, Spain). Science of

The Total Environment, 637-638, 561-576. https://doi.org/10.1016/j.scitotenv.2018.04.352

Hansson, S. V., Claustres, A., Probst, A., De Vleeschouwer, F., Baron, S., Galop, D., Mazier, F., & Le Roux, G. (2017). Atmospheric and terrigenous metal accumulation over 3000 years in a French mountain catchment: Local vs distal influences. Anthropocene, 19, 45-54. https://doi.org/10.1016/j.ancene.2017.09.002

Hillman, A. L., Abbott, M. B., Valero-Garcés, B. L., Morellon, M., Barreiro-Lostres, F., & Bain, D. J. (2017). Lead pollution resulting from Roman gold extraction in northwestern Spain. The Holocene, 27(10), 1465-1474.

Ho, J. C., Michalak, A. M., & Pahlevan, N. (2019). Widespread global increase in intense lake phytoplankton blooms since the 1980s. Nature, 574(7780), 7780. https://doi.org/10.1038/s41586-019-1648-7

Hock, R., Rasul, G., Adler, C., Cáceres, B., Gruber, S., Hirabayashi, Y., Jackson, M., Kääb, A., Kang, S., Kutuzov, S., Milner, A., Molau, U., Morin, S., Orlove, B., Stetzler, H., Allen, S., Arenson, L., Banjeree, S., Barr, I., & Zhang, Y. (2019). Chapter 2: High Mountain Areas (p. 94 pages).

Hooper, D. U., Adair, E. C., Cardinale, B. J., Byrnes, J. E. K., Hungate, B. A., Matulich, K. L., Gonzalez, A., Duffy, J. E., Gamfeldt, L., & O'Connor, M. I. (2012). A global synthesis reveals biodiversity loss as a major driver of ecosystem change. Nature, 486(7401), 7401. https://doi.org/10.1038/nature11118

Houghton, E. (1996). Climate change 1995: The science of climate change: Contribution of working group I to the second assessment report of the Intergovernmental Panel on Climate Change (Vol. 2). Cambridge University Press.

Huang, S., Zhang, K., Lin, Q., Liu, J., & Shen, J. (2022). Abrupt ecological shifts of lakes during the Anthropocene. Earth-Science Reviews, 227, 103981. https://doi.org/10.1016/j.earscirev.2022.103981

Ibanez, F., Fromentin, J.-M., & Castel, J. (1993). Application of the cumulated function to the processing of chronological data in oceanography. Comptes Rendus de l'Academie des Sciences - Series III, 316(8), 745-748. Scopus.

IPCC. (2021). Climate Change 2021: The Physical Science Basis. Contribution of Working Group I to the Sixth Assessment Report of the Intergovernmental Panel on Climate Change. Cambridge University Press. https://www.ipcc.ch/report/ar6/wg1/

IPCC (Ed.). (2022). High Mountain Areas. En The Ocean and Cryosphere in a Changing Climate: Special Report of the Intergovernmental Panel on Climate Change (pp. 131-202). Cambridge University Press. https://doi.org/10.1017/9781009157964.004

Irabien, M. J., Cearreta, A., & Urteaga, M. (2012). Historical signature of Roman mining activities in the Bidasoa estuary (Basque Country, northern Spain): An integrated micropalaeontological, geochemical and archaeological approach. Journal of Archaeological Science, 39(7), 2361-2370. https://doi.org/10.1016/j.jas.2012.02.023

Jane, S. F., Hansen, G. J. A., Kraemer, B. M., Leavitt, P. R., Mincer, J. L., North, R. L., Pilla, R. M., Stetler, J. T., Williamson, C. E., Woolway, R. I., Arvola, L., Chandra, S., DeGasperi, C. L., Diemer, L., Dunalska, J., Erina, O., Flaim, G., Grossart, H.-P., Hambright, K. D., … Rose, K. C. (2021). Widespread deoxygenation of temperate lakes. Nature, 594(7861), 7861. https://doi.org/10.1038/s41586-021-03550-y

Jenny, J.-P., Francus, P., Normandeau, A., Lapointe, F., Perga, M.-E., Ojala, A., Schimmelmann, A., & Zolitschka, B. (2016). Global spread of hypoxia in freshwater ecosystems during the last three centuries is caused by rising local human pressure. Global Change Biology, 22(4), 1481-1489. https://doi.org/10.1111/gcb.13193

Keck, F., Millet, L., Debroas, D., Etienne, D., Galop, D., Rius, D., & Domaizon, I. (2020). Assessing the response of micro-eukaryotic diversity to the Great Acceleration using lake sedimentary DNA. Nature Communications, 11(1), 1. https://doi.org/10.1038/s41467-020-17682-8

Keeling, R. F., Graven, H. D., Welp, L., Piper, S. C., Bollenbacher, A., Resplandy, L., & Meijer, H. A. J. (2016). Atmospheric evidence for a global secular increase in isotopic discrimination of land photosynthesis. 2016, B52D-07.

Kelts, K., & Hsü, K. J. (1978). Freshwater Carbonate Sedimentation. En A. Lerman (Ed.), Lakes: Chemistry, Geology, Physics (pp. 295-323). Springer. https://doi.org/10.1007/978-1-4757-1152-3_9

Körner, C. (2000). Why are there global gradients in species richness? Mountains might hold the answer. Trends in Ecology & Evolution, 15(12), 513-514. https://doi.org/10.1016/S0169-5347(00)02004-8

Krajick, K. (2004). All Downhill From Here? Science, 303(5664), 1600-1602. https://doi.org/10.1126/science.303.5664.1600

Kylander, M. E., Ampel, L., Wohlfarth, B., & Veres, D. (2011). High-resolution X-ray fluorescence core scanning analysis of Les Echets (France) sedimentary sequence: New insights from chemical proxies. Journal of Quaternary Science, 26(1), 109-117. https://doi.org/10.1002/jqs.1438

Lambs, L., Moussa, I., & Brunet, F. (2013). Air masses origin and isotopic tracers: A study case of the oceanic and Mediterranean rainfall southwest of France. Water, 5(2), 617-628.

Lana-Renault, N., Alvera, B., & García-Ruiz, J. M. (2011). Runoff and Sediment Transport during the Snowmelt Period in a Mediterranean High-Mountain Catchment. Arctic, Antarctic, and Alpine Research, 43(2), 213-222. https://doi.org/10.1657/1938-4246-43.2.213

Lasanta-Martínez, T., Vicente-Serrano, S. M., & Cuadrat-Prats, J. M. (2005). Mountain Mediterranean landscape evolution caused by the abandonment of traditional primary activities: A study of the Spanish Central Pyrenees. Applied Geography, 25(1), 47-65. https://doi.org/10.1016/j.apgeog.2004.11.001

Le Roux, G., Hansson, S. V., Claustres, A., Binet, S., De Vleeschouwer, F., Gandois, L., Mazier, F., Simonneau, A., Teisserenc, R., Allen, D., Rosset, T., Haver, M., Da Ros, L., Galop,

D., Durantez, P., Probst, A., Sánchez-Pérez, J. M., Sauvage, S., Laffaille, P., … Lofts, S. (2020). Trace Metal Legacy in Mountain Environments. En Biogeochemical Cycles (pp. 191-206). American Geophysical Union (AGU). https://doi.org/10.1002/9781119413332.ch9

Legendre, P., & Legendre, L. (2012). Numerical Ecology. Elsevier.

Lehman, J. T. (1975). Reconstructing the Rate of Accumulation of Lake Sediment: The Effect of Sediment Focusing. Quaternary Research, 5(4), 541-550. https://doi.org/10.1016/0033-5894(75)90015-0

Lenihan, J. M., Drapek, R., Bachelet, D., & Neilson, R. P. (2003). Climate change effects on vegetation distribution, carbon, and fire in California. Ecological Applications, 13(6), 1667-1681.

Lenton, T. M., Held, H., Kriegler, E., Hall, J. W., Lucht, W., Rahmstorf, S., & Schellnhuber, H. J. (2008). Tipping elements in the Earth's climate system. Proceedings of the National Academy of Sciences, 105(6), 1786-1793. https://doi.org/10.1073/pnas.0705414105

Leonard, E. M., & Reasoner, M. A. (1999). A Continuous Holocene Glacial Record Inferred from Proglacial Lake Sediments in Banff National Park, Alberta, Canada. Quaternary Research, 51(1), 1-13. https://doi.org/10.1006/qres.1998.2009

Leorri, E., Mitra, S., Irabien, M. J., Zimmerman, A. R., Blake, W. H., & Cearreta, A. (2014). A 700year record of combustion-derived pollution in northern Spain: Tools to identify the Holocene/Anthropocene transition in coastal environments. Science of The Total Environment, 470-471, 240-247. https://doi.org/10.1016/j.scitotenv.2013.09.064

Leunda, M., Gil-Romera, G., Daniau, A.-L., Benito, B. M., & González-Sampériz, P. (2020). Holocene fire and vegetation dynamics in the Central Pyrenees (Spain). CATENA, 188, 104411. https://doi.org/10.1016/j.catena.2019.104411

Leunda, M., González-Sampériz, P., Gil-Romera, G., Aranbarri, J., Moreno, A., Oliva-Urcia, B., Sevilla-Callejo, M., & Valero-Garcés, B. (2017). The Late-Glacial and Holocene Marboré Lake sequence (2612 m a.s.l., Central Pyrenees, Spain): Testing high altitude sites sensitivity to millennial scale vegetation and climate variability. Global and Planetary Change, 157, 214-231. https://doi.org/10.1016/j.gloplacha.2017.08.008

Lewis, S. L., & Maslin, M. A. (2015). Defining the Anthropocene. Nature, 519(7542), 7542. https://doi.org/10.1038/nature14258

Lionello, P. (2012). The climate of the Mediterranean region: From the past to the future. Elsevier.

Livingstone, D. M., Lotter, A. F., & Walkery, I. R. (1999). The Decrease in Summer Surface Water Temperature with Altitude in Swiss Alpine Lakes: A Comparison with Air Temperature Lapse Rates. Arctic, Antarctic, and Alpine Research, 31(4), 341-352. https://doi.org/10.1080/15230430.1999.12003319

Livingstone, S. J., Clark, C. D., Piotrowski, J. A., Tranter, M., Bentley, M. J., Hodson, A., Swift, D. A., & Woodward, J. (2012). Theoretical framework and diagnostic criteria for the

identification of palaeo-subglacial lakes. Quaternary Science Reviews, 53, 88-110. https://doi.org/10.1016/j.quascirev.2012.08.010

López-Merino, L., Moreno, A., Leira, M., Sigró, J., González-Sampériz, P., Valero-Garcés, B. L., López-Sáez, J. A., Brunet, M., & Aguilar, E. (2011). Two hundred years of environmental change in Picos de Europa National Park inferred from sediments of Lago Enol, northern Iberia. Journal of Paleolimnology, 46(3), 453-467. https://doi.org/10.1007/s10933-011-9546-5

López-Moreno, J. I., Alonso-González, E., Monserrat, O., Río, L. M. D., Otero, J., Lapazaran, J., Luzi, G., Dematteis, N., Serreta, A., Rico, I., Serrano-Cañadas, E., Bartolomé, M., Moreno, A., Buisan, S., & Revuelto, J. (2019). Ground-based remote-sensing techniques for diagnosis of the current state and recent evolution of the Monte Perdido Glacier, Spanish Pyrenees. Journal of Glaciology, 65(249), 85-100. https://doi.org/10.1017/jog.2018.96

López-Moreno, J. I., Goyette, S., & Beniston, M. (2009). Impact of climate change on snowpack in the Pyrenees: Horizontal spatial variability and vertical gradients. Journal of Hydrology, 374(3), 384-396. https://doi.org/10.1016/j.jhydrol.2009.06.049

López-Moreno, J. I., Goyette, S., Vicente-Serrano, S. M., & Beniston, M. (2011). Effects of climate change on the intensity and frequency of heavy snowfall events in the Pyrenees. Climatic Change, 105(3), 489-508. https://doi.org/10.1007/s10584-010-9889-3

Lorenzen, C. J. (1967). Determination of Chlorophyll and pheo-pigments: Spectrophotometric equations. Limnology and Oceanography, 12(2), 343-346. https://doi.org/10.4319/lo.1967.12.2.0343

Maberly, S. C., O'Donnell, R. A., Woolway, R. I., Cutler, M. E. J., Gong, M., Jones, I. D., Merchant, C. J., Miller, C. A., Politi, E., Scott, E. M., Thackeray, S. J., & Tyler, A. N. (2020). Global lake thermal regions shift under climate change. Nature Communications, 11(1), 1. https://doi.org/10.1038/s41467-020-15108-z

Machate, O., Schmeller, D. S., Schulze, T., & Brack, W. (2023). Review: Mountain lakes as freshwater resources at risk from chemical pollution. Environmental Sciences Europe, 35(1), 3. https://doi.org/10.1186/s12302-022-00710-3

Mackay, E. B., Jones, I. D., Folkard, A. M., & Barker, P. (2012). Contribution of sediment focussing to heterogeneity of organic carbon and phosphorus burial in small lakes. Freshwater Biology, 57(2), 290-304.

Mammides, C. (2020). A global assessment of the human pressure on the world's lakes. Global Environmental Change, 63, 102084. https://doi.org/10.1016/j.gloenvcha.2020.102084

Mangili, C., Brauer, A., Plessen, B., & Moscariello, A. (2007). Centennial-scale oscillations in oxygen and carbon isotopes of endogenic calcite from a 15,500 varve year record of the Piànico interglacial. Quaternary Science Reviews, 26(13), 1725-1735. https://doi.org/10.1016/j.quascirev.2007.04.012

Maris, M., Giraud, G., Durand, Y., Navarre, J.-P., & Mérindol, L. (2009). Results of 50 years of climate reanalysis in the French Pyrenees (1958-2008) using the SAFRAN and CROCUS models. Davos: International Snow Science Workshop, Proceedings.

Martínez Cortizas, A., López-Merino, L., Bindler, R., Mighall, T., & Kylander, M. (2013). Atmospheric Pb pollution in N Iberia during the late Iron Age/Roman times reconstructed using the high-resolution record of La Molina mire (Asturias, Spain). Journal of Paleolimnology, 50(1), 71-86. https://doi.org/10.1007/s10933-013-9705-y

Martín-Puertas, C., Jiménez-Espejo, F., Martínez-Ruiz, F., Nieto-Moreno, V., Rodrigo, M., Mata, M. d P., & Valero-Garcés, B. L. (2010). Late Holocene climate variability in the southwestern Mediterranean region: An integrated marine and terrestrial geochemical approach. Climate of the Past, 6(6), 807-816.

Martín-Puertas, C., Valero-Garcés, B. L., Brauer, A., Mata, M. P., Delgado-Huertas, A., & Dulski, P. (2009). The Iberian–Roman Humid Period (2600–1600 cal yr BP) in the Zoñar Lake varve record (Andalucía, southern Spain). Quaternary Research, 71(2), 108-120. https://doi.org/10.1016/j.yqres.2008.10.004

Martín-Puertas, C., Valero-Garcés, B. L., Pilar Mata, M., González-Sampériz, P., Bao, R., Moreno, A., & Stefanova, V. (2008). Arid and humid phases in southern Spain during the last 4000 years: The Zonar Lake record, Cordoba. The Holocene, 18(6), 907-921.

Mata Campo, M. P., Moreno Caballud, A., Oliva Urcia, B., Valero Garcés, B. L., & Rico, M. T. (2013). Registro histórico de la contaminación atmosférica por Pb en el Lago de Marboré (P.N. de Ordesa y Monteperdido). Macla: revista de la Sociedad Española de Mineralogía, 17, 71-72.

Matesanz, S., & Valladares, F. (2014). Ecological and evolutionary responses of Mediterranean plants to global change. Environmental and Experimental botany, 103, 53-67.

Mattauer, M. (1968). Les traits structuraux essentiels de la chaîne Pyrénéenne. Revue de Géologie Dynamique et de Géographie physique, 10(1), 3-11.

McConnell, J. R., Wilson, A. I., Stohl, A., Arienzo, M. M., Chellman, N. J., Eckhardt, S., Thompson, E. M., Pollard, A. M., & Steffensen, J. P. (2018). Lead pollution recorded in Greenland ice indicates European emissions tracked plagues, wars, and imperial expansion during antiquity. Proceedings of the National Academy of Sciences, 115(22), 5726-5731. https://doi.org/10.1073/pnas.1721818115

McKay, N. P., Emile-Geay, J., & Khider, D. (2021). GeoChronR – an R package to model, analyze, and visualize age-uncertain data. Geochronology, 3(1), 149-169. https://doi.org/10.5194/gchron-3-149-2021

McLauchlan, K. K., Williams, J. J., Craine, J. M., & Jeffers, E. S. (2013). Changes in global nitrogen cycling during the Holocene epoch. Nature, 495(7441), 352-355. https://doi.org/10.1038/nature11916

McNeill, J. R. (2001). Something new under the sun: An environmental history of the twentieth-century world (the global century series). WW Norton & Company.

Meyers, P. A., & Teranes, J. L. (2002). Sediment Organic Matter. En W. M. Last & J. P. Smol (Eds.), Tracking Environmental Change Using Lake Sediments (Vol. 2, pp. 239-269). Kluwer Academic Publishers. https://doi.org/10.1007/0-306-47670-3_9

Meza, F. J., Vicuna, S., Gironás, J., Poblete, D., Suárez, F., & Oertel, M. (2015). Water–food–energy nexus in Chile: The challenges due to global change in different regional contexts. Water International, 40(5-6), 839-855. https://doi.org/10.1080/02508060.2015.1087797

Michelutti, N., Wolfe, A. P., Cooke, C. A., Hobbs, W. O., Vuille, M., & Smol, J. P. (2015). Climate Change Forces New Ecological States in Tropical Andean Lakes. PLOS ONE, 10(2), e0115338. https://doi.org/10.1371/journal.pone.0115338

Morán-Tejeda, E., López-Moreno, J. I., & Sanmiguel-Vallelado, A. (2017). Changes in climate, snow and water resources in the Spanish Pyrenees: Observations and projections in a warming climate. En High Mountain Conservation in a Changing World (pp. 305-323). Springer, Cham.

Morellón, M., Anselmetti, F. S., Valero-Garcés, B., Giralt, S., Ariztegui, D., Sáez, A., Mata, M. P., Barreiro-Lostres, F., Rico, M., & Moreno, A. (2014). The influence of subaquatic springs in lacustrine sedimentation: Origin and paleoenvironmental significance of homogenites in karstic Lake Banyoles (NE Spain). Sedimentary Geology, 311, 96-111. https://doi.org/10.1016/j.sedgeo.2014.07.004

Morellón, M., Pérez-Sanz, A., Corella, J. P., Büntgen, U., Catalán, J., González-Sampériz, P., González-Trueba, J. J., López-Sáez, J. A., Moreno, A., Pla-Rabes, S., Saz-Sánchez, M. Á., Scussolini, P., Serrano, E., Steinhilber, F., Stefanova, V., Vegas-Vilarrúbia, T., & Valero-Garcés, B. (2012). A multi-proxy perspective on millennium-long climate variability in the Southern Pyrenees. Climate of the Past, 8(2), 683-700. https://doi.org/10.5194/cp-8-683-2012

Morellón, M., Valero-Garcés, B., González-Sampériz, P., Vegas-Vilarrúbia, T., Rubio, E., Rieradevall, M., Delgado-Huertas, A., Mata, P., Romero, Ó., Engstrom, D. R., López-Vicente, M., Navas, A., & Soto, J. (2011). Climate changes and human activities recorded in the sediments of Lake Estanya (NE Spain) during the Medieval Warm Period and Little Ice Age. Journal of Paleolimnology, 46(3), 423-452. https://doi.org/10.1007/s10933-009-9346-3

Morellón, M., Valero-Garcés, B., Vegas-Vilarrúbia, T., González-Sampériz, P., Romero, Ó., Delgado-Huertas, A., Mata, P., Moreno, A., Rico, M., & Corella, J. P. (2009). Lateglacial and Holocene palaeohydrology in the western Mediterranean region: The Lake Estanya record (NE Spain). Quaternary Science Reviews, 28(25-26), 2582-2599. https://doi.org/10.1016/j.quascirev.2009.05.014

Morellón, M., Vegas, J., Mata, M. P., de Vera, A. V., García, J. R., España, J. S., & Barreiro-Lostres, F. (2016). El impacto ambiental en la geomorfología de zonas de montaña: El registro sedimentario del Lago de La Cueva (Parque Natural de Somiedo, Asturias). Durán Valsero, JJ; Montes Santiago, M.; Robador Moreno, A., & Salazar Rincón,

Á.(eds.) Comprendiendo el relieve: del pasado al futuro. Actas de la XIV Reunión Nacional de Geomorfología Málaga, 22-25.

Moreno, A., Bartolomé, M., López-Moreno, J. I., Pey, J., Corella, J. P., García-Orellana, J., Sancho, C., Leunda, M., Gil-Romera, G., González-Sampériz, P., Pérez-Mejías, C., Navarro, F., Otero-García, J., Lapazaran, J., Alonso-González, E., Cid, C., López-Martínez, J., Oliva-Urcia, B., Faria, S. H., … García-Ruíz, J. M. (2021). The case of a southern European glacier which survived Roman and medieval warm periods but is disappearing under recent warming. The Cryosphere, 15(2), 1157-1172. https://doi.org/10.5194/tc-15-1157-2021

Moreno, A., López-Merino, L., Leira, M., Marco-Barba, J., González-Sampériz, P., Valero-Garcés, B. L., López-Sáez, J. A., Santos, L., Mata, P., & Ito, E. (2011). Revealing the last 13,500 years of environmental history from the multiproxy record of a mountain lake (Lago Enol, northern Iberian Peninsula). Journal of Paleolimnology, 46(3), 327-349. https://doi.org/10.1007/s10933-009-9387-7

Moreno, A., Pérez, A., Frigola, J., Nieto-Moreno, V., Rodrigo-Gámiz, M., Martrat, B., González-Sampériz, P., Morellón, M., Martín-Puertas, C., Corella, J. P., Belmonte, Á., Sancho, C., Cacho, I., Herrera, G., Canals, M., Grimalt, J. O., Jiménez-Espejo, F., Martínez-Ruiz, F., Vegas-Vilarrúbia, T., & Valero-Garcés, B. L. (2012). The Medieval Climate Anomaly in the Iberian Peninsula reconstructed from marine and lake records. Quaternary Science Reviews, 43, 16-32. https://doi.org/10.1016/j.quascirev.2012.04.007

Moreno, A., Stoll, H., Jiménez-Sánchez, M., Cacho, I., Valero-Garcés, B., Ito, E., & Edwards, R. L. (2010). A speleothem record of glacial (25–11.6kyr BP) rapid climatic changes from northern Iberian Peninsula. Global and Planetary Change, 71(3), 218-231. https://doi.org/10.1016/j.gloplacha.2009.10.002

Moreno, A., Valero-Garcés, B. L., González-Sampériz, P., & Rico, M. (2008). Flood response to rainfall variability during the last 2000 years inferred from the Taravilla Lake record (Central Iberian Range, Spain). Journal of paleolimnology, 40, 943-961.

Morice, C. P., Kennedy, J. J., Rayner, N. A., Winn, J. P., Hogan, E., Killick, R. E., Dunn, R. J. H., Osborn, T. J., Jones, P. D., & Simpson, I. R. (2021). An Updated Assessment of Near-Surface Temperature Change From 1850: The HadCRUT5 Data Set. Journal of Geophysical Research: Atmospheres, 126(3), e2019JD032361. https://doi.org/10.1029/2019JD032361

Mortlock, R. A., & Froelich, P. N. (1989). A simple method for the rapid determination of biogenic opal in pelagic marine sediments. Deep Sea Research Part A. Oceanographic Research Papers, 36(9), 1415-1426. https://doi.org/10.1016/0198-0149(89)90092-7

Moscariello, A. (2021). The Geomorphological Landscapes in the Geneva Basin. En E. Reynard (Ed.), Landscapes and Landforms of Switzerland (pp. 83-96). Springer International Publishing. https://doi.org/10.1007/978-3-030-43203-4_6

Moser, K. A., Baron, J. S., Brahney, J., Oleksy, I. A., Saros, J. E., Hundey, E. J., Sadro, S., Kopáček, J., Sommaruga, R., Kainz, M. J., Strecker, A. L., Chandra, S., Walters, D. M.,

Preston, D. L., Michelutti, N., Lepori, F., Spaulding, S. A., Christianson, K. R., Melack, J. M., & Smol, J. P. (2019). Mountain lakes: Eyes on global environmental change. Global and Planetary Change, 178, 77-95. https://doi.org/10.1016/j.gloplacha.2019.04.001

Muñoz, J. A. (1992). Evolution of a continental collision belt: ECORS-Pyrenees crustal balanced cross-section. Thrust tectonics, 235-246.

Muñoz-Rojas, M., Jordán, A., Zavala, L. M., De la Rosa, D., Abd-Elmabod, S. K., & Anaya-Romero, M. (2015). Impact of Land Use and Land Cover Changes on Organic Carbon Stocks in Mediterranean Soils (1956–2007). Land Degradation & Development, 26(2), 168-179. https://doi.org/10.1002/ldr.2194

Nadal-Romero, E., Lasanta Martínez, T., González-Hidalgo, J. C., Luis Arrillaga, M. de, & García-Ruiz, J. M. (2012). The effect of intense rainstorm events on the suspended sediment response under various land uses: The Aísa Valley Experimental Station.

Nicolás-Martínez, P. M. (1981). Morfología del circo de Tucarroya (Macizo de Monte Perdido, Pirineo aragonés). Cuadernos de Investigación Geográfica, 7, 51-80.

Nieto Callén, J. J. (1996). El proceso sidero-metarlúrgico altoaragonés: Los valles de Bielsa y Gistain en la Edad Moderna (1565-1800). Llull: Revista de la Sociedad Española de Historia de las Ciencias y de las Técnicas, 19(37), 471-508.

Nogués-Bravo, D., Araújo, M. B., Errea, M. P., & Martínez-Rica, J. P. (2007). Exposure of global mountain systems to climate warming during the 21st Century. Global Environmental Change, 17(3), 420-428. https://doi.org/10.1016/j.gloenvcha.2006.11.007

Noren, A., Bierman, P., Steig, E., Lini, A., & Southon, J. (2002). Millennial-scale storminess variability in the northeastern United States during the Holocene epoch. Nature, 419, 821-824. https://doi.org/10.1038/nature01132

Nriagu, J. O. (1979). Global inventory of natural and anthropogenic emissions of trace metals to the atmosphere. Nature, 279(5712), 5712. https://doi.org/10.1038/279409a0

Nriagu, J. O. (1996). A History of Global Metal Pollution. Science, 272(5259), 223-223. https://doi.org/10.1126/science.272.5259.223

Ohlendorf, C., & Sturm, M. (2001). Precipitation and Dissolution of Calcite in a Swiss High Alpine Lake. Arctic, Antarctic, and Alpine Research, 33(4), 410-417. https://doi.org/10.1080/15230430.2001.12003449

Ohlendorf, C., Sturm, M., & Hausmann, S. (2003). Natural environmental changes and human impact reflected in sediments of a high alpine lake in Switzerland. Journal of Paleolimnology, 30(3), 297-306. https://doi.org/10.1023/A:1026032829150

Oksanen, J., Blanchet, F. G., Friendly, M., Kindt, R., Legendre, P., McGlinn, D., Minchin, P. R., O'Hara, R. B., Simpson, G. L., Solymos, P., Stevens, M. H. H., Szoecs, E., & Wagner, H. (2019). Vegan: Community ecology package. http://CRAN.R-project.org/package=vegan

Oliva-Urcia, B., & Moreno, A. (2019). Discerning the major environmental processes that influence the magnetic properties in three northern Iberia mountain lakes. CATENA, 182, 104130. https://doi.org/10.1016/j.catena.2019.104130

Oliva-Urcia, B., Moreno, A., Leunda, M., Valero-Garcés, B., González-Sampériz, P., Gil-Romera, G., Mata, M. P., & HORDA Group. (2018). Last deglaciation and Holocene environmental change at high altitude in the Pyrenees: The geochemical and paleomagnetic record from Marboré Lake (N Spain). Journal of Paleolimnology, 59(3), 349-371. https://doi.org/10.1007/s10933-017-0013-9

Oliva-Urcia, B., Moreno Caballud, A., Valero-Garcés, B. L., Mata Campo, M. P., & Horda, G. (2013). Magnetismo y cambios ambientales en registros terrestres: El lago de Marboré, Parque Nacional de Ordesa y Monte Perdido (Huesca). https://digital.csic.es/handle/10261/87676

Oliva-Urcia, M., Ruiz-Fernández, J., Barriendos, M., Benito, G., Cuadrat, J. M., Domínguez-Castro, F., García-Ruiz, J. M., Giralt, S., Gómez-Ortiz, A., Hernández, A., López-Costas, O., López-Moreno, J. I., López-Sáez, J. A., Martínez-Cortizas, A., Moreno, A., Prohom, M., Saz, M. A., Serrano, E., Tejedor, E., … Vicente-Serrano, S. M. (2018). The Little Ice Age in Iberian mountains. Earth-Science Reviews, 177, 175-208. https://doi.org/10.1016/j.earscirev.2017.11.010

OPCC. (2019). Informe Final 2019. Resultados del proyecto OPCC2 y proyectos asociados: CLIM'PY, REPLIM, CANOPEE, FLORAPYR, PIRAGUA. Octubre 2019. https://opcc-ctp.org/sites/default/files/documentacion/opcc-informe-es-paginas.pdf

O'Reilly, C. M., Sharma, S., Gray, D. K., Hampton, S. E., Read, J. S., Rowley, R. J., Schneider, P., Lenters, J. D., McIntyre, P. B., Kraemer, B. M., Weyhenmeyer, G. A., Straile, D., Dong, B., Adrian, R., Allan, M. G., Anneville, O., Arvola, L., Austin, J., Bailey, J. L., … Zhang, G. (2015). Rapid and highly variable warming of lake surface waters around the globe. Geophysical Research Letters, 42(24), 10,773-10,781. https://doi.org/10.1002/2015GL066235

Osborn, T. J., Jones, P. D., Lister, D. H., Morice, C. P., Simpson, I. R., Winn, J. P., Hogan, E., & Harris, I. C. (2021). Land Surface Air Temperature Variations Across the Globe Updated to 2019: The CRUTEM5 Data Set. Journal of Geophysical Research: Atmospheres, 126(2), e2019JD032352. https://doi.org/10.1029/2019JD032352

Otto, J.-C. (2019). Proglacial Lakes in High Mountain Environments. En T. Heckmann & D. Morche (Eds.), Geomorphology of Proglacial Systems: Landform and Sediment Dynamics in Recently Deglaciated Alpine Landscapes (pp. 231-247). Springer International Publishing. https://doi.org/10.1007/978-3-319-94184-4_14

Pacyna, E. G., Pacyna, J. M., Fudala, J., Strzelecka-Jastrzab, E., Hlawiczka, S., Panasiuk, D., Nitter, S., Pregger, T., Pfeiffer, H., & Friedrich, R. (2007). Current and future emissions of selected heavy metals to the atmosphere from anthropogenic sources in Europe. Atmospheric Environment, 41(38), 8557-8566. https://doi.org/10.1016/j.atmosenv.2007.07.040

Parry, M. L., Canziani, O., Palutikof, J., Van der Linden, P., & Hanson, C. (2007). Climate change 2007-impacts, adaptation and vulnerability: Working group II contribution to the fourth assessment report of the IPCC (Vol. 4). Cambridge University Press.

Pèlachs, A., Nadal, J., Soriano, J. M., Molina, D., & Cunill, R. (2009). Changes in Pyrenean woodlands as a result of the intensity of human exploitation: 2,000 years of metallurgy in Vallferrera, northeast Iberian Peninsula. Vegetation History and Archaeobotany, 18(5), 403-416. https://doi.org/10.1007/s00334-009-0218-6

Penuelas, J., Poulter, B., Sardans, J., Ciais, P., Bopp, L., Boucher, O., Godderis, Y., Hinsinger, P., Llusia, J., Nardin, E., Vicca, S., Obersteiner, M., & Janssens, I. A. (2013). Human-induced nitrogen–phosphorus imbalances alter natural and managed ecosystems across the globe. Nature Communications, 10.

Pepin, N., Bradley, R. S., Diaz, H. F., Baraer, M., Caceres, E. B., Forsythe, N., Fowler, H., Greenwood, G., Hashmi, M. Z., Liu, X. D., Miller, J. R., Ning, L., Ohmura, A., Palazzi, E., Rangwala, I., Schöner, W., Severskiy, I., Shahgedanova, M., Wang, M. B., … Mountain Research Initiative EDW Working Group. (2015). Elevation-dependent warming in mountain regions of the world. Nature Climate Change, 5(5), 5. https://doi.org/10.1038/nclimate2563

Pérez, F. F., Boscolo, R., Bladé, I., Cacho, I., Castro-Díez, Y., Gomis, D., González-Sampériz, P., Miguez-Macho, G., Rodríguez-Fonseca, B., Rodríguez-Puebla, C., Sánchez, E., Sotillo, M. G., Valero-Garcés, B. L., & Vargas-Yáñez, M. (2010). Clima en España: Pasado, presente y futuro. Informe de Evaluación del Cambio Climático Regional. https://digital.csic.es/handle/10261/23600

Pérez-Sanz, A., González-Sampériz, P., Moreno, A., Valero-Garcés, B., Gil-Romera, G., Rieradevall, M., Tarrats, P., Lasheras-Álvarez, L., Morellón, M., Belmonte, A., Sancho, C., Sevilla-Callejo, M., & Navas, A. (2013). Holocene climate variability, vegetation dynamics and fire regime in the central Pyrenees: The Basa de la Mora sequence (NE Spain). Quaternary Science Reviews, 73, 149-169. https://doi.org/10.1016/j.quascirev.2013.05.010

Pérez-Zanón, N., Sigró, J., & Ashcroft, L. (2017). Temperature and precipitation regional climate series over the central Pyrenees during 1910-2013: REGIONAL CLIMATE SERIES OVER THE CENTRAL PYRENEES DURING 1910-2013. International Journal of Climatology, 37(4), 1922-1937. https://doi.org/10.1002/joc.4823

Perret, M.-F. (1988). Le passage du Dévonien au Carbonifère dans les Pyrénées. Zonation par conodontes. Courier Forschungsinstitut Senckenberg, 100, 39-52.

Pey, J., Larrasoaña, J. C., Pérez, N., Cerro, J. C., Castillo, S., Tobar, M. L., de Vergara, A., Vázquez, I., Reyes, J., Mata, M. P., Mochales, T., Orellana, J. M., & Causapé, J. (2020). Phenomenology and geographical gradients of atmospheric deposition in southwestern Europe: Results from a multi-site monitoring network. Science of The Total Environment, 744, 140745. https://doi.org/10.1016/j.scitotenv.2020.140745

Pla, S., Monteith, D., Flower, R., & Rose, N. (2009). The recent palaeolimnology of a remote Scottish loch with special reference to the relative impacts of regional warming and atmospheric contamination. Freshwater Biology, 54(3), 505-523. https://doi.org/10.1111/j.1365-2427.2008.02127.x

Pla-Rabes, S., & Catalan, J. (2005). Chrysophyte cysts from lake sediments reveal the submillennial winter/spring climate variability in the northwestern Mediterranean region throughout the Holocene. Climate Dynamics, 24(2-3), 263-278. https://doi.org/10.1007/s00382-004-0482-1

Pla-Rabes, S., & Catalan, J. (2011). Deciphering chrysophyte responses to climate seasonality. Journal of Paleolimnology, 46(1), 139-150. https://doi.org/10.1007/s10933-011-9529-6

Platt, N. H., & Wright, V. P. (1991). Lacustrine Carbonates: Facies Models, Facies Distributions and Hydrocarbon Aspects. En Lacustrine Facies Analysis (pp. 57-74). John Wiley & Sons, Ltd. https://doi.org/10.1002/9781444303919.ch3

Prudhomme, C., Giuntoli, I., Robinson, E. L., Clark, D. B., Arnell, N. W., Dankers, R., Fekete, B. M., Franssen, W., Gerten, D., & Gosling, S. N. (2014). Hydrological droughts in the 21st century, hotspots and uncertainties from a global multimodel ensemble experiment. Proceedings of the National Academy of Sciences, 111(9), 3262-3267.

Puigdefàbregas, C., & Souquet, P. (1986). Tecto-sedimentary cycles and depositional sequences of the Mesozoic and Tertiary from the Pyrenees. Tectonophysics, 129(1-4), 173-203.

Rangwala, I., & Miller, J. R. (2012). Climate change in mountains: A review of elevation-dependent warming and its possible causes. Climatic Change, 114(3), 527-547. https://doi.org/10.1007/s10584-012-0419-3

Redondo-Vega, J. M., Gómez-Villar, A., Santos-González, J., González-Gutiérrez, R. B., & Álvarez-Martínez, J. (2017). Changes in land use due to mining in the north-western mountains of Spain during the previous 50 years. Catena, 149, 844-856.

Renaut, R., & Gierlowski-Kordesch, E. (2010). Lakes. Facies Models 4. Toronto (Canada): Geological Association of Canada.

Richter, T. O., van der Gaast, S., Koster, B., Vaars, A., Gieles, R., de Stigter, H. C., De Haas, H., & van Weering, T. C. E. (2006). The Avaatech XRF Core Scanner: Technical description and applications to NE Atlantic sediments. Geological Society, London, Special Publications, 267(1), 39-50. https://doi.org/10.1144/GSL.SP.2006.267.01.03

Ríos Aragües, L. M., Galera Fernández, J. M., & Barettino Fraile, D. (1989). Mapa geológico y Memoria de la Hoja nº 146 (Bujaruelo). Mapa Geológico de España E. 1:50.000. ITGE.

Ríos Aragües, L. M., Galera Fernández, J. M., Barettino Fraile, D., & Charlet, J. M. (1991). Mapa geológico y Memoria de la Hoja nº 180 (Benasque). Mapa Geológico de España E. 1:50.000. ITGE.

Ríos Aragües, L. M., Lanaja del Busto, J. M., Ríos Mitchell, J. M., & Marín Blanco, F. J. (1982). Mapa geológico y Memoria de la Hoja nº 179 (Bielsa). Mapa Geológico de España E. 1:50.000.

Rivera-Rondón, C. A., & Catalan, J. (2017). Diatom diversity in the lakes of the Pyrenees: An iconographic reference. Limnetica, 36, 127-395. https://doi.org/10.23818/limn.36.10

Rivera-Rondón, C. A., & Catalan, J. (2020). Diatoms as indicators of the multivariate environment of mountain lakes. Science of The Total Environment, 703, 135517. https://doi.org/10.1016/j.scitotenv.2019.135517

Roberts, A. P. (2015). Magnetic mineral diagenesis. Earth-Science Reviews, 151, 1-47. https://doi.org/10.1016/j.earscirev.2015.09.010

Rockström, J., Steffen, W., Noone, K., Persson, Å., Chapin III, F. S., Lambin, E., Lenton, T. M., Scheffer, M., Folke, C., & Schellnhuber, H. J. (2009). Planetary boundaries: Exploring the safe operating space for humanity. Ecology and society, 14(2).

Rodriguez-Iruretagoiena, A., Elejoste, N., Gredilla, A., Fdez-Ortiz de Vallejuelo, S., Arana, G., Madariaga, J. M., & de Diego, A. (2016). Occurrence and geographical distribution of metals and metalloids in sediments of the Nerbioi-Ibaizabal estuary (Bilbao, Basque Country). Marine Chemistry, 185, 82-90. https://doi.org/10.1016/j.marchem.2016.04.005

Rogora, M., Buzzi, F., Dresti, C., Leoni, B., Lepori, F., Mosello, R., Patelli, M., & Salmaso, N. (2018). Climatic effects on vertical mixing and deep-water oxygen content in the subalpine lakes in Italy. Hydrobiologia, 824(1), 33-50. https://doi.org/10.1007/s10750-018-3623-y

Rogora, M., Mosello, R., & Arisci, S. (2003). The Effect of Climate Warming on the Hydrochemistry of Alpine Lakes. Water, Air, and Soil Pollution, 148(1), 347-361. https://doi.org/10.1023/A:1025489215491

Rosman, K. J. R., Chisholm, W., Hong, S., Candelone, J.-P., & Boutron, C. F. (1997). Lead from Carthaginian and Roman Spanish Mines Isotopically Identified in Greenland Ice Dated from 600 B.C. to 300 A.D. Environmental Science & Technology, 31(12), 3413-3416. https://doi.org/10.1021/es970038k

Rosman, K. J. R., Ly, C., Van de Velde, K., & Boutron, C. F. (2000). A two century record of lead isotopes in high altitude Alpine snow and ice. Earth and Planetary Science Letters, 176(3), 413-424. https://doi.org/10.1016/S0012-821X(00)00013-3

Ruddiman, W. F., Ellis, E. C., Kaplan, J. O., & Fuller, D. Q. (2015). Defining the epoch we live in. Science, 348(6230), 38-39. https://doi.org/10.1126/science.aaa7297

Rühland, K. M., Paterson, A. M., & Smol, J. P. (2015). Lake diatom responses to warming: Reviewing the evidence. Journal of Paleolimnology, 54(1), 1-35. https://doi.org/10.1007/s10933-015-9837-3

Rull, V., Vegas-Vilarrúbia, T., Corella, J. P., & Valero-Garcés, B. (2021). Bronze Age to Medieval vegetation dynamics and landscape anthropization in the southern-central Pyrenees. Palaeogeography, Palaeoclimatology, Palaeoecology, 571, 110392. https://doi.org/10.1016/j.palaeo.2021.110392

Sabás, I., Miró, A., Piera, J., Catalan, J., Camarero, L., Buchaca, T., & Ventura, M. (2021). Factors of surface thermal variation in high-mountain lakes of the Pyrenees. PLOS ONE, 16(8), e0254702. https://doi.org/10.1371/journal.pone.0254702

Sánchez, E., Rodríguez-Fonseca, B., Bladé, I., Brunet, M., Aznar, R., Cacho, I., Casado, M. J., Gimeno, L., Gutiérrez, J. M., Jordá, G., Lavín, A., López, J. A., Salat, J., & Valero-

Garcés, B. L. (2017). Progress in detection and projection of climate change in Spain since the 2010 CLIVAR-Spain regional climate change assessment report. https://digital.csic.es/handle/10261/158735

Sánchez España, F. J., Mata Campo, M. P., Vegas Salamanca, J., Morellón, M., Rodríguez García, J. A., Salazar Rincón, Á. E., & Yusta Arnal, I. (2018). Limnochemistry of the remote, high mountain Lake Marboré (Ordesa and Monte Perdido National Park, Central Pyrenees): Stratification dynamics and trace metal anomalies. https://doi.org/10.23818/limn.37.08

Sánchez-Canales, M., López-Benito, A., Acuña, V., Ziv, G., Hamel, P., Chaplin-Kramer, R., & Elorza, F. J. (2015). Sensitivity analysis of a sediment dynamics model applied in a Mediterranean river basin: Global change and management implications. Science of The Total Environment, 502, 602-610. https://doi.org/10.1016/j.scitotenv.2014.09.074

Sánchez-España, J., Vegas, J., Morellon, M., Mata, M. P., & Rodríguez García, J. A. (2019). Hydrogeochemical characteristics of the Saliencia lakes (Somiedo Natural Park, NW Spain): Trophic state and relationship with anthropogenic pressures. BOLETÍN GEOLÓGICO Y MINERO, 130(2), 251-269. https://doi.org/10.21701/bolgeomin.130.2.003

Sánchez-López, G., Hernández, A., Pla-Rabes, S., Trigo, R. M., Toro, M., Granados, I., Sáez, A., Masqué, P., Pueyo, J. J., Rubio-Inglés, M. J., & Giralt, S. (2016). Climate reconstruction for the last two millennia in central Iberia: The role of East Atlantic (EA), North Atlantic Oscillation (NAO) and their interplay over the Iberian Peninsula. Quaternary Science Reviews, 149, 135-150. https://doi.org/10.1016/j.quascirev.2016.07.021

Santisteban, J. I., Mediavilla, R., López-Pamo, E., Dabrio, C. J., Zapata, M. B. R., García, M. J. G., Castaño, S., & Martínez-Alfaro, P. E. (2004). Loss on ignition: A qualitative or quantitative method for organic matter and carbonate mineral content in sediments? Journal of Paleolimnology, 32(3), 287-299. https://doi.org/10.1023/B:JOPL.0000042999.30131.5b

Schaller, T., & Wehrli, B. (1996). Geochemical-focusing of manganese in lake sediments—An indicator of deep-water oxygen conditions. Aquatic Geochemistry, 2(4), 359-378. https://doi.org/10.1007/BF00115977

Schmidt, R., Kamenik, C., Lange-Bertalot, H., & Klee, R. (2004). Fragilaria and Staurosira (Bacillariophyceae) from sediment surfaces of 40 lakes in the Austrian Alps in relation to environmental variables, and their potential for palaeoclimatology. Journal of Limnology, 63(2), 171. https://doi.org/10.4081/jlimnol.2004.171

Schneider, P., & Hook, S. J. (2010). Space observations of inland water bodies show rapid surface warming since 1985. Geophysical Research Letters, 37(22). https://doi.org/10.1029/2010GL045059

Schnurrenberger, D., Russell, J., & Kelts, K. (2003). Classification of lacustrine sediments based on sedimentary components. Journal of Paleolimnology, 29(2), 141-154. https://doi.org/10.1023/A:1023270324800

Schwikowski, M., Barbante, C., Doering, T., Gaeggeler, H. W., Boutron, C., Schotterer, U., Tobler, L., Van de Velde, K., Ferrari, C., Cozzi, G., Rosman, K., & Cescon, P. (2004). Post-17th-Century Changes of European Lead Emissions Recorded in High-Altitude Alpine Snow and Ice. Environmental Science & Technology, 38(4), 957-964. https://doi.org/10.1021/es034715o

Shepard, F. P. (1954). Nomenclature Based on Sand-silt-clay Ratios. Journal of Sedimentary Research, 24, 151-158.

Shotyk, W., Weiss, D., Appleby, P. G., Cheburkin, A. K., Frei, R., Gloor, M., Kramers, J. D., Reese, S., & Van Der Knaap, W. O. (1998). History of Atmospheric Lead Deposition Since 12,370 14C yr BP from a Peat Bog, Jura Mountains, Switzerland. Science, 281(5383), 1635-1640. https://doi.org/10.1126/science.281.5383.1635

Simpson, G. (2023). Gratia: Graceful ggplot-Based Graphics and Other Functions for GAMs Fitted using mgcv. R package version 0.8.1.27. https://gavinsimpson.github.io/gratia/

Simpson, G. L. (2018). Modelling Palaeoecological Time Series Using Generalised Additive Models. Frontiers in Ecology and Evolution, 6, 149.

Smol, J., Birks, H., & Last, W. (2001). Tracking Environmental Change Using Lake Sediments: Volume 4: Zoological Indicators. https://doi.org/10.1007/0-306-47671-1

Smol, J. P. (2008). Pollution of Lake and Rivers: A paleoenvironmental perspective (2nd edition). Blackwell Publishing.

Smol, J. P. (2019). Under the radar: Long-term perspectives on ecological changes in lakes. Proceedings of the Royal Society B: Biological Sciences, 286(1906), 20190834. https://doi.org/10.1098/rspb.2019.0834

Souquet, P. (1967). Le crétacé supérieur sud-pyrénéen: En Catalogne, Aragon et Navarre. É. Privat.

Spagnoli, B., Planton, S., Déqué, M., Mestre, O., & Moisselin, J.-M. (2002). Detecting climate change at regional scale: The case of France. Geophysical Research Letters - GEOPHYS RES LETT, 29. https://doi.org/10.1029/2001GL014619

Šporka, F., Livingstone, D. M., Stuchlík, E., Turek, J., & Galas, J. (2006). Water temperatures and ice cover in lakes of the Tatra Mountains. Biologia, 61(18), S77-S90. https://doi.org/10.2478/s11756-006-0121-x

Stacklies, W., Redestig, H., Scholz, M., Walther, D., & Selbig, J. (2007). pcaMethods—A bioconductor package providing PCA methods for incomplete data. Bioinformatics (Oxford, England), 23(9), 1164-1167. https://doi.org/10.1093/bioinformatics/btm069

Steffen, W., Broadgate, W., Deutsch, L., Gaffney, O., & Ludwig, C. (2015). The trajectory of the Anthropocene: The Great Acceleration. The Anthropocene Review, 2(1), 81-98. https://doi.org/10.1177/2053019614564785

Steffen, W., Crutzen, P. J., & McNeill, J. R. (2007). The Anthropocene: Are humans now overwhelming the great forces of nature. Ambio-Journal of Human Environment Research and Management, 36(8), 614-621.

Steffen, W., Leinfelder, R., Zalasiewicz, J., Waters, C. N., Williams, M., Summerhayes, C., Barnosky, A. D., Cearreta, A., Crutzen, P., Edgeworth, M., Ellis, E. C., Fairchild, I. J., Galuszka, A., Grinevald, J., Haywood, A., Ivar do Sul, J., Jeandel, C., McNeill, J. r., Odada, E., … Schellnhuber, H. j. (2016). Stratigraphic and Earth System approaches to defining the Anthropocene. Earth's Future, 4(8), 324-345. https://doi.org/10.1002/2016EF000379

Stern, N. (2006). Stern Review: The economics of climate change.

Stocker, T. (2014). Climate change 2013: The physical science basis: Working Group I contribution to the Fifth assessment report of the Intergovernmental Panel on Climate Change. Cambridge university press.

Sturm, M., & Matter, A. (1978). Turbidites and Varves in Lake Brienz (Switzerland): Deposition of Clastic Detritus by Density Currents. En Modern and Ancient Lake Sediments (pp. 147-168). John Wiley & Sons, Ltd. https://doi.org/10.1002/9781444303698.ch8

Subías, I., Fanlo, I., & Billström, K. (2015). Ore-forming timing of polymetallic-fluorite low temperature veins from Central Pyrenees: A Pb, Nd and Sr isotope perspective. Ore Geology Reviews, 70, 241-251. https://doi.org/10.1016/j.oregeorev.2015.04.013

Subramanian, M. (2019). Anthropocene now: Influential panel votes to recognize Earth's new epoch. Nature.

Syvitski, J. P. M., Vörösmarty, C. J., Kettner, A. J., & Green, P. (2005). Impact of Humans on the Flux of Terrestrial Sediment to the Global Coastal Ocean. Science, 308(5720), 376-380. https://doi.org/10.1126/science.1109454

Talbot, M. R., & Allen, P. A. (1996). Lakes: Vol. Sedimentary Environments: Processes, Facies and Stratigraphy (3rd Edition). Blackwell Science.

Tammi, J., Appelberg, M., Beier, U., Hesthagen, T., Lappalainen, A., & Rask, M. (2003). Fish Status Survey of Nordic Lakes: Effects of Acidification, Eutrophication and Stocking Activity on Present Fish Species Composition. AMBIO: A Journal of the Human Environment, 32(2), 98-105. https://doi.org/10.1579/0044-7447-32.2.98

Taranu, Z. E., Gregory-Eaves, I., Leavitt, P. R., Bunting, L., Buchaca, T., Catalan, J., Domaizon, I., Guilizzoni, P., Lami, A., McGowan, S., Moorhouse, H., Morabito, G., Pick, F. R., Stevenson, M. A., Thompson, P. L., & Vinebrooke, R. D. (2015). Acceleration of cyanobacterial dominance in north temperate-subarctic lakes during the Anthropocene. Ecology Letters, 18(4), 375-384. https://doi.org/10.1111/ele.12420

Teixell, A., & García-Sansegundo, J. (1994). Mapa geológico y Memoria de la Hoja nº 118 (Zuriza). Mapa Geológico de España E. 1:50.000. ITGE.

Teranes, J. L., & Bernasconi, S. M. (2005). Factors controlling δ13C values of sedimentary carbon in hypertrophic Baldeggersee, Switzerland, and implications for interpreting

isotope excursions in lake sedimentary records. Limnology and Oceanography, 50(3), 914-922. https://doi.org/10.4319/lo.2005.50.3.0914

Tjallingii, R. (2007). Application and quality of X-Ray fluorescence core scanning in reconstructing late Pleistocene NW African continental margin sedimentation patterns and paleoclimate variations. En Http://elib.suub.uni-bremen.de/diss/docs/00010664.pdf.

Toro, M., Granados, I., Robles, S., & Montes, C. (2006). High mountain lakes of the Central Range (Iberian Peninsula): Regional limnology & environmental changes. Limnética, 25(1-2), 217-252.

Torres, I. C., Inglett, P. W., Brenner, M., Kenney, W. F., & Ramesh Reddy, K. (2012). Stable isotope (δ13C and δ15N) values of sediment organic matter in subtropical lakes of different trophic status. Journal of Paleolimnology, 47(4), 693-706. https://doi.org/10.1007/s10933-012-9593-6

Turner, B. L., Kasperson, R. E., Meyer, W. B., Dow, K. M., Golding, D., Kasperson, J. X., Mitchell, R. C., & Ratick, S. J. (1990). Two types of global environmental change: Definitional and spatial-scale issues in their human dimensions. Global Environmental Change, 1(1), 14-22. https://doi.org/10.1016/0959-3780(90)90004-S

Tylmann, W. (2005). Lithological and geochemical record of anthropogenic changes in recent sediments of a small and shallow lake (Lake Pusty Staw, northern Poland). Journal of Paleolimnology, 33(3), 313-325. https://doi.org/10.1007/s10933-004-5506-7

Urteaga, M. (2014). Minería romana en el Cantábrico oriental. Cuadernos de Prehistoria y Arqueología de la Universidad de Granada, 24, 267-300. https://doi.org/10.30827/cpag.v24i0.4095

Valero-Garcés, B. L., & Kelts, K. R. (1995). A sedimentary facies model for perennial and meromictic saline lakes: Holocene Medicine Lake Basin, South Dakota, USA. Journal of Paleolimnology, 14(2), 123-149. https://doi.org/10.1007/BF00735478

Valero-Garcés, B., Morellón, M., Moreno, A., Corella, J. P., Martín-Puertas, C., Barreiro, F., Pérez, A., Giralt, S., & Mata-Campo, M. P. (2014). Lacustrine carbonates of Iberian Karst Lakes: Sources, processes and depositional environments. Sedimentary Geology, 299, 1-29. https://doi.org/10.1016/j.sedgeo.2013.10.007

Vegas, J. (2007a). Los sistemas lacustres de las sierras de Neila y Urbión: Análisis sedimentológico y climático del pleistoceno superior y holoceno [Http://purl.org/dc/dcmitype/Text, Universidad Complutense de Madrid]. https://dialnet.unirioja.es/servlet/tesis?codigo=194249

Vegas, J. (2007b). … de eventos climáticos del Pleistoceno superior-Holoceno mediante el estudio sedimentológico de la Laguna Grande (Sierra de Neila, NO Sistema Ibérico). Revista de la Sociedad Geológica de España, 20.

Vegas, J., García-Cortés, A., Galán de Frutos, L., Pérez-González, A., Martín-Serrano, A., Vegas, J., García-Cortés, A., Galán de Frutos, L., Pérez-González, A., & Martín-Serrano, A. (2006). El registro sedimentario lacustre del maar de Fuentillejo (Ciudad

Real) [Info:eu-repo/semantics/article]. Instituto Geológico y Minero de España. https://eprints.ucm.es/id/eprint/30458/

Vegas, J., Ruiz-Zapata, B., Ortiz, J. E., Galán, L., Torres, T., García-Cortés, Á., Gil-García, M. J., Pérez-González, A., & Gallardo-Millán, J. L. (2010). Identification of arid phases during the last 50 cal. Ka BP from the Fuentillejo maar-lacustrine record (Campo de Calatrava Volcanic Field, Spain). Journal of Quaternary Science, 25(7), 1051-1062. https://doi.org/10.1002/jqs.1262

Vegas-Vilarrúbia, T., Corella, J. P., Sigró, J., Rull, V., Dorado-Liñan, I., Valero-Garcés, B., & Gutiérrez-Merino, E. (2022). Regional precipitation trends since 1500 CE reconstructed from calcite sublayers of a varved Mediterranean lake record (Central Pyrenees). Science of The Total Environment, 826, 153773. https://doi.org/10.1016/j.scitotenv.2022.153773

Ventura, M., Camarero, L., Buchaca, T., Bartumeus, F., Livingstone, D. M., & Catalan, J. (2000). The main features of seasonal variability in the external forcing and dynamics of a deep mountain lake (Redó, Pyrenees). Journal of Limnology, 59(1s), 97-108. https://doi.org/10.4081/jlimnol.2000.s1.97

Vera, J. A. (2004). Geología de españa. Igme.

Vicente-Serrano, S. M., Gouveia, C., Camarero, J. J., Beguería, S., Trigo, R., López-Moreno, J. I., Azorín-Molina, C., Pasho, E., Lorenzo-Lacruz, J., & Revuelto, J. (2013). Response of vegetation to drought time-scales across global land biomes. Proceedings of the National Academy of Sciences, 110(1), 52-57.

Vidaller, I., Revuelto, J., Izagirre, E., Rojas-Heredia, F., Alonso-González, E., Gascoin, S., René, P., Berthier, E., Rico, I., Moreno, A., Serrano, E., Serreta, A., & López-Moreno, J. I. (2021). Toward an Ice-Free Mountain Range: Demise of Pyrenean Glaciers During 2011–2020. Geophysical Research Letters, 48(18). https://doi.org/10.1029/2021GL094339

Vitousek, P. M., Mooney, H. A., Lubchenco, J., & Melillo, J. M. (1997). Human domination of Earth's ecosystems. Science, 277(5325), 494-499.

von Storch, H., Costa-Cabral, M., Hagner, C., Feser, F., Pacyna, J., Pacyna, E., & Kolb, S. (2003). Four decades of gasoline lead emissions and control policies in Europe: A retrospective assessment. Science of The Total Environment, 311(1), 151-176. https://doi.org/10.1016/S0048-9697(03)00051-2

Wilhelm, B., Arnaud, F., Enters, D., Allignol, F., Legaz, A., Magand, O., Revillon, S., Giguet-Covex, C., & Malet, E. (2012). Does global warming favour the occurrence of extreme floods in European Alps? First evidences from a NW Alps proglacial lake sediment record. Climatic Change, 113(3), 563-581. https://doi.org/10.1007/s10584-011-0376-2

Williamson, C. E., Saros, J. E., Vincent, W. F., & Smol, J. P. (2009). Lakes and reservoirs as sentinels, integrators, and regulators of climate change. Limnology and Oceanography, 54(6part2), 2273-2282. https://doi.org/10.4319/lo.2009.54.6_part_2.2273

Wilson, A. (2002). Machines, Power and the Ancient Economy. The Journal of Roman Studies, 92, 1-32. https://doi.org/10.2307/3184857

Wilson, E. O. (1992). The diversity of life Penguin. Penguin Books Ltd.: London, UK.

Wolfe, A. P., Cooke, C. A., & Hobbs, W. O. (2006). Are current rates of atmospheric nitrogen deposition influencing lakes in the eastern Canadian Arctic? Arctic, Antarctic, and Alpine Research, 38(3), 465-476.

Wood, S. (2022). mgcv R Package: Mixed GAM Computation Vehicle with Automatic Smoothness Estimation. https://CRAN.R-project.org/package=mgcv , R package version 1.8.33

Wood, S. N. (2017). Generalized Additive Models: An Introduction with R, Second Edition (2.ª ed.). Chapman and Hall/CRC. https://doi.org/10.1201/9781315370279

Woolway, R. I., M. Livingstone, D., & Kernan, M. (2015). Altitudinal dependence of a statistically significant diel temperature cycle in Scottish lochs. Inland Waters, 5(4), 311-316. https://doi.org/10.5268/IW-5.4.854

Wu, L., Wilson, D. J., Wang, R., Yin, X., Chen, Z., Xiao, W., & Huang, M. (2020). Evaluating Zr/Rb Ratio From XRF Scanning as an Indicator of Grain-Size Variations of Glaciomarine Sediments in the Southern Ocean. Geochemistry, Geophysics, Geosystems, 21(11), e2020GC009350.

Zaharescu, D. G., Hooda, P. S., Soler, A. P., Fernandez, J., & Burghelea, C. I. (2009). Trace metals and their source in the catchment of the high altitude Lake Respomuso, Central Pyrenees. Science of The Total Environment, 407(11), 3546-3553. https://doi.org/10.1016/j.scitotenv.2009.02.026

Zalasiewicz, J., Waters, C. N., Ellis, E. C., Head, M. J., Vidas, D., Steffen, W., Thomas, J. A., Horn, E., Summerhayes, C. P., Leinfelder, R., McNeill, J. R., Gałuszka, A., Williams, M., Barnosky, A. D., Richter, D. de B., Gibbard, P. L., Syvitski, J., Jeandel, C., Cearreta, A., … Zinke, J. (2021). The Anthropocene: Comparing Its Meaning in Geology (Chronostratigraphy) with Conceptual Approaches Arising in Other Disciplines. Earth's Future, 9(3), e2020EF001896. https://doi.org/10.1029/2020EF001896

Zalasiewicz, J., Williams, M., Haywood, A., & Ellis, M. (2011). The Anthropocene: A new epoch of geological time? Philosophical Transactions of the Royal Society A: Mathematical, Physical and Engineering Sciences, 369(1938), 835-841. https://doi.org/10.1098/rsta.2010.0339

Ziegler, M., Jilbert, T., de Lange, G. J., Lourens, L. J., & Reichart, G.-J. (2008). Bromine counts from XRF scanning as an estimate of the marine organic carbon content of sediment cores. Geochemistry, Geophysics, Geosystems, 9(5). https://doi.org/10.1029/2007GC001932

9. Appendix

The dataset for each lake where the data used in this thesis is collected is available here:

- Vicente de Vera, Alejandra. (2023). Alejandra Vicente de Vera PhD Thesis (2023) [Data set]. Zenodo. https://doi.org/10.5281/zenodo.7893501